MARTIN MARIETTA ENERGY SYSTEMS LIBRARIES

3 4456 0251538 4

CENTRAL RESEARCH LIBRARY
DOCUMENT COLLECTION

cy. 2

ORNL-4272
UC-10 – Chemical Separations Processes
for Plutonium and Uranium

CHEMICAL TECHNOLOGY DIVISION

ANNUAL PROGRESS REPORT

FOR PERIOD ENDING MAY 31, 1968

OAK RIDGE NATIONAL LABORATORY
CENTRAL RESEARCH LIBRARY
DOCUMENT COLLECTION
LIBRARY LOAN COPY
DO NOT TRANSFER TO ANOTHER PERSON
If you wish someone else to see this document, send in name with document and the library will arrange a loan.
UCN-7969
(3 3-67)

OAK RIDGE NATIONAL LABORATORY
operated by
UNION CARBIDE CORPORATION
for the
U.S. ATOMIC ENERGY COMMISSION

Printed in the United States of America. Available from Clearinghouse for Federal Scientific and Technical Information, National Bureau of Standards, U.S. Department of Commerce, Springfield, Virginia 22151
Price: Printed Copy $3.00; Microfiche $0.65

LEGAL NOTICE

This report was prepared as an account of Government sponsored work. Neither the United States, nor the Commission, nor any person acting on behalf of the Commission:

A. Makes any warranty or representation, expressed or implied, with respect to the accuracy, completeness, or usefulness of the information contained in this report, or that the use of any information, apparatus, method, or process disclosed in this report may not infringe privately owned rights; or

B. Assumes any liabilities with respect to the use of, or for damages resulting from the use of any information, apparatus, method, or process disclosed in this report.

As used in the above, "person acting on behalf of the Commission" includes any employee or contractor of the Commission, or employee of such contractor, to the extent that such employee or contractor of the Commission, or employee of such contractor prepares, disseminates, or provides access to, any information pursuant to his employment or contract with the Commission, or his employment with such contractor.

ORNL-4272

Contract No. W-7405-eng-26

CHEMICAL TECHNOLOGY DIVISION

ANNUAL PROGRESS REPORT

for Period Ending May 31, 1968

D. E. Ferguson – Division Director
K. B. Brown – Assistant Division Director
R. G. Wymer – Chemical Development Section A Chief
R. E. Blanco – Chemical Development Section B Chief
M. E. Whatley – Unit Operations Section Chief
H. E. Goeller – Process Design Section Chief
R. E. Brooksbank – Pilot Plant Section Chief

SEPTEMBER 1968

OAK RIDGE NATIONAL LABORATORY
Oak Ridge, Tennessee
operated by
UNION CARBIDE CORPORATION
for the
U. S. ATOMIC ENERGY COMMISSION

MARTIN MARIETTA ENERGY SYSTEMS LIBRARIES

3 4456 0251538 4

Reports previously issued in this series are as follows:

ORNL-2392	Period Ending August 31, 1957
ORNL-2576	Period Ending August 31, 1958
ORNL-2788	Period Ending August 31, 1959
ORNL-2993	Period Ending August 31, 1960
ORNL-3153	Period Ending May 31, 1961
ORNL-3314	Period Ending May 31, 1962
ORNL-3452	Period Ending May 31, 1963
ORNL-3627	Period Ending May 31, 1964
ORNL-3830	Period Ending May 31, 1965
ORNL-3945	Period Ending May 31, 1966
ORNL-4145	Period Ending May 31, 1967

Contents

SUMMARY vii

1. MOLTEN-SALT REACTOR PROCESSING 1
   - 1.1 Corrosion Control by Use of a Frozen Wall 1
   - 1.2 Relative Volatilities of Fission Product Fluorides in MSBR Salts 3
   - 1.3 Determination of Relative Volatilities by the Transpiration Method 3
   - 1.4 Distillation of MSRE Fuel Carrier Salt 8
   - 1.5 Measurement of Distribution Coefficients in Molten Metal-Salt Systems 10
   - 1.6 Removal of Protactinium from a Two-Fluid MSBR 14
   - 1.7 Removal of Protactinium from a Single-Fluid MSBR 17
   - 1.8 Engineering Studies of Continuous Reductive Extraction 21
   - 1.9 Recovery of Uranium from MSRE Fuel Salt by Fluorination 21
   - 1.10 MSRE Fuel Salt Processing 25
   - 1.11 Removal of Nickel, Iron, and Chromium Fluorides from MSRE Fuel Carrier Salt 25
   - 1.12 Preparation of ^{233}U Fuel for the MSRE 28

2. DEVELOPMENT OF AQUEOUS PROCESSES FOR FAST REACTOR FUELS 34
   - 2.1 Shipping and Head-End Mechanical Processing 35
   - 2.2 Head-End Treatment for Removal of Fission Products 41
   - 2.3 Dissolution 42
   - 2.4 Solvent Extraction with TBP 48
   - 2.5 Partitioning 50
   - 2.6 Solvent Stability 51
   - 2.7 Extraction of Plutonium with Amines 54

3. DEVELOPMENT OF PROCESSES FOR HTGR AND LWR FUELS 56
   - 3.1 Head-End Mechanical Methods for Processing HTGR Fuel 56
   - 3.2 Grind-Leach Process for HTGR Fuel 61
   - 3.3 Methods for Processing LWR Fuels 62

4. FLUORIDE-VOLATILITY PROCESSING 68
   - 4.1 Status of the Fluidized-Bed Volatility Pilot Plant 68
   - 4.2 Hot-Cell Studies of the Fluidized-Bed Volatility Process 69

4.3 Sorption of Fission Product Fluorides on Sodium Fluoride 69
4.4 Small-Scale Engineering Studies 71

5. WASTE TREATMENT AND DISPOSAL 72
5.1 High-Level Radioactive Waste 72
5.2 Intermediate-Level Radioactive Waste 74
5.3 Engineering, Economic, and Safety Evaluation 81
5.4 Separation of Noble Gases from Air by Using Permselective Membranes 85

6. TRANSURANIUM-ELEMENT PROCESSING 92
6.1 TRU Operations 92
6.2 Isolation and Purification of TRU Products 99
6.3 Development of Chemical Processes 102
6.4 Special Projects 112
6.5 Transplutonium Element Research 115

7. DEVELOPMENT OF THE THORIUM FUEL CYCLE 129
7.1 Preparation of Thorium-Uranium Oxide Sol by Solvent Extraction 129
7.2 Development of Microsphere Forming Equipment 129
7.3 Preparation of Sol-Gel Materials 136
7.4 Thorium-Uranium Recycle Facility 137
7.5 ^{233}U Storage and Distribution Facility 138

8. SOL-GEL PROCESSES FOR THE URANIUM FUEL CYCLE 142
8.1 Preparation of UO_2 Sols by Solvent Extraction 142
8.2 Plutonia and Urania-Plutonia 145
8.3 Preparation of Microspheres 149
8.4 Materials Development 157

9. SOL-GEL PROCESSES FOR ISOTOPIC HEAT SOURCES 161
9.1 Laboratory Studies of ^{238}Pu Sol-Gel Process 161
9.2 Development Studies in a Glove-Box System 166
9.3 Plutonium Sol-Gel Pilot Plant 168
9.4 Assistance to Mound Laboratory 170
9.5 Curium Sol-Gel Studies 170

10. SEPARATIONS CHEMISTRY RESEARCH 174
10.1 Extraction of Metal Sulfates and Nitrates by Amines 174
10.2 New Separations Agents 174
10.3 Beryllium Purification by Solvent Extraction 175
10.4 Recovery of Uranium from Commercial Phosphoric Acid 177
10.5 Equilibria and Mechanisms of Extraction 179
10.6 Kinetics of Metal-Ion Extractions by Organophosphorus Acids 181
10.7 Aggregation and Activity Coefficients in Solvent Phases 183

11. CHEMICAL APPLICATIONS OF NUCLEAR EXPLOSIONS 187
11.1 Copper Ores 187
11.2 Recovery of Oil from Shale 188
12. BIOCHEMICAL SEPARATIONS 192
MACROMOLECULAR SEPARATIONS 192
12.1. Development of Reversed-Phase Chromatography Systems for Transfer Ribonucleic Acid Separations 192
12.2 Engineering Scale-up of Biochemical Separations Techniques 194
12.3 Isolation of Purified Transfer Ribonucleic Acids 197
12.4 Solvent Extraction of Transfer Ribonucleic Acids 198
12.5 Behavior of Transfer Ribonucleic Acids on Polyacrylamide Gel Columns 200
BODY FLUID ANALYSIS 201
12.6 Prototype Analyzers 202
12.7 System Components 204
12.8 Parametric Studies 208
12.9 Identification of Body Fluid Constituents 209
12.10 Analytical Results 212
12.11 Data Acquisition and Analysis 217
12.12 Literature Survey 217
13. IRRADIATION EFFECTS ON HETEROGENEOUS SYSTEMS 218
13.1 The Radiolysis of Adsorbed Water 218
14. SPECTROPHOTOMETRIC STUDIES OF SOLUTIONS OF ALPHA-ACTIVE MATERIALS 219
14.1 Spectral Correlations of the Actinyl Ions 219
14.2 Modification and Testing of the Spectrophotometer System for High Alpha Levels 219
14.3 Emission Spectra of the Transuranium Elements 220
15. CHEMICAL ENGINEERING RESEARCH 221
15.1 Development of the Stacked-Clone Contactor 221
16. REACTOR EVALUATION STUDIES 225
16.1 Work in Support of the AEC Evaluation of Civilian Nuclear Power for the Period 1970–2020 225
16.2 Fuel Shipping Cost Studies 226
16.3 Cost Estimates for the Preparation, Reprocessing, and Reconversion of Fuel 228
16.4 Optimization Studies of the Reprocessing Industry in an Expanding Nuclear Economy 234
16.5 RIBDOR Fission Product Code 236
17. PREPARATION AND PROPERTIES OF ACTINIDE OXIDES 238
17.1 Fundamental Studies of Urania Sols 238
17.2 Preparation of Cermets from Mixed Sols 240

17.3 Fundamental Studies of Urania Gels 240
17.4 Comparative Investigation of Lanthanide and Actinide Sols 241

18. CHEMISTRY OF CARBIDES AND NITRIDES 243

19. SAFETY STUDIES OF FUEL TRANSPORT 249
19.1 The *Criteria* 249
19.2 AEC Assistance Program 253
19.3 CTD Cask Evaluation Program 254

20. THE NUCLEAR-POWERED AGRO-INDUSTRIAL COMPLEX: SPECIAL STUDY PROJECT 256

21. WATER RESEARCH PROGRAM 257

22. ASSISTANCE PROGRAMS 258
22.1 Eurochemic Assistance Program 258
22.2 Evaluation of the Radiation Resistance of Selected Protective Coatings (Paints) 258

PUBLICATIONS, SPEECHES, AND SEMINARS 261

Summary

1. MOLTEN-SALT REACTOR PROCESSING

The work on the development of methods for processing fuel streams of molten-salt breeder reactors has changed emphasis since the last reporting period. The fluorination-distillation flowsheet for processing two-fluid breeder reactor fuel has been discarded in favor of processes that are based on reductive extraction suitable for single-fluid breeder reactors. In the new system, protactinium can be isolated from the neutron flux by dynamically holding it in a decay tank between two reductive extraction cascades. The rare-earth fission products can probably be separated from thorium by reductive extraction and then concentrated to the limit of their solubilities (or to the economic limit imposed by the removal of decay heat). The determination of the separation factors for this system is under way. Fluorination, low-pressure distillation, and protection of surfaces from corrosion by frozen layers of salt are still being studied and are expected to find application in the new process.

1.1 Corrosion Control by Use of a Frozen Wall

Studies of the protection of a continuous fluorinator from corrosion by use of a layer of frozen salt on the vessel wall are under way. Operability of such a system was demonstrated by countercurrently contacting molten salt and an inert gas in the presence of a frozen layer of salt in a 5-in.-diam, 8-ft-long column. An internal heat source consisting of Calrod heaters in a $^3/_4$-in.-diam pipe located along the center line of the system was used to simulate the volume heat source provided by fission product decay in the molten salt. Generally, thicknesses of the frozen wall and the temperature profiles in the frozen salt were in good agreement with values that were predicted by relationships based on radial heat transfer from the expected volume heat source. The thickness of the frozen wall ranged from 0.3 to 0.8 in., depending on experimental conditions.

1.2 Relative Volatilities of Fission Product Fluorides in MSBR Salts

Relative volatilities, with respect to LiF, of several rare-earth trifluorides and alkaline-earth fluorides have been measured in an equilibrium still at 1000°C. The deviation between measured values and values predicted by Raoult's law (for fluorides for which sublimation pressure data are available) is within the combined errors involved in measuring the sublimation pressures and the relative volatilities.

1.3 Determination of Relative Volatilities by the Transpiration Method

Relative volatilities for several solutes were measured in the temperature range of 900 to 1050°C, using $LiF\text{-}BeF_2$ (90-10 mole %) as the solvent. Values obtained with respect to LiF at 1000°C were about 0.04 for UF_4, 25 for RbF, 95 for CsF, and about 2 for ZrF_4 (when present in solution at a concentration of 0.083 mole %). Some vapor-liquid equilibrium data were also obtained in $LiF\text{-}BeF_2\text{-}ThF_4$ systems.

1.4 Distillation of MSRE Fuel Carrier Salt

The low-pressure distillation of MSRE carrier salt is being studied in equipment that includes a 48-liter feed tank, a 12-liter still, a condenser, and a 48-liter condensate receiver. Two runs were made in which a still pot temperature of about 1000°C and a condenser pressure of 0.06 to 2 mm

Hg were used; the total salt volume distilled during the runs was about 60 liters. With the lower condenser pressures, distillation rates of 1.2 and 1.5 ft^3 of salt per day per square foot of vaporization surface were observed at still pot temperatures of 990 and 1005°C respectively.

1.5 Measurement of Distribution Coefficients in Molten Metal-Salt Systems

The distribution of uranium, thorium, and rare earths between selected molten fluoride salts and lithium-bismuth solutions is being studied in support of reductive extraction processes for molten-salt breeder reactor (MSBR) fuels. Data obtained so far show that uranium can easily be preferentially extracted from either the fuel salt of a two-fluid MSBR or from single-fluid MSBR fuel. The separation of uranium from rare earths is good (separation factors of at least 10^3) for each case. In the processing of single-fluid MSBR fuel, uranium can be separated from thorium by a factor of at least 10^4. Rare earths can probably be separated from thorium, but more data will be required to establish the optimum conditions.

1.6 Removal of Protactinium from a Two-Fluid MSBR

Protactinium removal processes based on reductive extraction, using liquid bismuth containing thorium, were evaluated to determine the feasibility of removing protactinium from the fertile stream of a two-fluid MSBR. Calculations based on a 1000-Mw (electrical) reactor indicate that adequate protactinium removal can be achieved with a system consisting of (1) an extraction column that is equivalent to about four ideal stages, (2) an electrolytic oxidizer-reducer, (3) a protactinium decay tank having a volume of about 400 ft^3, and (4) a fluorinator for removing uranium from salts in the decay tank. The required fertile salt and metal flow rates are about 25 and 0.2 gpm respectively.

1.7 Removal of Protactinium from a Single-Fluid MSBR

The steady-state performance of a system for isolating protactinium from a single-fluid MSBR by reductive extraction was examined. Calculations based on tentative equilibrium data indicate that protactinium can be adequately isolated by means of a system consisting of an extraction column that is equivalent to about 12 ideal stages, an electrolytic oxidizer-reducer, and a protactinium decay tank having a volume of about 400 ft^3. The required salt and metal flow rates are about 2 gpm. Calculations showed that the system would be quite sensitive to minor variations in operating conditions, and consequently several methods for stabilizing the system have been explored. Details will be revised as more accurate data become available; however, the qualitative conclusions presented here are believed to be valid.

1.8 Engineering Studies of Continuous Reductive Extraction

A facility is being installed in Building 3592 to permit experimental engineering studies of reductive extraction. This extraction process involves the continuous countercurrent contact of molten salt and liquid bismuth containing a reductant such as thorium. The transfer of uranium between the salt and the metal phases will be studied at 600°C, using salt of the composition $LiF-ThF_4-UF_4$ (23.7-76.0-0.3 mole %).

1.9 Recovery of Uranium from MSRE Fuel Salt by Fluorination

Small-scale tests are being made with simulated MSRE fuel salt to determine the effects of temperature, fluorine concentration, and fluorine flow rate on the rate of uranium volatilization and the rate of corrosion of Hastelloy N. Preliminary results indicate that uranium can readily be removed from the salt with fluorine at 450 or 500°C; however, corrosion rates of up to 0.5 mil/hr can be expected during the fluorination period.

Fluorination is also being considered for use as the first step in a precise method for analyzing for uranium in MSRE fuel salt. The resulting UF_6 product would be collected and decontaminated, using the NaF sorption-desorption method; then the UF_6-NaF complex could be transferred to a low-level radiation area, where the uranium would be analyzed by a precision coulometric method. Decontamination factors for ^{103}Ru, ^{95}Nb, and ^{132}Te

have been greater than 10^5; however, attempts to achieve an adequate decontamination factor (greater than 10^3) for iodine have been unsuccessful so far.

1.10 MSRE Fuel Salt Processing

We have completed modifications to the MSRE fuel processing facility to provide a backup system for the fluorine disposal and iodine sorption equipment. Also, a filter to remove metal corrosion products from the salt has been added. Four test runs were made with the SO_2 system for fluorine disposal. Because of operational difficulties, this system was replaced with a KOH-KI scrubber. Tests with the scrubber are now in progress.

1.11 Removal of Nickel, Iron, and Chromium Fluorides from MSRE Fuel Carrier Salt

During fluorination of the MSRE fuel salt for uranium removal, the salt will become contaminated with fluorides of nickel, iron, and chromium as a result of corrosion of the Hastelloy N fluorinator. The return of these fluorides to the reactor is undesirable. Experiments to evaluate corrosion product removal methods indicate that the reduction of Ni(II) by hydrogen sparging and the reduction of Fe(II) and Cr(II) by addition of zirconium metal are feasible. Filtration of the resulting mixture of salt and metals was shown to be effective for removing suspended metals.

1.12 Preparation of ^{233}U Fuel for the MSRE

Plans have been completed for refueling and operating the MSRE with ^{233}U fuel. Approximately 39.5 kg of 91.4%-enriched ^{233}U as ^{7}LiF-$^{233}UF_4$ (73-27 mole %) eutectic salt will be required by the MSRE. This material is being prepared in remotely operated equipment that is installed in cell G of the Thorium-Uranium Recycle Facility (Building 7930) because of the high ^{232}U content (222 ppm) of the ^{233}U. The process consists of reduction and hydrofluorination of $^{233}UO_3$ to yield $^{233}UF_4$. Lithium-7 fluoride is added and melted, and then the resulting eutectic salt is purified, filtered, and loaded into enriching capsules and salt cans for reactor refueling. The first third of the material has been successfully prepared.

2. DEVELOPMENT OF AQUEOUS PROCESSES FOR FAST REACTOR FUELS

2.1 Shipping and Head-End Mechanical Processing

A preliminary design and a cost estimate of an on-site fuel dismantling facility were completed. The operating cost of such a facility, unless shared by a number of reactors at the site, exceeds the saving in shipping costs. Heat transfer calculations indicate that a liquid coolant, probably sodium, will be required for normal shipping conditions if the temperature of the fuel cladding is not to exceed the temperature experienced when in the reactor (1275°F).

A small prototype semicontinuous shear that will accommodate a 5×5 array of LMFBR subassembly rods was operated at a shear rate that is equivalent to a throughput of 2 tons/day. The small size is a distinct maintenance advantage.

A prototype continuous leacher featuring an internal spiral screw performed satisfactorily in initial tests with sheared simulated General Electric LMFBR fuel rods.

2.2 Head-End Treatment for Removal of Fission Products

Preliminary tests of a head-end treatment for removing volatile fission products from UO_2-PuO_2 fuel prior to dissolution were encouraging. Heating high-burnup, long-decayed fuels ("spiked" with short-decayed UO_2 to provide ^{131}I and other short-lived fission products) to 450 to 750°C and oxidizing the UO_2 to U_3O_8 released 88 to 94% of the tritium and 82 to 98% of the ^{131}I.

2.3 Dissolution

In hot-cell dissolution tests with a number of irradiated stainless-steel-clad PuO_2-UO_2 fuels, the major portion of each of the fuel samples dissolved rapidly in 4 to 8 *M* HNO_3. However, in each case, a small fraction of the plutonium resisted dissolution. Essentially complete recovery of plutonium was obtained by releaching the residue. The fraction of iodine volatilized during dissolution varied from 15 to 88%, depending on the experimental conditions.

In dissolution studies with unirradiated UO_2 "spiked" with KI, more than 99.9% of the iodine was volatilized by using the proper conditions and equipment arrangement. Evolution of nitrogen oxides was prevented and the UO_2 dissolution rate was increased by adding hydrogen peroxide to the nitric acid dissolvent.

2.4 Solvent Extraction with TBP

Data were obtained for the extraction of Pu(VI) from 1 to 4 *M* HNO_3, and of Pu(IV) from 2 to 4 *M* HNO_3, with 15% TBP in *n*-dodecane. Coefficients for the extraction of Pu(VI) from 2 *M* HNO_3 were proportional to about the 1.4 power of the TBP concentration in the range of 4 to 30 vol %. In batch countercurrent tests of a coextraction flowsheet, metal recoveries of greater than 99.9% were demonstrated. Because of the relatively large concentrations of plutonium in this system, the recovery of plutonium is more sensitive to the concentration of metal in the solvent than it is in the processing of thermal reactor fuels. Therefore the system must be operated with relatively low solvent loadings in order to avoid excessive plutonium reflux.

2.5 Partitioning

Reductants that might serve as alternatives to ferrous sulfamate are being evaluated for reducing plutonium in the partitioning cycle. Favorable results were obtained by using ferrous nitrate stabilized with a small amount of hydrazine. In a batch countercurrent demonstration test, the stripping of plutonium from 15% TBP–*n*-dodecane was greater than 99.99% complete, and the Pu/U decontamination factor was 5×10^5. Studies of partitioning the plutonium by reducing it with hydrogen in the presence of a platinum catalyst continued to show promise.

2.6 Solvent Stability

A study is being made of the radiolytic and chemical stability of TBP–*n*-dodecane to obtain a better understanding of the extent of solvent damage that may result in processing high-burnup, short-cooled fast reactor fuels and its subsequent effect on process performance. Cyclic tests were completed in which the solvent was: (1) irradiated by a ^{60}Co source in increments of 0.3, 1.0, or 2.0 whr liter^{-1} cycle^{-1} while in contact with $UO_2(NO_3)_2$-HNO_3 (simulates the extraction step), (2) stripped of its uranium content with dilute HNO_3, and (3) washed with 0.3 *M* Na_2CO_3. This procedure was repeated until the integrated solvent radiation dose reached 6 to 10 whr/liter. The 0.3 whr liter^{-1} cycle^{-1} exposures (several times higher than estimated for processing short-cooled high-burnup fuels) had no observable effect on solvent performance, as compared with that of unirradiated solvent. At the higher per cycle exposures, the only changes observed were an increase in the extraction of ^{95}Zr and a slight increase in the retention of uranium by the irradiated solvent.

A study of the kinetics of the precipitation of ferric dibutylphosphate from 1 to 5 *M* HNO_3 aqueous solutions showed the rate of precipitation to be approximately proportional to the square of the excess Fe^{3+} concentration. The solubility product of $Fe(DBP)_3$ increases from 2×10^{-13} to 2×10^{-12} (mole/liter)^4 as the nitric acid concentration increases from 1 to 5 *M*. Preliminary experiments with zirconium at an initial concentration of 231 mg/liter in 1 to 5 *M* HNO_3 show that the precipitation process is essentially complete in 5 to 10 sec with initial concentrations of 0.1 to 1 g of HDBP per liter. Measurements at 50°C of the decomposition of TBP dissolved in 3 *M* HNO_3 show the rate to be somewhat less than 2 mg liter^{-1} hr^{-1}.

Studies of iodine extraction showed that extracted iodine reacts rapidly with the solvent to form compounds (presumably alkyl iodides) that are not readily removed from the solvent phase.

2.7 Extraction of Plutonium with Amines

Data for the extraction of Pu(IV) from 5 *M* HNO_3 were obtained with diethylbenzene solutions of four branched secondary amines. Each of these four amines has sufficient extraction power to permit its use in the final plutonium purification step. In addition, these amines have a potential advantage over tertiary and quaternary amines in that they are amenable to dilute acid stripping of the plutonium. Extractions of Pu(VI) were weak with a secondary amine but were moderately strong with tertiary and quaternary amines.

3. DEVELOPMENT OF PROCESSES FOR HTGR AND LWR FUELS

3.1 Head-End Mechanical Methods for Processing HTGR Fuel

Significant progress was made in the development of head-end mechanical methods for processing HTGR graphite-base fuels. In initial tests, an inexpensive hacksawing technique was shown to be feasible for converting a hexagon-shaped Public Service of Colorado (PSC) fuel block into pieces suitable for feed to a hammer mill or crusher. The cuts were made through coolant channels, thereby avoiding all contact with fuel particles. Hammer milling of sawed graphite PSC prototype fuel yielded a product that could be handled without difficulty and could be introduced easily into a fluidized bed. However, additional work with graphite fuel blocks containing coated particles will be necessary to establish the feasibility of the method.

Hydraulic jet erosion of fuel particles from a prototype PSC fuel stick was readily accomplished with a water jet operating at pressures of about 5000 to 6000 psig. However, an excessive number of fuel particles were broken by the jet as they were dislodged. Classification of dislodged particles by sieving showed that UO_2 and ThO_2 cannot be separated by a single screening operation. Additional studies of this method will be required.

Alteration and renovation of existing fluidized-bed equipment components were made in preparation for scoping studies of the burning of PSC fuel and the classifying of dislodged fuel particles.

3.2 Grind-Leach Process for HTGR Fuel

Duplex-coated sol-gel ThO_2 and $(Th,U)O_2$ particles that had been irradiated to burnups of 15,000 and 17,500 Mwd per ton of Th + U and had decayed for 10 and 19 months, respectively, were ground to −100 mesh to ensure fracture of the kernels and the pyrolytic-carbon coatings. They were then leached in boiling fluoride-catalyzed nitric acid to dissolve the thorium, uranium, and fission products. Recoveries of at least 99.6% of the uranium and 99.9% of the thorium were realized, and more than 86% of the gamma emitters were dissolved. These results contrast markedly with the uranium and thorium recoveries – as low as 95.4 and 93.1%, respectively – that were obtained in earlier grind-leach studies with laminar-coated $(Th,U)C_2$ particles in a graphite matrix. The grind-leach process may, therefore, be applicable to HTGR fuels containing pyrolytic-carbon-coated sol-gel oxide particles. However, the process may be of marginal value, since the leached residue must be stored as high-level radioactive waste.

3.3 Methods for Processing LWR Fuels

Studies of the shear-leach processing of third-generation LWR power reactor fuels were continued. Shearing of a tubular array having a cross section as large as 10 by 10 in. was found to be feasible. Prototype fuel assemblies containing 196, 327, and 484 stainless-steel-clad tubes filled with either porcelain or UO_2 were sheared satisfactorily. A shearing force of from $73\frac{1}{2}$ to 291 tons applied to a rectangular-shaped moving blade was required to sever the array.

An investigation of the factors responsible for the fires associated with the routine processing of NPR fuel at Nuclear Fuel Services, Inc., West Valley, New York, was begun. A literature search and initial bench-scale experiments allowed hypotheses to be made concerning the causes of the three incidents. A more comprehensive study, including the metallographic examination of fuel sheared and/or leached by NFS, is continuing.

4. FLUORIDE-VOLATILITY PROCESSING

The investigation of fluoride-volatility processing at ORNL was part of an intersite program to develop an alternative to the aqueous method for processing spent UO_2 fuels. Because of technical and budgetary factors, the program was canceled. Work at ORNL on the process has now been terminated.

Experimental work was brought to an orderly conclusion. The major equipment items that had been installed in the pilot plant were left in place; the pilot plant was put in standby.

4.1 Status of the Fluidized-Bed Volatility Pilot Plant

Most of the major equipment items for head-end processing (including the primary reactors, the pyrohydrolyzer, and the main cold trap) have been

installed. A cell ventilation system, to ensure safety, was also installed.

4.2 Hot-Cell Studies of the Fluidized-Bed Volatility Process

Bench-scale experiments were performed with irradiated UO_2 pellets. Overall decontamination of uranium from gross fission products was uniformly high.

4.3 Sorption of Fission Product Fluorides on Sodium Fluoride

We investigated the mechanism of sorption of niobium and ruthenium fluorides on NaF. Sorption of NbF_5 on NaF was found to be a function of temperature (with a maximum at 450°C) and of NbF_5 concentration in the gas stream.

Developmental work to determine the feasibility of recovering neptunium and uranium separately, using beds of NaF, was encouraging. The most promising process at this time involves the cosorption of NpF_6 and UF_6 on NaF and the subsequent desorption of UF_6 in the presence of an inert gas, followed by the desorption of NpF_6 in a stream of fluorine.

4.4 Small-Scale Engineering Studies

Decladding and oxidation studies were completed, but no fluorination experiments were run. Of the several in-line instrumentation systems that were tested, only one, a hydrogen analysis system for following the progress of the decladding reaction, was satisfactory. We did not complete the testing of the fluidized-bed sampler.

5. WASTE TREATMENT AND DISPOSAL

5.1 High-Level Radioactive Waste

Development work on the disposal of aqueous high-level waste by the Pot Calcination process is now complete except for the pilot-plant demonstration of this process at the Pacific Northwest Laboratory (PNL). Currently, the major objectives in high-level waste development are to develop and to demonstrate processes for preparing wastes from the High-Temperature Gas-Cooled Reactor (HTGR), the Molten-Salt Reactor (MSR), and fast breeder reactors (FBR's) for permanent disposal.

The Pot Calcination process was successfully demonstrated at PNL in a series of tests that involved wastes containing over 4,000,000 curies. In one test, a waste volume, which was equivalent to that from 1.2 tons of spent fuel and contained 1,300,000 curies, was calcined in a pot 8 in. in diameter by 8 ft long. Thus, one line of calcination equipment could process the waste from a 1-ton-of-uranium-per-day fuel processing plant, that is, one capable of serving about 7000 Mw of installed electrical capacity.

The burn-leach process for processing HTGR fuels produces two types of high-level waste – the solid leached alumina bed from the fluidized-bed burner and the liquid waste from the Thorex solvent extraction process. Simulated samples of the alumina bed and fission products were sealed in stainless steel pots, and the pressures were observed at 250, 550, and 850°C for three months. A pressure decrease was noted in each case. Bed samples were mixed with a lead silicate glass, and then the glass was melted at 850°C to form a continuous phase surrounding the solid waste particles. The product was a satisfactorily dense, hard, void-free solid containing 37 wt % powder and 63 wt % glass. The density and the viscosity of simulated Thorex liquid waste were determined as functions of temperature and concentration. In initial studies of MSR wastes, the stabilities of several fluoride salts were determined by thermal gravimetric methods. The ORNL computer code for retrieving data and for developing improved solid waste mixtures was modified for use with fast reactor wastes.

5.2 Intermediate-Level Radioactive Waste

Processes for incorporating all types of aqueous and organic intermediate-level wastes in asphalt, polyethylene, or other organic matrixes are being developed. These waste types include alkaline evaporator residues, second-cycle aqueous raffinates with added caustic, and organic wastes containing *n*-dodecane, carbon tetrachloride, tetrachloroethylene, tributyl phosphate (TBP), or mixtures of these compounds. Each type of waste is first mixed with emulsified asphalt (~35% water), molten polyethylene, or polyethylene emulsified

with an organic diluent or water, and the water or organic diluent is then volatilized by heating to about 160°C. The residue containing the radionuclides and other solids is drained into a steel barrel that can be stored temporarily or can be shipped directly to the burial ground.

Additives, such as attapulgite clay, are necessary to maintain a reasonably solid product when organic wastes are incorporated in asphalt. The amount of TBP that can be incorporated in asphalt is limited to about 25 wt % (37 wt % attapulgite clay–38 wt % asphalt). Up to 50% TBP, as compared with about 40 to 50 wt % inorganic solids from aqueous wastes, can be incorporated in polyethylene at the present stage of development of the process. The leach rates for both the waste-asphalt and the waste-polyethylene products in water were satisfactorily low. The fraction of total radionuclides that leached through a specific surface per day ranged from 4×10^{-4} to 4×10^{-6} $(cm^2/g)^{-1}$ day^{-1}. Asphalt and polyethylene products appeared to be satisfactory when irradiated to doses up to 10^8 rads and 10^9 rads respectively. No swelling, evolution of gases, or increase in leach rate of salts was noted for asphalt products that contained up to 52 curies of mixed radionuclides per gallon and had received a radiation dose as high as 1.1×10^8 rads over a two-year period.

The use of a wiped-film evaporator (with 4 ft^2 of heat transfer area) for incorporating simulated nonradioactive intermediate-level waste in asphalt was successfully demonstrated in a pilot plant that was designed for processing alkaline second-cycle Purex-type waste. Optimum processing conditions, based on residual water content and acceptable leach rate [$< 10^{-4}$ $(cm^2/g)^{-1}$ day^{-1}] of the product, were established. Waste feed rates of 7.5 and 5.0 gph, which were found to be optimal, resulted in products containing about 40 and 46 wt % solids respectively. The wiper rotation speed was 280 rpm, and the blade wear rate was 2 to 3 mils/hr along the leading edge. Solids did not accumulate on the evaporator wall. Condensate:feed decontamination factors ranged from 300 to 1500. In initial tests with another type of waste, alkaline evaporator waste concentrate, results were optimal at a waste feed rate of approximately 10 gph, which yielded a product containing about 45 wt % solids. The use of polyethylene and the incorporation of organic wastes have not been tested in the pilot plant.

Although small samples of asphalt containing large amounts of nitrate or nitrite burned much faster than pure asphalt, such products should not be classified as explosive mixtures. Ignition occurred at 275 to 330°C. Similar polyethylene-waste samples burned slowly with a steady candle-like flame, and ignition occurred at about 440°C. The fire hazard could be reduced by minimizing the time allowed for interim storage and by requiring the prompt burial of drums of waste-asphalt or waste-polyethylene product. However, careful evaluation of this fire hazard will be required.

Results of our studies thus far indicate that polyethylene products are superior to asphalt products with respect to radiation resistance and flammability and have comparable leach rates. However, the higher cost of polyethylene may limit its use to special applications such as the periodic disposal of used tributyl phosphate solvent. Other lower-cost polymers and paraffins are being studied as alternatives.

5.3 Engineering, Economic, and Safety Evaluation

Recent revised estimates of the volume of high-level wastes to be expected from the Civilian Nuclear Power Program indicate that about 75,000,000 gal of liquid waste containing 150,000 megacuries of fission product activity will have accumulated by the year 2000. If, as is currently planned, this waste is solidified for safer handling and disposal, it would occupy a volume of about 750,000 ft^3 and would require a total of about 1900 acres of salt-mine area for its disposal. These revised values are about twice those of previous estimates; however, we believe that they are still acceptable from the standpoints of safety and economy.

5.4 Separation of Noble Gases from Air by Using Permselective Membranes

A process is being developed for removing radioactive krypton and xenon from the air in a reactor containment shell, the off-gas from a fuel processing plant, or the blanket gas from a nuclear reactor. This process is based on the more rapid transport of krypton and xenon than of oxygen, nitrogen, argon, or helium through a thin sheet of dimethyl silicone rubber. The rates of transport of the various gases of interest have been measured as functions of pressure, temperature, gas mixture,

and other process parameters and have been compared with calculated values. The laborabory data have been used to estimate that a plant for removing the xenon and krypton from the cover gas from a 1000-Mw (electrical) sodium-cooled reactor would cost about $400,000 and that a plant for removing xenon and krypton from a reactor containment shell following a nuclear accident would cost about $1,100,000. The former amount is less than 0.3% of the total capital cost for a reactor, estimated at $150/kw.

6. TRANSURANIUM-ELEMENT PROCESSING

The USAEC Heavy Element Production Program at ORNL is centered in two main facilities, the High Flux Isotope Reactor (HFIR) and the Transuranium Processing Plant (TRU). These facilities gradually attained a semiroutine schedule during their second year of operation. Five milligrams of californium and the other associated actinide elements were recovered early in the year, and the major portion of the product was shipped to various research groups throughout the country. Many special projects to produce new and unique materials for special research now require a significant portion of the total effort. Three targets, each containing californium, ^{244}Pu, and ^{248}Cm, were fabricated and irradiated; the products were subsequently recovered and distributed. Other major accomplishments of the year included the startup of the remote target fabrication line and the demonstration of the sol-gel technique for producing americium-curium oxides on a 10-g scale.

Those phases of the program under the direction of the Chemical Technology Division, including operation of TRU, isolation and purification of products, development of chemical processes, and some chemical research with the actinide elements, are reported here. Target fabrication work is directed by the Metals and Ceramics Division and is described in detail in their reports.

6.1 TRU Operations

The Transuranium Processing Plant is primarily a production facility in which: (1) targets that have been irradiated in the HFIR are processed to isolate and purify the transuranium elements and (2) americium and curium are fabricated into recycle targets for additional irradiation in the HFIR.

Last year we reported that we had demonstrated, at full production level, processes for dissolving targets and preparing feed, for recovering plutonium, and for decontaminating the transplutonium elements from fission products (Tramex). This year, another processing step, an LiCl-based anion exchange process, which is used to partition the transplutonium elements, was scaled up and installed for use in the main-line processing plant. Isolation and purification of the transuranium elements continued to be done by using equipment that is installed temporarily in cell 5. More than 200 g of curium was processed. Feed materials included: (1) 17 targets that had been irradiated for about one year at the Savannah River Plant (SRP) and that had failed during subsequent irradiation in the HFIR, (2) miscellaneous targets that had been dissolved in laboratory-scale equipment to obtain more precise data, and (3) an americium-curium solution that was recovered from the original Savannah River raffinate solution that remained from the early plutonium recovery operation.

The startup of the remotely operated equipment used for target fabrication was a major accomplishment. Six recycle targets were fabricated from americium-curium oxide and are now being irradiated in the HFIR. The oxide, produced in a development facility, was prepared by the sol-gel method from curium that had been recovered in TRU.

The process for dissolving targets has been described previously. Briefly, the aluminum matrix is dissolved in caustic-nitrate solution, which is decanted, leaving the undissolved particles of actinide oxide. These particles are dissolved in 6 *M* HCl. Plutonium is recovered by batch extraction, using di(2-ethylhexyl)phosphoric acid (HDEHP), and subsequent stripping; di-*tert*-butylhydroquinone is used as a reductant. This process was introduced during the previous year as a possible replacement for the ill-fated chloride-based anion exchange process. Developmental and plant trials have proved its effectiveness for main-line use.

Two changes were made in the Tramex process. The first consisted in adopting a new, simpler method for controlling the loss (by radiolysis) of acid in the feed. The addition of methanol, a procedure which had been successful in the Curium Recovery Facility, was discontinued in favor of the periodic addition of concentrated HCl to the feed. The second change involved the method by which we prevent the oxidation of cerium to an

extractable form. We now add an organic-soluble reductant, di-*tert*-butylhydroquinone, to the extractant instead of adding $SnCl_2$ to the feed. Although both methods are equally effective, the $SnCl_2$ has the disadvantage of loading the solvent; this causes problems when recycle material is being processed.

The LiCl-based anion exchange process was scaled up by a factor of 2. The only other significant change in the process was the use of a batch extraction step to remove zirconium prior to the feed adjustment step. This eliminated problems with hydrolysis and precipitation of zirconium throughout the LiCl-based anion exchange processing. The largest single batch processed thus far contained 18 g of ^{244}Cm.

A two-stage batch solvent extraction process (Cleanex) was used to pretreat rework material and the SRP americium-curium solution to make them suitable for Tramex processing. In general, the actinides were extracted from either an HCl or an HNO_3 solution (0.2 *M* or less) into 1 *M* HDEHP in Amsco 125-82 diluent, and then stripped using HCl. The exact processing method depended upon the kinds and amounts of actinides and of impurities that were present.

We made some plant and equipment modifications, improvements, and repairs during a program that lasted about six weeks. We are still able to perform maintenance operations in the tank pits by direct contact with the equipment. Adequate working times were achieved by combining equipment flushing and the use of temporary unit shielding.

We found two sets of circumstances in which the corrosion rate of Zircaloy-2 equipment was unexpectedly catastrophic. The corrosion rate was much higher than we had anticipated in certain mixtures of HCl and HNO_3, and radiation increased the rate at which HCl corrodes Zircaloy-2 much more than we had anticipated. We made some corrosion tests to study these situations. The resulting data did not provide accurate values for low corrosion rates but did differentiate between low and catastrophic corrosion rates.

Zircaloy-2 was not attacked significantly by acid mixtures that were less than 2 *M* in HCl. In 3 *M* HCl the corrosion rate appeared to be significant ($\sim$5 mils/year) when the concentration of HNO_3 was as low as 0.5 *M* and was definitely catastrophic (75 to 200 mils/year) at 1 to 6 *M* HNO_3. Further, the attack was not uniform. In all HCl-HNO_3 mixtures in which the HCl concentration was greater than 3 *M* and the HNO_3 concentration was greater than a few tenths molar, the corrosion was catastrophic and the attack was not uniform.

The Zircaloy-2 corrosion rate in 6 *M* HCl at a solution power density of 37 w/liter was constant at about 60 mils/year. The data for a solution power density of 8 w/liter indicate that the corrosion rate was increasing throughout the test period. After 24 hr the rate was 1.3 mils/year, during the next 42.3 hr it was 14 mils/year, during the next 94 hr it was 18 mils/year, and during the final 46 hr it was 32 mils/year.

6.2 Isolation and Purification of TRU Products

Product finishing operations and final purification and isolation of transplutonium elements are accomplished in equipment that is installed in cell 5 in TRU and in supporting shielded-cave facilities. The final processing of main-line products in cell 5 is required because process methods are not fully developed. Product finishing operations and special separations will continue to be performed in the shielded-cave complex in cell 5 because progressively cleaner facilities are required to achieve high levels of purity.

The processing of product fractions obtained from LiCl-based anion exchange processing was continued in cell 5 by using the procedures reported last year. The americium and the curium in part of the americium-curium product were separated by selectively precipitating americium as an Am(V)-potassium double carbonate. Berkelium was separated from the residual actinides by extraction from 8 *M* HNO_3 into di(2-ethyhexyl)phosphoric acid. Einsteinium and californium were isolated from each other and from other residual actinides by selective elution from cation exchange resin with ammonium α-hydroxyisobutyrate. Purified products from these separations included 57 g of ^{244}Cm, 11 g of ^{243}Am, 300 μg of ^{249}Bk, 4.4 mg of ^{252}Cf, and 10 μg of ^{253}Es.

A high-pressure ion exchange column was used to separate microgram quantities of ^{253}Es from milligram quantities of ^{252}Cf and ^{244}Cm; it is anticipated that this column, as presently installed, can be used to process 100 mg of ^{252}Cf.

Various special separations were also made, including isolation of $\sim$1 μg of second-growth ^{253}Es (daughter of ^{253}Cf) and 97 μg of ^{248}Cm that had

grown into the purified californium products during storage, and separation of 55 μg of ^{249}Cf that had grown into 350 μg of ^{249}Bk. In additional processing, 65 g of ^{244}Cm obtained from Savannah River concentrate was highly purified for use in developing isotopic heat sources (by the Isotopes Division) and for shipment to other customers throughout the country.

6.3 Development of Chemical Processes

Laboratory support was provided to investigate chemical problems that arose during high-activity-level processing in TRU. We continued the development of processes for recovering plutonium, partitioning actinides, isolating berkelium, and recovering americium-curium from SRP concentrate by solvent extraction. Also, we continued to investigate methods for separating californium-einsteinium-fermium and for preparing americium-curium oxide for use in HFIR targets.

A solvent extraction plutonium recovery process (Pubex) was developed and successfully used in plant operations. In addition to isolating plutonium, this process also serves to decontaminate both the plutonium and the transplutonium-element fraction from corrosion product zirconium. In this process, tetravalent plutonium and zirconium are preferentially extracted from 6 *M* HCl into 1 *M* di(2-ethylhexyl)phosphoric acid in diethylbenzene. The transplutonium elements remain in the aqueous phase. The solvent is washed with dilute HCl, and the plutonium, after reduction to the trivalent form by use of the organic-soluble reductant 2,5-di-*tert*-butylhydroquinone, is stripped with concentrated HCl. The zirconium remains in the waste solvent, which is discarded.

The laboratory development of an extraction process for actinide partitioning was continued. In this process, the transcurium elements are separated from americium and curium by extraction into di(2-ethylhexyl)phosphoric acid from HCl. Single-stage separation factors between berkelium and curium are about 13. Multistage countercurrent experiments at tracer level have indicated that such a separation process is practicable; however, its effectiveness has not been evaluated with actual process solutions at high activity levels.

Continued laboratory development of the berkelium recovery process indicates that berkelium can be satisfactorily oxidized by chromate in 4 *M* HNO_3 and then extracted. Under these conditions, excellent separations of berkelium from curium were demonstrated at tracer levels. This oxidant avoids the marginal stability of bromate in 8 *M* HNO_3, which is used in the Berkex process.

A process was developed for recovering americium and curium from nitric acid solutions containing sodium and other ionic contaminants. This process involves careful addition of NaOH to obtain a low acid concentration ($\sim$0.1 *N*), extracting the actinides into 1 *M* HDEHP in Amsco 125-82, scrubbing with dilute HCl to remove nitrate, and stripping the actinides into 5 *M* HCl. This process was used in plant equipment as a two-stage batch extraction process to convert americium-curium from Savannah River concentrate into a chloride solution suitable for the preparation of Tramex feed. The process was also used to recover actinides from recycle streams that were contaminated with gross amounts of corrosion products and other ionic contaminants.

Laboratory studies of the high-pressure ion exchange column, which is used for separating californium, einsteinium, and fermium, were continued. Excellent actinide separations were demonstrated with samples of various process solutions, and the effects of experimental variables, with emphasis on very rapid separations, were studied. Adequate separations were achieved in about 2 min when 1-mg quantities of lanthanides were deposited on small columns that contained $\sim$1 ml of $<$10-μ-diam resin.

The sol-gel method for preparing americium-curium oxide for HFIR targets was successfully adapted for the preparation of mixed ^{244}Cm-^{243}Am sols. These sols were converted to gel microspheres, which were subsequently calcined to yield a dense oxide product. An in-cell development facility installed in Building 4507 was used to prepare 38 g of americium-curium oxide product in the desired size range (50 to 170 μ). This material was successfully fabricated into HFIR targets.

6.4 Special Projects

Numerous projects involving various groups at ORNL and at other sites require the services available at TRU for the preparation of unique or special materials not normally produced in main-line efforts. The phases of these projects involving

activities at TRU are reported here. The end results of the research are, of course, reported elsewhere.

Three special californium targets were fabricated and irradiated for the purpose of producing einsteinium. A second purpose of the irradiations was to refine some of the calculated values of the cross sections in the chain of isotopes above californium. Surprisingly, we learned that the capture cross section of ^{252}Cf is considerably higher than previously supposed, apparently in the range of 40 to 50 barns instead of 7 to 10 barns. The results of all three targets were in substantial agreement, thus ruling out the possibility that any substantial part of the starting material had been lost in the target preparation. Additional irradiation experiments will be necessary to further refine these measurements. Because of the high cross section, the irradiation times used were far too long for optimum einsteinium production, and a significant fraction of the californium was "burned up." About 6 μg of einsteinium, as compared with the 18 μg expected, was recovered for shipment to customers. Other special materials, including 1 mg of ^{244}Pu, a few micrograms of ^{248}Cm, and some aluminum alloy tensile specimens, were irradiated with the californium in these targets. The tensile specimens were used for studying the target failure problem.

The first significant neutron source was fabricated this year for fast-neutron activation studies in the Transuranium Research Laboratory. About 750 μg of ^{252}Cf (1.7×10^9 neutrons/sec) was loaded into a small aluminum source capsule, $^3/_8$ in. in diameter by $\sim$1 in. long, using a technique developed this year. The californium was precipitated as the hydroxide, adsorbed on the surface of aluminum powder, and retained on a pressed aluminum powder filter disk at the bottom of a standard target pellet liner. The liner and powder matrix were then dried and pressed in the usual manner; then the completed pellet was welded into an outer aluminum capsule.

Assistance was given in the preparation and irradiation of 50-mg quantities of U_3O_8 (42 mg of ^{236}U) in HFIR rabbits for the production of ^{237}U. The rabbits were subsequently processed by personnel at the Los Alamos Laboratory and were used for the measurement of the fission cross section of ^{237}U in an underground nuclear event.

6.5 Transplutonium Element Research

A systematic study of actinide element chemistry and of comparative lanthanide element chemistry is being made to increase our basic understanding of actinide systems. This program includes problems involving solution chemistry, with particular emphasis on complex formation and on preparation of solid actinide compounds that will be characterized by x-ray diffraction, electron microscopy, thermogravimetry, and differential thermal analysis.

The investigation of sulfate complexes of europium by means of amine extraction was continued. The existence of a previously unreported trisulfate complex, $Eu(SO_4)_3^{3-}$ (formation constant, $K_{03} = 1.8 \times 10^5$ at zero ionic strength), was indicated, and this suggested a dinuclear complex $Eu_2(SO_4)_3$, $K_{0n} = 3.5 \times 10^8$, in addition to the previously known complexes $EuSO_4^+$ and $Eu(SO_4)_2^-$. The formation constants found for the latter complexes were $K_{01} = 7.0 \times 10^3$ and $K_{02} = 5.2 \times 10^5$ respectively.

The spectrophotometric investigation to identify the complexes that Am^{3+} forms with aminopolyacetic acids was also continued. The compositions and pH stability ranges for 24 complexes with eight aminopolyacetic acids were determined. Instability constants were calculated for 13 of these complexes.

A program to prepare and evaluate new eluting agents for use in the ion exchange separation of the transplutonium elements was initiated. It was found that ethylmethylglycolic acid provides slightly greater separation factors than dimethylglycolic acid (α-hydroxyisobutyric acid); this indicates that the actinide separation factors are higher with increased branching of the α-hydroxycarboxylic acid.

In continued studies of the fundamental solution chemistry of berkelium, the absorption spectrum of Bk(III) was redetermined with $\sim$300 μg of highly purified ^{249}Bk.

In conjunction with actinide sol preparations, PuO_2, $Am(OH)_3$, and $Cm(OH)_3$ sols were examined by electron microscopy at various stages of preparation. Results of these studies confirmed that the colloidal characteristics of $Am(OH)_3$ and $Cm(OH)_3$ parallel those of the rare-earth sols. Electron diffraction experiments performed during these studies led to the positive identification of $Am(OH)_3$ for the first time. These studies also demonstrated that, while sols prepared from ^{244}Cm

are composed of colloidal crystallites of $Cm(OH)_3$, the crystallites are rapidly destroyed (in 10 to 20 hr) by self-radiation effects in aqueous media.

Examination of the thermal stability of americium hydroxide preparations was initiated, using the alpha-contained Ainsworth semimicro thermobalance.

7. DEVELOPMENT OF THE THORIUM FUEL CYCLE

During the past year an engineering demonstration of the preparation of ThO_2-UO_3 hydrosol by solvent extraction was carried out. The production rate was 1 kg of contained oxide per hour. The thorium-to-uranium mole ratio was 3, which is in the range of interest for use in HTGR fuel elements. Equipment very similar to that used in the above demonstration was fabricated for use with systems containing ^{233}U or ^{239}Pu. This equipment, which is critically safe and completely alpha-contained, includes three stages of extraction, with two interstage digesters, and a vacuum evaporator for sol concentration.

Dispersers for forming controlled-size sol droplets have been further developed. The two-fluid nozzle has been found to be useful for making microspheres of oxide in the 20-to-75-μ-diam range, and the vibrating capillary disperser has been improved to be more durable and to give more reproducible results over the 200-to-400-μ-diam range. The design of the pilot plant for preparing large samples of microspheres and for process demonstration has been simplified by eliminating all of the pumps except one.

The chemical reactions occurring among the 2-ethyl-1-hexanol (2EH) drying alcohol, the sol, the nitric acid present in the sol, and the surfactants employed have been studied. Although very complex, these reactions are now understood in a limited sense, and this understanding has led to some process improvements.

Mass transfer studies of the sol gelation process for ThO_2 in 2EH have led to correlations that will permit the prediction of gelation times when the initial sol molarity and the initial drop diameter are known.

Approximately 230 kg of ThO_2 microspheres were prepared in the microsphere preparation pilot plant as part of the developmental work and were used in a variety of ways both at ORNL and elsewhere.

The Thorium-Uranium Recycle Facility (TURF) was completed during the past year, and special equipment items such as manipulators and an in-cell crane have been installed. None of the process equipment has been installed.

Oak Ridge National Laboratory serves as a national storage, purification, and distribution center for ^{233}U. During the past year, 118 kg of ^{233}U (22 shipments) was received and 115 kg of ^{233}U (17 shipments) was disbursed by the center. Also, a special storage facility for 1100 kg of uranium (75% ^{235}U, 11% ^{233}U) as uranyl nitrate solution was built. This uranium is presently in the form of Indian Point Reactor fuel, which will be processed at the Nuclear Fuels Services plant prior to storage in the new facility. It contains 120 parts of ^{232}U per 10^6 parts of ^{233}U; thus it is moderately radioactive, with high-energy gamma emitters being prominent contributors.

8. SOL-GEL PROCESSES FOR THE URANIUM FUEL CYCLE

8.1 Preparation of UO_2 Sols by Solvent Extraction

The preparation of UO_2 sols from U(IV) nitrate-formate solutions by the solvent extraction method has been successfully scaled up and operated continuously in engineering equipment. Important process variables are the temperature and the duration of interstage digestion, and the method for preparing the U(IV) nitrate-formate solution from uranyl nitrate. Mixer-settlers are used for extraction; the design capacity of the equipment is 6 liters of 0.2 *M* sol per hour.

A slurry reductor that uses finely divided platinum (from PtO_2) as a catalyst and operates with 14-liter batches of 0.6 *M* $UO_2(NO_3)_2$–0.4 *M* HNO_3–0.3 *M* HCOOH feed has been developed. It has produced more than 40 kg of U(IV) which is suitable for use in preparing sol by solvent extraction methods.

Conditions during the digestion step between solvent extraction stages have been found to affect both the extent to which UO_2 sols can be concentrated without gelling and the shelf life of these sols. Too low a digestion temperature and too short a digestion period limit the sol concentration to less than 1 *M*. On the other hand, too high a temperature and too long a digestion period limit

the shelf life of the sol. A digestion time of about 1 hr and a temperature of about 60°C appear optimum after the first extraction stage. Further digestion after subsequent extraction also may be beneficial.

Generally, the 0.2 *M* UO_2 sols are concentrated to about 1 *M* by vacuum evaporation at about 35°C to facilitate microsphere formation. The concentrated sol is sensitive to air oxidation and must be kept under an inert atmosphere, since oxidation leads to thickening or even to flocculation of the sol. Seven 2-kg batches of sol have been successfully concentrated to 1 *M* in a forced-circulation vertical-tube evaporator.

8.2 Plutonia and Urania-Plutonia

The preparation of plutonia sols by the precipitation of polymer from Pu(IV) nitrate solution with ammonia followed by dispersion, baking, and redispersion in water has been studied further. The incorporation of an aging step prior to the first dispersion resulted in uniformly higher yields of acceptable product; the final PuO_2 sols had NO_3^-/Pu mole ratios that were lower than those of sols prepared without using this step.

Drying and firing procedures for PuO_2 and UO_2-PuO_2 have been modified to include a steam treatment. The steam enhances hydrocarbon removal (introduced in the sphere forming column) and suppresses or completely eliminates the thermal excursion that is occasionally observed in deep beds of microspheres. Also, it results in a somewhat more dense final product.

During the year, we prepared a variety of PuO_2 sols. Microspheres were made by using these sols alone or in mixtures. Altogether, more than 7 kg of plutonium was converted into PuO_2 sols.

8.3 Preparation of Microspheres

With only slight changes in procedures and equipment, the sol-gel process, which was originally developed to prepare ThO_2 microspheres, can also be used to prepare UO_2 microspheres. The characteristics of the sols are the most important variables with respect to the formation of good-quality spheres; consequently, the column operating conditions must be varied to allow for these characteristics. The problems inherent in the preparation of microspheres that are less than 100 μ in diameter can be somewhat simplified by changing the conditions of sol drop formation. Typical properties of the sol-gel product are illustrated by samples prepared for various parts of the Uranium Fuel Cycle program.

8.4 Materials Development

Applications of sol-gel processes based on the use of oxide-carbon sols as starting materials continue to appear promising as means for preparing special nuclear fuels of the more advanced type such as carbides, carbonitrides, nitrides, or porous oxides. In these processes, the oxide-carbon sols are converted to mono- or dicarbides by heating to temperatures of 1700 to 2000°C in argon or vacuum or to nitrides or carbonitrides by treating with nitrogen. In the preparation of porous oxides, the oxide matrix is set by firing in argon to 1200 to 1400°C; then the carbon is volatilized by chemical reaction with air at 800°C or with CO_2 or H_2O at 1000°C, depending on which oxide is being prepared.

Continued studies of the interactions between oxides and carbon in oxide-carbon sols showed that ThO_2, UO_2, or ThO_2-UO_3 strongly interacts with the carbon black aggregates to produce stable, fluid sols; the oxide acts as a protective colloid. Oxide-carbon sols containing carbon in sufficient amounts to produce carbides or porous oxides were prepared from ThO_2, UO_2, or ThO_2-UO_3 sols.

Further studies of the conversion of ThO_2-C gels showed that the most important variables for dense carbide preparations were the firing conditions and the carbon content. The method of firing ThO_2-C gel to dense ThC_2 involves a critical balance between chemical conversion, grain growth, and sintering. By proper choice of conversion temperature and CO pressure, ThC_2 microspheres having a density of 90 to 93% of theoretical were prepared. Excess carbon beyond that required to produce the carbide resulted in highly porous products; the optimum ratio of carbon to thoria in the initial ThO_2-C gel used to prepare dense carbides was found to be 3.9. Initial results obtained on converting UO_2-C to UC or ThO_2-UO_3-C gels to $(ThO_{0.78}UO_{0.22})C_2$ demonstrated the technical feasibility of preparing these carbides with densities that were 90 to 93% of theoretical. Initial results of the conversion of UO_2-C gels to uranium carbonitride microspheres

appeared encouraging and more easily controlled than conversion to the nitride by carbothermic reduction.

The preparation of porous ThO_2–22% UO_2 and porous UO_2 was demonstrated. Porous ThO_2–22% UO_2 was prepared from ThO_2-UO_3-C gels by using the same firing method that was previously used for the preparation of porous ThO_2. The oxide matrix was formed by firing to 1400°C in argon, and then the carbon was removed by firing in air at 800°C. In the case of the porous UO_2 preparations, however, the carbon had to be oxidized with CO_2 or H_2O to prevent oxidation of the UO_2 to U_3O_8 during the firing.

9. SOL-GEL PROCESSES FOR ISOTOPIC HEAT SOURCES

Several radioactive isotopes are useful as heat sources for self-contained power production units. Among these are ^{238}Pu and ^{244}Cm. Since significant progress had been made in sol-gel technology as applied to ^{239}Pu and to rare earths, sol-gel development programs for the preparation of isotopic heat sources have been initiated. Laboratory and pilot-plant studies are in progress, and a $^{238}PuO_2$ production unit has been fabricated.

9.1 Laboratory Studies of ^{238}Pu Sol-Gel Process

Development studies showed that ^{238}Pu sols can be made on a laboratory scale (10 g of ^{238}Pu) and that excellent microspheres (50 to 400 μ in diameter) can be obtained from these sols.

The properties of the ^{238}Pu spheres were generally comparable with those for ^{239}Pu; the ^{238}Pu spheres were more porous than ^{239}Pu spheres but had greater crushing strengths.

9.2 Development Studies in a Glove-Box System

A glove-box facility, capable of processing about 150 g of plutonium per day, is being used in the development program. Plutonium-239 is being used as a stand-in for ^{238}Pu in studies aimed at scaling up and improving the process.

In order to increase the density and the thermal stability of the plutonia, the drying and firing procedures were modified to include a moist atmosphere. Sodium (from the surfactants used in the process) appears to decrease thermal stability; use of a sodium-free surfactant (Amine O) resulted in a low level of sodium contamination in the final product, but the surfactant was ineffective. Residual carbon in the microspheres was eliminated by the change in the firing procedure mentioned above. A procedure was developed for the continuous washing of precipitated PuO_2.

9.3 Plutonium Sol-Gel Pilot Plant

A remotely operated, neutron-shielded pilot plant was constructed in cell 4 of Building 3019. The system design was patterned after the glove-box system discussed above. The system was successfully operated with ^{239}Pu. However, difficulties were encountered when ^{238}Pu was processed. Of four ^{238}Pu sol formation runs to date, none were completely successful. Process modifications that should permit formation of a satisfactory sol are being incorporated.

A sol prepared in the laboratory was used to form $^{238}PuO_2$ microspheres. Sphere formation, drying, and calcination were successful. Although the final product was of a slightly lower quality than the comparable ^{239}Pu product, it was generally satisfactory.

9.4 Assistance to Mound Laboratory

Equipment for the preparation of $^{238}PuO_2$ sols and for the subsequent forming, drying, and firing to dense $^{238}PuO_2$ microspheres was fabricated, installed in a stainless steel cubicle, and shipped to Mound Laboratory. The production capacity of the unit is one batch, containing 150 g of plutonium, per 24 hr.

9.5 Curium Sol-Gel Studies

Laboratory studies, aimed at adapting the sol-gel process to the preparation of actinide oxide microspheres, are under way. Mixed ^{244}Cm-^{243}Am oxide microspheres (84% curium) were successfully prepared on a 4- to 10-g scale. Purification of feed material, by oxalate precipitation and calcination, was found to be necessary. The final microspheres were free flowing, dust free, and showed no tendency to crack or disintegrate.

10. SEPARATIONS CHEMISTRY RESEARCH

New separations methods and reagents are being developed, principally for uses in radiochemical processing but also for other purposes extending from extractive metallurgy to biochemical separations. Reagents developed in the former ORNL raw-materials program and subsequent studies continue to show extended utility. The program in separations chemistry can be divided into three interdependent types of research activity: (1) descriptive chemical studies (Sects. 10.1–10.2) of the reactions of substances to be separated and of separations reagents, of the controlling variables in particular separations, and of new compounds that may be potential reagents; (2) development (Sects. 10.3–10.4) of selected separations into specific complete processes, both where no workable process has yet been devised and where existing processes can be improved, carried where warranted to the point that large-scale performance can be predicted; and (3) fundamental chemical studies (Sects. 10.5–10.7) of the species, equilibria, and reaction mechanisms involved in separations systems, both to increase knowledge and to help define potential applications.

10.1 Extraction of Metal Sulfates and Nitrates by Amines

As part of the program that is concerned with surveying the extraction characteristics of many metals from various systems, data were obtained for extractions of Co(II), V(IV), and hafnium from acidified lithium sulfate solutions (0.3 to 5 *N* SO_4^{2-}) with representative primary, secondary, tertiary, and quaternary amines. Hafnium was extracted very strongly by the primary amine at low sulfate concentrations but only moderately by the other types of amines over the total sulfate concentration range studied. Coefficients for extraction of V(IV) were weak (0.1 to 0.6) with all the amines; those for extraction of Co(II) were negligible (<0.02).

10.2 New Separations Agents

We are continuing to investigate, for potential utility in solvent extraction or other separations methods, compounds that are: (1) newly available commercially, (2) submitted by manufacturers for testing, or (3) specially procured for testing of class or structure.

We obtained a sample of a branched carboxylic acid with a fairly high molecular weight, $RR'MeCCO_2H$, $\Sigma R \approx C_{15}$, by distillation of a commercial developmental mixture, "Versatic Acid 1519." The acid is a strong extractant for alkaline-earth ions at a relatively high pH (8 to 9).

A new commercial sulfonic acid, nominally tridecylbenzenesulfonic acid, is acceptably soluble in hydrocarbons; however, its sodium salt is excessively soluble in all aqueous solutions tested.

1-Methylheptyl phenylphosphonic acid, a new extractant that is analogous to 2-ethylhexyl phenylphosphonic acid, appears to be superior to the latter for intralanthanide and intra-actinide separations in that it provides higher separation factors and permits less impairment of these factors by zirconium synergism.

Three new high-molecular-weight β-diketones were synthesized: tridecanoylacetone, 2-ethylhexanoylpivalylmethane, and tridecanoylpivalylmethane. All three compounds are effective for extracting lithium and for separating it from sodium and, especially, potassium. The first two require a modifier (trioctylphosphine oxide) in *n*-hexane solution to prevent precipitation of lithium; the modifier is optional with the third.

10.3 Beryllium Purification by Solvent Extraction

A process for preparing very pure beryllium hydroxide was demonstrated successfully in bench-scale tests. In this process beryllium is extracted from carbonate solution with a quaternary ammonium compound, stripped with NH_4HCO_3 solution, and precipitated from the strip solution by heating. Feed for solvent extraction was prepared by precipitating beryllium hydroxide from impure beryllium sulfate solution (total of 1.3×10^5 parts of metal contaminants per million parts of BeO) with ammonia and redissolving the precipitate in NH_4HCO_3-$(NH_4)_2CO_3$ solution. Total metal impurities detected in the final product were 120 parts per million parts of BeO.

10.4 Recovery of Uranium from Commercial Phosphoric Acid

By 1970, uranium that could be recovered from commercial phosphoric acid will represent a potential source of about 2000 tons of U_3O_8 annually. Usually, the uranium is present in the phosphoric acid (~5 *M*) at concentrations ranging from 50 to 200 ppm. Because of the strong complexing action of the phosphate, a solvent with very high extraction power is needed for effective recovery. A large number of organophosphorus compounds were tested for this purpose. Of these, the combination di(2-ethylhexyl)phosphoric acid plus tri-*n*-octylphosphine oxide has shown the most promise.

10.5 Equilibria and Mechanisms of Extraction

The study of the synergistic effect of zirconium (or hafnium) in enhancing the extraction of several metal ions by alkyl phenylphosphonic acids was extended to most of the metals and to a variety of organophosphorus acids. The most highly enhanced extractions were those of the alkaline earths and the lighter trivalent actinides and lanthanides. Other metals showing significantly enhanced extraction include Li, Ag, Tl(I), Mn(II), Co(II), Fe(III) in chloride, Y, Pb(IV), and Pu(IV), but not Cs, Be, Cu(II), Ni(II), Zn, Cr(III), Fe(III) in nitrate, nor Sc.

The equilibria of extraction of sodium and strontium by a moderately high-molecular-weight branched carboxylic acid (mixed $RR'MeCCO_2H$, mol. wt ≈ 260) are, in several ways, similar to those for di(2-ethylhexyl)phosphoric acid. The maximum strontium extraction and separation factors from sodium are nearly 100 times greater with the carboxylic acid than with HDEHP but require a higher pH: 8.5 to 9.5 vs 5 to 6. The most probable species present in the extract are $NaA\cdot 2HA$, $NaA\cdot 3HA$, $SrA_2\cdot 2HA$, $SrA_3\cdot 3HA$.

Two computer programs, SULFATE and CALACT, are available to speed up and refine the calculations of, respectively, (1) the Na_2SO_4:H_2SO_4 ratio to give a specified activity $a_{H_2SO_4}$ at a specified total sulfate concentration and to determine the resulting true sulfate ion concentration and the ionic strength and (2) the activity $a_{H_2SO_4}$, the true sulfate ion concentration, and the ionic strength resulting from a specified combination of Na_2SO_4 and H_2SO_4.

10.6 Kinetics of Metal-Ion Extractions by Organophosphorus Acids

The kinetics of the slow extraction of iron(III) from acid perchlorate solutions by hydrocarbon solutions of di(2-ethylhexyl)phosphoric acid (HA), at low loading and small fraction of the total iron extracted (so that the reverse reaction can be neglected), appears to be completely accounted for by the designated slow steps in the following reactions at the interface:

$$Fe(H_2O)_6^{3+} + HA_2^- \overset{1d}{\rightleftharpoons} (H_2O)_5FeOH^{2+} + (HA)_2 \rightleftharpoons (H_2O)_5FeA^{2+}\cdot HA + H_2O$$

$$HA \uparrow\downarrow$$

$$Fe(H_2O)_6^{3+} + A^- \overset{1m}{\rightleftharpoons} (H_2O)_5FeOH^{2+} + HA \rightleftharpoons (H_2O)_5FeA^{2+} + H_2O$$

$$HA$$

$$H^+ \uparrow\downarrow$$

$$(H_2O)_5FeA^{2+}\cdot HA \rightleftharpoons (H_2O)_5FeA^{2+}\cdot H^+ + A^- \overset{2,2s}{\rightleftharpoons} (H_2O)_4FeAOH^+ + HA + H^+ \rightleftharpoons (H_2O)_4FeA_2^+ + H_2O + H^+$$

$$(H_2O)_5FeA^{2+} + HA_2^- \overset{2d}{\rightleftharpoons} (H_2O)_4FeAOH^+ + (HA)_2 \rightleftharpoons (H_2O)_4FeA_2^+\cdot HA + H_2O\ .$$

The third ligand is presumably introduced by further (fast) reactions within the organic phase. Parallel steps $1m$ and $1d$ are in series with parallel steps $2s$ and $2d$. Hence, their individual contributions to the net rate/[Fe] = r combine as follows:

$$r = \frac{(r_{1m} + r_{1d})(r_{2s} + r_{2d})}{r_{1m} + r_{1d} + r_{2s} + r_{2d}} ,$$

where

$$r_{1m} = 4.0 \times 10^{-4}[\Sigma HA]^{0.5}/[H^+] ,$$

$$r_{1d} = 6.8 \times 10^{-3}[\Sigma HA]/[H^+] ,$$

$$r_{2s} = 1.03 \times 10^{-7}/[H^+][Fe] ,$$

$$r_{2d} = 2.1 \times 10^{-5}[\Sigma HA]^{1.5}/[H^+]^2 .$$

The four empirical coefficients were evaluated by least-squares fitting to the experimental data, and the resulting S-shaped curves of r vs $[\Sigma HA]$ at given [Fe] and $[H^+]$ agree well with the corresponding experimental points.

10.7 Aggregation and Activity Coefficients in Solvent Phases

A new commercial matched-thermistor vapor-pressure osmometer, which is advertised to be ten times as sensitive as similar instruments previously available, was tested. The sensitivity was confirmed, and the results were highly reproducible but appeared to be subject to a systematic error over much of the most sensitive range.

In order to extend the usefulness of benzil (dibenzoyl, $C_6H_5COCOC_6H_5$) as a reference standard in vapor-pressure measurements for determining activity coefficients or aggregation numbers, the deviations of its benzene solutions from ideality were determined by isopiestic comparison with triphenylmethane (TPM) solutions. The resulting values of the osmotic coefficient,

$$\phi = 1 - 0.8197m_{benzil} + 0.7970m^2_{benzil} , \; m \leqq 0.33 ,$$

show that the benzil solutions deviate only slightly more from ideality than do the TPM solutions, for which

$$\phi = 1 - 0.5743m_{TPM} + 0.3583m^2_{TPM} , \; m \leqq 0.33 .$$

Aggregation numbers of a branched carboxylic acid (mixed $RR'MeCCO_2H$, mol. wt ≈ 260) and its sodium salt in n-hexane were measured by a matched-thermistor vapor-pressure osmometer for use in equilibrium extraction studies. The aggregation number, $\bar{n}$, was 2 for HA, as expected for carboxylic acids in general, then rose with increasing sodium content to 4 at $NaA/\Sigma A = 0.25$ and to greater than 6 at $NaA/\Sigma A = 0.4$. Beyond this, the aggregation number exceeded the sensitivity of the instrument. There was no significant difference between 0.05 and 0.1 M ΣA.

The solubility of water in benzene solutions of tri-n-octylamine (TOA) and several of its salts was measured in a continued study of the role of water in organic solutions of extractants. The quantity of water extracted by up to 0.5 M free-base TOA, corrected for the quantity of water extracted by benzene alone, is summarized by the following equation:

$$\Delta M_w = M_w - M_{w/benzene} = 0.0275 M_{TOA} a_w .$$

Computer solution of the equations for hydrate formation indicated that a monohydrate $TOA{\cdot}H_2O$ was formed, with a concentration quotient, $Q_{Bw} = [TOA{\cdot}H_2O]/[TOA][H_2O]$, of 0.858 ± 0.006. The quantity of water extracted by 0.1 N benzene solutions of several salts (similarly corrected) followed Henry's law for part or all of the range of water activities. These solutions (with Henry's law constant on the molarity scale, and the a_w at the limit of linearity) were TOAHCl (0.101 M, $a_w = 1$), TOAH-acetate (0.012 M, $a_w = 1$), $TOAHNO_3$ (0.064 M, $a_w = 0.85$), $TOAHHSO_4$ (0.09 M, $a_w = 0.6$), and $(TOAH)_2SO_4$ (0.02 M, $a_w = 0.4$). The quantity of water extracted by the two sulfates increased rapidly at higher water activities, indicating the formation of $(TOAHHSO_4)_3{\cdot}8H_2O$ and $(TOAH)_2SO_4{\cdot}4H_2O$ in addition to the monohydrates.

Measurements such as the foregoing require sensitive and accurate measurement of the quantities of water extracted at various water activities by diluents alone. We developed a sensitive gravimetric method using vacuum distillation of an equilibrated sample through magnesium perchlorate in a weighing tube, and using tritium to estimate the completeness of water absorption. At the same time, the results evaluate the ratio, α, of H_2O and HTO distributions that are needed for use in collateral liquid-liquid distribution measurements.

The extraction of water followed Henry's law over all water activities in several common diluents as follows, with Henry's law constants on the molarity scale and $\alpha = D_a^\circ(H_2O)/D_a^\circ(HTO)$: benzene (0.0363 M, $\alpha = 1.07$), cyclohexane (0.00345 M, $\alpha = 1.27$), n-hexane (0.00362 M, $\alpha = 1.23$), and n-octane (0.00317 M, $\alpha = 1.22$).

11. CHEMICAL APPLICATIONS OF NUCLEAR EXPLOSIONS

11.1 Copper Ores

Small-scale test work has indicated that ^{106}Ru is probably the only radioisotope of importance with respect to radiocontamination of cement copper produced from ore broken by a nuclear blast. Copper products essentially free of ruthenium were produced recently by dissolving contaminated cement copper in sulfuric acid and electrolyzing the solution to deposit the copper on a copper anode. This is an alternative to the smelting-electrolysis method, which also produces ruthenium-free copper. Treating the cell electrolyte with ozone to volatilize ruthenium offers a means of limiting the ^{106}Ru buildup in the electrolyte.

11.2 Recovery of Oil from Shale

Preliminary tests indicate that the contamination of shale oil by fission products should not be a serious obstacle to using a nuclear device to break the shale prior to in situ retorting. Although oil heated with test-shot debris was slightly contaminated, the radioactive material remained in the pot residue when the oil was distilled. Most of the radioactive material present in the oil was in the form of finely dispersed solids.

The problem of tritium contamination of the oil appears to be more serious. Oil retorted from shale after prolonged exposure to tritiated water vapor (in a sealed flask at elevated temperatures) contained tritium; after the oil was distilled, each of the fractions also contained tritium. The tritium apparently is incorporated in the hydrocarbons of the shale during the exposure to tritiated water vapor. The extent of the incorporation varies with the tritium concentration in the water, the water-to-shale ratio, and the exposure time in the flask.

12. BIOCHEMICAL SEPARATIONS

MACROMOLECULAR SEPARATIONS

12.1 Development of Reversed-Phase Chromatography Systems for Transfer Ribonucleic Acid Separations

Additional reversed-phase chromatographic (RPC) systems for transfer ribonucleic acid (tRNA) separations have been developed. These systems, designated RPC-3 and RPC-4, which are similar to those described previously (RPC-1 and RPC-2), employ water-insoluble quaternary ammonium salts (as extractants) supported on hydrophobic diatomaceous earth. They have proved to be particularly useful for the separation of tRNA's that are eluted early in the chromatographic run.

12.2 Engineering Scale-Up of Biochemical Separations Techniques

In a previous production campaign, 1.5 g of phenylalanine tRNA product was separated from approximately 400 g of mixed tRNA. This product had a specific activity of 810 micromicromoles/ODU (as compared with 1350 micromicromoles/ODU for pure material) and was contaminated with about 130 micromicromoles/ODU of tryptophan tRNA. The relatively low product purity and the tryptophan tRNA contaminant had not been observed in earlier developmental runs. Various parameters, such as solution pH, flow rate, and column geometry were investigated to determine what combination of operating conditions would provide high-purity products. A feed pretreatment technique, in which the bulk of the phenylalanine tRNA is separated from a number of tRNA's (including tryptophan tRNA) on a DEAE cellulose, was also developed. In a final series of runs on both DEAE cellulose columns and reversed-phase columns, two phenylalanine tRNA products with specific activities of about 1200 micromicromoles/ODU were separated.

12.3 Isolation of Purified Transfer Ribonucleic Acids

Purified samples of two formylmethionine tRNA's (i.e., tRNA's that are involved in the initiation of

protein chains) and a valine tRNA have been prepared from *E. coli* B crude tRNA. The first formylmethionine tRNA was obtained directly from RPC-3 columns; the other two tRNA's were pooled after RPC-3 chromatography and then separated by rechromatography on RPC-4 columns.

12.4 Solvent Extraction of Transfer Ribonucleic Acids

Transfer RNA's were selectively extracted from aqueous NaCl solutions by a quaternary ammonium chloride, Adogen 464, dissolved in Freon 214. The extraction coefficients decreased with increasing NaCl concentration and increased with increasing temperature. Other parameters affecting the extraction coefficients were the quaternary ammonium chloride concentration in the organic phase and the Mg^{2+} concentration in the aqueous phase.

12.5 Behavior of Transfer Ribonucleic Acids on Polyacrylamide Gel Columns

Specific tRNA's were partially separated by chromatography on polyacrylamide gel columns. Melting curves (i.e., curves showing the change in absorbance with temperature) and osmotic pressure measurements indicated that the separation did not depend on differences in molecular weights but, possibly, resulted from conformational (shape) differences between the tRNA's.

BODY FLUID ANALYSIS

12.6 Prototype Analyzers

Prototype systems of an analyzer for determining the ultraviolet-absorbing constituents of body fluids and an analyzer for determining carbohydrates in body fluids have been designed and are presently being built. On completion, they will be sent to two research institutes for evaluation.

12.7 System Components

Improvements were made in the ion exchange separation media. The optimum properties of such media have now been established. Three new detection systems have been built and are being tested. An automated concentration gradient generator and a means of metering reagents by using pressurized reagent reservoirs have been developed.

12.8 Parametric Studies

A study of the effect of column dimensions on the resolution of the separation system has been made. The pressure drop across a high-pressure ion exchange column has been shown to be inversely dependent on the square of the mean diameter of the ion exchange resin particles and linearly dependent on the specific flow rate and the column length.

12.9 Identification of Body Fluid Constituents

The chromatographic positions of 60 ultraviolet-absorbing compounds and 40 carbohydrates were established; the positions of 53 ultraviolet-absorbing compounds and 29 carbohydrates were determined by cochromatography.

12.10 Analytical Results

The excretion rates of many urinary constituents of normal human subjects were determined to be nearly equal. Both the ultraviolet analyzer and the carbohydrate analyzer were evaluated, with regard to usefulness and performance, by analysis of body fluids from abnormal human subjects and from laboratory animals.

12.11 Data Acquisition and Analysis

An automated data acquisition system has been designed and built, and a simplified computer program has been written to analyze the ultraviolet chromatogram for peak position and peak area.

12.12 Literature Survey

About 4000 references have been accumulated from the pertinent literature of the two-year period 1964–66. An annotated bibliography containing these references is now being prepared.

13. IRRADIATION EFFECTS ON HETEROGENEOUS SYSTEMS

The study of the radiolysis of adsorbed water was completed. Energy adsorbed by the solid adsorbent is transferred to the surface in the form of electrons, which react with acid hydrogen sites to give enhanced gaseous hydrogen yields.

14. SPECTROPHOTOMETRIC STUDIES OF SOLUTIONS OF ALPHA-ACTIVE MATERIALS

Spectrophotometric techniques for studying aqueous solutions, especially of the lanthanides, actinides, and transition elements, are being developed and exploited. A special spectrophotometer system has been built to provide containment for alpha-active materials and to operate at temperatures up to 372°C and pressures up to 10,000 psi. This system is now being used for studying low-level-radioactive and nonradioactive materials.

Other studies include correlations of the spectra of penta- and hexavalent neptunium, plutonium, and americium with those of the uranyl ion and investigations of the emission spectra of some transuranium oxides. In these studies we have found that a single model is applicable to the electron distributions in all the known actinyl ions, and we have observed emission spectra which indicate that Am_2O_3 may have properties similar to those of laser materials.

15. CHEMICAL ENGINEERING RESEARCH

The 18-stage (14 extraction and 4 polishing stages) prototype stacked-clone solvent extraction contactor has been tested with simulated first-cycle LMFBR fuel processing solutions. Extraction operations using hydroclones are being evaluated for inclusion in the LMFBR conceptual reprocessing plant. A new 11-stage contactor, having nine hydroclones in each stage and representing a scaleup factor of 2.7, is being fabricated. The size of its hydroclones is three-eighths that of standard hydroclones. Tests of existing stacked-clone contactors with a variety of solutions that represent a wide range of physical properties are being made in both the aqueous- and the organic-phase-continuous modes of operation.

16. REACTOR EVALUATION STUDIES

This program, which is a joint effort with other ORNL Divisions, especially the Reactor Division and the Metals and Ceramics Division, consists of studies of various advanced reactor and fuel-cycle systems to determine engineering and economic feasibility. The work in this Division during the past year included cost studies of shipping fresh and spent nuclear fuel, reprocessing spent fuel, and preparing various virgin and recycle fuel materials (oxides, metals, fluorides, etc.), primarily in support of the USAEC evaluation of civilian nuclear power for the period 1970–2020. Computer codes were developed to calculate rational growth patterns for the fuel cycle industry and to make projections of cost vs time for the various steps in the fuel cycle, based on both marketplace (nonoptimal) and optimal economic models. A computer code, RIBDOR, was written to calculate activities and concentrations of individual fission product isotopes, fission product elements, groups of chemically similar elements, and their gross totals, as well as beta and gamma decay heat release rates. The program also calculates gamma photon release rates in terms of 16 energy groups for use in shielding calculations.

17. PREPARATION AND PROPERTIES OF ACTINIDE OXIDES

Electrophoretic studies of sols of UO_2 and various lanthanide hydroxide sols were made. Results of these studies indicate that chloride-stabilized UO_2 sols oxidize more slowly than nitrate-stabilized sols and that the U(VI) formed by oxidation is not uniformly distributed among the sol particles. In other studies, we found correlations between different techniques of measuring the charge on sol particles; also, we observed that the pH at the isoelectric point for lanthanide hydroxide sols decreases as the atomic number of the metal increases. Aging these sols at 80°C for two to four weeks can cause a reversal of the sign of the particle charge.

18. CHEMISTRY OF CARBIDES AND NITRIDES

Fundamental studies of the reactions of the uranium and thorium carbides, nitrides, and carboni-

trides with aqueous solutions were continued. In reactions of the uranium carbides with 2 to 18 *M* NaOH, some of the uranium in the carbides was oxidized to a higher valence state, with the accompanying evolution of hydrogen. Hydrocarbons similar to those produced in the reactions with water were also found. Uranium mononitride was inert at 80°C in water, in 3 to 12 *M* HCl, and in 1 *M* H_2SO_4. The nitride reacted with 0.5 to 15.8 *M* HNO_3, giving gaseous mixtures of N_2, N_2O, and NO_2 (when the acid concentration was 6 *M* or higher). In reactions of thorium monocarbide with 0.1 to 1 *M* HNO_3 at 90°C, both hydrolysis (yielding mainly methane) and oxidation (yielding CO_2 and nitrogen oxides) of the carbide occurred. At higher acid concentrations, only oxidation occurred. The main products from the reaction of uranium monocarbide or thorium monocarbide with 4 and 6 *M* NH_4F at 80°C were (U or Th)$F_4 \cdot NH_4F$, ammonia, and methane. Uranium carbonitride ($UC_{0.23}N_{0.77}$) was inert at 80°C in water and in 6 *M* NaOH. The carbonitride reacted with 6 *M* HCl and 6 *M* H_2SO_4 at 80°C, producing primarily CH_4, NH_4^+, H_2, and U^{4+}, and, in the case of 6 *M* H_2SO_4, $U(SO_4)_2 \cdot 4H_2O$. In reactions of the carbonitride with 1 to 8 *M* HNO_3, the nitride nitrogen was first converted to NH_4^+ and then slowly oxidized to free N_2. Nitrous acid and NO were also major products. About half the carbide carbon was found as CO_2; the other half was in the form of unidentified nitric acid–soluble organic compound(s).

19. SAFETY STUDIES OF FUEL TRANSPORT

This program was organized in the early part of 1966 to develop an *Irradiated Fuel Shipping Cask Criteria* for the Division of Reactor Development and Technology (DRDT). The *Criteria* will provide the AEC with a series of cask design standards and specifications that, if followed, should ensure adherence to the requirements set forth in AEC regulations.

The *Criteria* will establish suitable engineering standards for the design, fabrication, and inspection of irradiated fuel shipping casks by providing information on structural integrity, shielding, heat transfer, criticality, materials of construction, and fabrication techniques. Specifications and standards presented in the *Criteria* will be based on data that have been developed from experiments and analyses.

The writing of the *Criteria* has been interrupted frequently as the result of the many cask reviews that have been conducted for the AEC. During the past year we have been involved with seven cask projects of varying complexity. Five are now essentially complete, whereas two, which involve the PM-1 Navy cask and the uranium cask program at Paducah, are still in progress.

The Chemical Technology Division is in the process of analyzing all its casks to determine what modifications, if any, will be required to meet the regulations of the AEC and the new Department of Transportation (DOT). One new design has been approved by the AEC and DOT; two additional designs have been submitted for approval, and two others are currently being analyzed.

20. THE NUCLEAR-POWERED AGRO-INDUSTRIAL COMPLEX: SPECIAL STUDY PROJECT

During the Summer of 1967, ORNL undertook a special study, directed by Professor E. A. Mason of MIT, to determine the technical and economic feasibility of using low-cost nuclear power (and steam) from a nuclear reactor and low-cost water from a nuclear-powered seawater evaporator to provide the bases for a nuclear agro-industrial complex. Such a complex might enable developing countries to circumvent their normally slow industrial evolution, thereby increasing their rate of technological, and also economic, progress toward industrialization. The food produced in the food factory, the agricultural part of the complex, would be sufficient to feed 5,000,000 to 6,000,000 persons, and the fertilizer production would be sufficient to enhance crop yields in other farm areas that feed up to 80,000,000. Two bases were employed during the study: a near-term (10-year) base using light-water reactors and multistage flash evaporators, and a far-term (20-year) base utilizing advanced breeder reactors and vertical-tube evaporators. For each type of reactor, station capacities of 500 to 2500 Mw (electrical) were evaluated. Evaporator outputs of up to 1,200,000,000 gal of fresh water per day were considered.

Assistance provided by members of the Chemical Technology Division on this study was primarily, but not exclusively, devoted to the parts of the

study involving chemical and metallurgical industries. Technical and economic data for a number of processes were obtained from the literature, from consultants, and particularly from representatives of industry. These data enabled detailed production cost studies of a considerable number of parameters to be made. Processes utilizing large amounts of power and steam, and those providing basic fertilizers, were given high priority; the production of seawater chemicals was also studied because large amounts of concentrated brine are rejected from the seawater evaporator. Ammonia, elemental phosphorus, and phosphoric acid were the primary fertilizers or intermediates considered; urea, ammonium nitrate, and nitric phosphate were evaluated as secondary fertilizers. The electrolytic production of aluminum, magnesium, and caustic-chlorine was investigated. Seawater chemicals, including salt, potassium chloride and sulfate, anhydrous magnesium chloride, and gypsum for making sulfur and cement, were evaluated. Seven alternative methods for producing iron and steel in developing nations were studied.

Parameters that were evaluated included raw materials costs; plant capacities; power, steam, and water costs; and interest rates. In certain cases, special variables such as current densities for water electrolysis cells and phosphate rock assay for phosphoric acid manufacture were used. The production of ammonia was studied more completely than that of any other product. The production of hydrogen (for ammonia synthesis) in three different types of advanced water electrolysis cells was evaluated and compared with the production of ammonia from steam-naphtha (or methane) reforming. Use of off-peak power for hydrogen production by electrolysis for the subsequent synthesis of ammonia was also evaluated. The production of phosphorus by the electric furnace method was compared with the production of phosphoric acid by the acidulation of phosphate rock with sulfuric acid.

The results of the study indicate that the concept of a nuclear agro-industrial complex is feasible and economically viable and that rates of return in the range of 10 to 20% can be achieved for both industrial and agricultural products. With regard to basic products, the production of aluminum and caustic-chlorine would be very profitable when power costing 2 to 4 mills/kwhr is available. Assuming 4- to 5-mill/kwhr power to be available, the manufacture of phosphoric acid from electric furnace phosphorus was found to compete satisfactorily with the wet acid method. The production of ammonia from electrolytic hydrogen, using 2- to 3-mill/kwhr power, can compete with steam-naphtha reforming methods in foreign locations; use of off-peak power would improve the economic position for this process. The production of iron and steel, seawater chemicals, and magnesium may be relatively profitable; however, this will require further study. The development of water and steam electrolysis methods as sources of hydrogen appears to be worthy of further consideration.

21. WATER RESEARCH PROGRAM

Oak Ridge National Laboratory is carrying out a program of basic research on the properties of water and its solutions under the auspices of the Office of Saline Water, Department of the Interior. This program has as its long-range goal the development of methods for the economical purification of water in such amounts and of such purity that it may be used for irrigation and for drinking. Work in this interdivisional program is under the direction of K. A. Kraus. It is reported in part in a series of reports issued annually by the Department of the Interior. The most recent report in the series is *Saline Water Conversion Report, 1966*. Because the work is reported formally in the above series, only an abstract of the work carried out by Chemical Technology Division personnel is presented in this report.

Specific aspects of the economic feasibility of desalination by multistage hyperfiltration were investigated in the Chemical Technology Division during the past year. The engineering development of hyperfiltration must include optimization studies of plants that would use various membranes having a considerable range of possible characteristics. These studies will provide comparisons of the product water costs that are associated with various membrane characteristics, and they can serve in guiding the development of membranes that would be most suitable for use in hyperfiltration processes. We have established optimum operating conditions (with product water cost as the objective function) for one- and two-stage plants with various assumed membrane characteristics and with the assumption that the feedwater contains from 1000 to 5000 ppm of dissolved solids.

Some flowsheet design innovations were studied. It was assumed that each stage of the plant could be divided into any specified number of sections, with pumps for repressurizing the salt solution between sections and for recirculating part of the solution in each section. Each section would be composed of a number of membrane-lined tubes that could be assembled in parallel. The number of tubes per section could be varied along the stage, thereby allowing the inlet velocity to each section to be independent of the inlet velocities of the other sections. The product from each section of the first stage was fed to that section of the second stage where its composition was most closely matched.

In the optimization program, optimum inlet pressure, inlet velocity, and recycle ratio were determined for each section of each stage. After some exploratory studies of the effects of plant size and tube diameter, we investigated the effects of (1) membrane permeability, (2) water recovery, (3) capital costs per unit membrane area, (4) the number of sections per stage, and (5) assumed combinations of various types of membranes in the section of the first stage.

Two sets of membrane characteristics have been studied to date. One set, typical of those for dynamically deposited ion exchange membranes, gave 85% rejection for a 0.05 *M* salt solution when the rejection was undiminished by polarization and flux effects. Permeabilities were varied from 1 to 30 gal day^{-1} ft^{-2} atm^{-1}. Two-stage plants yielded lower water costs than one-stage plants for feeds containing 3000 to 5000 ppm of salts, and also for feeds containing 2000 ppm of salts over most of the permeability range.

Studies were made with another set of membrane characteristics, typical of cellulose acetate membranes, that gave a rejection of 99%, independent of the concentration of the salt solution, with a permeability of 0.5 gal day^{-1} ft^{-2} atm^{-1}. Except when feed containing 5000 ppm of solids was assumed, costs were higher for these characteristics than for higher-permeability, lower-rejection membranes.

22. ASSISTANCE PROGRAMS

22.1 Eurochemic Assistance Program

The Laboratory continued to coordinate the exchange of technical information between Eurochemic and USAEC production sites and national laboratories for the USAEC Division of International Affairs. E. M. Shank completed his sixth year at Mol, Belgium, as resident U.S. Technical Advisor to Eurochemic. Initial test runs to reprocess spent fuels from several European reactors were completed successfully, and a new campaign to reprocess highly enriched uranium fuel was begun.

22.2 Evaluation of the Radiation Resistance of Selected Protective Coatings (Paints)

Thirty-seven commercial protective coatings from five different manufacturers are being evaluated for possible use in nuclear facilities. Of the candidate materials, organic modified phenolic coatings were the least affected by exposure to ionizing radiation in this particular test series. The specimens were irradiated by exposure in a deionized water-filled or air-filled cavity to a ^{60}Co gamma source (intensity, 6×10^5 r/hr) at 40 to 50°C. In each case, the specimen always failed earlier when immersed in deionized water than when exposed in air.

A committee comprised of industrial, USAEC, and USAEC contractual and operating personnel issued a USA Standards Institute standard, N5.9-1967, "Protective Coatings (Paints) for the Nuclear Industry," under the sponsorship of the American Institute of Chemical Engineers.

1. Molten-Salt Reactor Processing

The concept of the molten-salt breeder reactor (MSBR) inherently simplifies the most difficult problem in the development of thermal breeder reactors (i.e., the chemical reprocessing of the fuel) by presenting its fuel to the reprocessing plant as a fluid. The development of a compact, low-inventory, continuous, high-performance processing plant to become an integral part of MSBR's is the responsibility of the Chemical Technology Division. The direction of this work has undergone a significant change since the last reporting period. This change resulted from the recognition and the acceptance of reductive extraction as a feasible and attractive means for isolating protactinium from the reactor and, possibly, for removing fission products. Since protactinium in these systems is less easily reduced (i.e., is less noble) than uranium but more easily reduced (i.e., is more noble) than thorium, it can be dynamically held between two reductive extraction cascades and concentrated in a vessel that is located at a distance from the neutron flux. This possibility, along with the recognition that a satisfactory breeding ratio can be achieved with a single-fluid system, has redirected the development of chemical processing methods toward both isolating protactinium and removing fission products from single-fluid reactor fuel salt that contains thorium fluoride.

While fluorination and distillation, as developed for a two-fluid reactor, will probably find applications as steps in the processing of a single-fluid machine, they will be secondary to reductive extraction, which will comprise the heart of the processing flowsheet. Our work on means for protecting exposed surfaces from corrosion by the use of a layer of frozen salt (a technique that was originally developed for the fluorination step) is also expected to find application in the new process.

This section contains some of the data that have suggested the feasibility of reductive extraction and presents the calculational analysis of some proposed flowsheets, with alternatives.

The Chemical Technology Division is also actively participating in the Molten-Salt Reactor Experiment (MSRE). This reactor has just successfully completed an extended period of operation with ^{235}U as fuel. In July 1968, the ^{235}U will be removed from the fuel salt by fluorination, the carrier salt will be processed to remove the corrosion products from the fluorination operation, and ^{233}U, in the form of an LiF-UF_4 eutectic, will be added to the salt for the next phase of MSRE operation. Our developmental work, facilities, and plans for the fuel salt processing, and the program which led to the preparation of the ^{233}U eutectic in our shielded facilities in the TURF facility, are discussed in this section.

1.1 CORROSION CONTROL BY USE OF A FROZEN WALL

Uranium must be removed from the fuel stream of a two-fluid MSBR prior to the distillation step because UF_4 cannot be completely volatilized during this step. Equipment is being developed to provide for the continuous removal of UF_4 from a salt stream by countercurrently contacting the salt with fluorine in a salt-phase-continuous system. A method for protecting the equipment from corrosion consists in freezing a layer of salt on the vessel wall; the heat flux necessary for maintaining molten salt adjacent to the frozen salt layer would be provided by the decay of fission products in the salt stream.

The feasibility of forming and maintaining a layer of frozen salt (which will protect the walls of a continuous fluorinator) was established by

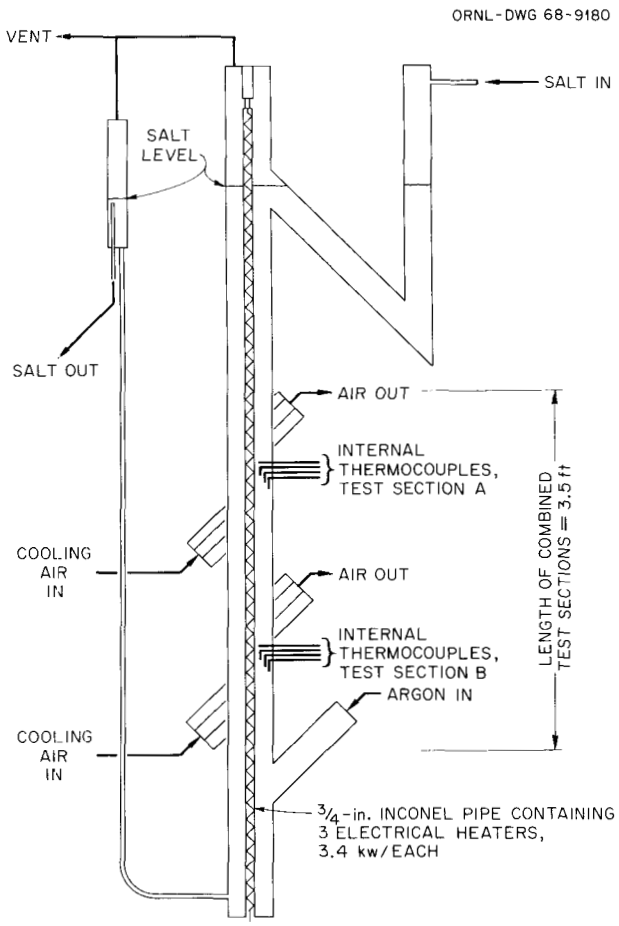

Fig. 1.1. Experimental Equipment for Studying the Formation of a Frozen Salt Layer for Corrosion Protection. All external surfaces were provided with electrical heaters and were heavily insulated.

laboratory experiments using a countercurrent flow of molten salt and an inert gas. The experimental equipment consisted of a 5-in.-diam by 8-ft-high column, fabricated from sched 40 nickel pipe (Fig. 1.1). An internal heat source consisting of three Calrod heaters contained in a $\frac{3}{4}$-in.-diam sched 40 Inconel pipe was used to simulate the volume heat source that will be provided by fission product decay in the molten salt. Two sets of internal thermocouples, located near the center of each of two test sections, measured the radial temperature gradient. The location of the interface between the molten and the frozen salt could then be established from these measurements. Each test section was independently cooled by air flowing through spirally wound $\frac{3}{8}$-in.-diam nickel tubing. Additional Calrod heaters were wound on the external surface of the fluorinator to provide auxiliary heat during heatup and to provide temperature control at the ends of the column. A 66-34 mole % $LiF\text{-}ZrF_4$ mixture, which has a liquidus temperature of 595°C and a phase diagram similar to the $LiF\text{-}BeF_2$ system, was metered from the feed tank for periods as long as 5 hr. This allowed data to be collected for a 1- to 2-hr period of steady-state operation.

The principal objective of the experiments (i.e., the demonstration that a layer of frozen salt can be formed and maintained under approximate operating conditions) was achieved. In Table 1.1, experimental conditions are compared with reference conditions for processing the fuel stream of a 1000-Mw (electrical) MSBR; the fluorinator has a salt throughput of 15 ft^3/day and an inlet uranium concentration of 0.8 kg per cubic foot of salt, with a 50% fluorine utilization.

In general, the thicknesses of the frozen wall and the temperature profiles in the frozen salt were in good agreement with the values that were obtained by assuming radial heat transfer from a volume heat source. The thickness of the frozen wall ranged from 0.3 to 0.8 in., depending on operating conditions. The effect of heat generation in the layer of frozen salt was not simulated in these experiments.

The thermal conductivity of the frozen salt was calculated for each run from the experimentally determined temperature gradient and the measured heat flux; the relative agreement of calculated values was assumed to be indicative of the consistency of the experimental data. Thermal conductivity values calculated from the upper test section data were closely grouped around 0.75 Btu hr^{-1} ft^{-1} $(°F)^{-1}$; however, values from the lower section were more widely scattered and were generally about 100% higher.

The heating-cooling system used on the column produced some variation in the temperature of the external wall (and hence the thickness of the frozen wall); in a typical run, the difference between the temperature of the salt liquidus and that of the wall ranged from 85 to 140°C.

Protection of the fluorine inlet nozzle from corrosion is an anticipated problem that is associated with operation of a frozen-wall fluorinator. A possible solution to this problem consists in introducing the fluorine through a short section of 3-in.-diam pipe that intersects the fluorinator at a 45° angle. The inlet section would be protected

Table 1.1. Comparison of Experimental and Reference Conditions for the Fluorination of 15 ft^3 of Molten Salt per Day

	Experimental	Reference
Salt flow rate, liters/hr	~3.3	17.7
Gas flow rate, std liters/min	0.5–2.0[a]	2.0[b]
Heat flux, w per foot of column height	600–1600	~2000

[a]Argon.
[b]Fluorine.

from corrosion by a layer of frozen salt as in the fluorinator. Results of tests with the present system indicate satisfactory operation when the surfaces of the inlet section are covered by a layer of frozen salt that is produced by maintaining wall temperatures below the temperature of the salt liquidus. Currently, heat is being supplied to this section by means of turbulence (caused by bubbles) in the molten salt; in an actual instance, heat would be generated in the salt as a result of fission product decay. This method of introducing gas appears to be feasible, although it will not produce small-diameter gas bubbles.

In future experiments, the heat flux will be increased to that of the reference value, and the salt flow rate will be increased to approximately 50% of the reference rate.

1.2 RELATIVE VOLATILITIES OF FISSION PRODUCT FLUORIDES IN MSBR SALTS

Relative volatilities, with respect to LiF, of several rare-earth trifluorides and alkaline-earth fluorides have been measured in an equilibrium still at 1000°C. The relative volatility of component i with respect to component j is defined as:

$$\alpha_{ij} \equiv \frac{Y_i/X_i}{Y_j/X_j}, \qquad (1)$$

where Y refers to the vapor-phase mole fraction and X refers to the liquid-phase mole fraction when the two phases are at equilibrium.

Experimental equipment and procedure for this work have been described previously.[1] Measured relative volatilities, with respect to LiF, of fluorides of several metals, including rare earths, barium, strontium, and beryllium, are summarized in Table 1.2. Calculated relative volatilities (based on Raoult's law) are also given for rare-earth trifluorides for which sublimation pressure data are available. The deviation between measured and predicted relative volatilities is within the combined errors involved in measurements of the sublimation pressures and the relative volatilities.

Errors (in relative volatilities) from several sources have been estimated; these estimates indicate that the values given are certainly within a factor of 5 (and probably within a factor of 2) of the equilibrium values. The relative volatilities of the rare earths, yttrium, barium, and strontium are low enough to allow adequate removal of these materials in a still of simple design. The removal of zirconium, however, will be insignificant.

1.3 DETERMINATION OF RELATIVE VOLATILITIES BY THE TRANSPIRATION METHOD

Liquid-vapor equilibrium data for LiF-BeF_2 and LiF-BeF_2-ThF_4 systems are being determined by the transpiration method in support of the development of possible distillation steps in the processing of both two-fluid MSBR fuel salt, LiF-BeF_2-UF_4 (66-34-0.3 mole %), and single-fluid MSBR fuel, LiF-BeF_2-ThF_4-UF_4 (about 68-20-12-0.3 mole %). The transpiration apparatus, shown schematically in Fig. 1.2, closely resembles that of Sense *et al.*[2] and Cantor.[3] High-purity argon is passed, for further purification, through a molecular sieve trap to remove water and through heated (450°C) metallic copper to remove oxygen. Then the argon is passed over the given salt (becoming saturated with it) and through a condenser, where the salt is deposited; finally the argon is passed into a wet test meter. After vapors have transpired for a predetermined time at a given temperature,

[1]J. R. Hightower and L. E. McNeese, *Measurement of the Relative Volatilities of Fluorides of Ce, La, Pr, Nd, Sm, Eu, Ba, Sr, Y, and Zr in Mixtures of LiF and BeF_2*, ORNL-TM-2058 (January 1968).

[2]K. A. Sense, M. J. Snyder, and J. W. Slegg, *J. Phys. Chem.* **58**, 223 (1954).

[3]W. R. Grimes, *Reactor Chem. Div. Ann. Progr. Rept. Dec. 31, 1965*, ORNL-3913.

Table 1.2. Relative Volatilities, with Respect to LiF, of Rare-Earth Trifluorides, SrF_2, YF_3, BaF_2, ZrF_4, and BeF_2 at 1000°C

Component, MF	Relative Volatility in $LiF\text{-}BeF_2\text{-}MF$[a]	Relative Volatility in LiF-MF Mixtures[b]	Relative Volatility Based on Raoult's Law[c]
CeF_3	1.8×10^{-4}	4.2×10^{-4}	2.5×10^{-4}
LaF_3	1.4×10^{-4}	3×10^{-4}	0.41×10^{-4}
NdF_3	1.4×10^{-4}	6×10^{-4}	3×10^{-4}
PrF_3	1.9×10^{-3}	6.3×10^{-4}	
SmF_3	8.4×10^{-5}	4.5×10^{-4}	
EuF_3	1.1×10^{-3}		
YF_3	3.4×10^{-5}		0.59×10^{-4}
BaF_2	1.1×10^{-4}		1.6×10^{-4}
SrF_2	5.0×10^{-5}		0.07×10^{-4}
ZrF_4	1.4, 0.76[d]		
BeF_2	4.73[e]		

[a]Pressure was 1.5 mm Hg; liquid composition was ~85-10-5 mole % $LiF\text{-}BeF_2\text{-}MF$.
[b]Pressure was 0.5 mm Hg; liquid composition was ~95-5 mole % LiF-MF.
[c]For systems obeying Raoult's law, $\alpha_{ij} = P_i^*/P_j^*$, where P_i^* is the vapor pressure of component i.
[d]Liquid concentrations of ZrF_4 were 0.96 and 0.03 mole % respectively.
[e]Average of 18 values.

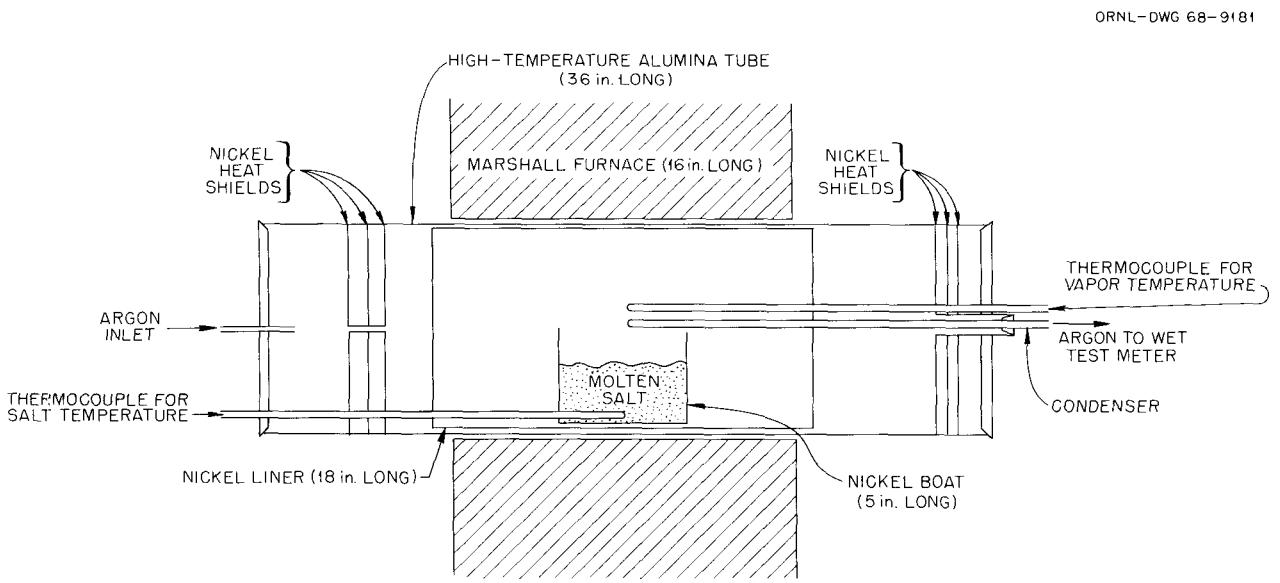

Fig. 1.2. Cross Section of Transpiration Apparatus Used to Determine Relative Volatilities in Molten Salt Systems.

the condenser is removed, and the salt contained in it is dissolved. Analyses of the solution, along with the pressure of the system and volume of argon used, provide the information necessary for calculating apparent partial pressures and relative volatilities.

Assuming ideal gas behavior and that Dalton's law of partial pressures is applicable, the following relationship is obtained:

$$P_A = \frac{m_A}{m_A + m_B + \ldots + m_N + M} P ,$$

in which

P_A = partial pressure of species A,

P = total pressure of vaporized salt and carrier gas,

m_A = total moles of species A collected in the condenser,

M = total moles of carrier gas passed through the system.

The transpiration method gives no direct information on the molecular formula of the vapor species or on the total vapor pressure of the system. Furthermore, in using this method, one must design the apparatus to avoid two possible errors. First, if the rate of gas flow is greater than the rate at which evaporation occurs at the liquid surface, the carrier gas will not become saturated, and the measured value for the vapor pressure will be low. Second, if the carrier gas flow rate is too low, thermal diffusion effects in the vapor will make the calculated value of P_A too large. For the experimental apparatus described above, the vapor pressure of a typical salt was found to be independent of the argon flow rate in the range of 15 to 50 cc (STP)/min. Therefore no correction was needed for diffusion or kinetic effects.

Relative volatility, which is a useful expression for representing vapor-liquid equilibrium data, is defined by:

$$\alpha_{AB} = \frac{y_A / y_B}{x_A / x_B},$$

where α_{AB} is the relative volatility of A with respect to B, y is the mole fraction of the designated component in the vapor phase, and x is the mole fraction in the liquid phase.

For a multicomponent system, the effective activity coefficient of component A at each temperature is given by:

$$\gamma_A = \frac{P_A}{N_A P_A^\circ},$$

where N_A is the mole fraction of A in the solution, P_A is the partial pressure of A, and P_A° is the vapor pressure of pure A.

Systems of Interest in Two-Fluid MSBR Fuel Processing

Data obtained for LiF-BeF_2 and LiF–BeF_2–metal-fluoride systems are given in Table 1.3. In the absence of any information regarding complex molecules in the vapor phase, the partial pressures of LiF, BeF_2, and solute fluorides were calculated on the assumption that only monomers existed in the vapor. In each experiment, the apparent partial pressures, P_A, could be described adequately by the linear expression

$$\log P_A \text{ (mm Hg)} = a - b/T \text{ (°K)} ,$$

in which a and b were constants over the temperature range investigated, 900 to 1050°C. Typical plots of log P vs $1/T$ are shown in Figs. 1.3 and 1.4.

The relative volatilities of BeF_2 (with respect to LiF) obtained in our experiments with LiF-BeF_2 binary systems are in reasonable agreement with those reported by Cantor,[4] who also used the transpiration method. For example, Cantor obtained values of 4.28 for LiF-BeF_2 (85-15 mole %) at 1000°C and 3.75 for LiF-BeF_2 (90-10 mole %); the corresponding values from our work were about 3.8 and 3.77 (Table 1.3). Our value obtained with LiF-BeF_2 (90-10 mole %) is somewhat lower than the average value of 4.71 reported by Hightower and McNeese,[5] who used an equilibrium still method, and is higher than the values obtained when the salt contained small amounts of RbF,

[4] R. B. Briggs, *MSR Program Semiann. Progr. Rept. Feb. 28, 1966*, ORNL-3936.

[5] J. R. Hightower, Jr., and L. E. McNeese, *Measurement of the Relative Volatilities of Fluorides of Ce, La, Pr, Nd, Sm, Eu, Ba, Sr, Y and Zr in Mixtures of LiF and BeF_2*, ORNL-TM-2058 (January 1968).

Table 1.3. Apparent Partial Pressures, Relative Volatilities, and Effective Activity Coefficients in $LiF-BeF_2$-Metal-Fluoride Systems

Salt Composition (mole %)			Species	Apparent Partial Pressure,* log P (mm) = $a - b/T$ (°K)		Effective Activity Coefficient at 1000°C	Relative Volatility, with Respect to LiF, at 1000°C
LiF	BeF_2	Third Component		a	b		
86	14		LiF	8.497	11,055	1.60	
			BeF_2	7.983	10,665	4.42×10^{-2}	3.82
90	10		LiF	7.604	10,070	1.30	
			BeF_2	8.707	11,884	3.55×10^{-2}	3.77
95	5		LiF	8.804	11,505	1.30	
			BeF_2	11.510	15,303	4.33×10^{-2}	4.60
90	10	UF_4: 0.02	LiF	9.481	12,386	1.33	
			BeF_2	9.339	12,411	5.96×10^{-2}	6.19
			UF_4	4.361	12,481	7.36×10^{-3}	2.9×10^{-2}
89.6	9.9	UF_4: 0.5	LiF	8.384	10,987	1.34	
			BeF_2	7.421	10,112	4.65×10^{-2}	4.78
			UF_4	6.686	13,443	1.09×10^{-2}	4.2×10^{-2}
86.4	9.6	UF_4: 4.0	LiF	10.790	13,992	1.55	
			BeF_2	10.177	13,726	3.84×10^{-2}	3.42
			UF_4	10.272	16,786	1.25 × 10–2	4.2×10^{-2}
90	10	RbF: 0.09	LiF	8.286	10,811	1.47	
			BeF_2	6.596	10,552	3.11×10^{-2}	2.93
			RbF	5.187	8,907	2.19	24.7
89.9	10	CsF: 0.03	LiF	9.654	13,459	1.99	
			BeF_2	8.310	11,313	4.07×10^{-2}	2.82
			CsF	0.819	3,375	1.17	95.1
90	10	ZrF_4: 0.083	LiF	7.915	10,358	1.41	
			BeF_2	7.167	10,070	2.83×10^{-2}	2.77
			ZrF_4	13.095	20,382	5.39×10^{-4}	2.19

*Temperature range: 900 to 1050°C. It was assumed that LiF, BeF_2, and the solute fluorides existed only as monomers in the vapor.

CsF, ZrF_4, or UF_4 (Table 1.3). This scatter in values is not surprising, because small variations in the composition of the liquid and/or vapor cause large changes in the relative volatility value. For example, it has been reported[5] that $LiF-BeF_2$ (66-34 mole %) is the vapor in equilibrium with $LiF-BeF_2$ (90-10 mole %) at 1000°C. This gives a value for

$$\alpha = \frac{36/66}{10/90} = 4.64 .$$

Another source[4] reports that the vapor in equilibrium with $LiF-BeF_2$ (88-12 mole %) has the composition $LiF-BeF_2$ (67-33 mole %), corresponding to an

$$\alpha \text{ of } \frac{33/67}{12/88} = 3.6 .$$

Our partial pressure data for $LiF-BeF_2$ systems are incompatible with some of the total pressure

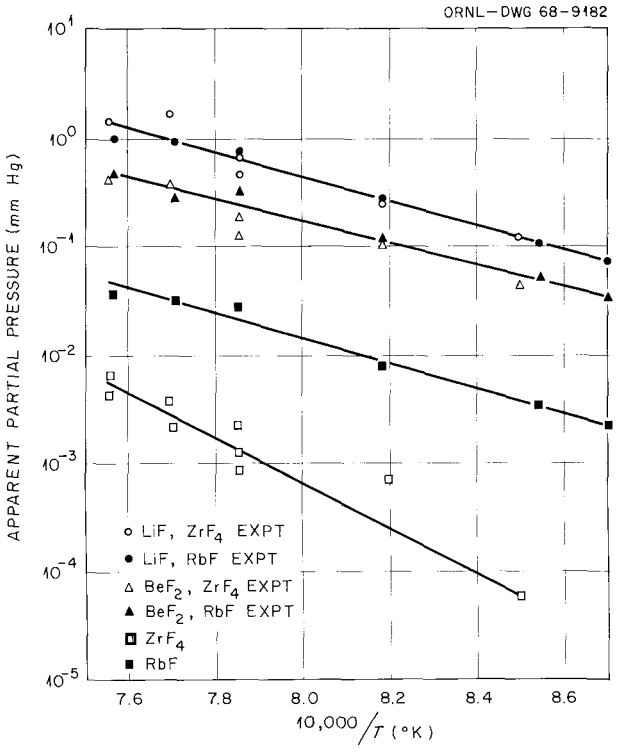

Fig. 1.3. Apparent Partial Pressure–Temperature Curves for the Systems $LiF-BeF_2-RbF$ (90-10-0.09 Mole %) and $LiF-BeF_2-ZrF_4$ (90-10-0.083 Mole %).

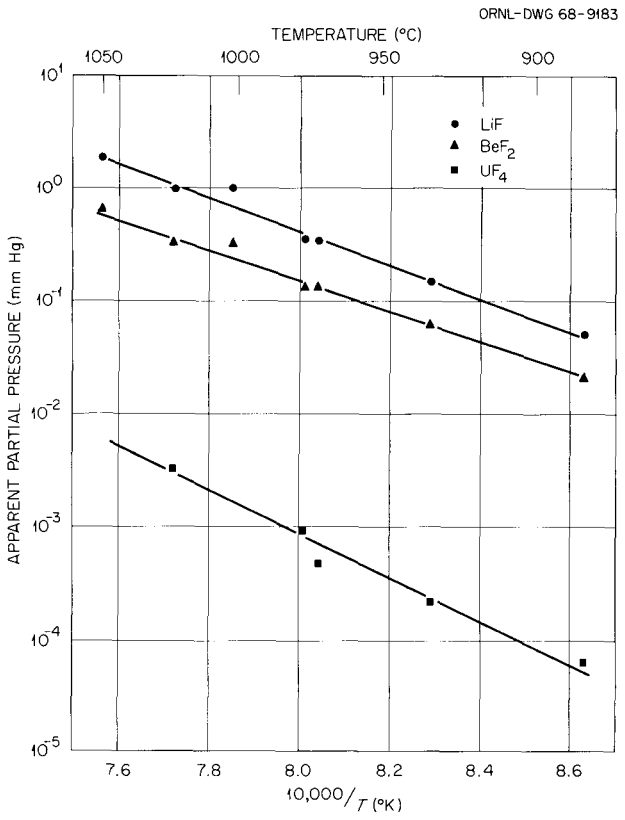

Fig. 1.4. Apparent Partial Pressure–Temperature Curves for the System $LiF-BeF_2-UF_4$ (86.4-9.6-4.0 Mole %).

data presented by Cantor.[6] He reports the total pressure of $LiF-BeF_2$ (90-10 mole %) to be 1.8 mm Hg at 1000°C. For the same system at 1000°C, we obtained the approximate values $P_{LiF} = 0.55$ and $P_{BeF_2} = 0.23$ mm Hg, corresponding to a total pressure of 0.78 mm (assuming that no association or dissociation occurred in the vapor phase). The total pressure calculated from our transpiration data should have been higher than the actual total pressure, because association in the vapor phase undoubtedly occurs; association in the vapors above pure LiF has been noted,[7] and complexation has been observed (by mass spectrometry) in the vapors above $LiF-BeF_2$ solutions.[6]

The activity coefficients obtained for BeF_2 are in good agreement with those reported by Kelly,[6] who used distillation data and assumed unit activity for LiF.

[6]W. R. Grimes, *Reactor Chem. Div. Ann. Progr. Rept. Dec. 31, 1966*, ORNL-4076.

[7]R. S. Scheffee and J. L. Margrave, *J. Chem. Phys.* 31, 1682 (1959).

The relative volatilities obtained for UF_4 (Table 1.3) confirm the prediction that adequate uranium recovery cannot be achieved in the distillation step. The values obtained for RbF and CsF (with respect to LiF) are within a factor of 2 of the theoretically predicted values.

Systems of Interest in Single-Fluid MSBR Fuel Processing

Preliminary vapor-liquid equilibrium data for $LiF-BeF_2-ThF_4$ systems have been obtained (Table 1.4) in support of possible distillation steps in the processing of single-fluid MSBR fuel. A typical partial-pressure–temperature plot is shown as Fig. 1.5. More work on systems like these will be done as soon as specific flowsheet applications are devised.

Table 1.4. Vapor-Liquid Equilibrium Data for the $LiF-BeF_2-ThF_4$ System at 1000°C[a]

Melt Composition (mole %)			Vapor Composition (mole %)			Apparent Partial Pressure (mm Hg)			Relative Volatilities with Respect to LiF		Predicted Total Pressure (mm Hg)
LiF	BeF_2	ThF_4	LiF	BeF_2	ThF_4	LiF	BeF_2	ThF_4	BeF_2	ThF_4	
68	20	12	27.4	72.5	0.14	0.598	1.59	0.0022	9.02	0.0212	2.18
70.5	7.5	22	36.7	63.1	0.20	0.391	0.724	0.0022	16.15	0.0179	1.12
75.4	3.6	21	54.6	44.2	1.2	0.407	0.380	0.00908	16.96	0.0738	0.796
53.5	1.5	45	12.0	86.4	1.65	0.0435	0.312	0.00599	260	0.158	0.361
34	1	65	16.0	79.6	4.55	0.0361	0.180	0.0103	165	0.149	0.226

[a]It was assumed that only three species, LiF, BeF_2, and ThF_4, existed in the vapor.

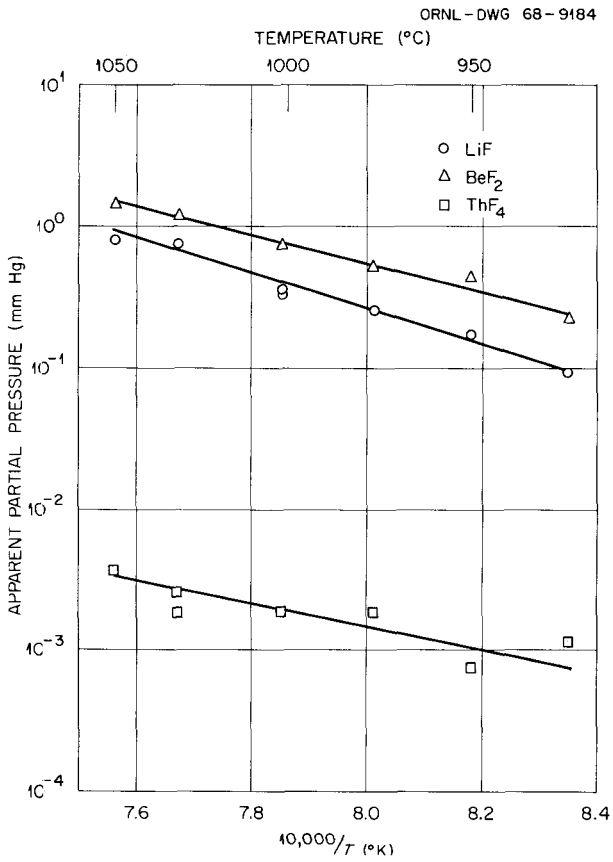

Fig. 1.5. Apparent Partial Pressure–Temperature Curves for the System $LiF-BeF_2-ThF_4$ (70.5-7.5-22 Mole %).

1.4 DISTILLATION OF MSRE FUEL CARRIER SALT

We have previously[8] described the equipment for use in the study of low-pressure distillation of MSRE fuel carrier salt. This equipment, which includes a 48-liter feed tank, a 12-liter still pot, a condenser, and a 48-liter condensate receiver, has been installed and checked out in a test facility; it is being used to perform nonradioactive experiments prior to operation with irradiated MSRE fuel carrier salt. During nonradioactive operation, four 48-liter batches of MSRE fuel carrier salt (65-30-5 mole % $LiF-BeF_2-ZrF_4$) will be distilled at 1000°C and at a pressure of about 1 mm Hg. Two experiments have been made to date; after the final two have been completed, the thermal insulation and heaters will be removed from the still, and a thorough examination of the equipment will be made. After examination, the still will be moved to a cell at the MSRE site for distillation of a 48-liter batch of fluorinated fuel salt from the reactor.

The first distillation run was completed in 83 hr, using approximately 48 liters of MSRE fuel carrier salt. At the beginning of the run, 9.4 liters of salt was transferred to the still pot, and the condenser pressure was reduced to 2.0 mm Hg.

[8]*MSRP Semiann. Progr. Rept. Feb. 28, 1967*, ORNL-4119, p. 211.

Table 1.5. Distillation Rates and Operating Conditions for Distillation of MSRE Fuel Carrier Salt

Condenser Pressure (mm Hg)	Distillation Rate: Kilograms per hour	Distillation Rate: Cubic Feet per day per Square Foot	Still Pot Temperature (°C)	Run Time (hr)
0.5	1.54	1.15	990	7.2
0.3	1.60	1.20	990	9.5
0.055	1.67	1.20	990	16.5
0.07	2.02	1.51	1005	29.8

Startup of the equipment was hampered by unsatisfactory operation of the liquid-level probes in the still pot. It is believed that argon that was dissolved in the molten salt formed bubbles on the probes initially as the pressure was reduced. After a period of approximately 4 hr, during which the system was held at 900°C and 2 mm Hg, the probes performed adequately. The system was then operated with a still pot temperature of 900 to 950°C and a condenser pressure of 0.65 to 2.0 mm Hg for approximately 40 hr. Salt was transferred to the still pot periodically in order to maintain a volume of about 9 liters. During this operating period, the concentration of BeF_2 in the still pot was reduced from the initial concentration of 30 mole %. The still pot temperature was increased to 990°C, and distillation rates were measured during a 40-hr period at condenser pressures of 0.5, 0.3, and 0.055 mm Hg. Results at these conditions are summarized in Table 1.5. Distillation rates were calculated from the rate of change of salt level in the feed tank and condensate receiver. During the last 40 hr of operation, the level of the liquid in the still and the salt feed rate were controlled automatically. Operation of the equipment was satisfactory. At the end of the run, approximately 8 liters of the initial salt mixture was used to flush the high-melting salt from the still pot in order to produce salt having a liquidus temperature of less than 700°C. The total volume of salt distilled during this run was approximately 30 liters.

The feed tank contained approximately 48 liters of MSRE fuel carrier salt in the second run. At the beginning of the run, salt was transferred to the still pot to yield a volume of about 9 liters. A still pot temperature of 900°C and a condenser pressure of 2 mm Hg were maintained for 1.5 hr; then the temperature was slowly increased (over a 13-hr period) to 1005°C, and the pressure was decreased to 0.07 mm Hg. These conditions were maintained for about 30 hr. The distillation rate during this period is given in Table 1.5. The total volume of salt distilled was 30 liters. The liquid level in the still pot and the salt feed rate were controlled automatically during the entire run. Minor difficulty was experienced in obtaining two condensate samples when small amounts of salt vapor condensed in the 1.5-in. line through which these samples were withdrawn.

Under the operating conditions in the still, the distillation rate is controlled by the provision that pressure drop in the passage connecting the vaporization and condensation surfaces must equal the difference between the vapor pressure of salt in the still pot and the pressure at the lower end of the condenser. For this reason, the distillation rate should be essentially independent of condenser pressure for condenser pressures much lower than the salt vapor pressure (1.0 to 1.5 mm Hg). When condenser pressures are much lower than the salt vapor pressure, the distillation rate should be proportional to the vapor pressure of the salt and hence quite dependent on the temperature of the still pot. A 21% increase in distillation rate was observed as the still pot temperature was increased from 990 to 1005°C; the corresponding increase in the vapor pressure of the salt was 28%.

Relative volatilities, with respect to LiF, were calculated from analyses of condensate samples to be 4.84 for BeF_2 and 10.4 for ZrF_4.

During distillation of the second batch of salt, the feed line to the still pot became partially obstructed; however, operation of the still was not interrupted. The obstructed section of line was replaced after unsuccessful attempts to melt or

dissolve the deposit by flowing salt through the line. The obstruction was located near the point where the feed line entered the still and consisted of a deposit of a spongy, magnetic material. Some of this material was gray, and some of it was brass-colored.

1.5 MEASUREMENT OF DISTRIBUTION COEFFICIENTS IN MOLTEN METAL-SALT SYSTEMS

Reductive extraction methods for the processing of molten-salt reactor fuels are being evaluated. The process currently under study involves the selective extraction of uranium, protactinium, and rare earths from the molten salt, using lithium-bismuth solutions. Initially[9,10] the effort was devoted to the processing of two-fluid MSBR salts, with emphasis on the removal of rare earths from the fuel salt and protactinium from the blanket salt. Subsequently, it was shown[11,12] that uranium and protactinium could probably be separated and recovered from a single-fluid MSBR salt. In addition, a preliminary evaluation[13] indicated that such a process was feasible from an engineering viewpoint. Before a more detailed evaluation of this method can be made, accurate distribution coefficients for uranium, thorium, protactinium, and rare earths must be determined. Laboratory work to provide these data is now in progress.

Extraction of Uranium and Rare Earths from the Fuel Salt of a Two-Fluid MSBR

The equilibrium distribution of a component M between a molten salt and a liquid metal phase can be expressed as a distribution coefficient D_M that is defined as:

$$D_M = \frac{\text{mole fraction of M in metal phase}}{\text{mole fraction of M in salt phase}}.$$

Thermodynamic treatment[14] (supported by experimental data) of the equilibria involved with salts containing LiF indicates that, at a fixed temperature, each distribution coefficient should vary with the lithium concentration in the metal phase according to the equation

$$\log D_M = n \log X_{Li(m)} + \log I$$

if the concentration of M in each phase is low. In this equation, n is the valence of the component (as its fluoride, MF_n) in the salt, $X_{Li(m)}$ is the equilibrium lithium concentration in the metal phase (atom fraction), and I is a constant. Presentation of equilibrium distribution data in the manner indicated by the above equation is desirable; however, in our initial experiments this was

[9] D. E. Ferguson, *Chem. Technol. Div. Ann. Progr. Rept. May 31, 1966*, ORNL-3945, p. 75.

[10] M. W. Rosenthal, *MSR Program Semiann. Progr. Rept. Aug. 31, 1967*, ORNL-4191, pp. 148 and 248.

[11] D. M. Moulton and J. H. Shaffer, Reactor Chemistry Division, internal memorandum (Jan. 2, 1968).

[12] M. W. Rosenthal, *MSR Program Semiann. Progr. Rept. Feb. 29, 1968*, ORNL-4254 (in press).

[13] M. E. Whatley, L. E. McNeese, and J. S. Watson, internal memorandum (Feb. 6, 1968).

[14] W. R. Grimes, *Reactor Chem. Div. Ann. Progr. Rept. Dec. 31, 1966*, ORNL-4076 (March 1967).

Table 1.6. Distribution of Europium, Lanthanum, and Uranium Between LiF-BeF_2 (66-34 Mole %) and Lithium-Bismuth Solutions at Various Temperatures

Temperature (°C)	Lithium Concentration in Metal Phase (at. %)	D_{Eu}	D_{La}	D_U
500	4.02	14.3		
583	4.95	16.4		
	3.46	17.1		
600	0.0133			1.74
	0.0232			5.41
	0.0313			53.6
602	2.56	5.41		
605	0.119		0.092	
	0.119		0.90	
	0.208		0.70	
	0.298		5.12	
	4.84	6.36		
608	0.85	0.82		
675	0.238		0.487	1021
	0.298		0.672	1788
	0.298		0.926	
	0.416		1.09	
	0.506		2.01	
700	5.11	8.66		

not possible because we usually obtained only a few data points at a given temperature. Our data can be compared with those obtained by others either in terms of the difference in standard reduction potentials (as defined by Moulton[15]),

$$E'_{0,M} - E'_{0,Li} = \Delta E'_0 = (RT/nF) \ln D_M - (RT/F) \ln D_{Li} ,$$

or in terms of the quantity Q, which is defined as:

$$Q_M = D_M X^{-n}_{Li(m)} .$$

The relationship between $\Delta E'_0$ and Q is easily shown to be:

$$\log Q = \frac{nF \Delta E'_0}{2.303RT} - n \log X_{LiF} ,$$

in which X_{LiF} is the mole fraction of LiF in the salt.

Data obtained on the distribution of several solutes between two-fluid MSBR fuel salt, LiF-BeF_2 (66-34 mole %), and lithium-bismuth solutions are given in Tables 1.6 and 1.7. In calculating values of $\Delta E'_0$, n was assumed to be 1 for lithium and sodium, 2 for europium, 3 for lanthanum, and 4 for uranium and thorium. At temperatures where more than one distribution coefficient was obtained, an average value for $\Delta E'_0$ is given. The values obtained for lanthanum and europium are in reasonable agreement with those reported by Shaffer and Moulton.[11,16,17] However, our value for uranium at 600°C is higher, by 0.14 v, than the value reported by Shaffer and Moulton.[17] At present, this difference cannot be explained.

The $\Delta E'_0$ value for a component appears to be practically constant over the temperature range of 500 to 700°C. If $\Delta E'_0$ is constant, then plots of log Q vs $1/T$ should be linear, with slopes of $nF \Delta E'_0/2.303R$. Plots of the data for europium

[15] M. W. Rosenthal, *MSR Program Semiann. Progr. Rept. Feb. 28, 1967*, ORNL-4119, pp. 150–52 (July 1967).

[16] M. W. Rosenthal, *MSR Program Semiann. Progr. Rept. Aug. 31, 1967*, ORNL-4191, pp. 155–56.

[17] D. M. Moulton and J. H. Shaffer, Reactor Chemistry Division, unpublished data (Dec. 14, 1967).

Table 1.7. $\Delta E'_0$ Values[a] for the Distribution of Various Solutes Between Different Fluoride Salts and Lithium-Bismuth Solutions

Salt Composition (mole %)			Temperature (°C)	$\Delta E'_0$				
LiF	BeF_2	ThF_4		U	La	Eu	Na	Th
66	34	0	500			0.27		
			600[b]			0.32		
			600[c]		0.40	0.30		
			600[d]	0.54	0.45	0.32		0.36
			600	0.68				
70	19	11	600	0.66		0.33		0.41
66	34	0	602			0.31		
			605		0.44	0.27	0.20	
			675	0.60	0.43			
			700			0.30		
			700[b]			0.34		

[a] $\Delta E'_0 = E'_{0,M} - E'_{0,Li}$, where M is the other metal involved; see text.

[b] D. M. Moulton and J. H. Shaffer, internal memorandum, Jan. 2, 1968.

[c] D. M. Moulton and J. H. Shaffer, ORNL-4191, p. 155.

[d] D. M. Moulton and J. H. Shaffer, ref. 17.

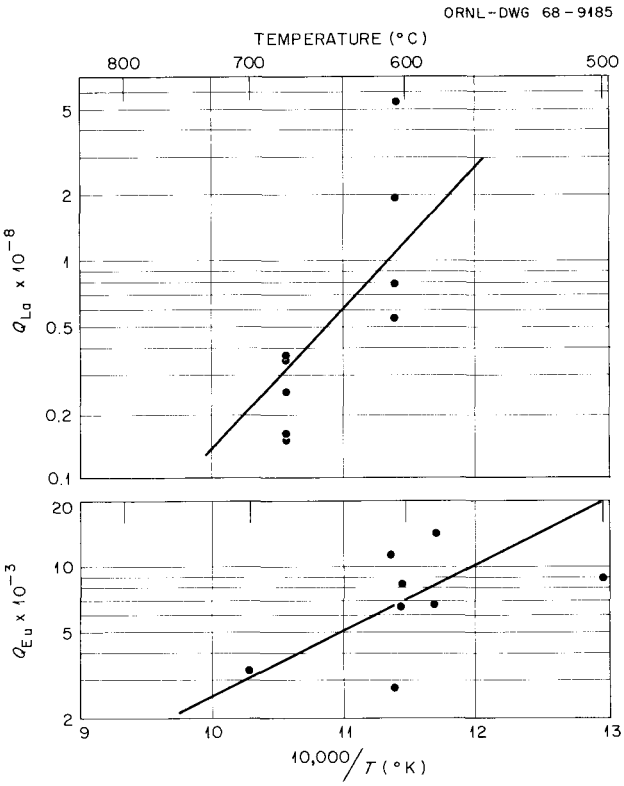

Fig. 1.6. Dependence of log Q on Temperature.

and lanthanum are shown in Fig. 1.6; average values of $\Delta E_0'$ of 0.43 and 0.30 for lanthanum and europium, respectively, were used in drawing the lines. Although the data points are widely scattered, Q appears to decrease with increasing temperature. This dependence of Q on temperature shows that the rare earths are more easily extracted at the lower temperatures. (Data for cerium[16] show the same type of temperature dependence as those for europium and lanthanum.)

The data given in Tables 1.6 and 1.7 show that uranium can be easily removed from the fuel salt of a two-fluid MSBR by reductive extraction and also that excellent separation from the rare earths can be achieved. At 600°C, the separation factors (D_U/D_{Ln}) are at least 10^3. Once uranium has been extracted, the rare earths can be removed from the salt by increasing the lithium concentration in the metal phase.

Extraction of Uranium, Thorium, and Rare Earths from Single-Fluid MSBR Fuel

The experiments with simulated single-fluid MSBR fuel salt were conducted by using a much better technique than that used in the earlier experiments with two-fluid reactor fuel salt. In the new procedure, pure bismuth, contained in a mild-steel crucible, was contacted with hydrogen for at least 24 hr at 700 to 800°C. The salt was treated in a separate, degassed graphite crucible with HF-H_2 mixtures at 600°C for 24 to 30 hr before being sparged with pure argon for about 20 hr. After purification, the salt ingot was physically transferred (in argon) to the crucible containing the bismuth. The two-phase system was then heated to the desired temperature under an argon purge; and lithium (as chunks of Li-Bi alloy) was added incrementally to the system. After each addition, the system was allowed to equilibrate 24 hr before filtered samples of each phase were taken. Each sample was weighed so that the weights of the respective phase could be calculated.

Analyses of the samples and determination of the weights of the phases provided the basis for calculating a reductant balance for the experiment. Assuming that lithium is consumed only by the reduction of metal fluoride species in the salt phase, analysis of the metal phase should show that:

$$\text{meq Li added} = [\text{meq of residual Li} + n_1(\text{mg-atoms } M_1) + n_2(\text{mg-atoms } M_2) + \ldots] .$$

in which M_1 and M_2 are metals of valences n_1 and n_2 respectively. Specifically, when the salt contains UF_4 and ThF_4, analysis of the metal phase should show that:

$$\text{meq Li added} = [\text{meq of residual Li} + 4(\text{mg-atoms U}) + 4(\text{mg-atoms Th})] .$$

Thus a plot of the sum of the milliequivalents of lithium, uranium, and thorium found in the metal phase vs the milliequivalents of lithium added to the system should have a slope of 1.

Graphs of practically all the data obtained in an experiment (experiment 2) involving the equilibration of LiF-BeF_2-ThF_4-UF_4-EuF_3 (initially 70-19-11-0.3-0.01 mole %) with Li-Bi solutions at 600°C are shown in Fig. 1.7. The first 6 or 7 meq of lithium added was probably consumed in reactions with FeF_2, OH^-, and other easily reduced species that were present in the salt. (Note that

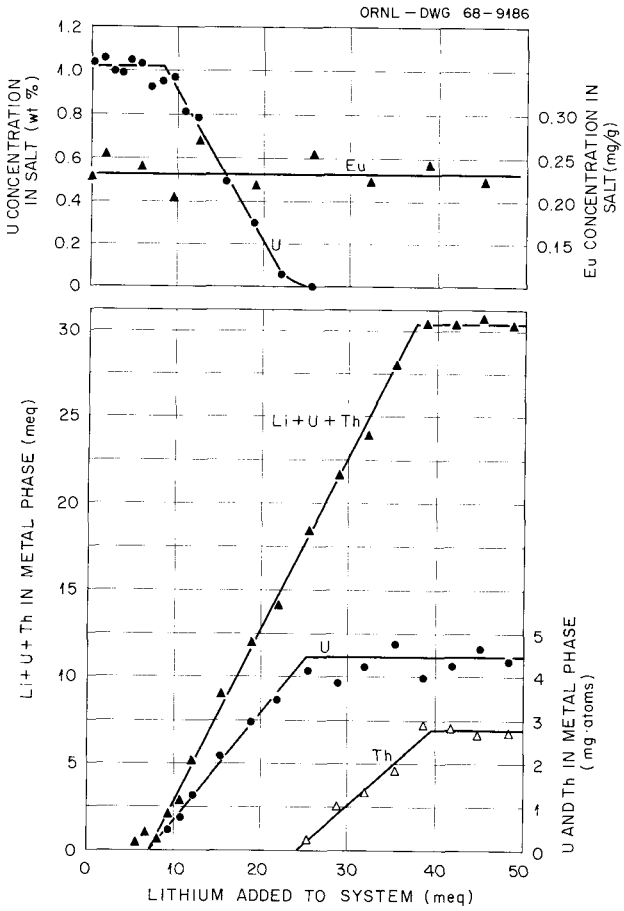

Fig. 1.7. Reductant Balance in Experiment Involving Equilibration of Li-Bi Solutions with $LiF-BeF_2-ThF_4-UF_4-EuF_3$ (Initially 70-19-11-0.3-0.01 Mole %) at 600°C.

the uranium concentration in the salt remained constant in this region.) Then, as more Li-Bi alloy was added to the system, the lithium was consumed, first by reduction of the UF_4 from the salt and then by reduction of some ThF_4. Within experimental error, the plot of the milligram-atoms of uranium found in the metal phase vs the milliequivalents of lithium added had a slope of 0.25 in accordance with the reaction $4Li + UF_4 \longrightarrow 4LiF + U$. This behavior shows that the uranium in the salt was tetravalent (undoubtedly as UF_4). After the uranium had been extracted from the salt, the addition of more lithium resulted in a systematic increase in the amount of thorium appearing in the metal phase. Finally the metal phase became saturated with respect to thorium, and each subsequent addition of lithium probably resulted only in the precipitation of Th_3Bi_4, while the composition of the metal phase remained practically constant. The reductant balance was excellent throughout the entire experiment; that is, the plot of the milliequivalents of U + Th + Li found in the metal phase vs the milliequivalents of lithium added was a straight line having a slope of 1 (until the metal phase became saturated with thorium).

Distribution coefficients obtained in two experiments involving the equilibration of simulated single-fluid MSBR fuel salt, $LiF-BeF_2-ThF_4-UF_4$ (initially 70-19-11-0.3 mole %), with Li-Bi solutions at 600°C are given in Table 1.8). One system contained EuF_3 (experiment 2), while LaF_3

Table 1.8. Distribution of Lithium, Uranium, Thorium and Europium Between $LiF-BeF_2-ThF_4$ (70-19-11 Mole %) and Bismuth Solutions at 600°C

Experiment Number	Li Concentration in Metal Phase (at. %)	D_U	D_{Th}	D_{Eu}
72	0.000672	0.00021		
72	0.00119	0.00013		
2	0.00321	0.0638		
2	0.00579	0.0267		
72	0.00584	0.311		
2	0.00726	0.132		
2	0.00747	0.238		
2	0.00827	0.417		
72	0.00873	0.134		
2	0.00988	2.47		
72	0.00997	0.827		
2	0.0112	1.12		
72	0.0128	1.47		
72	0.0133	2.28		
72	0.0136	4.08		
72	0.0176	5.07		
2	0.0182	15.1		
72	0.0285	15.2		
72	0.0376	26.1		
2	0.0570	102	0.00131	0.0041
72	0.0623	129	0.00229	
72	0.0786	168	0.00327	
72	0.0816	155	0.00573	
72	0.0855		0.00802	
2	0.0939		0.00998	0.011
2	0.0997	333	0.00712	0.014
72	0.114		0.0131	
2	0.175	759	0.0152	

was present in the other (experiment 72). The distribution coefficients for uranium can be represented by:

$$\log D_U = 4 \log C_{Li} + 7.874 ,$$

in which C_{Li} is the lithium concentration (at. %) in the metal phase. This equation was obtained by visually fitting what appeared to be the best line with a slope of 4 through the points in the lithium concentration range of 0.002 to 0.03 at. %, where the analyses were the most accurate. These data are shown in Fig. 1.8; the distribution coefficients obtained using LiF-BeF_2 (66-34 mole %) as the salt phase are included for comparison.

The distribution coefficients for thorium (Table 1.8) can be represented by the equation

$$\log D_{Th} = 4 \log C_{Li} + 2.00 ,$$

which was also obtained by a visual fit of the data (Fig. 1.8). The line through the three points obtained for europium was drawn with a slope of 2.

As Li-Bi alloy was added to the system in these experiments, the thorium concentration in the metal phase increased to a limiting value of 1700 ± 100 ppm. The corresponding uranium and lithium concentrations were 2500 ± 300 and 50 ± 10 ppm respectively. The distribution coefficients under this steady-state condition were about 0.014 for both thorium and europium and less than 0.07 for lanthanum (the lanthanum concentration in the metal phase was always less than 4 ppm). The data indicate that the solubility of thorium in bismuth is depressed by the presence of uranium and/or lithium, since the solubility of thorium in pure bismuth at 600°C is reported to be 3000 to 3900 ppm.[18,19]

The data presented here show that uranium can be easily extracted from single-fluid MSBR salt, leaving thorium and rare earths in the salt; the separation factors (D_U/D_{Th} and D_U/D_{Eu}) are at least 10^4. These data also show that the rare earths can probably be separated from thorium; however, further work will be required to determine the optimum conditions.

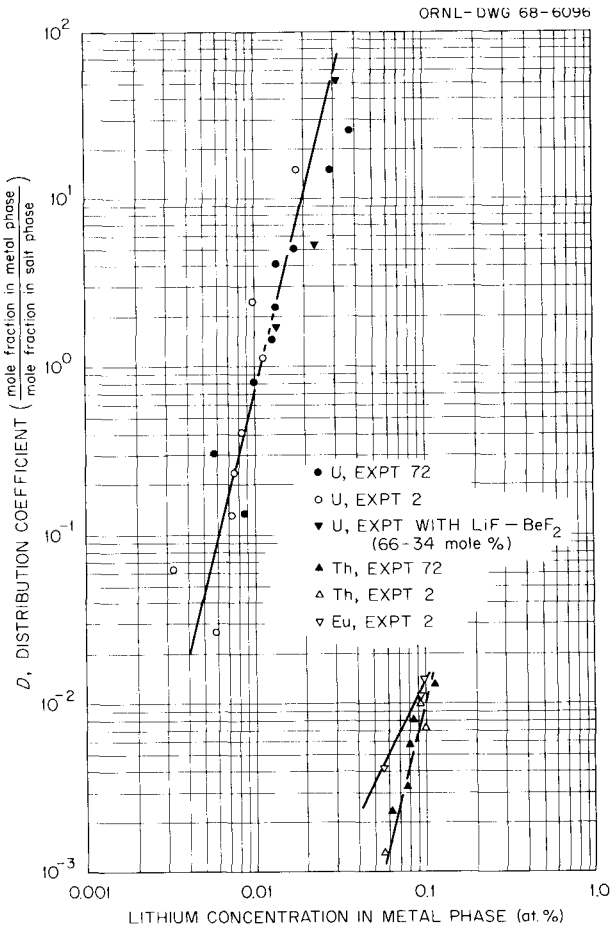

Fig. 1.8. Effect of Lithium Concentration in Metal Phase on the Distribution of Uranium, Thorium, and Europium Between LiF-BeF_2-ThF_4 (70-19-11 Mole %) and Bismuth at 600°C.

1.6 REMOVAL OF PROTACTINIUM FROM A TWO-FLUID MSBR

A higher breeding ratio can be achieved in molten-salt reactors if a low protactinium concentration is maintained in the regions of high neutron flux. This low concentration will serve to avoid parasitic capture by the protactinium before it decays to ^{233}U. One conceptual MSBR design is based on a two-fluid reactor in which the fertile stream circulates in separate channels through the high-flux core region as well as through the blanket surrounding the core. The protactinium concentration in the fertile stream would be kept low by processing the stream rapidly for removal of

[18] M. Hansen and K. Anderko, *Constitution of Binary Alloys*, 2d ed., p. 341, McGraw-Hill, New York, 1958.

[19] R. P. Elliott, *Constitution of Binary Alloys. First Supplement*, p. 202, McGraw-Hill, New York, 1965.

protactinium soon after it is formed, thereby leaving only a short time for neutron capture. Several prospective protactinium removal processes based on reductive extraction using liquid bismuth have been evaluated from the standpoint of feasibility.

The flowsheet chosen for study is shown in Fig. 1.9. A modification shown in Fig. 1.10 can be used if the development of a reliable electrolytic reducer proves to be more difficult than expected. Typical operating conditions are shown on each flowsheet. Although these conditions may not be optimum, they show the approximate flow rates and conditions expected. In each flowsheet, fertile salt from the reactor (stream 1) is contacted with liquid bismuth (stream 3) containing thorium (0.003 mole fraction). The bismuth has a lithium concentration such that no transfer of thorium or lithium occurs between the metal and the fertile salt. The

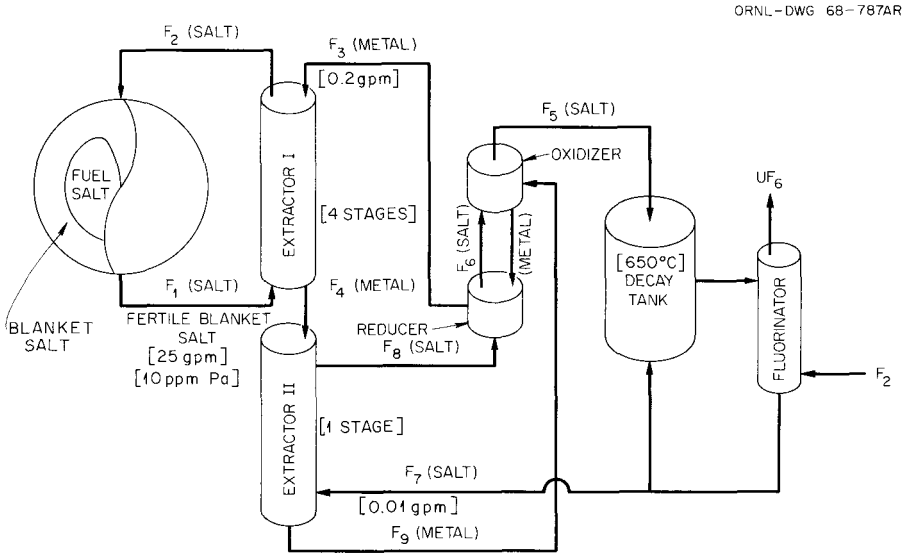

Fig. 1.9. Reference Flowsheet for Removing Protactinium from a Two-Fluid MSBR. Typical operating conditions are shown in brackets.

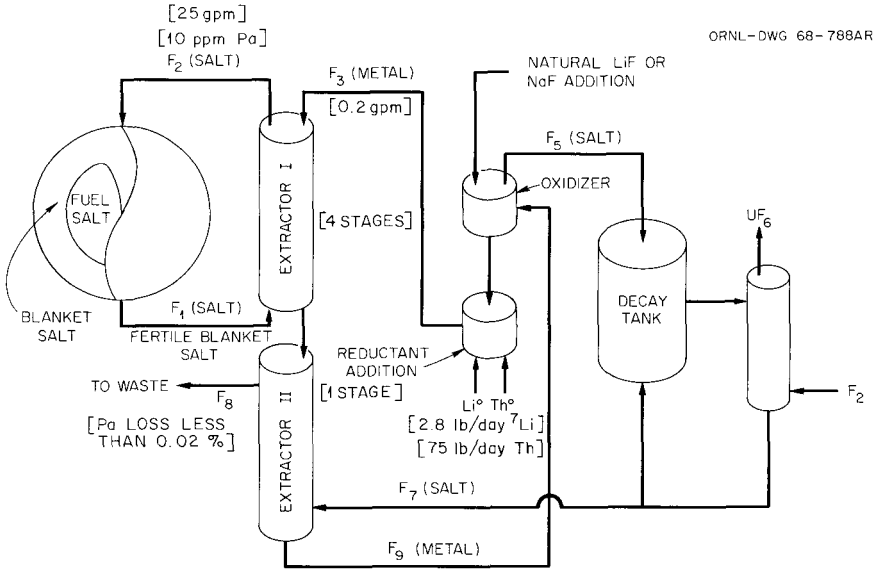

Fig. 1.10. "Throwaway" Flowsheet for Removing Protactinium from a Two-Fluid MSBR Without Use of an Electrolytic Oxidizer-Reducer. Typical operating conditions are shown in brackets.

metal stream (containing protactinium) from the extractor flows to an oxidizer, which converts the thorium, protactinium, and lithium to fluorides. The bismuth is not oxidized and is recycled to the extractor after the proper amounts of thorium and lithium have been added by electrolytically reducing all or part of a recycle salt stream from the decay tank (stream 7).

The salt mixture formed by the oxidation of stream 4 would have an undesirably high liquidus temperature; however, it is decreased in the preferred flowsheet (Fig. 1.9) by recycling salt from the decay tank through the reducer and into the oxidizer. To minimize the protactinium concentration in the stream that is returned to the extractor, salt recycled from the decay tank is contacted with the metal stream leaving the first or main extractor. This transfers most of the protactinium to the metal stream that flows to the oxidizer; the protactinium is then oxidized and is subsequently returned to the decay tank without passing through the main extractor.

In the modification shown in Fig. 1.10, fresh ^{7}Li and thorium metal are added to bismuth to form stream 3; no reducer is used. The metal stream from the first extractor is contacted with recycle salt from the decay tank, as shown in Fig. 1.9, before entering the oxidizer; however, the recycle salt is sent to waste. Lithium fluoride is added to the oxidizer to decrease the liquidus temperature of the resulting salt; since this material will not be returned to the reactor blanket, natural lithium can be used. Alternatively, another alkali-metal fluoride (e.g., sodium fluoride) can be used if it does not interfere with protactinium transfer in the second extractor.

To evaluate the relative merits of these flowsheets, the flow rates and compositions of all streams were calculated over a wide range of conditions for a 1000-Mw (electrical) reactor. The lithium and thorium concentrations in the blanket were fixed at 0.72 and 0.28 mole fraction, respectively, and the protactinium generation rate was fixed at 10.6 g-moles per day. All calculations were based on a processing rate of 5.81×10^6 g-moles of blanket salt per day, which is equivalent to 4750 ft^3 (i.e., approximately two blanket volumes) per day or 25 gpm. Results are shown in Figs. 1.11 and 1.12; typical operating conditions are given in Figs. 1.9 and 1.10.

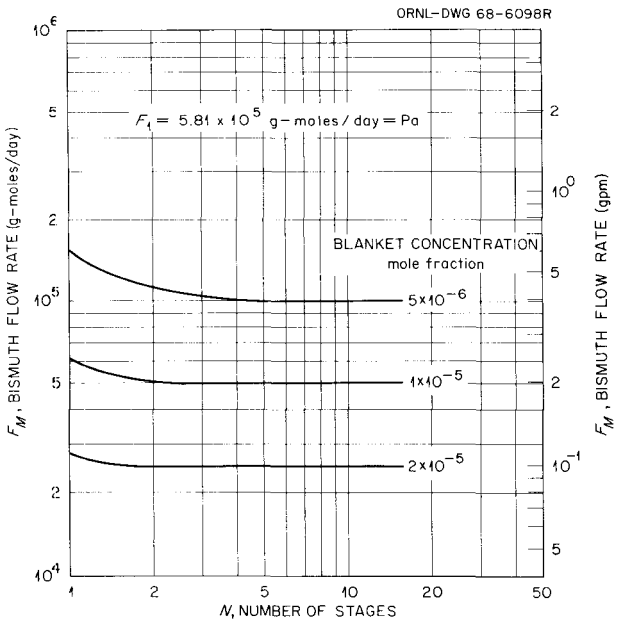

Fig. 1.11. Required Metal Flow Rate as a Function of the Number of Stages in the Extractor.

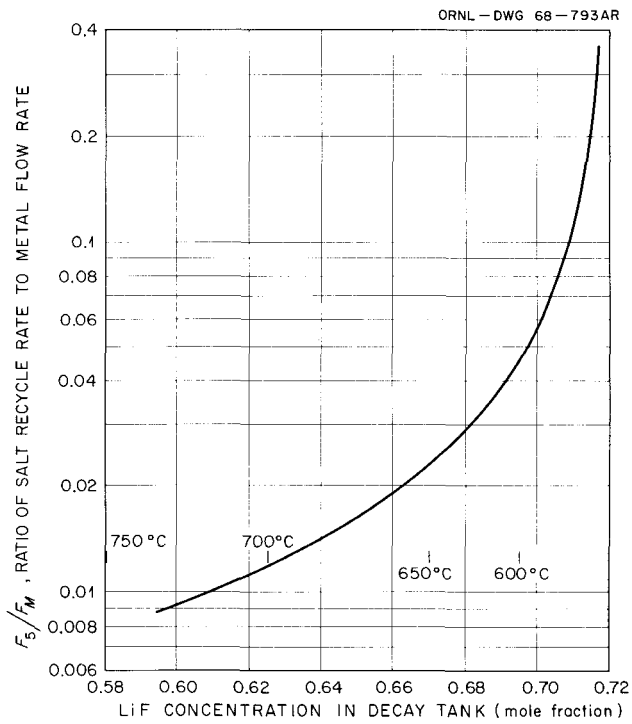

Fig. 1.12. Ratio of Salt Flow Rate from Oxidizer to Metal Flow Rate as a Function of LiF Concentration in Decay Tank.

Figure 1.11 shows the required metal flow rate in gram-moles per day (multiply by 3.9×10^{-6} to convert to gallons per minute) as a function of the number of stages in the extractor for three protactinium concentrations in the blanket (5×10^{-6}, 1×10^{-5}, and 2×10^{-5} mole fraction). Four stages were chosen as a "typical condition" since a greater number of stages provides only a slight improvement. The blanket concentrations shown in Fig. 1.11 may be compared with the value of approximately 8×10^{-5} mole fraction for the blanket of a "no-protactinium-removal" reactor system that has been considered.[20] Increasing the protactinium concentration in the blanket increases the equilibrium (or maximum) metal loading and decreases the required bismuth flow rate. A concentration of 1×10^{-5} mole fraction may be considered typical. The rate of flow of the metal stream is particularly important for two reasons: (1) it will affect the extractor design and bismuth inventory and (2) it determines the capacity of the reducer (or the ^{7}Li and thorium consumption in the "no-reducer" flowsheet). A low flow rate is desirable because the anode surface of the reducer may be expensive to maintain; the rate for the typical conditions shown in Fig. 1.9 is 5×10^4 g-moles/day or 0.2 gpm.

In the reference flowsheet, the rate at which the salt is recycled to the oxidizer is determined by the desired liquidus temperature. Figure 1.12 shows the composition of the decay tank as a function of the ratio of the salt recycle rate to the metal flow rate, F_M. With an infinite recycle rate, the lithium concentration in the recycle salt only approaches that of the blanket; therefore it is necessary to operate with a slightly lower lithium concentration in the decay salt than in the blanket. A liquidus temperature of 600°C is considered reasonable, and the flow rates indicated in Fig. 1.9 are based upon this value. However, the decay tank may be operated at a temperature as much as 50°C higher (e.g., at 650°C) to avoid freezing. The "no-reducer" flowsheet has the option of a lower reductant concentration, which increases the lithium-to-thorium ratio in the metal. This allows a lower salt recycle rate but requires higher metal circulation rates.

Although the volume of the decay tank is determined by the concentration of protactinium desired in the tank, it is subject to limitations. The tank must hold sufficient protactinium to allow 10.6 g-moles to decay in the tank per day (neglecting decay outside the tank). Under the conditions of interest, the volume of the tank will be limited by heat removal considerations rather than by the maximum concentration that could be achieved. A total of 6.7 Mw of heat will be generated in the decay tank from the decay of protactinium; this suggests a minimum tank volume of a few hundred cubic feet.

Important considerations unique to the "no-reducer" flowsheet are the consumption of ^{7}Li and thorium and the loss of protactinium. The ^{7}Li and thorium consumptions reflect both material transferred to fertile salt in extractor I (0.5 to 5% of material fed) and the material that remains in the effluent metal stream from this extractor and is ultimately sent to waste. The loss of protactinium results from incomplete removal of protactinium from the salt stream flowing through extractor II. The ^{7}Li consumption is 5.7 and 1.4 lb/day, respectively, for blanket protactinium concentrations of 5×10^{-6} and 2×10^{-5} mole fraction. The corresponding thorium consumption would be 150 and 38 lb/day. The "typical" conditions chosen for Fig. 1.10 give losses of 2.8 and 75 lb/day of ^{7}Li and thorium respectively. Although the consumption of these quantities of ^{7}Li and thorium could be tolerated, the costs would be significant. With a 400-ft^3 decay tank, the protactinium loss would be less than 0.02% of that produced in the reactor.

1.7 REMOVAL OF PROTACTINIUM FROM A SINGLE-FLUID MSBR

Laboratory experiments have shown that protactinium and uranium can be extracted into bismuth from molten salt that also contains fluorides of lithium, beryllium, and thorium by using metallic thorium as the reductant. A proposed flowsheet (Fig. 1.13) for isolating protactinium from a single-fluid MSBR has been developed, and results for steady-state system performance have been calculated. In the flowsheet, a salt stream from the reactor enters the bottom of the extraction column and flows countercurrently to a stream of bismuth containing reduced metals. Ideally, the metal stream entering the top of the column contains sufficient thorium and lithium to extract only the uranium entering the column. The system exploits the

[20] R. B. Briggs, *Summary of the Objectives, the Design, and a Program of Development of Molten-Salt Breeder Reactors*, ORNL-TM-1851 (June 12, 1967).

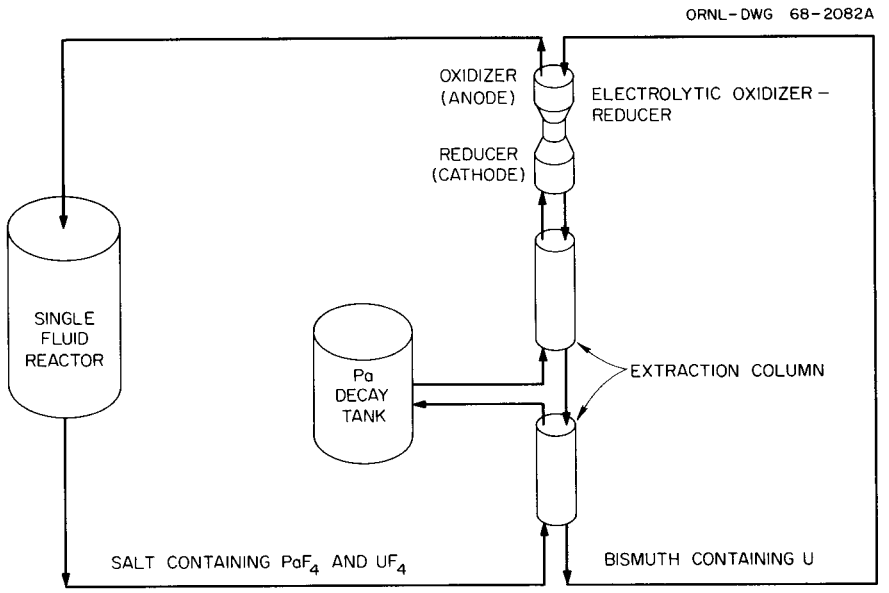

Fig. 1.13. Single-Fluid MSBR Processing by Reductive Extraction.

fact that protactinium is less noble than uranium but more noble than thorium. Hence, in the lower part of the column, uranium is preferentially extracted from the incoming salt, while the protactinium progresses farther up the column, where it is reduced by thorium. In this manner, protactinium refluxes in the center of the column, yielding relatively high protactinium concentrations. A molten-salt tank having a volume of about 400 ft^3 is provided at the center of the column, where the maximum protactinium concentration occurs, in order to retain the protactinium until it decays to uranium.

An essential part of the flowsheet is an electrolytic oxidizer-reducer, which serves the dual purpose of recovering the extracted uranium from the metal stream leaving the extraction column and preparing the lithium-thorium-bismuth stream that is fed to the extraction column. The metal phase containing the uranium extracted in the column serves as the cell anode, where uranium and lithium are oxidized to UF_4 and LiF. Salt from the top of the extraction column serves as the cell electrolyte and first passes over a pool of liquid bismuth that acts as the cathode, in which thorium and lithium are reduced.

Figure 1.14 shows typical performance of the protactinium isolation system for the following conditions: reactor volume, 1.5×10^6 g-moles; decay tank volume, 3×10^5 g-moles; salt flow rate, 5×10^5 g-moles/day (or ~2 gpm); extraction stages, 12. The minimum protactinium concentration in the reactor is obtained when the amount of bismuth added is just sufficient to extract the uranium entering the system. At slightly higher bismuth flow rates, protactinium will also be extracted since it is the next component in order of decreasing nobility. At bismuth flow rates slightly lower than the optimum rate (about 5×10^5 g-moles/day, or 2 gpm), some uranium will not be extracted; this uranium and most of the protactinium will flow out the top of the column. In either case, some protactinium would be allowed to return to the reactor, and the effectiveness of the system would be diminished. The protactinium isolation system becomes ineffective almost immediately when bismuth flow rates are lower than the optimum rate; for rates higher than the optimum, the reactor protactinium concentration increases from the minimum value of 22 ppm at the rate of 28 ppm for each percentage increase in metal flow rate under the conditions for this particular case. Thus far only the effect of the variation in bismuth flow rate on performance has been discussed, but similar effects will be produced by variations in the salt flow rate or in the total concentration of reduced metals (equivalents of reduced metals per mole of bismuth) fed to the column. Calculated concentration profiles in the extraction column for steady-state operation under optimum conditions are shown in Fig. 1.15. The concentration of uranium in the salt decreases from

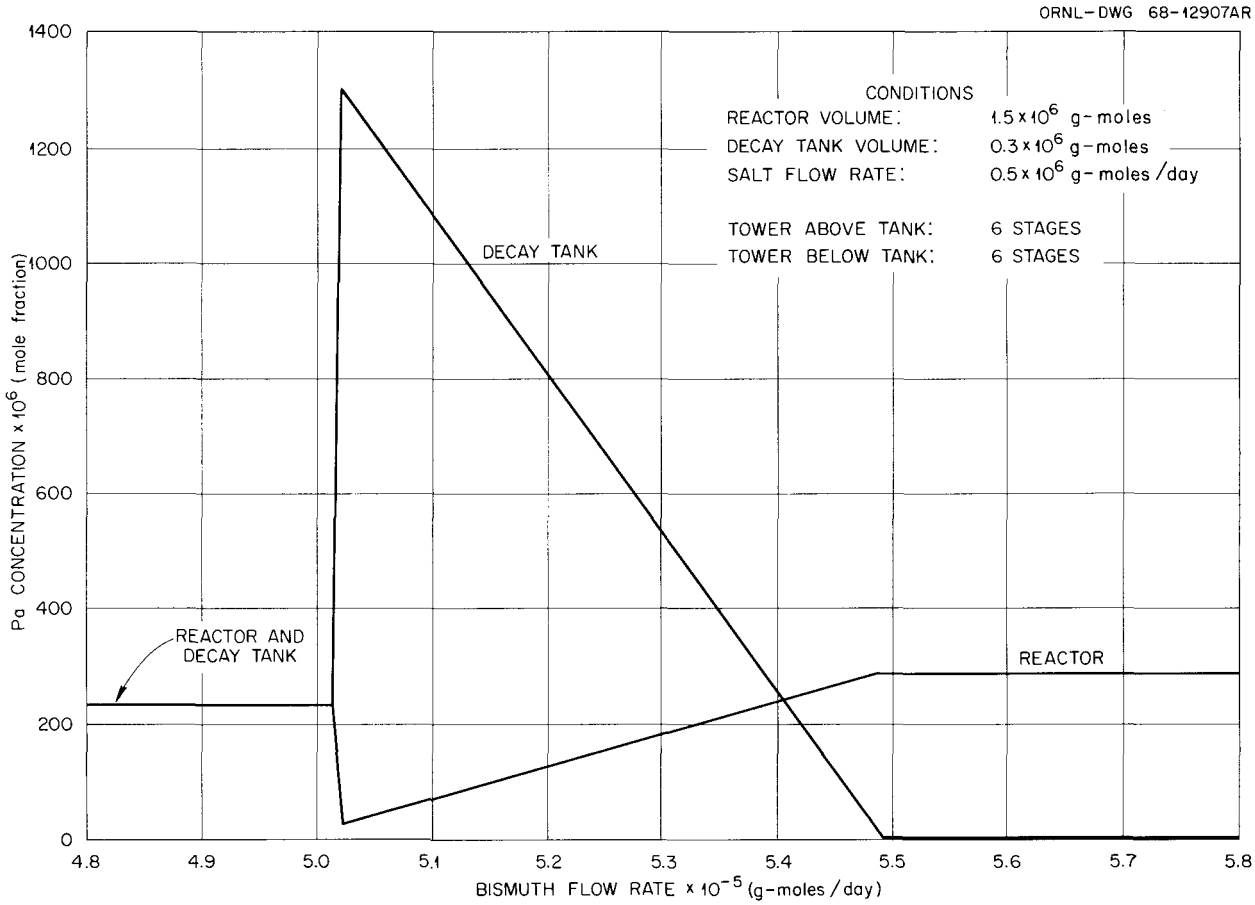

Fig. 1.14. Variation of Protactinium Concentration in Reactor and Protactinium Decay Tank with Bismuth Flow Rate.

the reactor concentration of 3×10^{-3} mole fraction to 6.3×10^{-5} mole fraction at the inlet to the protactinium decay tank, whereas the protactinium concentration increases from the reactor concentration of 2.2×10^{-5} mole fraction to 1.32×10^{-3} mole fraction at the inlet to the decay tank. The concentrations of protactinium and uranium in the decay tank are 1.3×10^{-3} and 8.3×10^{-5} mole fraction respectively. Above the decay tank, the uranium and protactinium concentrations decrease steadily to negligible values.

The flowsheet has several very desirable characteristics, including: (1) a negligible holdup of fissile ^{233}U in the processing plant, (2) an almost immediate return of newly produced ^{233}U to the reactor system, and (3) a closed system that precludes loss of protactinium, ^{233}U, or other components of the reactor fuel salt. The protactinium removal efficiency is, however, undesirably sensitive to minor variations in operating conditions such as the salt or bismuth flow rate and the concentration of reduced metals in the bismuth stream fed to the extraction column. Methods for making the system performance less sensitive to minor variations in operating conditions have been studied. The removal of uranium from the center of the column by fluorination of molten salt was found to make steady-state performance insensitive to small changes in operating conditions; the concentration of UF_6 in the fluorinator off-gas was found to be extremely sensitive to changes in operating conditions and can be used as a means of controlling the primary process.

The effectiveness of a system stabilized by uranium removal was compared with that of a nonstabilized system by assuming the error in the control of the bismuth flow rate to be distributed normally around a best mean flow rate FMB_0 with a standard

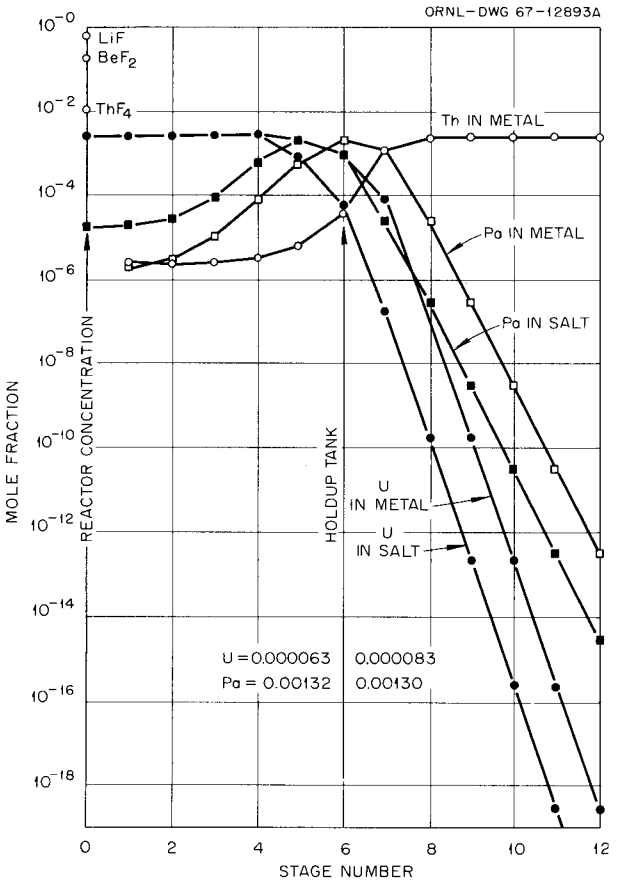

Fig. 1.15. Calculated Concentration Profiles in Reductive Extraction Tower Under Optimum Conditions.

deviation σ, so that an average reactor protactinium concentration $\bar{c}$ could be calculated by:

$$\bar{c} = \frac{1}{\sqrt{2\pi}} \int_{-\infty}^{\infty} c(x)\, e^{-x^2/2}\, dx ,$$

where

$$x = \frac{\mathrm{FMB} - \mathrm{FMB}_0}{\sigma} ,$$

FMB = bismuth flow rate,

$c(x)$ = steady-state reactor protactinium concentration at bismuth flow rate corresponding to x.

The average reactor protactinium concentration is shown in Fig. 1.16 as a function of the standard deviation in bismuth flow rate for cases with stabilization by uranium removal as well as for two cases with no uranium removal. In the latter two cases, the protactinium processing cycle times were three days and one day. For a standard deviation of 0.35% of FMB_{opt} (optimum bismuth flow rate), the minimum reactor protactinium concentration (22 ppm) is obtained if the fraction of uranium removed from the inlet to the decay tank is 2% or greater; with no uranium removal the average concentration is 38.5 ppm. With a one-day protactinium processing cycle time and a standard deviation

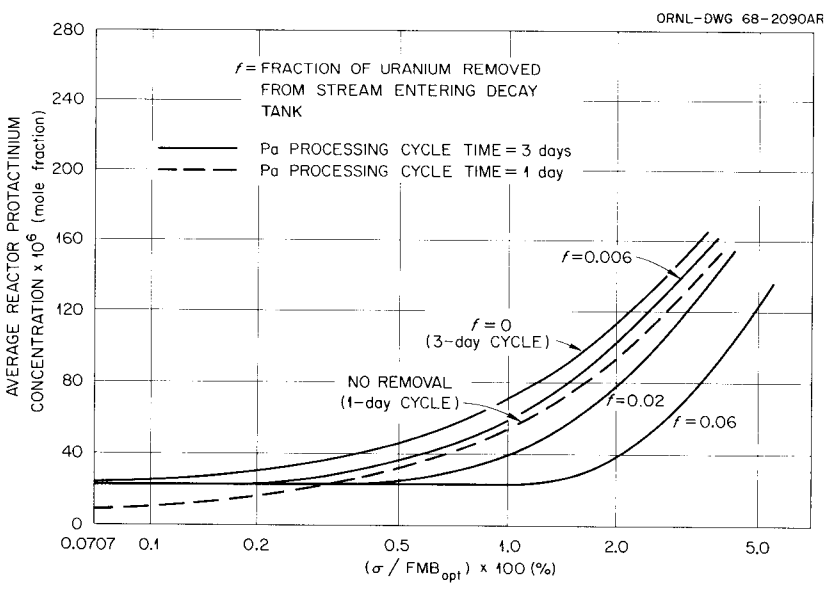

Fig. 1.16. Variation of Average Reactor Protactinium Concentration with Standard Deviation of Bismuth Flow Rate for Cases with Stabilization by Fluorination and with No Stabilization.

of 0.35%, an average concentration of 24.5 ppm is obtained. For standard deviations larger than about 0.35%, a protactinium isolation system having a one-day processing cycle time with no uranium removal produces approximately the same average reactor protactinium concentration as a system having a three-day cycle time with 1% removal of uranium from the salt stream entering the decay tank.

In choosing the optimum protactinium isolation system, we must consider the relative costs associated with higher processing rates, closer process control, and increased uranium removal, as well as the advantage of obtaining a given average reactor protactinium concentration.

1.8 ENGINEERING STUDIES OF CONTINUOUS REDUCTIVE EXTRACTION

An experimental facility is being installed in Building 3592 to permit engineering studies of reductive extraction to be made. The extraction process involves continuous countercurrent contact of molten salt and liquid bismuth containing a reductant such as thorium. The system consists of feed and catch tanks (effective volume of each, 15 liters) for the bismuth and salt phases, a graphite-lined salt and metal purification vessel, and an extraction column. The transfer of uranium between the salt and metal streams will be studied at 600°C, using salt of the composition $LiF-ThF_4-UF_4$ (23.7-76.0-0.3 mole %). The salt and the bismuth will be purified prior to each run. Samples of the metal and salt phases will be taken from the streams leaving the contactor during each run and from the feed tanks prior to a run. Gas displacement will be used to control the salt and metal flow rates.

1.9 RECOVERY OF URANIUM FROM MSRE FUEL SALT BY FLUORINATION

The future schedule of MSRE operation includes removal of the uranium (about 30% enriched in ^{235}U) from the carrier salt $LiF-BeF_2-ZrF_4$ (63-32-5 mole %) by fluorination. The purified carrier salt will then be reused for the subsequent operation of the MSRE with $^{233}UF_4$. Fluorination of UF_4, dissolved in a molten fluoride salt, with the attendant evolution of volatile UF_6 is quite corrosive to all known metallic containers. It is anticipated that significant amounts of chromium, iron, and nickel (as corrosion products) will accumulate in the salt, thus requiring the salt to be purified by hydrogen treatment and other means. A series of small-scale fluorination tests is being made with simulated MSRE salt to study the effects of temperature, fluorine concentration, and fluorine flow rate on the rate of uranium volatilization and the rate of corrosion of Hastelloy N. In addition, some experimental results are being obtained concerning the volatilization of chromium and molybdenum fluorides (corrosion products) and on the behavior of volatile fission products (Ru, Nb, I, and Te) in the fluorination of short-decayed fuel. Knowledge of fission product behavior is essential to the development of a special fluorination procedure to be used by the Analytical Chemistry Division for precisely analyzing the uranium in the fuel salt.

Fluorination-Corrosion Study

The fluorinator-corrosion tests are being made with MSRE-type salt in a 1.87-in.-ID Hastelloy N reactor under conditions that roughly approximate those being considered for use in the 49-in.-ID fluorination tank at the MSRE site. The uranium is being volatilized from the salt, with an intermediate period of sparging with inert gas being used to simulate the replacement of the NaF sorbent beds (i.e., beds for recovering the UF_6). A gas flow rate of 146 ml/min (STP) is being used in the 1.87-in.-ID reactor to simulate the flow rate of 100 liters/min in the 49-in.-ID reactor.

In the larger reactor, more uranium is involved, and the surface-to-volume ratio is lower. Hence the change in oxidation state of the salt during the course of UF_6 volatilization may be different in the two systems.

We have made two tests, one at 450°C and the other at 500°C; 340 g of $LiF-BeF_2-ZrF_4-UF_4$ (63-32-5-0.8 mole %) was used in each case. Salt samples were taken during the runs at intervals (after helium sparging) that were determined by the need to replace a 12-g NaF trap. In each test, 50% F_2–50% helium (146 ml/min) was used initially, followed by pure fluorine (146 ml/min) at the end of the run to ensure complete uranium recovery. In another test at 500°C, pure fluorine was used

Table 1.9. Uranium Volatilization and Corrosion Results in Fluorination Tests with MSRE Salt in Hastelloy N at Two Temperatures

Temperature (°C)	Fluorine Concentration (%)	Total Time (hr)	Corrosion (mg in salt[a])		Volatile Material		Fluorine Utilization Efficiency (%)
			Cr	Fe	U (%)	Cr (mg)	
450	50	0.5	13	4	5.4		4.0
	50	2.0	42	35	14.2		2.1
	50	3.5	93	60	44.7		7.5
	50	5.0	118	73	68.0		5.6
	100	6.0	103	82	92.2		2.2
	100	8.0	143	152	100	2.4	0.7
	100	12.0	128	93		5.5	
	100	16.0	117	96		14.7	
500	50	1.0	75	49	18.5		7.6
	50	1.75	153	95	38.5		11.0
	50	2.25	194	122	55.1		13.8
	100	2.75	224	126	83.4		11.7
	100	6.75	150	139	100	15	1.8
	100	10.75	140	180		27	
500	100	0.75	74	17	28.7		7.1
	100	1.25	112	48	59.4		11.4
	100	1.58	139	48	90.7		17.6
	100	2.58	136	71	98.9		1.5
	100	6.58	125	71	100	9	0.1
	100	10.58	102	82		12	

[a]Corrected for initial values at zero time.

throughout. A trap containing 2 *M* KOH was employed to sorb unused fluorine and volatile chromium and molybdenum compounds that passed through the NaF trap.

As shown in Table 1.9, the UF_6 volatilization rate and the degree of fluorine utilization were generally higher at 500°C than at 450°C. The amount of chromium leached from the Hastelloy N reactor increased with temperature. The effect of temperature on the solubilization of iron and nickel from the reactor is not as well defined. (The dip tube, the thermocouple well, and the bottom of the reactor were made of Ni-200.) Figure 1.17 shows the relationship between chromium and iron leaching and uranium volatilization with pure fluorine in the third run; corrosion appears to occur predominantly in the uranium volatilization period.

Estimates of the corrosion rate during the run can be calculated from the chromium data (Table 1.10). There is good agreement between the rate calculated for the period during which most of the chromium was leached and that for the period during which most of the uranium was volatilized. The estimates for the complete runs are somewhat arbitrary because fluorination was continued after the uranium had been removed in order to observe chromium behavior.

The volatility of chromium and molybdenum was also observed in these runs. A chromium compound (probably CrF_5) appeared to volatilize only after most of the uranium had been removed from the salt (Table 1.9). This compound was effectively trapped by NaF at 25°C, forming an orange-colored complex. Molybdenum (probably as MoF_6) volatilized to a large extent throughout each run and, as expected from the dissociation pressure of $MoF_6 \cdot 2NaF$, was not completely recovered in the 25°C NaF trap; most of it passed through to the KOH scrub solution.

Table 1.10. Estimates of Rates of Corrosion of Hastelloy N in Fluorination Tests

Temperature (°C)	Fluorine Concentration (%)	Corrosion Rate (mils/hr) During:		
		Period of Maximum Cr Leaching	Period of Maximum[a] U Volatilization	Complete Run
450	50 and 100	0.19	0.12	0.05
500	50 and 100	0.58	0.45	0.12
500	100	0.50	0.49	0.07

[a]80 to 95%.

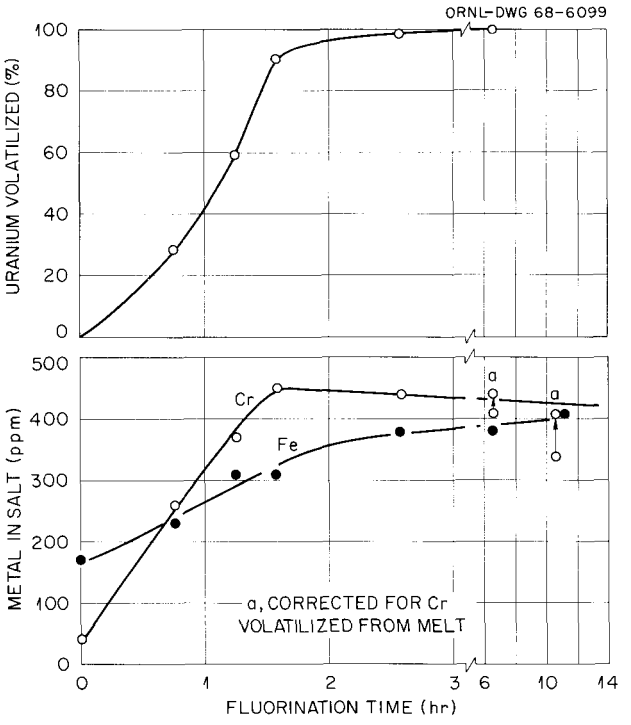

Fig. 1.17. Relationship Between Corrosion of Hastelloy N and UF_6 Volatilization in Fluorination of MSRE-Type Salt at 500°C.

Values for the fluorine utilization efficiency (calculated from UF_6 output and fluorine input) suggest that the utilization was highest during the first 2 hr of fluorination; however, this is not strictly true, since the method of calculation does not take into account the volume of fluorine that is consumed in changing the average oxidation number of the uranium. Also, the data do not imply that a definite consumption of fluorine must occur before any UF_6 is evolved. In recent fluorination tests, UF_6 was volatilized to a limited extent when the uranium oxidation number in the salt was as low as 4.3. This was calculated on the basis of complete consumption of the fluorine that was introduced in the first 1.5 min of fluorine flow.

Fission Product Behavior – Analytical Assistance Program

A precision of ±0.1% is needed in the analytical procedure currently proposed for determining uranium in MSRE fuel salt. Since it is anticipated that the use of remotely controlled hot-cell coulometric instrumentation will introduce an inherent error of ±1%, decontamination of the UF_6-NaF complex product from the first step (fluorination) to a level that is appropriate for analysis in a low-level radiation area will be essential. In addition, uranium losses in the waste salt and fluorination system (traps, etc.) must be less than 0.1 wt %. Encouraging results were obtained during preliminary tests in which uranium was volatilized (by fluorination) from simulated MSRE fuel salt containing some volatile fission products.

Four fluorination tests have been completed, using simulated MSRE fuel salt samples specially prepared by the Analytical Chemistry Division. The samples consisted of copper capsules, each containing about 46 g of LiF-BeF_2-ZrF_4-UF_4 (65.4-29.4-5.0-0.2 mole %). Each salt sample was melted under an inert atmosphere into a suitable nickel fluorinating vessel and then was "spiked" with about 0.1 mc of ^{103}Ru, ^{95}Nb, ^{131}I, or ^{132}Te. Solutions of these tracers were first evaporated to dryness with the corresponding carrier (about 40 to 50 mg) onto 0.5-g quantities of LiF. Fluorination was carried out by heating the salt to 550°C

in an inert atmosphere and then passing a mixture of 25% F_2–75% N_2 through the melt for 30 min, followed by pure fluorine for an additional 30 min at 100 ml/min (STP). The product gas stream (containing F_2, UF_6, and volatile fission products) was passed first through a 20-g NaF trap at 400°C to remove the fission products and then into a 10-g NaF trap (at 25°C), where the UF_6 product was sorbed. An additional 5-g NaF trap was installed downstream for determining uranium breakthrough.

Based on a makeup value of 1.185 wt % uranium in each of the initial salt samples, the total uranium found in three tests corresponded to recoveries of 99.27, 100.22, and 97.65%. However, corresponding uranium losses in the tests, based on analyses of the traps and waste salt, were 0.034, 0.059, and 0.076 wt %, indicating actual recoveries greater than 99.9% (see Table 1.11).

Decontamination factors obtained for ^{103}Ru, ^{95}Nb, and ^{132}Te during the fluorination step have been greater than 10^5; thus these nuclides apparently do not make a significant contribution to the overall activity level of the UF_6 product. The relative amounts volatilized from the salt during fluorination were, respectively, about 0.001, 10, and greater than 99%, with corresponding material balances of about 95, 10, and 0.1%. Essentially all of the volatilized ruthenium and niobium was retained by the 400°C NaF trap; however, no appreciable sorption of tellurium was detected (Table 1.12). Attempts to achieve an adequate decontamination factor (greater than 1000) for ^{131}I have been unsuccessful so far. In the first two tests, where the UF_6 sorption trap consisted of 10 g of NaF at 25°C, decontamination factors of 14 and 8 were obtained. In the third test, decreasing the amount of NaF to 5 g and increasing the sorption temperature to 100°C resulted in a higher, but still inadequate, decontamination factor (D. F.) of 35 (Table 1.13). In this test, the measurement of the temperature of the sorption bed may have been in error; therefore a duplicate test will be made for verification.

Table 1.11. Uranium Recoveries and Losses from MSRE-Type Salt During Fluorination and Sorption on NaF

Run No.	Uranium Makeup Value (wt %)	Uranium Recovery[a] (wt %)	Uranium Losses (wt % of Total Found)			
			Trap No. 1[b]	Trap No. 2[c]	Waste Salt	Total
1	1.185	99.27	0.012	0.009	0.013	0.034
2	1.185	100.22	0.051	0.006	0.002	0.059
3	1.185	97.65	0.026	0.022	0.022	0.076

[a]Based on analyses of all traps and scrubber solutions.
[b]400°C NaF trap.
[c]25°C NaF backup trap.

Table 1.12. Behavior of ^{103}Ru, ^{95}Nb, and ^{132}Te During Fluorination of Uranium from MSRE-Type Salt at 550°C

Nuclide	Total Activity (dis/min)					Amount of Nuclide Volatilized (%)	UF_6 Product D.F.
	MSRE Salt (Initial)	400°C NaF Trap	NaF Backup Trap	Waste Salt	UF_6 Product Trap		
^{103}Ru	$\sim 2 \times 10^8$	$<10^3$	$<10^3$	1.9×10^8	$<10^3$	10^{-3}	$>10^5$
^{95}Nb	$\sim 2 \times 10^8$	3×10^7	$<10^3$	9×10^7	$<10^3$	10	$>10^5$
^{132}Te	$\sim 2 \times 10^8$	$<10^3$	$<10^3$	4.3×10^5	$<10^3$	>99	$>10^5$

Table 1.13. Behavior of ^{131}I During Fluorination of Uranium from MSRE-Type Salt at 550°C

Run	Total Activity (dis/min)						Amount of ^{131}I Volatilized (%)	D.F.
	MSRE Salt (Initial)	400°C NaF Trap	Backup Trap	KOH Scrub Trap	Waste Salt	UF_6 Trap		
1	$\sim 2 \times 10^8$	$\sim 10^3$	1.3×10^6		$<10^3$	1.4×10^7	>99	14
2	$\sim 2 \times 10^8$	1.8×10^4	5.3×10^6	2×10^7	2×10^4	2.5×10^7	>99	8
3	$\sim 1 \times 10^9$	5.6×10^6	7.2×10^7		2.7×10^6	2.9×10^7	>99	35

1.10 MSRE FUEL SALT PROCESSING

The modifications to the MSRE fuel processing facility to provide a backup device for the fluorine disposal system and the iodine sorption trap were completed. Late in 1967 it was decided that the metal fluorides formed during fluorination should be removed from the salt before the salt is returned to the reactor system. The design, construction, and installation of a salt filter for removing the metals after reduction have been completed. The filter has a replaceable 9-ft^2 porous Inconel element.

Four cold test runs were made to determine the effectiveness of the SO_2 system for fluorine disposal. The backup device consisted of an activated alumina trap, which was heated during the last three runs to increase its fluorine capacity. After various difficulties with the flow rates of fluorine and SO_2 and the temperature control in early runs, the fourth run was made under desired conditions; however, a temperature increase in the alumina trap still occurred. Subsequent laboratory investigation showed that this increase was the result of SO_2F_2 decomposition (instead of unreacted fluorine, as originally believed). Because of the difficulty of demonstrating effective fluorine removal and of providing a satisfactory backup system for the SO_2-F_2 reactor, we decided to replace this system with a KOH-KI aqueous scrubber containing a soda-lime trap.

Two test runs with the new system (using the old alumina trap) demonstrated adequate fluorine removal. However, when the system was heated in the second run, the MoF_6 that was produced caused a heavy mist to form in the off-gas line from the scrubber and to plug this line. Installation of a filter to remove this mist is now in progress.

1.11 REMOVAL OF NICKEL, IRON, AND CHROMIUM FLUORIDES FROM MSRE FUEL CARRIER SALT

Current plans for the MSRE include operation of the reactor with ^{233}U rather than the present mixture of ^{235}U and ^{238}U. Most of the fission products now present in the reactor will be retained by fluorinating the fuel salt to remove uranium (as UF_6) and subsequently adding ^{233}U to the remaining salt mixture (65-30-5 mole % LiF-BeF_2-ZrF_4).

During fluorination, the salt will become contaminated with fluorides of nickel, iron, and chromium as a result of the corrosion of the Hastelloy N fluorinator. Although the expected concentrations of these corrosion product fluorides will not exceed their solubilities in the fuel salt, their return to the reactor is undesirable for several reasons. First, chromium in high concentrations decreases the sensitivity of chromium analyses and hence will decrease the accuracy of assessing generalized corrosion during operation. Second, fluorides of nickel and iron will react with chromium, which is the least noble constituent of Hastelloy N (the material of which the MSRE is fabricated). Experiments on corrosion product removal methods indicate that Ni(II) can be reduced to the metal by hydrogen sparging and that Fe(II) and Cr(II) can be reduced by the addition of zirconium metal. Filtration of the resulting mixture of salt and metals was shown to be effective in removing suspended metals.

Reduction of Corrosion Product Fluorides

An experiment was carried out in which a 104-kg batch of MSRE fuel carrier salt (65-30-5 mole %

$LiF-BeF_2-ZrF_4$) was prepared from the component fluoride salts by routine production procedures. In order to represent conditions expected after fluorination of the MSRE fuel salt, approximately 80 g of CrF_2, 50 g of FeF_2, and 800 g of NiF_2 were added to the salt. The resulting mixture was hydrofluorinated for 6 hr with 10 to 20 mole % HF in helium to ensure complete dissolution of the corrosion product fluorides. Analysis of a filtered salt sample taken after the hydrofluorination period is compared with expected concentrations in Table 1.14. The concentration of FeF_2 is somewhat higher than the calculated value and indicates that additional iron was oxidized during hydrofluorination.

Equilibrium data for reduction of the corrosion product fluorides indicate that, if equilibrium is achieved, a hydrogen sparge will reduce Ni(II) easily, Fe(II) with difficulty, and Cr(II) to a negligible extent in a practical time period. The aims of the first part of the experiment were to demonstrate Ni(II) reduction by use of a hydrogen sparge and to compare the utilization of hydrogen with that predicted from equilibrium data.

After the initial hydrofluorination, free HF was stripped from the salt mixture by helium sparging, and the molten salt was sparged for 9 hr with hydrogen at a rate of 10 std liters/min at 650°C. The 48.2-liter salt mixture was contained in a 12-in.-diam vessel, and the sparge line terminated 26 in. below the surface of the melt. The gas effluent from the treatment vessel was analyzed periodically for HF, and sparging was discontinued when the HF concentration decreased to a near-constant value (which was assumed to be the beginning of FeF_2 reduction). The quantity of HF produced during this period was equivalent to about 93% of the NiF_2 initially present in the salt mixture. Hydrogen utilization under these conditions was considerably lower than it would have been if equilibrium had been achieved; under equilibrium conditions a sparge time of 20.4 min would have resulted in the reduction of 99% of the NiF_2 initially present.

Table 1.14. Concentrations of Corrosion Product Fluorides After Hydrofluorination

Material	Estimated Concentration[a] (ppm)	Analysis[a] (ppm)
CrF_2	445	470
FeF_2	286	620
NiF_2	4680	3700

[a]Concentrations reported on a metal basis.

Since equilibrium data predict a very low hydrogen utilization during the reduction of FeF_2 and CrF_2, experiments were carried out in which these fluorides were reduced with zirconium metal. The zirconium was first machined in order to increase the surface area, thereby avoiding passivation of the surface by deposition of reduced iron and chromium. The turnings were pressed into $^3/_4$-in.-diam cylinders (density, ~ 3 g/cm^3), 0.3 to 1.0 in. long, to facilitate addition to the treatment vessel. The pressed zirconium slugs were added to the salt mixture after the Ni(II) had been reduced by hydrogen sparging. After each addition, the approximate extent of reduction was noted by sparging the melt with hydrogen and analyzing the effluent gas for HF. The HF concentration decreased steadily, and an arbitrary end point for the reduction reaction was established at an HF concentration of 0.02 meq of HF per liter of H_2. The calculated quantity of zirconium required to completely reduce the corrosion product fluorides was 115 g; this value was based on the analysis of the salt mixture shown in Table 1.14 and on the reduction of 12.2 equivalents of these metal fluorides during the hydrogen sparging period. Analyses of filtered samples taken near the conclusion of the zirconium addition period are as follows:

Zirconium Added (g)	Metals Found (ppm by wt)		
	Cr	Fe	Ni
253	9	60	<30
327	26	44	36

These values are below the limits established for the initial MSRE fuel carrier salt. On the basis of these data, zirconium utilization was at least 46 to 65%.

Salt Filtration Studies

Since suspension or entrainment of much of the solids during the transfer of the fuel salt to the reactor drain tank could adversely affect filter

performance, tests of salt filtration characteristics were made under conditions that approximate those anticipated in the reactor application. Filtration tests were made with three filters: a sintered nickel filter (Micro Metallics Corporation) having a mean pore diameter of 40 μ, and two grades of Feltmetal (Huyck Metals Company). The first grade of Feltmetal consisted of Monel having 20-μ-diam pores, while the second consisted of 347 stainless steel having 41-μ-diam pores. The Feltmetal (designated FM250 by the manufacturer) had a porosity of 78% and a stated removal efficiency of 98% for particles larger than 10 μ in diameter. This material was chosen for application in the reactor system because of its adaptability to fabrication requirements and its satisfactory performance during the filtration tests.

The experimental assembly used for the filtration tests was essentially that used for the routine production of fluoride mixtures. The salt preparation vessel was connected by a $\frac{1}{2}$-in.-diam Inconel tube to a heated salt receiver vessel. The transfer tube extended to within $\frac{1}{4}$ to $\frac{1}{2}$ in. of the bottom of the salt preparation vessel and only penetrated the top of the receiver. The filter was mounted vertically in the transfer line above the receiver. A salt return line extended from near the bottom of the receiver to the salt preparation vessel. This arrangement permitted eight filtration tests to be made with the same batch of salt.

In tests made under settled conditions, the melt was allowed to remain quiescent for a minimum time of 4 hr prior to transfer; tests were also made under agitated conditions by rapidly sparging the melt with helium just prior to transfer of the salt. The first set simulated expected conditions in application, while the second gave a test of filter loading capacity. The temperature of the melt was controlled at 650°C in each case. The temperature of the salt transfer line was maintained at about 565°C during the transfer operations.

Table 1.15. Summary of Filtration Tests

Salt composition: $LiF-BeF_2-ZrF_4$ (65-30-5 mole %)
Weight of salt mixture: 104.1 kg
Volume of salt at 650°C: 1.7 ft^3
Indicated pressure differential: 11 psig (forepressure vs vacuum)

Test No.	Filter Material	Pore Diameter (μ)	Salt Conditions	Transfer Time (hr)	Weight Gain (g)	Remarks
1	Monel Feltmetal	20	Static		22	Test terminated after 2 hr; essentially no salt transfer.
2	Sintered nickel	40	Static	0.5	7	No visible material on filter or evidence of failure.
3	Sintered nickel	40	Agitated	1.75	44	
4	347 SS Feltmetal	41	Static	2.0	77	Test stopped after transfer of 90 kg.
5	Sintered nickel	40	Static	2.17	63	Filter plugged after transfer of 40 kg. Material on filter predominantly salt.
6	Sintered nickel	40	Static	1.84	19	Balance of salt transferred; filter ruptured.
7	347 SS Feltmetal	41	Agitated	2.0	67	
8	Sintered nickel	40	Static	1.75	22	Back transfer of 80 kg of salt from receiver to treatment vessel; filter plugged.

Table 1.16. Summary of Analyses of Salt Samples Withdrawn During Filtration Tests

Sample Interval	Impurity Concentration (ppm)			
	Cr	Ni	Fe	Total
Before test 1[a]	26	36	44	106
After test 4	15	84	66	165
After test 6	16	256	132	404
After test 7	17	19	49	85

[a]Filter stick sample.

The salt was transferred by pressurizing the treatment vessel with helium to 11 psig and evacuating the receiver vessel; hence the pressure drop across the filter varied from 22.5 to 20.8 psi as the level of salt in the treatment vessel decreased. A summary of the filtration tests is shown in Table 1.15. The occasional plugging of the filter in tests 4 and 5 suggests that the loading capacity of the 40-μ filters may be about 50 to 75 g of metal particles.

Samples of the salt mixture were withdrawn by means of a filter stick prior to the first filtration experiment and by a composite sampler located downstream from the filter plate after tests 4, 6, and 7. Analyses of these samples are given in Table 1.16. Although the filter ruptured in test 6, chemical analyses did not show excessive concentrations of metals in the filtered salt. Variations in the other results are probably within the combined reproducibility of the analytical methods and the test procedure. Only 1.8 to 3.4% of metals reduced from solution passed through the filter material that is proposed for use in the reactor application.

1.12 PREPARATION OF ^{233}U FUEL FOR THE MSRE

Plans have been completed for refueling and operating the MSRE with ^{233}U fuel. Approximately 39.5 kg of 91.4%-enriched ^{233}U in the form of ^{7}LiF-$^{233}UF_4$ (73-27 mole %) eutectic salt will be required by the MSRE. This material is being prepared in remotely operated equipment that is installed in cell G of the Thorium-Uranium Recycle Facility (Building 7930) because of the high ^{232}U content (222 ppm) of the ^{233}U.

Process and Equipment

Preliminary process and equipment concepts were briefly described in the preceding report.[21] During the cold shakedown run, several operational difficulties pointed out the need for changes in the process. These changes, along with the associated equipment modifications, have now been made. The revised process has proved to be highly satisfactory and has successfully been used to produce the first third of the material.

Originally, the preparation process consisted of opening the aluminum cans of $^{233}UO_3$ by remote means, dumping the $^{233}UO_3$ into a nickel-lined, 8-in.-diam by 3-ft-high heated reaction vessel, adding the ^{7}LiF to the vessel, and melting the material to produce a slurry. This slurry was first treated with hydrogen to reduce the oxide to $^{233}UO_2$ and was then hydrofluorinated to convert $^{233}UO_2$ to $^{233}UF_4$. Operational difficulties were associated with the high temperature required (900°C) to melt pure ^{7}LiF, the highly exothermic reactions that occurred, and the inherently heterogeneous nature of the system.

In the revised process, the $^{233}UO_3$ powder was first treated with hydrogen to reduce to $^{233}UO_2$, and then the $^{233}UO_2$ was hydrofluorinated to yield $^{233}UF_4$. The ^{7}LiF was subsequently added to the $^{233}UF_4$ to form the eutectic melt. Thus we were able to avoid simultaneous high temperatures and exothermic reactions in the process, as well as the corrosive conditions associated with molten salt and HF at these temperatures.

The formation of the eutectic is followed by sparging, first with H_2-HF to convert the small residual amount of UO_2 to UF_4 and then with highly pure hydrogen to reduce the iron and nickel corrosion product fluorides to metals. The salt is then sampled, filtered, and transferred via a heated line into a temporary storage container. From there the salt is transferred into 45 enriching capsules, each of which contains about 98 g of uranium, and into nine 2½-in.-OD cans ranging in capacity from 0.5 to 7 kg of uranium. These salt cans and capsules will be shipped to the MSRE in shielded carriers. A schematic diagram of the process equipment is given in Fig. 1.18.

[21]*Chem. Technol. Div. Ann. Progr. Rept. May 31, 1967*, ORNL-4145, pp. 102–3.

ORNL DWG 67-11638 R1

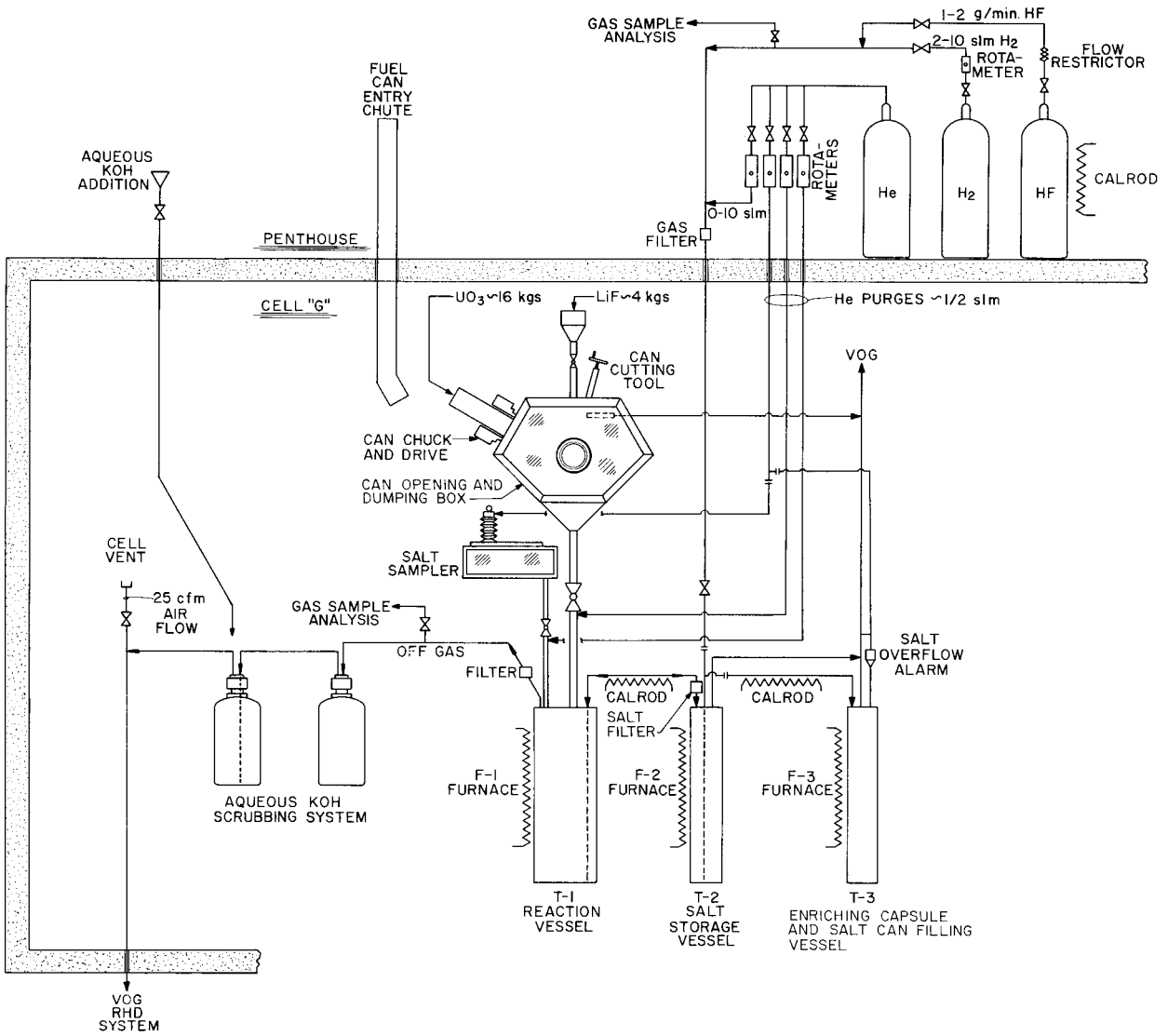

Fig. 1.18. Schematic Flowsheet for ^{233}U Fuel Salt Preparation, Cell G, Building 7930.

Construction

The TURF building was released to ORNL by the construction contractor on September 15, 1967, which was about 1½ months later than we had anticipated. The cost-plus-fixed-fee contractor then spent approximately one month installing the cell platform, the electrical power supply system, the charging chute, the roof and slot closure plugs, the PAR manipulator, the gas supply system, and the instrument panel. ORNL craft forces completed installation of the process equipment in January 1968 (Figs. 1.19–1.21).

The $^{233}UO_3$ oxide can opener and dumping box was originally designed using drawings and sample cans from Savannah River. Unfortunately, after the box was completed, it was found that the actual cans were 1.75 in. shorter than the drawings and

Fig. 1.19. Control Panel and Gas Supply for ^{233}U Fuel Salt Preparation, Cell G, Building 7930.

the samples had indicated. Since modification of the box to accommodate the shorter cans was impractical, equipment was provided to allow each can to be lengthened the desired amount by cementing an extension cap on it. The design of the cell G equipment and installation required 138 drawings, plus more than 280 field sketches. Reviews of the pressure vessels, criticality, building, and radiochemical plant were made in order to obtain approval for operating the ^{233}U fuel preparation process in the TURF facility.

Cold Test

One full-scale cold test run, using $^{238}UO_3$ (11.59 kg of U) and ^{7}LiF, was made to test the equipment included in the original process flowsheet. Modifications were made to the can opener and dumper box and to the salt sampler to improve operability. The densification and thermal reduction of the UO_3 to approximately $UO_{2.6}$, as well as reduction of the $UO_{2.6}$ to UO_2 with hydrogen, apparently proceeded satisfactorily at 900°C. After 295 hr of hydrofluorination, a period of time estimated to be sufficient to attain complete conversion, analysis of a sample of the melt showed that only 15% of the UO_2 had been converted to UF_4. The low conversion rate had not been detected because of difficulties with the off-gas titration system (for determining the HF utilization) and the problems associated with attempts to measure the freezing point of the charge. When a reliable off-gas titration system was installed, the low HF utilization was confirmed; it was found to result from failure of the HF sparger line, which had corroded at the gas-salt interface. When this line was replaced, the

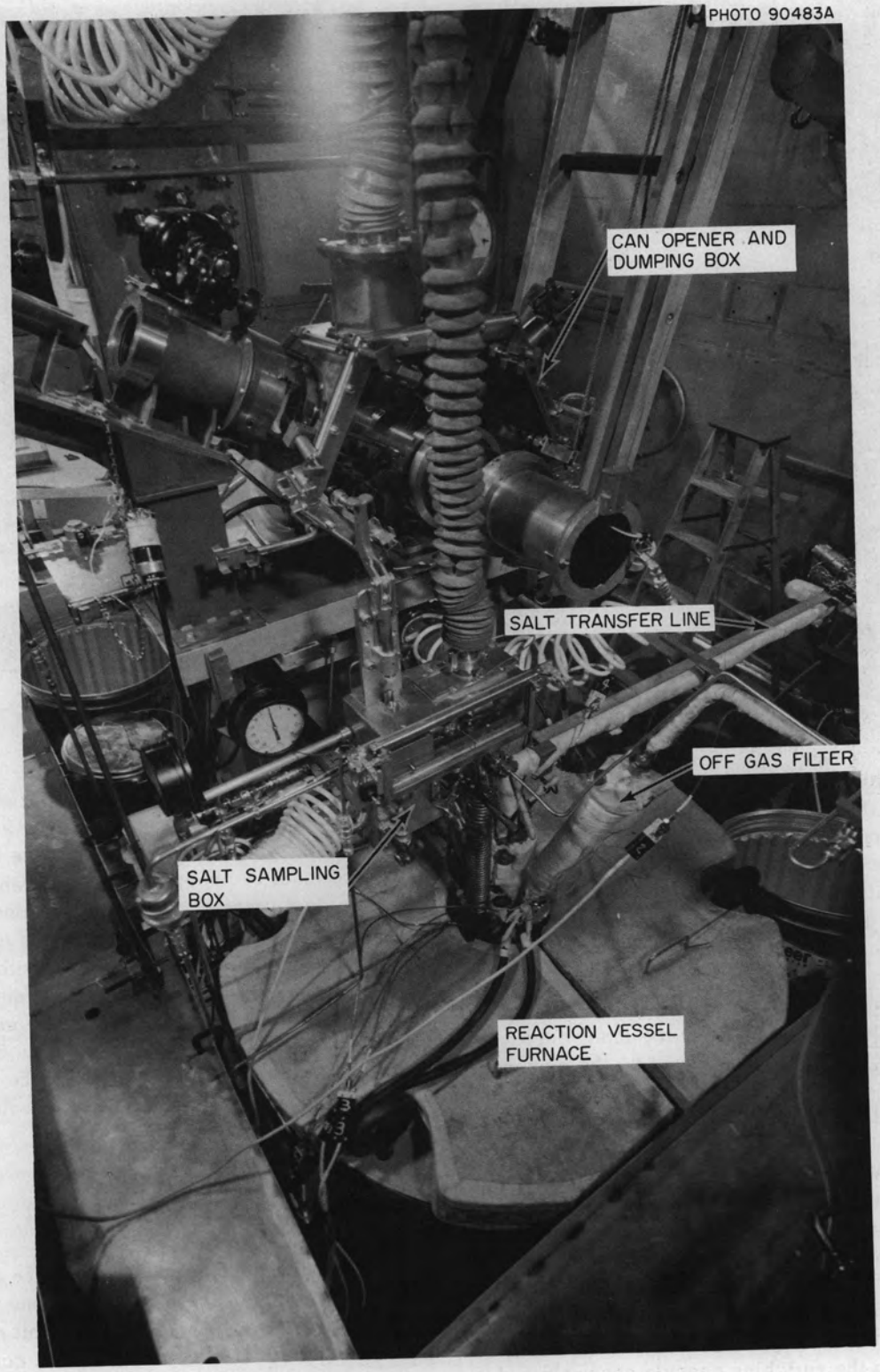

Fig. 1.20. Main Reaction Vessel Furnace and Auxiliary Equipment for ^{233}U Fuel Salt Preparation, Cell G, Building 7930.

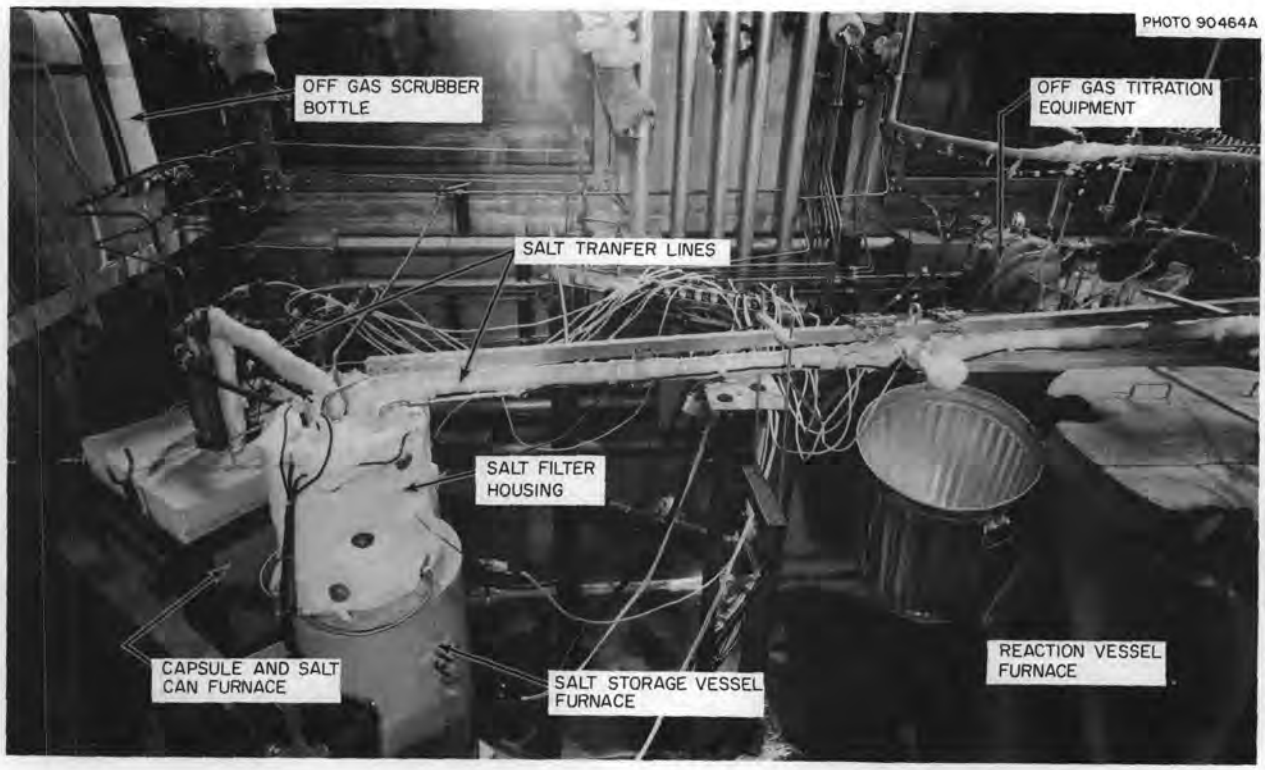

Fig. 1.21. Auxiliary Furnaces and Equipment for ^{233}U Fuel Salt Preparation, Cell G, Building 7930.

HF utilization increased to about 70%. A contact microphone (to amplify the sound of the gas bubbling through the salt) was attached to a vessel nozzle to permit verification of performance.

Another difficulty, that is, plugging of the dip line by UO_2 deposits, was traced to a cylinder of wet, off-specification hydrogen; to solve this problem, dryers were installed on the hydrogen and helium systems. High and variable oxide analyses of the salt samples in the later stages of the run were found to be caused by the presence of atmospheric air, which was probably admitted to the vessel during the sampling procedure or during premature exposure of the hot sample cup to the air. After some revisions in the procedures were made, an improvement in sample quality and uniformity was evident. The run was concluded by sparging with high-purity hydrogen to reduce the iron and nickel corrosion product fluorides to the corresponding metals. The salt was filtered and placed in the salt storage vessel; then it was transferred to the enriching capsule assembly and the $2\frac{1}{2}$-in.-diam salt can assembly. The product salt, which contained 61.05% U, 60 ppm of Ni, 80 ppm of Fe, and 111 ppm of O_2, was satisfactory. The run required approximately 2000 hr at temperatures ranging from 700 to 900°C. Ample evidence of severe local overheating was found when the reaction vessel was cut open and examined. The reaction vessel for the ^{233}U production runs was modified by replacing the flat bottom with a conical bottom to improve mixing and contact of the gas with the powder charge and the salt melt. Also, a heated nickel-mesh-packed trap was installed on the HF supply to remove the small amount of sulfur that is usually present in commercial-grade HF.

Low-Temperature Flowsheet

The difficulties experienced during the cold run prompted revision of the flowsheet to one that would specify lower temperatures, permit more effective temperature control, minimize corrosion, and provide rapid, more complete conversion of the UO_3 to UF_4. On the basis of one experiment in the laboratory, the following conditions

were used in the plant with completely satisfactory results: The reduction of UO_3 to UO_2 was accomplished at a temperature that was gradually increased from 400 to 550°C, using 2 std liters of H_2-He (containing $\leq$ 40% H_2) per minute. A multipoint thermocouple probe in the oxide bed was used to follow the progress of the reaction through the bed and to determine when it was safe to increase the initially low H_2 content of the gas to the maximum value of 40%. The maximum temperature difference between the center-line and the furnace control temperatures was $\leq$100°C. Hydrogen utilization was complete. Hydrofluorination was done similarly with a flow of 2 std liters of 40% HF–60% H_2 per minute, starting at a temperature of 400°C and gradually increasing to a final temperature of 650°C. The maximum temperature rise of the bed was 30°C. The overall utilization of HF was 95 to 97%; however, the utilization decreased very sharply at the conclusion of the run. In the laboratory development run, less than 0.2% O_2 was found in the bed; this indicated that a high conversion of UF_4 had been achieved. The ^{7}LiF was added, and the vessel was heated briefly to 850 to 875°C to melt the LiF. After the melt had been sparged at 700°C for 24 hr with 2 std liters of 20% HF–80% H_2 per minute, samples of the melt were analyzed and found to contain less than 200 ppm of oxygen. The melt was then sparged with highly pure hydrogen for 24 hr to reduce the iron(II) and nickel(II) to the metals. Finally, the melt was filtered (through a sintered nickel filter) into the storage vessel and was subsequently transferred from this vessel to the enriching capsules and salt cans.

^{233}U Fuel Salt Production Runs

The first of three ^{233}U production runs was started on May 9, 1968, when cans containing a total of 13.08 kg of $^{233}UO_3$ (91.4% ^{233}U) were opened and their contents dumped into the reaction vessel. Because the powder was quite variable in appearance and flow properties, considerable manual manipulation was required to move it through the charging box to the reaction vessel. We repaired some minor damage to the charging box, made a few changes to improve operability, and added vibrators to the box, all by remote means, to correct the problem during the remaining runs. The chemical phase of the run, which began on May 20, 1968, went very smoothly; the resulting data confirmed the laboratory results. Examination of the multipoint thermocouple probe, which was removed from the vessel after hydrofluorination of the melt so that the salt could be sampled through the same vessel nozzle, indicated that corrosion had been negligible and that no overheating of the metal had occurred. The filtered salt from this run was found to be satisfactory for use in reactor refueling. Chemical analysis showed that it contained 61.7 wt % U (i.e., ~27.5 mole % ^{233}U) and the following elements (in parts per million): Ni, 68; Fe, 56; Cr, 45; O, 62; and S, <20. Isotopic analysis revealed that ^{233}U, ^{234}U, ^{235}U, ^{236}U, and ^{238}U were present in the following concentrations (atomic percent) respectively: 91.47, 7.48, 0.80, 0.057, and 0.186.

2. Development of Aqueous Processes for Fast Reactor Fuels

Beginning in the 1980's, reprocessing of large quantities of fissile material from LMFBR reactors will be required. The problems that will be encountered during the reprocessing of this material will be different from those that have been encountered with light-water reactor (LWR) fuels for the following reasons: (1) The major fissile material in LMFBR reactors is plutonium rather than ^{235}U. (2) The fissile content of the LMFBR fuel is higher, by a factor of about 7 in the core section and by a factor of about 3 when all the material to be processed is considered, than that of the LWR fuel. (3) The average fission product content will be somewhat higher (the localized fission product content may be three times higher) than that encountered in LWR fuel. (4) The specific power of the LMFBR is higher, by a factor of about 5, than that of the LWR. (5) Processing of the LMFBR fuel after short decay periods will be advantageous, owing to the high fissile content (and high inventory costs) of the core material.

Fortunately, the Purex solvent extraction process, which is employed by nearly every major fuel processing facility in existence today, will be applicable in the processing of LMFBR fuels. The unexcelled separation efficiency, the process versatility, the ease of adaptation of the process to continuous high-capacity throughput, and the vast operating experience that has been attained in the major processing facilities make this aqueous solvent extraction process an obvious and reliable choice.

Aqueous reprocessing is most economically accomplished in large central facilities to which fuel is shipped from various reactor sites. The problem of fuel shipment, which is difficult even with LWR fuels, is aggravated in the case of LMFBR fuels by the high specific power of the fuel and the need to ship after only short decay times. We have been working toward development of equipment and techniques for shipment that will ensure safety and containment under accident conditions, as well as the adequate dissipation of fission product decay heat by natural (unaided) means.

The preparation of LMFBR fuel for solvent extraction is more difficult than that of LWR fuel because of increased heat generation, vastly increased amounts of radioiodine (if the fuel is processed after short decay periods), and the presence of substantial quantities of relatively difficult-to-dissolve plutonium and fission products. We are making studies of the dissolution rates for irradiated fuel and of equipment that will be suitable for the accomplishment of certain of the mechanical operations (e.g., shearing). Improved containment of each equipment item and reduction of the quantity of contaminated off-gas are among the primary goals.

Disposal of the tritium that is produced during the fissioning of uranium and plutonium is not currently a problem because of the relatively small amount being produced. However, when the nuclear capacity expands by several orders of magnitude and the size and number of processing facilities increase, there will be a definite need to minimize the discharge of tritium to the environment. A process that, hopefully, will isolate the tritium prior to its dilution with dissolver solution is under development. (If the tritium becomes mixed with the dissolver solution, its isolation and recovery will be impractical.) This process involves an oxidative heat treatment, which will also liberate other volatile fission products such as iodine, xenon, and krypton.

The treatment of off-gas is a major consideration in the processing of fuels that have been cooled less than 120 days. Removal efficiencies for radioiodine of 10^8 will be required for large-scale plants which process fuel that has been cooled for about 30 days. While no processing facility in ex-

istence today has the capacity (or the need) for this degree of removal, we believe that such a plant is not beyond reasonable attainment. In the processing of short-decayed fuels, substantial quantities of radioactive xenon will also be present in the off-gas streams; it, along with ^{85}Kr, can be removed by various known means and by other rare gas removal methods that are being developed.

The solvent extraction processing of LMFBR fuels must take into consideration (1) higher plutonium contents and (2) increased fission product activity in the feed. The second problem will cause difficulty in both plutonium valence control (necessary for good plutonium recovery) and solvent stability. The first will affect process and/or equipment design (to avoid criticality), as well as the choice of reductant to be used in the partitioning step. Neither of these problems appears to be serious in view of currently available information and of existing means for operating within the limitations.

Our work in the past has been directed, in a considerable measure, toward clear definitions of the problems and a delineation of the most profitable areas of investigation. In the future we expect to develop the equipment and the process flowsheet conditions that are required to demonstrate safe and economic shipment and the processing of short-cooled LMFBR fuel. While this is a challenging problem, we are confident that the solution lies in the extension of current practice and/or technology.

2.1 SHIPPING AND HEAD-END MECHANICAL PROCESSING

The shipping and the mechanical head-end processing of spend short-cooled LMFBR fuel involve several consecutive steps, principally mechanical in nature, of preshipment preparation, shipping, receiving, cleaning and storage, disassembly, shearing, removal of volatile fission products, and leaching. All of these operations should be conducted in a manner that will permit a short turnaround time of the reprocessed plutonium. Some of these steps may also include a chemical processing operation, for example, the deactivation of sodium during the cleaning of the elements or the dissolution of the fuel cores in the leaching step. In contrast to LWR fuel, the mechanical and chemical treatment steps for LMFBR fuel are complicated by criticality considerations (high plutonium content), a high rate of emission of decay heat, and the presence of highly reactive sodium.

During the past year, certain steps of the shipping and the mechanical head-end flowsheet were investigated. A conceptual study was made to determine the feasibility of complete disassembly and canning of spent fuel at the reactor site to facilitate the release of heat from the shipping cask. In addition to this study, we completed the conceptual design for a shipping cask and made some initial heat-transfer calculations. Methods of sealing a cask and shipping cans were surveyed, and a unique type of can closure was designed. Initial tests to determine practical methods for the removal (deactivation) of sodium from fuel assemblies were begun. In addition, a small continuous prototype shear that would be applicable to small bundles of LMFBR fuel was fabricated; this shear, along with a prototype continuous leacher, was subjected to initial tests. Future work will include an engineering evaluation of various mechanical concepts to determine the most practical approach to each step included in the flowsheet.

Preshipment Preparation

A preliminary design study and cost estimate of a facility located at a 1000-Mw (electrical) LMFBR site for the preshipment preparation of 20-day-cooled spent fuel[1] assemblies has been made.[2] In this study, it was assumed that the neutron shields have been removed and that the fuel rod assemblies

[1]The fuel chosen for the study is the General Electric reference fuel as described in GEAP-4939. This fuel consists of UO_2-PuO_2 pellets clad in stainless steel and assembled in a hexagonal multitubular array measuring ~7.8 in. across the flats and containing 490 or 546 (combination of fuel rods and BeO rods) 0.267-in.-OD rods. Each tube is wrapped with $\frac{1}{32}$-in.-diam wire in a spiral fashion to prevent adjacent rods from touching and to provide channels through which sodium coolant is pumped. A fuel assembly, approximately 77 in. long, has a fission gas plenum chamber, an 18-in. upper axial blanket, a 16-in. core, and an 18-in. lower axial blanket. The tubular axial blankets are composed of depleted UO_2 pellets clad in stainless steel. Each assembly contains a 13-ft neutron shield attached at the upper end; this results in an overall length of 24 ft (neutron shield, fuel rod assembly, and end adapter) for the assembly.

[2]B. C. Finney, R. S. Lowrie, and C. D. Watson, *A Conceptual Design and a Cost Estimate of an On-Site Facility for Cleaning, Disassembling, and Canning Short-Cooled LMFBR Fuel in Preparation for Shipment to a Central Reprocessing Plant*, ORNL-TM-2050 (May 20, 1968).

have been cleaned of sodium and stored in a water-filled pool. Each of the bundles is disassembled into individual tubular fuel rods with the gas plenum chamber removed; then the BeO rods are separated from the fuel rods, the wire wrap is stripped from each fuel rod, 21 fuel rods are inserted into a can, and the can is sealed and placed in a 100-ton shipping cask for shipment to a central reprocessing plant. The conceptual design of the on-site facility (including structures, auxiliary equipment, and processing equipment) is detailed only to the extent required for a scoping type of cost estimate. The economic inducement for prompt shipment will probably dictate duplicate operator-aided automatic or semiautomatic equipment to prevent expensive delays in certain phases of the operation. In general, automated high-speed equipment handling large quantities of highly irradiated, short-decayed fuel has never been operated in a shielded cell; consequently the design of the facility (and cost estimate) is based on present-day technology extended to this concept. A summary of capital costs follows:

A. Capital costs	
1. Sodium removal	$419,000
2. Fuel assembly storage pool	434,000
3. Mechanical cell	1,999,000
4. Mechanical cell disassembly equipment	745,000
5. Fuel can storage and cask loading	924,000
6. Decontamination cell	367,000
7. Service facility (staff shop)	162,000
	$5,050,000
B. Annual costs	
1. Amortization ($6\frac{2}{3}$ years at 15%/year)	$758,000
2. Operating	300,000
3. Waste disposal	4,000
Subtotal	$1,062,000
4. Shipping (based on $11.20 per kilogram of Pu + U, as determined by R. Salmon, Chemical Technology Division, ORNL)	202,000
Total	$1,264,000
C. Unit costs	
1. Preshipment preparation (cleaning, disassembly, sorting, canning, and cask loading)	0.152 mill/kwhr
2. Shipping (based on $11.20 per kilogram of Pu + U, as determined by R. Salmon, Chemical Technology Division, ORNL)	0.029 mill/kwhr
Total unit cost	0.181 mill/kwhr

The unit cost is based on an 80% load factor for the 1000-Mw (electrical) General Electric Reference Oxide Fast Breeder Reactor (an annual electrical output of 7×10^9 kwhr). Although the study is preliminary, it indicates that a disassembly facility as described, operated perhaps only one month during each year, would be uneconomical if the costs were absorbed by a single reactor. It is apparent that the amount of reactor-site disassembly that can be economically justified is a direct function of the quantity of fuel generated at that station. If five reactors were sharing the same disassembly facilities, the preshipment preparation costs would be reduced to ~0.03 mill. Because of the increased weight of the casks, shipping costs for intact fuel will probably be twice those for fuel that has been fully disassembled. A profitable trade-off between increased shipping costs and decreased disassembly costs could probably be made for a large single-reactor station.

Shipping Cask Design Studies

Aqueous reprocessing is most economically accomplished in large central facilities. This necessitates the shipping of short-cooled (~20 days), high-burnup (up to 127,000 Mwd/metric ton) fuel. Therefore additional studies were begun to design a shipping container in which such fuel, with its concomitant radiation and heat dissipation problems, can be safely handled. We considered a hypothetical on-site facility in which spent fuel assemblies (General Electric reference fuel) were cleaned of residual sodium and disassembled and then the individual fuel rods were loaded into stainless steel cans. The sealed cans were then placed in an artificially cooled lead-shielded cask for shipment to the reprocessing plant. Because the economics of such an on-site shipping facility appear unattractive,[2] we are now concentrating our efforts on designing a cask in which complete fuel assemblies, probably canned in sodium, can be shipped safely. The design criteria of such a cask are listed below.

1. The heat load of the cask will be based on the decay heat released from complete fuel assemblies from the center zone of the reactor. The decay heat from a single assembly is calculated to be ~56,000 Btu/hr, with ~47,000 Btu/hr being released in the 16-in.-long core section of the 11-ft-long assembly.
2. The maximum temperature of the cladding of a fuel pin in the center of the fuel assembly under normal shipping conditions will not exceed 1275°F, which approximates the temperature experienced by the cladding during reactor operation.

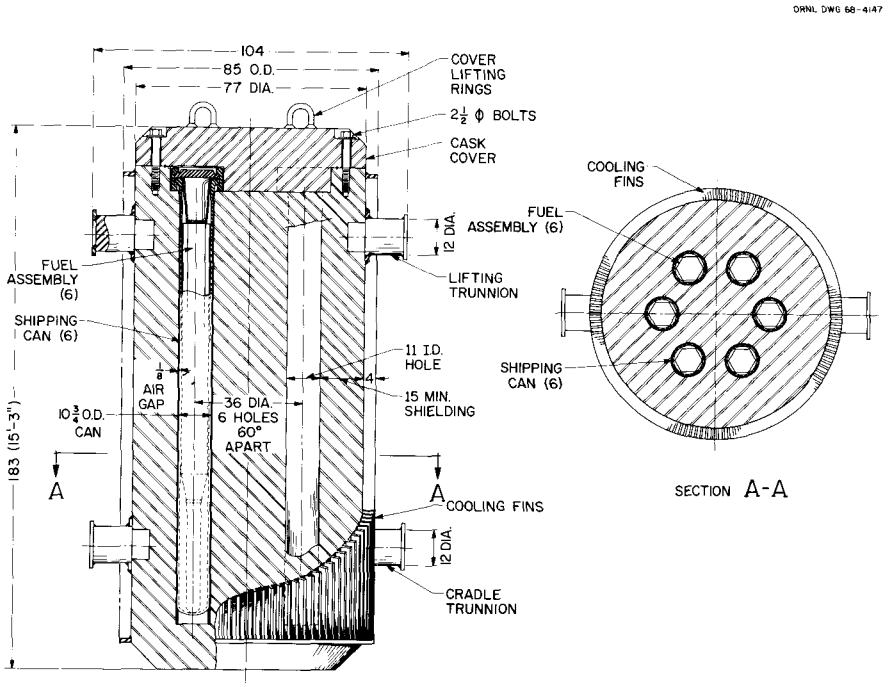

Fig. 2.1. Conceptual Design of Shipping Cask for LMFBR Fuel Assemblies. Weight of cask, 115 tons.

3. The sodium-filled can in which the fuel assembly (or assemblies) will be placed will act as the primary containment vessel. The General Electric reference fuel is vented; however, even with unvented fuel, the possibility of ruptured fuel pins exists.
4. The maximum temperature of the wall of the sodium-filled can will not exceed 1500°F during accident conditions.

With these criteria as a guide, a number of configurations were evaluated before the conceptual cask design (Fig. 2.1) was established. In this design, six fuel assemblies, each in its own sodium-filled can, are located symmetrically in a circle inside a steel shipping cask. Because the diameter of the cask depends on the diameter of the can closure, a breech-lock closure (see the following section, "Cask and Can Closures") is proposed to minimize the size of the cask. The dimensions of a finned cask are 85 in. OD by 15.25 ft long. The cask will weigh approximately 125 tons when empty.

The computer code SIFT-TOSS (applicable to three-dimensional heat transfer analyses) was used to calculate the steady-state conditions existing in a conceptual shipping cask (Fig. 2.1) containing six General Electric reference fuel assemblies canned in sodium. Three cases for fuel burned to 110,000 Mwd/metric ton and cooled 20 days were considered:

Case I: All heat is dissipated to the atmosphere by natural convection and radiation. An air gap, $\frac{1}{8}$ in. wide, exists between the shipping can and the surrounding steel shielding. Heat transfer within the shipping can is assumed to be by conduction only (no convective flow).

Case II: Case II is the same as case I except that the finned external cask surface is cooled by means of forced air.

Case III: Forced-air cooling of the finned external cask surface is provided as in case II, but the annular space between the cask and the can is filled with sodium, which serves as a noncirculating heat transfer agent.

Calculated temperature profiles of a radial cross section of the cask through the active core of the fuel assembly for the three cases are shown in Fig. 2.2. Center-line temperatures of the fuel assembly were 2200, 2170, and 1870°F for case I, case II,

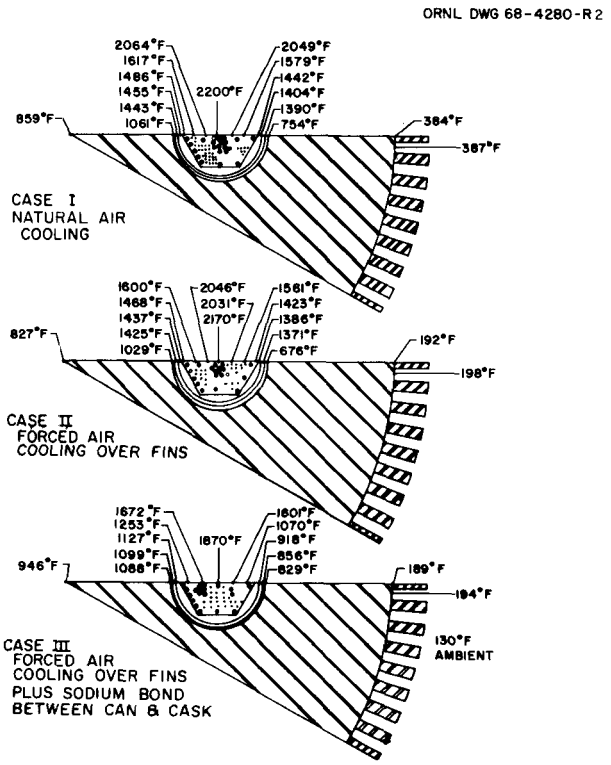

Fig. 2.2. Calculated Temperature Profiles for LMFBR Shipping Cask.

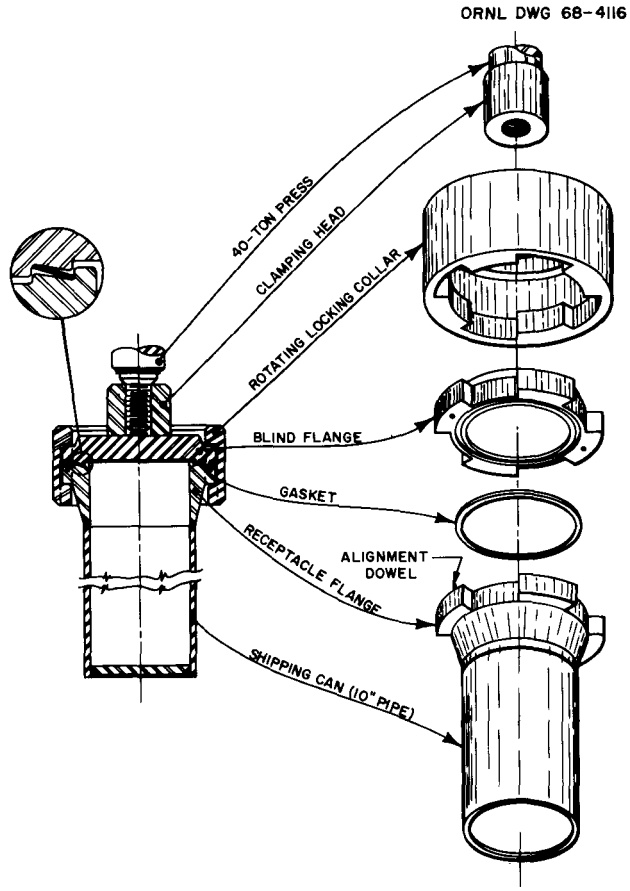

Fig. 2.3. Breech Lock Closure for Shipping Cans.

and case III respectively; all of these temperatures are above 1275°F. It is apparent that, for this system, either circulation of sodium through the fuel assemblies, by either forced or natural convection, or passage of coolant around the shipping cans will be required to limit the center-line temperature to 1275°F during shipment of short-cooled fuels.

Cask and Can Closures

A survey of mechanical seals and design concepts of closures was made to develop a leak-tight closure for Inconel X shipping cans (10-in. sched 80 IPS) containing 15- to 25-day-cooled fuel. The cans must maintain their structural integrity under accident conditions to prevent release of radioactivity from the cans. Presently, a shipping can will contain one fuel assembly (containing a large quantity of radioactive ^{131}I) surrounded with sodium as a heat transfer medium. The design criteria require the closure and seal to be leak-tight at a pressure of 100 psi and at a temperature of 1500°F. The closure and seal developed for the shipping cans may also be adaptable to the cask closure and many other in-cell remote operations.

Three manufacturers of special closures are considering the development of new closures (or alteration of their present closures) to seal the shipping cans. ORNL engineers have developed five different concepts of closures and have considered seven different types of seals. A breech-lock closure (Fig. 2.3) with a hydraulic actuator and a Conoseal or Naflex seal appears to be more acceptable than the other concepts.

The breech-lock type of closure is being favorably considered because: (1) it appears to meet the design specifications, (2) it is more compact (16.5 in. OD) than other high-pressure and -temperature seals for this pipe size, (3) its assembly and disassembly are the easiest to accomplish remotely, and (4) its seal ring is easy to replace. A model is being fabricated to demonstrate operability

and sealing characteristics. This type of closure is designed to be operated as follows: (1) a 40-ton hydraulic press forces the blind flange down on the can flange, thus flexing a metallic ring gasket. (2) A collar with a breech-lock thread is then rotated and locked in position, thereby clamping the blind flange to the can. (3) The hydraulic press is removed to allow the ring gasket to flex and to take up the clearance between the collar and its mating surfaces.

Studies of the Deactivation of Sodium

Methods are being evaluated for safely deactivating and disposing of the sodium that is associated with spent LMFBR fuel assemblies. These procedures must be capable of handling sodium that adheres to the external surfaces of the fuel assembly as well as the sodium that is present inside a fuel rod. Sodium may be present internally as a result of leakage through ruptured cladding or vented fuel, or it may have been added as a heat-transfer bond. Adequate provisions must be made to remove the heat of the deactivation reaction and the fission product decay heat resulting from the short-cooled, high-burnup fuel. In the case of unbonded, unvented stainless-steel-clad UO_2-PuO_2 fuels, the external sodium will probably be deactivated by reacting it with controlled amounts of water, either as a vapor or a liquid spray, in an inert gas such as argon. A proposed cleaning facility using this flowsheet has been discussed previously.[1]

Studies to measure the amount of sodium adhering to prototype General Electric reference fuel were begun. Results of preliminary tests made with small-scale prototype fuel rod clusters immersed in heated sodium indicate that a full-sized fuel assembly may retain greater than 4 kg of sodium. In a single deactivation test with a prototype cluster, argon containing water was passed across and through the cluster until the off-gas was free of hydrogen. When the cleaned cluster was dipped into water, several violent reactions occurred, indicating that small pockets of sodium had survived the deactivation reaction. A high-velocity gas stream, which could serve to eliminate the sodium pockets, will be evaluated in future tests.

Disposal of sodium inside fuel rods is more difficult, since the sodium must first be exposed by mechanically shearing the fuel. Two approaches will be investigated: (1) volatilization of sodium from the sheared pieces in a heated chamber and (2) deactivation of the sodium with a suitable reagent. Deactivation should be accomplished prior to the leaching step.

Prototype Semicontinuous Shear

Initial tests of a semicontinuous shear (Fig. 2.4) of a new design have been successful.

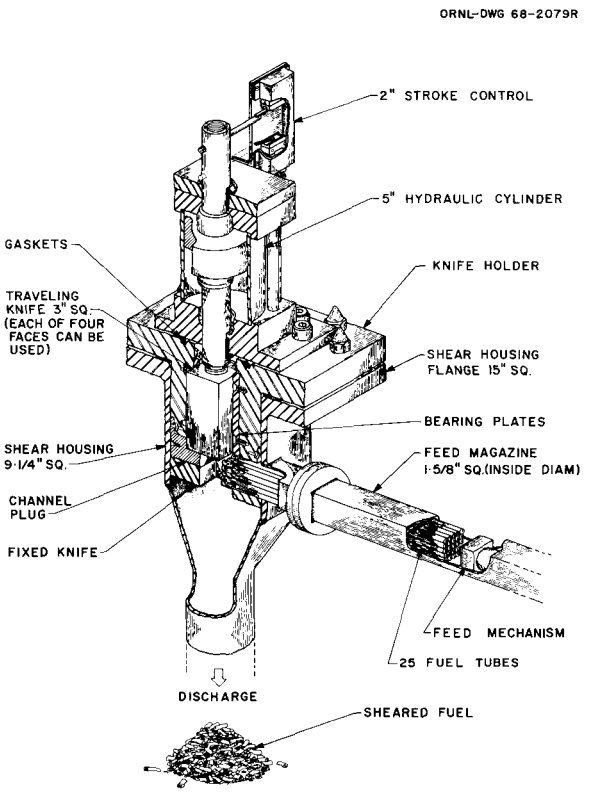

Fig. 2.4. ORNL Semicontinuous Prototype Shear (5 × 5 Tube Bundle).

Prototype General Electric reference fuel bundles consisting of 25 porcelain-filled stainless steel tubes (0.250 in. OD × 0.010 in. wall thickness × 52 in. long) were sheared into 1-, 2-, and $2\frac{3}{4}$-in. lengths at 15 strokes/min. The amount of dislodged material (stainless steel fines and porcelain) for the sheared lengths was 7.5, 3.4, and 2.2% respectively. The force required to shear the 25-rod bundle was about 9 tons. If two units were operated at 15 strokes/min (with one in operation while the other was being loaded) to shear bundles of 25 rods into 1-in. lengths, 2.5 metric tons of product would be produced every 16 hr. A 5 × 5 tube bundle was chosen because calculations indicate that the release of decay heat from this bundle will not cause excessive temperatures, even at burnups as high as 100,000 Mwd/metric ton and a 30-day cooling period.

The shear is compact, measuring approximately 15 × 15 × 34 in. high, and can be operated both manually and automatically. The knife holder can be remotely located at any one of four positions by loosening the conical head bolts and rotating the holder 90°, thereby making it possible to use the four cutting edges of the moving and fixed blades before replacement is required. Clearance between the traveling knife and the fixed knife is, by design, 2 to 6 mils; this eliminates the necessity for remote adjustment of blade clearances. The design is unique in that no holding mechanism (gag) is required for restraining the 25 tubes during shearing. The feeding mechanism is sufficiently strong to withstand the back pressure caused by the shearing operation.

Prototype Continuous Leacher

A prototype rotary leacher (Fig. 2.5), featuring a spiral screw for material transport, was fabricated, and initial tests were successful. The 18-in.-diam spiral screw has 13 flights with a 6-in. pitch. The sheared sections of stainless-steel-clad porcelain generated by the small shear serve as the feed for the leacher. Initial evaluation studies are being made to determine if the sheared material can be moved without being jammed between the rotating spiral screw and the housing. Final feasibility testing will include other fuel configurations with a heavier wire wrap.

ORNL DWG 68-4162R

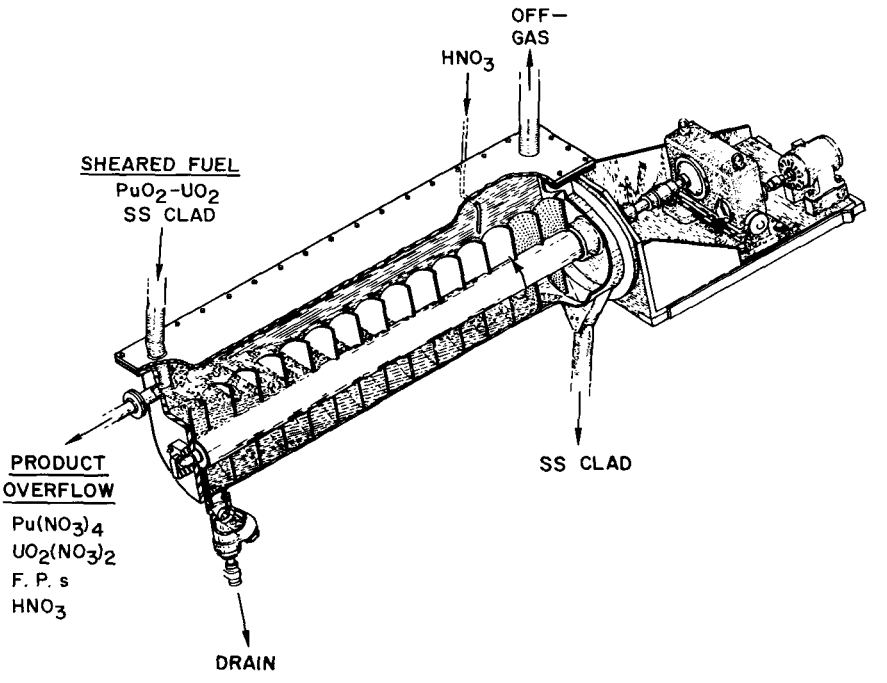

Fig. 2.5. Prototype Continuous-Flooded Rotary Leacher.

2.2 HEAD-END TREATMENT FOR REMOVAL OF FISSION PRODUCTS

As the nuclear power industry grows and the number and size of the fuel reprocessing plants increase, the release of radioactive noble gases, tritium, and iodine to the environment will become a much more important consideration than at present. In the future, the removal of essentially all radionuclides from the plant off-gas may be required. The removal of iodine from process off-gases, which requires careful control even in present reprocessing plants, will become much more difficult when short-cooled fast reactor fuels are processed. Earlier work[3] at Atomics International showed that noble gases and certain other volatile fission products could be effectively removed from irradiated UO_2 during the phase change that occurred when the UO_2 was oxidized to U_3O_8 at elevated temperatures. Similar results have been obtained in pyrometallurgical processing studies at Argonne.[4] Recent experiments at ORNL (Sect. 4.2) on the application of fluidized-bed volatility processes to power reactor fuels showed that most of the tritium was released when highly irradiated UO_2 was heated to 450°C and oxidized to U_3O_8.

[3]G. E. Brand and E. W. Murbach, *Pyrochemical Reprocessing of UO_2 by Airox*, NAA-SR-11389 (August 1965).

[4]R. C. Vogel *et al.*, *Chemical Engineering Division Research Highlights, May 1965—April 1966*, ANL-7175.

We are studying the heating-oxidation of irradiated fast reactor oxide fuels to determine if this may be an attractive head-end treatment to provide early removal of the volatile fission products. Our objective is to release these fission products into a relatively small volume of gas from which they can be efficiently removed in concentrated form for storage. There is an important advantage in the removal of tritium before it contacts hydrogen-containing process reagents from which its subsequent separation would be impractical. Preliminary results have been encouraging.

Most of the experiments were made with sectioned metallographic remnants of stainless-steel-clad PuO_2-UO_2. These specimens were supplied by Nuclear Materials and Equipment Corporation (NUMEC). They had decayed for as long as three years. To provide ^{131}I and other short-lived fission products, we "spiked" the fuel with sol-gel UO_2 microspheres that had been irradiated in the Oak Ridge Research Reactor and cooled less than 30 days. The fuel was heated in a vertical tube in a stream of gas (~25 cm^3/min); the off-gas was passed through a series of traps for capturing the fission products (Fig. 2.6).

Tritium Behavior

Analysis of a sample of declad UO_2 from the core of the Yankee Atomic Electric Reactor showed that it contained 0.15 mc of tritium per gram. The fuel had been irradiated to about 35,000 Mwd/ton and

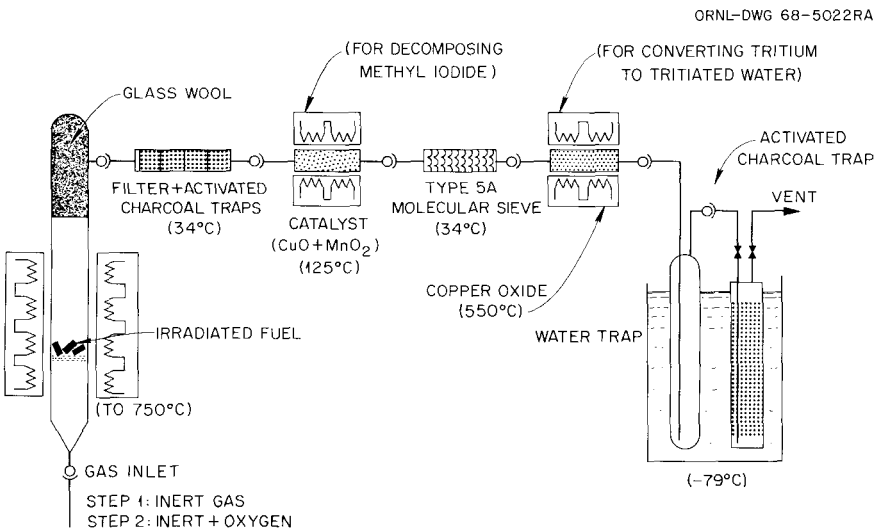

Fig. 2.6. Heating-Oxidation Treatment for Volatilizing Fission Products from Irradiated Fuel.

had decayed 1.5 years. Tritium was determined by dissolving the fuel in nitric acid and analyzing the fuel solution and off-gas streams. A sample of the UO_2 was heated to 450°C in a stream of argon–4% hydrogen over a 0.5-hr period and then oxidized to U_3O_8 by heating for 4 hr at 450°C in a 1:1 mixture of oxygen and argon–4% hydrogen. This treatment removed about 88% of the tritium that was originally present in the fuel.

A similar experiment was made with 20% PuO_2–80% UO_2 fuel that had been irradiated by NUMEC to a burnup of 20,000 Mwd/ton and decayed 30 months. Heating a 2.1-g sample of the fuel to 450°C in argon–4% hydrogen and then in a 1:1 mixture of oxygen and argon–4% hydrogen for 3 hr at 450°C removed 94% of the tritium.

In these experiments, the tritium (as tritiated water) was efficiently removed from the gas stream by sorption on Linde type 5A molecular sieve. It was later desorbed by heating the molecular sieve to 400°C at a pressure of less than 1 mm Hg and was trapped by freezing the water from the gas phase in a liquid-nitrogen cold trap.

Iodine Behavior

The addition of short-decayed UO_2 to the highly irradiated but long-decayed PuO_2-UO_2 permitted us to follow the behavior of iodine during the heating-oxidation treatment. In the experiment described above, in which NUMEC 20,000-Mwd/ton material was heated at 450°C for 3 hr in oxygen plus argon–4% hydrogen, 98.3% of the iodine was volatilized from the fuel. A film or "tarlike" material deposited on the walls of the furnace tube just outside the heated zone. At the end of the test, the equipment was leached with CCl_4 and HNO_3. Although only a portion of the brown deposit was soluble in CCl_4, the remainder dissolved completely in warm 8 *M* HNO_3. The activity of the material was due mostly to ^{131}I; however, ruthenium and some other fission products were also detected. Of the total iodine found in the experiment, about 48% was on the walls of the quartz tube just above the furnace, 32% was in the head of the burner packed with glass wool (roughing filter), and 18% was adsorbed on the activated charcoal and molecular sieve traps.

In another test, 20% PuO_2–80% UO_2 fuel that had been irradiated to a burnup of 49,000 Mwd/ton was heated at 750°C, first in a stream of nitrogen for 3 hr and then in a stream of oxygen for 3 hr. This treatment removed about 90% of the ^{131}I from the fuel. About 71% of the total ^{131}I was found in the tubing located just beyond the heated zone. Of the total ^{131}I collected (~18%) in traps beyond this point, 94% volatilized during the 3-hr heatup in nitrogen and 6% volatilized during the 3-hr oxidation.

We determined the relative amounts of iodine volatilized from the fuel at various temperatures during heatup and during the oxidation step. In this experiment, a sample of 20% PuO_2–80% UO_2 that had been irradiated to a burnup of 50,000 Mwd was heated to 750°C stepwise (1 hr at each of these temperatures: 450, 550, 650, and 750°C) in a stream of argon–4% hydrogen. The gas stream was then changed to pure oxygen, and heating at 750°C was continued for 3 hr. The charcoal trap located just beyond the burner was replaced after each step. About 56% of the total ^{131}I was found on the walls of the burner just outside the heated zone, while about 18% was left in the oxidized fuel. About 14, 0.9, 0.6, and 1% of the ^{131}I were found in charcoal traps removed after heating at 450, 550, 650, and 750°C, respectively; 9% was collected in the charcoal trap during the oxidation step. Analyses showed that about 85% of the collected ^{133}Xe was in the cooled charcoal trap at the end of the trapping system; the balance was found in the other charcoal traps and in the molecular sieve. Krypton-85 was detected only in the cooled charcoal trap. The oxidized fuel was not analyzed for ^{133}Xe and ^{85}Kr.

2.3 DISSOLUTION

Data on the leaching of fast reactor fuels are very limited. Information is needed concerning the dissolution rate and the metal recoveries to be expected as a function of the preparation history, the burnup, and the postirradiation temperature history of the fuel. We are procuring irradiated oxide fuels from as many sources as possible for testing. In addition to metal recovery data, information concerning the composition and physical characteristics of the leach residues is being obtained. Particular attention is also being given, both in laboratory and hot-cell studies, to the behavior of iodine in the dissolver-condenser system and to the use of fumeless dissolving techniques for minimizing the volume and the fume content of the off-gas to allow easier separation and containment of the radioactive rare gases and iodine.

Dissolution of Irradiated Fuels in HNO_3

Dissolution tests were made with sectioned remnants (from metallographic examination) of specimens of stainless-steel-clad PuO_2-UO_2 that had been prepared by different fabrication routes and that ranged in PuO_2 content from 5 to 28% and in burnup from 2000 to 64,000 Mwd/ton. Initial tests were made with fuel specimens that were supplied by NUMEC from their irradiation capsules NU-15, -16, -17, and -18. In experiments NU-15 and -16, stainless-steel-clad 5% PuO_2–95% UO_2 that had been irradiated in the General Electric Test Reactor (GETR) to burnups of 10,000 and 20,000 Mwd/ton was used. Experiments NU-17 and -18 were made with 20% PuO_2–80% UO_2 that had been irradiated in the GETR to burnups of 20,000 and 50,000 Mwd/ton and decayed about 2.5 years. Each capsule contained three to five individual pins of mechanically blended or coprecipitated mixed oxide. (We could not identify the type of oxide in the remains of NU-15 and -16.) In each dissolution test, the fuel was "spiked" with <30-day-cooled UO_2 to provide short-lived fission products. The oxide was leached from its cladding in Pyrex vessels equipped with either an Allihn reflux (updraft) condenser or a specially made downdraft reflux condenser. Usually, a purge gas of nitrogen or oxygen was fed to the vapor space of the dissolver to carry the noncondensable vapors to caustic scrubbers or adsorption columns.

Table 2.1 summarizes the results of experiments with the NUMEC specimens. In general, the dissolution of the major portion of each fuel sample in 4 to 8 *M* HNO_3 appeared to be quite rapid; bubbling and evolution of nitrogen oxides ceased within 0.5 hr, often before the acid reached its boiling point. In almost all these tests, however, the leaching times were not sufficiently long to permit complete recovery of the plutonium.

Multiple Leaches. – Additional leaching tests were made with 1-in. segments of irradiated $(U,Pu)O_2$ clad with 0.25-in.-OD stainless steel tubing. In these tests the fuel samples were leached either three or four times with boiling nitric acid, each time for 2 to 3 hr. Three of the fuel samples consisted of remains from the metallographic examination of GE-APO Fast Ceramic Reactor Experiments C3C, C3E, and F1A. The first two samples were 28% PuO_2–72% UO_2 that had been irradiated in the GETR to 64,000 and 63,000 Mwd/ton, respectively, and the third sample was 20% PuO_2–80% UO_2 that had been irradiated in the EBR-II to a burnup of 2000 Mwd/ton. A sample of 20% PuO_2–80% UO_2, prepared by the sol-gel process and irradiated to a burnup of 20,000 Mwd/ton, was also leached. After each leaching period, the solution was cooled, filtered, and sampled. The residue, along with the cladding and the filter paper, was returned to the dissolver for additional contacts with fresh leachant.

Figure 2.7 and Table 2.2 summarize results of the experiments. Various nitric acid concentrations, ranging from 4 to 13 *M*, were used for leaching in these tests. The results reflect this difference, as well as differences in the plutonium content and the preparation and irradiation histories of the samples. In each test, essentially complete recovery of the plutonium was obtained. Uranium leaching data are not shown; however, the recovery of uranium closely paralleled that for plutonium. The highest plutonium loss occurred during the leaching of coprecipitated oxide with 4 *M* HNO_3; 0.16% of the plutonium in this sample remained undissolved after four leaches (totaling 9.5 hr). Coprecipitated oxide dissolved much more rapidly in 8 and 13 *M* HNO_3, with more than 99.9% of the plutonium being dissolved in two 2-hr leaches. The sol-gel oxide sample dissolved more readily in 4 *M* HNO_3 than did the coprecipitated oxide sample. However, the latter contained a higher concentration of plutonium, and this, as well as the preparation method, could have been an important factor in controlling the dissolution rate.

These dissolution data suggest that, since the major portion of each of the fuel samples (Tables 2.1 and 2.2) dissolved very readily, a small fraction of the plutonium in each sample is in a refractory form which is much more difficult to dissolve than the bulk of the plutonium. It may be attractive, therefore, to dissolve the major fraction of the fuel by using a short leach treatment and to separate the fuel residue from the fuel solution (and cladding) for a later, more stringent treatment.

Adjustment of Plutonium Valence. – Analyses of two of the dissolver solutions from the leaching studies showed that 19 and 33%, respectively, of the total plutonium was Pu(VI). [Plutonium(IV) is the preferred form for solvent extraction.] Addition of $NaNO_2$ to the latter solution (to 0.1 *M*) increased the Pu(IV) concentration to 98% of the total. Four days later the Pu(IV) content of this solution was still about 94%, showing that the tetravalent form is reasonably stable at the moderate beta-gamma

Table 2.1. Dissolution of Irradiated PuO_2-UO_2 Specimens Supplied by NUMEC

Experiment No.	Fuel Description				Leaching Conditions		Residue Weight (% of initial fuel weight)	Amount in Residue (% of total)	
	Percent Pu	Oxide Type[a]	Burnup (Mwd/ton)	Weight[b] (g)	Solution	Time[c] (hr)		U	Pu
1	5	U	10,000	7.1	8 *M* HNO_3	3.5	0.11	0.06	0.11
2	5	U	10,000	6.4	8 *M* HNO_3	7.5	0.65	0.13	1.0
3	5	U	20,000	6.4	8 *M* HNO_3[d]	7.5	0.18	0.01	0.04
4	5	U	20,000	6.0	8 *M* HNO_3	3	2.0	0.05	11.4[e]
5[f]	20	U	20,000	2.1	4 *M* HNO_3	3	0.68	0.18	0.47
6	20	CP	20,000	1.2	4 *M* HNO_3	12	3.8	2.5	4.7
7	20	MB	20,000	1.0	8 *M* HNO_3	6	2.4	1.3	1.3
8[f]	20	CP	50,000	1.8	4 *M* HNO_3 (first)	3			
					8 *M* HNO_3 (second)	4	4.8	0.16	1.5
9[f]	20	MB	50,000	1.4	4 *M* HNO_3–0.05 *M* HF (first)	5			
					8 *M* HNO_3–0.05 *M* HF (second)	3	6.8	0.04	0.41

[a]U = unidentified; CP = coprecipitated; MB = mechanically blended.

[b]Fuel was "spiked" in each test with an additional 1.0 g of <30-day cooled, low-burnup UO_2.

[c]Includes ~15 min to heat to boiling temperature; balance of leach was at boiling temperature.

[d]Leak in apparatus; solution boiled dry at about 4 hr; redissolved in 8 *M* HNO_3–0.05 *M* HF.

[e]Probably special fuel rod containing discrete PuO_2 particles pressed into UO_2 matrix.

[f]Fuel (and cladding) heated in oxygen at 450 to 750°C before leaching.

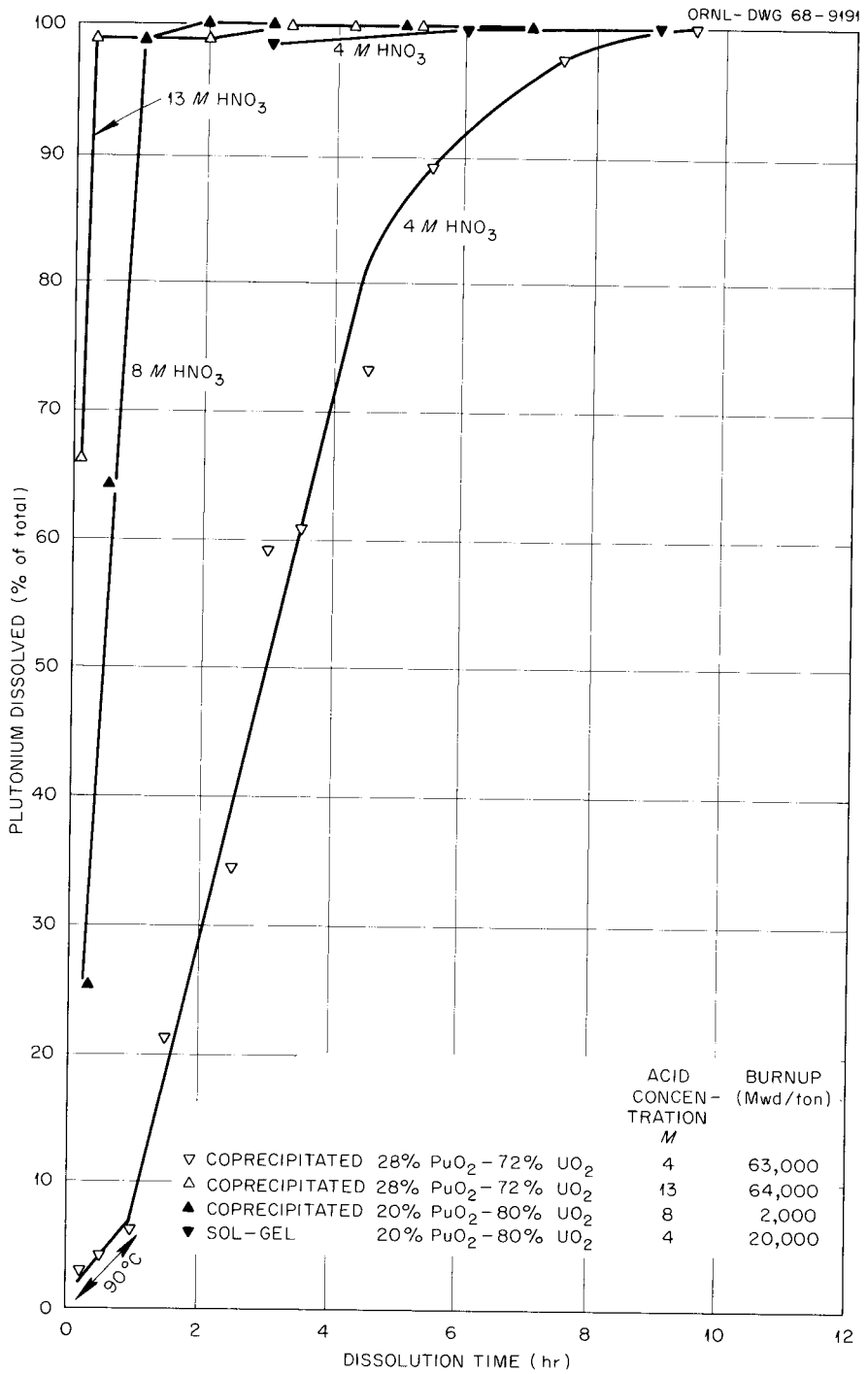

Fig. 2.7. Recovery of Plutonium from 1-in. Sections of Stainless-Steel-Clad $(Pu,U)O_2$ by Multiple 2- to 3-hr Leaches with Boiling Nitric Acid.

Table 2.2. Recovery of Plutonium by Multiple Leaches[a] of PuO_2-UO_2 with Boiling Nitric Acid

HNO_3 Concentration (*M*)	Oxide Preparation Method	Plutonium Undissolved After Leaching (% of total)			
		First Leach	Second Leach	Third Leach	Fourth Leach
4	Coprecipitated	65.4	10.8	2.1	0.16
4	Sol-gel	1.5	0.2	<0.01	
8	Coprecipitated	1.28	0.03	<0.01	<0.01
13	Coprecipitated	1.14	0.09	0.01	<0.01

[a]Either three or four 2- to 3-hr leaches.

Table 2.3. Volatility of ^{131}I During Fuel Dissolution

HNO_3 Concentration (*M*)	Leaching Time (hr)	Purge Gas	Condenser Type[a]	Iodine Volatilized from Dissolver Solution (% of Total)
8	3.5	O_2	DD	61
8	7.5	N_2	DD	80
8	7	O_2	DD	84
4	9	None	UD	15
8	8[b]	O_2	UD	84[c]
8	6	O_2	UD	85
4	10[b]	O_2	DD	88

[a]DD = downdraft reflux condenser; UD = updraft reflux condenser.

[b]KI added (to 0.02 *M*) 4 hr before end of test; $NaNO_2$ added (to 0.05 *M*) 2 hr before end of test.

[c]In this test, 68 and 79% of the iodine had volatilized after 4 hr and 6 hr respectively.

activity levels of these feeds; the stability of Pu(IV) at high activity levels will be examined in future tests.

Composition of Leach Residues. – Some of the residue from experiment 9, Table 2.1, was dissolved in aqua regia. Emission spectroscopy of the solution showed that it contained, primarily, the following metals: Fe, Cr, Ni, Mn, Al, Mo, and Pd; the activity of the residue resulted almost entirely from the presence of ^{103}Ru-Rh and ^{106}Ru-Rh. A black solid precipitated from the solution after it had been allowed to stand for a few days. Spectrographic analysis of the precipitate gave emissions that were very strong from Ru, strong from Rh and Si, moderate from Fe, Ni, and Pd, and weak from Al, Co, Cr, Mo, and Zr.

The gamma spectrum for one of the leach residues (experiment 8, Table 2.1) showed the following principal radionuclides with the indicated activity levels (in dis min^{-1} g^{-1}): ^{106}Ru, 20.9×10^{12}; ^{103}Ru, 8.5×10^{11}; ^{144}Ce, 7.2×10^{11}; ^{95}Zr-Nb, 5.1×10^{11}; ^{125}Sb, $<3.0 \times 10^{11}$; ^{140}Ba-La, 7.0×10^{11}.

Evolution of ^{131}I During Dissolution. – Some scouting tests were made to determine the amount of ^{131}I that was volatilized from the fuel solution under various dissolution conditions. To provide ^{131}I, the long-decayed $(U,Pu)O_2$ fuel was "spiked" with short-decayed sol-gel UO_2. The amount of iodine volatilized in these tests varied from 15 to 88% (Table 2.3). The results show that, at least with these equipment arrangements, a purge gas is

needed to remove the iodine effectively. In two of the tests, KI was added to the dissolver to reduce any iodate to volatile elemental iodine, and $NaNO_2$ was added near the end of the run to oxidize any residual iodide to elemental iodine. The amount of iodine removed in these tests was 84 to 88%. The use of reflux condensers hampers the removal of iodine. We could see a deposit of iodine crystals on the cold wall of the condenser, and some of this iodine was probably washed back into the dissolver by the returning condensate. Other equipment arrangements that may allow more efficient iodine removal are being tested.

Dissolution of Unirradiated Fuels in HNO_3

Iodine Behavior. – If reactor fuel elements are processed only 30 days after discharge from the reactor, the ^{131}I concentration in the processing solutions will be at least 2000 times that present after the more conventional 120-day cooling. In addition, there will be a much greater quantity of total iodine (predominantly ^{129}I) in high-burnup fast reactor fuels (core) than in the relatively low-burnup thermal fuels now being processed. Consequently, the behavior of iodine in, for example, the dissolver and the solvent extraction systems must be considered when the optimum chemical flowsheet and the equipment design for a processing plant are chosen.

Other workers have reported that from 30 to 95% of the ^{131}I is volatilized when metal fuels are dissolved in nitric acid. We are studying the dissolution of unirradiated UO_2 in nitric acid with iodine present to obtain a better understanding of iodine behavior under a variety of dissolution conditions and equipment arrangements. Two general approaches are being considered: (1) control of conditions during fuel dissolution and feed adjustment so that essentially all the iodine is evolved from the dissolver solution into a small volume of gas from which it can be efficiently removed and (2) control of conditions so that essentially all the iodine remains in the aqueous solution during the dissolution and solvent extraction operation and, finally, decays in the raffinate. Since elemental iodine volatilizes readily from hot nitric acid, the second method would require addition of a holding reductant to retain the iodine in solution (as iodide ion) or oxidation of the iodine to retain it as the iodate. Converting the iodine to the reduced form (the iodide) and holding it in solution in that form during dissolution do not appear practicable since the iodide and any holding reductant would be oxidized readily by the hot nitric acid. Similarly, initial tests indicate that converting all the iodine in the system to the iodate would be a difficult task. Up to 60% of the iodine was converted to the iodate in laboratory dissolution tests using extreme conditions (11 *M* HNO_3 containing H_2O_2); higher conversions could undoubtedly be obtained, although whether this would be practicable on a commercial scale is questionable. In addition, recent tests have shown that treatment of the feed solution with nitrite to reduce Pu(VI) to Pu(IV) prior to solvent extraction reduces some of the iodate to elemental iodine. For these reasons, therefore, the present emphasis in our experimental work involves the removal of essentially all the iodine from the feed solution[5] prior to solvent extraction.

Our initial tests show that, when unirradiated UO_2 microspheres are dissolved in boiling 5 to 8 *M* HNO_3 containing KI (and ^{131}I tracer), essentially all the iodine is retained in the dissolver and updraft reflux condenser if no gas stream is passed through the system. The iodine volatilizes readily and forms a visible deposit on a small area of the cold surface of the condenser. When the UO_2 is dissolved with an air stream entering the vapor space of the dissolver (and subsequently passing through the condenser), the iodine volatilizes rapidly during the initial stages of dissolution and deposits on the condenser as before, but then it is eventually carried out of the system in the off-gas. More than 99% of the iodine initially present in the dissolver solution has been removed by this procedure. Iodine removal is favored by operation without a reflux condenser. In a test without a condenser, 99.93% of the iodine was evolved during dissolution. The dissolution temperature in this test was kept below 90°C to avoid evaporating a significant volume of solution from the dissolver. Near the end of the run, KI was added to reduce any iodate in the solution to elemental iodine, and

[5]The decay of fission product ^{132}Te (half-life, 3.3 days), which yields 2.3-hr ^{132}I, is a complicating factor in treating very short-cooled fuels. After a 30-day cooling period, the activity of ^{132}Te would be about 4% of the ^{131}I activity. Even if all the iodine is evolved (or fixed as the iodate) during dissolution and feed adjustment, ^{132}I will grow back rapidly from the ^{132}Te present in the solution. This potential problem, of course, rapidly becomes less important as the cooling time is increased.

nitrite was subsequently added to oxidize any residual iodide to elemental iodine. These results are encouraging but must be confirmed in hot-cell tests where the iodine will be derived from irradiated fuels. To date, highly efficient removal of iodine during dissolution has not been achieved in hot-cell tests (see above). This may be the result of certain differences in dissolution procedures and equipment design for the hot-cell tests, as compared with laboratory tests. On the other hand, it may indicate that at least some of the iodine in irradiated fuels is present in a chemical form other than I^-, I_2, or IO_3^- (e.g., as organic iodide).

Dissolution of UO_2 in Nitric Acid–Peroxide Solution. – When UO_2 dissolves in nitric acid, oxides of nitrogen are released, thereby complicating off-gas handling procedures. In a recent test, UO_2 microspheres dissolved readily in 3.6 *M* HNO_3–0.8 *M* H_2O_2, and analyses of the final solution for nitrate showed that the loss of nitrogen oxides from the dissolver was negligible. No brown fumes were observed at any time during the dissolution. The amount of H_2O_2 used in this test was 2.8 times the stoichiometric amount required to oxidize the UO_2 (on a mole:mole basis). Dissolution began when the temperature was below 50°C. The UO_2 was completely dissolved in 45 min, during which time the temperature was raised to 86°C. Dissolution of UO_2 under the same conditions but without the peroxide was much slower.

2.4 SOLVENT EXTRACTION WITH TBP

Initial emphasis in the solvent extraction studies has been on establishing flowsheet conditions for the interim processing of fast reactor fuels in an existing plant.[2] The first-cycle solvent extraction flowsheet is based on the use of 15% TBP and feeds of subcritical concentrations (≦5.0 g of fissile plutonium per liter) in existing geometrically unrestricted equipment. The overall process calls for coextraction and partitioning of plutonium from uranium in the first cycle, followed by a TBP cycle and an ion exchange cycle for further purification of the plutonium.

Extraction of Plutonium

Depending on dissolution conditions, a large fraction of the plutonium in the dissolver solution may be hexavalent and will require reduction to the more extractable Pu(IV). British[6] and French[7] studies indicate that adjusting the plutonium, quantitatively, to the quadrivalent state and maintaining it in that form in a high radiation field are difficult. It seems reasonable to assume that a small percentage of the plutonium in the solvent extraction feed may be present as Pu(VI) and that the Pu(VI) will be more important than the Pu(IV) in controlling the plutonium recoveries. Since adequate Pu(VI) and Pu(IV) extraction data (particularly at high solvent loadings) were not available, we obtained data with 15% TBP–*n*-dodecane as a function of nitric acid and uranium concentrations.

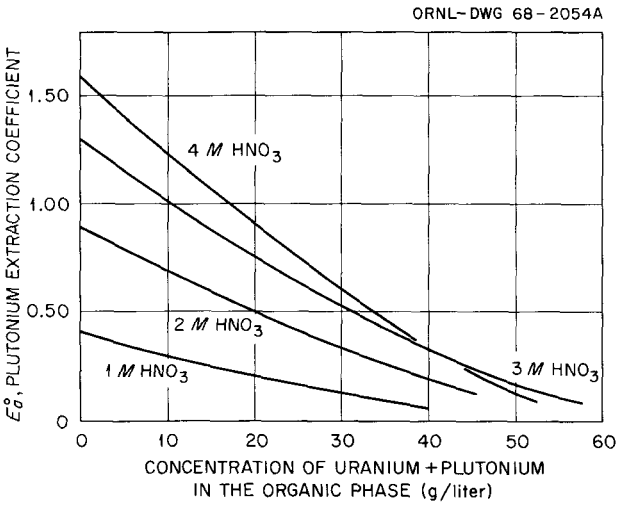

Fig. 2.8. Extraction of Pu(VI) from HNO_3 with 15 vol % TBP in *n*-Dodecane. Data obtained in extractions at a phase ratio of 1:1 from HNO_3 containing 1 to 10 g of Pu(VI) and 0 to 100 g of uranium per liter.

At low solvent loadings, the Pu(VI) extraction coefficients (Fig. 2.8) from 2 *M* HNO_3 (specified scrub acid concentration in our present flowsheet) and 3 *M* HNO_3 (extraction section acid concentration) were about 0.8 and 1.3 respectively. For comparison, Pu(IV) coefficients at these acid concentrations were 2.2 and 4.2, or about three times those for Pu(VI) (Fig. 2.9). Increasing the metal loading of the solvent to 45 g/liter decreased the

[6] D. M. Donaldson, K. Hartley, P. Lees, and N. Parkinson, "Reprocessing Fast Reactor Fuels at Dounreay," *Trans. Met. Soc. AIME* **227**, 191–202 (1963).

[7] *Semiannual Report of the Department of Chemistry, Centre d'Etudes Nucléaires, Fontenay-aux-Roses, November 1965–May 1966.*

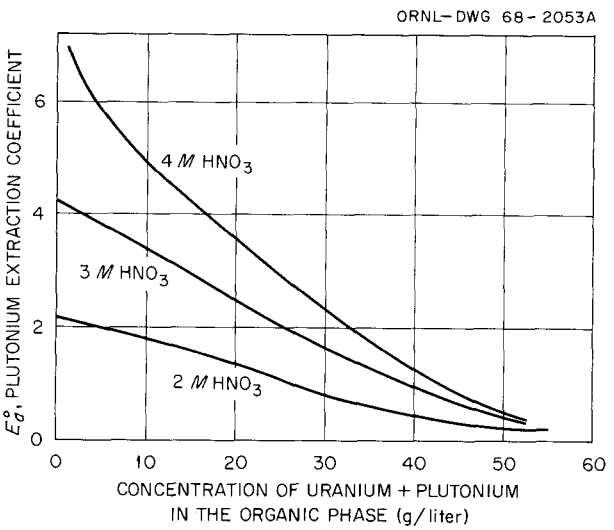

Fig. 2.9. Extraction of Pu(IV) from HNO_3 with 15 vol % TBP in *n*-Dodecane. Data obtained in extractions at a phase ratio of 1: 1 from HNO_3 containing 1 to 10 g of Pu(IV) and 0 to 100 g of uranium per liter.

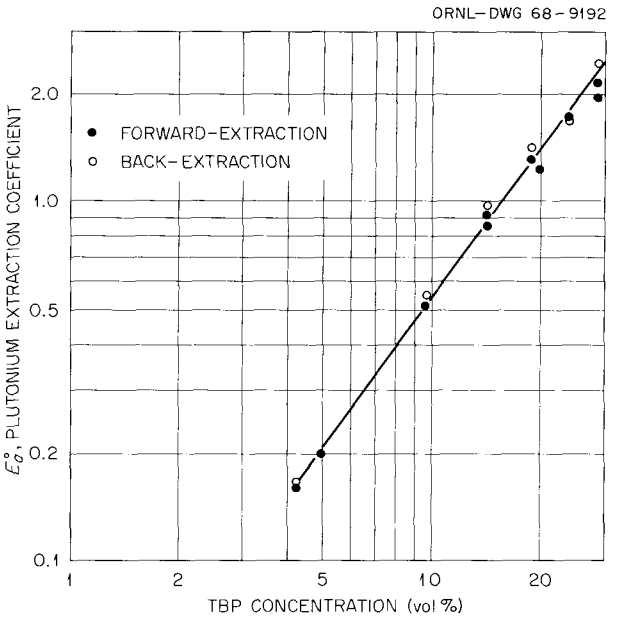

Fig. 2.10. Effect of TBP Concentration on the Extraction of Pu(VI) from 2 *M* HNO_3. Back-extraction data were obtained by contacting an extract with 2 *M* HNO_3. Plutonium concentration in the solvent at equilibrium was 0.3 to 0.6 g/liter in each test.

Pu(VI) and the Pu(IV) extraction coefficients from 2 *M* HNO_3 to about 0.1 and about 0.3 respectively. These data indicate that, in treating feeds containing a significant fraction (e.g., 10%) of the plutonium as Pu(VI) by the proposed flowsheet, the metal content of the solvent leaving the scrub section must be limited to less than 39 g/liter (i.e., to less than 60% of the theoretical loading limit of 0.5 mole of metal per mole of TBP). Otherwise, the plutonium reflux will be excessive, resulting in high plutonium losses. Even with all the plutonium in the quadrivalent state, the solvent loading should probably be limited to 65% of the theoretical maximum in order to avoid excessive plutonium reflux.

Study of the effect of TBP concentration, in the range of 4 to 30 vol %, on the extraction of Pu(VI) from 2 *M* HNO_3 showed that the extraction coefficient is directly proportional to about the 1.4 power of the TBP concentration (see Fig. 2.10).

Data were also obtained for the extraction of Pu(VI) with dibutyl butylphosphonate (DBBP), an extractant that is a potential alternative to TBP. In extractions from 2 *M* HNO_3 with 15 vol % DBBP in *n*-dodecane, extraction coefficients varied from 8.5 at low solvent loadings to 0.95 at a solvent loading of 50 g of (U + Pu) per liter. These coefficients are higher, by about a factor of 10, than those for TBP at equivalent solvent loadings. Of course, DBBP has the disadvantage of being less responsive than TBP to dilute acid stripping of uranium and plutonium.

Batch Countercurrent Tests

Several batch countercurrent runs were made in a glove box to demonstrate the first extraction cycle (coextraction of uranium and plutonium with 15% TBP) with feeds containing different amounts of Pu(VI). The uranium and total plutonium concentrations were 65 and 7 g/liter respectively. The nitric acid concentration was 3 *M* in the feed and 2 *M* in the scrub solution. Eight extraction and three scrub stages were used. With a feed containing less than 2% of the plutonium as Pu(VI) and a solvent/feed ratio of 1.8/1, the plutonium (as well as the uranium) recovery was greater than 99.9%. When about 10% of the plutonium was in the form of Pu(VI), a solvent/feed ratio of 2.1/1 was required to give a plutonium recovery of about 99.9%. An attempt to operate with this feed and a solvent/feed ratio of 1.6/1 demonstrated convincingly, as predicted from the data in Figs. 2.9 and

2.10, that the reflux and loss of plutonium would be excessive under these conditions.

Second-Cycle Studies. – Because of the large amount of plutonium present, the use of ferrous sulfamate for reducing plutonium in the partitioning cycle results in a second-cycle feed containing sulfate at a relatively high concentration (0.3 to 0.4 *M*). Sulfate at concentrations in this range interferes severely with the second-cycle extraction of plutonium by TBP. This interference was overcome by salting the feed with 0.6 *M* $Al(NO_3)_3$ and operating with a relatively low plutonium loading of the solvent. Use of a plutonium reductant that does not contribute sulfate (see Sect. 2.5), however, should provide a much better solution to this problem.

2.5 PARTITIONING

Ferrous sulfamate is used to reduce plutonium in the partitioning cycle in reprocessing plants employing the Purex process. However, its use in fast reactor fuels processing would add large amounts of iron and sulfate to the system because of the large amounts of plutonium present. The sulfate interferes with plutonium extraction in the second TBP cycle (Sect. 2.4), and, in addition, both iron and sulfate would add significantly to the solids content of the waste and thereby limit desirable volume reductions. We are evaluating alternative reductants, including uranous nitrate, which has been studied extensively, particularly in Europe. Other reductants that have shown promise in preliminary tests at ORNL are ferrous nitrate and hydrogen gas.

The use of ferrous nitrate (instead of ferrous sulfamate) avoids the problems caused by sulfate. A small amount of a holding reductant (capable of destroying nitrite) such as hydrazine is necessary to stabilize the Fe^{2+} and to avoid reoxidation of the plutonium. The plutonium reduces very rapidly. More than 99% of the plutonium was stripped from the solvent in 1 min when it was contacted with one-seventh volume of 0.25 *M* $Fe(NO_3)_2$ (two equivalents of Fe^{2+} per equivalent of Pu^{4+}) containing hydrazine, hydroxylamine, sulfamic acid, or hydroquinone (Table 2.4). Excellent results were obtained in a batch countercurrent test demonstrating the use of ferrous nitrate–hydrazine as the reductant. In a system with four partitioning and five uranium reextraction stages, the stripping of plutonium was greater than 99.99% complete; the Pu/U and U/Pu decontamination factors were 5×10^5 and 1×10^4 respectively (see Fig. 2.11). It should be noted that the amount of holding reductant needed in actual process practice would depend on the amount of nitrite produced in the system under process conditions. Hot-cell tests are being run to determine whether effective partitioning can be achieved at high radiation levels.

Table 2.4. Reductive Stripping of Plutonium with Ferrous Nitrate

Organic: 15% TBP in *n*-dodecane containing 4.4 g of Pu(IV) and 40 g of uranium per liter
Aqueous: 0.2 *M* HNO_3 and reductants as shown
Contact: Batch contact at organic/aqueous phase ratio of 7/1

Reductant	Plutonium Stripped (%)		
	1 min	5 min	30 min
0.25 *M* ferrous nitrate	74	71	71
0.25 *M* ferrous nitrate–0.025 *M* sulfamic acid	>99	>99	99
0.13 *M* ferrous nitrate–0.025 *M* sulfamic acid	98.4	98.3	
0.25 *M* ferrous nitrate–0.025 *M* hydrazine	>99	>99	>99
0.13 *M* ferrous nitrate–0.013 *M* hydrazine	98.0	98.3	
0.25 *M* ferrous nitrate–0.025 *M* hydroxylamine nitrate	99	>99	>99
0.25 *M* ferrous nitrate–0.025 *M* hydroquinone	>99	>99	

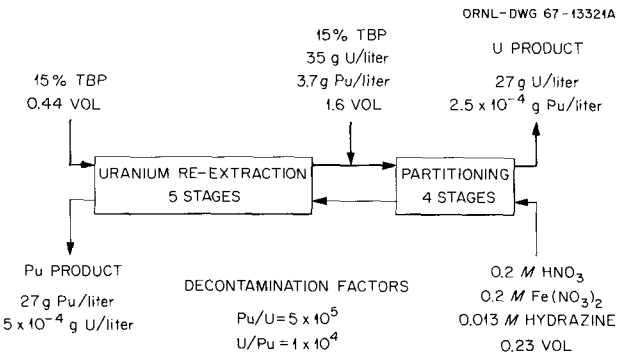

Fig. 2.11. Batch Countercurrent Test of Plutonium-Uranium Partitioning with Ferrous Nitrate plus Hydrazine.

Reduction of Plutonium with Hydrogen

Plutonium was reduced by passing the solvent extract and 4% H_2–argon cocurrently with dilute HNO_3 (containing a small amount of hydrazine) up through a column of platinized alumina.[8] In tests with 30% TBP in *n*-dodecane (loaded with 80 g of uranium and 16 g of plutonium per liter), using a 37-cm-long column having a cross-sectional area of 3 cm^2, operation was satisfactory with an organic flow of 2 to 3 ml/min, an aqueous flow of 0.5 to 1.5 ml/min, and a gas flow of 100 to 400 ml/min. With these conditions, 90 to 95% of the plutonium was stripped into the aqueous phase. The residence time of the solutions in this small column was only a few seconds; more efficient stripping might be expected with a longer column. Sufficient data have been accumulated to indicate that this partitioning method shows promise. Experimental work on hydrogen reduction has been terminated, pending results of an engineering-scale comparison of the different partitioning methods.

2.6 SOLVENT STABILITY

Because of the expected high burnup of fast reactor fuels and the economic desirability of processing them after short cooling periods, the aqueous feeds to solvent extraction will have high radiation power densities. It is known that solvent degradation products (TBP hydrolysis products and nitration products of both TBP and the hydrocarbon diluent) can decrease separations from fission products, increase plutonium retention by the solvent, and contribute to "crud" and emulsion formation. Consequently, we are making a thorough study of the system to obtain a better understanding of the extent of solvent damage that may occur (during the processing of fast reactor fuels) and its effect on process performance. As the first step in this study, past laboratory studies and production experience concerning solvent stability were reviewed and assessed.[9] Most of the available information was found to have little or no value in predicting solvent performance in the processing of short-cooled high-burnup fuels.

A study[10] by E. L. Nicholson showed that, in spite of the high activity of the aqueous feed, the radiation dose to the solvent in pulsed-column processing of fast reactor fuels (average burnup, 40,000 Mwd/metric ton; cooling period, 30 days) should be relatively low (<0.1 whr $liter^{-1}$ $cycle^{-1}$). This reassuring estimate, coupled with the favorable results obtained recently in cyclic irradiation tests, leads us to the preliminary conclusion that problems arising from solvent radiation damage sustained during the treatment of short-cooled high-burnup fuels will be minimal.

Cyclic Solvent Irradiation Tests

In most of the solvent irradiation tests described in the literature, the solvent was first given a relatively large radiation exposure (in some cases, without nitric acid present), and then its extraction characteristics were evaluated. Unfortunately, results of such tests are not useful for predicting solvent performance in an actual process system in which the solvent receives a relatively small dose in each cycle and is washed between cycles to remove degradation products. We are trying to simulate process conditions more closely in cyclic tests in which: (1) 15% TBP in *n*-dodecane is mixed with 0.4 *M* $UO_2(NO_3)_2$–3 *M* HNO_3 while being irradiated by a ^{60}Co source (to simulate the extraction step), (2) the uranium is stripped from the extract with dilute nitric acid, and (3) the stripped solvent is washed with 0.3 *M* Na_2CO_3 solution. Samples of the irradiated solvent are withdrawn during each cycle for characterization tests with respect to fission product extraction, extraction and retention of plutonium, etc.

We have completed three cyclic tests in which the solvent was irradiated in increments of 0.3, 1.0, or 2.0 whr $liter^{-1}$ $cycle^{-1}$ until the integrated radiation doses reached 6 to 10 whr/liter. In each test, phase separations were rapid and well defined; no formation of solids was observed. The 0.3 whr $liter^{-1}$ $cycle^{-1}$ exposures (several times higher than estimated for processing short-cooled high-burnup fuels) had no observable effect on the solvent. Results obtained from the extraction and stripping of uranium and plutonium, and from the

[8] R. H. Rainey, "Hydrogen Reduction of Pu(IV) to Pu(III)," *Nucl. Appl.* 1(4), 310 (1965).

[9] C. A. Blake, Jr., *Solvent Stability in Nuclear Fuel Processing: Evaluation of the Literature, Calculation of Radiation Dose, and Effects of Iodine and Plutonium*, ORNL-4212 (March 1968).

[10] E. L. Nicholson, *Preliminary Investigation of Processing of Fast-Reactor Fuel in an Existing Plant*, ORNL-TM-1784 (May 8, 1967).

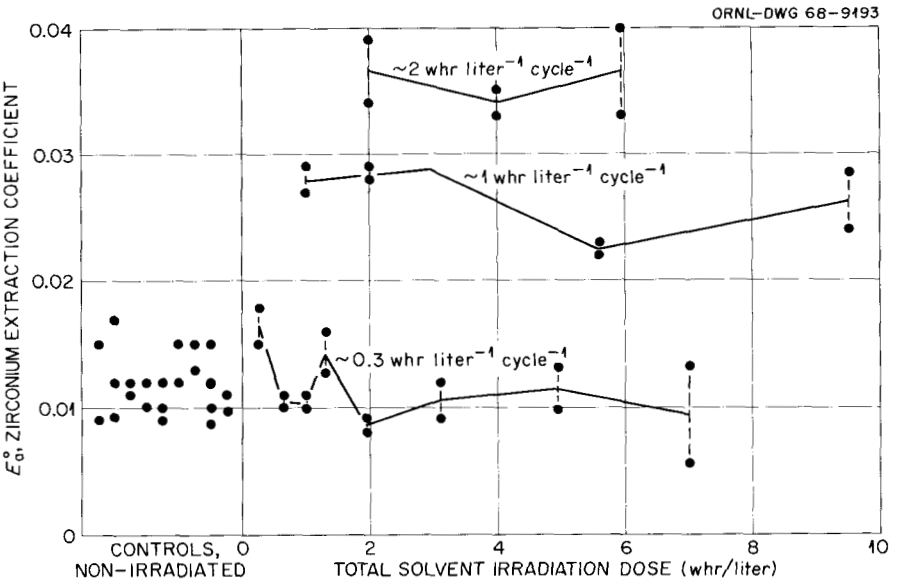

Fig. 2.12. Extraction of ^{95}Zr by Irradiated 15 vol % TBP–*n*-Dodecane. *Extractions were from 3 M* HNO_3 containing 0.9 g of Zr, ^{95}Zr-Nb tracer, and uranium (to maintain solvent uranium loading at 35–40 g/liter).

extraction of ruthenium and zirconium, were essentially identical to those obtained in comparative tests with unirradiated solvent. At the higher exposures per cycle, the only observed change was an increase in the extraction of ^{95}Zr (Fig. 2.12) and a slight increase in the retention of uranium by the irradiated solvent. Although the data were somewhat scattered, the average zirconium extraction coefficient obtained with unirradiated solvent was 0.013; average coefficients of 0.011, 0.027, and 0.036 were obtained when the exposures per cycle were 0.3, 1.0, and 2.0 whr/liter respectively. At the two highest exposure levels, the zirconium extraction coefficients did not increase with cycling; this indicated that the degradation products (presumably, mostly dibutylphosphoric acid) responsible for the increased zirconium extraction had been effectively removed by the alkaline wash treatment.

At each radiation level, more than 99.99% of the uranium was stripped by contacting the uranium extract with five 0.5 volumes of 0.01 *M* HNO_3. In the characterization tests, the plutonium retention was verified by loading the uranium-containing solvent from the irradiation contact with about 0.5 g of plutonium per liter and stripping the plutonium by contacting this extract three times with 0.1 *M* $Fe(NH_2SO_3)_2$–0.17 *M* HNO_3. In each case, at least 99.99% of the plutonium was stripped by this procedure. Ruthenium extractions were made from 3 *M* HNO_3 solution containing 0.3 g of ruthenium per liter, ^{106}Ru tracer, and sufficient uranium to maintain a solvent uranium loading of 35 to 40 g/liter. Ruthenium extraction coefficients with irradiated solvent were about 0.002; this value was equal to, or slightly less than, the coefficients obtained with nonirradiated solvent.

Stability of TBP and Precipitation of Its Decomposition Products

As part of the study of the stability of TBP in nuclear fuel processing, we are measuring the rate of decomposition of TBP when it is dissolved (to saturation) in aqueous 1 to 5 *M* HNO_3. In addition, we are measuring the rates of precipitation of some of the fission product cations (such as zirconium) with dibutylphosphate (DBP) and monobutylphosphate (MBP). Each of these butylphosphates is produced by the radiolytic and thermal decomposition of TBP. The initial precipitation experiments were made with a single-phase (aqueous-phase) system. Later we will study the two-phase system.

The kinetics of precipitation of ferric dibutylphosphate were determined from aqueous 1, 3, and 5 *M* HNO_3 solutions. Using an initial concentration of 231 mg of Fe^{3+} per liter (4.1 m*M*) and 3.06

or 1.53 g of HDBP per liter (14.6 or 7.3 m*M*), it was found[11] that the Fe^{3+} concentration (*C*, moles/liter), as determined by the use of ^{59}Fe tracer, could be expressed in terms of an integrated form of the rate equation

$$dC/dt = -k(C - S_{Fe})^n . \quad (1)$$

Here we assumed that the reaction is:

$$Fe^{3+} + 3HDBP \rightleftharpoons Fe(DBP)_3 + 3H^+ . \quad (2)$$

The order of the reaction, *n*, is approximately 2; the solubility of ferric ion, S_{Fe}, increases with increasing acidity; and the rate constant, *k*, is of the order 10^{-3} to 10^{-2} when time is expressed in minutes. The value of the solubility product $[Fe^{3+}] \times [DBP^-]^3$ increases from about 2×10^{-13} to 2×10^{-12} (mole/liter)^4 as the nitric acid concentration increases from 1 to 5 *M*.

We have initiated studies of the precipitation of zirconium dibutylphosphate in 1 to 5 *M* HNO_3. The rate of precipitation of zirconium dibutylphosphate is so rapid that we have not yet been able to obtain kinetic data for it. For example, three tests with initial HDBP concentrations of 0.1, 0.316, and 1.0 g/liter, respectively, were made; the solutions were 1 *M* in HNO_3 and contained 231 mg of zirconium per liter. In each test, precipitation was essentially complete when the first sample was withdrawn for ^{95}Zr-Nb analyses. Visually, precipitation appears to be complete in about 5 sec. This rate is much faster than that observed for ferric dibutylphosphate (e.g., several minutes to several tens of minutes were required for half of the iron to precipitate).

Solubilities of zirconium in the two solutions initially containing 0.316 and 1.0 g of HDBP per liter in 1 *M* HNO_3 were about 160 and 28 mg/liter respectively. In both tests the mole ratio of HDBP initially present to zirconium precipitated was about 2; this suggests that the precipitate may have the composition $ZrO(DBP)_2$. However, it was noted that the amount of precipitate reached a minimum at times on the order of 5 to 30 min after the zirconium and HDBP solutions were mixed, thereby indicating a change in the composition of the precipitate.

[11] W. Davis, Jr., and D. O. Rester, "Kinetics of Precipitation of Ferric Dibutylphosphate from Aqueous HNO_3 Solutions," accepted for publication in the *Journal of Inorganic and Nuclear Chemistry*.

Quantitative determinations of HDBP, H_2MBP, and H_3PO_4 have been the most uncertain features of studies of the thermal or radiolytic decomposition of TBP. Hardy[12] showed that these products can be determined by gas chromatography if they are first converted to the corresponding methyl esters by reaction with an ethereal solution of diazomethane. We have adapted this technique to the measurement of quantities of TBP decomposition products formed in aqueous nitric acid solution. To avoid consumption of gross amounts of diazomethane with nitric acid, we first freeze about 10 cc of the solution and remove both water and nitric acid by sublimation in a vacuum system. About 10 to 15 cc of 0.1 *M* CH_2N_2 in ether is added to the residue from the sublimation step, and, preferably before all of the ether has evaporated, we add a carefully measured volume (usually 1 cc) of distilled TBP to serve as an internal standard in the gas chromatographic technique. From this standard we subsequently obtain the numbers of moles of methyl dibutylphosphate (MDBP), dimethyl monobutylphosphate (M_2MBP), and trimethyl phosphate (TMP) that are produced, respectively, from HDBP, H_2MBP, and H_3PO_4.

On the basis of three sets of calibrations with known quantities of the three acids (originally in 1 *M* HNO_3 solution), separately and combined, we have drawn the following conclusions: (1) Six- to thirty-two-milligram quantities of HDBP are converted to MDBP with an overall yield and standard deviation of 71 ± 2% and with an uncertainty of ±0.95 mg. (2) Two- to eleven-milligram quantities of H_2MBP are converted to M_2MBP with a yield of 75 ± 8% and with an uncertainty of ±1.5 mg. (3) One- to five-milligram quantities of H_3PO_4 are converted to TMP with a yield of only 39 ± 4% and an uncertainty of ±0.31 mg. These values are sufficiently accurate to permit us to obtain adequate data on the decomposition of TBP dissolved in aqueous HNO_3 solutions.

Two tests have been performed to measure the rate of decomposition of TBP in 3 *M* HNO_3 at 50°C; the gas chromatographic technique described above was used to measure the quantities of acid decomposition products. Although reproducibility was not good, we found the TBP decomposition rate to be on the order of 7×10^{-3} millimole liter^{-1} hr^{-1}, or somewhat less than 2 mg liter^{-1}

[12] C. J. Hardy, *J. Chromatog.* **13**, 373–76 (1964).

hr^{-1}. In these tests, in which stirring was employed, 0 to 0.5 ml of TBP was usually in contact with 300 ml of nitric acid solution (to maintain saturation with respect to TBP).

As an extension of these studies of the thermal decomposition, we have now assembled equipment for measuring the combined rate of thermal and radiolytic decomposition of TBP dissolved in nitric acid solutions.

Reaction of Iodine with the Solvent

Relatively large amounts of iodine will be present in high-burnup fuels, with ^{131}I constituting about 0.2% of the total iodine in 30-day-cooled fuel. We expect to remove most of the iodine from the fuel in a head-end treatment (Sect. 2.2) or during dissolution (Sect. 2.3). Nevertheless, it is important to understand the behavior of iodine in the solvent extraction system since quantitative iodine removal may not be possible in these earlier processing steps. In addition, unless these steps also quantitatively remove tellurium, radioactive ^{132}I will grow back rapidly into the fuel solution from its precursor, ^{132}Te.

Elemental iodine is rapidly, and almost quantitatively, extracted into the solvent (TBP–*n*-dodecane) phase. Also, any iodide ion in the aqueous phase is oxidized rapidly to elemental iodine and subsequently extracted into the solvent. The rapid oxidation presumably is related to the ease of extraction (into TBP) of the oxidant nitrous acid, which is usually present in low concentration in nitric acid. Neither iodate nor periodate ions are extracted. Elemental iodine is stripped readily from the organic extract by scrubbing it with dilute sodium carbonate solution; it can be stripped slightly more efficiently with dilute solutions of sodium thiosulfate or carbonate-thiosulfate mixtures.

Elemental iodine in the extractant phase eventually reacts with the organic molecules, apparently to form alkyl iodides. These compounds are not stripped with carbonate or thiosulfate solutions. We have initiated a program to study the variables affecting the reaction, to identify the products, and to develop methods for removing the products from the organic phase. In one test, in which 10^{-3} *M* iodine (traced with ^{131}I) was extracted from 3 *M* HNO_3 into a 20% TBP solution in *n*-dodecane, 10% of the extracted iodine could not be stripped from the extract with 0.05 *M* aqueous sodium thiosulfate 1 hr after the extraction. Such behavior indicated that this fraction of the total iodine had already reacted to form alkyl iodides. The amount increased to 30% after one day and to 80% after one week. Alkyl iodides are known to have limited stabilities in alkaline systems, and these stabilities vary with structure. In one test, 70% of the bound iodine was removed by contacting the one-day-old organic extract (described above) for 2 hr with 0.5 *M* KOH in methanol.

2.7 EXTRACTION OF PLUTONIUM WITH AMINES

Studies of long-chain amines for use in extracting plutonium were continued. Extraction with amines is a potential alternative to extraction with TBP in the first plutonium purification cycle and is also a potential alternative to ion exchange processing for final purification of the plutonium. Our earlier interest[13] was principally concerned with the first-cycle application, since the radiation degradation products from long-chain amines are reportedly less troublesome than those of TBP. However, radiation damage to TBP, even during the treatment of short-cooled high-burnup fuels, does not now appear to represent a difficult process problem (Sect. 2.6), and the use of TBP in the first cycle for co-recovery of the plutonium and uranium (conventional Purex process) should be satisfactory. Consequently, emphasis in the amine studies has been shifted to evaluating the use of these amines for final purification of the plutonium. For this purpose, secondary amines may be particularly attractive since they can be stripped with dilute acid to give a plutonium product solution that possibly can be fed directly to the process (e.g., sol-gel) for reconstituting the fuel. Also, the chemical degradation products of secondary amines should be less troublesome than those of, for example, trilaurylamine.

Curves showing the extraction of Pu(IV) from 5 *M* HNO_3 with 0.3 *M* solutions of four different branched secondary amines in diethylbenzene are shown in Fig. 2.13. At low solvent loadings, the extraction coefficients were about 11, 6, 3, and 2, respectively, for di(tridecyl)amine, Amberlite LA-1, *N*-benzylheptadecylamine, and Amine S-24. The

[13] *Chem. Technol. Div. Ann. Progr. Rept. May 31, 1967*, ORNL-4145, p. 55.

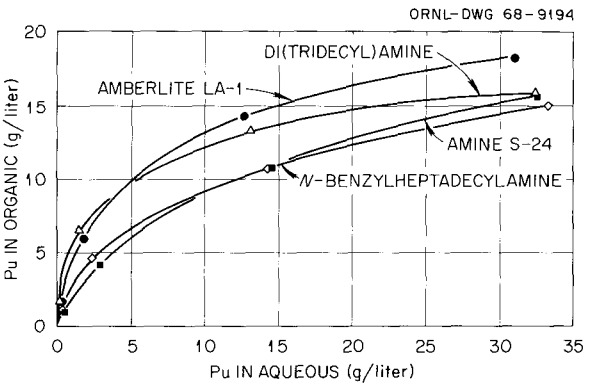

Fig. 2.13. Extraction of Pu(IV) from 5 *M* HNO_3 with 0.3 *M* Amino Solutions in Diethylbenzene.

maximum plutonium loading of the solvent phase (~30 g of plutonium per liter in the aqueous phase) was about 18 g/liter for Amberlite LA-1, as compared with 15 to 16 g/liter for the other three amines. Each of these amines has sufficient extraction power to allow essentially complete recovery of plutonium in a reasonable number of stages (<6). These amines are also being comparatively evaluated from the standpoint of other pertinent properties (amenability to stripping, selectivity, phase separation, etc.).

Sulfate may be present in the aqueous feed to the amine process if ferrous sulfamate or sulfuric acid is used for stripping plutonium from TBP in prior extraction cycles. Comparison of the extraction data of Fig. 2.13 with data for plutonium extractions from 5 *M* HNO_3–0.15 *M* H_2SO_4 (data not shown) show very little interference from sulfate. At low solvent loadings the extraction coefficients were essentially the same, regardless of whether sulfate was or was not present. Maximum solvent loadings were 5 to 15% higher, however, from the sulfate-free solutions.

Extraction of Pu(VI)

In extractions of Pu(VI) from HNO_3–$UO_2(NO_3)_2$ solutions [5 *M* in total NO_3^- and containing 1 g of Pu(VI) per liter and 0 to 75 g of U(VI) per liter] with 0.3 *M* di(tridecyl)amine in diethylbenzene, the plutonium extraction coefficients were about 0.3, showing no variation with changes in uranium concentrations in the aqueous (and solvent) phase. Coefficients obtained with 0.3 *M* solutions (in diethylbenzene) of the tertiary amine Adogen-363 and the quaternary amine Adogen-464 were 6.2 and 9.1, respectively, with no uranium present and 1.6 and 5.0, respectively, at the maximum uranium concentration. These data indicate that, in using di(tridecyl)amine, essentially quantitative adjustment of the plutonium to the tetravalent state would be required. However, the tertiary or quaternary amines could be used successfully even if a significant fraction of the plutonium was present as Pu(VI).

3. Development of Processes for HTGR and LWR Fuels

3.1 HEAD-END MECHANICAL METHODS FOR PROCESSING HTGR FUEL

The engineering evaluation and development of the head-end portion of a processing flowsheet (Fig. 3.1) for the recovery of fissile and fertile particles from the Public Service of Colorado (PSC) HTGR graphite fuel block was continued by the investigation of: (1) hacksawing as a method for reducing the hexagon-shaped graphite fuel block (14 in. across the flats × 30 in. high) to a size suitable for feed to a hammer mill or crusher, (2) the crushing characteristics of an unfueled section of the PSC graphite fuel block, using a hammer mill, (3) a jet penetration technique, using high-pressure water as a possible method for removing unirradiated pyrocarbon-coated UO_2 and ThO_2 particles from a prototype PSC fuel stick, and (4) fluidized-bed burning and sizing.

Hacksawing

A preliminary investigation indicated that a hacksaw (Fig. 3.2) could be used to convert a Public Service of Colorado (PSC) graphite fuel block to pieces of suitable size for feed to a hammer mill or crusher. The unfueled graphite fuel block was a 12-in.-high section of a hexagonal-shaped PSC prototype measuring 14 in. across the flats. Three saw cuts were made across the block; each cut progressed vertically in a downward direction through rows of coolant holes, producing six pie-shaped pieces 12 in. long and 7.3 in. across the longest dimension. The distance between the coolant holes was $\frac{3}{4}$ in. Dust produced by the saw fell through the coolant holes and was removed from the cutting area, thereby producing ideal cutting conditions for a short-stroke hacksaw. At maximum operating speed, the saw easily cut through the 12-in.-thick block in 2.9 min. At this rate, a 30-in.-thick block could be sawed in 7.5 min. The amount of graphite removed by the saw in the 12-in. cut was equivalent to that in a rectangular slab of carbon $7\frac{3}{8} \times \frac{1}{8} \times 12$ in. (~ 11 in.^{3}).

Crushing

In an investigation of methods for crushing graphite fuels in preparation for fluidized-bed burning, two unfueled sections of a prototype PSC-type graphite fuel block (approximately $7 \times 7\frac{1}{4} \times 11\frac{3}{4}$ in.) were crushed in a Jeffery type A Swing Hammer Pulverizer. The resulting product was sieved, and the particle size distribution was determined (Table 3.1).

The largest piece in the $+\frac{3}{4}$ in. size fraction for run 2 was approximately $4 \times 2\frac{1}{2} \times 1$ in. The remainder of the pieces were $<2 \times 2 \times 2$ in. Increasing the width of the grate opening from $\frac{3}{4}$ in. to $2\frac{1}{2}$ in. resulted in a desirable decrease in the $-297\ \mu$ fraction. The graphite section was crushed in 6 sec at a calculated power of 11.8 hp. Additional testing is planned, using graphite fuel block sections fueled with unirradiated pyrocarbon-coated UO_2 and ThO_2 particles. Tests of unfueled sections will also be performed in the evaluation and testing laboratories of producers of commercial crushing and breaking equipment.

Jet Penetration

Tests were conducted, using the equipment shown in Fig. 3.3, to evaluate hydraulic jet penetration as a possible method for removing unirradiated pyrocarbon-coated UO_2 and ThO_2 particles from a prototype PSC fuel stick contained in a graphite sleeve. The prototype fuel stick contained 3.3 g of pyrocarbon-coated UO_2 particles ($<480\ \mu$ in diameter) and 61.7 g of pyrocarbon-coated ThO_2 particles ($>530\ \mu$ in diameter) bonded with a mixture

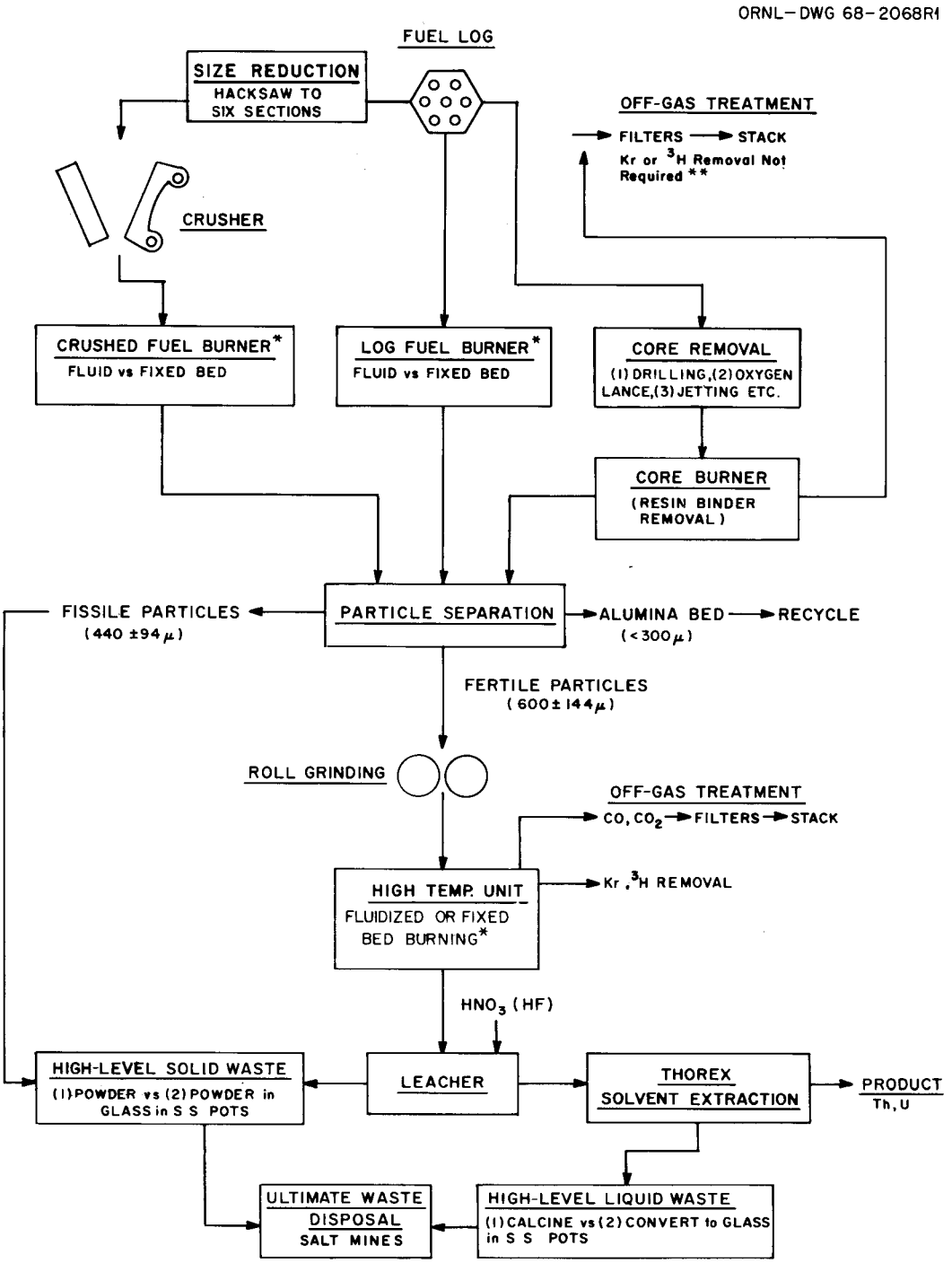

* GRIND LEACH NOT CONSIDERED SATISFACTORY
** Kr or ^{3}H NOT PRESENT BECAUSE OF SiC COATING ON ALL PARTICLES

Fig. 3.1. Fuel Processing and Waste Disposal Flowsheet for HTGR Fuels. Processing alternatives for Ft. St. Vrain and interim reference fuels, where all fuel particles have SiC coatings.

Table 3.1. Particle Size Distribution of a Pulverized Unfueled PSC Graphite Fuel Block

Device:	Jeffery type A Swing Hammer Pulverizer
Hammers:	10, $1\frac{1}{2}$ in. thick, spaced $1\frac{1}{2}$ in. apart, arranged 3, 2, 3, 2 on the periphery at 0, 90, 180, and 270°
Grating:	$\frac{3}{4}$- by $8\frac{5}{8}$-in. or $2\frac{1}{2}$- by $8\frac{5}{8}$-in. opening separated by $\frac{1}{2}$-in. bars
Clearance:	$\frac{1}{4}$ in. between hammer tips and grating
Rpm:	900
Hammer tip peripheral speed:	54 fps

Mesh Screen Size	Size Distribution of Product			
	Run 1[a]		Run 2[b]	
	Wt (g)	Wt (% of total)	Wt (g)	Wt (% of total)
$+\frac{3}{4}$ in.	222	3.53	1880	30.10
$\frac{3}{4}$ in./$\frac{1}{2}$ in.	1315	20.90	1597	25.50
$\frac{1}{2}$ in./4760 μ	2299	36.54	1411	22.60
4760 μ/1680 μ	992	15.77	566	9.05
1680 μ/840 μ	488	7.75	276	4.40
840 μ/590 μ	202	3.21	113	1.71
590 μ/297 μ	312	4.97	171	2.23
-297 μ	462	7.34	253	4.05

[a]Grate opening, $\frac{3}{4} \times 8\frac{5}{8}$ in.
[b]Grate opening, $2\frac{1}{2} \times 8\frac{5}{8}$ in.

of P-514 resin, 15 wt % graphite powder, and 10 wt % maleic anhydride and cured to 80°C (Table 3.2). The fuel stick was inserted into a graphite tube (1 in. OD × 0.5 in. ID × 12 in. long) and carbonized at 1000°C to simulate the PSC fuel. A general description of the microspheres is given in Table 3.2.

No erosion of the fuel stick occurred, and no particles were dislodged at an initial water pressure of 4000 psig or less. The nozzle used for these tests is $\frac{3}{8}$ in. OD and has seven 0.028-in.-diam holes. Four of the water jets were directed forward against the fuel stick, whereas three were directed to the rear and downward against the sides of the graphite tube. The high-pressure water was accumulated in a neoprene rubber bladder surrounded by nitrogen; the pressure decreased as the water was exhausted from the accumulator.

A fuel stick in a graphite sleeve was eroded at an average rate of 2 in./sec (26 cm^3 of H_2O per gram of particles plus binder) by water over a pressure range of 6000 to 4850 psig. The force exerted on the fuel stick by each jet is about 2 lb/in.^{3}. The particles were dried and then sized by screening (Table 3.3).

The resin binder adhered to some of the particles, and a considerable number of the pyrocarbon coatings were fractured (Fig. 3.4). The particles were leached with Thorex dissolvent (13 *M* HNO_3, 0.04 *M* F^-, 0.10 *M* Al^{3+}) to determine the number of particles fractured. Analysis of the leachate indicated that the pyrocarbon coatings on 24.8% of the UO_2 particles and 14% of the ThO_2 particles had been fractured. Tentative limits established for the fracture of these particles are 0.1 and 10% respectively.

In a similar test, a fuel stick was eroded at $2\frac{1}{2}$ in./sec with water (21 cm^3 of H_2O per gram of particles plus binder) in the pressure range 5100 to 3900 psig. The results were similar to those for

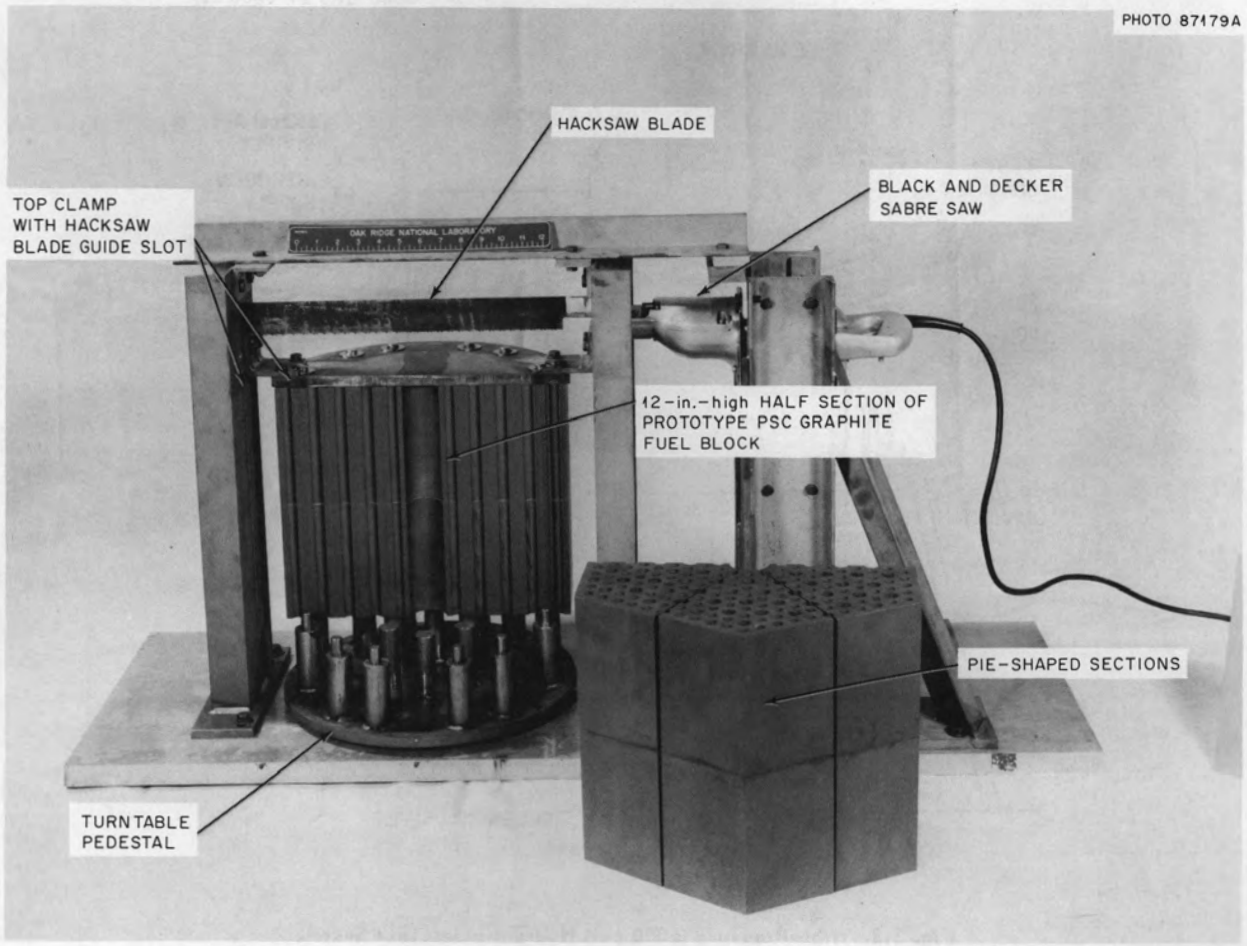

Fig. 3.2. Hacksaw Equipment Showing Pie-Shaped Sections and Unsawed Half of a Public Service of Colorado Graphite Fuel Block in Place. Blade: 21 × 1.75 × 0.090 in.; 6 teeth/in. Saber saw motor: Black and Decker, 115 v, 6 amp, six speeds, 480–2310 strokes/min, 1.25-in. stroke. Feed: gravity.

Table 3.2. Microspheres Used in Jet Penetration Studies

UO_2 Microspheres[a]		ThO_2 Microspheres[b]	
Coating	Thickness (μ)	Coating	Thickness (μ)
Inner porous carbon layer	40	Inner porous carbon layer	60
Dense carbon sealer layer	5	Dense carbon layer	40
SiC layer	30	Carbon sealer layer	5
Dense carbon layer	20	Sacrificial bonding layer	10
Outer carbon sealer layer	5		

[a]210 to 250 μ in diameter.
[b]330 to 360 μ in diameter.

ORNL DWG 67-5285 R2

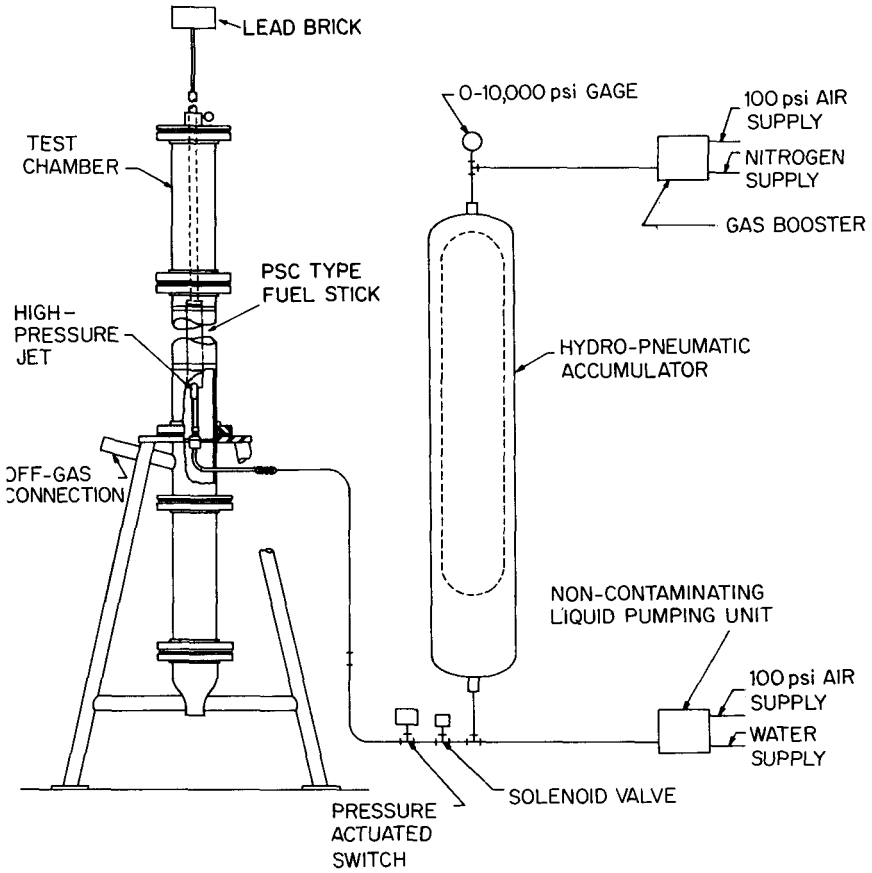

Fig. 3.3. High-Pressure (6000 psi) Hydraulic Jet Test System.

the previous test. The pyrocarbon coatings on 3.7% of the UO_2 particles and 13.8% of the ThO_2 particles were fractured.

The results of the tests with unirradiated fuel sticks indicate that particles removed by jet penetration cannot be separated by a single screening operation because the binder adheres to the coating and because excessive fracturing of the pyrocarbon coating occurs. Additional tests are planned when new fuel sticks become available.

Table 3.3. Particle Size Distribution of PSC Fuel After Jet Erosion Test

Sieve Fraction (Mesh)	Particle Size (μ)	Weight[a] (g)
+20	>840	3.3
20/30	840–590	39.9
30/35	590–500	15.9
35/50	500–297	8.2
−50	<297	5.1

[a]Overall material balance, 99.23%.

Combustion Studies with Unirradiated Fuel

Two fluidized-bed reactors (2- and 4-in. ID) that had been used previously in fluidized-bed volatility studies were modified to permit their use in HTGR burning studies. Tests of the instrumentation that measures the internal temperature of the bed and monitors the CO and CO_2 content of the off-gas stream have been completed. The components of a 5-in.-ID fixed-bed burner are available and may be installed to permit evaluation of this type of burner. We have begun to modify a 2-in.-diam

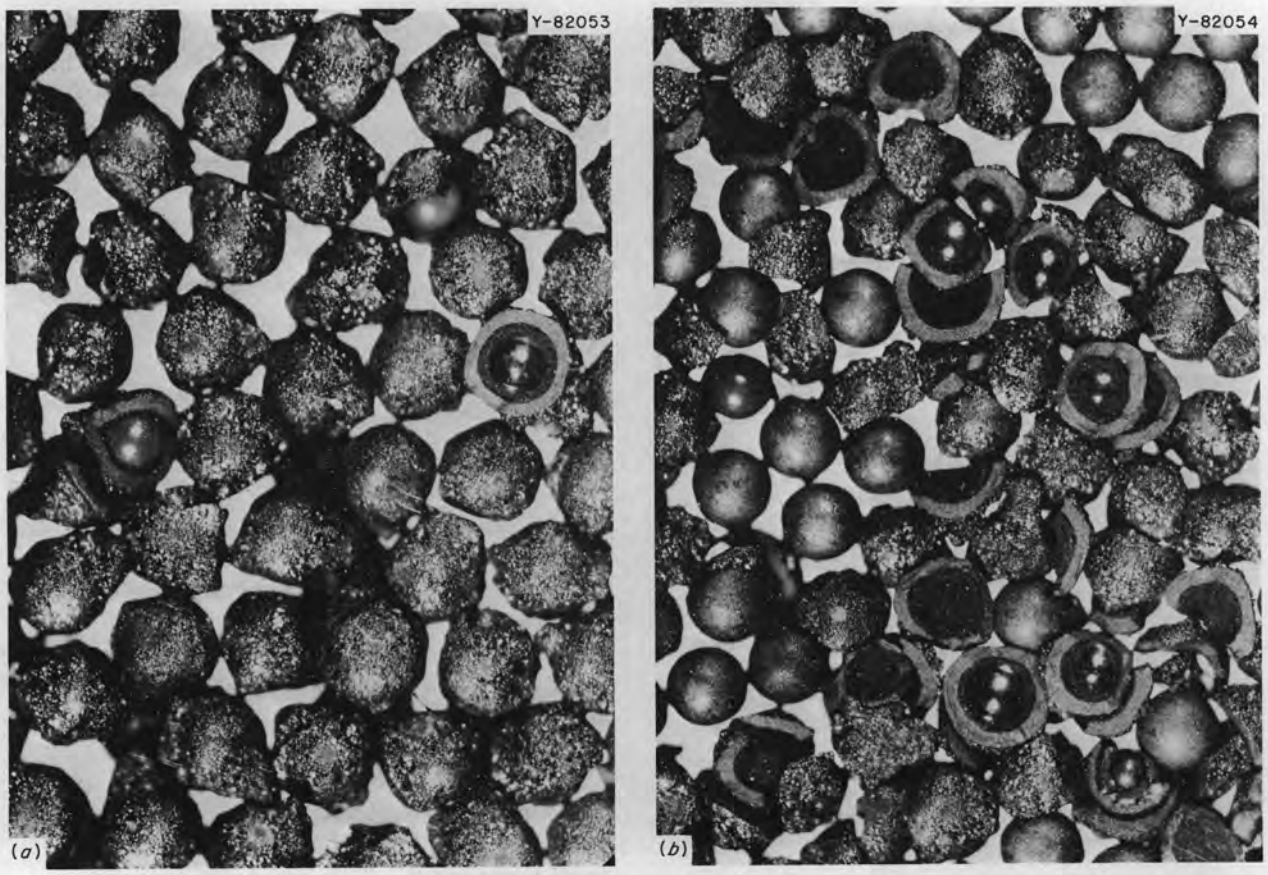

Fig. 3.4. Photomicrographs (33×) of Pyrocarbon-Coated UO_2 and ThO_2 Microspheres Removed from a Prototype PSC Fuel Stick, Using a High-Pressure Water Jet. (*a*) 30-to-35-μ fraction. (*b*) 35-to-50-μ fraction. Reduced 28%.

glass fluidized-bed column prior to the investigation of air classification as a method for separating the mixed aluminum, uranium, and thoria particles in the bed material (discharged from fluidized- or fixed-bed burners) into component fractions.

3.2 GRIND-LEACH PROCESS FOR HTGR FUEL

An earlier hot-cell evaluation of the grind-leach process with Peach Bottom fuel compacts and experimental AVR fuel spheres showed that the leached residues (pyrolytic carbon and matrix graphite) contained excessive amounts of thorium (6.9% of the total), uranium (4.5%), and fission products (up to 35%).[1] The tests involved grinding coarsely crushed fuel compacts to -100 mesh to ensure fracture of the (Th,U) C_2 kernels and pyrolytic carbon coatings of the particles, followed by multiple leachings with boiling 13 *M* HNO_3–0.05 *M* HF–0.1 *M* $Al(NO_3)_3$.

During the past year, similar tests were made to test the effectiveness of the grind-leach process for treating pyrolytic-carbon-coated $(Th,U)O_2$ particles, a proposed second-generation HTGR fuel.[2] Two batches of duplex-coated sol-gel $(Th,U)O_2$ particles were irradiated in loops in the Oak Ridge Research Reactor (by the Reactor Chemistry Division as a part of the ORNL Gas-Cooled Reactor Program) to burnups of 15,000 and 17,500 Mwd per ton of Th + U. These particles had decayed 10 and 19 months, respectively, prior to our tests.

[1] J. R. Flanary and J. H. Goode, *Hot-Cell Evaluation of the Grind-Leach Process. I. Irradiated Pyrocarbon-Coated $(Th,U)O_2$ Particle-Graphite Matrix HTGR Candidate Fuels*, ORNL-4117 (August 1967).

[2] J. H. Goode and J. R. Flanary, *Hot-Cell Evaluation of the Grind-Leach Process. II. Recovery of Uranium and Thorium from Irradiated Pyrolytic-Carbon-Coated Sol-Gel Thoria-Urania Particles*, ORNL-4213 (March 1968).

Table 3.4. Leaching[a] of Minus 100-Mesh Pyrolytic-Carbon-Coated $(Th,U)O_2$ Particles[b]

	Distribution (% of total)		
	First Leach Solution	Second and Third Leach Solutions	Residue
Uranium	99.8	0.08	0.04
Thorium	99.7	0.23	0.07
Gross gamma	74.2	11.7	14.1
^{95}Zr	94.5	Not analyzed	5.5
^{95}Nb	46.1	27.4	26.5
^{106}Ru	86.2	9.1	4.7
^{137}Cs	92.6	0.30	7.1
^{144}Ce	91.9	0.17	8.0

[a]With boiling 13 *M* HNO_3–0.05 *M* HF–0.1 *M* $Al(NO_3)_3$. First leach, 5 hr; second and third leaches, 2 hr each.

[b]Irradiated to a burnup of 15,000 Mwd per ton of Th + U; decayed ten months.

Postirradiation examination of the particles revealed no failures or damage to the pyrolytic carbon coatings. Table 3.4 shows typical results obtained by dissolving particles that had been irradiated to the lower burnup. The leached residue contained 0.04% of the total uranium, 0.07% of the thorium, and 14% of the gross gamma emitters. The residue from the particles irradiated to the higher burnup contained about the same quantities of uranium and thorium, but only about 2% of the gamma emitters. The difference was primarily due to the smaller concentration of ^{95}Nb in the longer-decayed particles.

A similar test was made with a mixture of duplex-coated $(Th,U)C_2$ particles (13% of the total weight) and duplex-coated ThO_2 particles (87%) that had been irradiated to a burnup of 15,000 Mwd/ton and cooled for ten months. Losses of uranium (0.4%) and thorium (0.1%) to the residue were much lower than in the Peach Bottom experiments, but fission product migration out of the $(Th,U)C_2$ particles into the coating was much higher. About 61% of the gross gamma emitters were found in the residue; this included 60% of the total ^{95}Zr, 97% of the ^{95}Nb, 67% of the ^{106}Ru, 19% of the ^{137}Cs, and 21% of the ^{144}Ce.

The results of these tests indicate that the grind-leach process can probably be applied successfully to HTGR fuels containing pyrolytic-carbon-coated sol-gel oxide particles. The economics of the process, however, may not be attractive because of the high retention of fission products by the leached carbon residue. Even with long-decayed fuel, the residues would have to be treated as intermediate- to high-level solid wastes, and their storage would add significantly to the processing costs.

3.3 METHODS FOR PROCESSING LWR FUELS

The engineering development and evaluation of the shear-leach process was continued in a series of three tests to determine the feasibility of shearing large prototype fuel assemblies that are representative of third-generation LWR power reactor fuels. Fuel assemblies of this type are comprised of UO_2-filled Zircaloy-2 tubes encased in brazed grids.

In the first test, a 10 × 10 × 21 in. long unirradiated prototype fuel assembly (Fig. 3.5), consisting of 484 0.340-in.-OD (0.11-in. wall thickness) porcelain-filled stainless steel tubes inserted into two Westinghouse-type brazed leaf spring grids, was successfully sheared into 1- to $2\frac{1}{4}$-in. lengths. Because of the void space in the assembly (56.4%), the tubes were bent inward by the moving blade. The resulting sheared length was slightly less than the set length. The force required for shearing varied from $73\frac{1}{2}$ tons for a cross section consisting solely of tubes to 291 tons when the tubes were encased in a brazed grid. The maximum length of the pieces of the terminal cut was 3 in. A maximum back pressure of 1421 lb was exerted on the 10 × 10 in. pusher head feeding the assembly into the shear when a grid was sheared. The holding force applied to the assembly by the outer gag (57.9 in.^{2}) was 41,400 lb at the time the back pressure was measured. Some difficulty was encountered in feeding the test assembly into the shear because of the tendency of the grids to wedge in the gag guide (Fig. 3.6). This problem was eliminated by increasing the air pressure on the feed mechanism from 87 to 150 psig, thereby giving a forward feeding force of 3135 lb, which was sufficient to displace the jammed grids.

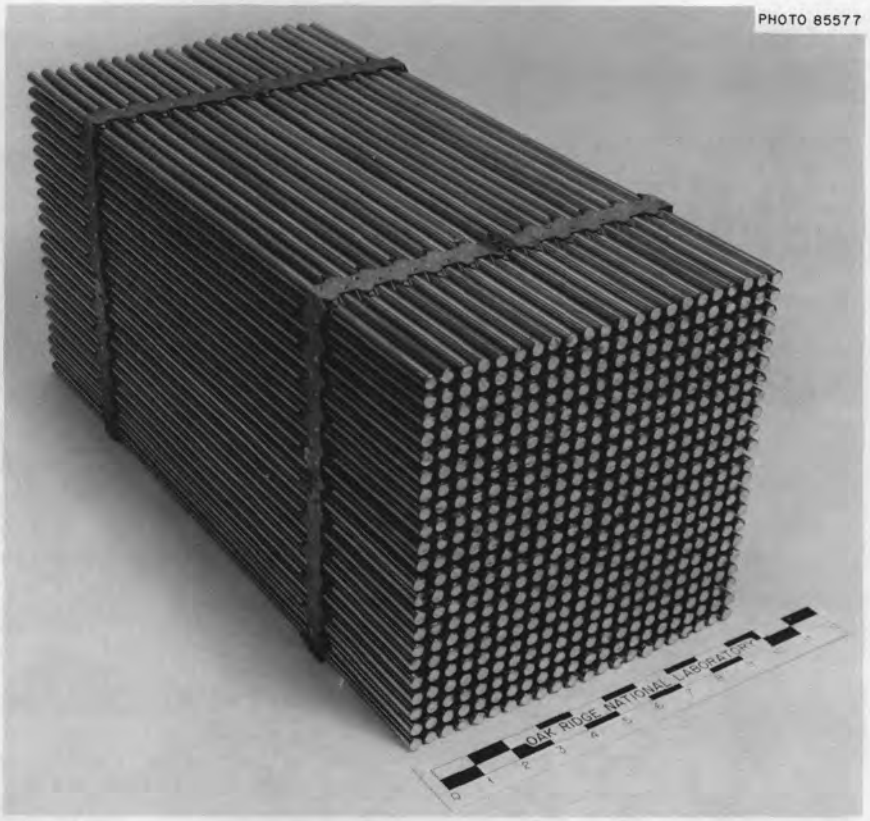

Fig. 3.5. Prototype Fuel Assembly, 10 × 10 × 21 in., Containing 484 0.340-in.-OD Porcelain-Filled Stainless Steel Tubes Inserted into Two Westinghouse-Type Leaf-Spring Grids.

In the second test, a prototype fuel assembly $7\frac{3}{4} \times 7\frac{3}{4} \times 36$ in. long, containing 196 0.4375-in.-OD by 0.028-in.-thick-wall porcelain-filled stainless steel tubes and two brazed Westinghouse-type grids placed on 12-in. centers, was sheared into approximately $2\frac{1}{4}$-in. lengths, using an inverted, stepped moving blade. (This assembly is similar to that shown in Fig. 3.5.) The required shearing force varied from 153 tons for the tubes alone to 283 tons in the vicinity of a grid. The fuel was fed and sheared satisfactorily. However, 1-in.-thick rubber facing on the outer gag was dislodged on the third cut. This loss of 1 in. of gag stroke and the excessive clearance between the gags caused the outer gag to become "cocked," thus bending the gag arm and making further shearing difficult. On the 17th cut ($6\frac{1}{2}$ in. of fuel remaining), the moving blade (weakened by a dimensional error in fabrication) was broken.

The third and final test consisted of shearing a $9\frac{1}{8} \times 9\frac{3}{8} \times 105$ in. fuel assembly containing 327 0.340-in.-OD by 105-in.-long UO_2-filled stainless steel tubes and 105 0.300-in.-OD by 96-in.-long (0.010-in. wall thickness) UO_2-filled stainless steel tubes inserted in ten Westinghouse core B type leaf-spring grids on $10\frac{5}{8}$-in. centers (Fig. 3.7). The use of the 96-in.-long tubes resulted in a void region, approximately $3\frac{5}{8} \times 2\frac{3}{4} \times 9$ in., at one end of the assembly. The end containing the void was fed into the shear first, with the void on the gag side. This allowed the outer gag to become "cocked" in the vertical direction (as shown in Fig. 3.8), again bending the gag arm. In spite of the damage to the gag and the gag arm, the assembly was satisfactorily fed and sheared into lengths varying from 1 to $2\frac{1}{4}$ in., using a rectangular-shaped moving blade with a straight cutting face. The terminal pieces were about 4 in. long. The required shearing forces varied from 119 tons for the tubes alone to 269 tons in the vicinity of a grid.

In order to demonstrate the feasibility of shearing large prototype fuel assemblies, the shear (in these tests) was operated beyond design specifications

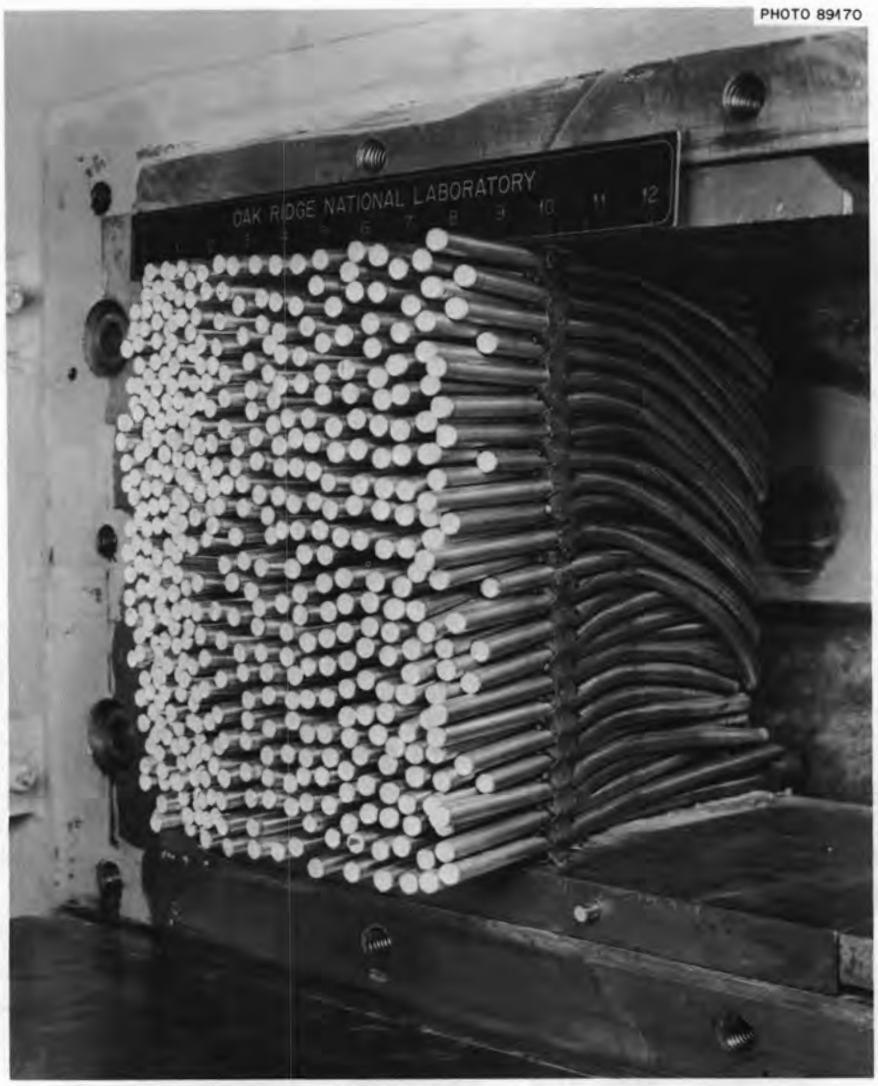

Fig. 3.6. Short Section of 10 × 10 × 21 in. Prototype Fuel Showing Compressed Leaf-Spring Grid Wedged in Gag Guide.

with regard to shear stoke, gag stroke, and gag pressures. Although some malfunctions were encountered, it was concluded that very large multitubular fuel assemblies can be sheared satisfactorily; the malfunctions simply emphasized the importance of properly designed gags and the limitations that are imposed by the strength of materials used in fabrication.

The tests were observed by representatives of Allied Chemical Corporation, Bechtel Corporation, Nuclear Fuel Services, Inc., and Argonne National Laboratory.

Processing Incidents with Zirconium-Clad Uranium Metal Fuel

From mid-July of 1967 to late January of 1968, Nuclear Fuel Services, Inc., experienced seven incidents involving melting or burning of spent NPR fuel during reprocessing. This type of fuel (coextruded zirconium-clad uranium metal) reputedly contains an intermetallic phase of UZr_2, which is known to react violently in boiling nitric acid. The incidents are of interest to the head-end process developmental studies since

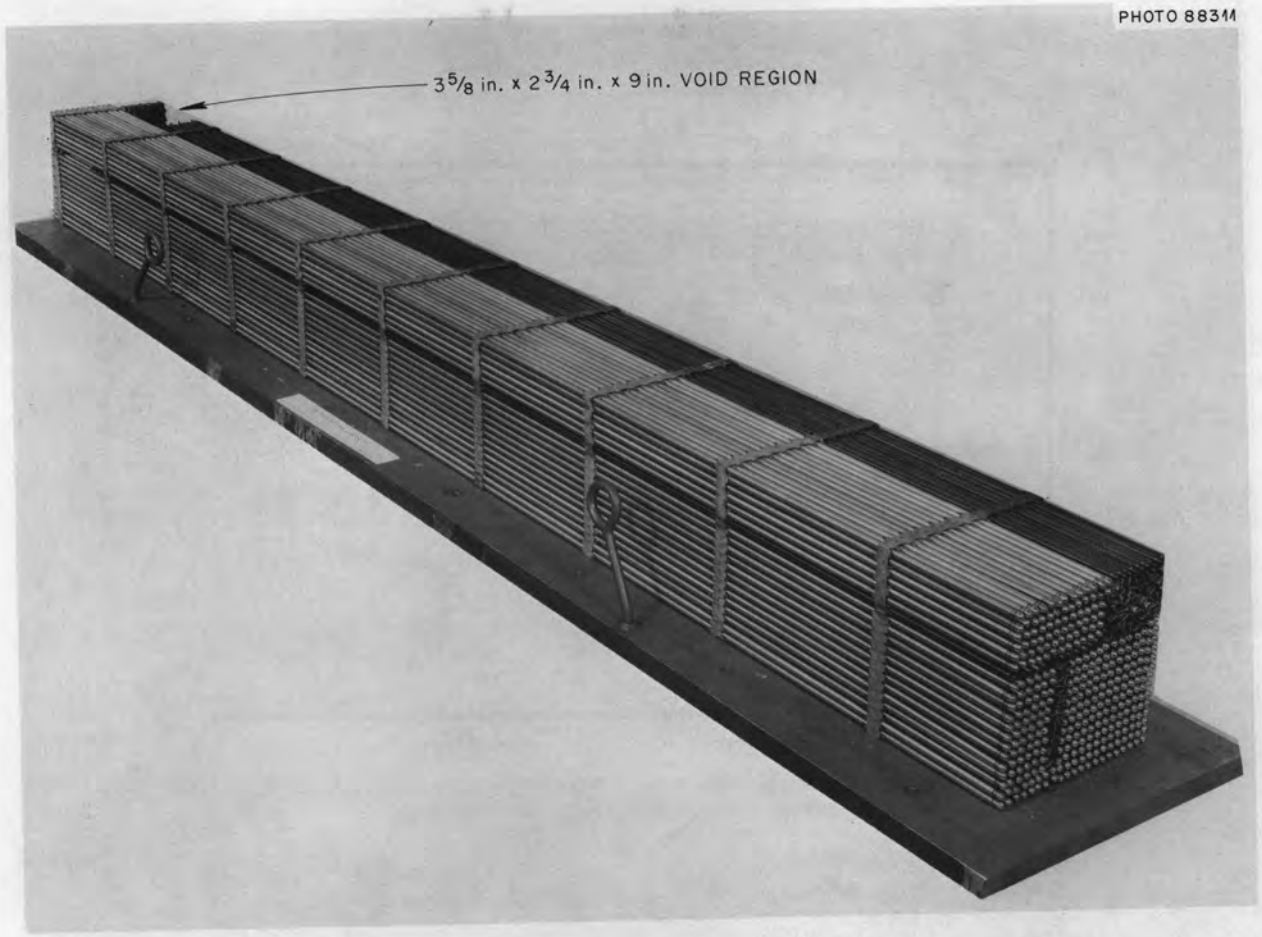

Fig. 3.7. Prototype Fuel Assembly, $9\frac{1}{8} \times 9\frac{3}{8} \times 105$ in., Containing 327 0.340-in.-OD by 105-in.-long and 105 0.300-in.-OD by 96-in.-long UO_2-Filled Stainless Steel Tubes Inserted in Ten Westinghouse Leaf-Spring Grids.

they may have revealed a potential hazard in the shear-leach processing of spent Zircaloy-2-clad UO_2 LWR fuel.

A limited investigation, including a literature search and crude small-scale laboratory experiments with unirradiated NPR fuel, resulted in the following hypotheses of the incidents:

1. The oxidation of fuel slugs in an aluminum storage container located under 11 ft of water was caused by water that leaked into the fuel from breaks in the zirconium cladding and reacted with metallic fines. The breaks in the cladding were caused by irradiation and/or mechanical damage sustained in handling and in shipping and storage.
2. Runaway reactions in the dissolver probably resulted from the reaction of finely divided and broken uranium metal and boiling HNO_3 (vapor and liquid). Such incidents might be triggered locally by U_3O_8 and UH_3 (from "leakers") and by the vigorous reaction of boiling HNO_3 with the carbon steel liner. The finely divided uranium results from embrittlement of the metal by irradiation and subsequent crumbling during mechanical handling, especially during shearing.
3. The ignition and slow burning of zirconium hulls after leaching were apparently caused by the reaction of the UZr_2 diffusion layer with O_2 or HNO_3. Mechanical abrasion or attrition that occurs when the hulls are poured from a basket onto an examination table or into a hopper could be the triggering device.

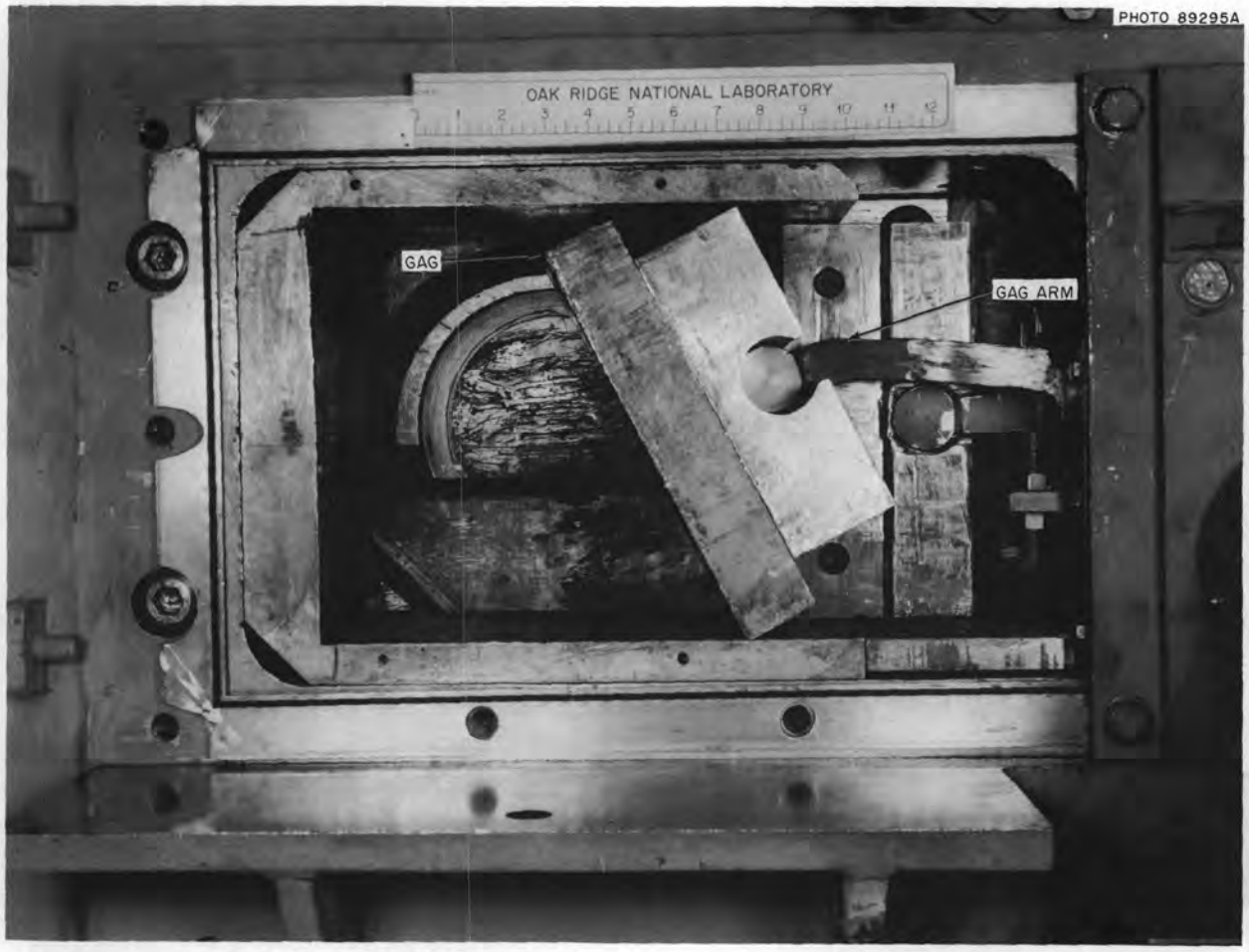

Fig. 3.8. "Cocked" Outer Gag and Bent Gag Arm That Resulted During the Shearing of the $9\frac{1}{8} \times 9\frac{3}{8} \times 105$ in. UO_2-Filled Prototype Fuel Assembly.

Sheared NPR fuel is being obtained for hot-cell metallurgical examination; the results of this examination will be compared with those for irradiated Zircaloy-2-clad UO_2 when the latter fuel becomes available. An attempt to reproduce the NFS incidents will be made if the information obtained from the hot-cell examination suggests that such an experiment would yield data that would prove useful in the processing of LWR fuel.

Delayed-Neutron Leached-Hull Monitor

Monitoring of leached fuel cladding is desired in order to prevent significant amounts of uranium and plutonium from being inadvertently discarded with the cladding. Evaluation of a delayed-neutron leached-hull monitor has been completed.[3] The monitor, which was designed for use in the shear-leach process for recovering LWR and FBR spent reactor fuels, is capable of detecting as little as 10 mg of ^{235}U in the presence of a 10^5-r/hr gamma-radiation field. An experimental unit that was designed to analyze directly a 20-cm-diam by 150-cm-long dissolver basket (typical of the shear-leach equipment) is shown in Fig. 3.9.

The electronics (amplifiers and scalers) associated with monitoring for unleached fuel in a high gamma background (>500 r/hr) should have nano-

[3] J. E. Strain, W. J. Ross, G. A. West, and J. W. Landry, *The Design and Evaluation of a Delayed-Neutron Leached-Hull Monitor*, ORNL-4135 (February 1968).

Fig. 3.9. Prototype Single-Compartment Leached-Hull Monitor. The target of the neutron generator is inserted in the polyethylene moderator. The radiation shield for the ^{60}Co gamma source can be seen beneath the moderator support.

second-response circuitry. Conventional electronics systems (microsecond-response circuitry) may be used if the radiation field near the detectors does not exceed 500 r/hr. Five different types of neutron detector units were evaluated. The tests revealed that two of these would be suitable for use in gamma radiation fields:

1. ^{10}B-lined counters for high gamma backgrounds, <40 up to 10^5 r/hr, and
2. $^{10}BF_3$-filled proportional counter for gamma fields <40 r/hr.

The cost of a completely installed leached-hull monitor, including the ^{10}B-lined neutron detectors, fast electronic systems, and a neutron generator, was estimated to be less than $50,000. This monitoring system offers the following advantages over other methods: (1) faster analysis, (2) quantitative data that are independent of cladding material, cooling time, and burnup, (3) analyses of samples of uranium-containing process solutions, as well as of solid materials, and (4) operation by automatic means or by nontechnical personnel.

4. Fluoride-Volatility Processing

The investigation of fluoride-volatility processing at ORNL was part of an intersite program; the aim of this program was to develop an alternative to the aqueous method for recovering valuable components that are present in spent UO_2 fuel from power reactors. The main effort at ORNL was to have been the installation and operation of a pilot plant for processing irradiated fuels.

Early in the year the AEC reviewed the overall volatility program. Based on both technical and budgetary considerations, a decision to terminate the program was reached. Accordingly, the ORNL portion of the program was shut down in an orderly manner.

Design work for the pilot plant was terminated almost immediately. Purchase orders were canceled where feasible, and no additional purchase orders were issued. Equipment fabrication was halted; materials and equipment on hand were made available to other programs. Equipment installation that was already in progress was completed, and some additional construction work was initiated and completed in order to achieve a safe standby status for the pilot plant cells.

Laboratory developmental work was carried to a logical early conclusion. The processing of irradiated UO_2 pellets was studied in hot-cell equipment. In studies of the sorption of fission products on NaF, we found that the removal of NbF_5 is a function of temperature, with a maximum at about 450°C, and is a second-order function of NbF_5 concentration in the gas stream. Experiments concerned with developing a process for recovering neptunium showed promise.

Small-scale engineering studies were concluded almost immediately after the decision to terminate the program was reached.

4.1 STATUS OF THE FLUIDIZED-BED VOLATILITY PILOT PLANT

The Fluidized-Bed Volatility Pilot Plant was scheduled for installation in Building 3019 as part of an intersite program. However, design and construction efforts were terminated according to the directive issued by the AEC. Completed portions of the pilot plant have been placed in standby.

The fluidized-bed volatility process and most of the equipment items were described previously.[1] The design, fabrication, and installation of the decladding, oxidizing, and fluorinating equipment were essentially completed. Equipment for the purification of UF_6 had been partially designed at the time the project was canceled; however, this phase of the work will not be completed. A safety analysis of the pilot plant, which also serves as the terminal design report, has been published.[2]

The major items of equipment required for head-end processing were installed in cell 3. These items include: the primary reactor, the reactor gas cooler, the primary reactor filter housing, the pyrohydrolyzer (with its filter housing), and the main cold trap. Very little piping was completed, but most of the shielding was installed in the cell. The vessel off-gas scrubbing system was about 70% complete when construction was stopped. The equipment in cell 3 will be left in place until the cell is needed for other developmental work; some

[1] *Chem. Technol. Div. Ann. Progr. Rept. May 31, 1967,* ORNL-4145, p. 58.

[2] E. L. Youngblood and F. W. Miles, *Hazards Evaluation for the Fluidized-Bed Volatility Pilot Plant,* ORNL-TM-2092 (July 1968).

of the items may possibly prove to be useful in future experiments.

Other installed equipment includes a new caustic makeup and storage station (at the southeast corner of the building) and a cell ventilation system. The off-gas systems from cells 2 and 3 were separated to provide greater flexibility. The off-gas ducts from these two cells join those from cell 1 before entering a caustic scrubber. The scrubbed off-gas is routed through a new filter station before it is combined with the cell off-gas from the rest of the building.

4.2 HOT-CELL STUDIES OF THE FLUIDIZED-BED VOLATILITY PROCESS

The major portion of the laboratory developmental studies of the fluidized-bed volatility process was done at Argonne National Laboratory. The laboratory efforts at ORNL were confined to pilot plant support, but they included some bench-scale experiments with irradiated fuel.

Experiments with UO_2 that had been irradiated to a burnup of 34,000 Mwd/metric ton and cooled for two years were performed, using a 0.94-in.-ID fluidized-bed reactor.[3] In these studies, the UO_2 was first oxidized with 20% O_2–80% N_2 at 450°C, then treated with BrF_5-N_2 mixtures (5 to 10% BrF_5) at 700°C to volatilize the uranium and most of the ruthenium, molybedenum, and technetium, and finally fluorinated (with fluorine) at 300 to 500°C to volatilize the plutonium. In some runs, BrF_3 was used as a cleanup agent after the BrF_5 treatment. The UF_6 was purified by passage, first, through a 400°C NaF bed (primarily to remove ruthenium and niobium) and, then, by sorption (100°C) on and desorption (400°C) from NaF. The PuF_6 was recovered by irreversible sorption on a small NaF bed at 500 to 600°C. The principal results are summarized as follows:

1. A major fraction of the tritium present in the fuel was evolved during the oxidation with air at 450°C, which converted the UO_2 pellets to powdered U_3O_8.
2. The effectiveness of NaF at 400°C for removing many fission product fluorides from a gaseous UF_6-BrF_5-F_2 stream was confirmed.
3. Treatment of the fluidized-bed fluorinator with BrF_3 after the BrF_5 step allowed cleanup of the disengaging part of the reactor, the sintered metal filter, and the lines. This treatment resulted in lower uranium and ruthenium concentrations in the PuF_6 product.
4. The overall decontamination of uranium from gross fission products was uniformly high; however, decontamination factors for molybdenum and technetium (ionic contaminants) were not satisfactory. An MgF_2 bed at 100°C was not effective in removing TcF_6 from the UF_6 product.
5. The major radioactive contaminant in the PuF_6 product was ruthenium. The use of BrF_3 in the uranium volatilization step reduced the contamination to a limited extent. Another process step, which was more effective, was passage of the PuF_6 through a bed of NaF at 550 to 600°C. The PuF_6 was trapped, while most of the ruthenium passed through. Presumably, some further decontamination of the plutonium (PuF_4-NaF complex) could be achieved by extraction of the NaF with anhydrous HF.

4.3 SORPTION OF FISSION PRODUCT FLUORIDES ON SODIUM FLUORIDE

In support of the anticipated program for the Fluidized-Bed Volatility Pilot Plant, we studied the sorption of several fission product fluorides on NaF. This study included a basic investigation of the mechanism of sorption of niobium and ruthenium fluorides and some developmental work involving the separation of neptunium from uranium.

Sorption of Niobium and Ruthenium Fluorides on Sodium Fluoride

A study of the mechanism of the sorption of some fission product (niobium and ruthenium) fluorides on fixed beds of NaF was made to obtain a better understanding of the sorption-desorption methods for purifying UF_6.[4]

Two types of experiments were conducted in this study. First, deep beds subdivided into sections

[3] J. C. Mailen and G. I. Cathers, *Hot-Cell Studies of the Fluidized-Bed Volatility Process*, ORNL-TM-2170 (in preparation).

[4] E. D. Nogueira and G. I. Cathers, *Sorption of Fission Product (Niobium, Ruthenium) Fluorides on Sodium Fluoride*, ORNL-TM-2169 (in preparation).

were used in order to investigate the removal of niobium (and ruthenium) pentafluoride from a gas stream as a function of temperature and bed height. Later, single layers of sodium fluoride particles were used to study the removal of niobium pentafluoride as a function of gas concentration and solid surface area. The sorption process was followed by means of a tracer technique using ^{95}Nb and ^{103}Ru.

Experimental data were obtained in the temperature range of 100 to 600°C and at niobium pentafluoride concentrations below a partial pressure of 5×10^{-2} mm Hg.

The results of this study indicate that the decontamination of the gas stream from niobium pentafluoride is a function of temperature, with a maximum at about 450°C, and of niobium pentafluoride concentration in the gas stream (apparent second-order dependence). The decontamination factor does not depend on the surface area of the solid.

One of the proposed mechanisms involves the existence (in the gas) of a dimeric niobium pentafluoride (Nb_2F_{10}), which is sorbed on sodium fluoride with an apparent activation energy of about 9.0 kcal/g-mole. Data presented in several literature references also seem to suggest the existence of this dimer.

Recovery of Neptunium by a Sorption Process

The recovery of neptunium in the processing of thermal reactor fuels is desirable. In fluoride volatility processes, neptunium hexafluoride, which has properties similar to those of uranium hexafluoride, is formed. The low ratio of neptunium to uranium (about 10^{-4} at a burnup of 30,000 Mwd/metric ton) makes the use of sorption processes attractive.

Laboratory tests demonstrated that NpF_6 was sorbed by LiF, NaF, MgF_2, and CaF_2 (Table 4.1); however, sorption by NaF at 150 to 200°C appeared to be the most effective. The complex compound formed by the interaction of NpF_6 with NaF appeared to be sufficiently stable in the presence of fluorine to allow determination of the equilibrium dissociation pressure, using a transpiration technique, over the range of 250 to 450°C. The dissociation pressure data conformed to the equation

$$\log p_{mm} = 7.9 - \frac{5.0 \times 10^3}{T} .$$

Table 4.1. Sorption of Neptunium Hexafluoride by Lithium, Sodium, Magnesium, and Calcium Fluorides

Conditions: about 30 mg of NpF_6 used per test; trap residence time, 2.4 sec

Sorbent Temperature (°C)	Percentage of Available NpF_6 Sorbed on:			
	LiF	NaF	MgF_2	CaF_2
100–110	29	15	17	19
150		68.5		
200	37	99.7	28	
240			16	32
400	22			27

Table 4.2. Distribution of Neptunium and Uranium After Uranium Hexafluoride Desorption Step

Conditions: desorption at 250 to 275°C for 4 hr from 1.8 g of NaF with 200 ml of N_2 or He per minute; Np/U atom ratio ~0.037

Run	Amount Remaining on Sorbent Bed (mg)		Amount Desorbed and Collected on Backup Trap (mg)	
	Np	U	Np	U
9-12-He	33.55	14.5	1.61	676
10-3-N_2	30.61	9.6	1.43	698
9-26-He	29.71	19.1	1.81	626
9-25-He	29.71	11.1	1.54	620
9-13-N_2	17.03	16.6	1.23	692
9-27-He	12.28	28.5	1.18	642
Total	152.89	99.4	8.80	3954
% of Total Np or U	94.56	2.45	5.44	97.55

The dissociation pressures for the NpF_6-NaF complex were generally about one one-hundredth of those determined for the $UF_6 \cdot 2NaF$ system. This indicated that a separation of neptunium and uranium, based on the difference in equilibrium pressures for the two complexes, would not be practicable for neptunium-to-uranium atom ratios that are much greater than 0.01.

Some consideration was given to the possibility of cosorbing NpF_6 and UF_6 on NaF at about 200°C, desorbing the UF_6 at 200 to 400°C with inert gas (with the neptunium being held on the NaF in a reduced, nonvolatile state), and, finally, desorbing NpF_6 in a stream of fluorine at 400°C (with the fluorine serving both as an oxidant and as the transpiration gas). In the six tests where this process method was tested (Table 4.2), the overall neptunium-to-uranium atom ratio was 0.037, which is considerably higher than the ratio (10^{-4}) expected in actual processing. Further work with this process appears desirable.

4.4 SMALL-SCALE ENGINEERING STUDIES

Small-scale engineering studies to obtain experience with remotely operated fluidized-bed equipment were terminated in August 1967. At that time, the HCl decladding and UO_2 pellet oxidation steps in the Fluidized-Bed Volatility Pilot Plant flowsheet for Zircaloy-clad fuel had been studied, and modifications of the small-scale engineering test facility to permit the use of BrF_5 in the fluorination step had been completed. However, no actual tests had been made.

A system to monitor the HCl–Zircaloy-2 reaction by measurement of the hydrogen concentration in the pyrohydrolyzer off-gas stream with a thermal conductivity cell was built and tested. Changes in hydrogen concentration as low as 0.05% were readily detected. A system based on a paramagnetic type of oxygen detector (to measure the oxygen concentration in the off-gas stream from the primary reactor during the oxidation step) was also fabricated and tested. The reaction could be followed qualitatively; however, the rather low oxygen utilization and the high flow rates severely limited our ability to determine the end point of the reaction. Tests were made to determine the capability of a gas chromatograph (equipped with a column loaded with Kel-F 10 on an alumina support and using Freon 114 as the carrier gas) for following bromine, BrF_3, and UF_6 in the off-gas stream from the BrF_5 fluorination step. From the standpoint of development of an in-line instrument for use in the pilot plant, the results were not encouraging.

Tests of the prototype gas-powered jet sampling loop for obtaining representative material from fluidized-bed reactors were not completed. While the bed material could be circulated through the sample loop and the flow could be readily started and stopped, we could not correlate the uranium content of the sample with the total amount of uranium in the bed. This difficulty was caused by a malfunction of the valves that were used to isolate and drain the section of the loop containing the sample.

5. Waste Treatment and Disposal

The objectives of the waste treatment and disposal development program are to develop a comprehensive waste-management system for nuclear wastes, including their final disposal, and to estimate the cost of this operation. Economical management of radioactive effluents is a prerequisite to the natural growth of a nuclear power industry. A comprehensive waste-management flowsheet, which was presented previously,[1] includes the following operations: (1) High-level radioactive wastes (HLW), which contain nearly all the fission products, are converted to solids. (2) Intermediate-level radioactive wastes (ILW), which are characterized by their generally high salt content, are incorporated in asphalt or polyethylene; any contained water is simultaneously volatilized. (3) Low-level radioactive wastes (LLW) are treated to remove the radionuclides, and the decontaminated water is discharged to the environment or recycled for reuse; the recovered solids are combined with the ILW. Both the HLW and ILW solid products can be shipped to a final disposal site.

5.1 HIGH-LEVEL RADIOACTIVE WASTE

The problems associated with the processing of wastes from the High-Temperature Gas-Cooled Reactor, the Molten Salt Reactor (MSR), and various types of fast reactors are being studied. The burn-leach head-end treatment for HTGR fuels produces a high-level aqueous waste stream and a high-level solid waste composed of leached alumina powder. Preliminary tests showed that the alumina powder can be sealed in a stainless steel container or can be dispersed in a lead silicate glass at 800°C for additional safety. Densities and viscosities of the aqueous waste stream were measured as a function of concentration (after evaporation) and temperature to define potential problems in processing the aqueous waste by the Pot Calcination method. Studies were initiated to determine the temperature at which MSR waste salts can be safely stored. Thermal gravimetric (TGA) studies of the waste component fluorides are being conducted at temperatures up to 850°C to determine thermal effects prior to similar tests in the presence of radiation. An option to the ORNL computer code for storing and retrieving data and for developing improved solid mixtures for the fixation of highly radioactive wastes was developed to aid in the initial studies associated with the processing of fast-reactor wastes.

Chemical Development

High-Temperature Gas-Cooled Reactor (HTGR) Waste. – The burn-leach process for graphite-base fuels containing carbon-coated fuel particles produces a high-level aqueous waste stream and a high-level solid waste composed of leached alumina powder. After being crushed, the graphite fuel blocks are burned in a fluidized bed of alumina. Thorium and uranium oxide ash is leached from the alumina bed, and the thorium and uranium are recovered by solvent extraction (Thorex process). Based on results of hot-cell tests of the burn-leach process,[2] as much as 15% of the fission product activity remains in the alumina bed after leaching. The bed can also contain silicon carbide since this material is sometimes used to coat the particles containing

[1] *Chem. Technol. Div. Ann. Progr. Rept. May 31, 1965*, ORNL-3830, p. 96.

[2] J. R. Flanary *et al.*, *Hot-Cell Evaluation of the Burn-Leach Process Using Graphite-Base HTGR Fuels*, ORNL-4120 (in preparation).

^{235}U. A simple and direct approach to disposal of this powder involves drying and sealing it in a suitable container. Added safety can be obtained by dispersing it in a glass.

Synthetic waste was prepared by burning and leaching nonradioactive fission products (to which the appropriate amount of graphite had been added) corresponding to a fuel burnup of 70,000 Mwd/ton and a cooling period of 100 days. Pressure tests were conducted on 15-g samples of the synthetic waste powders sealed in stainless steel containers at 250, 550, and 850°C. After three months at temperature, the gage pressures in the samples were −20, −80, and −400 in. H_2O respectively. The waste powder was dispersed in a lead silicate glass at 800°C to yield a dense, hard, void-free solid containing 37 wt % powder and 63 wt % glass. In this case, the waste powder was mixed with the glass powder, and the glass was melted to form a continuous phase surrounding the solid waste particles. The density and the viscosity of the HTGR-Thorex waste were determined as functions of concentration and temperature in order to evaluate the problems associated with evaporating, storing, and calcining the aqueous waste (Table 5.1). Densities ranged from 1.183 g/ml at 25°C for the unconcentrated waste to 1.509 g/ml at 100°C for waste that had been concentrated by a factor of 4. Viscosities ranged from 4 centipoises at 25°C for the unconcentrated waste to 16.4 centipoises at 75°C for waste that had been concentrated by a factor of 4. For comparative purposes, measurements of simulated solutions containing no fission products were also made.

Molten Salt Reactor (MSR) Waste. – Waste management for a molten-salt reactor presents problems that have not been encountered previously. These problems are caused by the appearance of significant amounts of fission products in several parts of the fuel processing system; they collect in the residues, the NaF and MgF_2 sorbents, and the off-gas cleanup equipment. Procedures similar to those used for aqueous wastes could be used for interim storage of the solidified salt residues and other solids until procedures for safe permanent disposal are established. Several tanks, integrated directly into the fuel processing system, could be used to store the bulk of the MSR waste for the lifetime of a given reactor. Following this interim cooling period, the waste would be processed for permanent disposal.

Table 5.1. Densities and Viscosities of Simulated HTGR-Thorex Waste Solutions as Functions of Boildown and Temperature

Temp (°C)	Density (g/cc)						Viscosity (centipoises)					
	Conc × 1[a]		Conc × 2[b]		Conc × 4[c]		Conc × 1[a]		Conc × 2[b]		Conc × 4[c]	
	Run 4[d]	Run 5[e]	Run 4	Run 5	Run 4	Run 5	Run 4	Run 5	Run 4	Run 5	Run 4	Run 5
25	1.198	1.183	1.370	1.358		1.574	4.0	4.1	7.7	7.3		
50	1.183	1.168	1.349	1.337		1.549	3.0	3.1	5.5	4.9		
75	1.170	1.157	1.331	1.320	1.543	1.526	2.6	2.7	4.2	4.1	16.4	
100	1.160	1.150	1.315	1.304	1.540	1.509	4.0	2.9	4.4	3.8	11.6	

[a]Solution with initial concentration:

Component	Concentration (*N*)
H^+	2.5
Al	0.93
F	0.3
NO_3^-	4.99
Total FP's (run 5 only)	13.4 g/liter

[b]Solution after concentration by a factor of 2.

[c]Solution after concentration by a factor of 4.

[d]Contains no simulated fission products.

[e]Contains simulated fission products expected from processing fuel that has been irradiated to a burnup of 70,000 Mwd/metric ton.

Although fluorine is not evolved from the molten fluoride salts in an MSR at the normal operating temperature (~600°C), the radiolytic decomposition and recombination of these salts is expected to be different at other temperatures, particularly in the solidified salt residues. Studies have been initiated to determine the temperatures at which waste salts from an MSR can be safely stored without evolution of fluorine. Thermal gravimetric (TGA) studies at temperatures up to 850°C were made of the fluorides of rubidium, cesium, strontium, lanthanum, cerium, neodymium, samarium, terbium, and erbium. If a vacuum distillation step is used in the fuel processing system, the residue should have a melting point slightly lower than 850°C. These studies with pure fluorides in the absence of radiation will help to distinguish thermal from radiation-induced effects on salts that are expected to be stored.

Fast-Reactor Waste. – An option[3] to the ORNL computer code, which is used for storing data and for determining improved solid mixtures for the fixation of highly radioactive wastes, was developed to aid in initial studies of fast-reactor wastes. This option is extremely useful for evaluating solidified waste products as a function of physical properties.

Liaison with Pacific Northwest Laboratory. – The Pot Calcination process was developed at ORNL to solidify high-level radioactive wastes by evaporating them to dryness in stainless steel pots and calcining the residues. When filled with residue, the pots would be welded shut and then shipped to a remote site, such as a salt mine, for permanent disposal. The technical feasibility of this process was demonstrated during the past year at Pacific Northwest Laboratory (PNL) where, as part of a cooperative program with ORNL, wastes containing nearly 4,000,000 curies of radioactivity were solidified. Gaseous and liquid effluents from the process were sufficiently low in radioactivity that little or no additional decontamination was required before they could be released to the environment. In one test, a volume of waste, which was equivalent to that obtained by processing 1.2 tons of spent fuel (the waste contained 1,300,000 curies of radioactivity), was converted to solids. The solids were then sealed in an 8-in.-diam by 8-ft-long pot. The 5100 w of power, produced by radioactive decay of fission products, resulted in a maximum internal temperature of 940°C when the pot was suspended in air. The results of this test are particularly significant since the calcined product contained more radioactivity than any previously reported product from a waste calcination process. The tests showed that a single line of calcination equipment could successfully process the waste produced by a 1-ton-of-uranium-per-day fuel processing plant, which is adequate to serve about 7000 Mw of installed electrical capacity. Additional tests are planned to obtain further data on the operational reliability, safety, and economics of the process. A report[4] that summarizes the initial test series has been prepared by PNL and ORNL personnel.

5.2 INTERMEDIATE-LEVEL RADIOACTIVE WASTE

Incorporation in asphalt or polyethylene constitutes a promising new method for preparing aqueous or organic intermediate-level wastes for storage or burial. The aqueous intermediate-level wastes (ILW) generated in nuclear installations have generally been stored in tanks, discharged to the earth in controlled areas, or mixed with cement and buried in specially designated land areas above the water table. Aqueous intermediate-level wastes include second- and third-cycle raffinates; solutions from solvent cleanup, off-gas scrubbers, and the decladding of spent reactor fuel; and slurries containing solids arising from the decontamination of process waters. These aqueous wastes are characterized by their modest levels of radioactivity (heating and radiation dose levels are not serious problems) and by their high salt or solids content, which prevents their efficient treatment by a conventional method such as ion exchange or precipitation. Both tank storage and solidification in cement have limitations. Tank storage is a temporary measure that requires constant surveillance, and the products formed by mixing the waste with

[3] C. L. Fitzgerald, H. W. Godbee, M. H. Davis, and W. E. Clark, *A Computer Code for Storing and Retrieving Data and Developing Improved Solids for Fixation of Highly Radioactive Wastes*, ORNL-3824, Supplement 1 (March 1968).

[4] C. R. Cooley, J. L. McElroy, W. V. DeMeir, J. E. Mendel, J. C. Suddath, and J. O. Blomeke, *Pot Calcination Performance During Radioactive Test in Waste Solidification Engineering Prototype. Waste Solidification Program, Vol. 4* (BNWL-814) (in press).

cement are only moderately insoluble. The integrity of cement decreases greatly as the concentration of insoluble salts increases. If low concentrations of waste salts are used in the cement, the volume of the final product to be stored is much larger than the original waste volume. In addition, most operations with cement are dusty, good mixing is difficult to achieve, and the operations are cumbersome.

Organic intermediate-level wastes are composed of solvents that are used in fuel processing plants and of miscellaneous solid and liquid organic materials that are used in all nuclear installations. These wastes are modest in volume and radioactivity content and are incompatible with disposal systems for low-level aqueous wastes. Presently, such organic wastes are stored in tanks, discharged to the earth in controlled areas, volatilized and discharged to the atmosphere, buried, or burned in open trays. Many of these current aqueous or organic waste disposal methods are questionable on a long-term basis from the standpoint of immobilization, volume reduction, economics, and pollution control.

Immobilization of intermediate-level wastes by incorporation in a cheap insoluble material, such as asphalt, polyethylene, or other organic matrixes, before burial or other types of disposal, would reduce the actual or potential rate of flow of radioactivity to the environment by several orders of magnitude; it might also decrease overall treatment costs. Plants for incorporating intermediate-level aqueous wastes in asphalt are already in operation at Mol, Belgium,[5] and Marcoule, France,[6] while a plant similar to that in Belgium is being constructed at Harwell, England.[7] The processes at these plants have been confined to the incorporation of inert solids, such as hydrous oxides; incorporation of salts such as sodium nitrate has not been attempted. The barrels of waste-asphalt product are either stored above ground, along with other miscellaneous wastes (pending a national decision to permit burial of wastes), or dumped into the ocean.

The process being developed at ORNL[8–12] is designed to incorporate all types of organic and alkaline aqueous wastes or slurries in asphalt or polyethylene by using continuous processing equipment. The products would be collected in barrels that could be stored, for economically optimized periods, prior to final disposal in national burial grounds or in salt mines. Solids, such as contaminated equipment and various residues, that cannot pass through the processing system could be surrounded by asphalt in a burial ground. Incorporating the wastes in asphalt or polyethylene will reduce the actual or potential release of radioactivity to the environment by several orders of magnitude, particularly where groundwater might accidentally contact the buried wastes. In this concept, the waste treatment and disposal system is largely independent of geography, since the barrels of product can be transported to any designated burial ground.

Status of the Incorporation of Wastes in Asphalt or Polyethylene

Process Description. – In the ORNL process, aqueous or organic wastes are first mixed with emulsified asphalt (35% H_2O) or with molten polyethylene (or polyethylene emulsified with an

[5] N. Van de Voorde and P. Dejonghe, "Insolubilization of Radioactive Concentrates by Incorporation into Asphalt," SM-71/4, pp. 569–600 in *Practices in the Treatment of Low- and Intermediate-Level Radioactive Wastes*, IAEA, Vienna, 1966, STI/PUB/116 (ORNL-Tr-1431).

[6] J. Rodier, M. Alles, P. Auchapt, and G. Lefillatre, "Solidification of Radioactive Sludges Using Asphalt," SM-71/52, pp. 713–29 in *Practices in the Treatment of Low- and Intermediate-Level Radioactive Wastes*, IAEA, Vienna, 1966, STI/PUB/116 (ORNL-Tr-1432).

[7] R. H. Burns, J. H. Clarke, T. D. Wright, and J. H. Myatt, "Present Practices in the Treatment of Liquid Wastes at the Atomic Energy Research Establishment, Harwell," SM-71/58, pp. 17–29 in *Practices in the Treatment of Low- and Intermediate-Level Radioactive Wastes*, IAEA, Vienna, 1966, STI/PUB/116.

[8] H. W. Godbee, R. E. Blanco, E. J. Frederick, W. E. Clark, and N. S. S. Rajan, *Laboratory Development of a Process for Incorporation of Radioactive Solutions and Slurries in Emulsified Asphalt*, ORNL-4003 (April 1967).

[9] J. H. Goode, *Fixation of Intermediate-Level Radioactive Waste in Asphalt: Hot-Cell Tests*, ORNL-TM-1343 (Nov. 18, 1965).

[10] J. H. Goode and J. R. Flanary, *Fixation of Three Intermediate-Level Radioactive Waste Concentrates in Asphalt: Hot-Cell Evaluation*, ORNL-4059 (January 1968).

[11] A. M. Rom, *Development of the Waste-Asphalt Process on a Semiworks Scale: Design and Installation of Evaporator Equipment in Building 4505*, ORNL-TM-1637 (September 1966).

[12] A. M. Rom, *Incorporation of Intermediate-Level Waste in Asphalt: Preliminary Design and Cost Estimate of a Full-Scale Plant for ORNL*, ORNL-TM-1697 (January 1967).

organic diluent or water) at temperatures of about 100°C or less, the water or organic solvent is then volatilized by heating to about 160°C, and, finally, the residue containing the waste is drained into a steel barrel. The vapors are condensed, and the inert gases are passed through high-efficiency filters prior to discharge. The condensed organic solvent could be reused; the aqueous condensate could be either reused or combined with other low-level aqueous wastes for further decontamination. Alternatively, all the solvent could be retained in the polyethylene or asphalt matrix by operating at a lower temperature.

Laboratory tests have been performed with a 4- by 6½-in. batch mixer in which most of the aqueous waste types listed above have been incorporated in asphalt to yield products containing up to 60 wt % solids (including up to 35 wt % nitrate) and 50 curies of radioactivity per gallon. The amount of tributyl phosphate (TBP) that can be incorporated in asphalt is limited to about 25 wt % TBP (37 wt % attapulgite clay–38 wt % asphalt) to maintain a reasonably solid product. Up to 50% TBP, but only about 40 to 50 wt % inorganic solids from aqueous wastes, can be incorporated in polyethylene at the present stage of development of the process. The leach rates for both the waste-asphalt and the waste-polyethylene products in water were satisfactorily low. The fraction of total radionuclides that was leached through a specific surface per day ranged from 4×10^{-4} to 4×10^{-6} $(cm^2/g)^{-1}$ day^{-1}. Asphalt and polyethylene products appear satisfactory when irradiated at doses up to 10^8 rads and 10^9 rads respectively.

The large-scale continuous incorporation of nonradioactive simulated aqueous wastes in asphalt was successfully demonstrated in pilot plant tests. A 12-in.-diam by 16-in.-high Pfaudler wiped-film evaporator with 4 ft^2 of heat-transfer area processed 5 to 10 gal of aqueous waste per hour to produce approximately 2.5 to 5 gph of asphalt product containing 40 to 45 wt % solids. Moderate blade wear has been experienced in about 200 hr of normal operation. No solids have accumulated on heat-transfer surfaces. The use of polyethylene and the incorporation of organic wastes have not been tested in the pilot plant.

Chemical Development

Organic Wastes in Asphalt. – The feasibility of extending the ORNL emulsified asphalt process to the disposal of the waste organic solvents generated in fuel processing was confirmed in laboratory studies. Since organic liquids tend to dilute asphalt, the use of thickeners (clays with large surface areas) was necessary to obtain acceptable products, that is, those which would flow from a wiped-film evaporator at 160°C but which would not flow at storage temperatures near ambient. Products containing 10 to 40 wt % TBP, 10 to 56 wt % asphalt, and 5 to 70 wt % thickener were prepared. Thickeners tested included powdered natural clays (attapulgite, bentonite, and Grundite) and portland cement, as well as colloidal alumina, carbon, and silica. Representative products are shown in Table 5.2. The product that seemed to have the best flow properties contained 25 wt % TBP, 38 wt % asphalt, and 37 wt % attapulgite-150 (Table 5.2, Mixture No. 1). This product showed no apparent change when irradiated to 10^8 rads by a ^{60}Co source (Fig. 5.1). In burning tests, 1- to 2-g samples burned at a much slower rate than pure asphalt. In leaching tests with water, the fraction of the original ^{137}Cs that leached through a unit of specific surface area per unit of time was 4.5×10^{-5} $(cm^2/g)^{-1}$ day^{-1} at the end of seven weeks. Thus, only 1/300,000 of the original activity was being leached from this sample during each day.

Organic Wastes in Polyethylene. – Laboratory studies showed that organic compounds such as *n*-dodecane, carbon tetrachloride, tetrachloroethylene, and TBP, as well as mixtures of these, can be incorporated in polyethylene to yield solid products containing a higher percentage of organics than the best asphalt product. Polyethylene products containing 20 to 50 wt % TBP were prepared. Samples of a product containing 40 wt % TBP and 60 wt % polyethylene were irradiated to doses of up to 10^9 rads by an external ^{60}Co source. No radiation damage was apparent at accumulated doses of 10^6 and 10^7 rads. However, the sample that was irradiated to 10^8 rads discolored slightly; the color of the one irradiated to 10^9 rads was light brown. The samples appeared to become more crystalline as the dose was increased, probably from additional cross-linking. In leaching tests with water, the leached fraction of the original ^{106}Ru was low, that is, 1.5×10^{-5} $(cm^2/g)^{-1}$ day^{-1}, while that for ^{95}Zr-^{95}Nb was 4.3×10^{-5} $(cm^2/g)^{-1}$ day^{-1}.

Aqueous Waste in Polyethylene. – Initial tests showed that polyethylene products containing up

Table 5.2. Representative Products of Organic Waste[a] Incorporated with Mineral Fillers in Asphalt

Mixture Number	Composition (wt %)			Comments on Product	
	TBP[a]	Base Asphalt	Filler	At 160°C	At 25°C
			Attapulgite-150 Filler[b]		
1	25	38	37	Will pour	Firm, but bleeds
2	10	50	40	Too stiff to pour	Firm
3	20	50	30	Will pour	Firm
			Grundite Filler[c]		
4	25	35	40	Will pour	Soft and tacky
5	20	10	70	Too stiff to pour	Firm
			Attacote Filler[d]		
6	25	37	38	Will pour	Firm, but bleeds
7	25	19	56	Will pour	Firm, but bleeds
			Attasorb Filler[e]		
8	25	37	38	Will pour	Firm, but bleeds
9	29	43	28	Will pour	Soft and tacky
			Attaclay Filler[f]		
10	25	37	38	Will pour	Soft and tacky
			Neospectra Mark I Filler[g]		
11	36	54	10	Will pour	Soft and spongy
12	38	56	6	Will pour	Soft and spongy
			Cab-o-sil Filler[h]		
13	48	47	5		Soft and creamy
14	46	45	9	Too stiff to pour	Soft and creamy

[a]Tributyl phosphate.
[b]Attapulgite-150 is a magnesium aluminum silicate drilling clay produced by Minerals and Chemicals Philipp Corp.
[c]Grundite is a high-strength bonding clay produced by the Illinois Clay Products Co.
[d]Attacote is a magnesium aluminum silicate coating clay produced by Minerals and Chemicals Philipp Corp.
[e]Attasorb is a magnesium aluminum silicate high-sorption clay produced by Minerals and Chemicals Philipp Corp.
[f]Attaclay is a magnesium aluminum silicate clay produced by Minerals and Chemicals Philipp Corp.
[g]Neosprecta Mark I is a carbon black produced by Columbian Carbon Co.
[h]Cab-o-sil is a high-surface-area silica produced by Cabot Corp.

to 50 wt % solids can be prepared from aqueous intermediate-level wastes (ILW) that simulate evaporator residues. The composition of ILW is shown in Table 5.3.

Thermal Conductivity. – Thermal conductivity measurements are required in order to estimate the temperature rise during the storage of wastes. The thermal conductivity of asphalt is low (i.e., 0.062 Btu hr^{-1} ft^{-1} $°F^{-1}$) at 100°F, although the conductivities of the inorganic salts that are expected to be included in asphalt are relatively high (e.g., 1 to 3 Btu hr^{-1} ft^{-1} $°F^{-1}$) at 100°F. The thermal conductivity of a salts-asphalt mixture containing 62.2 wt % salts was measured, using a steady-state radial-heat-flow technique.[13] It varied from 0.145 Btu hr^{-1} ft^{-1} $°F^{-1}$ at 85°F to 0.153 Btu hr^{-1} ft^{-1} $°F^{-1}$ at 215°F. These

[13]Letter, "Thermal Conductivity Measurements on Salts-Asphalt-Sample," from D. L. McElroy and Peter Spinder to H. W. Godbee, ORNL, dated Mar. 1, 1968.

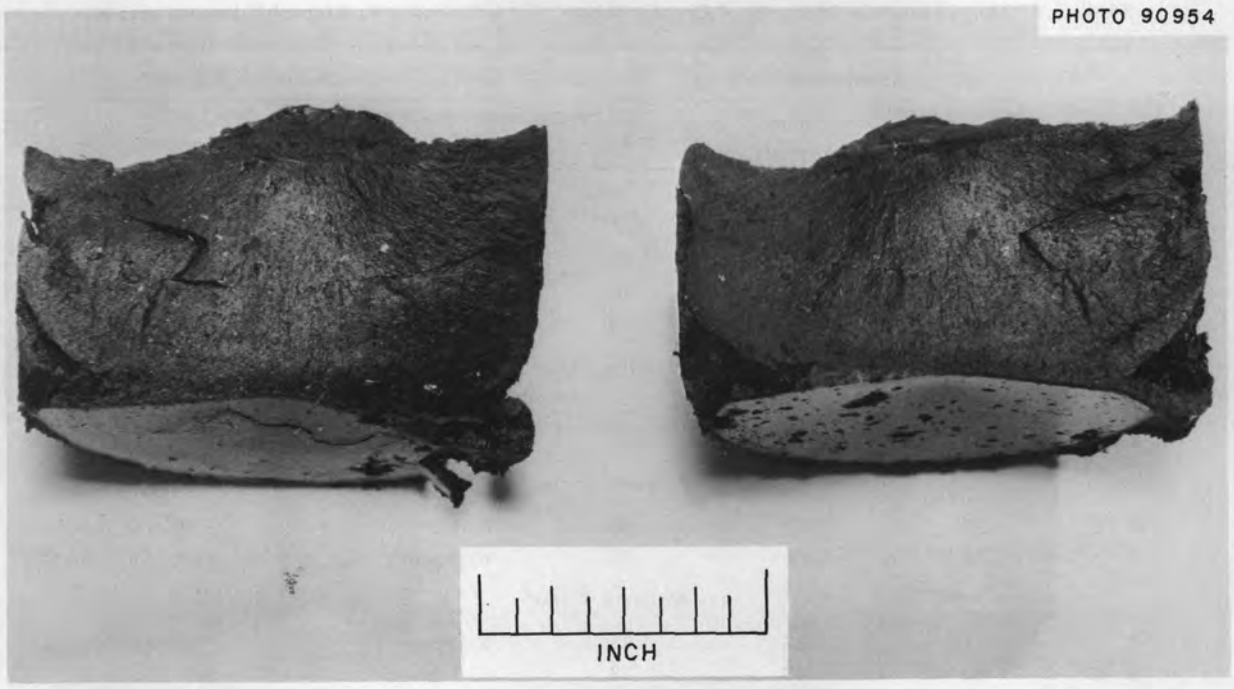

Fig. 5.1. Product Containing 25 wt % Tributyl Phosphate, 38 wt % Asphalt, and 37 wt % Attapulgite-150 After Being Irradiated to 10^8 Rads by an External ^{60}Co Source.

results conform to Maxwell's equation for the effective conductivity, k_e, of a heterogeneous body of spheres of one conductivity, k_d, embedded in a matrix having another conductivity, k_c, namely:

$$k_e = k_c \frac{k_d + 2k_c - 2V_d(k_c - k_d)}{k_d + 2k_c + V_d(k_c - k_d)},$$

where V_d is the volume fraction of the spheres. Thus, the conductivity of the continuous phase (the asphalt) controls the effective conductivity of the two-phase system.

Aqueous Wastes in Asphalt. – Water analyses and continued measurements of the pressure above the water covering the asphalt–60 wt % solids products, which had been prepared in earlier hot-cell campaigns[9,14] and had been irradiated to doses up to 1.1×10^8 rads over a two-year period, showed that no gases were evolved. No swelling of the product or increase in the water leach rate was observed.

[14]*Chem. Technol. Div. Ann. Progr. Rept. May 31, 1967*, ORNL-4145, pp. 114–15.

Table 5.3. Composition of Wastes Used in Pilot-Plant Asphalt Incorporation Tests

	Waste Type	
	2CW1[a]	ILW[b]
Na^+, mg/ml	161	151
Al^{3+}, mg/ml		5.97
Fe^{3+}, mg/ml	21.9	
NO_3^-, mg/ml	279	275
OH^-, *N*	2.05	2.06
Cl^-, mg/ml		1.98
SO_4^{2-}, mg/ml	78.4	33.6
Density, g/ml	1.366	1.315

[a]Concentrated Purex second-cycle plutonium waste (neutralized with 10% excess caustic).

[b]ORNL intermediate-level waste evaporator concentrate.

Flammability. – Results obtained by burning small samples of asphalt products indicated a sharply enhanced burning rate for asphalt containing large amounts of nitrate or nitrite, as compared with pure asphalt, but did not imply that such

products should be classified as explosive mixtures. (Nitrite-bearing samples were not evaluated in the standard explosive tests.[8]) Spontaneous ignition occurred at 330°C when 1- to 2-g samples containing 60 wt % solids (35 wt % nitrate) were heated on a hot plate. Samples containing 65 wt % solids (22 wt % nitrate–16 wt % nitrite) spontaneously ignited at 275°C. However, base asphalt did not spontaneously ignite at temperatures up to 460°C. The melting of $NaNO_3$ and $NaNO_2$ at 308°C and 271°C, respectively, and the tendency of solids to settle to the bottom as the asphalt mass liquified at higher temperatures may be significant. The burning rate in each case was much faster for the simulated waste products than for pure asphalt. Further work would be required to fully assess the effects of impurities, such as nitrite, on the burning rate of asphalt mixtures.

Standard drop-weight, autoignition, shock sensitivity, and flame-propagation tests of small samples containing 20, 40, and 60 wt % solids, including up to 35 wt % nitrate, were made and reported previously.[8] It was concluded from these tests that such materials should not be classified as explosives. In tests with 30-gal-drum samples, the salts-asphalt mixtures burned vigorously, as would be expected, but did not explode or show a significant increase in burning rate over that for pure asphalt. However, the initial temperature in the asphalt mass was not monitored. A careful evaluation of the fire hazard would be required in order to permit storage of the waste-asphalt product either in barrels prior to burial or in massive quantities in tanks. The restrictions on shipping the products are not expected to be significantly different from the present regulations for shipping aqueous solutions containing similar amounts of radionuclides. In either case, radionuclides could be volatilized in a large accidental fire. Asphalt is not classified as flammable by the ICC; and a sample of waste-asphalt product containing 60 wt % solids and 35 wt % nitrate, as tested by the Bureau of Explosives, did not fall into their classifications for dangerous goods.[8]

Manufacturers state that polyethylene will not flash or support a roaring fire. This low flammability also applies to waste-polyethylene mixtures. In hot-plate tests of small samples of polyethylene containing 40 wt % solids (~20 wt % nitrate), spontaneous ignition occurred at 440°C; however, the burning was characterized by a steady yellow flame, in contrast to the rapid burning observed with asphalt samples. Polyethylene did not spontaneously ignite up to 550°C.

Economics. – In quantities of 15 tons or more, polyethylene costs about 24 times more than emulsified asphalt (i.e., ~24¢ vs ~1.0¢/lb f.o.b.). A processing plant handling 6 tons of fuel per day would produce about 2400 gal of intermediate-level wastes (second- and third-cycle raffinates, scrubber solutions, evaporator bottoms, etc.) and would require about 3 tons of asphalt or polyethylene per day. The estimated capital cost of a plant at ORNL for annually incorporating in asphalt 400,000 gal of waste, containing 5 curies/gal, was $330,500.[11] The estimated cost of treatment was 37¢/gal, assuming 20-year amortization at 4% interest, a burial charge of 57¢/ft^3, and barrels at $3.00 each. Use of polyethylene may be limited to special operations such as the periodic disposal of used TBP solvent.

Engineering Development

The waste-asphalt pilot plant (Fig. 5.2) was operated to: (1) evaluate the use of the Pfaudler wiped-film evaporator for incorporating intermediate-level waste in asphalt, (2) obtain information concerning scaleup of the plant, and (3) verify data obtained in laboratory-scale development. Seventeen runs were completed; in these, nonradioactive simulated second-cycle Purex waste, neutralized with 10% excess caustic (2CW1), or ORNL intermediate-level waste evaporator concentrate (ILW) was incorporated in asphalt under various operating conditions. The product quality, as determined by residual water content and sodium leach rate (a substitute for radioactive cesium), determined the optimum operating conditions. Standard type RS-2 emulsified asphalt (i.e., the type generally used for constructing roads) was used in all cases.

Neutralization of second-cycle Purex waste with caustic prior to processing is necessary in order to prevent reaction of the acid with the asphalt. Iron hydroxide is precipitated during the neutralization step. In the 2CW1 runs (Table 5.4), the use of a high-speed agitator in the waste feed tank adequately dispersed and suspended the precipitate. This permitted accurate metering of the waste solution to the evaporator without plugging either the internal orifice or the control valve of

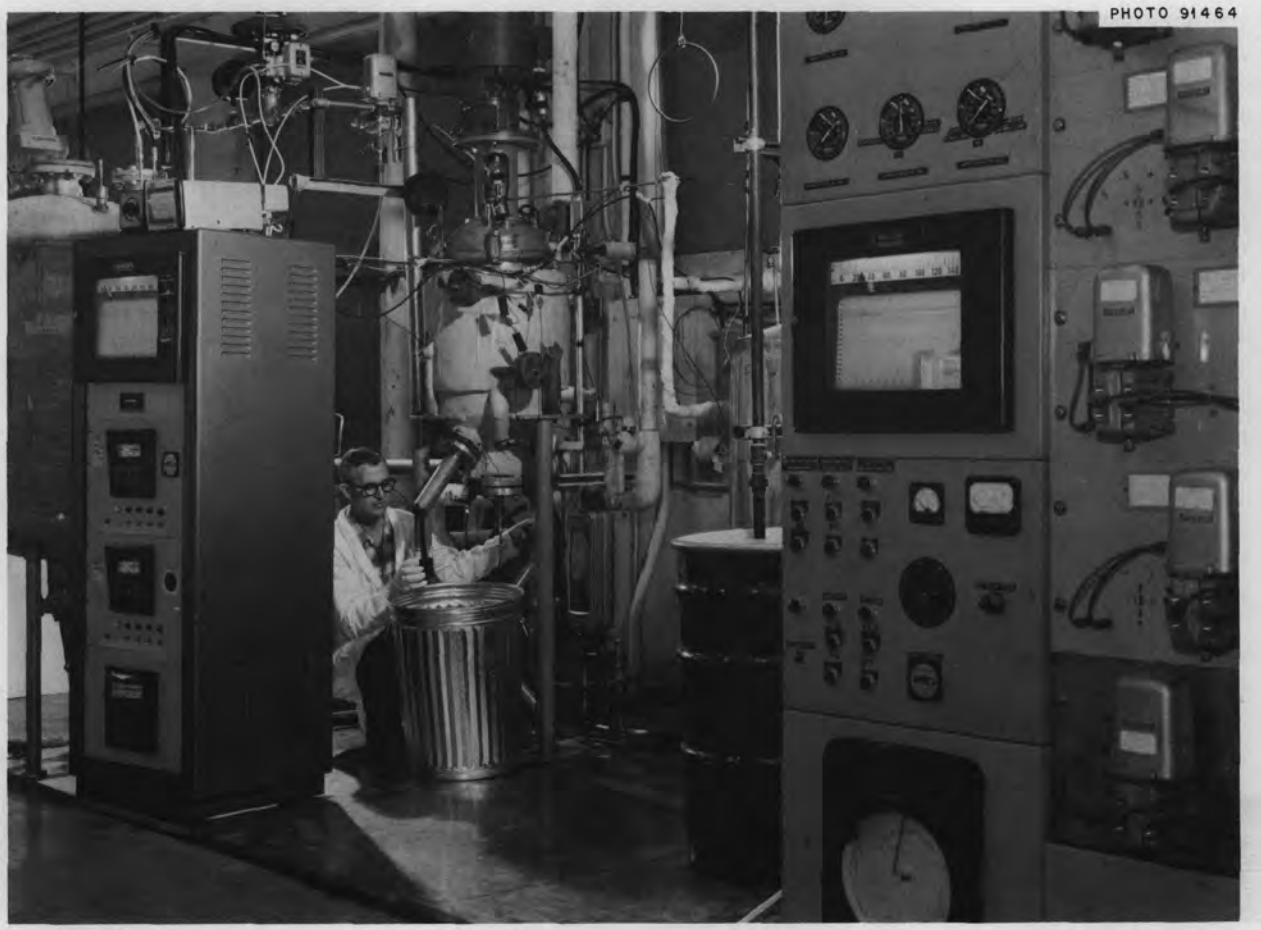

Fig. 5.2. Pilot Plant for Incorporating Intermediate-Level Waste in Asphalt.

the automatic feed system. Laboratory-scale tests had indicated that about 50 wt % was the maximum feasible solids concentration for 2CW1 waste in order to achieve a smooth homogeneous product. The 2CW1 waste was processed at the rate of 5 to 10 gph to yield products having solids contents of 30 to 50 wt %. The optimum waste feed rates were 7.5 and 5.0 gph, giving products that contained about 40 and 46 wt % solids respectively. The residual water content varied from 5 to 19 wt %, and the average sodium leach rate at the end of four weeks was 3×10^{-5} to 5×10^{-5} fraction leached $(cm^2/g)^{-1}$ day^{-1}. The fact that these water contents were much higher than the essentially zero water content obtained in laboratory tests is readily explainable. The total time at temperatures greater than 100°C in the laboratory batch mixer was 1 to 2 hr, as compared with less than 5 min in the large continuous wiped-film evaporator. The higher water content in the wiped-film product was not undesirable in terms of the leach rate; however, it did serve to decrease the relative concentration of solids in the product. The leach rates for the products obtained in the pilot plant are comparable with those obtained for laboratory products of similar salt content. Pilot-plant tests showed that, by reducing the waste feed rate to the lower optimum of 5.0 gph, a product with a slightly higher salt content and a much lower residual water content can be obtained. However, the initial leach rate and the leach rate at the end of four weeks for this product were about the same as those observed for the product obtained at the higher waste feed rate. Processing at a feed rate of approximately 10 gph gave products having high initial leach rates regardless of salt content; this suggests that the mixing capacity of the 4-ft^2 evaporator had been exceeded.

Table 5.4. Incorporation of 2CW1 Waste in Asphalt

Evaporator wall temperature – 200°C, except 193°C in runs 1A and 1B
Evaporator rotor speed – 280 rpm, except 164 in run 5A, 206 in run 5B, and 380 rpm in run 6

Run No.	Run Time (hr)	Waste Feed Rate (gph)	Asphalt Feed Rate (gph)	Evaporator D.F.[a]	Waste Solids (wt %)	Residual Water (wt %)	Sodium Leached[b]
1A	1.67	10.14	6.47	1010	49.3	11.0	5.44×10^{-2}
1B	0.75	9.50	6.15		50.0	11.4	1.54×10^{-2}
2	3.87	10.1	6.34	1030	51.9	11.6	5.12×10^{-2}
3	4.50	5.02	5.02	790	46.3	4.6	2.59×10^{-4}
4	5.00	7.45	6.82	1222	42.4	11.6	4.20×10^{-4}
5A	3.50	7.36	6.89	693	39.8	19.2	1.51×10^{-3}
5B	1.50	7.36	6.89		38.7	19.5	
6	5.00	7.60	6.81	1430	43.2	13.6	2.37×10^{-4}
7	4.50	7.61	10.3	835	32.0	17.5	1.99×10^{-4}
8	5.00	7.52	6.97	1500	42.2	14.5	1.52×10^{-4}
9	2.95	7.52	7.21	368	44.4	10.3	1.41×10^{-4}
10	3.00	7.45	10.6	330	34.5	13.3	2.06×10^{-4}
11	2.50	10.0	9.20	643	40.8	18.0	1.13×10^{-3}

[a]Ratio of total sodium fed to evaporator vs total sodium in evaporator condensate.
[b]Fraction sodium leached $(cm^2/g)^{-1}$ day^{-1} in 7-day period.

The rotational speed of the evaporator wiper blade apparently has some influence on product quality. At speeds of less than 280 rpm, the product exhibited high residual water content and high initial leach rates. However, speeds in excess of 280 rpm had no noticeable effect on the quality of the product. We have considered redesigning the wiper blade to decrease the wear (2 to 3 mils/hr at 280 rpm) along the leading edge. The blade is designed to be replaceable in a plant unit.

The potential entrainment of nonvolatile fission products in the vapor was determined by comparing the ratio of the amount of sodium fed to the evaporator to the amount found in the evaporator condensate. Values for 11 runs varied from 300 to 1500. There was no logical explanation for the fluctuation and inconsistency.

Runs to verify the results described above and to define optimum conditions for incorporating ILW waste in asphalt are being conducted. Waste feed rates of 8 to 13 gph to yield products containing 40 to 55 wt % waste solids have been investigated. Initial results indicate that a waste feed rate of about 10 gph will be optimum and will give a product having a solids content of about 45 wt %.

Conclusion

Tests thus far indicate that polyethylene is superior to asphalt with respect to radiation resistance and flammability and comparable from the standpoint of leach rate. However, the higher cost of polyethylene may limit its use to special applications such as the periodic disposal of used tributyl phosphate solvent. The degree of fire hazard can be reduced by minimizing interim storage and by prompt burial of the drums of waste-asphalt or waste-polyethylene product. A careful evaluation of the fire hazard is required just as in operations at a fuel processing plant where large amounts of flammable solvents are used.

5.3 ENGINEERING, ECONOMIC, AND SAFETY EVALUATION

Projected Wastes from the U.S. Nuclear Power Economy

As part of a long-range waste management study performed jointly with the Health Physics Division,

the volumes of high-level waste expected to accumulate in the United States during the remainder of this century were estimated. As a basis for these projections, the total installed nuclear generating capacity was assumed to increase from 12,000 Mw (electrical) in 1970 to 123,000 Mw in 1980 and to reach 675,000 Mw in the year 2000 (Fig. 5.3). At present, light-water reactors constitute the only source of nuclear-produced electrical power; however, fast breeders will assume an increasingly significant role after 1985. In estimating the production and the characteristics of waste, these two types of reactors are considered separately; then the results are combined to obtain a composite that represents the entire economy.

In the case of light-water reactors (Table 5.5), it is assumed that the fuel is exposed to 33,000 Mwd/ton at a specific power of 35.5 Mw/ton and that the reactors operate with an average load factor of 0.85. Based on these assumptions, the amount of fuel to be processed annually would increase from 300 tons in 1970 to 17,000 tons in 2000. Assuming that the fuel is processed by aqueous methods and that the resulting waste is concentrated to 100 gal per 10,000 Mwd (thermal) exposure, the annual production of waste would increase from 100,000 gal in 1970 to 5,600,000 gal in 2000. If this waste is stored in the form of liquid, 72,000,000 gal will have accumulated by the year 2000; on the other hand, if it is converted to a solid form, the waste volume may be reduced by a factor of about 13. Fission-product levels were calculated on the basis of continuous reactor operation at a specific power of 30.1 Mw/ton and a cooling period of 150 days for the spent fuel. The heat-generation rate in one ton of spent fuel as a function of the time after its discharge from the reactor is shown by curve *a* in Fig. 5.4.

Power generation by liquid-metal fast breeder reactors (LMFBR's) will probably begin in 1985 (Table 5.6). In the case of LMFBR's, it is assumed that all the power is generated in the core and that the reactor operates with a specific power (in the core) of 113 Mw/ton, a spent fuel exposure of 80,000 Mwd/ton, and a load factor of 0.83. Based on these assumptions, the quantities of fuel

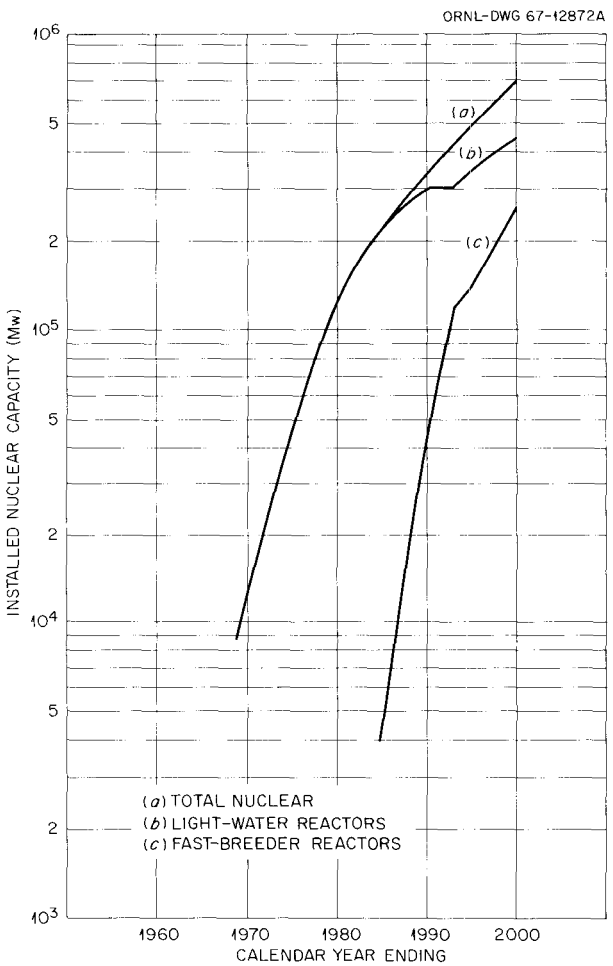

Fig. 5.3. Projected U.S. Nuclear Power Economy over the Remainder of This Century.

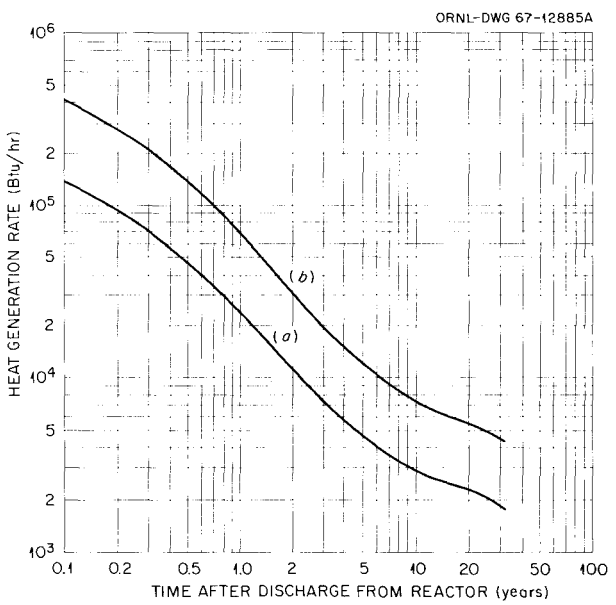

Fig. 5.4. Variation of Fission Product Heat-Generation Rate with Time for 1 Ton of Spent Fuel from (*a*) Light-Water Reactors and (*b*) Fast Breeder Reactors.

Table 5.5. Estimated Wastes From Light-Water Reactors

	Calendar Year			
	1970	1980	1990	2000
Installed capacity, 10^3 Mw (electrical)	12	123	294	430
Fuel processed, 10^3 tons/year	0.3	3.5	11	17
Volume waste produced, as liquid[a]				
Annually, 10^6 gal/year	0.1	1.2	3.6	5.6
Accumulated, 10^6 gal	0.2	4.8	27	72
Volume waste produced, as solid[b]				
Annually, 10^3 ft^3/year	1.0	12	36	56
Accumulated, 10^3 ft^3	2.0	48	270	720
Accumulated fission products[c]				
Total weight, metric tons	8	490	3,000	7,600
Total beta activity, megacuries	1000	17,000	72,000	140,000
Total heat generation rate, 10^6 Btu/hr	11	170	690	1,3000
^{90}Sr, megacuries	15	660	4,600	11,000
^{85}Kr, megacuries	2	84	470	1,000
^{3}H, megacuries	0.05	2.4	14	33
^{144}Ce, megacuries	100	1,100	4,400	6,000
^{137}Cs, megacuries	15	660	4,600	11,000

[a]Assumes fuel exposure of 33,000 Mwd/ton and 330 gal of waste per ton of fuel.

[b]Assumes 3.3 ft^3 of solidified waste per ton of fuel.

[c]Assumes that fuel is continuously irradiated at 30.1 Mw/ton to a burnup of 33,000 Mwd/ton and that fuel is processed 150 days after discharge from reactor.

Table 5.6. Estimated Wastes from LMFBR's

	Calendar Year		
	1985	1990	2000
Installed capacity, 10^3 Mw (electrical)	4	41	245
Quantity of fuel and blanket processed, 10^3 tons/year	0	0.5	2.7
Volume of waste produced, aqueous processing			
As liquid[a]			
Annually, 10^6 gal/year	0	0.08	0.5
Accumulated, 10^6 gal	0	0.2	3.3
As solid[b]			
Annually, 10^3 ft^3/year	0	0.8	5.0
Accumulated, 10^3 ft^3	0	1.7	33
Accumulated fission products[c]			
Total weight, metric tons	0	20	370
Total beta activity, megacuries	0	1400	13,000
Total heat generation rate, 10^6 Btu/hr	0	15	130
^{90}Sr, megacuries	0	11	290
^{85}Kr, megacuries	0	7	160
^{3}H, megacuries	0	0.06	2.4
^{144}Ce, megacuries	0	42	570
^{137}Cs, megacuries	0	30	780

[a]Assumes fuel exposure of 80,000 Mwd/ton and 800 gal of waste per ton.

[b]Assumes 8 ft^3 of solidified waste per ton of fuel.

[c]Assumes that fuel is continuously irradiated at 94 Mw/ton to a burnup of 80,000 Mwd/ton and that fuel is processed 75 days after discharge from reactor.

Table 5.7. Estimated Waste[a] from U.S. Nuclear Power Economy

	Calendar Year			
	1970	1980	1990	2000
Installed capacity, 10^3 Mw (electrical)	12	123	335	675
Electricity generated, 10^9 kwhr/year	89	880	2230	4170
Fuel processed, 10^3 tons/year	0.3	3.5	11.5	19.7
Volume of waste produced, as liquid[b]				
Annually, 10^6 gal/year	0.1	1.2	3.7	6.1
Accumulated production, 10^6 gal	0.2	4.8	27	75
Volume of waste produced, as solid[b]				
Annually, 10^3 ft^3/year	1.0	12	37	61
Accumulated production, 10^3 ft^3	2.0	4.8	270	750
Accumulated fission products[b]				
Total weight, metric tons	8	490	3000	8000
Total beta activity, megacuries	1000	17,000	73,000	150,000
Total heat generation rate, 10^6 Btu/hr	11	170	700	1400
^{90}Sr, megacuries	15	660	4600	11,000
^{85}Kr, megacuries	2	84	480	1200
^{3}H, megacuries	0.05	2.4	14	35
^{144}Ce, megacuries	100	1100	4400	6600
^{137}Cs, megacuries	15	660	4600	11,000

[a]Assuming that all spent fuels are processed by aqueous methods.

[b]Based on sum of results shown in Tables 5.5 and 5.6, as explained by footnotes in those tables.

and blanket to be processed annually would increase from 500 tons in 1990 to 2700 tons in the year 2000. If this material is processed by aqueous methods, it is estimated that 3,300,000 gal of liquid waste, concentrated to a volume of 100 gal per 10,000 Mwd (thermal), will have accumulated by the year 2000. If it is converted to solids, 33,000 ft^3 will be produced by the year 2000. Fission product levels in these wastes were calculated on the basis of continuous reactor operation at a specific power of 94 Mw/ton and a 75-day cooling period for the spent fuel. In estimating the *total* fission product activities and heat-generation rates, ^{235}U thermal fission yields were used since they have been found to give results that are in reasonable agreement with calculations based on fast fission yields. For individual isotopes, however, fast fission yields for ^{3}H, ^{85}Kr, ^{90}Sr, ^{137}Cs, and ^{144}Ce of 0.01, 0.6, 2.5, 6.6, and 3.9, respectively, were used. Curve *b*, Fig. 5.4, shows the variation of fission product heat-generation rate with time for 1 ton of spent fuel from an LMFBR.

The total fuel processing requirements, volumes of waste produced and accumulated, and fission product levels for the projected U.S. nuclear power economy are presented in Table 5.7.

Conditions to be encountered under the currently proposed conversion-to-solids concept are shown in Table 5.8. According to this concept, the waste produced by the aqueous processing of all fuels will be converted to solids immediately and will be packaged in 6-in.-diam by 10-ft-long pots. After storage for 30 years in water-filled canals, these pots will then be shipped 1000 miles to salt mines for final disposal. Estimates of the annual rates of waste solidification, the required lengths of storage canals, the number of shipments per year, and the necessary salt-mine space are about twice those that were presented previously;[15] however,

[15]R. E. Blanco, J. O. Blomeke, and J. T. Roberts, "Future Magnitude and Proposed Solutions of the Waste Disposal Problem," pp. 3–14 in *Proceedings of the Symposium on the Solidification and Long-Term Storage of Highly Radioactive Wastes, February 14–18, 1966, Richland, Washington*, CONF-660208.

Table 5.8. Waste Management Data for Conversion-to-Solids Concept

	Calendar Year			
	1970	1980	2000	2030[a]
Solid waste production, ft^3/year[b]	1000	12,000	61,000	
30-year interim solid storage				
Volume in storage, ft^3	2000	48,000	750,000	
Length of 48-ft-wide canals, ft	22	530	8300	
1000-mile shipment to salt mines[c]				
Number of shipments per year	0	0	20	1200
Number of casks in transit	0	0	1	7
Disposal in salt mines				
Area required, acres/year	0	0	2.6	157
Accumulated area used, acres	0	0	5.1	1930

[a]Commitments made in the year 2000.

[b]One cubic foot of solid waste per 10,000 Mwd (thermal) of fuel exposure.

[c]Thirty-six 6-in.-diam cylinders per shipping cask.

we do not believe that they are of a sufficient magnitude to cause concern.

5.4 SEPARATION OF NOBLE GASES FROM AIR BY USING PERMSELECTIVE MEMBRANES

A process is being developed jointly by ORNL, ORGDP, and the General Electric Company for separating radioactive krypton and xenon from other gases by use of a permselective membrane. This separation is based on differences in the solubilities of the gases in, and different rates of transport of the gases through, the membrane. Applications include the removal of the noble gases from: (1) the air within a reactor containment building, for instance, after an accidental release of fission products; (2) the off-gas from a processing plant for spent reactor fuels; and (3) the gas that blankets nuclear reactors, such as the molten salt and the sodium-cooled breeder reactors, which continuously vent volatile fission products.

The removal of noble gases from air has been studied extensively in AEC-sponsored research. Except for the permselective membrane process and the Freon extraction process currently being considered by J. R. Merriman at ORGDP, all of the separation processes require either low temperatures (less than $-70°C$) or facilities that occupy large volumes.[16] The processes that occupy a small volume and can be conducted at ambient temperatures may have advantages in cost, reliability, and transportability.

The different rates of transport of gases through solids have been known for many years;[17] however, separation of gases by this method became practical only after the development of thin plastic sheets that are free of holes.[18] Although any membrane may be used for separation of gases, silicone rubber has a much higher permeability than any other material that has been tested.[19] Scientists at the Research and Development Center of the General Electric Company have developed a method for preparing approximately 2-mil-thick silicone rubber membranes that are free of holes and are supported on a Dacron mat for physical support. They found the permeability factors of

[16]G. W. Keilholtz, "Removal of Radioactive Noble Gases from Off-Gas Streams," *Nucl. Safety* 8(2), 155–60 (Winter 1966–67).

[17]J. H. Michell, "On the Penetrativeness of Fluids," *J. Roy. Inst.* 2, 101–8, 307–21 (1831).

[18]S. A. Stern, "Industrial Applications of Membrane Processes: The Separation of Gas Mixtures," *Proceedings of Symposium, Membrane Processes for Industry, Birmingham, Alabama, May 19–20, 1966.*

[19]Karl Kammermeyer, "Silicone Rubber as a Selective Barrier," *Ind. Eng. Chem.* 49(10), 1685–86 (1957).

unsupported membranes, as measured at room temperature and zero back pressure, for xenon, krypton, oxygen, and nitrogen to be 203, 98, 60, and 28 respectively.[20] The permeability factor is the flow (cm^3/sec) per unit of area (cm^2) times 10^9, divided by the membrane thickness (cm) and the difference in pressure across the membrane (cm Hg).

Permeabilities of Nitrogen, Oxygen, Argon, Krypton, and Xenon Through a Dimethyl Silicone Rubber Membrane

The ORNL-measured permeabilities of nitrogen, oxygen, argon, krypton, and xenon through a sheet of dimethyl silicone rubber supported on a Dacron mat at room temperature were approximately one-half the permeabilities measured by Robb[20] for an unsupported membrane. The permeability factors decreased, but the separation factors increased, with increasing pressure across the membrane. The permeability of diluted mixtures of noble gases varied with the permeability of the diluent gas, with the percentage of gas that passed through the membrane, and with temperature.

The rubber membrane used in these experiments was about 1.8 mils thick and was supported between two sheets of 4-mil-thick Dacron mat. This mat has a void volume of about 50%. The combination of the rubber membrane and its two attached Dacron supports is called the membrane package. This membrane package is, in turn, supported on each side by a 23-mesh plastic screen. A 1- by 2-ft sheet of the membrane was mounted in a steel holder in such a way that the gas flowed across the top of the membrane through a space about $\frac{1}{16}$ in. thick. On the low-pressure side (atmospheric pressure), the screen was placed directly on the steel holder. The gases that passed through the membrane (the "extract") and those which did not (the "raffinate") could be removed either at the same end of the membrane holder or at opposite ends, depending on the type of flow employed (i.e., cocurrent or countercurrent flow respectively). Equipment was provided to measure the pressure and the flow rate of the feed, the extract, and the raffinate. Also, each of these streams could be diverted through a radiation detector, where their radioactivity could be measured (Fig. 5.5). Except where indicated, experiments were made at room temperature, using the 30% product cut. Product cut is defined as the flow rate of the extract times 100, divided by the flow rate of the feed.

The permeabilities of pure oxygen, argon, nitrogen (see Fig. 5.6), and helium were determined by measuring the flow of these gases through the membrane at various pressure differences across the membrane. The large amount of gas required to fill our equipment made permeability measurements of pure xenon and krypton impractical. The decrease in permeability as the pressure difference across the membrane increases has been attributed to the compression of the Dacron mats and the increased pressure of the membrane package against the screen. This, in effect, increases the back pressure of the gas on the rubber membrane.

The permeability of the noble gases xenon and krypton in gas mixtures was determined by using oxygen, nitrogen, or helium containing less than 0.3% xenon or krypton and tracer $^{133-135}Xe$ or ^{95}Kr. The permeabilities, which were calculated by taking advantage of the difference between the average partial pressure on the high-pressure side (average of the feed and raffinate) and the partial pressure in the extract, were found to vary directly with the permeability of the carrier gas (Fig. 5.7). The permeability decreased more rapidly with increasing cut than expected, based on calculations. Both experimental and theoretical studies are continuing in an attempt to resolve this problem.

Our laboratory data demonstrated an increase in separation of krypton from nitrogen when: (1) the gases in the separation unit are flowing in a countercurrent instead of a cocurrent mode, (2) the percentage of the gas flowing through the membrane (i.e., the cut) is increasing, or (3) the pressure across the membrane is increasing (Fig. 5.8). The stage separation factor α, which is the ratio of the concentrations of the noble gas in the product and raffinate streams at zero cut, is given by the equation[21]

$$\alpha = \frac{\alpha_0}{1 + R(\alpha_0 - 1)},$$

[20] W. R. Robb, "Thin Silicone Membranes – Their Permselective Properties and Some Applications," Report 65-C-031, General Electric Company (October 1965).

[21] Samuel Blumkin, "A Method for Calculating Cascade Gradients for Multicomponent Systems Involving Large Separation Factors," K-OA-1559, Oak Ridge Gaseous Diffusion Plant (Jan. 15, 1968).

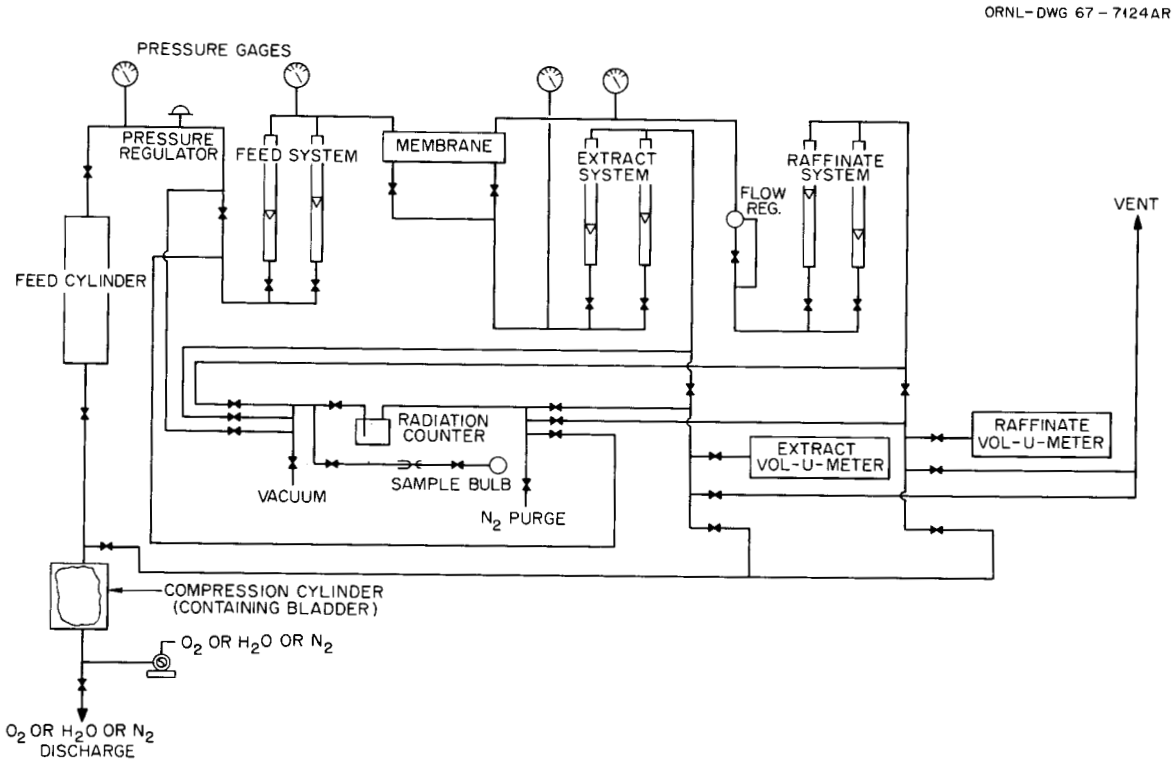

Fig. 5.5. Equipment for Measuring the Permeabilities of Gases Through a Permselective Membrane.

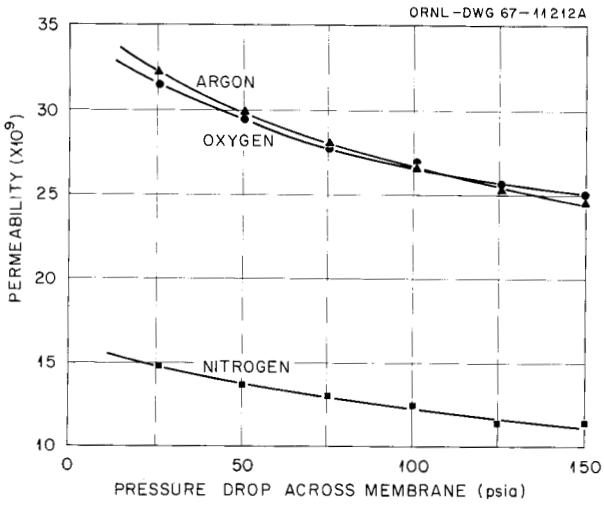

Fig. 5.6. Decrease in Permeabilities of Nitrogen, Oxygen, and Argon with Increasing Pressure Across a Permselective Membrane.

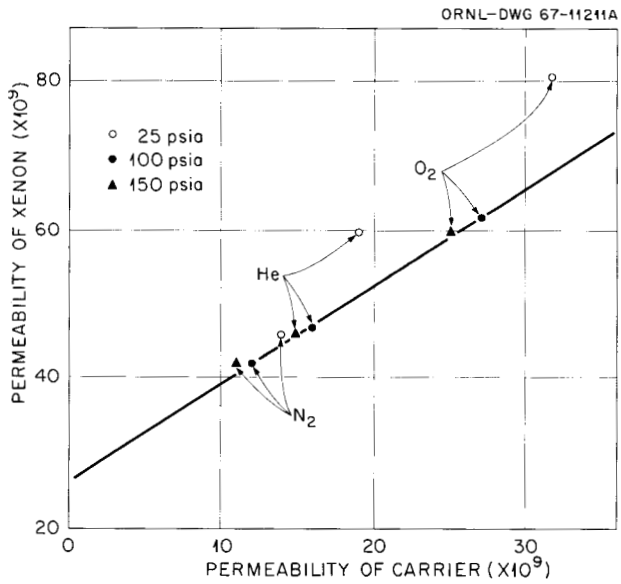

Fig. 5.7. Effect of Permeability of Carrier Gas on Permeability of Xenon Through a Permselective Membrane.

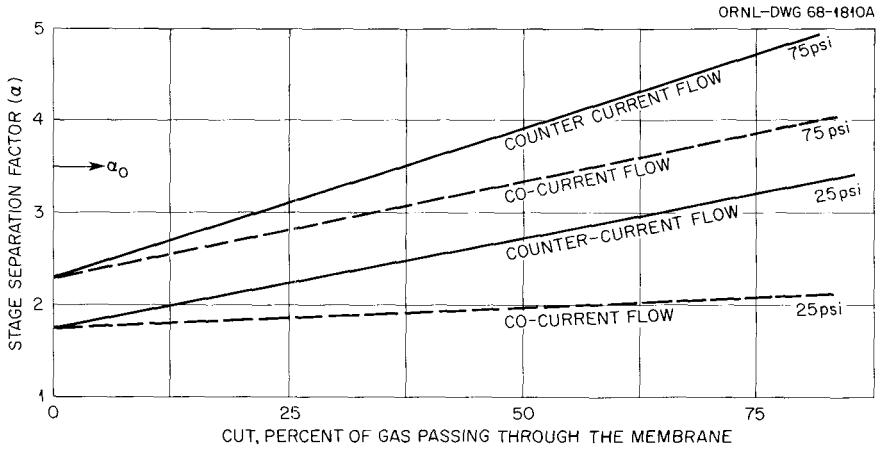

Fig. 5.8. Separation of Krypton from Nitrogen as a Function of Flow Mode, Cut, and Pressure Across the Membrane.

where R is the ratio of the pressure on the low-pressure side to that on the high-pressure side of the membrane and α_0 is the ratio of the permeabilities of the two gases at zero back pressure. Our experimental data extrapolated to zero cut agreed well with this equation when the high-pressure side was at 25 psi and the low-pressure side was at atmospheric but not when the higher pressure was 75 psi.

S. Blumkin[21] and E. Von Halle (ORGDP) have prepared a computer code that calculates gas permeability and binary separation factors for a permselective membrane as functions of pressure, fraction of gas flowing through the membrane, ratio of the permeabilities of the two gases, and cocurrent or countercurrent operation. The calculated values agreed reasonably well with the experimental values obtained at low operating pressures and cocurrent flow but were significantly different under other conditions.

D. E. Fain *et al.* (ORGDP) showed that the permeabilities of krypton, oxygen, and nitrogen increased approximately linearly in the temperature range −20 to 80°C (see Fig. 5.9 for data in upper part of temperature range). The separation factor of krypton from the oxygen or nitrogen decreased with increasing temperature. These data, obtained by using five different membrane samples, showed a scatter in the permeability values; however, the ratios of the permeabilities of the different gases were constant. This scatter may be

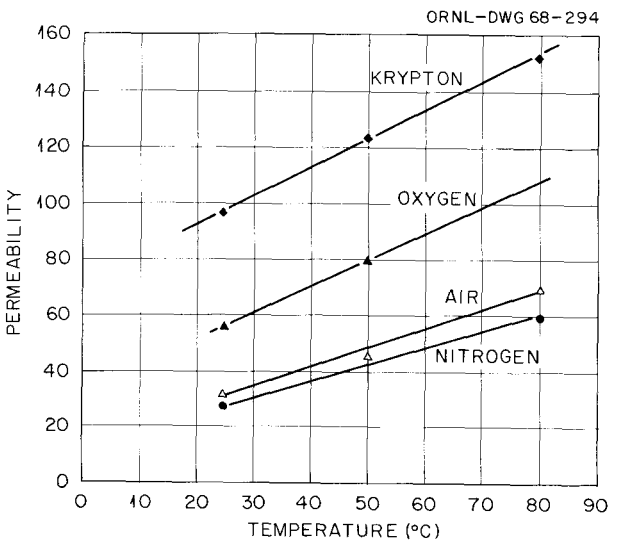

Fig. 5.9. Effect of Temperature on Permeabilities of Gases Through a Permselective Membrane.

the result of variation in the thicknesses of the small pieces of membrane. The separation factors of krypton from nitrogen and oxygen at 25°C were about 10% greater than those reported by the General Electric Company. The permeability decreased slightly, but the separation factor increased, with increasing ΔP across the membrane; this is in agreement with data from the General Electric Company and ORNL.

Development of Improved Membrane and Multimembrane Package

The General Electric Company's Research and Development Center in Schenectady, New York, is working, under a subcontract, to develop a membrane with improved permeability and to design a compact multimembrane single-stage unit that is suitable for use in a plant for separating gases.

The permeability of the membrane when it is supported between two Dacron mats is about half that observed when the membrane is unsupported. Scientists at General Electric have found that the loss in permeability is decreased by use of a Dacron mat containing only long fibers. A membrane supported by Dacron only on the low-pressure side is also being studied; this arrangement could decrease the concentration gradient of gases (polarization) perpendicular to the membrane.

A 6- by 6-in. multimembrane single-stage unit was successfully fabricated. It contains about 500 ft^2 of membrane per cubic foot of active volume (membrane, spacers, and intermembrane space, but not end plates) and exhibits satisfactory operating characteristics. Construction of a larger (1- by 2-ft) multimembrane single-stage unit is now in progress. This unit will contain 10 yd^2 of membrane and forty-five 2-ft^2 membranes.

The membrane sheet with improved permeability will be used in laboratory studies, and the 10-yd^2 membrane package will be used in engineering experiments at ORNL to determine stage efficiency, life, power requirements, etc. Its capability for removing radioactive noble gases from the off-gas in an ORNL reactor, a fuel processing pilot plant, or the Nuclear Safety Pilot Plant will then be determined.

Removal of Noble Gases from the Cover Gas of a Sodium-Cooled Breeder Reactor

The use of a cascade of permselective membrane units was evaluated for removing the radioactive krypton and xenon from argon gas used to blanket the sodium coolant in a reactor designed by the Babcock and Wilcox Company. This reactor is a sodium-cooled 1000-Mw (electrical) fast breeder with vented fuel elements. The xenon and krypton migrate to the argon, which is used to blanket the sodium, and must be removed before the argon is recycled or vented to the atmosphere.

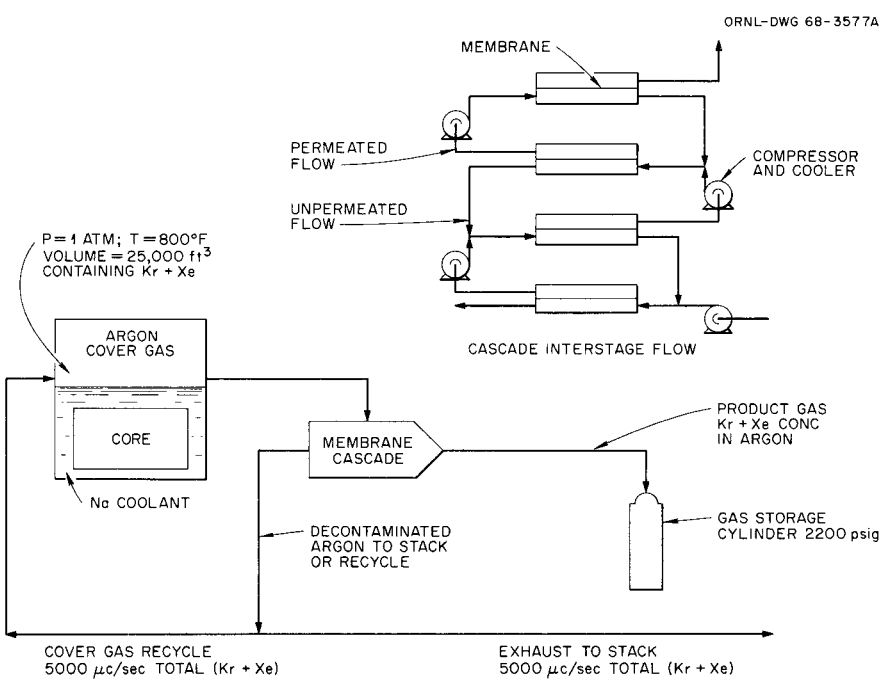

Fig. 5.10. Proposed Scheme for Removing Noble Gases from the Argon Covering the Sodium Coolant of a 1000-Mw (Electrical) Reactor Designed by the Babcock and Wilcox Company.

The size and the cost of a cascade that will remove and concentrate the noble gases in the cover gas have been estimated for a system that operates as shown in Fig. 5.10. The plant would continuously process a small stream (0.01 to 10 scfm) of the cover gas, decontaminating it sufficiently to permit greater than 90% of the gas to be recycled to the reactor or to be discharged to the atmosphere. The concentrated gas from the top of the cascade would be compressed to 2200 psi and would be stored in conventional gas cylinders. The activity of the cover gas at equilibrium is a function of the processing rate; data are given in Table 5.9 for rates of 0.01, 1.0, and 10 scfm. The activity in the gas increases from 5.5×10^6 to 3.1×10^7 curies in the 25,000-ft^3 gas space as the processing rate decreases from 10 to 0.01 scfm. Xenon-133 accounts for 80 to 95% of the total activity.

The data in Table 5.10 show the performance, size, and cost of a cascade for three modes of operation at a feed rate of 10 scfm. The first column presents the results for recycling 90% of the feed; the second column gives the results for recycling 99%, and the third column for recycling 99.8%. In each case, the radioactivity of the recycle gas is reduced to slightly less than 5000 μc/sec, a level that is acceptable for either recycle or discharge to the atmosphere. The estimated capital cost of the gas separation system is \$289,000, \$342,000, or \$366,000, respectively, for concentrating the xenon and krypton by factors of 10, 100, or 500. This cost is less than 0.3% of the total capital cost for a reactor, estimated at \$150/kw.

Table 5.9. Calculated Concentration of Noble Gases Above the Sodium Coolant in a 1000-Mw (Electrical) Reactor Designed by the Babcock and Wilcox Company

	Average Rate = 10 scfm		Average Rate = 1.0 scfm		Average Rate = 0.01 scfm	
	Curies	Atoms/ft^3	Curies	Atoms/ft^3	Curies	Atoms/ft^3
^{83m}Kr	9,800	0.140135×10^{15}	10,600	0.151575×10^{15}	10,700	0.153005×10^{15}
^{85m}Kr	39,800	0.134638×10^{16}	46,500	0.157303×10^{16}	47,300	0.160009×10^{16}
^{85}Kr	43	0.311655×10^{17}	418	0.302958×10^{18}	4,310	0.312380×10^{19}
^{87}Kr	70,000	0.681579×10^{15}	73,600	0.716632×10^{15}	74,000	0.720526×10^{15}
^{88}Kr	108,000	0.232494×10^{16}	119,000	0.256174×10^{16}	121,000	0.260480×10^{16}
^{89}Kr	9,660	0.396253×10^{13}	9,680	0.397073×10^{13}	9,680	0.397073×10^{13}
^{131m}Xe	16,300	0.360976×10^{17}	97,500	0.215921×10^{18}	216,000	0.478348×10^{18}
^{133m}Xe	89,400	0.379552×10^{17}	245,000	0.104016×10^{18}	302,000	0.128216×10^{18}
^{133}Xe	4,470,000	0.434665×10^{19}	18,800,000	0.182812×10^{20}	29,000,000	0.281997×10^{20}
^{135m}Xe	62,200	0.127519×10^{15}	66,800	0.136950×10^{15}	66,900	0.137155×10^{15}
^{135}Xe	356,000	0.251855×10^{17}	479,000	0.338872×10^{17}	498,000	0.352314×10^{17}
^{137}Xe	33,900	0.182444×10^{14}	34,000	0.182982×10^{14}	34,000	0.182982×10^{14}
^{138}Xe	258,000	0.562025×10^{15}	261,000	0.568560×10^{15}	261,000	0.568560×10^{15}
^{41}Ar	2,200	0.309506×10^{14}	2,200	0.309506×10^{14}	2,200	0.309506×10^{14}
Total Kr	237,303		259,798		266,990	
Total Xe	5,285,800		19,983,300		30,377,900	
	5,523,103		20,243,098		30,644,890	

Table 5.10. Performance, Size, and Cost of Several Cascades of Permselective Membranes for Separating Krypton and Xenon from Argon

Gas feed rate to cascade = 10 scfm

	Product Gas Rate		
	1 scfm	0.1 scfm	0.02 scfm
Cascade			
Number enriching stages	9	15	20
Number stripping stages	19	23	24
Membrane area, yd^2	4630	5020	5140
Cascade volume, ft^3	~9	~10	~11
Power requirement, kw	126	136	140
Largest compressor, hp	9.2	7.9	7.7
High pressure side of membrane, psig	150	150	150
Low pressure side of membrane, psig	0	0	0
Feed gas			
Kr concentration, at. %	0.004	0.004	0.004
Xe concentration, at. %	0.136	0.136	0.136
Kr activity, curies/ft^3	24.4	24.4	24.4
Xe activity, curies/ft^3	542.6	542.6	542.6
Recycle (or vented) gas			
Kr concentration, at. %	0.47×10^{-5}	0.49×10^{-5}	0.46×10^{-5}
Xe concentration, at. %	0.53×10^{-9}	0.51×10^{-10}	0.25×10^{-10}
Kr + Xe activity, curies/ft^3	0.029	0.030	0.028
Product gas (to be stored)			
Kr concentration, at. %	0.04	0.4	2
Xe concentration, at. %	1.4	14	68
Ar concentration, at. %	98.6	85.0	30
Kr activity, curies/ft^3	244	2440	12,200
Xe activity, curies/ft^3	5426	54,260	271,300
Concentration factor, product/feed	10	100	500
Number storage cylinders per week[a]	50	5	1
Installed cost, dollars	289,000	342,000	366,000
Estimated space requirement, ft × ft × ft	10 × 10 × 15	10 × 10 × 15	10 × 10 × 15

[a]Standard N_2 cylinder at 2200 psig pressure.

6. Transuranium-Element Processing

The Transuranium Processing Plant (TRU) and the High Flux Isotope Reactor (HFIR) were built at ORNL to produce sizable quantities of the heavy actinide elements for research. The production for the USAEC Heavy Element Program is centered at these facilities. The program began several years ago with the long-term irradiation of ^{239}Pu in a Savannah River production reactor. Subsequent irradiations of part of the recovered ^{242}Pu in a high-flux demonstration run at Savannah River in 1965 provided the first heavy elements, which were separated and purified in TRU during the first year of its operation. During this report period (the second year of operation), irradiated rods from HFIR were processed as the production program progressed. Seventeen targets processed in 1967 yielded about 5 mg of californium, along with the normal complement of other actinide elements. Except for some californium that was held for irradiation purposes, the entire quantity of heavy actinides (berkelium, californium, and einsteinium) was made available to research workers throughout the country. A major campaign to recover, purify, and make available multigram amounts of ^{243}Am and ^{244}Cm from the original Savannah River raffinate solution (from the early plutonium processing) was conducted. Products, which were shipped to about a dozen customers, included 70 g of curium and 25 g of americium. Many special projects, which were directed toward making available certain isotopes and elements not recovered in the normal processing operations, were initiated and completed.

Startup of the remote fabrication line was accomplished. Six curium recycle targets and three special californium targets were fabricated and have been inserted in HFIR for irradiation. This work is under the direction of the Metals and Ceramics Division and is reported in detail elsewhere.

6.1 TRU OPERATIONS

The major functions of the Transuranium Processing Plant (TRU) are: (1) to process targets that have been irradiated in the High Flux Isotope Reactor (HFIR) and to subsequently isolate and purify the transuranium elements and distribute the transcurium elements to researchers, and (2) to fabricate recycle targets containing americium and curium for additional irradiation in HFIR. TRU is primarily a production facility; however, many of the processes that are being used are new and are being developed at the same time that the materials are being processed. For the foreseeable future, processes that are "routine" will be modified, processes that were thought to be suitable only for laboratory-scale operations will be scaled up and installed for use in main-line processing, and entirely new processes will be developed.

The purpose of this section is to report the production of transuranium materials and to describe recent changes in the equipment and the processes that are being used.

Status and Progress

TRU became operational in 1966. Ten targets that had been irradiated at the Savannah River Plant (SRP) were processed. Dissolution of the targets, preparation of feed, recovery of plutonium, and decontamination of the transplutonium elements from fission products were demonstrated.

During this report period, the LiCl-based anion exchange process for partitioning the transplutonium elements was scaled up (in glass and plastic equipment) and installed for use in the main-line processing plant.

None of the processes that are proposed for use (in the main-line plant) following LiCl-based anion exchange processing has been developed sufficiently to be installed. Isolation and purification of the transuranium elements are still being done in equipment that is installed temporarily in cell 5 (see Sect. 6.2). The design of permanent equipment for several isolation and purification steps (the separation and purification of americium and curium, the first-stage berkelium isolation, and the formation of oxide microspheres by sol-gel techniques) is well under way; this equipment will be fabricated and installed in early 1969.

A major accomplishment was the final check-out and startup of the remote target fabrication line. Six curium oxide recycle targets were fabricated. The curium oxide was produced, in a development facility, by the sol-gel method from curium that had been recovered in TRU (see Sect. 6.3). These targets are now being irradiated in the HFIR.

Seventeen targets that had been irradiated at SRP for about one year, and then additionally irradiated from six to eight months in the HFIR, were processed. Premature discharge of these targets was necessary because of unexpected failure of the cladding. Investigation of the mode of failure has not yet pinpointed the exact mechanism that caused the embrittlement of the aluminum, but a model describing the accumulation of fission products and the buildup of pressure within the target has led to an apparent solution to the general problem of target failures. Reduction of pellet density from 90 to 80% of theoretical should provide sufficient space for fission product accumulation for any desired irradiation time. Six new test targets are now being irradiated to substantiate this hypothesis. To some extent, the failures reduced the availability of heavy elements during the past year. Only about 5 mg of californium was recovered from the 17 targets mentioned above. More than 200 g of curium, including 130 g that was recovered from the original Savannah River raffinate solution (from the plutonium recovery operation of several years ago), was processed in TRU during this report period.

Production and Processing

Table 6.1 shows the amounts of transuranium materials processed to date in the main-line plant. Campaigns 4 through 8 were made in 1967.

Table 6.1. Materials Processed During Major Campaigns in the Transuranium Processing Plant Prior to January 1, 1968

Listed values are measurements or estimates of feed solutions

Campaign No.	Description of Campaign	^{242}Pu (g)	^{243}Am (g)	^{244}Cm (g)
1	Tracer-level tests			
2	Four prototype HFIR targets	10.5	4.5	12.4
3	Six SRP reactor slugs	49.5	19.3	76.5
4	Five ruptured HFIR targets	12.0	5.7	22.1
5	Miscellaneous targets[a]	26.5[b]	7.7[b]	17.0
6	Twelve ruptured HFIR targets	26.3	15.2	46.4
7	Am-Cm solution from SRP		118.7	131.5
8	Rework material from other campaigns		(14)	(31)
	Total (excluding rework material)	124.8	171.1	305.9

[a]Six targets were dissolved in laboratory-scale equipment to obtain more precise data.

[b]Estimated from product measurements.

Each of the 18 SRP-HFIR targets (campaigns 4 and 6) originally contained 9.57 g of ^{242}Pu in the form of calcined oxide. They had been irradiated at SRP for 16,500 Mwd, which is equivalent to 165 days in the HFIR. One target was held as a reference, whereas 17 were irradiated in the HFIR for an additional 12,000 to 17,300 Mwd; this resulted in a total burnup of 75 to 77% of the ^{242}Pu.

The history of the americium-curium solution from SRP (campaign 7) is as follows: Long-term irradiation of two 10-kg batches of ^{239}Pu in an SRP production reactor produced about 1 kg of ^{242}Pu, which was recovered and decontaminated at SRP. The raffinate of the plutonium recovery step was processed to recover the ^{243}Am and ^{244}Cm, which had been produced during the irradiation, in an impure solution containing the rare-earth fission products. About two years ago, this solution was transferred to the Curium Recovery Facility (Building 4507), where a total of about 75 g of americium and curium was recovered and purified. The remainder, about 280 g of ^{244}Cm and 220 g of ^{243}Am (in 1000 liters of solution), was transferred to TRU. The americium and curium from about half of this solution was recovered during the past year.

Campaign 8 was made to recover the transuranium elements from all of the rework material that had been collected.

Process Flowsheet

Figure 6.1 is a block diagram showing the processing steps that are being used for transuranium element production; these steps are discussed individually in later sections.

The steps include: (1) preparation of a feed solution by dissolving irradiated targets, (2) recovery of the plutonium by solvent extraction (Pubex), (3) decontamination of all the transplutonium elements from fission products by countercurrent solvent extraction (Tramex), and (4) separation of the actinides into three product fractions, using an LiCl-based anion exchange process; the fractions are processed subsequently in laboratory-scale equipment to purify the individual transuranium elements. These four steps are being performed routinely in TRU.

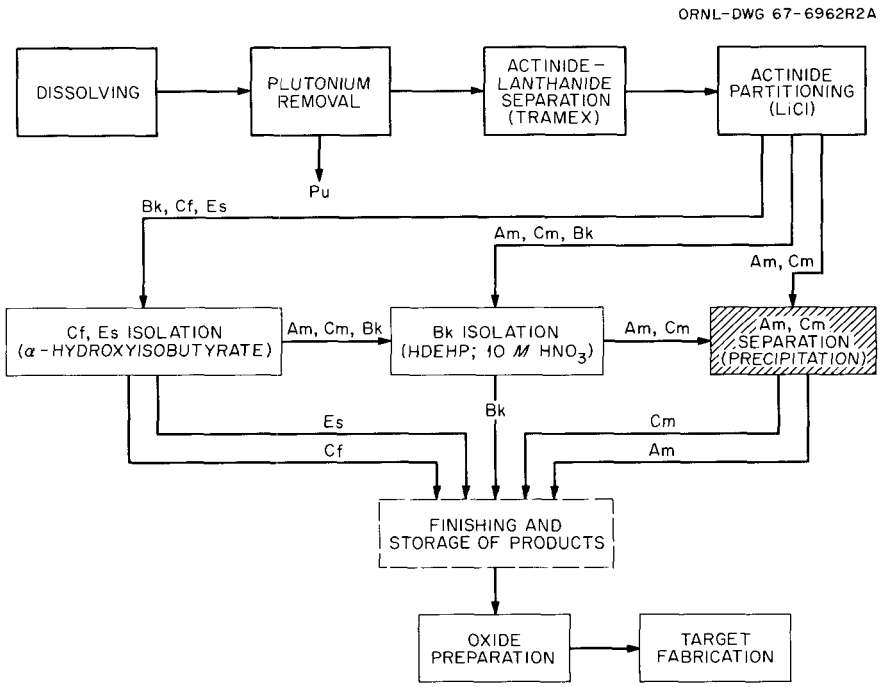

Fig. 6.1. Block Diagram of Operations Required in the Transuranium Processing Plant.

Plant-scale processes and equipment for separating and purifying the transcurium elements are still being developed; in the interim, scaled-up versions of laboratory isolation methods are being used for final isolation and purification of products.

Dissolution

The aluminum jacket and matrix material is dissolved first in 6 *M* NaOH–3 *M* $NaNO_3$, which is decanted through a filter, leaving the undissolved particles of actinide oxide. These latter particles are then dissolved in 6 *M* HCl. Twenty targets, which contained a total of 60 g of ^{242}Pu and 112 g of ^{244}Cm, have been dissolved in seven runs. No difficulty in retaining the actinide residue while removing the caustic solutions has been noted.

Recovery of Plutonium

Plutonium is recovered using a simple batch extraction process (Pubex). Initial work with this flowsheet had appeared quite promising; and development work, as well as plant use during this report period, proved the effectiveness of the process in TRU (see Sect. 6.3). The plutonium is extracted into 1 *M* di(2-ethylhexyl)phosphoric acid (HDEHP) in diethylbenzene (DEB). Then di-*tert*-butylhydroquinone is used to reduce the plutonium in the organic phase so it can be stripped into concentrated HCl.

First-Cycle Solvent Extraction Process (Tramex)

The Tramex solvent extraction process[1] is used to separate the transplutonium elements from the lanthanide rare-earth elements and other major fission products. The process has performed well; only a few minor operational upsets have been experienced.

Two changes have been made in the process during the past year. For unknown reasons we were not able to control the loss of acid in the feed (due to radiolysis) by the addition of methanol, a procedure which had been successful in the Curium Recovery Facility.[2] However, we found it to be a simple matter to add concentrated HCl to the feed periodically to compensate for acid loss.

We have also modified the method by which we prevent the oxidation of cerium to an extractable form. Previously, $SnCl_2$ was added to the feed for this purpose. Currently, the organic-soluble reductant di-*tert*-butylhydroquinone is included in the extractant at a concentration of 0.05 *M*. Although both methods are equally effective, the $SnCl_2$ had the disadvantage of loading the solvent, which was particularly troublesome when processing recycle material.

In the two years that TRU has been in operation, a total of 309 g of ^{244}Cm (plus associated transuranium elements) has been processed in 13 Tramex processing runs.

Separation of Transuranium Elements

The next required step is the separation of the transcurium elements from the americium and curium. To accomplish this, we are now using an LiCl-based anion exchange process, which was described last year.[3] This process partially separates the actinides into three fractions: (1) about 90% of the americium and curium, nearly free of ionic and radioactive contaminants and containing no transcurium elements, (2) an americium-curium-berkelium fraction containing about 10% of the americium and curium and about 60% of the berkelium, and (3) the remaining berkelium and the transberkelium elements, along with about 0.5% of the americium and curium.

A typical Tramex product from the processing of irradiated targets of ^{242}Pu contains up to 10,000 times as much americium and curium as the total amount of transcurium elements.

This process, which has been used for many years to make separations in the laboratory, was scaled up during the previous report period for processing the Tramex product solutions from the prototype targets and three SRP slugs. During the current report period, the same equipment was used for processing three additional SRP slugs and five of the SRP-HFIR targets. New equipment (of glass and plastic) was installed for processing on an even larger scale in the TRU processing

[1] D. E. Ferguson *et al.*, *Chem. Technol. Div. Ann. Progr. Rept. May 31, 1967*, ORNL-4145, p. 133.

[2] F. L. Culler *et al.*, *Chem. Technol. Div. Ann. Progr. Rept. May 31, 1964*, ORNL-3627, pp. 136–52.

[3] D. E. Ferguson *et al.*, *Chem. Technol. Div. Ann. Progr. Rept. May 31, 1967*, ORNL-4145, p. 137.

cells. We are now installing permanent equipment that is fabricated from tantalum.

The largest single batch processed thus far contained 18 g of ^{244}Cm. Except for scale-up by a factor of 2, the only significant change has been in the feed preparation step. Simple batch extraction of zirconium, preceding the feed adjustment, has reduced the concentration of this contaminant significantly. Previous problems with hydrolysis and precipitates are now nonexistent. A procedure similar to that for Tramex feed adjustment permits the handling of up to 1 g of zirconium in a batch of feed.

Preparation of Tramex Feed from SRP Raffinate and Rework Solutions

A two-stage batch solvent extraction process (Cleanex) has been used to pretreat rework material and the SRP americium-curium solution to make them suitable for Tramex processing. In general, the actinides are extracted from either an HCl or an HNO_3 solution (0.2 *M* or less) into 1 *M* HDEHP in Amsco 125-82 diluent, and then stripped with HCl. The exact processing method depends upon the kinds and amounts of actinides and of impurities that are present.

The SRP americium-curium solution was processed in 14 batches, each containing up to 10 g of ^{244}Cm, to remove excess sodium and, simultaneously, to convert from a nitrate to a chloride medium. A batch of the nitrate solution was transferred from the storage tank to a process tank (T-72), where the HNO_3 concentration was adjusted to 0.1 *M* by adding caustic and water. This solution was contacted with an equal volume of extractant (1 *M* HDEHP in Amsco 125-82) by air sparging. The aqueous phase was transferred to another tank (T-71), where it was contacted with another equal volume of extractant. The aqueous phase from this second extraction stage was discarded. The actinide-bearing solvent in T-72 was scrubbed twice with 0.5-volume batches of 0.03 *M* HCl; then the resulting solution was transferred to T-71 to scrub the second-stage extractant. The aqueous phase was discarded. The extractant in T-71 was eventually recycled to T-72, where it was used as the first-stage extractant for processing the next batch of feed. Three 0.5-volume batches of HCl were used to strip the americium and curium from the first-stage solvent; 5 *M* HCl was used for the first seven batches, and 2 *M* HCl was used for the last seven batches to improve the iron decontamination factor (DF). No iron was separated when 5 *M* HCl was used; the iron DF was 40 when 2 *M* HCl was used. It was possible to use this lower acid concentration because the SRP solutions contain only insignificant amounts of transcurium elements, which might not be stripped quantitatively in 2 *M* HCl.

The rework material included process wastes from the product finishing in cell 5, unused portions of samples from the analytical laboratories, and solutions that had been collected in the rework tank during processing. The latter solutions contained various large amounts of lithium, sodium, nitrate, chloride, and corrosion products of Hastelloy C.

Emulsions that occurred during the extractions made it impossible to determine the aqueous-organic interfaces during phase separations. It was necessary to stop the aqueous transfers when about 5 liters of aqueous remained in the tank. Therefore, one or two extra stripping steps were required per batch to dilute the tank heel.

About 30 g of ^{244}Cm and 800 μg of ^{252}Cf were recovered. Measured losses were less than 2%. The material balances indicated recoveries of 92% of the curium and 125% of the californium present (by analysis) in the feed.

Target Fabrication

Most of the americium and curium that is recovered from irradiated targets is incorporated into recycle targets and reirradiated in the HFIR to produce transcurium elements. During this report period, the first six recycle targets were fabricated in TRU, using the remote equipment installed in cells 1, 2, and 3. This equipment has been described previously.[4]

For each of the six target assemblies, actinide oxide powder, which was prepared during developmental work on the curium sol-gel process (see Sect. 6.3), was blended with aluminum powder, and the resulting mixture was pressed into aluminum-clad pellets. The pellets were inspected to ensure conformity to size and weight requirements, cleaned ultrasonically, and dried under vacuum at

[4] *Metals and Ceramics Div. Ann. Progr. Rept. May 31, 1962*, ORNL-3313, pp. 108–11.

400°C. From 34 to 36 pellets (total length, 20 ± 0.5 in.) were loaded into a target tube that had previously had a bottom end cap welded in place. A top support liner, cut to the proper length for the target, was inserted. The tube was evacuated and filled with helium; then the top end cap was installed and welded to the tube. The tube was examined for leaks in a helium leak detector; was cleaned, dried, and smeared for contamination; and was x rayed to ensure the integrity of the welds and to determine that the end spacers and pellets were in place. The tube was pressed hydrostatically (at 10 tons/in.^{2}) to make a good heat transfer bond between the pellets and the tube, and the tube was helium-leak-tested again. Finally, the hexagonal coolant-flow tube was mechanically staked to fins on the target rod, and the finished target assembly was cleaned and transferred to the HFIR.

Although numerous minor problems have been encountered, as might be expected for equipment of this complexity, this equipment is considered to be fully operational.

Maintenance and Modification of Equipment

During a program that lasted about six weeks early in 1968, we made some modifications, improvements, and repairs. The dissolver, T-70, which was fabricated from Zircaloy-2 and which had undergone serious corrosion (see the next section), was replaced by a duplicate vessel. Dip probes, which had been badly corroded, were replaced in two tanks. An additional tantalum-lined evaporator was installed for concentrating and for adjusting the composition of products from the Tramex process and from subsequent processing steps. The drive system (gears and chains) for the intercell conveyor was extensively overhauled.

The cubicle 6 back equipment rack, which is primarily a pump distribution system for Tramex products and subsequent processing steps, was replaced with an improved system. Phase separators were added to the back equipment rack in cubicle 7, which contains the pump distribution system for the dissolver and the Pubex and Tramex processes. These changes made the pump distribution systems conform to the most recent flowsheets as they evolved, and minimized the use of makeshift piping systems.

A permanent in-cell vacuum system was installed in cubicles 4, 5, 6, and 7 to replace a temporary system that we had found to be useful for transferring solutions, assisting sluggish samplers, and picking up solutions from the cubicle floors. This system is separate from the plant vacuum system.

We were still able to perform maintenance operations in the tank pits by direct contact with the equipment. Adequate working times were achieved by combining equipment flushing and the use of temporary unit shielding.

Corrosion of Zircaloy-2

Extensive corrosion testing was done before the decision was made to use Zircaloy-2 as a major material of construction in TRU. We thought that we had defined the problem areas and knew how to avoid them. However, we have found two sets of circumstances in which the corrosion of equipment was unexpectedly catastrophic.

The first involved corrosion by mixtures of HCl and HNO_3. Although such mixtures are not used in any of the processing steps in TRU, both acids are used (separately) in the plant; therefore, solutions of the mixed acids appear in the condensate collection system and in the rework collection system. Our attempts to avoid concentrations of mixed acids that would cause catastrophic corrosion were apparently not successful. Zircaloy-2 dip probes in both the condensate collection tank, T-34, and the rework collection tank, T-77, had to be replaced two and three times, respectively, even though heels of caustic were maintained in the tanks. We have recently installed dip probes constructed of Hastelloy C in these tanks (which are of Hastelloy C) to circumvent this corrosion problem. In general, Hastelloy C is much less resistant to corrosion by HCl than Zircaloy-2 is; however, it does not undergo catastrophic attack in HNO_3-HCl solutions.

The second situation stemmed from the effect of radiation on the rate at which HCl corrodes Zircaloy-2. Early tests indicated that the corrosion rate of Zircaloy-2 in HCl was only 1 to 2 mils/year in the absence of radiation. There was a slight increase in the corrosion rate in HCl solutions having a power density of up to 2 w/liter, but it did not appear to be significant. However, our dissolver solutions contained much more zirconium than was expected, and thus indicated

very high corrosion rates. The Zircaloy-2 dip probes in the dissolver finally became so badly corroded that they were useless. Since the dissolver was constructed entirely of Zircaloy-2 and the probes were welded to the vessel, we replaced the entire unit. We are planning to use a dissolution technique that will not require the Zircaloy-2 dissolver to be exposed to HCl solutions having high power densities. We expect to dejacket (dissolve the aluminum) in the dissolver, T-70, using caustic-nitrate solution, and then to transfer a slurry of actinide oxides to a tantalum-lined vessel for dissolution in 6 *M* HCl. (Since caustic causes catastrophic corrosion of tantalum, we cannot perform the dejacketing operation in vessels fabricated of this metal.)

Corrosion Tests

To further study the two problems noted above, we exposed Zircaloy-2 to various mixtures of HCl and HNO_3 in the absence of radiation, and to chloride solutions containing ^{244}Cm at concentrations that gave solution power densities up to 37 w/liter (13 g/liter). These tests did not yield accurate results in the case of low corrosion rates, but they did differentiate between low corrosion rates and catastrophic corrosion rates.

Corrosion specimens for the nonradioactive tests consisted of 49-mil-wall Zircaloy-2 tubing that was $^3/_8$ in. in diameter by 1 in. long. They were exposed to the solutions at room temperature, and the corrosion rates were determined by measuring the weight lost in a given time interval (24, 48, or 72 hr).

Zircaloy-2 was not attacked significantly by mixtures containing HCl at a lower concentration than 2 *M*; nitric acid concentrations from 0 to 6 *M* were studied. The corrosion rate for 3 *M* HCl appeared to be significant ($\sim$5 mils/year) when the concentration of HNO_3 was as low as 0.5 *M* and was definitely catastrophic (75 to 200 mils/year) at HNO_3 concentrations of 1 to 6 *M*. Further, the attack was not uniform. The corrosion was catastrophic and the attack was nonuniform in each HCl-HNO_3 mixture in which the HCl concentration was greater than 3 *M* and the HNO_3 concentration was greater than a few tenths molar.

Next, the effect of radiation on corrosion rates was studied. The chloride solutions and the power density levels used in this study were as follows: (1) 6 *M* HCl at 37 w/liter, (2) 6 *M* HCl at 8 w/liter, (3) 11 *M* LiCl–0.3 *M* HCl at 32.2 w/liter, and (4) 11 *M* LiCl–0.3 *M* HCl at 10.3 w/liter.

The Zircaloy-2 coupons used in the radioactive tests were 0.5 in. × 1 in. × $^1/_4$ in. thick. The solution temperatures were not controlled; we estimated that they varied between 35 and 60°C. This lack of temperature control detracts from the results of the tests; however, results of other, "cold" tests have shown that corrosion of Zircaloy-2 by HCl solutions is not markedly dependent on temperature. Corrosion rates were determined by measuring the weight change in a given time interval. The longest exposure was 207 hr in HCl and 156 hr in LiCl.

The Zircaloy-2 corrosion rate in 6 *M* HCl at a power density of 37 w/liter was constant at about 60 mils/year. The 8-w/liter data indicate that the corrosion rate was increasing throughout the test period. After 24 hr, the rate was 1.3 mils/year; during the next 42.3 hr it was 14 mils/year; throughout the following 94 hr it was 18 mils/year; and during the final 46 hr it was 32 mils/year.

The Zircaloy-2 coupons gained weight in LiCl-HCl solutions for up to 43 hr and then started to lose weight, but at much lower rates than in the tests in 6 *M* HCl. The surfaces of the specimens appeared unchanged. No apparent deposits were noted.

HFIR Target Rod Failures

Last year we reported that several TRU target rods had ruptured during irradiation in the HFIR. These were part of a group of 17 targets that had been irradiated for about one year in a Savannah River Plant reactor. Sixteen of them ruptured after irradiation in the HFIR for 125 to 175 days at a power of 100 Mw.

The Metals and Ceramics Division began an extensive program to determine the mechanisms that caused the failures and to develop an improved target design. Details of their efforts to date have recently been reported.[5] The nature of the problem precludes rapid solution; proof of a new target design will require a minimum of 18 months of irradiation in the HFIR. Because of our vital interest

[5] A. L. Lotts *et al.*, *Analysis of Failure of HFIR Target Elements Irradiated in SRL and in HFIR – an Interim Status Report*, ORNL-TM-2236 (to be published).

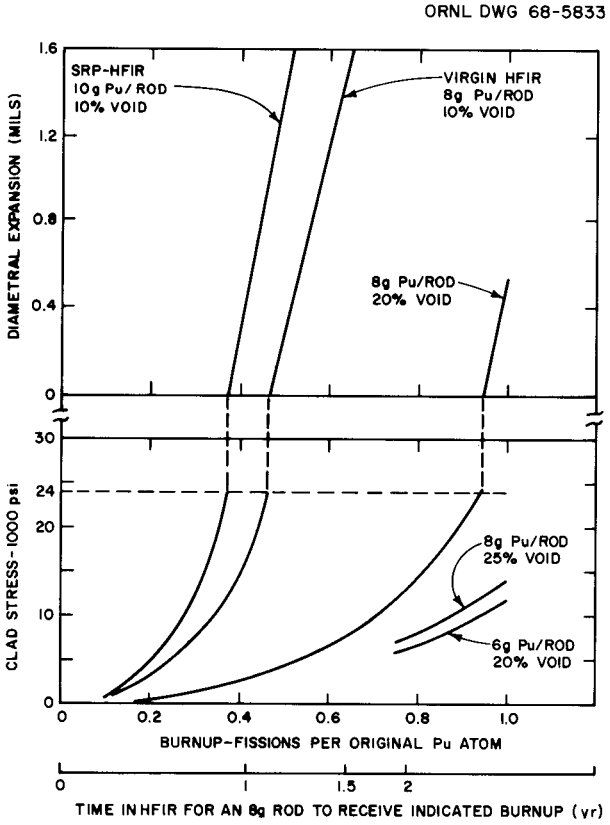

Fig. 6.2. Effect of Burnup and Fabrication Variables on Clad Stress.

in this matter, the status of the work is summarized here.

Various techniques were used in analyzing the failure: visual inspection, measurement of dimensional changes, metallography, vacuum-fusion gas analysis, determination of mechanical properties, electron microscopy, and x-ray diffraction. It was concluded that the exposure of the aluminum alloy cladding material to the high fast-neutron flux in the HFIR causes a rapid decrease in the ductility. Fission products accumulate and fill the void volume in the pellets, and the gases increase the pressure in the remaining voids. This results in a gradual increase in the stresses in the cladding. When the stresses reach the yield point of the cladding, the embrittled cladding fractures instead of yielding.

We have developed an engineering model to guide the development of an improved design. Figure 6.2 summarizes the results of calculations that have been made. The lower family of curves shows the stress in the cladding of various targets as a function of the burnup. The abscissa is the number of fissions occurring per atom of plutonium in the original target rod. The dashed line at 24,000 psi indicates the probable stress at which the SRP-HFIR targets failed. This value, which was determined from specimens of the aluminum coolant-flow tubes that were on the targets, was used as a typical stress at which the cladding on any target might fail. The upper graph has, as its ordinate, the diametral expansion that would occur if the target sheath yielded (instead of rupturing).

The curve for the SRP-HFIR targets (10 g of ^{242}Pu per target and 10% void space in the pellets) is in fair agreement with the failure data. The model indicates failure at 0.375 fission per original plutonium atom; the targets actually failed at burnups of from 0.21 to 0.33 fission per original plutonium atom. The early failures might be attributed to nonuniform loading and variation in pellet densities. The curve for "virgin HFIR targets containing 8 g of ^{242}Pu and having 10% void volume" represents a group of 13 targets that are now being irradiated in the HFIR. It indicates that these targets will fail at a burnup of 0.43 fission per original plutonium atom. This burnup will be achieved near the end of HFIR cycle No. 21, which is scheduled to end in mid-June 1968. No failures occurred prior to mid-May.

Each of the three curves labeled "8 g plutonium/rod, 20% void," "8 g plutonium/rod, 25% void," and "6 g plutonium/rod, 20% void" represents pairs of special targets that were fabricated during the past year and are now being irradiated to determine whether smaller loading and/or pressing of pellets to lower densities (and larger void volumes) will result in longer target lifetimes. Calculations indicate that none of these targets will fail prior to the time that the irradiations are scheduled to be terminated. If this proves to be true, the failure problem will be resolved, for all practical purposes, in a way that does not restrict future production. Of course, there will still be great interest in, and further work will be done to study, the aluminum embrittlement phenomenon.

6.2 ISOLATION AND PURIFICATION OF TRU PRODUCTS

Product finishing operations and final purification and isolation of transplutonium elements are

accomplished in equipment that is installed in cell 5 in TRU and in supporting shielded-cave facilities.

The final processing of main-line products in cell 5 is required because of the lack of a fully developed process method. When such a process becomes available, equipment for it will be installed in the main-line processing area, and the temporary equipment will be removed from cell 5.

Product finishing operations and special separations will continue to be performed in the cell 5 shielded-cave complex indefinitely. When products reach certain levels of purity, they must be moved to progressively cleaner facilities and, finally, to shielded caves or to glove boxes that are used only for handling products. These operations are the main subject of this section.

Status and Progress

Tramex products are processed by an LiCl-based anion exchange method to provide additional decontamination and to separate the products into three fractions: an americium-curium fraction, a berkelium fraction, and a transberkelium fraction. The processing of these fractions was continued in cell 5 by the procedure described in the last annual report.[6] Part of the americium-curium product was processed to separate the contained elements by selectively precipitating americium as an Am(V)-potassium double carbonate. Berkelium was separated from residual actinides by extraction of tetravalent berkelium from 8 *M* HNO_3 into di(2-ethylhexyl)phosphoric acid. Einsteinium and californium were isolated from each other and from other residual actinides by selective elution from cation exchange resin with ammonium α-hydroxyisobutyrate. Purified products from these separations included 57 g of ^{244}Cm, 11 g of ^{243}Am, 300 μg of ^{249}Bk, 4.4 mg of ^{252}Cf, and 10 μg of ^{253}Es.

A high-pressure ion exchange column was used to separate microgram quantities of ^{253}Es from milligram quantities of ^{252}Cf and ^{244}Cm. This marked the first use of such equipment in high-activity-level processing. It is anticipated that the column presently installed can be used to process 100 mg of ^{252}Cf.

[6]D. E. Ferguson *et al.*, *Chem. Technol. Div. Ann. Progr. Rept. May 31, 1967*, ORNL-4145, pp. 136–51.

Various special separations were also made; these include: isolation of ~1 μg of second-growth ^{253}Es (daughter of ^{253}Cf) and 97 μg of ^{248}Cm, both of which had grown into the purified californium products during storage, and separation of 55 μg of ^{249}Cf that had grown into 350 μg of ^{249}Bk. In other processing, 65 g of ^{244}Cm obtained from Savannah River concentrate was highly purified for use in isotopic heat sources by the Isotopes Division and for distribution to numerous customers around the country.

Californium-Einsteinium-Fermium Separations

The results obtained with the high-pressure ion exchange column for californium-einsteinium separations at high activity levels have been very encouraging. In this separation, which involves chromatographic elution from cation exchange resin with α-hydroxyisobutyrate solution, a high-pressure feed pump makes it possible to maintain a constant, rapid flow through a long bed of very fine resin. The shorter processing time decreases radiation damage to the resin and suppresses the formation of radiolytic gas during processing. Typical elutions with this system produce product fractions that contain ~99% of the desired element with <1% cross contamination. This compares with 80 to 90% yields in the product fraction and 10% cross contamination for conventional ion exchange column operation.

Process Equipment. – A photograph of the equipment rack installed in cell 5 is shown in Fig. 6.3. Two 48-in.-high ion exchange columns, water-jacketed for temperature control at 80°C, are located in the center of the rack. These columns are 0.3 and 0.4 in. in diameter and have resin capacities of 40 and 100 ml respectively. In-line alpha detectors and external neutron detectors were used to monitor the elution of the transcurium elements.

Operating Experience. – The columns were packed with Dowex 50-X8 resin that was 20 to 40 μ in diameter. Elution was accomplished with 0.25 *M* ammonium α-hydroxyisobutyrate adjusted to a pH of 4.2. Process solutions were pumped through the column at flow rates of 5 to 10 ml min^{-1} cm^{-2}, which generated pressures on the order of 500 to 1000 psig.

Numerous separations were made in which the feed, typically, contained californium-einsteinium

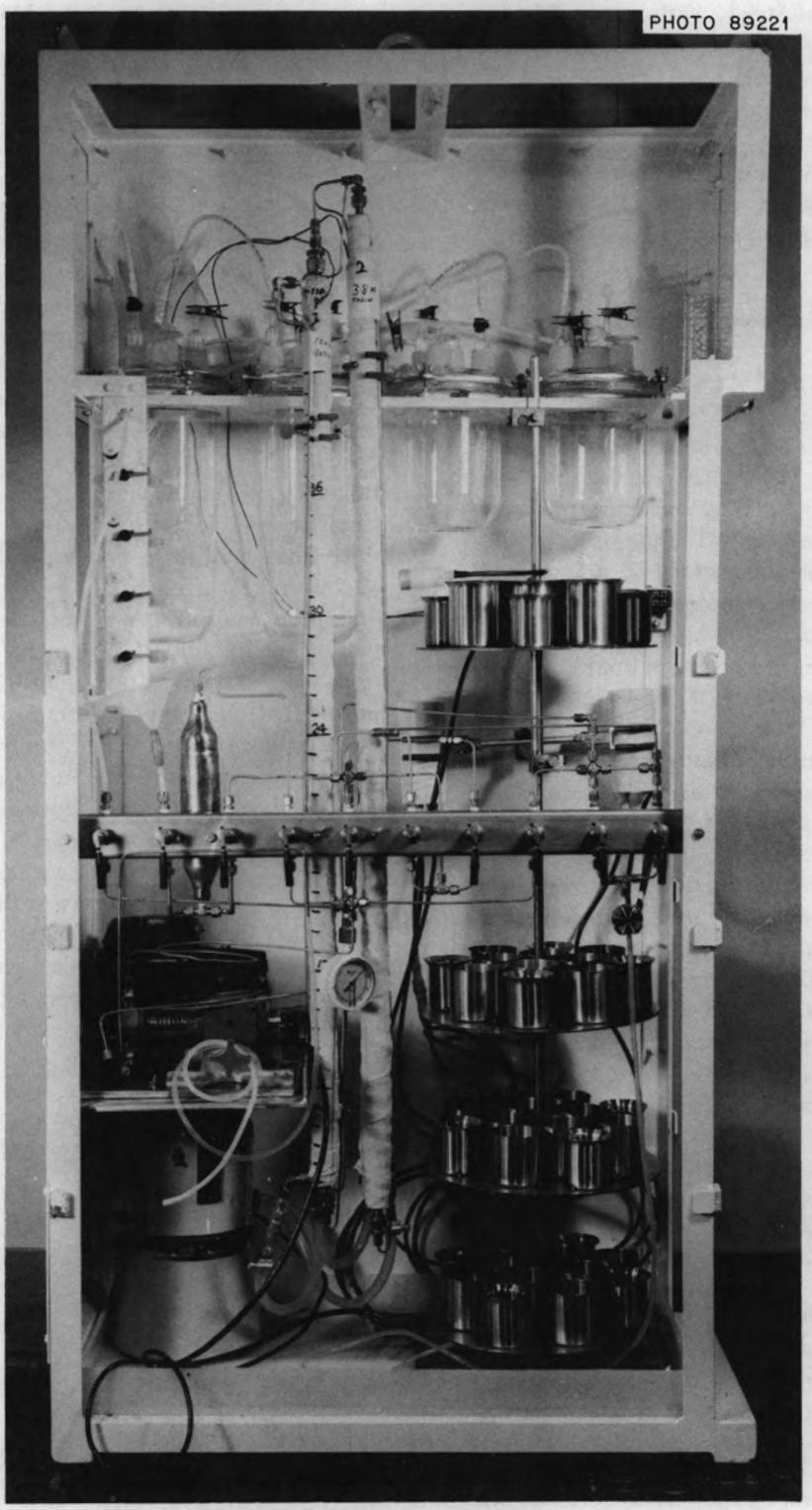

Fig. 6.3. High-Pressure Ion Exchange Column Equipment Rack.

with a mass ratio of 500:1, while product fractions contained >99% of the respective elements, with <1% cross contamination. The largest quantity of material processed in a single run was ~200 mg of ^{244}Cm, 3 mg of ^{252}Cf, and 6 μg of ^{253}Es. The einsteinium fraction contained <0.5 μg of ^{252}Cf, which represents a californium decontamination factor greater than 1000.

Isolation of Second-Growth Isotopes

A total of 55 μg of ^{249}Cf was separated from 350 μg of its parent, ^{249}Bk. The berkelium was oxidized to Bk(IV) and extracted into HDEHP in the usual manner. The ^{249}Cf was then recovered from the raffinate by adding iron carrier and precipitating the hydroxides. The precipitate was dissolved in a small volume of HCl and passed through an anion exchange column to remove the iron. The gamma radiation level of the final product was 8 mr/hr; no neutrons could be detected. Alpha pulse analysis indicated that the product was pure ^{249}Cf.

The ^{252}Cf product was processed, after storage for about six weeks, by the high-pressure ion exchange method to recover the ^{248}Cm and ^{253}Es that had grown in. About 1 μg of pure ^{253}Es and 95 μg of ^{248}Cm were recovered. The overall separation factor between curium and californium in two separation stages was 49,000; however, the ^{248}Cm was contaminated with ^{244}Cm, as shown in Table 6.2. This material will be used for neutron cross-section experiments, and part of it will be irradiated later in a further effort to produce significant amounts of ^{250}Cm.

Table 6.2. Isotopic Composition of ^{248}Cm Product

Isotope	Abundance (%)	Percent of Alpha Emission	Percent of Neutron Emission
^{244}Cm	57.14	99.96	30.4
^{245}Cm	0.43		
^{246}Cm	5.82	0.03	2.7
^{247}Cm	0.11		
^{248}Cm	36.50	0.003	66.8

Purification of ^{244}Cm

A special project required the preparation of about 65 g of highly purified curium oxide for use both in experiments directed toward fabrication of heat sources by the Isotopes Division and for various research groups throughout the country. The curium was separated from associated ^{243}Am by selectively precipitating an Am(V)-potassium double carbonate as described previously.[6] The separated curium was first purified from metal ion contaminants by a series of three oxalate precipitations and then calcined to the oxide at 800°C.

Oxalate precipitations were made at an HNO_3 concentration of 0.5–0.7 *M* with 0.2 *M* oxalic acid. Under these conditions, calcium and most other metallic ions do not precipitate; however, since these ions tend to be carried with the curium oxalate it was necessary to make three successive precipitations in order to sufficiently remove potassium and calcium. The successive precipitations were made by dissolving the curium oxalate in 6 *M* HNO_3 and then diluting to 0.5 *M* HNO_3 with 0.1 *M* oxalic acid to reprecipitate the curium oxalate. This procedure was subsequently repeated. Curium losses in the oxalate filtrate were less than 1%, with solubilities of <10 mg/liter.

The final curium oxalate was calcined at 800°C to form the oxide. Analysis of the oxide showed that, other than residual ^{243}Am, the curium contained <0.5% impurities. The americium content varied from 0.5 to 2 wt % over a period of several runs. A trace of ^{106}Ru(Rh) was the only detectable radiochemical impurity.

The americium was further purified from residual curium by a second cycle. This reduced the curium content to 0.005 wt %. The americium was purified through two oxalate precipitations and converted to oxide by calcination at 800°C. The only detectable metal ion impurity was ~0.4 wt % Ca.

6.3 DEVELOPMENT OF CHEMICAL PROCESSES

Laboratory support was provided to investigate chemical problems that arose during high-activity-level processing in TRU. We continued the development of processes for recovering plutonium, partitioning actinides, isolating berkelium, and recovering americium-curium from Savannah River

Plant concentrate by solvent extraction. Also, we continued to investigate methods for separating californium-einsteinium-fermium and for preparing americium-curium oxide for use in HFIR targets.

Status and Progress

Difficulties experienced during plant operation of the ion exchange system for recovering plutonium from HCl solution led to the development of a batch solvent extraction process (Pubex) that has proved successful in routine use. In addition to isolating plutonium, this process also serves to decontaminate both the plutonium and the transplutonium-element fraction from corrosion product zirconium. In this process, tetravalent plutonium and zirconium are preferentially extracted from 6 *M* HCl into 1 *M* di(2-ethylhexyl)phosphoric acid in diethylbenzene. The transplutonium elements remain in the aqueous phase. The solvent is washed with dilute HCl, and the plutonium is stripped with 6 to 8 *M* HCl after reduction to the trivalent form with the organic-soluble reductant 2,5-di-*tert*-butylhydroquinone. The zirconium remains in the waste solvent, which is discarded.

The laboratory development of an extraction process for actinide partitioning (Hepex) was continued. This process, which is a possible alternative to partitioning by LiCl-based anion exchange, may be attractive for very large-scale processing. In the Hepex process, the transcurium elements are separated from americium and curium by extraction into di(2-ethylhexyl)phosphoric acid from HCl. Single-stage separation factors between berkelium and curium are about 13. Multistage countercurrent experiments at tracer level have indicated that a separation process using this method is practicable; however, the process has not been tested with actual process solutions at high activity levels.

Laboratory development of the berkelium recovery process was continued. This process (Berkex), which involves oxidation of the berkelium to Bk^{4+} with $NaBrO_3$ and extraction from 8 *M* HNO_3 into di(2-ethylhexyl)phosphoric acid, has operated satisfactorily; however, stability of the oxidant in 8 *M* HNO_3 is marginal. Recent results indicate that berkelium can be satisfactorily oxidized by chromate in 4 *M* HNO_3 and then extracted, thereby eliminating difficulties that stem from the decomposition of bromate. Although excellent separations of berkelium from curium have been demonstrated at tracer levels, process conditions have not been fully optimized, and the fate of chromium in the process has not yet been determined.

Laboratory studies were conducted to develop a process (Cleanex) for recovering americium and curium from nitric acid solutions containing sodium and other ionic contaminants. This process involves careful neutralization with NaOH to obtain a low acid concentration ($\sim$0.1 *N*), extracting the actinides into 1 *M* HDEHP in Amsco 125-82, scrubbing with dilute HCl to remove nitrate, and stripping the actinides into 5 *M* HCl. This process was used in plant equipment as a two-stage batch extraction process to convert americium-curium from Savannah River concentrate into a chloride solution suitable for use as Tramex feed. The process was also used to recover actinides from recycle streams that contained gross amounts of corrosion products and other ionic contaminants, as well as various solids.

The laboratory development of the high-pressure ion exchange column that has been used for separating californium, einsteinium, and fermium was continued (see Sect. 6.2). Similar systems have also been effectively used for analytical applications. The effects of experimental variables were studied, with emphasis on very rapid separations; when 1-mg quantities of lanthanides were applied to small columns containing about 1 ml of resin that was less than 10 μ in diameter, adequate separations were achieved in about 2 min.

The sol-gel method for preparing americium-curium oxide for HFIR targets was successfully adapted for preparing mixed ^{244}Cm-^{243}Am sols. The sols were first converted to gel microspheres and then calcined to dense oxide spheres. A development facility installed in-cell in Building 4507 was used to prepare 38 g of americium-curium oxide product in the desired size range (50 to 170 μ). This material was successfully fabricated into HFIR targets. Additional development work will be required to simplify the equipment for permanent plant facilities and to better understand the process variables.

Plutonium Recovery by Solvent Extraction

The Pubex process was designed to selectively extract tetravalent plutonium and zirconium from transplutonium elements in HCl media. Following

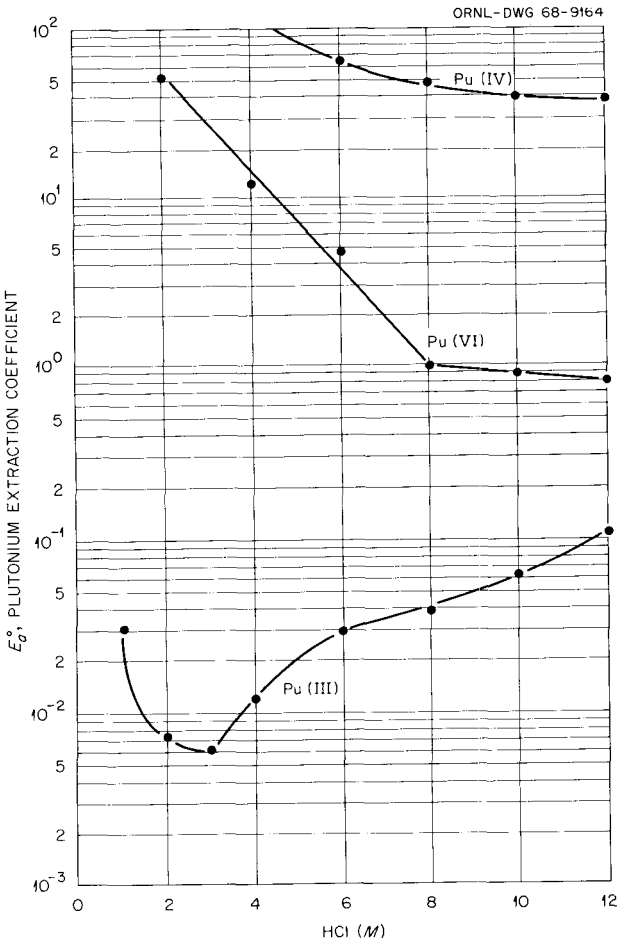

Fig. 6.4. Extraction of Plutonium by 1 *M* HDEHP in Diethylbenzene from HCl Solutions as a Function of HCl Concentration.

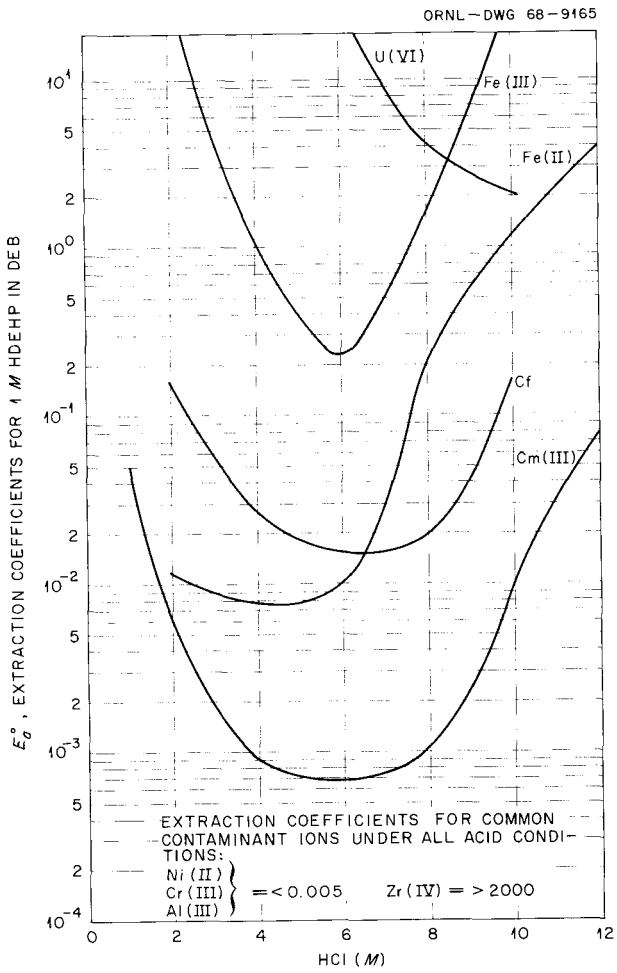

Fig. 6.5. Extraction Coefficients, E_a^o, for Various Metals Dissolved in 1 *M* HDEHP–DEB.

its reduction to the trivalent state, plutonium can be stripped from the organic phase, leaving zirconium in the waste solvent. High separation factors and efficient plutonium stripping permit simple batch extraction operations.

Plutonium and zirconium are extracted from 6 *M* HCl into 1 *M* di(2-ethylhexyl)phosphoric acid (HDEHP) in diethylbenzene (DEB). The transplutonium elements remain in the aqueous phase. The solvent is washed with 5 *M* HCl, and the plutonium is reduced to the trivalent form with the organic-soluble reductant 2,5-di-*tert*-butylhydroquinone (DBHQ). The trivalent plutonium is then stripped into 8 *M* HCl, leaving the zirconium in the waste solvent.

Extraction Coefficients (E_a^o). – Coefficients for the extraction of Pu(III), Pu(IV), and Pu(VI) from 1 *M* HDEHP in DEB as a function of HCl concentration are shown in Fig. 6.4. The extraction coefficients obtained for tetravalent plutonium decrease with increasing acid concentration. However, optimum separation from curium and other ions is obtained at 6 *M* HCl, where the extraction curves of many metal ions show a pronounced minimum (Fig. 6.5).

The extraction of Pu(IV) is first-order dependent on the HDEHP concentration in the organic phase (Fig. 6.6) and shows only a slight dependence on the nature of the diluent. A small decrease in extraction occurs when the dielectric constant of the diluent is increased.

Solvent Scrub. – A wash cycle is included in the Pubex process both to back-extract the transplutonium elements and to remove extracted HNO_3, which is present in the feed for plutonium valence

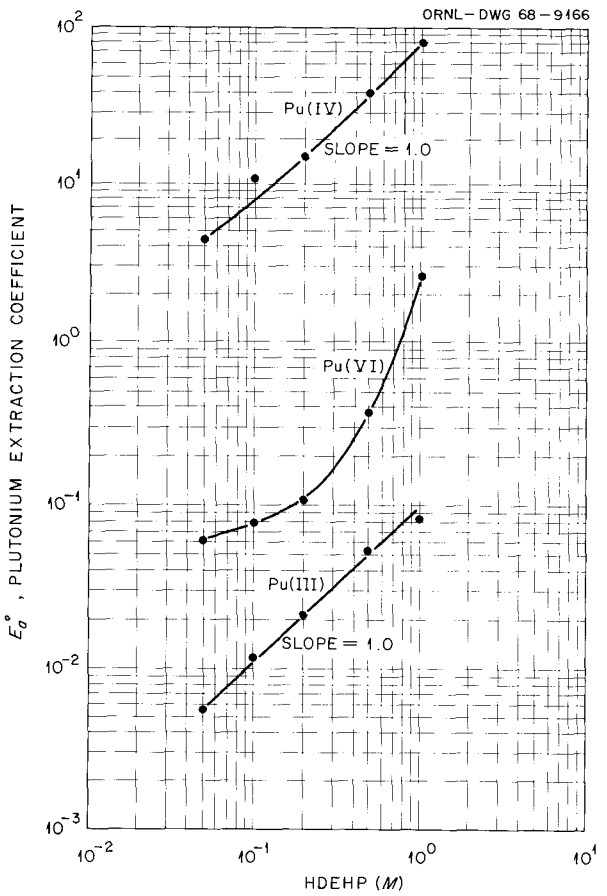

Fig. 6.6. Plutonium Extraction from 6 *M* HCl as a Function of HDEHP Concentration.

control. Any residual HNO_3 in the organic phase oxidizes DBHQ and thereby interferes with plutonium reduction. Solutions with very low acid concentrations remove nitrate most efficiently, but they result in poor phase separation. A 1 *M* HCl solution is optimum for nitrate removal and good phase separation; however, 5 *M* HCl is preferred because it not only removes nitrate satisfactorily but is more efficient in removing transplutonium elements from the solvent.

Plutonium Stripping. – When the organic phase is adjusted to contain 25 vol % of the reducing mixture 2-ethylhexanol–0.2 *M* DBHQ, 90% of the plutonium can be stripped by a single equal-volume contact with 8 *M* HCl. If the organic phase is adjusted to contain less than 20 vol %, however, a significant decrease in stripping efficiency is observed.

Hydrochloric acid solutions at concentrations from 5 to 9 *M* effectively strip the reduced plutonium from the organic phase. Although the Pu(III) extraction data (see Fig. 6.4) indicate that optimum stripping would occur at 3 *M* HCl, the addition of 2-ethylhexanol shifts the extraction minimum to an acid concentration of 7 *M*.

Table 6.3. Stripping of Pu(IV) from 1.0 *M* HDEHP in Diethylbenzene by Aqueous-Soluble Reductants in 6 *M* HCl

Aqueous-Soluble Reductant	Temperature (°C)	Equilibration Time (min)	S_o^a
0.1 *M* hydroxylamine hydrochloride	25	5	0.0068
0.1 *M* ascorbic acid	25	5	0.16
0.1 *M* hydroquinone	25	5	0.16
0.2 *M* hydroquinone	25	5	0.22
0.2 *M* hydroquinone	25	40	0.41
0.2 *M* hydroquinone	50	5	14.3

During early developmental work, various reducing agents were evaluated as plutonium reductants. Reductants that are soluble in the aqueous phase were not highly effective at 25°C (Table 6.3), although it has recently been found that their effectiveness can be greatly increased at elevated temperatures (50°C).

In the examination of several complexing agents for use in stripping plutonium from HDEHP in chloride systems, oxalic acid was found to be effective for stripping both plutonium and zirconium. This technique is useful for analytical purposes; however, since there is no separation of plutonium and zirconium, it has no process value.

Second-Cycle Plutonium Purification. – Separation from nearly all contaminants except antimony is obtained by a second-cycle batch extraction. Prior to the second extraction, the plutonium must be reoxidized to Pu(IV). The inclusion of hydroxylamine hydrochloride as a holding reductant in the first-cycle strip solution retards plutonium oxidation; however, complete oxidation can be obtained by the addition of lithium hypochlorite and nitric acid (to 0.05 *M* HNO_3), followed by extensive air sparging.

Although separation from radioantimony (^{125}Sb) is not obtained in this system, a decontamination

factor of 20 can be obtained by use of a single cycle of an anion exchange process. Antimony can be selectively sorbed, under reducing conditions, from 3 *M* HCl–0.1 *M* hydroxylamine hydrochloride.

Heavy-Element Partitioning (Hepex)

Laboratory development of a solvent extraction process for partitioning the transplutonium elements into two groups was continued. In this process, the transcurium elements are extracted and separated from the less-extractable americium and curium. A single-stage separation factor of about 13 between berkelium and curium was demonstrated repeatedly in extractions by aliphatic hydrocarbon solutions of di(2-ethylhexyl)phosphoric acid from dilute hydrochloric acid solutions (with and without impurities that were likely to be encountered in processing). In extractions by 0.8 *M* HDEHP from 0.5 *N* HCl, distribution coefficients for berkelium and curium were 8 and 0.6 respectively. These values were confirmed by operation of a six-stage mixer-settler system, which resulted in the separations indicated in Fig. 6.7. The berkelium can be easily recovered from the extract by stripping with 5 *N* HCl or 5 *N* HNO_3. A greater yield or higher purity of the berkelium could be obtained by proper adjustments of relative flow rates or of the extractant concentration. High concentrations of salts derived from previous processing would require further adjustments; for example, a lithium chloride concentration of 1 *M* decreases distribution coefficients by a factor of 2. When present in expected concentrations, corrosion products such as iron, nickel, chromium, tin, and zirconium do not significantly affect distribution coefficients.

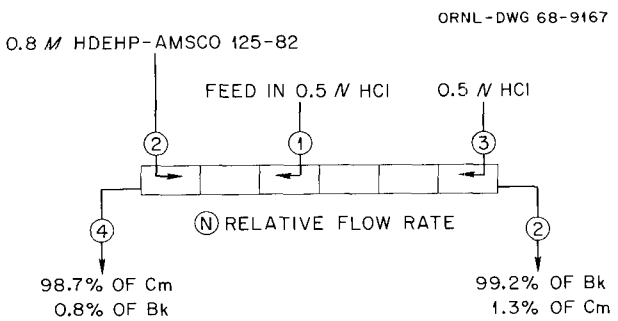

Fig. 6.7. Six-Stage HEPEX Separation of Berkelium and Curium.

As yet, the Hepex process has not been tested with actual process solutions at high activity levels.

Berkelium Isolation by Solvent Extraction (Berkex)

The present method for separating berkelium from other transplutonium elements consists in oxidizing Bk(III) to Bk(IV) by bromate ions in 8 to 10 *M* HNO_3 and then extracting with di(2-ethylhexyl)phosphoric acid (HDEHP). Instability of the bromate in concentrated acid, especially at elevated temperatures and in the presence of radiation, can cause erratic results in the oxidation and extraction of the berkelium. We found that supplementing or replacing the bromate with chromate permits efficient extraction of berkelium from 4 *M* HNO_3.

Berkelium extraction coefficients were measured as a function of CrO_3, HNO_3, and extractant concentrations (see Figs. 6.8–6.10). Berkelium distribution coefficients in extractions with 0.1 to 0.5 *M* HDEHP in *n*-dodecane from 0.8 *M* CrO_3 in 4 *N* HNO_3 exceeded 10^3, while curium distribution coefficients under the same conditions were 10^{-2} to $<10^{-4}$. The berkelium is easily recovered from the extract by stripping with 8 *N* HNO_3 containing H_2O_2.

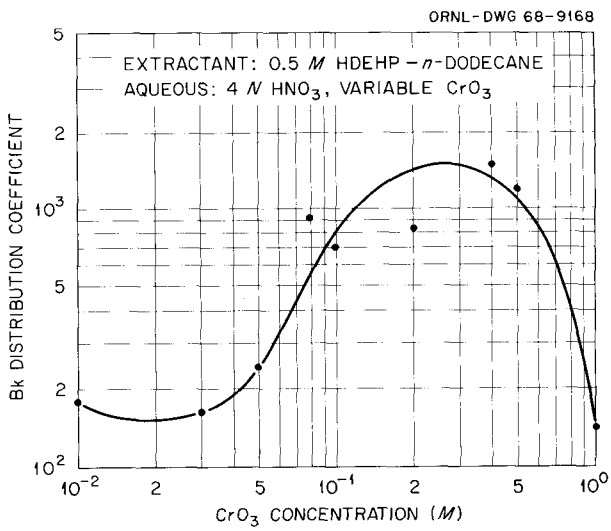

Fig. 6.8. Dependence of Berkelium Extraction on CrO_3 Concentration.

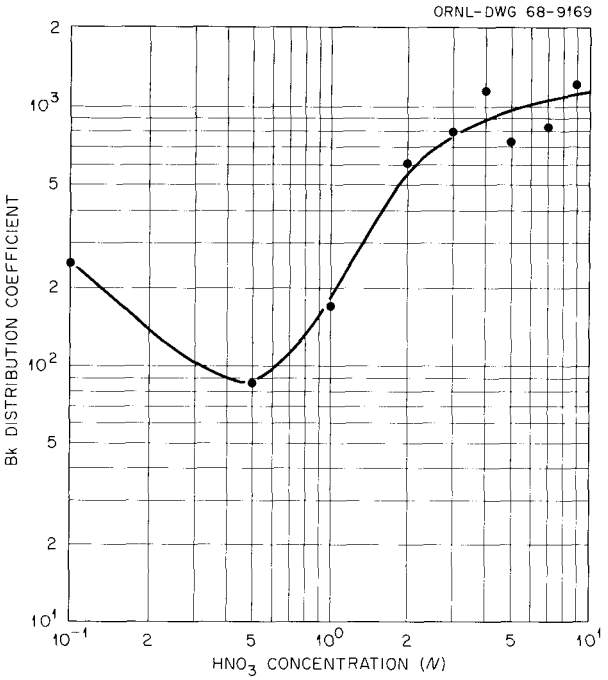

Fig. 6.9. Dependence of Berkelium Extraction on HNO_3 Concentration. Extractant: 0.5 *M* HDEHP–*n*-dodecane; aqueous: 0.08 *M* CrO_3, variable HNO_3.

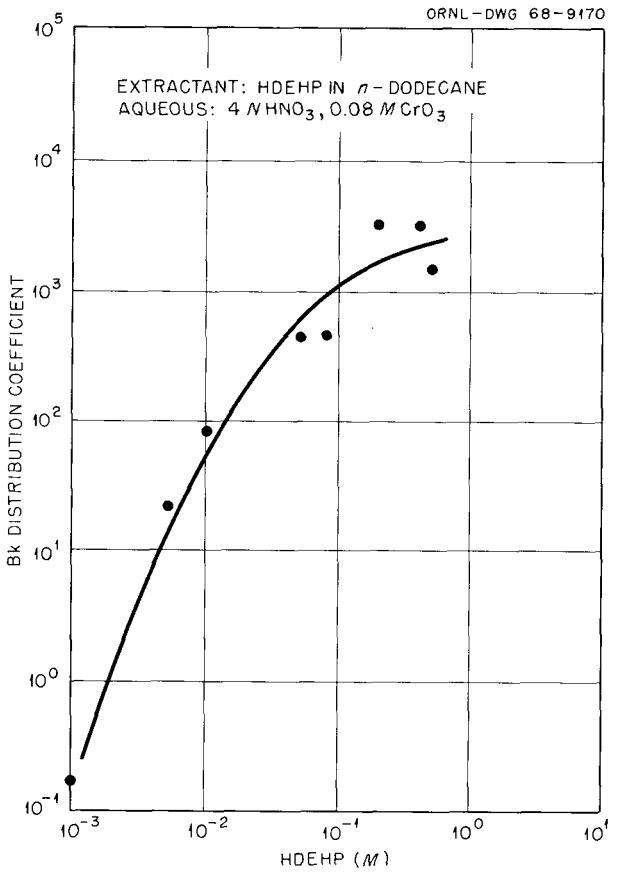

Fig. 6.10. Dependence of Berkelium(IV) Extraction on Extractant Concentrations.

Development of the Cleanex Process

About 278 g of ^{244}Cm and 251 g of ^{243}Am (produced in the ^{239}Pu irradiation program at Savannah River), along with kilogram quantities of rare-earth fission products, were contained in 562 liters of HNO_3 solution. Prior to the separation of americium-curium from rare earths by the Tramex process, it was necessary to convert this nitrate medium to a chloride medium in order to permit removal of gross amounts of the interfering ions – sodium, iron, zirconium, nickel, chromium, molybdenum, sulfate, and phosphate. Thus, an alternative process that might circumvent this conversion was desirable.

A solvent extraction process (termed Cleanex), in which trivalent actinides and lanthanides can be extracted from nitrate media with di(2-ethylhexyl)phosphoric acid (HDEHP) and subsequently stripped with HCl, appeared to be suitable. Laboratory studies were conducted with both simulated rare-earth feed solutions and actual process solution to define suitable process conditions.

Although these studies indicated that the process was amenable to continuous countercurrent extraction operations, a simpler two-stage batch process was found to be highly effective. The batch process also proved to be capable of operation with very "dirty" recycle material that could not be easily handled in continuous contactors.

In the Cleanex process, the aqueous feed (1 *M* in HNO_3) is adjusted to a low acid concentration (0.2 *M* or less) by the addition of caustic, and the curium, americium, and rare earths are extracted into 1 *M* HDEHP in Amsco 125–82. Nitrate that is extracted along with these metals is then removed by scrubbing with 0.03 *M* HCl, and the actinides and lanthanides are finally stripped with 2 *M* HCl.

The principal difficulty, as indicated by initial experiments that were conducted with synthetic feed containing mixed rare earths as a stand-in for the actinides, was the formation of a voluminous

precipitate during neutralization. Tests with actual feed samples showed that this difficulty could be alleviated by diluting the feed 1:1 with water and carefully adding caustic to effect neutralization to 0.2 *M* HNO_3; a feed that remained stable (i.e., was essentially free of precipitates) for 12 hr was obtained. In plant operations the acid concentration of the feed was first reduced to 0.3 *M*, and then the final adjustment to 0.08–0.1 *M* was made in the mixing tank during the first extraction stage; we found that the small amount of precipitate which formed during this procedure could be accommodated.

Extraction. – The extraction coefficients are extremely sensitive to the acid concentration of the aqueous phase. For example, the extraction coefficient for rare earths decreased from 72 at an acid concentration of 0.15 *M* to 4.5 at 0.26 *M*. Comparable curium data indicated extraction coefficients of 4 and about 10 at acid concentrations of 0.15 *M* and 0.1 *M* respectively. Extraction data also indicated that solvent loading by rare earths in excess of 3.5 g/liter seriously depresses extraction coefficients.

Nitrate is readily washed from the solvent with 0.03 *M* HCl solutions. A decontamination factor of 1800 was obtained for a single equal-volume contact. Under the conditions selected, good decontamination from sodium, iron, and zirconium is also obtained. Sodium is not significantly extracted; iron and zirconium are extracted but are retained in the solvent during the final stripping with 2 *M* HCl.

Californium-Einsteinium-Fermium Separations

The separation of californium-einsteinium-fermium and the purification of some final products will be effected by ion exchange methods. A new high-pressure technique that improves control and decreases processing time was reported last year. Studies of this system were continued, and a high-pressure ion exchange column was installed in-cell and successfully used to separate californium from einsteinium (see Sect. 6.2).

Actinide Separations. – A high-pressure ion exchange system was used to separate the actinide elements (from americium to fermium) in laboratory-scale studies, using samples of actual plant solutions. Chromatographic elution from Dowex 50-X12 resin with partially neutralized (to pH 4.4) α-hydroxyisobutyric acid (AHIB) solutions was used. Excellent separations were obtained from both synthetic feeds and TRU process solutions, which include Tramex product, target dissolver solution, and LiCl anion exchange column product. Each separation was accomplished in about 1 hr at flow rates up to 25 ml cm^{-2} min^{-1}.

When a run was made using a Tramex product solution containing the actinides, more than 99.8% of the alpha activity was due to ^{244}Cm; yet, good separations were obtained between the fermium, einsteinium, and californium that were present. A peak, located under the curium tail, was also observed for ^{243}Am, although the experimental conditions did not favor separation of americium from curium. Beta counting of product fractions that were taken between the californium and curium peaks showed a broad band resulting from a combination of ^{249}Bk and ^{155}Eu-^{156}Eu, which were not resolved in this separation.

A similar separation was made, using HFIR target dissolver solution, to determine the behavior of fission products. Elements that gave reasonably sharp bands, like the actinides, included ^{160}Tb (just behind einsteinium), europium (between californium and curium), ^{137}Cs (just ahead of curium), and ^{60}Co (in combination with americium); large amounts of ^{144}Ce-^{144}Pr were found in the cleanup solution that was used to flush the column after the actinide elution. In addition, ruthenium and ^{95}Zr-^{95}Nb were found to be present in all product fractions.

A typical separation obtained by using the heavy-element fraction previously separated on an LiCl column is shown in Fig. 6.11; this feed material contained much less curium and americium than the above-discussed Tramex product solution. Fermium was detected in two fractions; and high-purity einsteinium, californium, and curium products were obtained. Yields and purities depend on the product collection techniques; however, in this case, 98% of the einsteinium was obtained; it contained about 1% ^{240}Pu and less than 1% curium, as determined by alpha counting techniques. About 99.6% of the californium was recovered; it contained 0.1% einsteinium and less than 0.1% of other alpha emitters.

The curve labeled "Bk" is based on the beta counting of product fractions between californium and curium. Beta and gamma spectral measurements, decay studies, and determinations of ^{249}Cf growth support the conclusion that beta counting

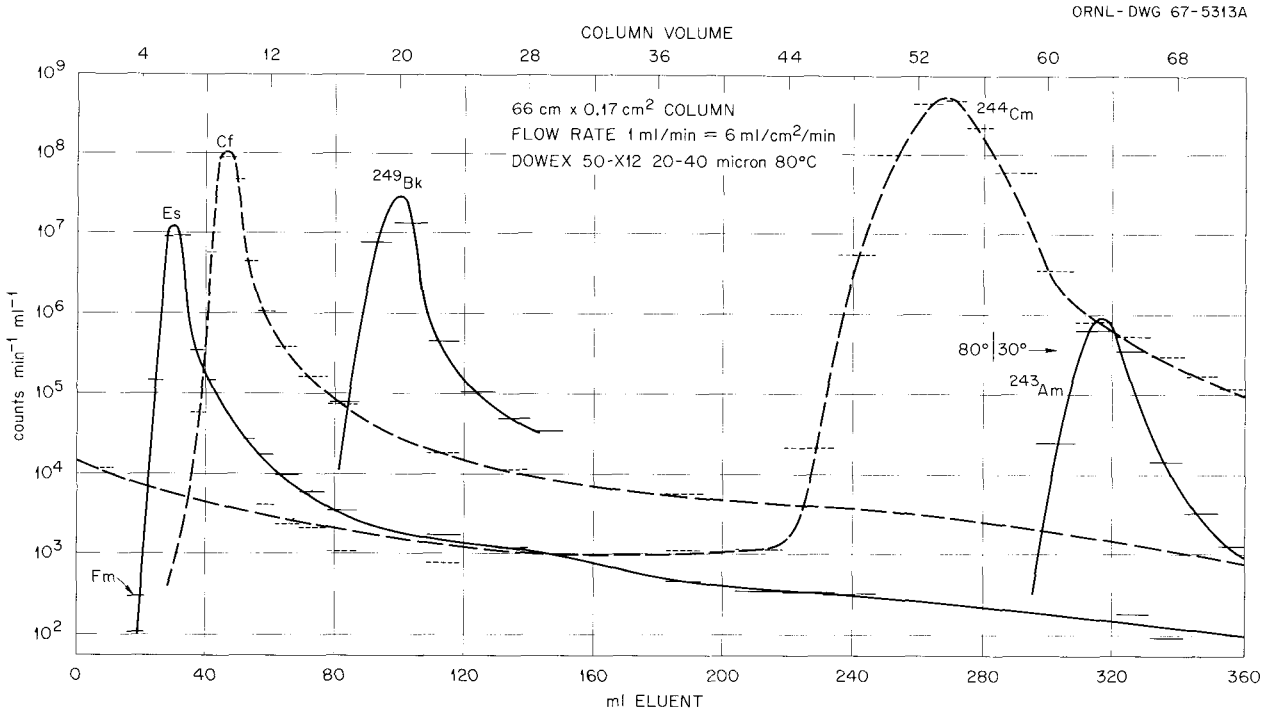

Fig. 6.11. Typical Separation of Actinide Elements on a High-Pressure Column.

provides a quantitative measurement of berkelium content when the berkelium is sufficiently free of radioactive impurities. Based on these studies, an analytical procedure has been developed in which berkelium is first isolated on a high-pressure column, then purified, and finally, counted by direct beta counting techniques.

In this chemical system (cation resin vs an aqueous elutriant containing an organic complexing agent), each elution band is characterized by tailing. That is, the concentration of the eluate rises to a sharp peak from very low levels but then decreases slowly at a concentration in the range of a few hundred to 10^4 times less than the peak. Tailing of this type is not a unique property of the high-pressure system, or of stainless steel equipment in general; it also occurs with conventional glass and plastic equipment. Several experimental variations made in attempts to decrease the tailing of bands met with only limited success. Tailing was generally greatest, however, when the system had long lines, provision for volume holdup in which mixing could occur, or stagnant pockets such as those that can occur in valves, branch lines, or tubing connections. In the least amount of tailing observed, the concentration was lower, by about a factor of 10,000, than the peak concentration; this separation was obtained when dilute eluents were used.

Chromatographic Column Studies. – Chromatographic column studies with rare earths were continued to evaluate loading techniques and rapid separation methods.

A useful technique for column loading, in which the feed material is applied to a very small column, was developed. The material on the small column can then be eluted through a larger column to achieve chromatographic separation. In demonstration runs, feed was loaded, quantitatively, on a 0.15-ml resin bed at the rate of 2 ml cm^{-2} min^{-1}; this resulted in a residence time in the resin bed of about 2 sec. The material on this column was eluted through an 11-ml column with AHIB; results were satisfactory.

This procedure has two advantages. First, very short columns may be used for loading. This permits the use of very fine resin and high flow rates without the development of excessively high pressure; also, the radiation exposure is minimized. Second, undesirable constituents in the feed are

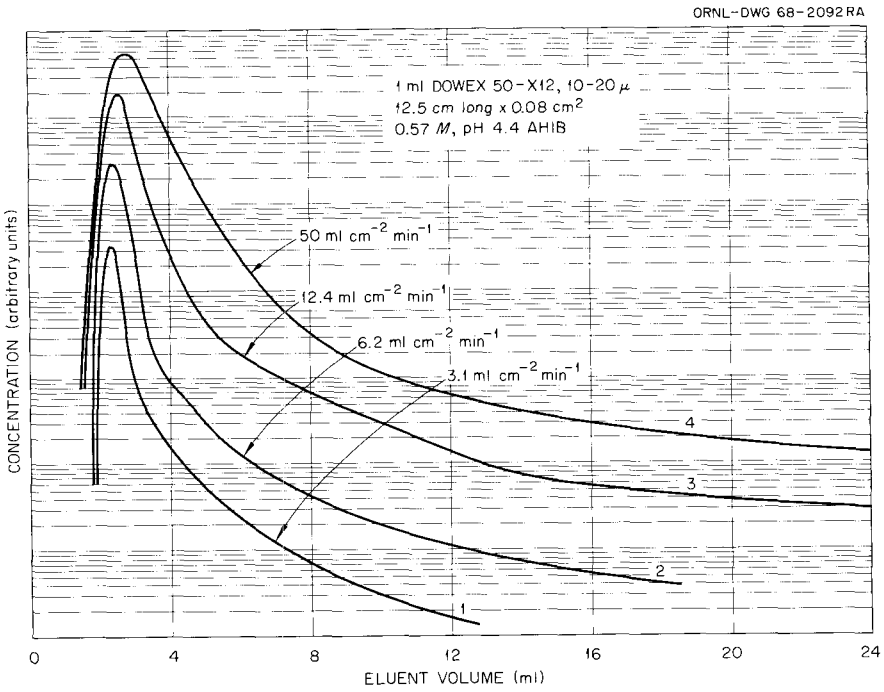

Fig. 6.12. Elution of a Single Element from a High-Pressure Column at Different Flow Rates.

found to load to only a limited extent because of the small resin volume of the column. This includes hydrogen ion (which can be present in large amounts in practical processing situations and which can interfere with the elution), and contaminants and fission products (such as ruthenium, zirconium-niobium, and some corrosion products) that have small to intermediate distribution coefficients.

The study of numerous short-lived isotopes would be substantially aided if chromatographic separations could be achieved rapidly (in times on the order of 1 min). Results of experiments performed with small resin columns, fine resin, and high flow rates with lanthanide isotopes indicate that adequate separations can be achieved in about 2 min.

Elution curves for a series of experiments with a 1-ml resin column are shown in Fig. 6.12. Here, only single elements were studied; however, a narrow elution band indicates that separations of adjacent actinides could be achieved. Except for flow rate, all experimental conditions were the same in each test. The increase in the width of the bands was proportional to the cube root of the flow rate. It was interesting to note that tailing, as previously discussed, was not greatly affected by flow rate; the ratio of peak height to tailing is about the same in each case. The elution bands were sufficiently narrow to suggest capability for satisfactory separations in the lower two curves and partial separation in curve 3; curve 4, however, indicates unsatisfactory separation.

Although these results show that separations can be achieved very rapidly, we have not yet observed a good elution band in less than 1 min; the use of an even shorter column with still finer resin may lead to improved results. The detailed study of the shape of elution bands such as these, under a wide range of conditions, should lead to a much better understanding of rate-limiting processes in high-pressure ion exchange systems. This, in turn, would permit optimization of column design.

Preparation of Actinide Oxides for HFIR Targets

Actinide oxides in the form of pressed pellets of aluminum powder and the oxide are loaded into HFIR targets. The aluminum phase must be continuous to ensure satisfactory heat transfer during irradiation, and oxide particles of proper size are required to achieve a continuous aluminum phase.

As reported last year,[7] a sol-gel process for preparing oxide microspheres of controlled particle size from rare earths as stand-ins for americium and curium was developed; and several methods for preparing 10-g batches of sol were evaluated with rare earths and ^{241}Am. During this report period, the rare-earth sol-gel process was successfully adapted for the preparation of mixed ^{244}Cm-^{243}Am sols and used to obtain 38 g of americium-curium oxide. The results of these experiments clearly demonstrate our ability to produce 10-g batches of mixed ^{243}Am-^{244}Cm sols and oxide microspheres of controlled size by this method.

A development facility to house the curium experiments was installed in cell 4 (Building 4507). Sol preparations were made in modified laboratory glassware, and spheres were formed in an equipment rack that contained the microsphere forming column, the solvent circulation system, and various process and storage vessels required for curium purification.

Sol Preparation. – Prior to sol preparation, feed material was purified by either a single or a double oxalate precipitation-calcination cycle. High-purity material appears to be required for optimum sol preparation. The impurity level of the original feed, which contained 150 mg of zirconium per gram of curium and smaller amounts of other ionic impurities, was sufficiently high to prevent sol formation. However, a single oxalate cycle reduced the zirconium concentration to <10 mg per gram of curium.

Batch sizes in these experiments varied from 4 to 9 g of total metal (16% ^{243}Am, 78% ^{244}Cm, 6% higher curium isotopes). In initial efforts to prepare americium-curium sols, stock solution purified by one oxalate cycle was used. The metal hydroxide was precipitated by adding a dilute solution of the metal nitrate to a large excess of 8 *M* NH_4OH, filtered and washed with water in a jacketed filter funnel to a final pH of 8 to 9, and heated for 1 to 2 hr at 85°C. During heating, the paste was converted to a fluid sol that could be collected by filtration through the filter medium.

Americium-curium sols were prepared in this way; however, the yields of fluid sol were very low (10 to 15%). It appeared that prolonged contact between the sintered-glass frit and the hydroxide under static conditions had deleterious effects; in subsequent experiments, essentially complete conversion to sol was obtained by fluidizing the filter cake during the washing procedure and removing the hydroxide from the filter immediately after washing. The hydroxide was digested at 85°C in a glass beaker. Conversion to a fluid sol required about 2 hr under these conditions. These sols were milk-white in color, had NO_3^-/metal mole ratios of 0.4 to 0.7, and did not foam excessively. The sols were quite fluid at a concentration of 0.1 to 0.15 *M* but exhibited a tendency to thicken at a concentration of about 0.2 *M*.

Three subsequent runs, using americium-curium stock solution that had been highly purified by a double oxalate precipitation cycle, produced a high yield of sols that were superior to previous preparations in several respects. The NO_3^-/metal mole ratios were reduced from about 0.7 to 0.2, the digestion time required for conversion of washed hydroxide to crystalline sol was reduced from 2 hr to 1 hr or less, and the sols were very fluid at metal concentrations of 0.2 to 0.25 *M*. The sols were characterized by excellent colloidal stability; no foaming was observed.

Microsphere Preparation. – Gel microspheres were formed from 0.1 to 0.25 *M* americium-curium sols, using standard sphere forming techniques. The plugging of the column feed line, which had occurred in early runs, was virtually eliminated by using a larger orifice in the column nozzle and by water-cooling the sol during storage. This apparently eliminated the formation of solids, caused by self-drying, on the storage container walls.

The gel spheres were removed from the column and air-dried overnight in an open container prior to calcination in air at 1150°C. The calcined spheres were free flowing, dust-free in appearance, and showed no tendency to crack or disintegrate. A photomicrograph of calcined spheres is shown in Fig. 6.13. The particle size varied from 40 to 177 μ in diameter, which is suitable for use in HFIR target preparation.

As yet, these products have only been analyzed by visual inspection; crushing strengths, densities, and similar parameters have not been determined. The characteristic pit seen in each of the larger spheres is believed to result, primarily, from low sol concentration; similar effects are observed when dilute rare-earth sols are formed.

[7] D. E. Ferguson *et al.*, *Chem. Technol. Div. Ann. Progr. Rept. May 31, 1967*, ORNL-4145, pp. 149–51.

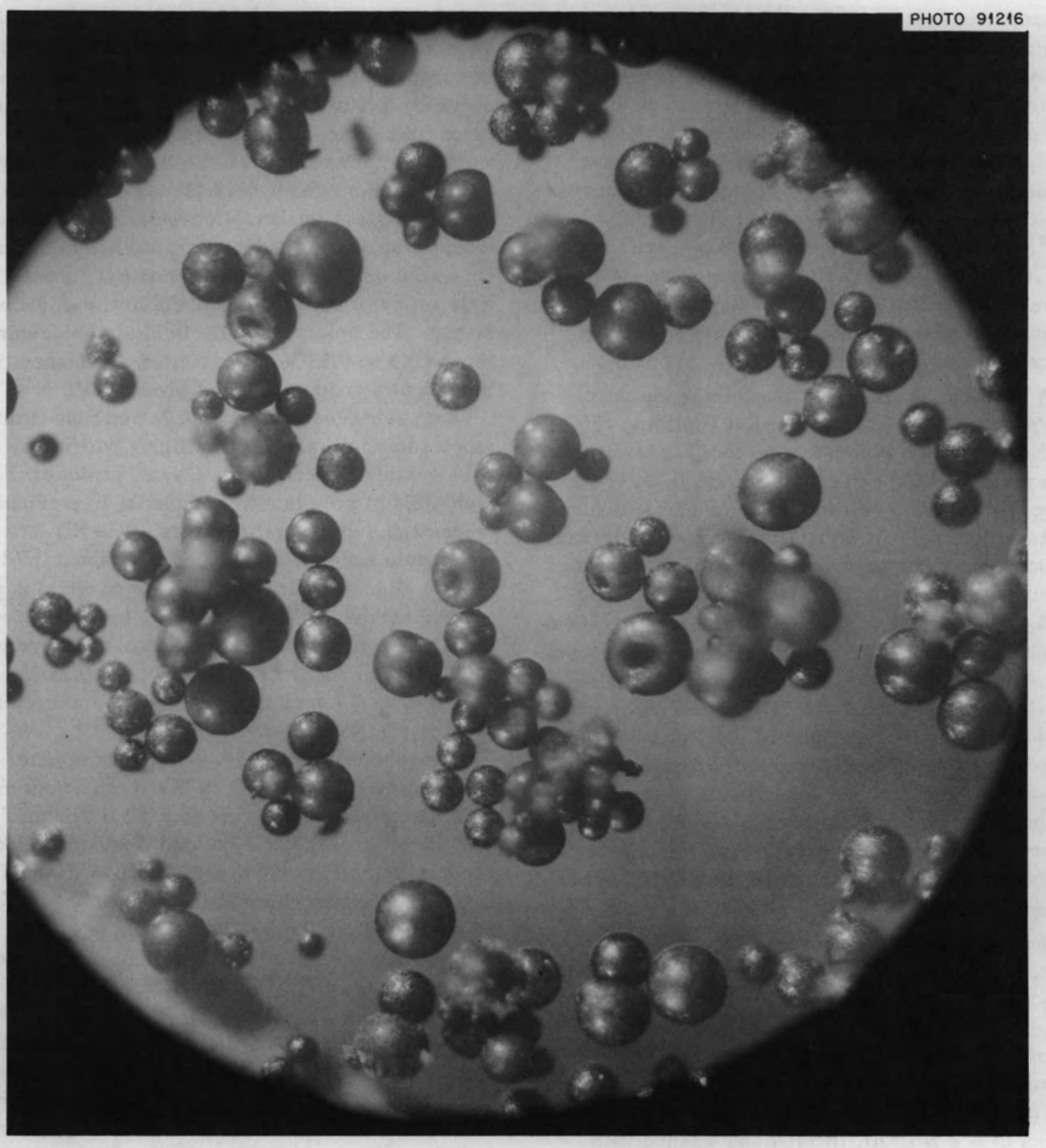

Fig. 6.13. Calcined 40- to 177-μ-diam AmO_2-CmO_2 Microspheres.

6.4 SPECIAL PROJECTS

Projects not associated with main-line processing steps are becoming an increasingly important phase of the transplutonium element program, involving the efforts of many groups at ORNL and elsewhere. Such projects are described in this section. No attempt is made to describe the end results of the research efforts; however, some general background information concerning these projects, along with somewhat more-detailed reports of the specific work done in the TRU facility, is presented.

Status and Progress

Three special targets containing a total of 3 mg of californium were fabricated, irradiated, and processed during the past year. Surprisingly, the burnup of the californium was much higher than calculations, based on previously used cross sections, had predicted. The data indicate that the capture cross section for ^{252}Cf is in the range of 40 to 50 barns instead of the 7 to 10 barns previously assumed. Approximately 6 μg of ^{253}Es was recovered for shipment to customers. Specimens of ^{244}Pu and ^{248}Cm were also included in these special targets.

A neutron source containing about 750 μg of ^{252}Cf (1.7×10^9 neutrons/sec) was fabricated for neutron activation studies in the Transuranium Research Laboratory.

Assistance was given to Los Alamos in an experiment that involved measurement of the fission cross section of ^{237}U in an underground nuclear event. Rabbits containing 42 mg of ^{236}U were fabricated, irradiated in HFIR, and shipped to LASL.

Special Californium Targets

About 3 mg of ^{252}Cf that had been recovered from processed HFIR and SRP targets was recycled to the HFIR in three special targets to produce additional amounts of ^{253}Es and heavier nuclides. The first two targets (ST-1 and ST-2) contained a number of special materials in addition to the californium. The third (ST-3) was a "production" target. ST-1 contained 0.36 mg of ^{252}Cf in two pellets and was irradiated for three reactor cycles (69 days). ST-2 contained 0.49 mg of ^{252}Cf, also in two pellets, and was irradiated for five reactor cycles (110 days). The objective of these irradiations was to learn more about the effective production cross sections of the heavy isotopes as well as to produce significant amounts of einsteinium for experimenters. Later, an additional 2 mg of ^{252}Cf was fabricated into a third target, ST-3, which was also irradiated for three cycles.

When ST-1 was processed in mid-March, only 44% of the expected amount of ^{252}Cf was found. It seemed logical either that half of the material had been physically lost in the process of fabricating the target or that the burnout cross section of ^{252}Cf was much higher than the 7 to 10 barns we had previously calculated. To account for the loss of ^{252}Cf in our experiment by the latter explanation, we would have to assume a ^{252}Cf capture cross section (σ_c) of 40 to 50 barns. However, such a high cross section should have resulted in the formation of a much larger amount of ^{253}Cf than was actually found. It seems reasonable to assume, therefore, that ^{253}Cf must have a very high fission cross section (σ_f), which causes its nonproductive removal from the production process. The measured quantity of short-lived fission products (such as ^{132}Te and ^{143}Ce) found in the irradiated californium supported this hypothesis.

When the second two targets were processed in early April, we obtained additional evidence of a high fission cross section. Each of these two targets also contained only one-fourth to one-half of the expected californium and activation products. Currently, the best estimates for the cross sections are as follows:

	^{252}Cf σ_c (barns)	^{253}Cf σ_f (barns)
ST-1 (3 cycles)	38 ± 7	2600 ± 300
ST-2 (5 cycles)	45 ± 8	3100 ± 500
ST-3 (3 cycles)	50 ± 10	2300 ± 500

As a consequence of these unexpectedly high cross sections, the irradiation period was much longer than would have been optimum for the production of einsteinium. The quantity produced was only 5.7 μg, as compared with the 18 μg that was predicted.

The high burnup cross section for ^{252}Cf will cause the steady-state production rate of ^{252}Cf and heavier isotopes to be lower than previously supposed, perhaps by a factor of 2. However, it may mean *higher* production rates of ^{249}Bk and ^{249}Cf, because now the optimum irradiation cycles for ^{252}Cf will become shorter (i.e., closer to the optimum cycles for these nuclides).

A number of other experiments were included in the first two target rods. These experiments are discussed below.

Target ST-1 contained two 0.5-mg ^{244}Pu pellets, one for an ORNL-sponsored experiment and one for an ANL-sponsored experiment. Target ST-2 contained only an ORNL-sponsored ^{244}Pu experiment.

The ^{244}Pu was irradiated to burn out some of the less-desirable ^{242}Pu and also to produce high-specific-activity sources of 10.85-day ^{246}Pu. The ^{246}Pu was separated and reirradiated in an attempt

to produce ^{247}Pu; however, this effort was unsuccessful.

One 13-μg ^{248}Cm (58% ^{248}Cm, 37% ^{244}Cm) pellet was included in each target. The ^{248}Cm was irradiated to provide more accurate cross-section data on the heavier curium isotopes and also to produce a small amount of ^{250}Cm. Although the quantitative loading of microgram quantities of material into a single pellet constituted a formidable handling problem, it was readily solved by a technique that is discussed below.

In addition to the actinide-loaded pellets, six aluminum alloy tensile specimens were included in each of the targets to study radiation damage to aluminum as it relates to the target-failure problem.

Flux monitors in the form of special pellets called SPAM's (Spacer Assembly, Monitor) were alternated with the actinide-fueled pellets to facilitate disassembly and to provide for flux monitoring. An SPAM consists of a dummy pressed pellet of aluminum powder in which a small quartz ampul containing two flux monitor wires is embedded; one wire is a cobalt-aluminum alloy, and the other is relatively pure niobium. Each wire weighs about 6 mg.

Preparation of ^{252}Cf, ^{248}Cm, and ^{244}Pu Pellets for Special HFIR Irradiations

The procedure for preparing pellets involved making a miniature filter funnel out of a pellet liner by pressing powder (pure aluminum) to ~70% of theoretical density in the bottom cap. In effect, the bottom cap became a porous disk that was strong enough to survive the succeeding procedures.

First, the matrix aluminum powder was slurried in a solution of the actinide to be loaded into the pellet, and the actinide was then precipitated onto the surfaces of the aluminum powder by use of excess NH_4OH. Next, the slurry was transferred into the pellet liners, and the excess liquid was aspirated through the porous disk. The filter cake was washed with water and methanol and air dried; then it was calcined at about 350°C for 4 hr. Finally, the liners were loaded into dies, filled with pure aluminum powder to form a top or sealing layer, and compacted to approximately 90% of theoretical density by pressing at 20 tons/in.^{2}.

Using this technique, about 20 pellets, containing from 1 to 200 μg of ^{252}Cf, were made. The less heavily loaded pellets will be incorporated into special targets and rabbits from time to time to gain better knowledge of the cross sections of the nuclides around ^{252}Cf. The size of the loading was chosen so that sufficient material would be available in the product to allow mass-spectrometer analyses of the californium and einsteinium fractions to be made. The more heavily loaded pellets were fabricated into the three special targets to be used for einsteinium and fermium production. In addition, two pellets containing 13 μg of ^{248}Cm each, two pellets containing 0.5 mg of ^{244}Pu each, and one pellet containing 0.6 mg of ^{244}Pu were prepared by this method.

The finished pellets were combined with SPAM assemblies, loaded remotely into the target tubes, and fabricated into completed target assemblies by techniques similar to those used for americium-curium recycle targets described in Sect. 6.1.

Preparation of a Californium Source for Neutron-Activation Studies

Enzo Ricci, of the Analytical Chemistry Division, is working with personnel in the Transuranium Research Laboratory (TRL) on the development of a system for fast-neutron activation studies, using spontaneous neutrons from ^{252}Cf fissions. This technique, while similar in many respects to conventional methods of thermal neutron activation, will be selective for a different set of elements. At the higher energies, reactions such as (n,α), (n,p), and $(n,2n)$ are possible, thus potentially giving rise to an entirely different set of activated products. However, since the fast-neutron cross sections tend to be small, fairly intense sources are required. The first source that was prepared for these studies contained 750 μg of ^{252}Cf (1.7×10^9 neutrons/sec) loaded into a single pellet by the filter funnel method described above. The pellet was subsequently sealed in a cylindrical aluminum container that was $\frac{3}{8}$ in. in diameter and 1 in. long.

Special techniques to weld the aluminum source container shut were developed. After suitable test welds were made, the closure weld on the actual ^{252}Cf source container was made and x rayed. It was found to be acceptable; therefore, the remaining container hardware was assembled.

The neutron source was delivered to the Transuranium Research Laboratory on February 12, 1968.

Immediately prior to shipment, a 17-hr test was made to determine the activity of the source. Several aluminum coupons were exposed to its fast neutrons, thereby creating the 15.4-hr ^{24}Na by an (n,α) reaction. Exact interpretation of the source strength requires a knowledge of either the effective cross section of aluminum for fast neutrons from the ^{252}Cf fission spectrum, or both the cross section at all energies and the actual fission neutron spectrum. An attempt to graphically integrate the aluminum activation cross section multiplied by the ^{252}Cf fission neutron energy spectrum did not give results that agreed closely with the known source strength. In the future, this should prove to be a simple method for measuring the activities of sources, once the effective cross sections are known.

Preparation of ^{236}U Rabbit Capsules

Three pellets containing ^{236}U were prepared for a project sponsored by LASL. The objective of this project was to make measurements of the fission cross section of ^{237}U as a function of neutron energy. These pellets were fabricated into capsules for irradiation in the HFIR hydraulic rabbit facility. The rabbit capsules were flown to LASL to minimize the decay of the ^{237}U and the growth of the undesirable ^{237}Np. At LASL, the uranium was purified, and the ^{237}U was isotopically separated for the measurements, which were made by using neutrons from an underground nuclear explosion. Since the timing of the entire operation was crucial, a practice run was made before the actual test.

Each of the pellets was made by blending 50 mg of U_3O_8 powder (42 mg of ^{236}U) with aluminum powder and pressing the mixture into pellets.

Because the scheduling of the entire operation was crucial, we had to know the necessary cooling time before the irradiated rabbit could be shipped. A "white" rabbit, that is, one containing no neutron absorber, was irradiated for 36 hr in the rabbit facility, loaded into the shipping carrier (shielded with 6.75 in. of lead) that LASL had supplied for shipment of their irradiated ^{236}U capsules, and the radiation levels were observed for about 24 hr. From these measurements the complex decay curve for ^{236}U was resolved into three components. From 10 min until 17 min after discharge, the radiation level at the surface of the cask was controlled, primarily, by that of the 2.3-min ^{28}Al which is produced by an (n,γ) reaction on ^{27}Al, the principal constituent of the rabbit (12 g). From 17 min until 2 hr after discharge, the principal gamma activity detected at the surface of the cask was the 2.58-hr ^{56}Mn which is produced by an (n,γ) reaction on ^{55}Mn, a minor constituent (0.01%) of the X-8001 aluminum alloy from which the capsule is fabricated. From 2 to 24 hr after discharge, the gamma activity at the surface of the cask was dominated by the 15.4-hr ^{24}Na which is produced by an (n,α) reaction on the ^{27}Al. There was no gamma radiation that would indicate the presence of 9.5-min ^{27}Mg, which is produced by an (n,p) reaction on the aluminum.

On the basis of this experiment, we calculated that the actual rabbit to be irradiated for ten days in the HFIR could be shipped 2.7 hr after discharge from the reactor. Observed radiation levels were about 50% higher than expected, probably due to the activation of copper impurities in the 1100 aluminum spacers used in the rabbit.

6.5 TRANSPLUTONIUM ELEMENT RESEARCH

As significant quantities of new isotopes become available, a systematic study of actinide element chemistry and of comparative lanthanide element chemistry will be carried out. Such a study will materially increase our basic understanding of actinide systems. This part of the transplutonium element program includes work on problems involving solution chemistry, with particular emphasis on complex formation, and the preparation of solid actinide compounds that will be characterized by x-ray diffraction, electron microscopy, thermogravimetry, differential thermal analysis, and metallographic examination.

Status and Progress

The investigation of sulfate complexes of europium by means of amine extraction was continued. The existence of a previously unreported trisulfate complex $Eu(SO_4)_3^{3-}$ (formation constant, $K_{03} = 1.8 \times 10^5$ at zero ionic strength) was indicated, and the results also suggested that a dinuclear complex $Eu_2(SO_4)_3$, $K_{0n} = 3.5 \times 10^8$, exists in addition to the previously known complexes $EuSO_4^+$ and $Eu(SO_4)_2^-$. The formation constants found for

the latter, $K_{01} = 7.0 \times 10^3$ and $K_{02} = 5.2 \times 10^5$, respectively, and their ratio $K_{12} = 75$, agree as well with the literature values as the literature values do with each other. An alpha spectrometer and alpha-contained equipment have been assembled for a parallel study of americium sulfate complexes.

We continued the spectrophotometric investigation to identify the complexes that are formed between Am^{3+} and aminopolyacetic acids. The pH ranges of stability were determined for 24 of the complexes formed with eight aminopolyacetic acids; instability constants for 13 were calculated. The general behavior of the ligands studied in this series indicates a correlation between the magnitude of the instability constant and the number of coordination sites available for a given ligand.

A program was initiated to prepare and evaluate new eluents to be used in the ion exchange separation of the transplutonium elements. Ethylmethylglycolic acid has been shown to provide slightly higher separation factors than dimethylglycolic acid (α-hydroxyisobutyric acid); this indicates that higher actinide separation factors can be obtained with increased branching on the α-hydroxycarboxylic acid. An investigation of this trend is being continued.

In continued studies of the fundamental solution chemistry of berkelium, the absorption spectrum of Bk(III) was redetermined with ~300 μg of highly purified ^{249}Bk. Twenty-five absorption bands were identified, and their molar extinction coefficients were determined.

In conjunction with the preparation of actinide sols, electron microscopy was used to examine PuO_2, $Am(OH)_3$, and $Cm(OH)_3$ sols at various stages of preparation. Results of this investigation confirmed that the colloidal characteristics of $Am(OH)_3$ and $Cm(OH)_3$ parallel those of rare-earth sols. Electron diffraction experiments that were performed during these studies led to the first positive identification of $Am(OH)_3$ that has ever been made. Since only 0.01 μg of ^{241}Am was used in each experiment, the techniques developed will be of great interest in identifying highly radioactive actinide compounds when only very small amounts of material are available. These studies also demonstrated that sols prepared from ^{244}Cm are composed of colloidal $Cm(OH)_3$ crystallites that are rapidly destroyed (in 10 to 20 hr) by self-radiation effects in aqueous media. Therefore, curium sols cannot be stored but must be immediately converted into microspheres. These studies were made at Baylor University in cooperation with Dr. W. O. Milligan.

Examination of the thermal stability of americium hydroxide preparations was initiated using the alpha-contained Ainsworth semimicro thermobalance. Installation of a Cahn microbalance system is nearly complete. This unit will provide similar capability for the thermoanalysis of berkelium.

Lanthanide and Actinide Sulfate Complexes

The continuing study of the aqueous sulfate complexes of europium by means of amine extraction[8] indicated the existence of a previously unreported trisulfate complex, $Eu(SO_4)_3^{3-}$, and suggested the existence of a dinuclear complex, $Eu_2(SO_4)_3$.

The amine extraction method was described previously.[8,9] Briefly, we determine the sodium sulfate and sulfuric acid concentrations required so that a series of prepared aqueous solutions will vary in actual sulfate ion concentration but each solution will still be in equilibrium with a single organic (amine sulfate-bisulfate) phase. Then, when an extractable metal is also present at tracer level, the thermodynamic activity of each extractable species is constant throughout the series of aqueous phases, since the thermodynamic activity is always proportional to the unchanging activity of that same species in the constant organic phase. We need to know the concentration of each species, that is, its activity divided by its activity coefficient. We estimate the variation of the activity coefficient of each possible complex species, as a function of its own ionic charge and of the ionic strength of the solution, by means of a Debye-Hückel expression. According to this expression, the activity coefficient of a neutral complex does not change with changing ionic strength; hence, its concentration as well as its activity is constant throughout the series. The concentration of each of the other possible complex species can then be expressed as the product of the real or hypothetical concentration of a neutral complex

---

[8] *Chem. Technol. Div. Ann. Progr. Rept. May 31, 1967*, ORNL-4145, p. 225.

[9] K. A. Allen and W. J. McDowell, *J. Phys. Chem.* **67**, 1138 (1963).

times the ratio of the appropriate formation constant and the activity coefficient. The sum of these individual concentrations is equated to the measured total metal concentration in each equilibrated aqueous phase, and the resulting series of material-balance equations is solved for the formation constants by simultaneous least-squares analysis.

The actual sulfate ion concentration and the ionic strength are calculated for each aqueous solution by using a computer program (see Sect. 10.5) based on the relation originally used by Baes.[10] Figure 6.14 shows a typical set of experimental data, together with the smooth curve obtained with the formation constants. The minimum aqueous europium concentration necessarily occurs where the average of the complex species is neutral. The increasing concentrations on both sides reflect increasing proportions of positive complexes to the left and negative complexes to the right. With the assumption that the possible species are Eu^{3+}, $EuSO_4^{+}$, $Eu(SO_4)_2^{-}$, $Eu(SO_4)_3^{3-}$, and $Eu_2(SO_4)_3$, analysis of the extraction data so far obtained gives the following formation constants (at zero ionic strength) relative to the neutral complex:

$$\tfrac{1}{2}Eu_2(SO_4)_3 \rightleftharpoons Eu^{3+} + \tfrac{3}{2}SO_4^{2-} , \qquad K_{n0} = 2.9 \times 10^{-9} ;$$

$$\tfrac{1}{2}Eu_2(SO_4)_3 \rightleftharpoons EuSO_4^{+} + \tfrac{1}{2}SO_4^{2-} , \qquad K_{n1} = 2.0 \times 10^{-5} ;$$

$$\tfrac{1}{2}Eu_2(SO_4)_3 + \tfrac{1}{2}SO_4^{2-} \rightleftharpoons Eu(SO_4)_2^{-} , \qquad K_{n2} = 1.5 \times 10^{-3} ;$$

$$\tfrac{1}{2}Eu_2(SO_4)_3 + \tfrac{3}{2}SO_4^{2-} \rightleftharpoons Eu(SO_4)_3^{3-} , \qquad K_{n3} = 5.1 \times 10^{-4} .$$

These values were calculated by a patterned-search computer procedure. Values obtained by a different computer procedure, using derivatives, are in good agreement. The confidence limits have not been estimated.

[10] C. F. Baes, *J. Am. Chem. Soc.* **79**, 5611 (1957).

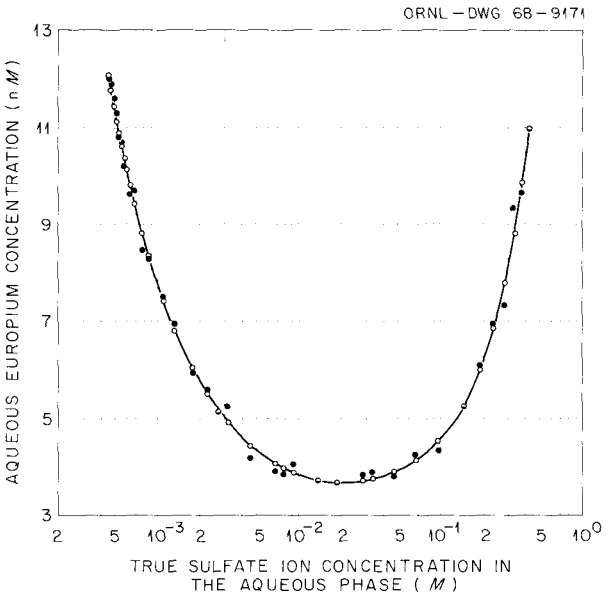

Fig. 6.14. Effect of Sulfate Ion Concentration on the Aqueous Europium Concentration That Is in Equilibrium with the Constant Organic-Phase Europium Concentration.

After the foregoing constants were converted to the usual form (i.e., for formation of each complex from the uncomplexed ion Eu^{3+}), they were compared with literature values (see Table 6.4). The latter values, which were measured at approximately constant ionic strengths of 1 and 2 *M*, have been adjusted to zero ionic strength by the Debye-Hückel expression.

The constants and the corresponding smooth curve of Fig. 6.14 were obtained with the assumption that the dinuclear complex $Eu_2(SO_4)_3$ is a real species, comprising up to, for example, ~5 mole % of the europium at 0.015 *M* total sulfate, pH 3. So far, this assumption permits slightly better overall fitting to the experimental data than does the opposite assumption [i.e., that there is no $Eu_2(SO_4)_3$]. Curves of the cation exchange extraction over the same range of sulfate ion concentrations showed more curvature than could be accounted for by Eu^{3+}, $EuSO_4^{+}$, and $Eu(SO_4)_2^{-}$, but (at constant ionic strength) this method could not distinguish between $Eu_2(SO_4)_3$ and $Eu(SO_4)_3^{3-}$.

An alpha spectrometer and other equipment have been assembled for the parallel study (in a glove box) of the americium sulfate complexes.

Table 6.4. Formation Constants for Europium Sulfate Complexes

Calculated at zero ionic strength by means of the Debye-Hückel relation

Complex	Constant	Value of Constant		
		This Work	Sekine[a]	DeCarvalho and Choppin[b]
$EuSO_4^+$	K_{01}	7.0×10^3	9.5×10^3	1.5×10^4
$Eu(SO_4)_2^-$	K_{02}	5.2×10^5	8.9×10^5	4.7×10^5
$Eu(SO_4)_3^{3-}$	K_{03}	1.8×10^5		
$Eu_2(SO_4)_3$	K_{0n}	3.5×10^8		
	K_{12}[c]	75	93	32

[a]Tatsuya Sekine, *Acta Chem. Scand.* **19**, 1469 (1965).
[b]R. G. DeCarvalho and G. R. Choppin, *J. Inorg. Nucl. Chem.* **29**, 725 (1967).
[c]$K_{12} = K_{02}/K_{01}$.

Spectrophotometric Analysis of the Complexes Formed by Am^{3+} and Certain Aminopolyacetic Acids

An effort was made to identify the complexes that Am^{3+} forms with certain aminopolyacetic acids. Absorption spectrophotometry of Am^{3+} was used since successive complex formation causes the Am^{3+} band at 5028 A to shift to longer wavelengths, with each complex having a characteristic absorption band.

The americium complexing was determined with the following ligands: iminodiacetic acid (IDA), hydroxyethyliminodiacetic acid (HIMDA), hydroxyethylethylenediaminetriacetic acid (HEEDTA), ethylenediaminetetraacetic acid (EDTA), 2-hydroxypropane-1,3-diaminetetraacetic acid (HPDTA), diethylenetriaminepentaacetic acid (DTPA), triethylenetetraaminehexaacetic acid (TTHA), and tetraethylenepentaaminheptaacetic acid (TPHA).

Figure 6.15 shows the absorption band shift on complexation for the iminodiacetic acid system. The first complex is a 1:1 americium-to-ligand composition and is formed in the pH range 3.5 to 5.3, with the americium absorption band shifting from 5028 to 5048 A. The second complex is a 1:2 americium-to-ligand composition and is stable in the pH range 5.1 to 6.7. The absorption band for the 1:2 complex is at 5064 A. The third complex has a 1:3 relationship and shows stability in

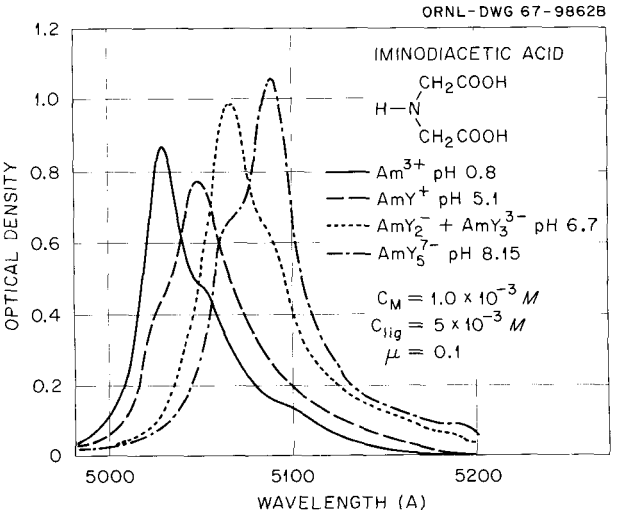

Fig. 6.15. Changes in Am^{3+} Spectrum Due to the Formation of Complexes with IDA.

the pH range 6.5 to 7.2 and maximum absorption at 5075 A. The final complex is formed in the pH range 7.0 to 9.5 and has a 1:5 americium-to-ligand composition. The absorption band is at 5088 A. A similar absorption band shift on successive complex formation was noted for the other ligands studied.

A summary of the compositions of the complexes, their pH ranges of stability, and their calculated instability constants is given in Table 6.5.

Table 6.5. Summary of Am^{3+} Complexing with Aminopolyacetic Acids as Determined Spectrophotometrically

Ligand	Composition of Complex, Am:Lig	λ max (A)	pH Range of Formation	Instability Constant, pK_i	Complexation Reaction
IDA	1:1	5048	3.5–5.3	6.93	$Am^{3+} + HY^- \rightleftharpoons AmY^+ + H^+$
	1:2	5064	5.1–6.7		$AmY^+ + HY^- \rightleftharpoons AmY_2^- + H^+$
	1:3	5075	6.5–7.2		$AmY_2^- + HY^- \rightleftharpoons AmY_3^{3-} + H^+$
	1:5	5088	7.0–9.5	8.31	$AmY_3^{3-} + 2HY^- \rightleftharpoons AmY_5^{7-} + 2H^+$
HIMDA	1:1	5046	1.3–2.0	10.03	$Am^{3+} + H_2Y \rightleftharpoons AmY^+ + 2H^+$
			2.0–2.8	9.57	$Am^{3+} + HY^- \rightleftharpoons AmY^+ + H^+$
	1:2	5068	2.6–6.5	7.21	$AmY^+ + HY^- \rightleftharpoons AmY_2^- + H^+$
HEEDTA	1:1	5061	0.7–2.0	16.18	$Am^{3+} + H_3Y \rightleftharpoons AmY + 3H^+$
	2:3	5064	3.0–6.0		$2AmY + HY^{2-} \rightleftharpoons Am_2Y_3^{3-} + H^+$
	1:2	5075	6.3–9.7	0.72	$Am_2Y_3^{3-} + HY^{2-} \rightleftharpoons 2AmY_2^{3-} + H^+$
EDTA	1:1	5061	1.0–2.1	18.06	$Am^{3+} + H_4Y \rightleftharpoons AmY^- + 4H^+$
	2:3	5064	3.7–7.3		$2AmY^- + HY^{3-} \rightleftharpoons Am_2Y_3^{6-} + H^+$
	1:2	5075	7.0–12.0		$Am_2Y_3^{6-} + HY^{3-} \rightleftharpoons 2AmY_2^{5-} + H^+$
DTPA	1:1	5074	0.7–1.6	24.03	$Am^{3+} + H_5Y \rightleftharpoons AmY^{2-} + 5H^+$
TTHA	2:1	5072	1.3–2.3	30.97	$2Am^{3+} + H_6Y \rightleftharpoons Am_2Y + 6H^+$
	1:1	5073	1.7–2.4	27.61	$Am^{3+} + H_6Y \rightleftharpoons AmY^{3-} + 6H^+$
	2:3	5075	2.4–3.5	9.15	$2AmY^{3-} + H_4Y^{2-} \rightleftharpoons Am_2H_2Y_3^{10-} + 2H^+$
			3.5–4.2	13.40	$2AmY^{3-} + H_3Y^{3-} \rightleftharpoons Am_2HY_3^{11-} + 2H^+$

The general behavior of the pK_i's for the ligands studied in this report seems to indicate that a correlation exists between the magnitude of the pK_i and the available ligand coordination sites. In Fig. 6.16 the pK_i's for the Am^{3+}-polyaminopolyacetic acid complexes are plotted as a function of available ligand coordination sites. The linear increase in strength indicates the probable coordination number of the americium-ligand complex. The DTPA ligand appears to be octadentate with americium, whereas TTHA is nona- or decadentate.

In summary, the study of this series of complexes has shown several interesting points:

1. Small ligands, such as IDA, form a series of complexes with Am^{3+} in which as many as five molecules of the ligand are accommodated around the metal ion. It seems that only a slight difference exists between the small and the large ligands with regard to the maximum Am^{3+} coordinate bonding. The large ligands, such as TTHA, are apparently able to pack around the central metal ion to the same extent as the smaller ligands such as IDA.

2. The larger ligands, such as HEEDTA, EDTA, and TTHA, are capable of forming complexes of the type 2:3 and 1:2. This tendency may give an increased value for the coordination number, although a more detailed study would be required to prove this.

3. The ligand DTPA forms only one complex, which has a metal-to-ligand ratio of 1:1. The ability to coordinate as an octadentate ligand apparently completely satisfies the requirements of the Am^{3+} ion, and further complexation is prevented.

4. The regular trend of stability constants as a function of the available ligand coordination sites (Fig. 6.16) suggests the participation of OH bonding in the case of the ligands HIMDA and HEEDTA.

5. The behavior of HPDTA is irregular with respect to the series. The formation of a 2:1 complex is unexpected for a ligand of this size. The presence of CH-OH in the middle of the chain is very important in inducing polynuclear complexes.

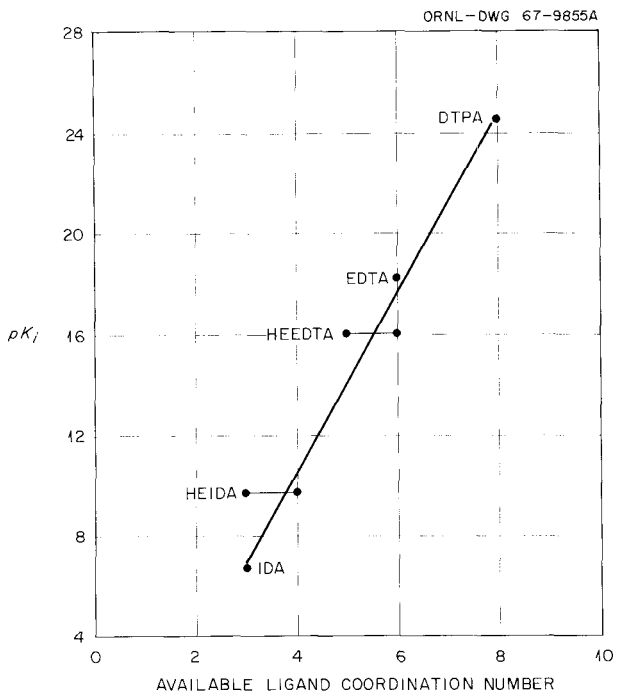

Fig. 6.16. Instability Constants for Am^{3+}-Aminopolyacetic Acid Complexes.

New Ion Exchange Eluents

A program has been initiated to prepare and evaluate new ion exchange eluents for use in the separation of the transplutonium elements. Up to the present time, the most effective reagent for the chromatographic separation of these elements has been α-hydroxyisobutyric acid (dimethylglycolic acid) (Table 6.6). It appears that, as branching increases on the α-hydroxycarboxylic acid (glycolate), the separations increase. An investigation of this trend was extended to the next reagent, α-hydroxy-2-methylbutyric acid (ethylmethylglycolic acid).

The ion exchange behavior of the transplutonium elements was investigated with α-hydroxy-2-methylbutyric acid (HMBA) to determine the effect of ligand concentration and temperature upon the separation factors between Am, Cm, Cf, and Es. In general, increasing the HMBA concentration of the elutriant decreased the number of column volumes needed to elute the elements but had no significant effect on the separation factors. Increasing the temperature (80°C) gave sharper peaks but no significant change in the separation factors between the transplutonium elements.

Laboratory-scale runs were made in a glove box that contained a high-pressure stainless steel ion exchange column, 24 in. long, packed with 11 ml of 20- to 40-μ mesh Dowex 50-X8 resin. The column had an active bed volume of 20 in. The feed containing Am, Cm, Cf, and Es was adjusted to about 0.05 *M* HNO_3 and fed to the column. After loading, the column was washed consecutively with water, ammonium formate, and water and then

Table 6.6. Transplutonium Element Separation Factors for α-Hydroxycarboxylic Acids

Element	Glycolic Acid	Methylglycolic Acid[a]	Dimethylglycolic Acid[b]	Ethylmethylglycolic Acid[c]
Am	1.14	1.21	1.41	1.46
Cm	1.00	1.00	1.00	1.00
Bk	0.70	0.65	0.45	
Cf	0.60	0.41	0.20	0.17
Es		0.33	0.13	0.12

[a]Lactic acid.

[b]α-Hydroxyisobutyric acid.

[c]α-Hydroxy-2-methylbutyric acid.

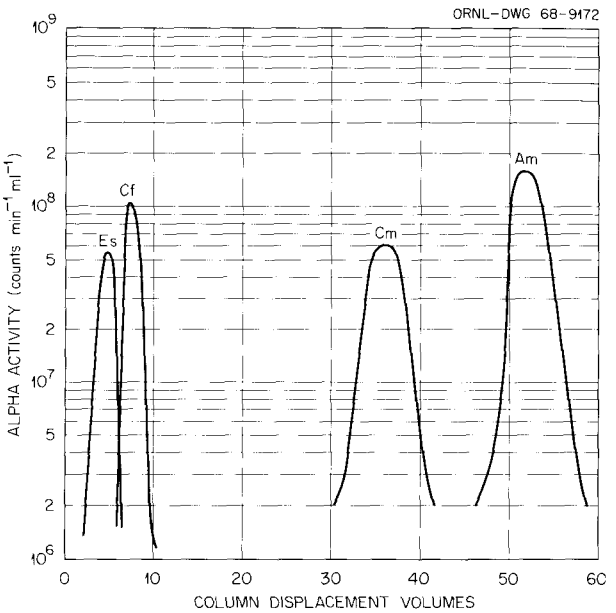

Fig. 6.17. Positions at Which Transplutonium Elements Are Eluted with 0.4 *M* Ethylmethylglycolic Acid at pH 3.80.

eluted with 0.4 *M* HMBA, pH 3.8, at a flow rate of 2 ml/min. The temperature of the column was maintained at 80°C. The elution peaks for Es, Cf, Cm, and Am are shown in Fig. 6.17. As expected, ethylmethylglycolic acid gave slightly greater separation factors than dimethylglycolic acid. The investigation to determine whether this trend will continue with increasing reagent complexity is being continued.

A summary of transplutonium element separation factors with the α-hydroxycarboxylic acids is given in Table 6.6.

Solution Absorption Spectrum of Trivalent Berkelium

A reevaluation of the solution absorption spectrum of berkelium was made in order to better define the positions and intensities of the absorption bands. Because the earlier work of Gutmacher *et al.*[11] was done using a total of only about 30 μg of berkelium, observation of the weak absorption lines of berkelium was limited. Since the quantity of available ^{249}Bk has now increased tenfold, it seemed advisable to repeat this work.

[11]R. G. Gutmacher *et al.*, *J. Inorg. Nucl. Chem.* **29**, 2341 (1967).

A total of about 350 μg of ^{249}Bk was available for the spectrophotometric studies. The methods used for the initial isolation of the berkelium from the HFIR target rods included solvent extraction by the Tramex process, LiCl anion exchange, and solvent extraction of berkelium in four different valence states with HDEHP. The recovered berkelium was then further purified by a series of oxidation-reduction solvent extraction cycles with HDEHP to ensure complete decontamination from all elements except cerium. The cerium was removed by chromatographic elution from a Dowex 50-X12 cation exchange column with α-hydroxyisobutyric acid. In this procedure a Bk/Ce separation factor of 7.8 is obtained, which indicates an excellent decontamination. Europium, which is the only rare earth that would elute in the same position as berkelium, was completely removed in the solvent extraction cycles. The berkelium was then further decontaminated from light elements (contaminants) by elution from a Dowex 50-X4 cation column with 2 *M* HCl until the start of the berkelium breakthrough; at this point, 6 *M* HCl was used for elution. The last two ion exchange columns were made of all quartz; only quartz-distilled reagents were used.

Only the center fractions were taken from the ion exchange elution bands for the spectral studies; about 300 μg of ^{249}Bk was used. When the 6 *M* HCl solution from the final column was evaporated to dryness, a slight deposit of $BkCl_3$ was visible as a yellow-green salt.

The most satisfactory absorption spectrum of Bk^{3+} was obtained in the $DClO_4$ and the D_2SO_4 solutions. A reproduction of the Bk^{3+} spectrum in 1 *M* $DClO_4$ is shown in Figs. 6.18 and 6.19. The graph in Fig. 6.18 is a plot of the optical density of the visible region; in Fig. 6.19 the spectrum is plotted as a function of molar absorptivity. Twenty-five bands were found in the spectral region 2500 to 13,500 A; a list of these bands and their molar absorptivities is given in Table 6.7. The large value for absorptivity at wavelengths below 3100 A was initially thought to be the result of the ultraviolet cutoff; however, Bk^{3+} was found to have a very strong absorption band at 2900 A.

The absorption spectrum of Bk^{3+} in 0.14 *M* D_2SO_4–D_2O (Fig. 6.20) is very similar to that found in 1 *M* $DClO_4$. The bands at 4180 and 4740 A are in similar positions and have essentially the same molar absorptivities. Since the

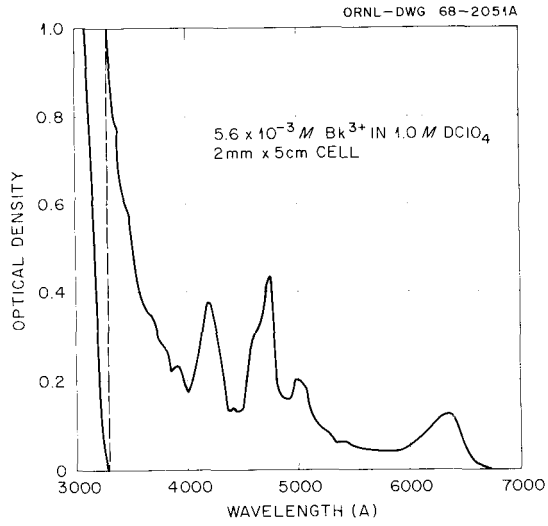

Fig. 6.18. Optical Density of Bk^{3+} in 1 *M* $DClO_4$.

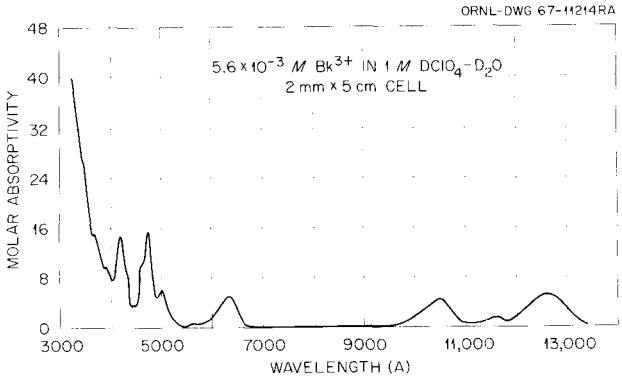

Fig. 6.19. Molar Absorptivity of Bk^{3+} in 1 *M* $DClO_4$.

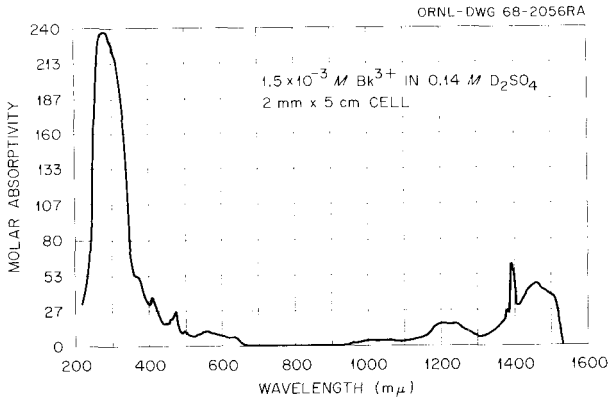

Fig. 6.20. Molar Absorptivity of Bk^{3+} in 0.14 *M* D_2SO_4.

Table 6.7. Absorption Bands of Bk^{3+} in 1 *M* $DClO_4$ Solution

Wavelength (A)	Molar Absorptivity
2,900	260
3,270	2
3,360	1.5
3,670	1.5
3,740	1
3,780	1
3,910	1.5
3,980	1
4,180	8.6
4,300	1.5
4,430	0.7
4,620	2
4,740	14
4,860	0.7
5,010	5
5,050	1.5
5,200	1.5
5,400	0.5
6,000	0.7
6,200	1
6,350	4
10,100	0.7
10,470	4.6
11,640	1.8
12,700	4.7

Bk^{3+} concentration in the D_2SO_4 solution was less, by a factor of ~4, than in the $DClO_4$ solution, direct resolution of the 2900-A absorption band was possible. The molar absorptivity of the 2900-A band was found to be 236, which agrees fairly closely with the value (260) determined for the $DClO_4$ solution. The shoulder at 3250 A in the D_2SO_4 solution was not found in the $DClO_4$ solution. The other difference is in the Bk-D_2SO_4 absorption in the infrared region of 13,000 to 15,500 A, where there are several absorption bands not observed in the Bk-$DClO_4$ solution. Apparently, some complexing of the dilute D_2SO_4 and the Bk^{3+} does take place, which accounts for the minor variation in the absorption spectra for the two solvents.

The final spectral observation of trivalent berkelium was made in the 1 *M* KCNS–D_2O system; the

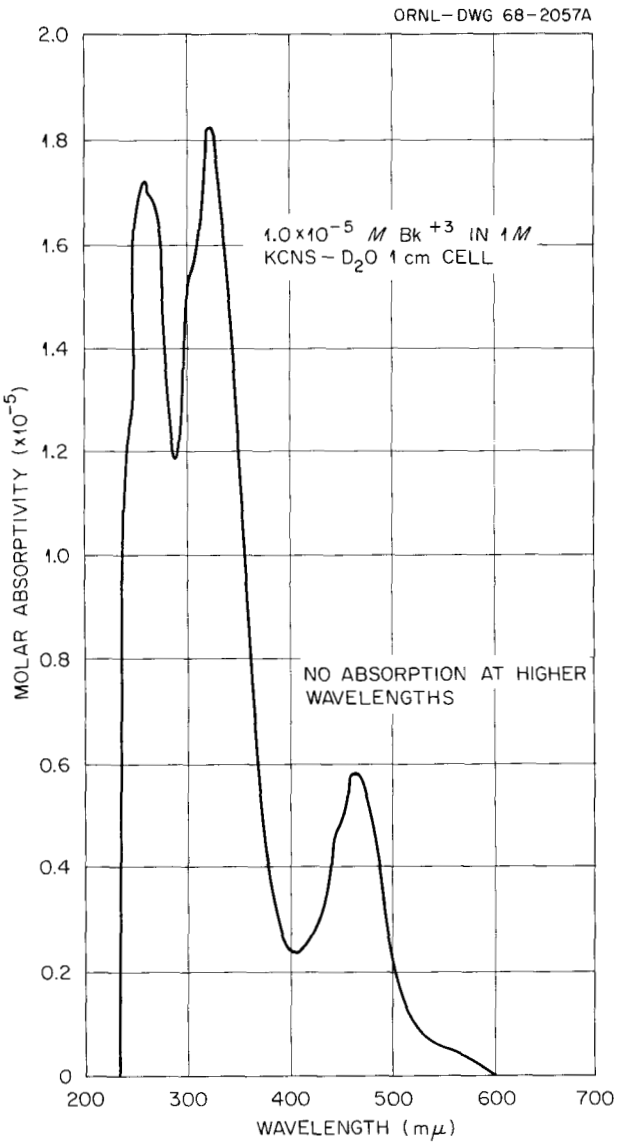

Fig. 6.21. Molar Absorptivity of Bk^{3+} in 1 *M* KCNS-D_2O.

absorption spectra are shown in Fig. 6.21. The very strong absorption bands at 2625, 3310, and 4680 A, with molar absorptivities of $\sim 10^5$, would make this system attractive from an analytical standpoint.

Investigation of Actinide Hydroxides by Electron Microscopy

Electron microscopy and electron diffraction have been used to investigate actinide hydroxide and actinide oxide preparations that are of interest in the ORNL transuranium sol-gel programs. Similar investigations by other workers on thorium and uranium have been previously reported.[12–14] The results of more recent work involving plutonium, americium, and curium are reported here.

The americium and curium sol-gel process, which is essentially the same as that reported for the rare earths (see Sect. 6.3), consists in precipitating the trivalent metal ion with NH_4OH, washing with water, and digesting at elevated temperatures.

Electron microscopy and electron diffraction were used to follow the changes that take place during the process. For these experiments, high-purity ^{241}Am and ^{244}Cm (i.e., ^{244}Cm plus small amounts of higher isotopes) were used. Examination of precipitates after washing showed that the material consisted of symmetrical 15- to 20-A particles. Diffraction patterns indicated that the particles were amorphous. Aging the colloidal preparations at 80°C in water for 1 to 2 hr converted the small particles into crystalline needles or rodlike structures. The needles are about 200 A wide and 2000 A long, with the curium needles being slightly larger than those of americium. The needles are similar to the needle structures observed with the lanthanides.[15] Figure 6.22 shows an electron micrograph of the americium needles. The diffraction pattern showed that the americium compound was isostructural to $Nd(OH)_3$, indicating that the crystalline material was the trihydroxide of americium. The diffraction pattern for the americium compound is shown in Fig. 6.23.

Examination of colloidal solutions after standing at ambient temperatures indicated a change in the appearance of the needle structure; this is believed to be the result of self-radiation damage. The change in curium sols was noticed after only a few hours, and complete destruction of the crystallite structure occurred within about 24 hr. Similar effects were noted for americium sols, but much

---

[12] K. H. McCorkle, *Surface Chemistry and Viscosity of Thoria Sols*, ORNL-TM-2056 (July 1966).

[13] C. J. Hardy, *Examination of Hydrous Uranium Dioxide Precipitates and Sols by Electron Microscopy, Electron Diffraction and Spectrophotometry*, ORNL-3963 (August 1966).

[14] N. A. Krohn *et al.*, *Preparation and Preliminary Studies of Chloride-Stabilized UO_2 Sols*, ORNL-TM-2056 (February 1968).

[15] C. J. Hardy *et al.*, *Preparation of Lanthanide Oxide Microspheres by Sol-Gel Methods*, ORNL-4000 (August 1967).

Fig. 6.22. Electron Micrograph of Aged $Am(OH)_3$.

Fig. 6.23. Electron Diffraction Pattern of Aged $Am(OH)_3$.

longer times were involved; this is in accord with the difference in the half-lives of the isotopes.

The plutonia sol-gel process used at ORNL was described last year.[16] The first step in the process involves a hydroxide precipitation of tetravalent plutonium. This precipitate is believed to be a hydrous form of PuO_2, since the first diffraction pattern obtained from washed precipitates is identical to PuO_2 diffraction patterns. The same pattern is obtained for the material, from the dispersed precipitate to the final denitrated sol, as it progresses through the different steps of the flowsheet. It is of interest to note that the colloidal PuO_2 particles have an absorption spectrum which is identical to that reported in the literature for plutonium(IV) polymer.

Examination of plutonium precipitates by electron microscopy has shown that the material is composed of small (10- to 20-A), symmetrical primary particles. Secondary aggregates of these primary particles are believed to be present also. The primary particles have essentially the same sizes as those determined by x-ray line-broadening techniques. The effect of aging the precipitate at reflux temperatures, as indicated in the flowsheet, was also investigated. The major difference between aged and unaged precipitates was found to be in the degree of crystallinity rather than in the size of the crystallites present.

The final sol is obtained by thermal denitration at elevated temperatures. During the denitration, the x-ray crystallite size increases to about 80 A. Examination of this material by electron microscopy showed that the material consists of symmetrical 80- to 100-A particles (or particles having about the same size as the crystallites). The general appearance of these particles is shown in Fig. 6.24. The majority of the particles are 80 to 100 A wide, but larger aggregates of these particles are undoubtedly present. The extent of aggregation is reduced considerably for sols made from aged precipitates. This is in agreement with the difference in the physical properties of the sols. Figure 6.25 shows the diffraction pattern for the PuO_2 sol.

[16] D. E. Ferguson *et al.*, *Chem. Technol. Div. Ann. Progr. Rept. May 31, 1967*, ORNL-4145, pp. 195–203.

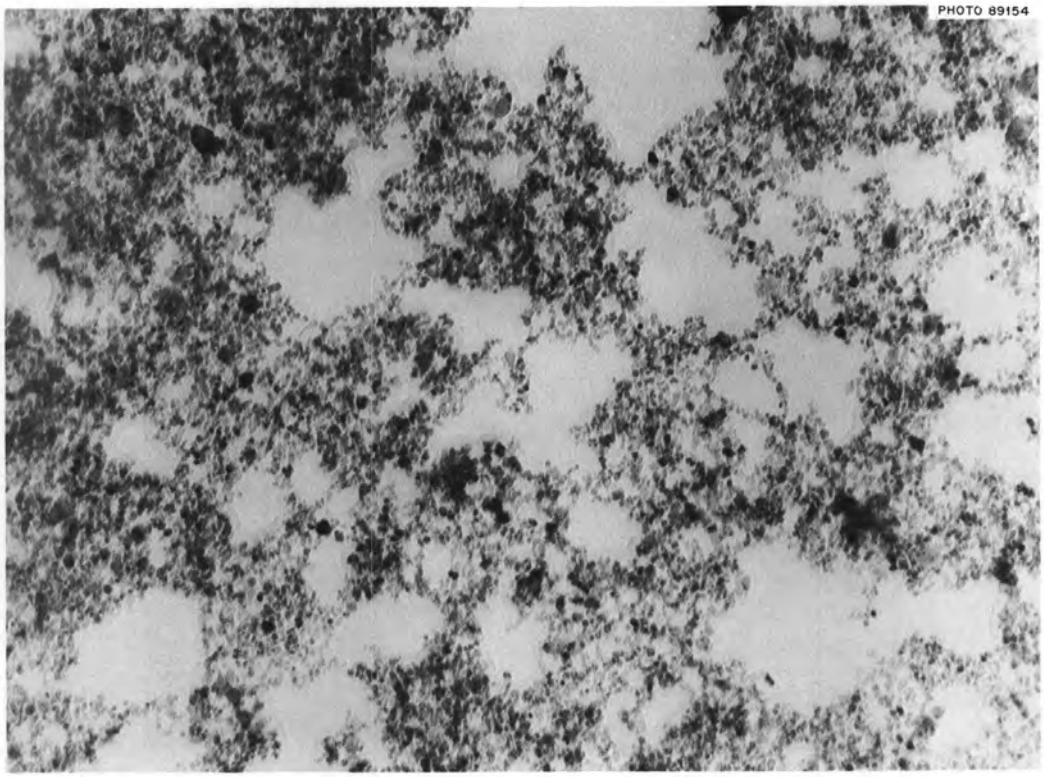

Fig. 6.24. Final Plutonium Sol from an Aged Precipitate.

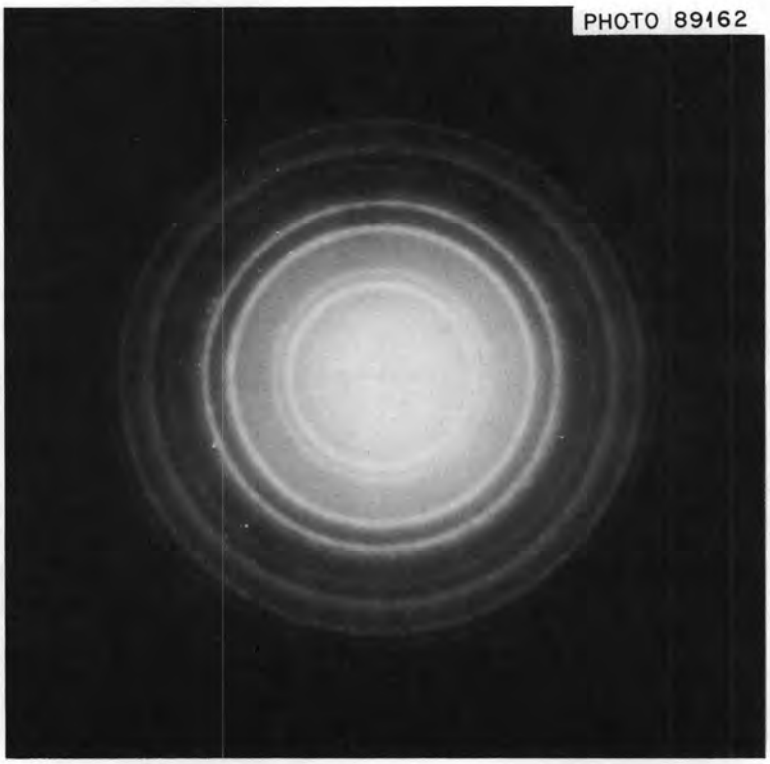

Fig. 6.25. Electron Diffraction Pattern of PuO_2 Sol from an Aged Precipitate.

Thermal Analysis of Actinide Compounds

Previously described[17] thermogravimetric and differential thermal analysis equipment for studying actinide compounds was used to evaluate the thermal stability of americium hydroxide preparations. This material has been examined up to 1600°C in air, oxygen, and in vacuum using the Ainsworth balance. In each case, the final product obtained after cooling to room temperature was confirmed by x-ray analysis to be AmO_2. In vacuum (10 μ Hg), a gradual weight loss above 1400°C was assumed to be due to partial decomposition of the dioxide. In atmospheres containing oxygen, the weight loss occurring from 1400 to 1600°C was less noticeable. The thermogram for the decomposition in oxygen is shown in Fig. 6.26. The weight changes below 600°C are continuous rather than discrete. The sample is known to contain a small amount of nitrate and carbonate. Although the DTA peaks and the TGA changes are only tentatively assigned at this time, the change at 1000°C is believed to be due to the decomposition of carbonate, and the change at about 300°C is thought to result from a loss of nitrate. Changes below 300°C have been assigned to loss of water. When the decomposition was allowed to take place in vacuum, a thermogram similar to that in Fig. 6.26 was observed, except that the high-temperature change occurred just after 800°C. Further work will be done on other preparations to confirm these results.

After installation of the Cahn microbalance (see Fig. 6.27) is complete, the system will be checked and tested with cold samples; it will be operated as a TGA unit only. The same flexible design used for the Ainsworth system was incorporated in the Cahn unit. The alpha enclosure contains two separate compartments that are connected by a stainless steel coupling. The Cahn electrobalance is supported by a frame which permits alignment of either of the two beam positions of the balance with the coupling. In the lower compartment, the bottom of the coupling serves as a center for vacuum ports, gas inlet and exhaust tubes, and thermocouple leads. The furnace tubes are also connected to the coupling. A variety of furnace tubes and sizes may be used with the coupling, and the tubes can be readily replaced. In Fig. 6.27, three different tubes are shown: a $\frac{3}{4}$-in.-OD quartz tube, a $\frac{3}{4}$-in.-OD alumina tube,

[17] *Chemical Application of Nuclear Explosions (CANE): Progress Report for July 1 to September 30, 1966*, ORNL-TM-1688 (Nov. 9, 1966).

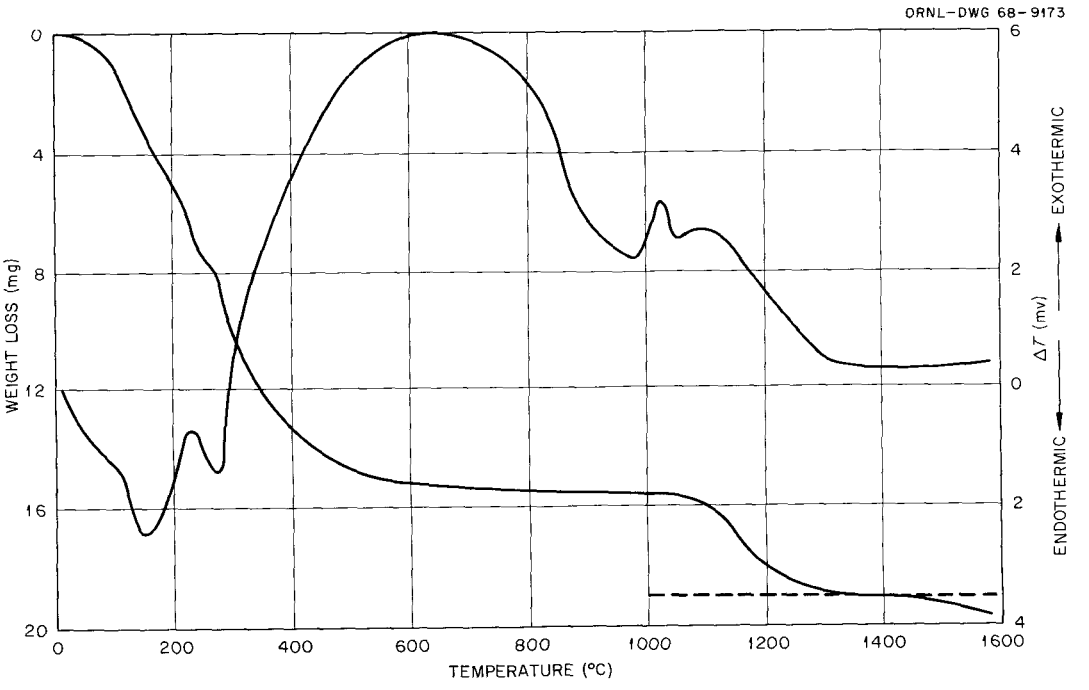

Fig. 6.26. Thermogram of an Americium Hydroxide Preparation.

and a $1\frac{1}{2}$-in.-OD alumina tube. In its final form, the unit will be capable of operation in vacuum or in various atmospheres up to 1600°C. The temperature limit can be extended by using induction heating or special furnaces. The Cahn balance has a maximum full-scale sensitivity of 20 μg but may be used at several lower sensitivities.

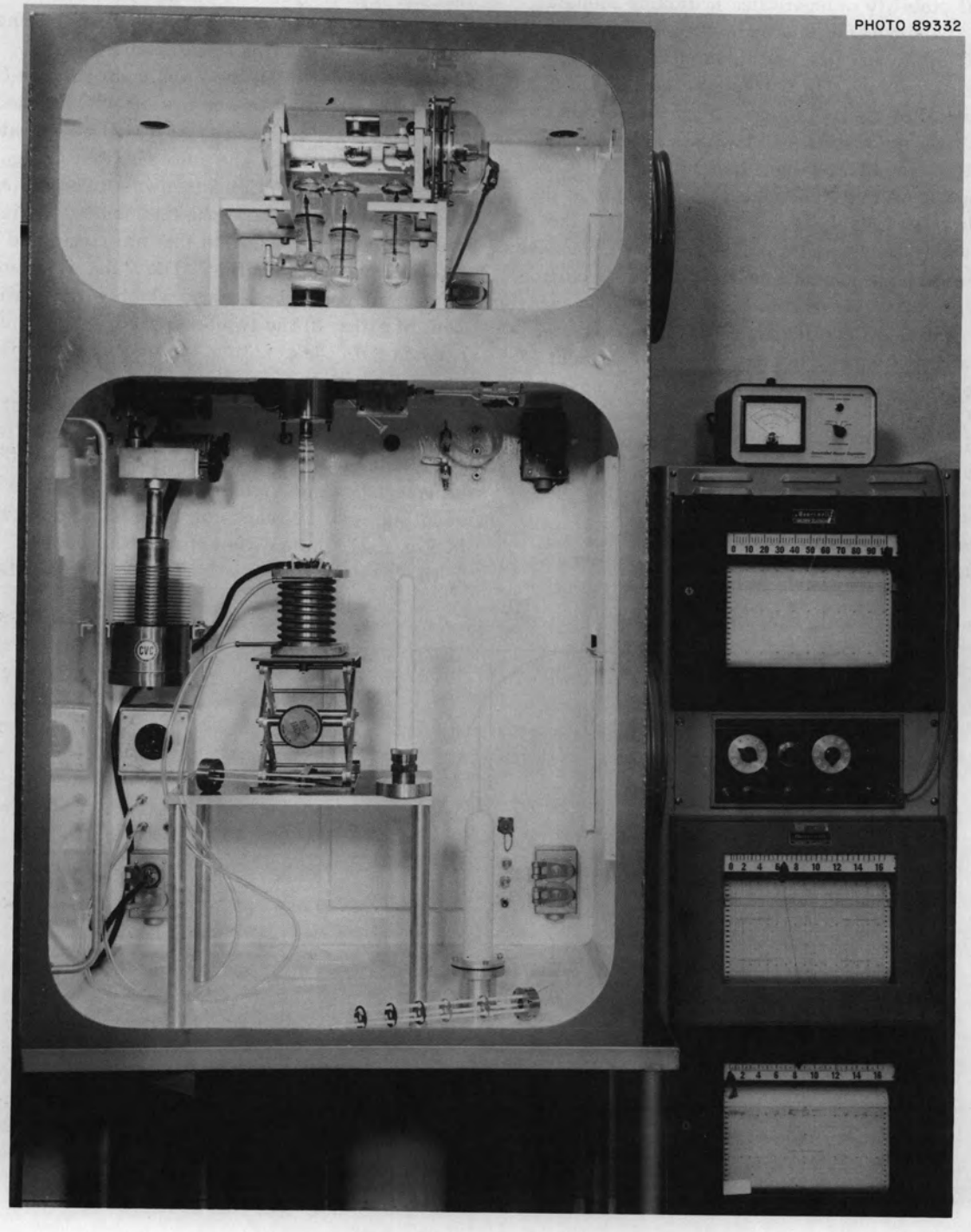

Fig. 6.27. Alpha-Contained Cahn Thermobalance.

7. Development of the Thorium Fuel Cycle

7.1 PREPARATION OF THORIUM-URANIUM OXIDE SOL BY SOLVENT EXTRACTION

An engineering-scale test of the amine extraction process was performed, and the production of ThO_2-UO_3 hydrosols with suitable microsphere-forming properties was demonstrated. A batch of 1.5 *M* hydrosol, with an NO_3^-/total metal mole ratio of 0.11 and a Th/U atom ratio of 3, was formed into microspheres in the Coated Particle Development Laboratory. This hydrosol had been prepared and concentrated in the amine extraction equipment shown in the previous report.[1] The hydrosol was produced at a rate that is equivalent to 1 kg of oxide per hour.

Seven kilograms of 350- to 500-μ-diam microspheres were formed, dried in a steam atmosphere, and then calcined to 1150°C in an argon atmosphere. Two surfactants, Ethomeen S/15 (0.6 vol %) and Span 80 (0.5 vol %), were used in the 2-ethyl-1-hexanol. No microsphere cracking was detected in either the drying or calcining steps. The appearance of these microspheres was excellent.

Engineering studies of the amine extraction process are being extended to include high-specific-alpha materials, that is, ^{233}U and ^{239}Pu. Toward this end, an alpha-contained amine extraction system has been designed.[2] This system will permit the preparation of concentrated hydrosols containing fissionable isotopes at a rate of 1 kg/day.

A simplified diagram of equipment for producing ThO_2-$^{233}UO_3$ concentrated hydrosols is shown in Fig. 7.1. Three stages of amine extraction, with two stages of interstage digestion, are permissible in this equipment. Three contactors without the interstage digester are used for amine regeneration. The six contactors are mounted on a frame, with the utilities being located between the hydrosol forming stages and the amine regeneration stages (Fig. 7.2). The entire equipment assembly fits onto a track inside an alpha enclosure to facilitate equipment modifications (Fig. 7.3).

Concurrent flow of the amine and aqueous phases through six agitated back-mix compartments provides the necessary contact time for nitrate removal in each contactor. The first and second nitrate extraction stages are equipped with interstage digesters. The post-extraction digestion step is essential to the process. The heights of the aqueous and organic weirs may be adjusted in order to obtain proper interface control whenever flowsheet conditions are altered (Fig. 7.4).

A second alpha enclosure of identical design contains the critically safe vacuum evaporator. This evaporator, which is designed for batch operation, is capable of removing about 4 liters of condensate per hour (Fig. 7.5).

7.2 DEVELOPMENT OF MICROSPHERE FORMING EQUIPMENT

The development of equipment and procedures for preparing small spherical particles (microspheres) and the production of test batches of the particles have continued. In these processes, droplets of the aqueous sol are gelled by extracting the water into an immiscible organic liquid such as 2-ethyl-1-hexanol (2EH). At a characteristic sol concentration, gelation occurs.

---

[1] D. E. Ferguson, *Chem. Technol. Div. Ann. Progr. Rept. May 31, 1967*, ORNL-4145, pp. 156–59.

[2] J. W. Snider, *The Design of Pilot-Plant-Scale Solex Equipment*, ORNL-4256 (in press).

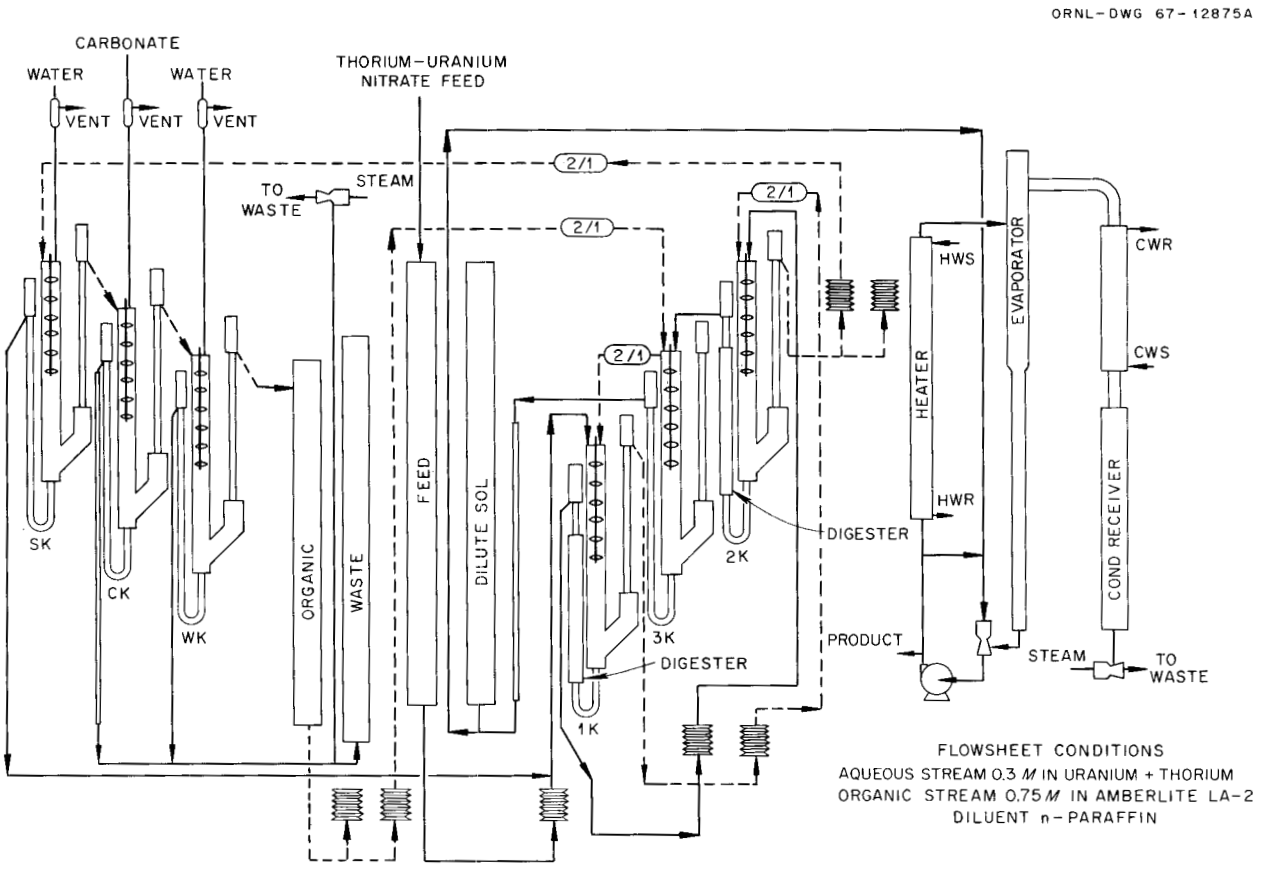

Fig. 7.1. Diagram of Solvent Extraction Equipment Used to Produce ThO_2-UO_3 Sol.

Dispersion of Sol into Drops

The first step in the preparation of microspheres is dispersion of the sol into droplets. The yield of product is maximized, and many column operation problems are minimized, when the sol disperser gives drops of controlled and uniform diameters. The types of dispersion devices previously described[3] have been developed and tested further. The two-fluid nozzle operated to perform according to the varicose breakup mechanism continues to be the most useful and reliable dispersion device for producing droplets in the 300- to 2000-μ range. We have found that breakup of the sol, using turbulent flow of the drive fluid, is also a useful dispersion mechanism. However, it is applicable to the preparation of small spheres only (see Sect. 8.3).

The vibrating capillary dispersers described in the last annual report have been modified. The reproducibility and durability were greatly improved by suspending the capillary at the end of a pivoted arm and by using more-rugged and more-powerful sources of vibration.[4,5] Stable operation,

[3] *Chem. Technol. Div. Ann. Progr. Rept. May 31, 1967*, ORNL-4145, pp. 171–72.

[4] R. J. Bates and P. I. Bachelder, ORNL-MIT-14 (Jan. 25, 1967).

[5] R. N. Leslie and J. M. Eloy, ORNL-MIT-18 (Mar. 29, 1967).

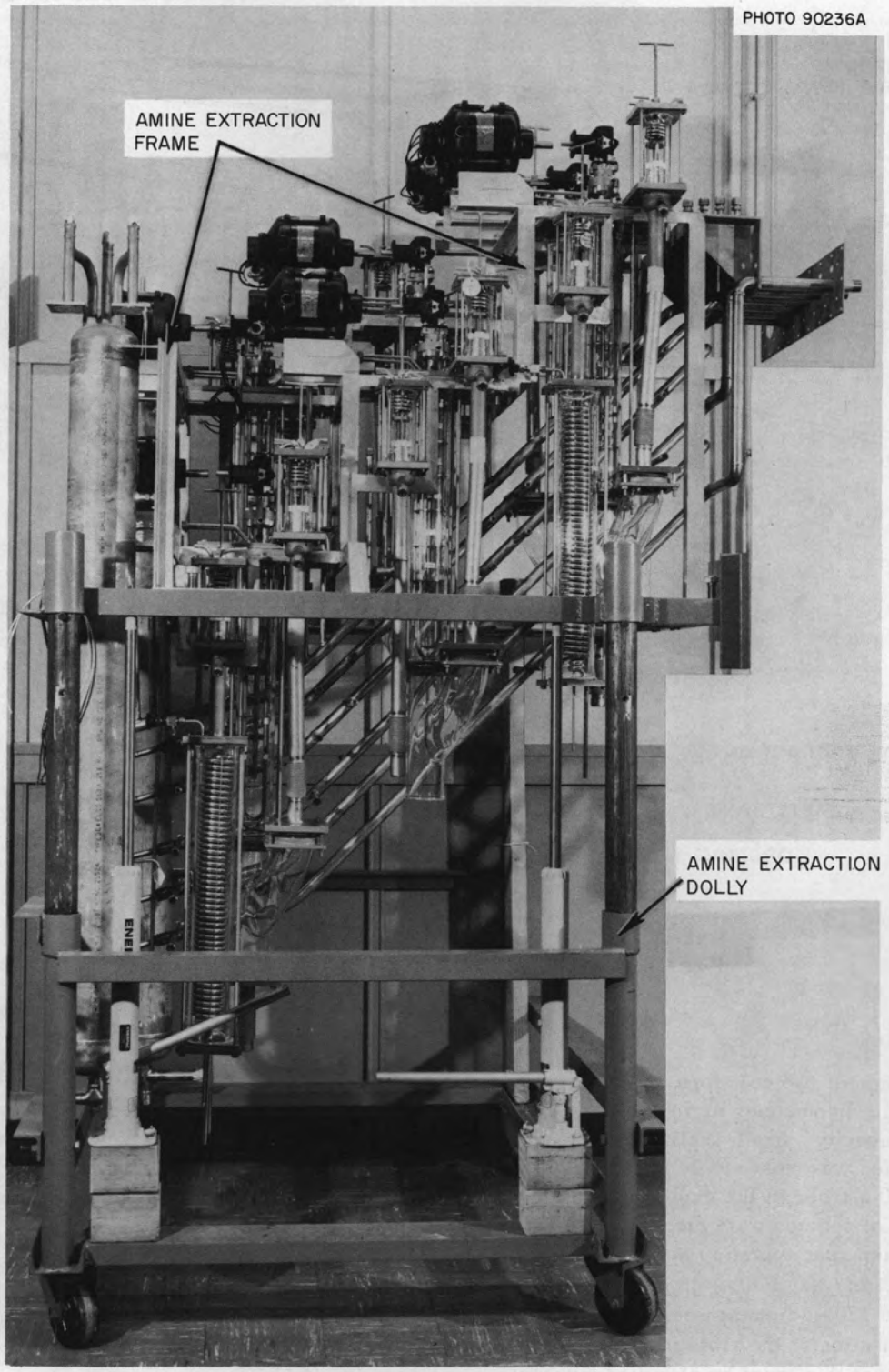

Fig. 7.2. Partially Assembled Solvent Extraction Equipment for Producing ThO_2-UO_3 Sol.

ORNL-DWG 67-12897R2A

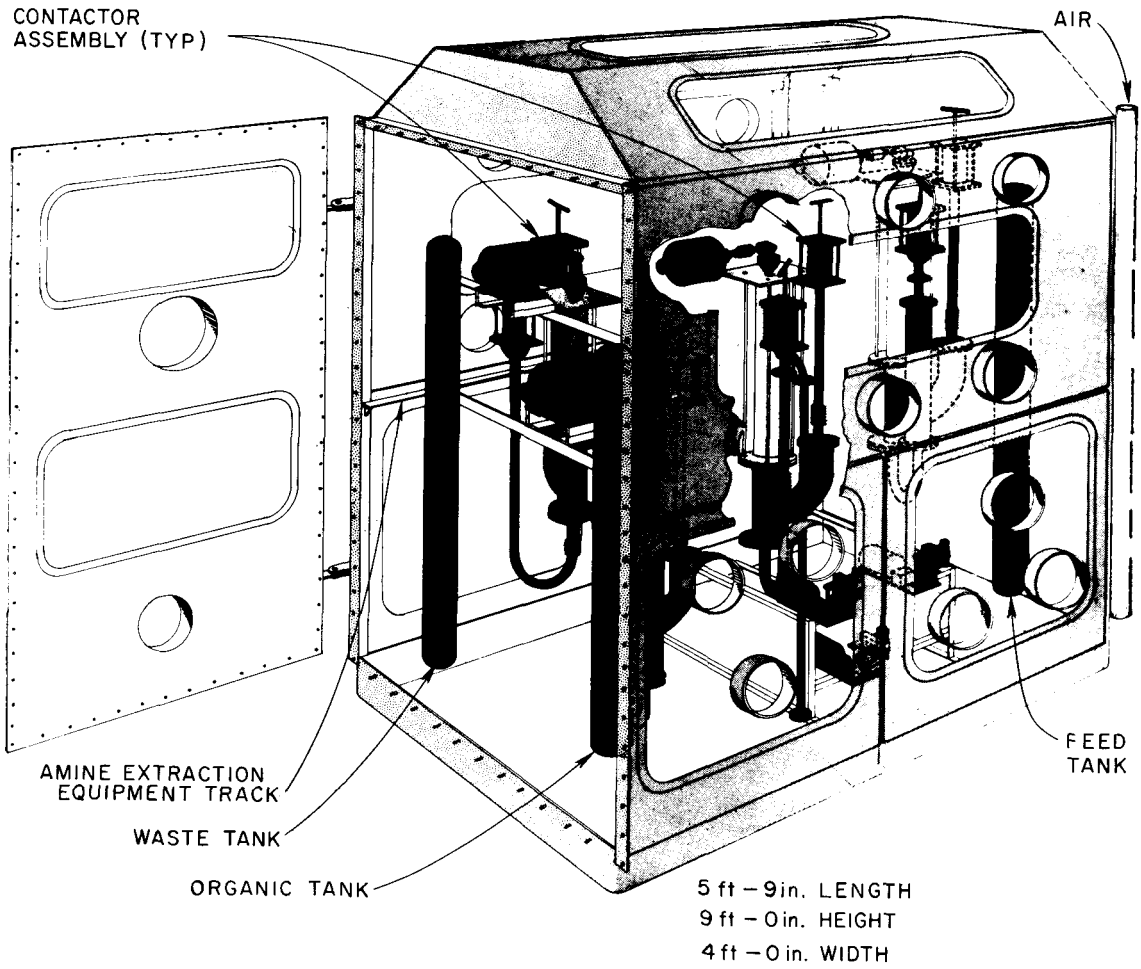

Fig. 7.3. Alpha Enclosure for Amine Extraction Equipment.

with formation of two sol drops per cycle, was possible with frequencies up to 800 Hz. At the higher frequencies, small amplitudes were required. The operation was most stable for sol flow rates of 50 to 100 cm/sec in the capillaries. In one test, 14 kg of spheres were prepared with a three-capillary disperser operating at 120 Hz. The yield was 55 wt % of (460 ± 40)-μ-diam spheres or 91 wt % (460 ± 120)-μ-diam spheres. The most serious limitation of the vibrating capillary dispersers is that they must be observed visually and "tuned" with respect to amplitude and frequency; also, their operation is more difficult with sols of either high viscosity or low density.

The following table shows the types of dispersers we have used successfully to produce several size ranges of fired microsphere product.

Device and Mechanism	Mean Diameter of Product (μ)
Two-fluid nozzle, varicose mechanism	50–500
Two-fluid nozzle, modified free-fall drop	200–600
Plastic bucket with orifices, free-fall drop mechanism	$\geq$400
Vibrating capillary	150–600

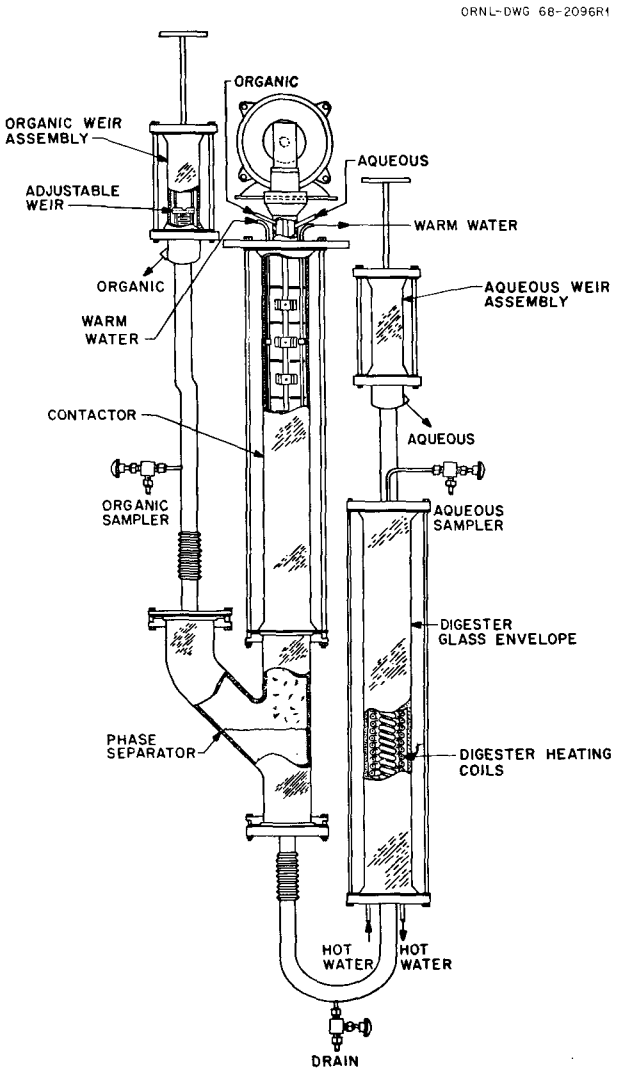

Fig. 7.4. Contactor-Digester Assembly for Preparing ThO_2-UO_3 Sols by Solvent Extraction.

Microsphere Preparation Pilot Plant (Coated Particle Development Laboratory)

The pilot plant was rebuilt, using a simplified one-pump flowsheet (Fig. 7.6). Of the original equipment, only the distillation train and the glass sphere-forming column were retained. Settlers were placed in the circuit at the overflow of the forming column and on the inlet side of the dryer. Appropriate elevations were selected for each equipment piece to allow unimpeded gravity-flow return of the 2EH to a single surge tank. This simplified system was used to prepare both mixed oxide microspheres (Th/U atom ratio of 3) and ThO_2 microspheres. During a four-month period of operation, no equipment breakdowns or process upsets were experienced, and the equipment appears to be suitable for remote operation. The settler in the column circuit effectively dries and removes fines; thus, turbidity of the 2EH (due to suspended ThO_2 fines) is no longer a problem. Additional particulate removal and flexibility in operation of the microsphere transfer jet are afforded by use of a settler in the dryer circuit.

Sintering of loose ThO_2 microspheres and apparent devitrification of the alumina crucibles (99% Al_2O_3) were observed in firing. The sinters of ThO_2 microspheres are easily broken, but they may prove troublesome in the operation of the proposed deep-bed calciner. Devitrification can probably be eliminated by prefiring (to 500°C) the microspheres to remove moisture. This prefiring step could easily be included as an extension of dryer operation.

An in-line hydraulic transfer sampling device for removing microspheres from the bottom of the column was built and used successfully. The microspheres can be optically examined in the sampler for shape and surface characteristics and can then be returned to the system. The optical requirements necessary for this examination and for the observation of the dispersion of the sol were defined.

Surfactants and 2-Ethyl-1-Hexanol: Chemical Considerations and Long-Term Operation

The optimum operating conditions for the microsphere forming column have been determined empirically for each new sol. To stabilize the droplets during water extraction, small amounts of surfactants are required. A combination of a nonionic surfactant, Span 80,[6] and a cationic surfactant, Ethomeen S/15,[7] is most commonly used. Previous experience[8] has shown that, as nitrate is extracted from the sol during operation, additional surfactant must be added.

---

[6]Product of Atlas Chemical Co.; trade name for sorbitan monooleate.

[7]Product of Armour Industrial Chemical Co.; trade name for the condensation products of ethylene oxide with primary fatty amines.

[8]*Chem. Technol. Div. Ann. Progr. Rept. May 31, 1967*, ORNL-4145, pp. 167–71.

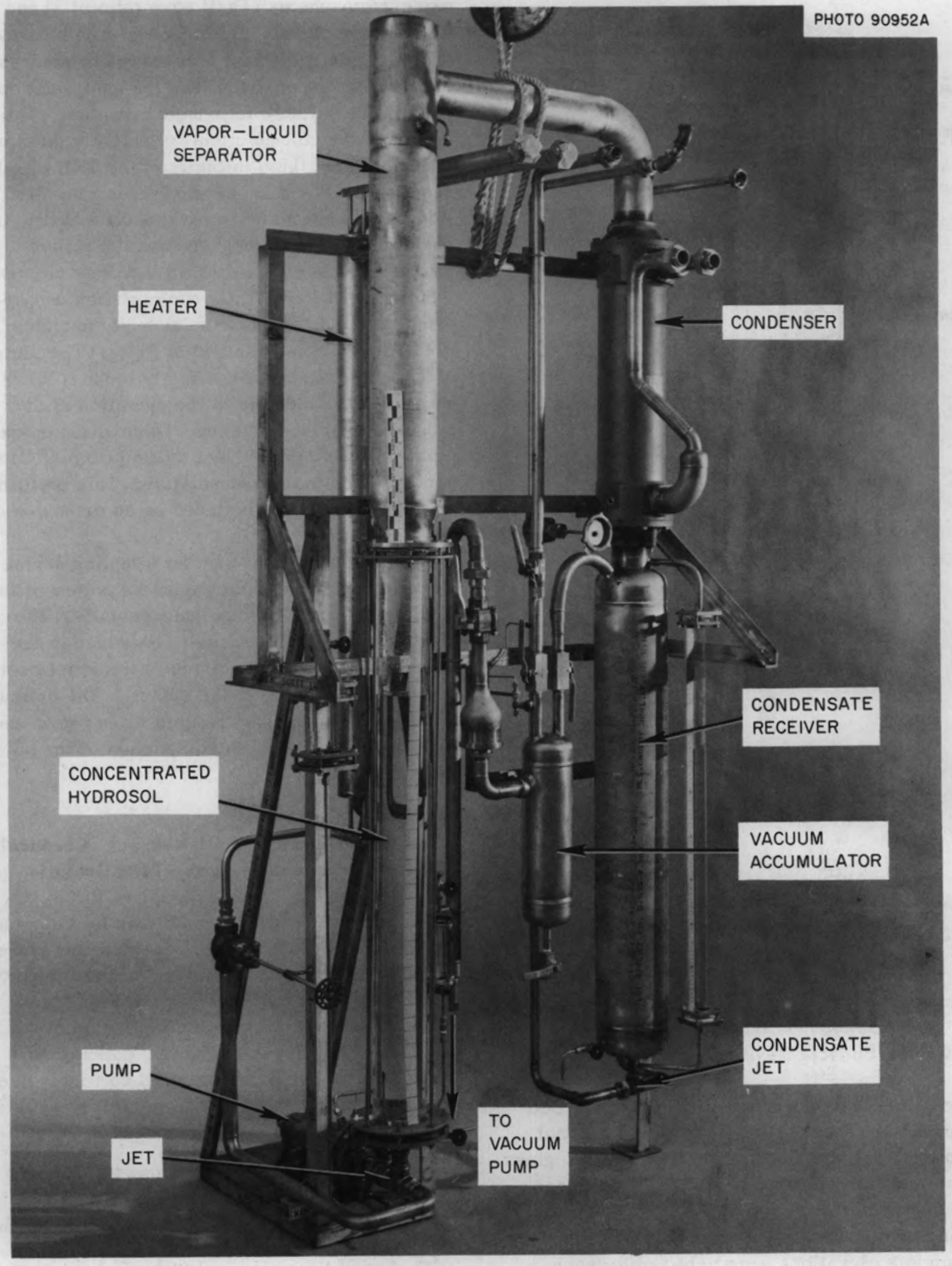

Fig. 7.5. Critically Safe Vacuum Evaporator.

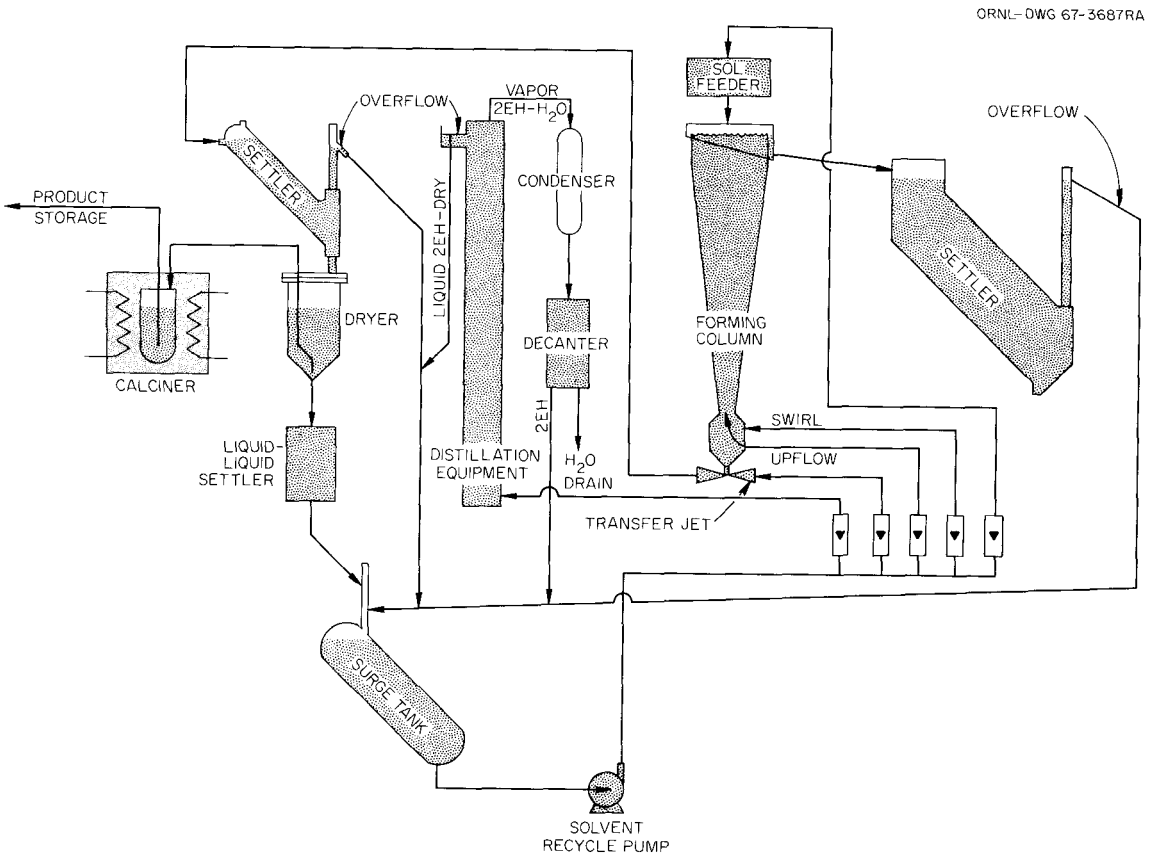

Fig. 7.6. Improved and Simplified Equipment Flowsheet for a One-Pump Solvent Recycle System.

Equilibration studies are being made in the laboratory to elucidate the interactions of the constituents of the organic phase with the surfaces of the sol crystallites and with the electrolytes HNO_3 and HCOOH that are used to stabilize the colloidal oxides. In a typical equilibration test, a given volume of the alcohol (containing the surfactants) is agitated with an equal volume of aqueous phase. The resulting emulsion is separated by centrifugation, and the phases are analyzed. Also, relative emulsification power is noted by measuring the time it takes for the emulsion to break. Conductivity and pH measurements of the aqueous phase were used to detect and analyze the electrolytes. Pure 2EH or 2EH containing Span 80 had only a slight tendency to extract HNO_3 or HCOOH; however, strong extraction occurred when Ethomeen S/15 was present in the alcohol. This presumably was due to formation of amine or formate salts. Ethomeen S/15 extracts nitric acid in preference to formic acid, as was expected. Ionic impurities associated with the surfactants are readily extracted by the aqueous phase.

Ethomeen S/15 showed its strongest emulsifying power at a pH of 4 to 6, whereas Span 80 was more effective at a pH of 6 to 8. Thus, to ensure the most satisfactory operation when fresh 2EH is used, the acid concentration of the organic phase should be adjusted to the pH of the sol on startup; this has been demonstrated in the laboratory-scale column and in the glove-box production facility.

We presently use infrared absorption to analyze for Span 80; however, this method does not differentiate it from closely related compounds having carbonyl groups. For example, we observe

interfering absorption by carbonyl-containing compounds that are produced when nitric acid is heated with 2EH, 2EH plus Ethomeen, or 2EH plus Span 80. Since nitric acid that is extracted from the sols appears to be the chief cause of surfactant losses, we plan to examine means for removing nitrates prior to distillation.

Mass Transfer During Gelation

The rate that water is extracted from thoria sols was investigated by fluidizing single thoria sol droplets in 2EH and measuring their diameters, as a function of time, until shrinkage no longer occurred. Data for drops of both water and sol were obtained at 25°C. The experimental variables were drop diameter (0.1 to 0.2 cm), sol molarity (0 to 2.5 *M*), and water concentration in the bulk solvent (2 to 12 mg of H_2O per milliliter of 2EH). The procedures were described and the results were reported previously.[9]

[9]S. D. Clinton, *Mass Transfer of Water from Single Thoria Sol Droplets Fluidized in 2-Ethyl-1-hexanol*, ORNL-TM-2163 (June 1968).

A linear relationship was found for the water and sol droplet data when the Sherwood number was plotted vs the product of the Reynolds number to the $\frac{1}{2}$ power and the Schmidt number to the $\frac{1}{3}$ power. The common correlation for the fluidized water and sol drops verified a proposed mass-transfer model that is based on an organic-phase film surrounding the drop as the rate-controlling resistance. The drop Reynolds number, which was based on an average organic fluidizing velocity, varied from 0.2 to 7. The Schmidt number for the system was fixed at 35,700.

During the extraction of water, the mass-transfer coefficients for fluidized sol drops were shown to depend only on the increasing thoria concentration or molarity. By correlating the mass-transfer coefficients with the density difference between the sol and the 2-ethyl-1-hexanol, an expression was derived to predict the gelation times required for any initial sol molarity and drop diameter.

7.3 PREPARATION OF SOL-GEL MATERIALS

Kilogram batches of microspheres prepared from ThO_2 or ThO_2-UO_3 sol in the microsphere prepa-

Table 7.1. Quantities and Uses of ThO_2 Microspheres Prepared in the CPDL Microsphere Preparation Pilot Plant

Particle Size Range (μ)	Amount Delivered (kg)	Destination	Ultimate Use
88–125	10	ORNL Metals and Ceramics Div.	To be coated with pyrolytic carbon
210–250	95	ORNL Metals and Ceramics Div.	Development of pyrolytic-carbon coatings
250–297	10	ORNL Metals and Ceramics Div.	Development of pyrolytic-carbon coatings
297–420	42	ORNL Metals and Ceramics Div.	Development of pyrolytic-carbon coatings
350–500	40	ORNL Metals and Ceramics Div.	Development of pyrolytic-carbon coatings
350–500	20		For HTGR fuel sticks – processing studies
420–500	2		For power reactor fuel reprocessing studies
350–500[a]	7[a]		For firing studies
420–500	1	Babcock and Wilcox Co.	
420–590	5	ORNL Metals and Ceramics Div.	For thermal conductivity measurements

[a]ThO_2-UO_2 from ThO_2-UO_3 sol prepared by the solvent extraction technique.

Table 7.2. Typical Properties of Thorium Fuel Cycle Microspheres

Composition	Size (μ)	Density (g/cc)	Surface Area (m^2/g)
ThO_2	350–500	10.08[a]	
ThO_2	210–250	9.98[a]	
ThO_2	44–53	9.64[b]	0.020
ThO_2–11% UO_2	210–250	10.16[a]	
ThO_2–22% UO_2	210–250	10.12[a]	

[a]By mercury porosimetry at 100 or 200 psi.
[b]By helium pycnometry.

ration pilot plant were supplied to various projects associated with the Thorium Utilization Program and other related programs. Quantities and uses of some of these batches are listed in Table 7.1. Smaller-sized batches with special compositions or diameter ranges were prepared in process development equipment (Table 7.2).

7.4 THORIUM-URANIUM RECYCLE FACILITY

A fixed-price contract for the construction of the Thorium-Uranium Fuel Cycle Facility was signed with Blount Brothers Construction Company on May 6, 1965. The major portion of the facility was completed and accepted by the Laboratory for occupancy by September 15, 1967. The remaining work was completed and accepted on October 2, 1967, 85 days after the date specified in the contract. Partial acceptance of the facility prior to total completion of the facility permitted an early starting date for the installation of processing equipment in cell G for the MSRE ^{233}U fuel preparation experiment (see Sect. 1.12).

Upon partial acceptance of the facility, Rust Engineering Company began installing the in-cell crane and manipulator systems, the out-of-cell processing equipment for cell G, various service plugs in service sleeves throughout the cell bank, the viewing windows at the various cell operating modules, and the equipment mounting pads on the floor in cells C and D. This cost-plus-fixed-fee (CPFF) portion of the construction program was completed on January 15, 1968, for approximately 85% of the estimated cost. Certain painting work, which was transferred from the fixed-price construction contract to the CPFF participation, was completed on March 9, 1968.

The installation of special equipment in the facility by the Laboratory was begun on November 1, 1967, and was completed on March 15, 1968. This work consisted primarily of the installation of master-slave manipulators; special sampling equipment for the liquid waste tanks; a pneumatic-tube, solid-sample conveyor system for cells C, D, and E; the facility radiation and contamination monitoring and control equipment; and the cleaning and filling of zinc bromide window tanks installed in cells G and F. The filling of the remainder of the window tanks has been deferred until facility operations will require shielded viewing windows in other cells.

The Laboratory's participation in the construction project has included the procurement and installation of the special equipment mentioned above, the total cost of which was $1,753,000.

The incomplete phases of the project include procurement of the sol-gel sphere-forming equipment and the zinc bromide for the window tanks that will be filled in the future. Purchase of these items has been deferred until the end of 1969. Construction and installation of the fuel fabrication equipment have not yet been authorized.

Previously reported problems with the screw drives for radiation shielding doors Nos. 2 and 3 have apparently been resolved by the installation of ball screw and nut assemblies to replace the modified square-thread mechanical screw jacks. These assemblies were tested and found to be satisfactory in January 1968.

Methods for cleaning the copper lining inside the viewing window tanks have been studied for the past three years. Results of these studies showed that a cleaning procedure with the following major steps would be effective: (1) degreasing with alcohol; (2) washing with a solution of acetic acid, sodium chloride, and demineralized water; (3) rinsing and drying with alcohol; (4) washing with a solution of 10% zinc bromide and demineralized water; and (5) rinsing with demineralized water containing hydroxylamine.

The safety analysis was prepared for the facility during the latter part of 1967, and the facility received preoperational review by the USAEC on

January 21, 1968. The facility was approved to carry out the MSRE ^{233}U fuel preparation experiment, and tentative overall approval for operation of the facility was given.

7.5 ^{233}U STORAGE AND DISTRIBUTION FACILITY

Oak Ridge National Laboratory serves as a national distribution center for ^{233}U. The center is equipped with facilities to store as much as 120 kg of ^{233}U in solid form in shielded wells or 500 kg in nitrate solution (up to 250 g/liter) in borosilicate-glass-poisoned tanks. During the past year an existing building was converted to serve as a shielded vault and was approved for the storage of 70 kg of ^{233}U or ^{239}Pu in shipping containers.

The facility accepts ^{233}U in nitrate form or as properly packaged metal or solid compounds which can be dissolved in solutions that are compatible with the stainless steel equipment.

The purification facilities consist of a one-cycle solvent extraction system that is capable of purifying ^{233}U at the rate of 25 kg per week. All ^{233}U shipped from the facility is in the form of nitrate solution.

Summary of Operations

During the past year, 118 kg of ^{233}U (22 shipments) was received by the facility and 115 kg of ^{233}U (17 shipments) was disbursed. A total of 34 dissolutions of solids were made to provide feed for four solvent extraction runs for the purification of 72 kg of ^{233}U.

The largest receipt of material was 75 kg from the ORNL Neutron Physics Division, following completion of criticality experiments. The largest quantity transferred was 50 kg (as UO_2) to the Thorium-Uranium Fuel Cycle Development Facility for conversion to the LiF-UF_4 eutectic salt for the Molten Salt Reactor Experiment. The activity of the ^{233}U handling facility for 1967, as compared with previous years, is shown in Fig. 7.7. The present inventory of ^{233}U in the facility, along with the form, isotopic purity, and ^{232}U content, is shown in Table 7.3.

Table 7.3. ^{233}U Inventory – April 1, 1968

Form	Purity (at. % ^{233}U)	^{232}U Content (ppm)	Quantity (kg)
Nitrate	91	13	24.1
Oxide	91	250	98.0
Nitrate	97	5	49.0
Oxide	97	5	36.7
Scrap (oxide, slag, etc.)	97	5	0.7
Nitrate	97	34	14.7
Oxide	97	50	13.6
Metal	97	50	5.6
Total			242.4

TRUST Facility

The TRUST (Thorium Reactor Uranium Storage Tank) facility was built to receive, transfer, and store 1100 kg of highly enriched uranium (75% ^{235}U, 11% ^{233}U) in the form of a uranyl nitrate solution. This material is the uranium product from Indian Point Reactor fuel and is to be purified by solvent extraction at the Nuclear Fuels Services Plant in West Valley, New York. The solution will be stored in the TRUST facility indefinitely because it contains sufficient ^{232}U (120 parts per 10^6 parts ^{233}U) to prohibit the direct refabrication into fuel elements.

The TRUST facility was constructed by modifying several of the installations in Building 3019 (Fig 7.8). The penthouse area, including a newly installed glove box, is used for transient storage of the uranium shipping containers and charging of shipping bottles into cell 4. A modified shielded cubicle on the third level of cell 4 contains process equipment for removing solution from shipping bottles and transferring solution to and from the uranium storage tank. The 5000-gal uranium storage tank, packed with 1.5-in. Pyrex Raschig rings that displace 34% of the volume, is located in a heavily shielded compartment of the thorium storage pit south of the building. This compartment is sealed and reinforced to contain the maximum credible explosion; it is ventilated to cell 5 of Building 3019.

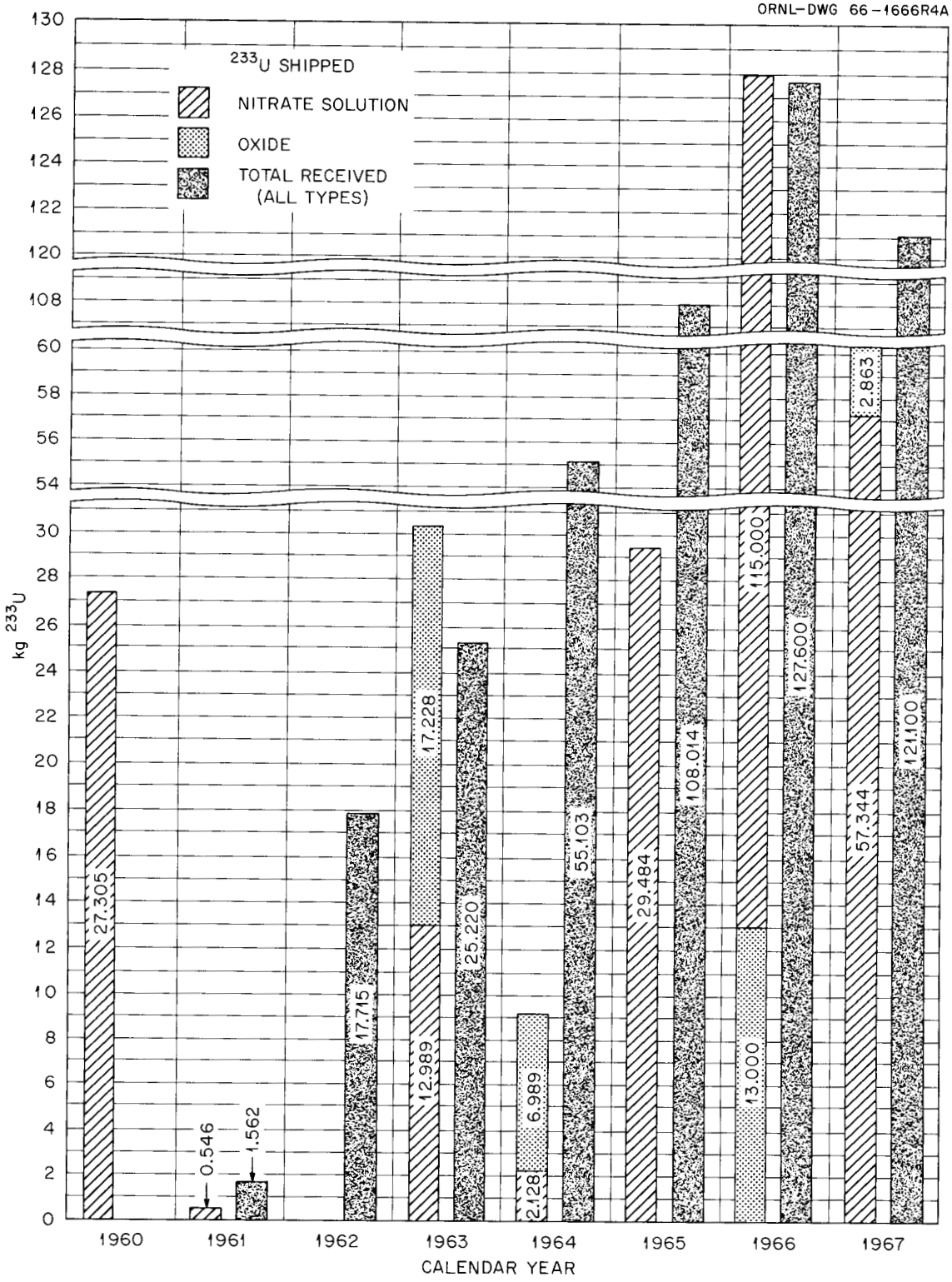

Fig. 7.7. Summary of ^{233}U Receipts and Shipments.

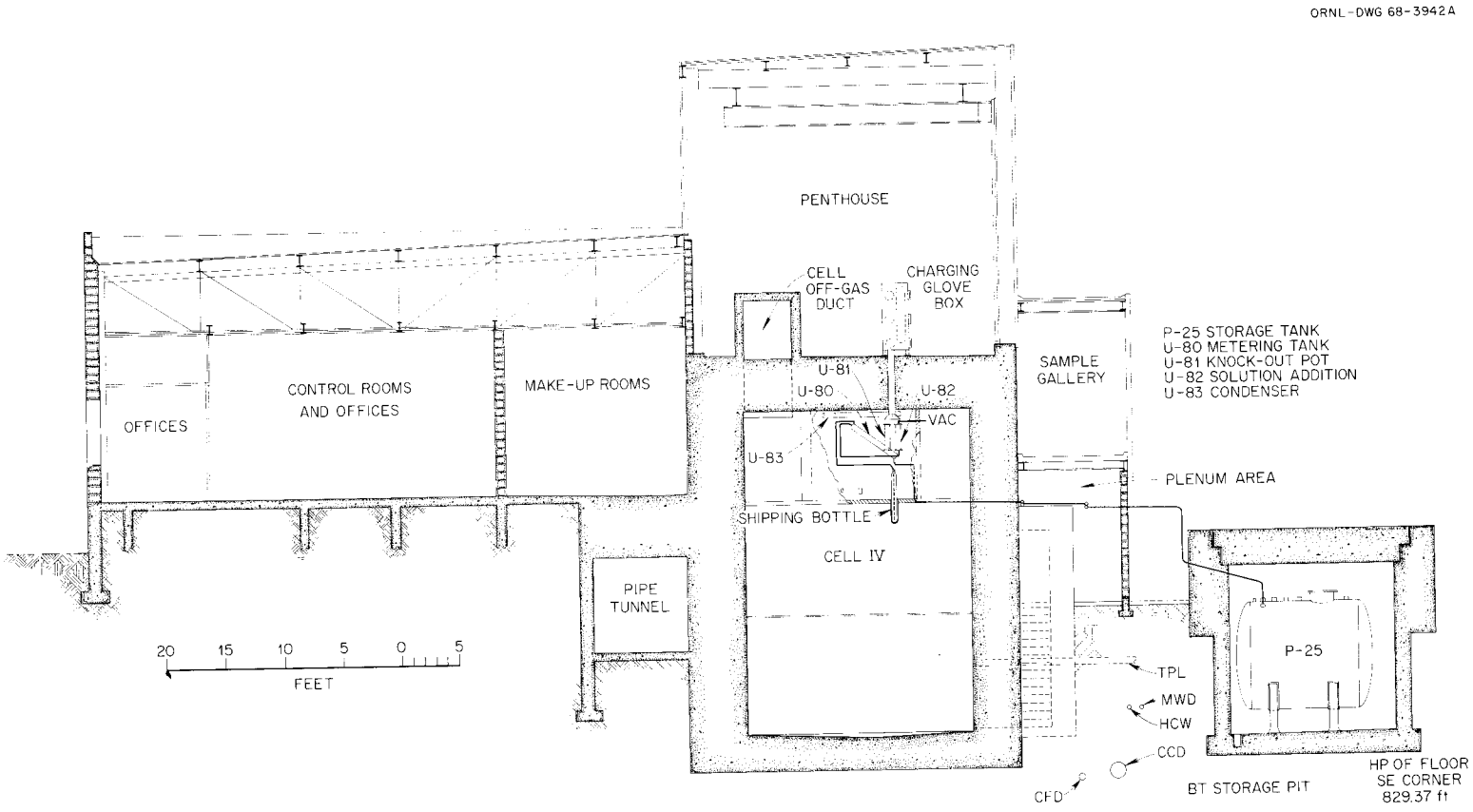

Fig. 7.8. TRUST Facility, Building 3019.

Upon receipt at ORNL, the uranium solution will be mixed with cadmium and gadolinium nitrates (in the uranium storage tank) to form a solution that contains 150 g of uranium per liter and is 3.9 *M* in HNO_3, 0.2 *M* in $Cd(NO_3)_2$, and 0.0168 *M* in $Gd(NO_3)_3$. The Raschig rings in the tank will provide primary criticality control during filling operations. These rings and the solubilized cadmium and gadolinium will ensure the subcriticality of the solution in the tank under all anticipated storage conditions. The presence of the neutron absorbers in solution will be the sole means of criticality control in the improbable event that solution rises above the level of the rings or that the solution leaks to the stainless steel floor pan. In the latter case, the solution would be transferred to a 10,000-gal tank located in an adjacent compartment of the pit.

Off-Gas Modifications

During the year, the vessel off-gas filtration system that handles off-gas from all process vessels as well as the building glove boxes was replaced. The previously used deep-bed fiber-glass filter was discarded in favor of replaceable CWS roughing and absolute filters. The deep-bed filter had required constant flushing to verify the absence of uranium and plutonium and had operated at an efficiency (93%) well below the ORNL requirements (99.95%). The new filters can be changed by the bag-out technique and are located in a filter house at the southeast corner of the building. A deentrainment device and heating coils were installed to prevent the collection of moisture on the filter media.

8. Sol-Gel Processes for the Uranium Fuel Cycle

8.1 PREPARATION OF UO_2 SOLS BY SOLVENT EXTRACTION

The preparation of UO_2 sols by the solvent extraction method has been continued. The process has been successfully scaled up and operated continuously in engineering experiments. Forty runs, each producing about 2 kg of UO_2 in the form of a dilute (about 0.2 *M*) sol, have been made. Laboratory studies to characterize the sol and aid in the engineering studies are still in progress. We have studied three operating parameters that affect sol properties: nitrate-to-uranium mole ratio during digestion, digestion temperature, and method for preparing the initial U(IV) solution.

The basic method for preparing UO_2 sol by solvent extraction (see the reference flowsheet in Fig. 8.1) was developed from laboratory batch studies.[1] It consists in extracting nitrate from an aqueous solution of U(IV) nitrate-formate with a long-chain amine (e.g., Amberlite LA-2[2]) dissolved in a paraffin. Digestion of the resulting nitrate-deficient solution produces the UO_2 sol. Final nitrate adjustment is obtained in subsequent extractions. The amine, which is regenerated by contact with sodium carbonate, is recycled.

The equipment for the engineering study of the process is the same as that used for the preparation of ThO_2-UO_3 sol.[3] The contacting devices for extraction, water scrubbing, and amine regeneration consist of mixer-settlers. These mixer-settlers are geometrically safe with regard to criticality. Each

[1] *Chem. Technol. Div. Ann. Progr. Rept. May 31, 1967*, ORNL-4145, p. 184.

[2] Product of Rohm and Haas Co.

[3] *Chem. Technol. Div. Ann. Progr. Rept. May 31, 1967*, ORNL-4145, p. 156.

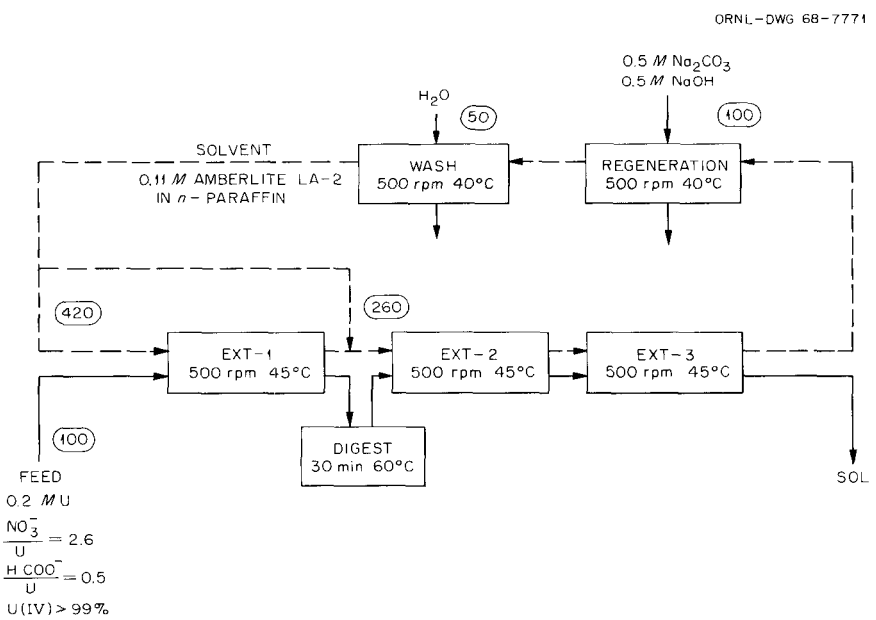

Fig. 8.1. Reference Flowsheet for the Preparation of UO_2 Sol by Solvent Extraction.

mixer has six compartments, which, with cocurrent flow of the solvent and aqueous phases, give the same effect as mixing vessels in series. The phases separate in the settler section below the mixer. The position of the interface is controlled by adjustable weirs on both the solvent outlet and the aqueous outlet. Maintaining the interface below the mixer helps to produce a water-in-oil type of dispersion, which is important in minimizing emulsions. At shutdown the aqueous phase is drained out of the mixer, so that at subsequent startup the incoming aqueous is readily dispersed into the solvent phase. The digester is an enlargement of the aqueous jackleg on the first extraction mixer-settler stage. The temperature in each stage and in the digester is controlled by circulating water through internal coils. The design capacity of the equipment is 6 liters of sol per hour; the capacity is determined by the size of the digester and the required residence time in the digester (30 min).

Preparation of U(IV) Solution

During the laboratory studies, U(IV) solution was prepared by contacting 0.2 *M* $UO_2(NO_3)_2$–0.1 *M* HCOOH with hydrogen, using platinized Al_2O_3 powder as the catalyst. Although this procedure usually produced good results, it did not appear very practical for the larger engineering tests because of the time required for removing (by settling and filtration) the catalyst. Consequently, several alternative methods of reduction were evaluated. One of these consisted of continuous reduction in a pressurized fixed bed of platinized Al_2O_3 pellets. Attempts to make sol by using U(IV) from this reductor failed because of the formation of viscous sol in the second extraction stage. Another method involved batch operation of the fixed catalyst bed at approximately atmospheric pressure. This allowed better control of the reduction; therefore, the resulting sol was improved and no thickening of the dilute sol occurred. However, the sol could not be concentrated (by vacuum evaporation) to 1 *M* without thickening or gelling. The U(IV) solution contained a nitrogen-bearing basic material that behaved like ammonia during chemical analysis but degraded on standing. [Ammonia was shown, in laboratory tests, to cause thick sol when it was added (NH_3/U mole ratio = 0.02) to laboratory-prepared U(IV) solution, which was then formed into sol by the usual batch extraction technique.]

Most of the recent runs have been made by using U(IV) feed that had been prepared in a slurry-type reductor, where finely divided PtO_2 catalyst is suspended in a well-mixed uranium nitrate solution and the hydrogen enters through a sparger. Since the catalyst is reduced to metal that becomes flocculated in the presence of excess hydrogen, it settles very rapidly and is readily retained on a filter when reduction of the uranium is nearly complete. The filter consists of a flat disk of porous stainless steel (10-μ pore) that forms the bottom of the reductor. The reduction is monitored by measuring the redox potential of the solution, using a platinum electrode vs a reference glass electrode system. (Other reference electrodes such as silver–silver chloride or calomel can also be used but are not as rugged and trouble-free as glass.) The end point is readily detected as a sharp break in emf which occurs when reduction has progressed to between 96 and 100% U(IV). The feed composition was fixed at 0.6 *M* $UO_2(NO_3)_2$–0.4 *M* HNO_3–0.3 *M* HCOOH, so that the NO_3^-/U mole ratio was 2.6 and the HCOOH/U mole ratio was 0.5.

Both a small laboratory slurry reductor (1.6-liter capacity) and a larger unit (14-liter capacity) have been evaluated as devices for supplying feed for the engineering tests of the solvent extraction sol process. About 10 kg of uranium was reduced in the small reductor, thus demonstrating the feasibility of the slurry catalyst. The large reductor was designed and built using the laboratory data. The results of 20 runs, producing a total of 40 kg of U(IV), show excellent performance. The platinum catalyst has shown no sign of loss in activity or of decrease in filtration efficiency (filtration time by gravity was 12 min for 14 liters). Reduction of greater than 99.5% of the uranium was easily obtained, very little ammonia was formed (NH_3/U mole ratio $\leq$ 0.002), and less than 10% of the HCOOH was lost. (Some reduction techniques lead to a substantial HCOOH loss.) The rate of uranium reduction with 30 g of PtO_2 ranged from 2 moles/hr when only a small excess of hydrogen was used (96% utilization) to 3.3 moles/hr at 77% utilization.

Operation of the Solvent Extraction Equipment

The solvent extraction equipment has operated very satisfactorily (in 20 runs, about 1000 liters of

Table 8.1. UO_2 Sol Prepared by Solvent Extraction in Continuous-Flow Engineering Tests

Run No.	Excess Amine (%)	Digester Temperature (°C)	NO_3^-/U Mole Ratio	Shelf Life[a] of 1 *M* Sol (days)
15	50	50	0.17	13
16A	50	50	0.26	50
16B	50	65	0.08	90
17	50	50	0.27	43
18	50	50	0.24	40
19	70	50	0.24	60
20	50	60	0.09	35
21	50	60	0.09	36
22	50	60	0.10	60
23A	65	60	0.17	25
23B	65	50	0.24	
24	50	50	0.24	50
27	20	60	0.13	50
28	20	60	0.14	50
29	50	60	0.10	50
30	50	60	0.09	10
31	50	60	0.09	25
32	50	60	0.09	15
33	50	70	0.07	8
35	50	60	0.10	
36	50	60	0.09	

[a]Shelf life refers to the number of days the sol remained fluid. In some cases the sol thickened after the interval listed; in others, it gelled.

0.2 *M* UO_2 sol was produced). Table 8.1 summarizes some operating conditions and sol product properties. No emulsion or entrainment difficulties have been encountered. The entrainment of solvent in the sol product has been consistently less than 0.01 vol %. A small amount of entrained sol in the used solvent is removed by scrubbing with water to prevent loss of uranium to the waste. Although three extraction stages have been used in most of the runs, only two are needed because the nitrate content of the sol changes only slightly in the third stage. The stage efficiency has been consistently greater than 90% at a mixer speed of 500 rpm.

Variation of the uranium concentration from 0.15 to 0.3 *M* (the reference concentration is 0.2 *M*) did not cause any difficulty, and good-quality sols were produced; however, two attempts with a sol having a uranium concentration of 0.6 *M* were unsuccessful because the sol became thick in the second extraction stage.

The digestion temperature was found to be an important variable. At 50°C the sol contains a significant amount of amorphous UO_2 (as determined by x-ray diffraction). The sol gels at a uranium concentration of about 0.5 *M* if it is evaporated immediately after preparation; however, after aging overnight it can be concentrated to greater than 1.0 *M* and will remain fluid for more than 30 days. When the digestion temperature is increased to 60°C, the sol contains more UO_2 crystallites, and the fresh sol can be concentrated without gelling. To minimize oxidation of the uranium at the higher digestion temperature, the laboratory flowsheet was modified to include the use of an excess of amine in the first stage. This amine extracts sufficient nitrate to give an NO_3^-/U mole ratio of less than 0.5. At a digester temperature of 70°C, the sol has a shorter shelf life after concentration, perhaps because extensive oxidation of uranium occurs even at the low NO_3^-/U mole ratio. The digester temperature also

affects the NO_3^-/U mole ratio in the sol product; the ratio averages 0.24, 0.10, and 0.07 when digestion is carried out at 50, 60, and 70°C respectively. From 20 to 70% excess amine (i.e., 20 to 70% more than the stoichiometric quantity required to extract the nitrate from the feed) has very little effect on the nitrate content of the sol. The average size of the UO_2 crystallites in the sol product is 35 to 40 A and does not seem to depend on either the digester temperature or the period of aging.

A digestion period of about 1 hr and a temperature of about 60°C appear optimum after the first extraction stage. Further digestion after subsequent extraction may also be beneficial.

Evaporation of Sol

Dilute sol (~0.2 *M*) must be concentrated until it is about 1 *M* in uranium in order to facilitate the formation of microspheres. Vacuum evaporation is used to avoid overheating the sol. The temperature is kept below about 35°C. Because the sol is quite sensitive to oxidation, exposure to air is a common cause of thickening or, in extreme cases, flocculation of the sol.

Representative samples from each run have been concentrated to 1 *M* in uranium in a small laboratory evaporator (Roto Vac), in order to determine the effects of variables on the shelf life of the concentrated sol. Most of the sols formed by the reference flowsheet remain fluid at a uranium concentration of 1 *M* for 50 days or more.

Seven batches (each containing 2 kg of uranium) of dilute sol have been successfully concentrated in the forced-circulation vertical-tube evaporator[4] to yield 1 *M* sol for use in making microspheres. The evaporation has been satisfactory at the design boilup rate of 15 liters/hr and at an absolute pressure of 30 torrs. No foaming or scaling has been observed. Shelf lives of the large batches of concentrated sol were shorter than the shelf life of the product from the small laboratory evaporator. We believe that the reason for this is inleakage of air and the resultant oxidation of uranium in the large evaporator. In several runs where large leaks were discovered, the sol thickened overnight; in other runs, the sols were still fluid after 30 days.

[4]*Chem. Technol. Div. Ann. Progr. Rept. May 31, 1967*, ORNL-4145, p. 158.

8.2 PLUTONIA AND URANIA-PLUTONIA

The plutonia sol-gel studies are directed toward the economical production of fast-reactor fuels. The initial program objective was the development of a process for preparing stable aqueous PuO_2 sols that: (1) would yield dense PuO_2, (2) would be compatible with other oxide sols, and (3) would be capable of being formed into microspheres by the techniques already developed at ORNL. The chemical flowsheet and the process equipment for preparing stable PuO_2 sols and for, subsequently, forming these sols into dense microspheres were described in a previous progress report.[5] Stable plutonia sols up to 3 *M* in plutonium, with NO_3^-/Pu mole ratios of less than 0.15, can be prepared. They are compatible with the thoria and urania sols made at ORNL[5–8] and have been formed into spheres both alone and in combination with UO_2, ThO_2, or ZrO_2.

The program includes preparation of material in laboratory, as well as larger, equipment. In the laboratory, we investigated process variables in the existing flowsheet, alternative methods for producing plutonia sols, and procedures for the preparation of mixed sols and microspheres of PuO_2-UO_2. Work was also directed toward preparing PuO_2 sols for use in the UO_2-PuO_2 fuel fabrication development and testing program at ORNL, which is conducted jointly with the Metals and Ceramics Division of ORNL and with groups at other sites.

Plutonium Storage and Distribution Facility

A plutonium storage and distribution facility, which will serve as a centralized source of feed material to support the sol-gel effort at ORNL, will be built in the basement of Building 3019. The facility will allow storage of as much as 100 kg of plutonium in solid or liquid form.

Plutonium will be received as PuF_4 (solid) and $Pu(NO_3)_4$ (solution). The PuF_4 will be stored in

[5]*Chem. Technol. Div. Ann. Progr. Rept. May 31, 1967*, ORNL-4145, pp. 196–203.

[6]*Chem. Technol. Div. Ann. Progr. Rept. May 31, 1966*, ORNL-3945, pp. 170–75.

[7]*Chem. Technol. Div. Ann. Progr. Rept. May 31, 1965*, ORNL-3830, pp. 174–75.

[8]C. J. Hardy, S. R. Buxton, and M. H. Lloyd, *Preparation of Lanthanide Oxide Microspheres by Sol-Gel Methods*, ORNL-4000 (August 1967).

shielded wells in a glove box. The nitrate solution will be stored in a large tank poisoned with borosilicate-glass Raschig rings.

The design of the facility is complete. Equipment that is no longer in use and is not needed for this facility is being removed from the planned location. All surfaces will be decontaminated before the new equipment is installed.

Laboratory Studies

Preparation of Plutonia Sols. – The undesirable effects observed when high HNO_3 concentrations were used for the peptization of plutonia precipitates, and when concentrated ammonia and plutonium solutions were used during precipitation, were reported last year.[5] Subsequent experience has confirmed these observations. Incorporation of an "aging" step prior to the first dispersion in the PuO_2 sol preparation process has proved to be a significant improvement.[5] Aging in NH_4OH solutions and in water gives similar results; however, the simplicity of aging in water led to its adoption as the procedure to be included in the flowsheet. With the use of the aging step, laboratory yields of PuO_2 sol from $Pu(NO_3)_4$ solutions have been routinely nearly 100%, and lower NO_3^-/Pu mole ratios have been attained without sacrificing stability of fluidity of the sols. These sols are characterized by a translucent appearance; this is in contrast to the opaque appearance of sols that have comparable NO_3^-/Pu ratios but were prepared without the aging step. Such behavior is in accord with other results, which indicate that much less aggregation of small particles is present in sols made by the method featuring this step.

Preparation of Mixed Urania-Plutonia Sols. – Interest in mixed UO_2-PuO_2 fuels for fast breeder reactors prompted a study of the preparation of mixed sols directly from ionic solutions of the elements rather than by mixing the respective sols together. One of the problems encountered in this approach was the reaction of tetravalent uranium with tetravalent plutonium when solutions of the elements in these valence states were mixed. This reaction resulted in solutions that contained the elements in several oxidation states. The procedure used in these experiments was the same as that for preparing UO_2 sols by precipitation-peptization.[9] The starting solutions were 1 *M* uranium(IV) nitrate-formate solutions (as used for the urania flowsheet) and 0.1 *M* plutonium nitrate solutions. The plutonium was used in both the trivalent and tetravalent forms, 1 *M* in HNO_3. These solutions were mixed under an argon atmosphere, and the order of the addition of solutions was varied. The final pH of precipitation was 7.5 to 8.0. Mixed sols were obtained in both cases. Concentrations of the sols (uranium plus plutonium) ranged from 1 to 2 *M*. The NO_3^-/metal mole ratios of the sols varied from 0.13 to 0.30; the $HCOO^-$/metal mole ratios were about 0.1. The plutonium content of the mixtures ranged from 10 to 17 wt % of the total metal. Excellent gel microspheres were obtained from some of the sols. They were fired according to the accepted procedure for pure uranium.[10] Figure 8.2 shows metallographic sections of some of the PuO_2-UO_2 microspheres that were prepared.

Drying and Firing of Plutonia Microspheres. – During the year, the gel microsphere drying technique was modified to include steam drying at 95 to 105°C over a period of 4 to 5 hr to remove the residual drying solvent; then, further drying was carried out in steam up to 150 to 170°C for 5 to 6 hr. Approximately 3 to 4 g of steam per gram of plutonium was passed through the bed of PuO_2 microspheres. This technique yielded microspheres of fairly high density, and a process advantage was realized in that steam either suppressed or eliminated the thermal excursion that is occasionally observed during the drying of deep beds of gel. To reduce microporosity in the product microspheres, humidified air was passed over the microsphere bed throughout the firing step.

Preparation of Materials

A total of 7.4 kg of plutonium was converted into stable PuO_2 sols during the year. Approximately 90% of this quantity was formed into PuO_2 microspheres having a density greater than 94% of theoretical. The remainder was mixed with UO_2 sols and formed into microspheres for fuel fabrication studies (see Sect. 8.3).

---

[9] *Chem. Technol. Div. Ann. Progr. Rept. May 31, 1967*, ORNL-4145, p. 180.

[10] *Chem. Technol. Div. Ann. Progr. Rept. May 31, 1967*, ORNL-4145, p. 189.

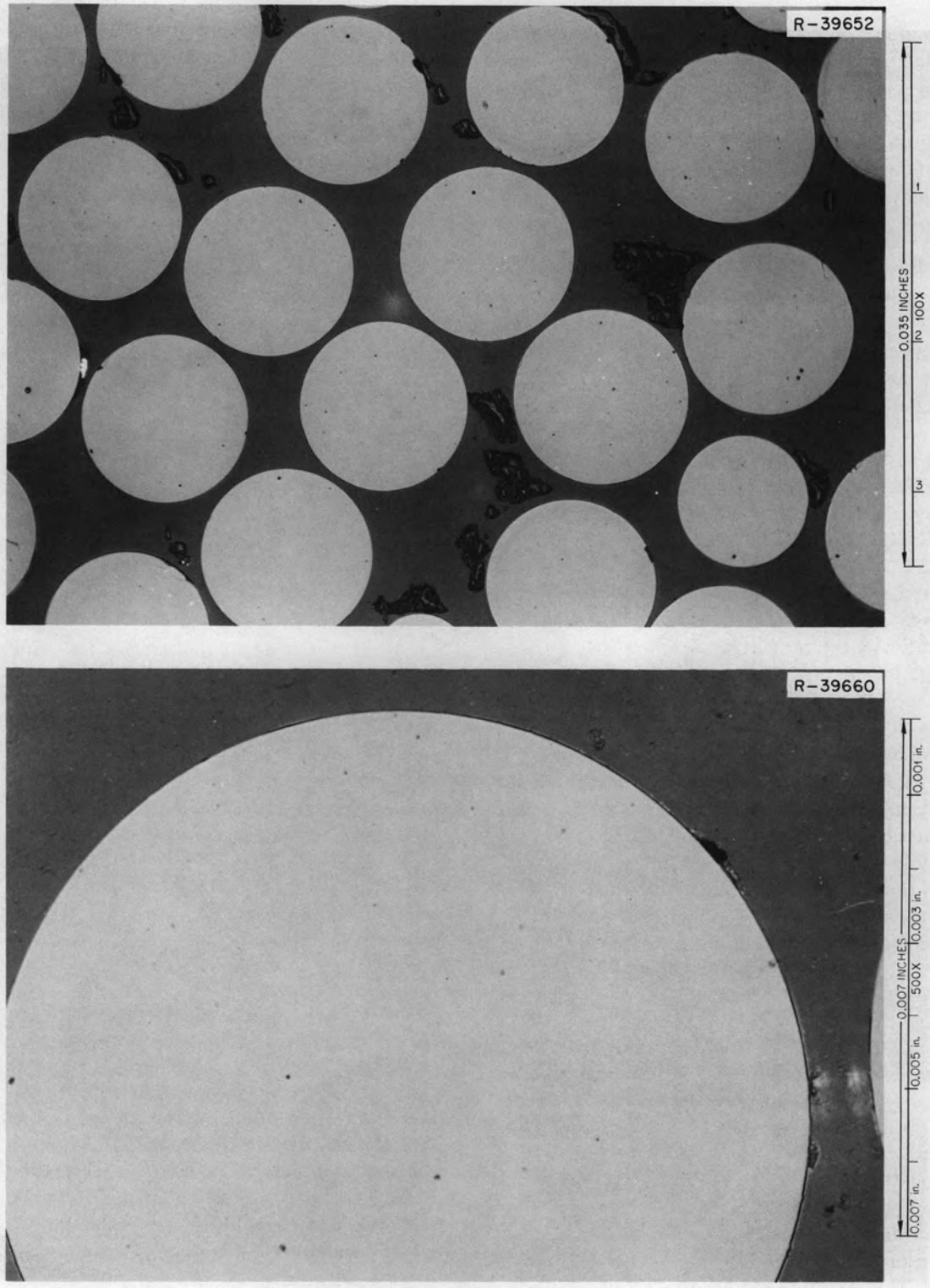

Fig. 8.2. Metallographic Sections of PuO_2-UO_2 Microspheres Formed from Sols Prepared by Mixing Solutions of Plutonium and Uranium.

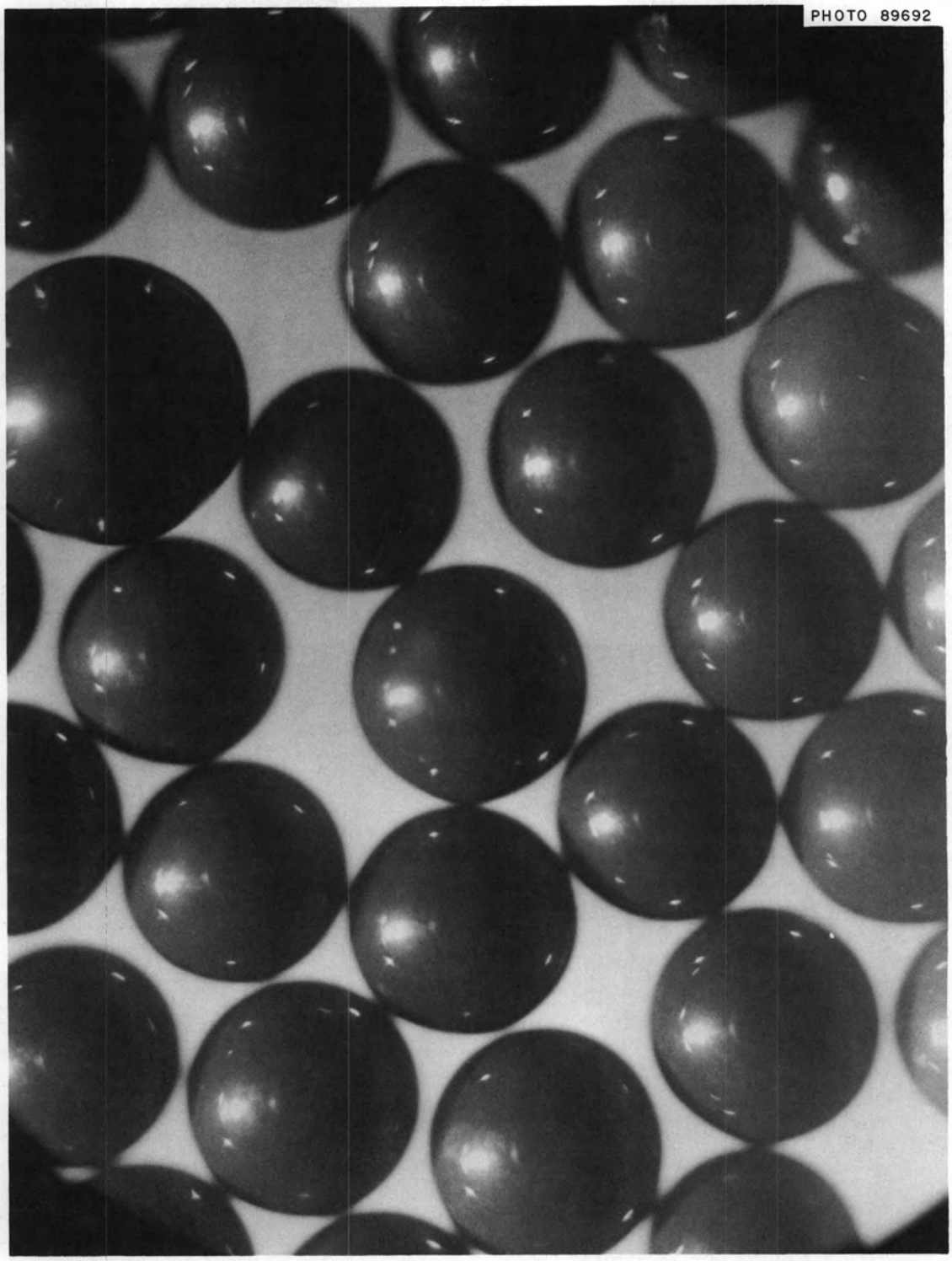

Fig. 8.3. Calcined Microspheres of PuO_2-ZrO_2 (15% Pu). Average diameter, 300 μ.

A special PuO_2-ZrO_2 sol was formed into dense microspheres containing 8 wt % PuO_2 for use in physics experiments at Battelle Northwest Laboratory. The microspheres were coated with pyrolytic carbon by the Metals and Ceramics Division prior to shipment.

Preparation of Plutonia-Urania Microspheres. – Sols of PuO_2 were mixed with UO_2 sols to give sols having Pu/U atom ratios of $\frac{1}{3}$ and $\frac{1}{4}$. These sols were formed into gel microspheres (cf. Sect. 8.3) for fuel fabrication studies. About 1.7 kg of gel microspheres having a Pu/U atom ratio of $\frac{1}{3}$ were dried in argon at 170°C. These microspheres were transferred to Battelle Northwest Laboratory and to the Metals and Ceramics Division at ORNL. About 0.5 kg of dense, fired microspheres that had been prepared from sols having a Pu/U atom ratio of $\frac{1}{4}$ were transferred to the Metals and Ceramics Division.

Preparation of PuO_2-ZrO_2 Microspheres. – Microspheres of PuO_2-ZrO_2 were made by mixing plutonia and zirconia sols and forming the microspheres by standard ORNL techniques (cf. Sect. 8.3). The zirconia sols (4 *M*), which had a low nitrate content, had been produced by autoclaving zirconyl nitrate.[11] The plutonia sols (2 *M*) had been prepared according to the regular plutonia flowsheet. The NO_3^-/metal mole ratios for the mixed sols varied from 0.1 to 0.2. In the preparation of mixed sols with a low plutonium content (<10 wt % of total metal), a high-nitrate plutonia sol was found to be satisfactory for mixing with the zirconia sol. These high-nitrate plutonia sols were prepared by using sufficient nitric acid to achieve an NO_3^-/Pu mole ratio of 1 during peptization of the precipitate (instead of the mole ratio of 2.5 used in the regular plutonia flowsheet) and were concentrated to 2 *M* in plutonium prior to mixing with the zirconia sol. Microspheres of PuO_2-ZrO_2 were made from mixed sols of several compositions. Figure 8.3 shows some microspheres of PuO_2-ZrO_2 containing 15 wt % plutonium. Firing up to 1150°C was done in air. Microspheres were made that contained 8, 15, 25, 37, and 50 wt % plutonium, based on total metal content.

During the year a special project was undertaken to provide 250 g of pyrocarbon-coated PuO_2-ZrO_2 microspheres for use in a physics experiment at Battelle Northwest Laboratory. In this preparation, a 5 to 6 *M* ZrO_2 sol was mixed with a PuO_2 sol to give a sol having a Pu/(Pu + Zr) ratio of 0.08. Dense, strong microspheres were formed by the usual sphere-forming operation, followed by steam treatment as with PuO_2 spheres. The final firing lasted 12 hr and was carried out at 1200°C in moist air. The microspheres were coated with pyrocarbon by the ORNL Metals and Ceramics Division.

[11] *Chem. Technol. Div. Ann. Progr. Rept. May 31, 1967*, ORNL-4145, p. 195.

8.3 PREPARATION OF MICROSPHERES

The microsphere forming equipment that was originally developed to prepare small spheres of ThO_2 has been used, with only slight changes, for the preparation of UO_2 spheres. The continuing equipment development studies are reported in Sect. 7. There are minor differences between the urania-plutonia materials and thoria with regard to the optimum chemical conditions in the sphere forming column and in the gel drying and firing schedules. Since microspheres having diameters of less than 100 μ are important for several applications, more efficient procedures were developed to prepare these smaller spheres.

Column Operating Conditions: Sols, Surfactants, and Organic Liquids

While many sols can be formed into gel spheres by using the equipment and procedures that are used for thoria sols, the optimum conditions are often different. The characteristics of the sol constitute important variables for determining the behavior of the sol in the column, although varying the column conditions permits some control. For the most part, our sol-gel developmental studies have been concentrated on determining improved conditions for forming spheres. We cannot predict which column operating problems will be most significant until we have formed a sol into gel spheres of the required diameter. Once the operating problems have been identified experimentally, previous experience will suggest changes that will be likely to provide solutions. Most of our experience with ThO_2 and UO_2 sols can be described by generalizations (Table 8.2), which may also be of value for other sols. However, some sols, such as UO_2-C, show behavior that does not agree with

Table 8.2. Generalizations for Forming ThO_2 and UO_2 Microspheres

Problem Observed in Column Operation	Changes in Surfactant Concentration to Minimize Problem		Change in Drop Diameter to Minimize Problem	Remarks
	Change	Order of Effect[a]		
Coalescence of fluidized drops	Increase	S-80, A-O, E/15	Not certain	Not a controlling problem
Drops sticking to column wall[b]	Increase	S-80, A-O, E/15	Increase	Much more likely for poor-quality sols and nonuniform drops
Clustering of partially dried drops	Increase	S-80	Increase	Much more likely for poor-quality sols
Sphere distortions of dimple type[c]	Decrease amine Increase Span	E/15, A-O S-80	Decrease	Not a problem for a pure ThO_2 sol
Other sphere distortions[d]	Decrease Span Increase amine[e] Decrease amine[e]	S-80 E/15, A-O A-O, E/15	Decrease	More likely for good-quality sols
Cracking of spheres	Decrease	E/15, A-O, S-80	Decrease	Properties of sol are important, but cracking also depends on the amount of H_2O in 2EH and on drying and firing conditions

[a]Listed in order of effectiveness. S-80 = Span-80, A-O = Amine-O, and E/15 = Ethomeen S/15.
[b]Usually near top.
[c]Extreme case is shell. This condition is probably the result of premature gelation on the surface of the sphere.
[d]Extreme case is raisin shape. This condition is probably the result of low interfacial tension.
[e]Amines can compete with and decrease the effect of Span-80; amines can also cause distortions.

that for ThO_2 or UO_2 sols. In general, 2-ethyl-1-hexanol (2EH) is the drying alcohol used in the columns.

The selection of the types and the amounts of surfactants to be added to 2EH in the sphere-forming column to minimize sticking, clustering, distortions, and cracking is a complex matter. Generally, sticking and clustering are minimized by using either a larger volume of surfactant or a more-effective surfactant and more rapid extraction of water (gelation); distortions and cracking, on the other hand, are minimized by using smaller volumes of surfactants and a slower extraction of water (Table 8.2). When nitrate is used as the peptizing ion, the "good" oxide sols (those which disperse relatively completely at low nitrate/metal ratios and which are relatively nonviscous and nonthixotropic) have less sticking-clustering problems and more distortion-cracking problems. Previously, we used about 1 to 2 vol % surfactant for "poor" UO_2 sols, but we have steadily reduced the surfactant concentrations as the properties of our UO_2 sols have improved.

In order to minimize the effects of column operating variables when sols or drying and firing conditions are compared, we use "standard conditions" for the operations not being studied. The current standard conditions for forming UO_2 sols into gel microspheres are listed below. Evaluations of UO_2 sols are always made under these conditions unless exceptions are specifically noted.

1. Average holdup time of UO_2 in column: 30 to 60 min.
2. Conditions for distillation apparatus: 85 to 100 psig steam; 2EH flow/sol feed volume ratios of 70 to 120 are maintained to give about 1.5 vol % H_2O in column; 0.5 vol % H_2O in dry 2EH from still.
3. Sol drop size: appropriate size to give theoretically dense UO_2 spheres having a mean diameter of 400 ± 50 μ. In some cases, spheres having a mean calcined diameter of 190 ± 30 μ are desired.
4. Age of 2EH: used for $\geq$ 4 hr of operation prior to any sol evaluation test.
5. 2EH charge for solvent-extraction-prepared UO_2 sol: 0.1 vol % Span 80; no Ethomeen S/15.
6. 2EH charge for UO_2 sols prepared by precipitation at pH = 7.5: 0.4 vol % Span 80; 0.05 vol % Ethomeen S/15.

Plutonia sols were formed into about 10 kg of oxide microspheres – about 7 kg of PuO_2 spheres and 3 kg of UO_2-PuO_2 spheres containing 8 to 25% PuO_2. The PuO_2 spheres can be formed by using 0.3 to 0.5 vol % Ethomeen S/15 alone as the surfactant.[12] Clustering has been an important problem in forming UO_2-PuO_2 spheres. Increasing the surfactant to high levels (0.3 vol % Ethomeen S/15 and up to 3 vol % Span 80) inhibited this tendency but did not entirely eliminate it. Acidifying the solvent to 0.01 *M* in HNO_3 completely suppressed the clustering tendencies and resulted in microspheres that were exceptionally uniform in size and sphericity.

Preparation of Small (< 100-μ-diam) Spheres

The relative importance of operating problems for forming small (50 to 300 μ in mean diameter) sol drops is much different from that for large (300 to 2000 μ in mean diameter) sol drops. Products having smaller diameters are important for some uranium fuel cycle applications; therefore, we tested procedures and equipment for preparing the smaller spheres more efficiently.

None of the disperser mechanisms that were used to give uniform drops in the 300- to 2000-μ mean diameter range (see Sect. 7.2) were practical for making 50- to 300-μ drops. The capacity of the two-fluid nozzle as used for the larger drops was too small. The other mechanisms were ineffective for the small sizes. Several other dispersers were tested for uniformity and control of mean diameter in the preparation of drops 50 to 300 μ in mean diameter. A paddle agitator in a baffled vessel containing 2EH gave sol drops with mean diameters of up to 200 μ; the size depended on the speed of the agitator. The uniformity of size was poor. A vibrating-plate mixer (Vibro-Mischer) operated at 60 Hz gave uniform drops within a 20- to 60-μ mean diameter range, depending on the amplitude; however, it was not effective for larger drops. Both the paddle agitator and the vibrating-plate mixer could be controlled to give larger drops if an organic liquid of higher density was substituted for the 2EH. We presently use an apparatus based upon turbulent flow of the alcohol to give sol drops with 20- to 150-μ mean diameters. The uniformity of size is poor compared with that obtained with the varicose breakup for streamline flow, but it is good when compared with that obtained by other dispersers producing small drops of the same size. The mean drop diameter decreases as the turbulence, or Reynolds number, of the organic drive fluid increases. Other parameters such as the sol flow rate, viscosity, and density are much less important and are not yet well understood. Results for two sols are tabulated in Table 8.3.

Small sol droplets are easier to suspend during gelation than large droplets. The higher surface-to-volume ratio results in faster gelation and, along with lower settling velocities, eliminates the need for fluidization. Small drops are less likely to crack or to give hollow particles if the rate of mass transfer of water is increased by using drier 2EH or an alcohol with a higher solubility of water. Smaller drops show more clustering and sticking to the vessel walls; however, small drops can be gelled without fluidization, and either a larger volume of surfactant or a more-effective surfactant can be used to prevent cracking or distortion. Therefore, clustering and sticking do not seriously restrict the preparation of smaller spheres.

The separation of the gel microspheres from an organic liquid becomes increasingly troublesome as smaller spheres are formed. The sizes of equipment are limited to those having critically safe geometries for fissionable materials. Since the

[12] *Chem. Technol. Div. Ann. Progr. Rept. May 31, 1967*, ORNL-4145, pp. 195–202.

Table 8.3. Size Distributions of UO_2 Microspheres, Using Turbulent Flow of the Alcohol

	Test Number			
	1	2	3	4
Sol flow, cc/min	9.6	9.6	4.8	4.8
Sol drop diameter/product diameter ratio	3.8	3.8	3.8	3.4
Product size distribution, wt %				
−325[a] or −44 μ	81	87	51	58
270/325[a] or 44–53 μ	11	6	15	18
200/270[a] or 53–74 μ	4	4	17	14
140/200[a] or 74–105 μ	4	3	17	10
Estimated mean diameter of product, μ	25	20	45	40
Estimated mean diameter of sol drop, μ	100	75	170	140

[a]U.S. sieve series screens.

solubility of water in 2EH requires a 2EH/sol volume ratio of about 100, alternative methods of gelation were tested to simplify the gel sphere separation problem. From tests of chemical gelation with NH_3 or organic amines, it appears that the gel spheres having diameters of less than 100 μ must be partially dehydrated before they are collected in settled beds. The "wet" gel of this size shows excessive caking or coalescence when collected in multilayer beds. Also, the chemical gelations can be so rapid that they interfere with the formation of spherical sol drops.

Drying and Firing of Urania Gel Microspheres

We are continuing studies of the optimum firing conditions for producing UO_2 microspheres of low carbon content (< 50 ppm) and high density (> 95% of theoretical). In order to obtain the desired product properties, it is necessary to remove the sorbed organic compounds prior to sintering and densification of the gel.[13,14] The source of the sorbed organic compounds is the drying solvent that is used in the sphere forming process. Products having the desired properties can be obtained by firing the gels to 1000°C in a steam atmosphere and reducing the UO_{2+x} in Ar–4% H_2. A small volume of Ar or Ar–4% H_2 is used in conjunction with the steam to ensure that no back diffusion of oxygen occurs when the use of steam is concluded.

Sorbed organics are more difficult to remove from UO_2 microspheres prior to densification than from other types of sol-gel spheres such as ThO_2, PuO_2, PuO_2-UO_2, and UO_2-ThO_2. This is because the pure UO_2 begins to sinter fairly rapidly at the relatively low temperatures of 400 to 500°C and because the removal of sorbed organics is slow below this temperature.

In our previous studies,[13,14] other atmospheres such as CO_2, air and argon, and Ar–3% H_2O did not reproducibly yield UO_2 products of the desired properties. Also, adjustment of the oxidizing potential of CO_2 by the introduction of controlled amounts of CO did not produce reproducible results. Firing in air to 200°C to remove the sorbed organics was very effective for removing carbon; however, it was difficult to prevent overoxidation of the UO_2. Because the reaction of the sorbed organics with air was very rapid and produced excessive temperature rises, the temperature of oxidation could not be controlled. A mixture of 3% H_2O in argon was not sufficiently oxidizing to remove the organics prior to the start of sintering.

The removal of sorbed organics with steam prior to sintering is slow, and moderately long heating cycles are required to effectively carry out the

[13]*Chem. Technol. Div. Ann. Progr. Rept. May 31, 1967*, ORNL-4145, p. 189.

[14]J. P. McBride (compiler), *Laboratory Studies of Sol-Gel Processes at Oak Ridge National Laboratory*, ORNL-TM-1980 (September 1967); also presented at CNEN Symposium on Sol-Gel Processes for Ceramic Nuclear Fuels, Turin, Italy, Oct. 2–3, 1967 (to be published in the Proceedings).

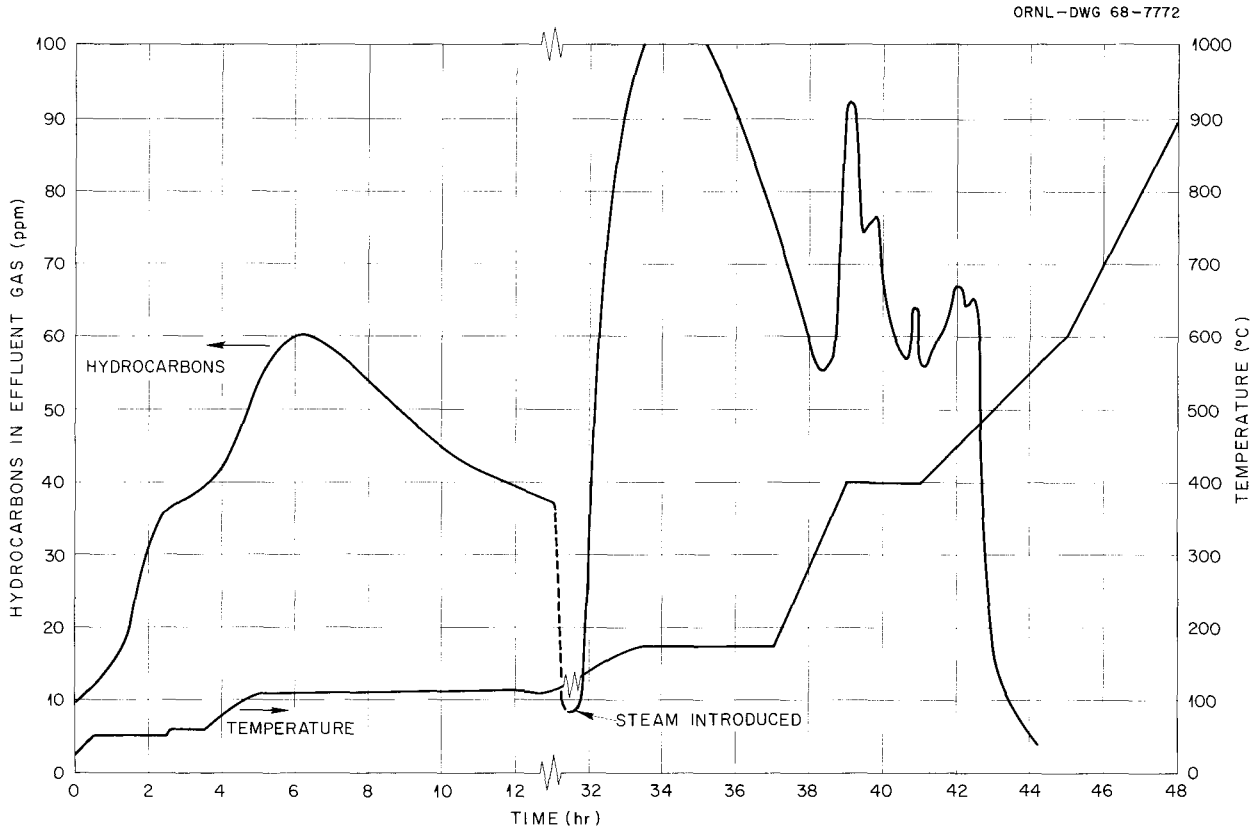

Fig. 8.4. Hydrocarbon Content in Off-Gas from UO_2 Gel Microspheres as a Function of Firing Time and Temperature During Firing. Slow schedule. Conditions: 30 g of UO_2; 1 std ft^3/hr of argon to 110°C and hold overnight; 5 std ft^3/hr of steam and 0.5 std ft^3/hr of argon to 900°C.

firings. Different rates of removal are observed for the different gel preparations. This may be due to small differences in the crystallite size, nitric acid content, viscosity, and O/U atom ratio of the sol, or differences in the sphere forming process. We find that an in-line hydrocarbon analyzer (for carbon-hydrogen bonds) for the effluent gas is helpful in conducting the firings so that desired product properties are achieved. A typical curve of hydrocarbon removal as a function of time and temperature is shown in Fig. 8.4. Rise rates and soaking times in the steam atmosphere were selected so that the hydrocarbons are removed at a temperature as low as is practically possible. The peaks of maximum evolution of hydrocarbons correspond to those previously observed for maximum weight loss in thermogravimetric studies.[14] On heating the gel in argon, the sorbed 2EH was evolved; the evolution increased with increasing temperature (Fig. 8.4). When steam was introduced, the rate of removal increased dramatically and reached a maximum during the 175°C hold period. The gas continued to be evolved in steadily decreasing amounts to about 350°C, where the evolution began to increase. Another maximum was reached at about 400°C. Two other smaller gas evolution peaks occurred between 450 and 500°C. The evolution then steadily decreased from 500 to about 600°C; at 600°C it was complete. The largest peak occurred at 150 to 200°C, as expected. (The boiling point of 2EH is 183–185°C, and maximum evolution of alcohol would be expected at 150 to 200°C.) However, it was observed that insignificant amounts of alcohol remained after steam treatment to 200°C; this indicates that the alcohol is strongly sorbed. Heating the gel at rates too rapid to permit removal of the sorbed alcohol (Fig. 8.5) (temperature rise rates of 300°C/hr) resulted in hydrocarbon evolution up to 950°C and also during cooldown of the sample in argon.

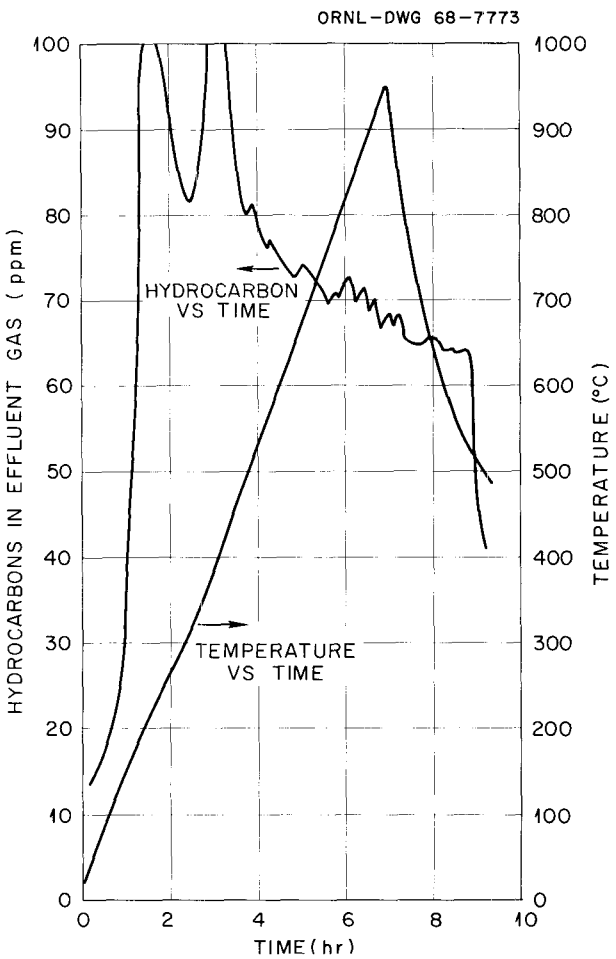

Fig. 8.5. Hydrocarbon Content in Off-Gas from UO_2 Gel Microspheres as a Function of Firing Time and Temperature. Fast schedule. Conditions: 10 g of UO_2 microspheres; 1 std ft^3/hr of argon to 110°C; 5 std ft^3/hr of steam and 0.5 std ft^3/hr of argon to 950°C; cool in argon.

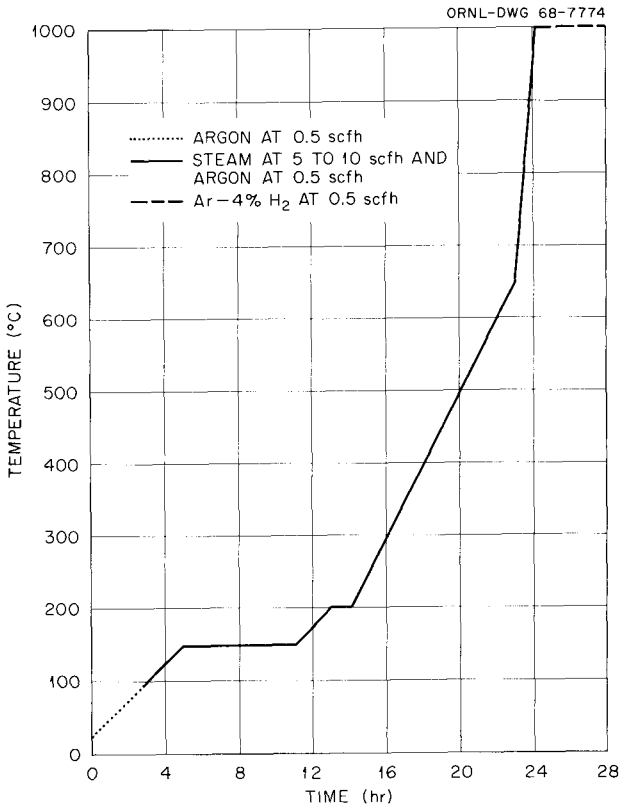

Fig. 8.6. Soaking Conditions for the Firing of UO_2 Gel Microspheres.

Firing in steam to 1000°C consistently produced good results when organic materials were removed prior to sintering (Table 8.4). Products had a uniform black color, a density that was to 95 to 99% of theoretical, a carbon content of <50 ppm, and an O/U atom ratio of <2.005. X-ray diffraction measurements showed that crystallite sizes were 500 to 800 A; 400-μ-diam spheres resisted crushing loads of 1500 to 2000 g.

The soaking conditions used for most of the firings are given in Fig. 8.6. The flow rates used were: steam, 5 to 10 std ft^3/hr; Ar–4% H_2 or Ar, 0.5 std ft^3/hr. The hydrocarbon analyzer was used to monitor most of the firings. We found that shorter soaking times could be used with some, but not all, of the preparations shown in Table 8.4. A few of the preparations were heated to 1000°C at the rate of 300°C/hr after the usual soaking to 200°C. The desired product properties were obtained; however, the faster rise rate generally resulted in a low-density product. A few of the gel preparations could be fired to high density at 850°C, but most required firing at 1000°C.

Except for cracking of the spheres, no apparent differences were observed in the firing characteristics of UO_2 gel spheres that were formed from sol prepared by amine extraction and those formed from sol prepared by precipitation. A few of the products from sols that had been prepared by amine extraction cracked badly when fired at temperature rise rates as low as 25°C/hr; however, the majority of these gel products could be dried and fired without cracking. It is believed that the cracking was the result of insufficient crystallite growth in the sol preparations.

Table 8.4. Properties of UO_2 Gel Microspheres Fired in a Steam Atmosphere at 1000°C

Sol Preparation Method	Gel Preparation	Amount Fired (g)	Density by Hg Intrusion at 210 psi (% theoretical)[a]	Carbon (ppm)
Precipitation	P-11-2-1504	130	97.5	<20
	P-6-16-1545	65	96.7	10
	P-9-11-1545	82	97.2	<20
Amine extraction	P-7-27-1408	40	99.3	30
	P-9-8-1049	55	97.3	<20
	P-7-31-1040	65	100.1	30
	P-219-1310	30	97.7	20
	P-2-20-1107	15	95.6	30
	P-2-12-1248	45	97.9	<20

[a]Calculated by using 10.97 g/cc as the x-ray crystal density of UO_2.

Table 8.5. Materials Prepared in Process Development or Laboratory Equipment and Used in Other Programs

Material	Size (μ)	Amount (g)	Density[a] (g/cm^3)	Surface Area (m^2/g)	Analyses	
					Carbon (ppm)	O/U Atom Ratio
$^{235}UO_2$[b]	210–250	125	10.54		180	<2.002
$^{235}UO_2$[b]	210–250	97	10.18		150	<2.002
$^{235}UO_2$[b]	350–420	549	10.62	0.006	140	2.0022
UO_2	150–250	617	10.01	0.011	400	2.000
UO_2	350–500	510	10.60	0.008	30	2.002
UO_2	150–500	380	10.91		<20	2.007
UO_2	~400	190	10.59	0.017	50	2.007
ZrO_2–8% $^{235}UO_2$	100–250	375	5.79	0.556	<20	2.083
22% $^{235}UO_2$–ThO_2	210–250	627	10.16		<10	<2.01
11% $^{235}UO_2$–ThO_2	210–250	1060	10.12		<10	<2.01

[a]By mercury porosimetry at 100 or 200 psi.
[b]Enrichment, 97%.

Table 8.6. Microsphere Production in the Glove Box Facility

Composition	Size (μ)	Pu (g)	No. of Pu Sols	Density (g/cm^3) Bulk	Density (g/cm^3) *a*	Surface Area (m^2/g)	Carbon (ppm)	Resistance to Crushing (g)	Disposition
PuO_2	88–250	6180	46	11.2	11.4	0.0200	<20	475	BMI-Columbus, LASL, ANL
25% PuO_2–75% UO_2	88–595	417[b]	3						M&C Division (ORNL), Battelle NW
20% PuO_2–80% UO_2	420–595	110	1	10.9	11.1			~1300	M&C Division (ORNL)
8% PuO_2–92% ZrO_2	250–420	30	1	5.58	5.77	0.2665	64	225	Battelle NW
8% $^{233}UO_2$–92% ZrO_2	250–420	41[c]	1[d]	5.55	5.90	0.3900	60	450	Battelle NW
Misc. PuO_2		705	5[e]						M&C Division (ORNL)

[a]By mercury porosimetry at 10,000 psig.

[b]Gel microspheres were not calcined; they were transferred to the Metals and Ceramics Division, ORNL, for fuel fabrication studies.

[c]^{233}U.

[d]Data reported for one batch made by mixing UO_2 and ZrO_2 sols.

[e]These sols diverted to fuel fabrication experiments by Metals and Ceramics Division, ORNL.

Sample Preparation

In the course of our developmental studies and flowsheet demonstrations of sol-gel microsphere preparations, samples of the various preparations have been made available, on request, to other related programs. Most of the samples are used for irradiation testing and fuel fabrication studies. Samples of sol-gel oxide microspheres have been prepared for the ORNL Metals and Ceramics Division, Babcock and Wilcox Company, Pacific Northwest Laboratory, Argonne National Laboratory, Los Alamos Scientific Laboratory, Battelle Memorial Institute, and others. The kinds, amounts, and some of the properties of the sol-gel materials that have been provided are listed in Tables 8.5 and 8.6.

Samples of $^{238}UO_2$ were prepared entirely in the process development equipment. Samples of materials containing ^{235}U were made from sols prepared in small laboratory equipment and were formed in the microsphere process development equipment. Samples containing ^{239}Pu or ^{233}U were prepared by using the glove-box equipment previously described.[15]

8.4 MATERIALS DEVELOPMENT

The materials development work is concerned with the preparation of nuclear fuels of the more advanced types. Work thus far has been centered on the laboratory-scale preparation of carbides, nitrides, and carbonitrides and on the preparation of porous oxides of interest as nuclear fuels. Sol-gel methods for carrying out these processes are being investigated. In the sol-gel methods, aqueous hydrosols of the oxides plus carbon are prepared by ultrasonically dispersing carbon black in the oxide sol. The mixed sol is then converted to gel shards or gel microspheres by suitable means. The oxide-carbon gel is heated in a vacuum or in an inert atmosphere such as argon, or is heated in nitrogen under the appropriate conditions, to form either carbonitrides or nitrides. Temperatures of 1700 to 2100°C are required to obtain a dense product. Metal-oxide–carbon gels also appear to be a general route to the preparation of porous oxides. After the oxide matrix is set by heating the gels to 1200 to 1400°C, the carbon is removed by reaction with air at 800°C or with CO_2 or H_2O at 1000°C. The volume of porosity introduced is approximately equal to the volume of carbon introduced in the oxide.

Aside from the remote fabrication advantages of sol-gel methods, it is believed that the conversion of oxide-carbon gels to carbides, carbonitrides, nitrides, or porous oxides will have advantages that conventional methods employing blending of oxide powders and carbon blacks will not have. The main advantage involves the intimate association of the oxides and carbon in the sols and gels. Conceivably, this association could lead to better control of conversion conditions and to better distribution of porosity in porous oxides.

Results thus far have demonstrated the feasibility of this approach for the preparation of ThC_2, UC, $(Th,U)C_2$, and uranium carbonitride, starting with ThO_2, UO_2, or ThO_2–25% UO_3 sols that were prepared by standard methods used at ORNL.[16–18] The preparation and characterization of the oxide-carbon sols and the conversion of ThO_2-C gels to ThC_2 or porous ThO_2 have been studied extensively. A few laboratory-scale demonstration runs have shown the technical feasibility of the preparation of $(Th_{0.78},U_{0.22})C_2$, UC, and UC-UN microspheres and of porous $(Th_{0.78},U_{0.22})O_2$ and UO_2. We believe that similar sol-gel processes will be applicable to the preparation of pure nitrides, PuC, UC-PuC, and solid solutions of uranium and plutonium carbonitrides.

Preparation and Properties of Oxide-Carbon Sols

Extensive studies of the preparation of oxide-carbon sols are being made since fluid, stable hydrosols containing the required amounts of carbon are essential to the process. In addition, an understanding of the interactions between the oxides and carbon in our presently used oxide-carbon sols will be useful in the preparation of other sols such

[15] *Chem. Technol. Div. Ann. Progr. Rept. May 31, 1967*, ORNL-4145, p. 197.

[16] *Chem. Technol. Div. Ann. Progr. Rept. May 31, 1967*, ORNL-4145, pp. 159–65.

[17] K. J. Notz, *Preparations of Porous Thoria by Incorporations of Carbon in Sols*, ORNL-TM-1780 (in press).

[18] J. P. McBride (compiler), *Laboratory Studies of Sol-Gel Processes at Oak Ridge National Laboratory*, ORNL-TM-1980 (September 1967); presented at CNEN Symposium on Sol-Gel Processes for Ceramic Nuclear Fuels, Turin, Italy, Oct. 2–3, 1967 (to be published in the Proceedings).

as PuO_2-C, UO_2-PuO_2-C, and UO_2-ZrO_2-C, which will be of future interest.

We are continuing fundamental studies of the interaction of oxides with carbon. Results to date have shown that the oxide crystallites in our ThO_2, UO_2, or ThO_2-UO_3 sols disperse carbon aggregates by means of a strong interaction with them. In this interaction, the oxide crystallites are sorbed on the surface of the carbon aggregates, and the oxide acts as a protective colloid. The extent of sorption of the oxide depends primarily on the relative surface areas of the oxides and the carbon. As yet, we have not determined the roles of surface charge and the nature of the surface groups of the oxides in the sorption process. We know that some colloidal oxides do not show this strong type of interaction.[16–18] For example, ORNL-prepared ZrO_2 and $Eu(OH)_3$, boehmite (Baymal[19]), and silica (Ludox[20]) do not disperse carbon to the extent that the ThO_2, UO_2, or ThO_2-UO_3 sols do. In fact, they have virtually no dispersion power toward carbon black. Plutonia sols prepared at ORNL interact sufficiently to produce a mixed sol containing the amount of carbon required for conversion to carbide or nitride.

Electron microscopic techniques and viscosity, electrophoretic, and specific surface area measurements are employed in studies of the oxide-carbon interactions. As reported last year,[16] the nature of the interactions between ThO_2 and C in ThO_2-C could not be determined unambiguously by electron microscopy. Electron micrographs of sols that contained carbon in excess of the amount required by the ThO_2 surface area showed the presence of carbon aggregates that were identical in appearance to those in the original carbon black. On the other hand, when the quantity of carbon present was less than that required by the ThO_2 surface area, none of the aggregates could be observed. The results could be explained in one of two ways. Either the ThO_2 particles were being adsorbed on the carbon aggregates, thereby preventing their detection by the electron beam, or the thoria was dispersing the carbon aggregates to their individual crystallites by some unusually strong surface interaction. The detection of carbon aggregates in the sol did not necessarily prove that surface adsorption of the ThO_2 crystallites occurred only on the aggregates. It is possible that the breakup of additional aggregates to crystallites was kinetically blocked when all of the ThO_2 crystallites present were already held tightly by carbon crystallites. However, this ambiguity was resolved by dissolving the ThO_2 present in the sol by refluxing the mixed ThO_2-C sol in 4 *M* HCl and subjecting the recovered carbon to electron microscopic examination. The electron micrographs showed more or less spherical particles having the same size and shape as the original carbon (Spheron 9, Cabot Corporation); this carbon black has a specific surface area of 105 m^2/g and an electron microscopic size of 250 to 450 A. The surface area of this residue was 90 m^2/g, which is slightly less than that of the starting material. It is unlikely that the dispersed individual crystallites would reagglomerate to a size and shape virtually identical to the original aggregates in the carbon black. Further, surface area measurements of gels prepared from ThO_2-C sols gave values that were in good agreement with those calculated from the sizes of the original materials. Therefore, it appears that the interaction occurs between the ThO_2 crystallites and the carbon aggregates, and that the thoria acts as a protective colloid. The behavior of urania and ThO_2-UO_3 sols is virtually identical to that of thoria sols. The extent to which carbon was dispersed by all of these sols was dependent upon the relative surface areas of the oxide and carbon and was demonstrated by viscometric titration.

Stable, fluid sols containing carbon in sufficient quantity to produce mono- or dicarbides or to produce porous oxides could be prepared from UO_2, ThO_2, or ThO_2-UO_3 sols made at ORNL. The amounts of dispersed carbon required to produce mono- and dicarbides from these oxides are 3 and 4 moles per mole of oxide respectively. The amount of carbon required to produce porous oxides over the range of 10 to 60% porosity is 0.5 to 6 moles per mole of oxide.

Conversion of Metal-Oxide–Carbon Gels to Carbides

Studies of process variables that affect the conversion of ThO_2-C gel to ThC_2 were extended. The technical feasibility of converting UO_2-C gels to UC or UC-UN and of converting ThO_2-UO_3-C gels to $(Th_{0.78},U_{0.22})C_2$ was demonstrated.

[19]Trade name for AlO(OH). Product of E. I. du Pont de Nemours and Co.

[20]Product of E. I. du Pont de Nemours and Co.

The most important variables in the sol-gel method for preparing ThC_2 are the firing conditions during conversion and the carbon content in the ThO_2-C gel. To obtain densities that are greater than 90% of the theoretical density of ThC_2 (9.6 g/cc), the conversion must be effected under a controlled CO overpressure at temperatures where a critical balance among the rate of chemical conversions, grain growth, and sintering is maintained. If porous carbides are the desired product, the reactions can be carried out under vacuum. Products having densities of 91 to 93% were obtained when the reaction was carried out at a controlled rate under argon until nearly complete and then vacuum was applied to complete the reaction. The argon sweep gas, after passage over the sample, contained about 4000 ppm of CO, which was maintained by controlled diffusion out of the sample crucible. An infrared in-line CO analyzer (Beckman model 315) was used to monitor the progress of the reactions. This conversion technique also produced $(Th_{0.78},U_{0.22})C_2$ and UC microspheres that had densities 90 to 93% of theoretical in a few demonstration runs.

Control of the carbon-to-metal-oxide mole ratio in the gel starting material is important for efficient conversion to the carbide and preparation of a high-density product. When the initial carbon-to-ThO_2 mole ratio was too low, objectionable amounts of monocarbide were formed; when it was too high, a highly porous product was obtained. Excess carbon contents of 0.50 to 2.58% in ThC_2 resulted in highly porous products. A carbon-to-oxide mole ratio of 3.9 appears optimum for preparing dense ThC_2. In practice, the carbon-to-metal-oxide ratio must be adjusted empirically. This adjustment is necessary because additional carbon is acquired by the sorption of the carbon-bearing organic materials in the sphere forming process and because of the reaction of carbon with the nitric acid during firing of the gel. A few attempts were made to remove the additional carbon imbibed during sphere formation by oxidizing it with air on a recording thermogravimetric balance, where the rate of reaction could be carefully monitored; however, the degree of oxidation was found to be difficult to control. We have not yet tried to remove the sorbed organic material by treating with steam to 600°C; this is a method found to be effective for removing organics from UO_2 gel spheres.

A few experiments involving the conversion of ThO_2-UO_3-C gel spheres to $(Th_{0.78},U_{0.22})C_2$ spheres gave very encouraging results (Table 8.7).

Table 8.7. Analyses of $(Th_{0.78}, U_{0.22})C_2$ Microspheres

Conversions in argon at 1900°C

	Run Number		
	IV-82	IV-84	IV-86
Carbon-to-metal mole ratio of reactants	4.00	4.06	4.15
Composition of product, %			
Thorium	70.3	69.7	69.4
Uranium	20.4	20.2	20.0
Carbon	8.87	9.02	9.37
Oxygen	0.081	0.127	0.173
Free carbon	0.097	0.264	0.146
Material balance	99.65	99.05	98.94
Mercury density of product, g/cm^3			
1 atm	9.45	8.92	7.75
10,000 psi	9.56	9.09	8.65

The products were solid solutions of the monoclinic ThC_2 structure, with slightly contracted parameters due to the uranium content. A reaction temperature of 1900°C was sufficient for complete reaction, whereas approximately 2000°C was necessary for ThC_2. The presence of the uranium permitted conversion at a lower temperature and also seemed to promote a desirable sintering pattern. Densities were 76 to 94% of the theoretical value, depending on the original carbon content. Even at the higher porosities the spheres had a uniform cross section, and the pores were $\sim 1\ \mu$ in diameter. Preliminary results, equally encouraging to those obtained in preparing $(Th,U)C_2$, were obtained on converting UO_2-C gel spheres to UC and UC-UN microspheres.

Preparation of Porous Oxides

We have shown previously that ThO_2 microspheres or shards of controlled porosity can be prepared from ThO_2-C gels by volatilizing the carbon by oxidation with air after the oxide structure has been preset by firing to 1400°C in argon.[16–18] The amount of porosity can be controlled by varying the amount of carbon added (i.e., the volume of porosity introduced is nearly equal to the volume of carbon added). In subsequent work the technical feasibility of preparing porous ThO_2-UO_2 and UO_2 by this same approach was demonstrated. For the ThO_2-UO_2 preparations, ThO_2-UO_3-C gels were employed, and air oxidation was used to volatilize the carbon. However, in the porous UO_2 preparations, CO_2 or H_2O was the preferred reactant for removing the carbon because the air caused extensive oxidation of the UO_2.

Experiments involving the preparation of 60% porous ThO_2–22% UO_2 indicated that higher porosities could be obtained with ThO_2-UO_3-C gel shards than would have been expected by analogy with ThO_2-C gel shards of the same O/C atom ratio. The amount of carbon that produced 47% porosity in ThO_2 produced 59% porosity in ThO_2-UO_2. Also, the pores were slightly larger. The pores in the ThO_2-UO_2 were 400 to 800 A in diameter, whereas those in the ThO_2 were about 400 A.

In our attempts to prepare porous UO_2 in a way that would prevent excessive air oxidation of the UO_2, two methods for removing carbon from the prefired UO_2-C have been tested: the reaction $H_2O + C \rightleftharpoons CO + H_2$ and the Boudouard reaction ($CO_2 + C \rightleftharpoons 2CO$). Both require a temperature of about 1000°C to remove the carbon at a practical rate. The technical feasibility of preparing porous UO_2 by this approach was demonstrated by removing carbon from a sample of gel shards containing 6 moles of carbon per mole of urania. Although, in these experiments, only 80% of the original carbon was reacted, a product having a porosity of 48 vol % was obtained.

9. Sol-Gel Processes for Isotopic Heat Sources

Several radioactive isotopes are useful as heat sources for self-contained power production units. These devices could furnish energy for such purposes as auxiliary power for space missions, pacemakers for heart patients, and possibly an "artificial heart that can be surgically implanted in the patient."[1]

Plutonium-238 and curium-244 are two of the isotopes of primary interest in the isotopic power program. In November 1966, because of the significant progress in sol-gel technology as applied to ^{239}Pu,[2,3] the AEC requested that ORNL initiate development of a $^{238}PuO_2$ sol-gel process as an alternative to the production procedure then in use. This work was later expanded to include curium oxide.

In laboratory-scale studies of the sol-gel process, we developed a procedure for preparing dense $^{238}PuO_2$ microspheres. Studies aimed at scaling up the process (using ^{239}Pu rather than ^{238}Pu) are being made, using pilot-scale equipment in glove boxes. A plutonium sol-gel pilot plant has been built and is now in operation; preliminary runs with ^{239}Pu were satisfactory, but difficulties are being encountered with ^{238}Pu. A plutonium sol-gel production unit was designed, built, and shipped to Mound Laboratory. Small-scale curium sol-gel studies are in progress.

9.1 LABORATORY STUDIES OF ^{238}Pu SOL-GEL PROCESS

The successful preparation of ^{239}Pu sols and microspheres on a laboratory and pilot-plant scale has been reported.[2,3] Additional laboratory work with ^{238}Pu was needed in order to determine the effects of increased radiolysis and of self-heating on the process. The studies showed that, with a few minor flowsheet modifications, ^{238}Pu sols could be made on a laboratory scale (10 g of ^{238}Pu) and that excellent microspheres could be obtained from these sols.

Investigation of Process Variables

The laboratory studies were designed to: (1) develop procedures for making ^{238}Pu sols, (2) determine the stability of the sols, and (3) develop procedures for forming good microspheres from the sols. The starting material in all the experimental work was calcined $^{238}PuO_2$. The oxide was dissolved in HNO_3, and the valence was then adjusted with nitric oxide; the resulting solution was used for several experiments.

Our initial approach was to proceed rapidly through the steps of the ^{239}Pu flowsheet[2] to avoid radiolysis and self-heating effects. High concentrations of acid were used to maintain valence stability and to provide convenience in handling. In these experiments, 4 to 8 *M* HNO_3 solutions of tetravalent plutonium were precipitated in 4 to 10 *M* NH_4OH. Peptization was done at NO_3^-/Pu mole ratios of 2.5, and the peptized solution was evaporated under partial vacuum at 80°C. Thermal denitration of these preparations was unsuccessful; the resulting solids would not resuspend in water, although the NO_3^-/Pu mole ratios were about 0.3.

Efforts were then made to adhere more closely to the ^{239}Pu flowsheet. Valence stability data indicated that tetravalent ^{238}Pu would be stable in 2 *M* HNO_3 for reasonable periods of time. This permitted the use of plutonium stock solutions with a low concentration of free acid (2 *M* HNO_3) and a

[1] Glenn T. Seaborg, "HFIR, TRU, and TRL – a Transuranium Team," November 8, 1966 (AEC News Release S-43-66).

[2] *Chem. Technol. Div. Ann. Progr. Rept. May 31, 1966*, ORNL-3945, p. 170.

[3] *Chem. Technol. Div. Ann. Progr. Rept. May 31, 1967*, ORNL-4145, p. 195.

dilute base for precipitation (2 *M* NH_4OH). In addition to the use of more dilute reagents, two other procedural controls were instituted. (1) During filtration, the precipitate was not allowed to form a dry filter cake. (2) When it became necessary to hold the preparation at an intermediate step, the solutions were maintained at low plutonium concentrations. Thermal denitration of these preparations was successful, and high yields of ^{238}Pu sols with NO_3^-/Pu mole ratios of 0.15 to 0.20 were obtained. However, the opaque sols were more viscous than desired, and the formation of foam as a result of radiolysis was very apparent. The foam presented some mechanical problems in adding the sol to the column. Microspheres made from these sols displayed surface imperfections, generally characterized by deep pits or holes. These effects were independent of the types of surfactants used and the concentrations of surfactants in the microsphere forming column. Since the sols appeared less fluid and more opaque than ^{239}Pu sols of comparable NO_3^-/Pu ratios, and since the microspheres were not of the desired quality, further efforts were made to improve the ^{238}Pu sols.

We found that sols of a superior quality could be made by incorporating an "aging" step in the flowsheet. Aging could be accomplished by refluxing the washed precipitate in either water or dilute NH_4OH for about 2 hr. Because of the simplicity of aging in water, this procedure has been adopted in the general flowsheet. The aging step improves the crystallinity of the plutonium precipitate and increases the polymer's resistance to radiolysis and chemical degradation. Subsequent thermal denitration of material made by using this step gave 100% yields of dark-green translucent sols. The sols were more fluid and had lower NO_3^-/Pu mole ratios than those made without the aging step. Formation of foam was scarcely noticeable. These sols were generally concentrated until they were 1 to 1.5 *M* in plutonium prior to the formation of microspheres; however, they were still fluid at concentrations greater than 2 *M*. Excellent microspheres, which did not show surface imperfections or holes under microscopic examination, were made from these sols. The sols appeared to be stable on standing and showed no tendency to settle after several days; after periods of about one week, the only visible change was the loss of water through the vented caps of the containers. The sols were generally used about one day after preparation.

Laboratory Flowsheet

The flowsheet used for the laboratory experiments with ^{238}Pu is shown in Fig. 9.1. The starting material was PuO_2. The oxide was dissolved in concentrated HNO_3; HF was added two or three times in quantities sufficient to make the solution 0.02 *M* in HF. The solution was diluted to 6 *M* HNO_3, and the valence of the plutonium was adjusted by bubbling nitric oxide through the solution while the temperature was maintained at 60 to 70°C. The final stock solution was 1.5 to 2.0 *M* in HNO_3 and 0.1 *M* in plutonium. Precipitation and peptization were carried out according to the general procedure;[2] the above-mentioned aging step was incorporated into the flowsheet following the precipitation step. Denitration was accomplished in 4 to 6 hr at 240°C in a covered heating unit machined from stainless steel. To increase the rate of denitration at NO_3^-/Pu mole ratios below 0.2, the cover was generally removed. The final sols were made by dispersing the solids in water and concentrating the sols until they were 1 to 1.5 *M* in plutonium. The final NO_3^-/Pu mole ratios were 0.1 to 0.15.

Evaluation of Microspheres

Plutonium-238 microspheres with diameters of 50 to 400 μ were made in a laboratory column, using the standard ORNL techniques. Amine O or Span 80 (0.1 vol %) was used as the surfactant, and the drying solvent was 20% octanol in 2-ethyl-1-hexanol. The sols were fed from an inverted syringe pump that was mounted at an angle of approximately 45°. This permitted radiolytic gases to collect above the sol and maintained a better flow of sol to the column. After being dried in the column, the microspheres were then dried and calcined (in air) at 1150°C.

The general appearance of the microspheres was excellent (e.g., see Fig. 9.2). Densities of the microspheres, as determined by mercury porosimetry, were as high as 97% of the theoretical crystal density. Crushing strengths, which averaged almost 1200 g per 300-μ-diam microsphere, were about twice the values normally obtained for ^{239}Pu spheres. Metallographic examination of the microspheres indicated high density, although more porosity was evident than was generally observed with ^{239}Pu microspheres. Two polished sections

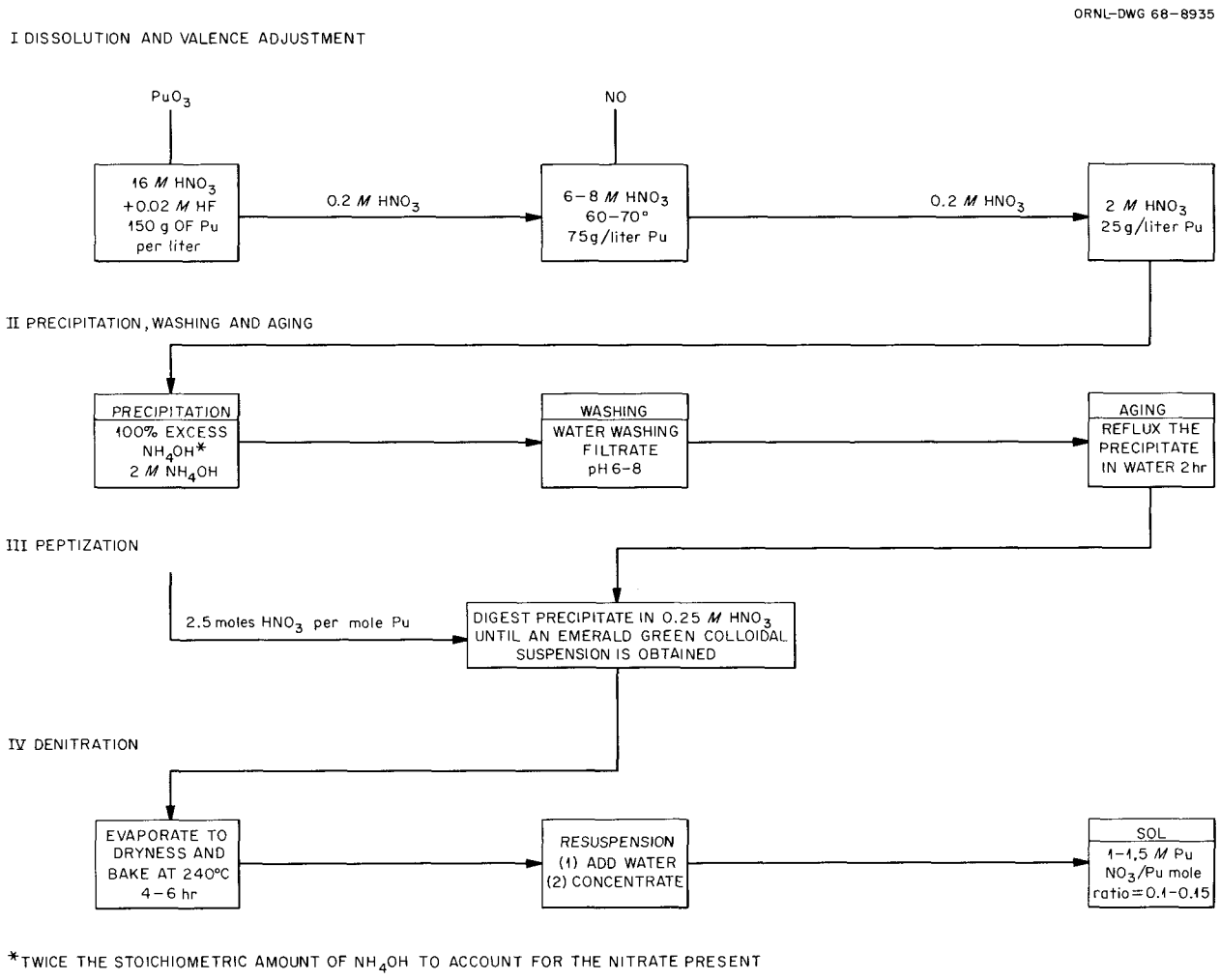

Fig. 9.1. Flowsheet for Laboratory Preparation of ^{238}Pu Sol.

are shown in Fig. 9.3. There is an indication of some included material, which could be silica since glass equipment was used during sol preparation.

Scouting experiments were performed to estimate the amount of water-leachable contamination at the surface of calcined microspheres. Microspheres were first washed rapidly with water to remove general contamination before they were added to the test solution. The washed microspheres were then soaked in water for 4 hr (0.1 g of microspheres per 25 ml of water); activity of the leachate was 2×10^4 dis min^{-1} ml^{-1}. The leachable activity could be reduced to 4×10^3 dis min^{-1} ml^{-1} by soaking the spheres in 8 *M* HNO_3 for 30 min at 25°C prior to water leaching, or to 400 dis min^{-1} ml^{-1} by boiling the spheres in 8 *M* HNO_3 for 5 min prior to leaching.

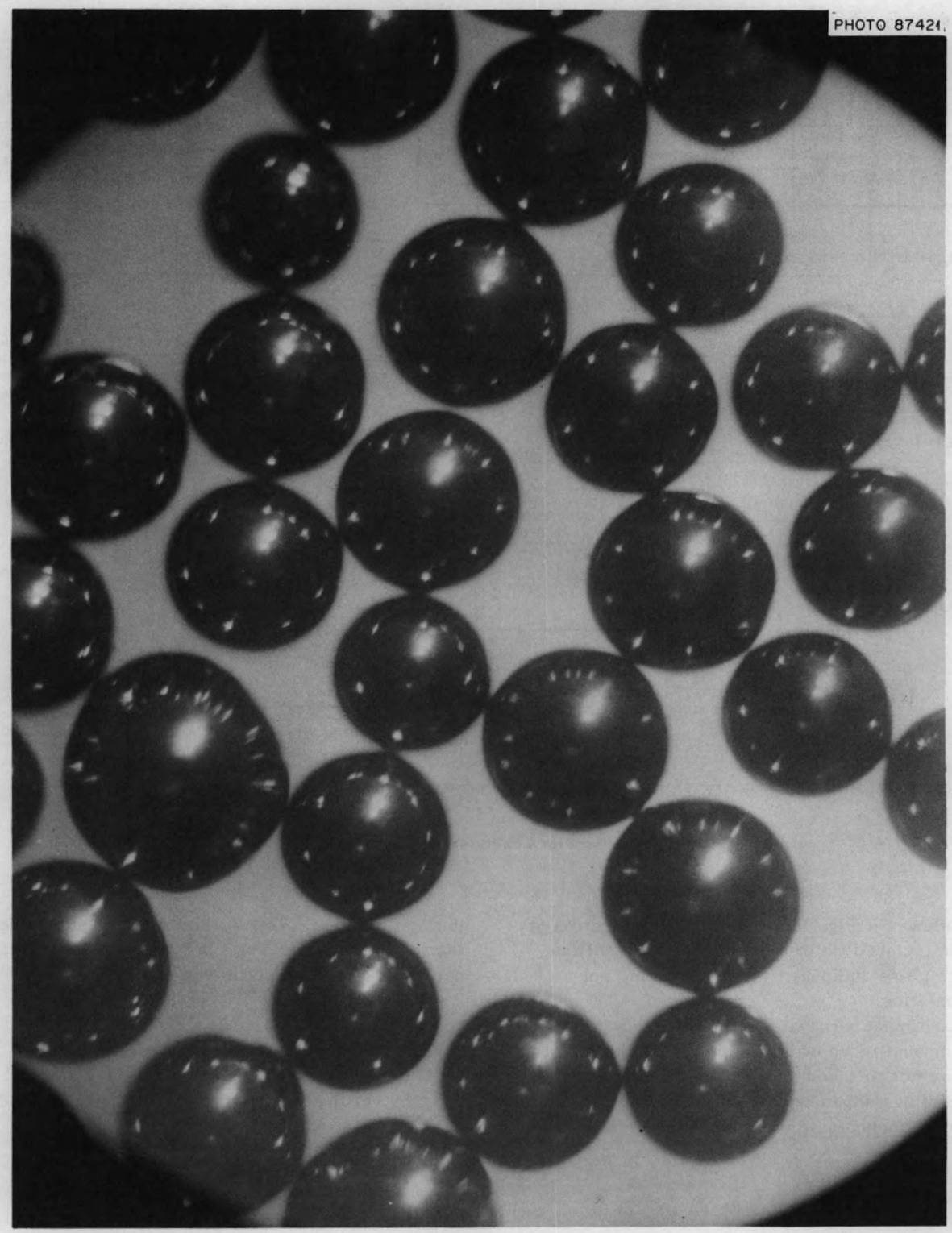

Fig. 9.2. Calcined Microspheres (300-μ diameter) of $^{238}PuO_2$.

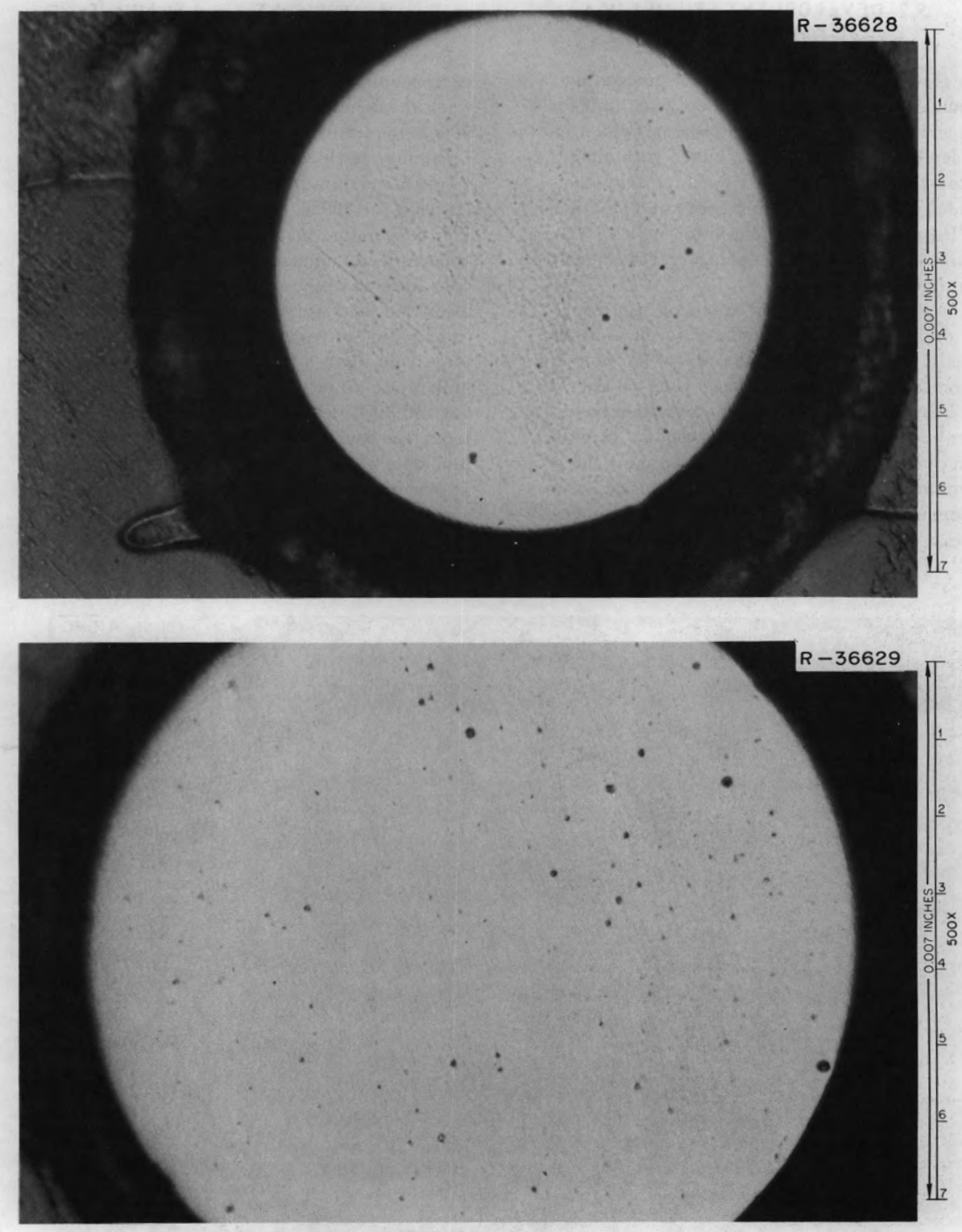

Fig. 9.3. Polished Sections of $^{238}PuO_2$ Microspheres.

9.2 DEVELOPMENT STUDIES IN A GLOVE-BOX SYSTEM

A glove-box facility, capable of processing about 150 g of plutonium per day, was built for use in the overall plutonium program (which includes the use of plutonium mixed with other metals). This facility was used for developmental work in the isotopic heat source program; ^{239}Pu was used as a stand-in for ^{238}Pu. The basic flowsheet and the equipment have been described previously.[3]

The developmental work included improving the drying and firing procedures to increase the density and the thermal stability of the plutonia, determining the effects of impurities on the product, and evaluating surfactants that have been proposed for use in the process. In addition, a continuous procedure for washing the precipitated PuO_2 was tested successfully; this procedure is much faster than the batch procedure.

Densification and Thermal Stability Studies

Earlier studies had revealed the presence of microscopic pores in PuO_2 microspheres, even when the density of the spheres was greater than 99% of theoretical. An empirical test for determining the thermal stability of dense microspheres consists in heating the spheres rapidly (15 min) to 1800°C at 10^{-5} torr and holding at this temperature for 30 min. When PuO_2 microspheres were subjected to this test, a significant fraction of the spheres shattered, and about 2% of the total weight was lost. Metallographic examination of tested microspheres showed that large void spaces had appeared and that possibly some sintering had occurred (see Figs. 9.4 and 9.5). In an effort to reduce these effects, the drying procedure was modified to provide a steam atmosphere (rather than argon) at temperatures up to 170°C; the firing procedure was also modified to include a sweep of humidified air. Microspheres that were dried and fired

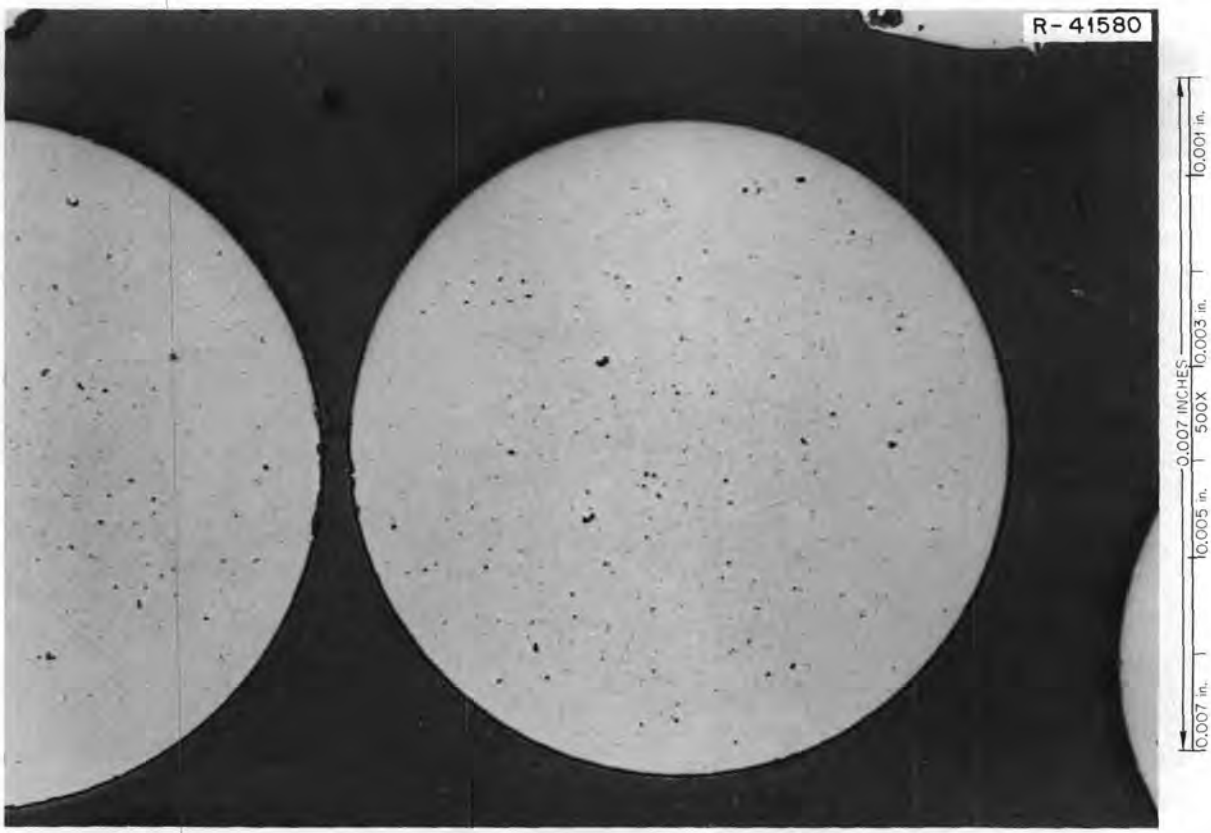

Fig. 9.4. PuO_2 Prepared Without Steam Drying. As received.

Fig. 9.5. PuO_2 Prepared Without Steam Drying. After heating for 15 min at 1800°C and 2×10^{-3} torr.

according to the new schedule were characterized by high density and low microporosity. When these spheres were heated to 1800°C, the porosity was less than had been previously encountered (see Fig. 9.6); however, the weight loss was still about 2%.

Correlations between results of the tests described above and the impurities in the microspheres were not conclusive, but the greatest destruction appeared to occur among microspheres having high sodium contents. (The source of the sodium was the surfactants; the sodium concentrations in Ethomeen S/12 and Span 80 were 0.6 and 1.2 g/liter respectively.) When Amine O, with a sodium content of less than 1 ppm, was used as the surfactant in a series of runs, the final microspheres were relatively free of sodium; however, the density of the product (about 93% of theoretical) was lower than desired. In addition, the Amine O did not prevent agglomeration of the gel droplets during the gelation step.

Steam-dried gel microspheres contained about 0.8% residual carbon (as organic material), which could be reduced to less than 20 ppm by firing with a sweep of moist air. Spheres that were calcined without an air sweep had a final carbon content concentration of 0.55% and a bulk density of only 94% of theoretical. When these microspheres were recalcined with an air sweep, they shattered, and their density was reduced to 83% of theoretical.

Continuous Washing of Precipitated PuO_2

After the hydrated PuO_2 is precipitated from the aqueous nitrate system, soluble ionic materials are removed by washing the precipitate with water. Batch washing and filtering through sintered stainless steel is very slow. In an effort to reduce the time required for this step, the equipment was modified to permit continuous washing. A test was conducted with 150 g of plutonium in a total slurry volume of 2 liters.

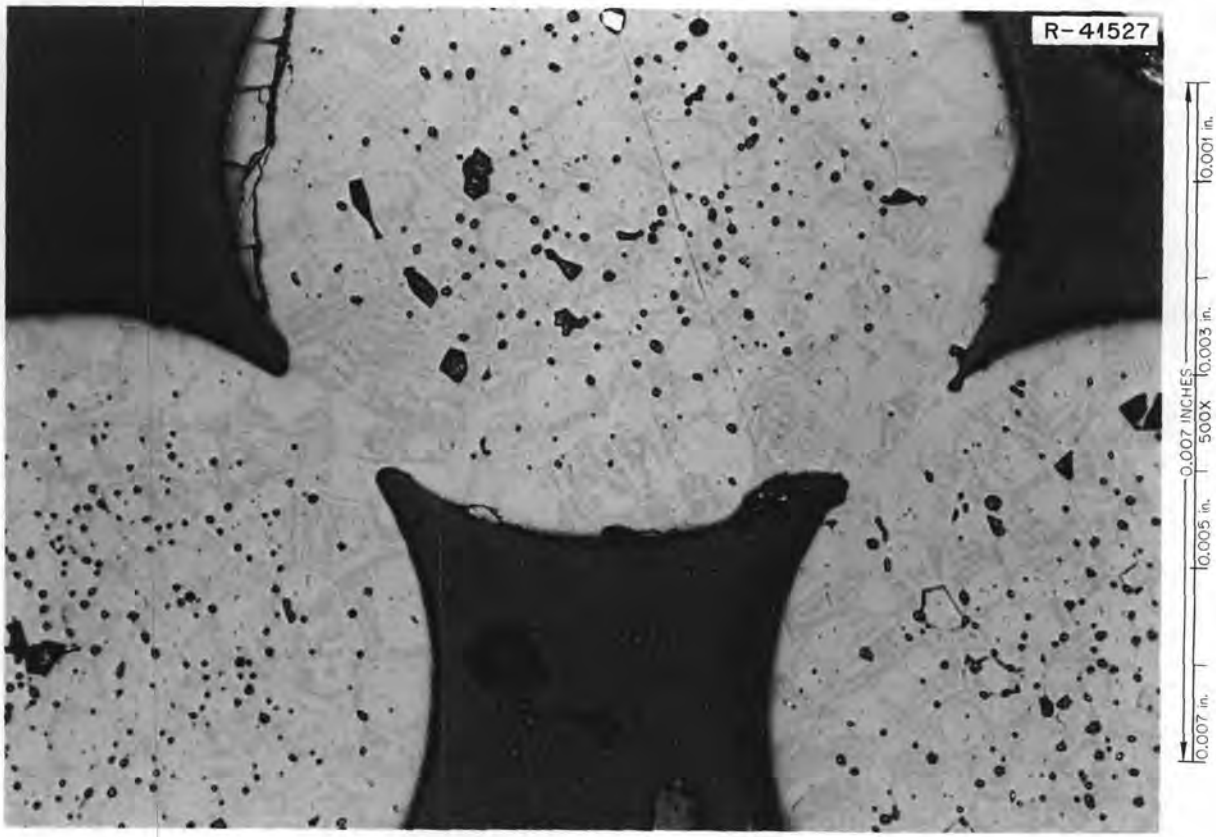

Fig. 9.6. PuO_2 Prepared with Steam Drying. After heating for 15 min at 1800°C and 2×10^{-3} torr.

The pH of the filtrate decreased to less than 8 after 18 liters of wash water had been used; this volume may be compared with the 12 liters that would have been required for batch washing. However, the total time required was significantly reduced, since the filtration rate for continuous washing was 200 ml/min as compared with 60 ml/min for batch washing.

9.3 PLUTONIUM SOL-GEL PILOT PLANT

A remotely operated, neutron-shielded facility was constructed in cell 4, Building 3019, to demonstrate the sol-gel process as a method for producing dense $^{238}PuO_2$ microspheres. The equipment was sized to process 200 g of plutonium per day, or 1 kg of mixed oxides (containing up to 25% fissile material) per day. The system was designed as a remotely operated replica of the ^{239}Pu glove-box system that was discussed in Sect. 9.2. After the equipment components were fabricated, they were installed in a plywood mockup for vessel calibration and for hydraulic testing of the piping system. The use of this mockup was necessitated by the space limitations in cell 4. The equipment and piping were then moved to cell 4, where they were permanently installed; a front view of the pilot plant is shown in Fig. 9.7.

Demonstration of ^{239}Pu Microsphere Production

The sol-gel pilot plant was initially operated with ^{239}Pu in order to characterize the equipment and to establish operating parameters. A total of four 150-g runs were made prior to the introduction of ^{238}Pu into the system. The first three were partially successful, and the fourth was completely successful; microspheres of good quality were produced, but only about 50% of them were within the desired size range (88 to 250 μ in diameter).

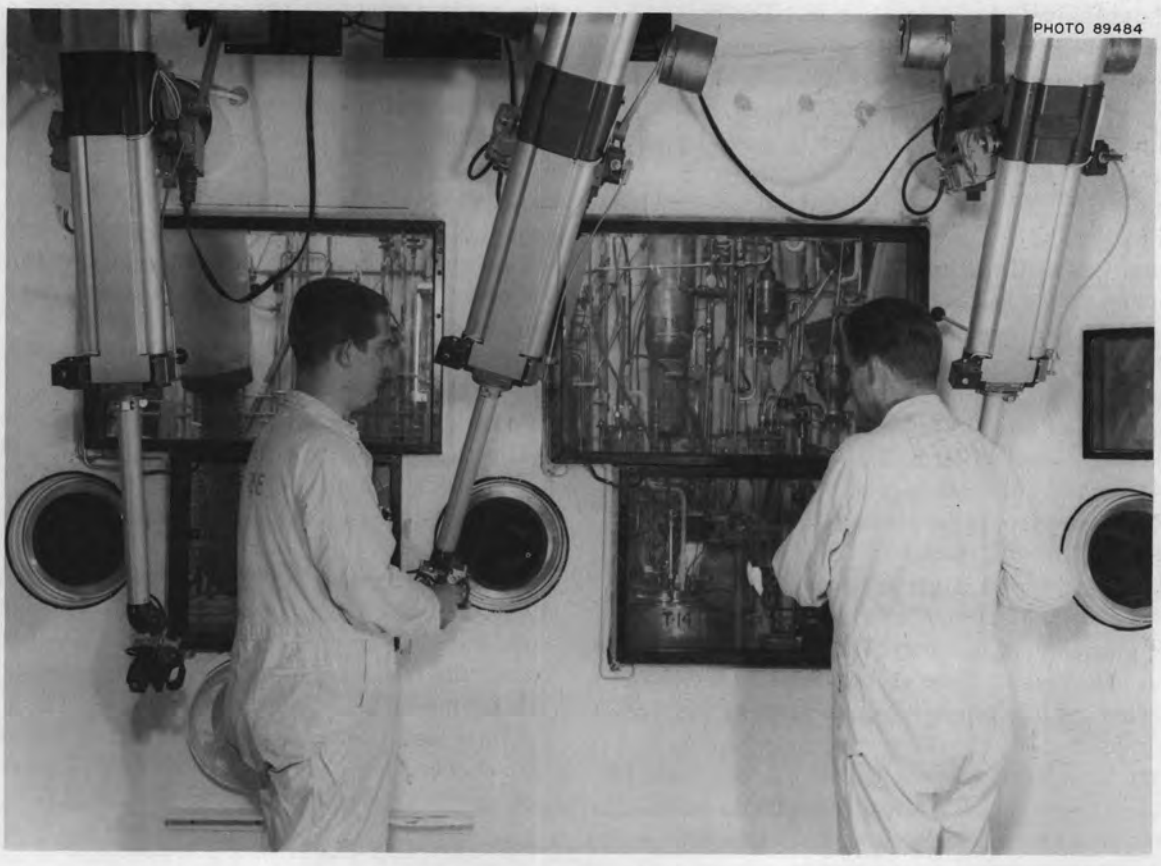

Fig. 9.7. Front View of the Plutonium Sol-Gel Pilot Plant.

Following this operating period, the cell face was shielded with 5 in. of Benelex 100-A in preparation for the processing of ^{238}Pu.

Demonstration of ^{238}Pu Microsphere Production

The basic ^{239}Pu flowsheet was followed in work with ^{238}Pu (80% ^{238}Pu, 16% ^{239}Pu, and 4% other plutonium isotopes); but, as a result of experience with this plutonium isotope in earlier laboratory studies, more stringent control of conditions was applied at times. Of the four sol runs (50 to 160 g of plutonium per run) that were made, none was completely successful in preparing a sol suitable for microsphere preparation. However, each of the attempts has contributed to a better understanding of the special difficulties of remote sol preparation, of the limitations of the physical equipment, and of the special radiolytic problems inherently associated with ^{238}Pu (specific activity of 3.8×10^{10} dis min^{-1} ml^{-1} and heat generation of 0.55 w/g). Current operational modifications include: (1) dissolution of plutonium oxides in glassware to eliminate the accumulation of stainless steel corrosion products (from the condenser system) when fluoride is used as a catalyst; (2) continuous washing of suspended precipitate to decrease washing time and to prevent caking of the precipitate, which would cause damage to the plutonium polymer as a result of localized overheating or radiolytic effects; (3) peptization at NO_3^-/Pu mole ratios of at least 2.0, with subsequent rapid concentration by evaporation and final concentration (to dryness) by "fuming" at 95°C, to reduce the polymer damage from the combined effects of high HNO_3 concentration

and high temperature; and (4) denitration without an air sweep through the baking furnace to prevent excessively rapid denitration. The first three of these modifications were incorporated in the fourth run; excellent results were achieved prior to the denitration step. In this run, a sol was prepared from the filter cake by partially resuspending the solids in water. Although the average NO_3^-/Pu mole ratio for the entire batch was extremely low, the NO_3^-/Pu mole ratio of the sol was still too high to permit the formation of spheres. We believe that a ^{238}Pu sol suitable for sphere forming can be prepared by incorporating the fourth modification into the procedure.

Sphere forming equipment was successfully operated to produce $^{238}PuO_2$ microspheres from a sol (NO_3^-/Pu mole ratio, 0.18) prepared by Chemical Development Section A. The microspheres were formed in 2-ethyl-1-hexanol containing 0.3 vol % Ethomeen S/15. The gel spheres were dried in air at temperatures up to 140°C and then calcined at 1200°C. Two problems were encountered in the ^{238}Pu microsphere formation: (1) excessive gas evolution from the sol introduced a surge capacity in the sol feed system and caused uneven feed flow to the column and (2) the final microspheres had such a high initial static charge that very few of them could be removed from the calcining furnace. The final microspheres were characterized by a dimple, or "cherry pit," and, in general, had slightly less desirable physical characteristics than comparable ^{239}Pu microspheres.

9.4 ASSISTANCE TO MOUND LABORATORY

Equipment for the preparation of $^{238}PuO_2$ sols and for the subsequent forming, drying, and firing to dense $^{238}PuO_2$ microspheres was fabricated, installed in a stainless steel cubicle, and shipped to Mound Laboratory, Miamisburg, Ohio. The box, 10 ft long by 7 ft 3 in. high and 42 in. deep, has been installed as part of a new, shielded production facility, where it is to be operated remotely, using four model G manipulators; one end of the box is shown in Fig. 9.8. The production capacity of the unit is one batch of sol, containing 150 g of plutonium, per 24 hr. The equipment was designed in accordance with the standard precipitation-peptization-denitration flowsheet for producing sol.[3] Microspheres are to be made by forming droplets of sol in a two-fluid nozzle, fluidizing the droplets in a stream of 2-ethyl-1-hexanol in a tapered glass column until they are dried to a gel, drying the gel spheres in hot air and steam at temperatures up to 160°C, and, finally, firing the spheres in air at temperatures up to 1200°C.

The sol forming equipment includes: (1) feed adjustment tank, (2) precipitation-peptization vessel, (3) high-nitrate sol evaporator, (4) denitration vessel, (5) final sol evaporator, and (6) sol surge tank. (The precipitation-peptization and the denitration vessels were described earlier.[3]) Also included are separate filtrate (basic) and condensate (acid) waste systems (two tanks each) and vacuum and vessel off-gas systems. An infusion pump meters the sol to the microsphere forming column; a surge tank with a submerged centrifugal pump, a cooler, a filter, and a still for removing H_2O from the 2-ethylhexanol comprise the system for recirculating the solvent. A surge vessel for gel spheres, a dryer with associated steam generator, and a firing furnace constitute the remainder of the process equipment. The equipment was checked for operability after the final installation, and the box was closed and leak-checked prior to shipment to Mound Laboratory.

9.5 CURIUM SOL-GEL STUDIES

A development program was initiated to prepare curium and mixed curium-americium oxides of controlled particle size for incorporation into HFIR targets (see Sect. 6.3). The development of a sol-gel process for preparing oxide microspheres of controlled particle size from rare earths (as stand-ins for americium and curium) and the evaluation of equipment for preparing 10-g batches of sol with rare earths and ^{241}Am were discussed in the last annual report.[4] During the past year, the process was successfully adapted to the preparation of mixed ^{244}Cm-^{243}Am sols (78% ^{244}Cm, 6% higher curium isotopes, 16% ^{243}Am) and was used to prepare 30 g of curium-americium oxide microspheres. These experiments demonstrated our ability to prepare 10-g batches of mixed ^{244}Cm-^{243}Am oxide sols and oxide microspheres of controlled size by the modified method.

[4] *Chem. Technol. Div. Ann. Progr. Rept. May 31, 1966*, ORNL-3945, p. 149.

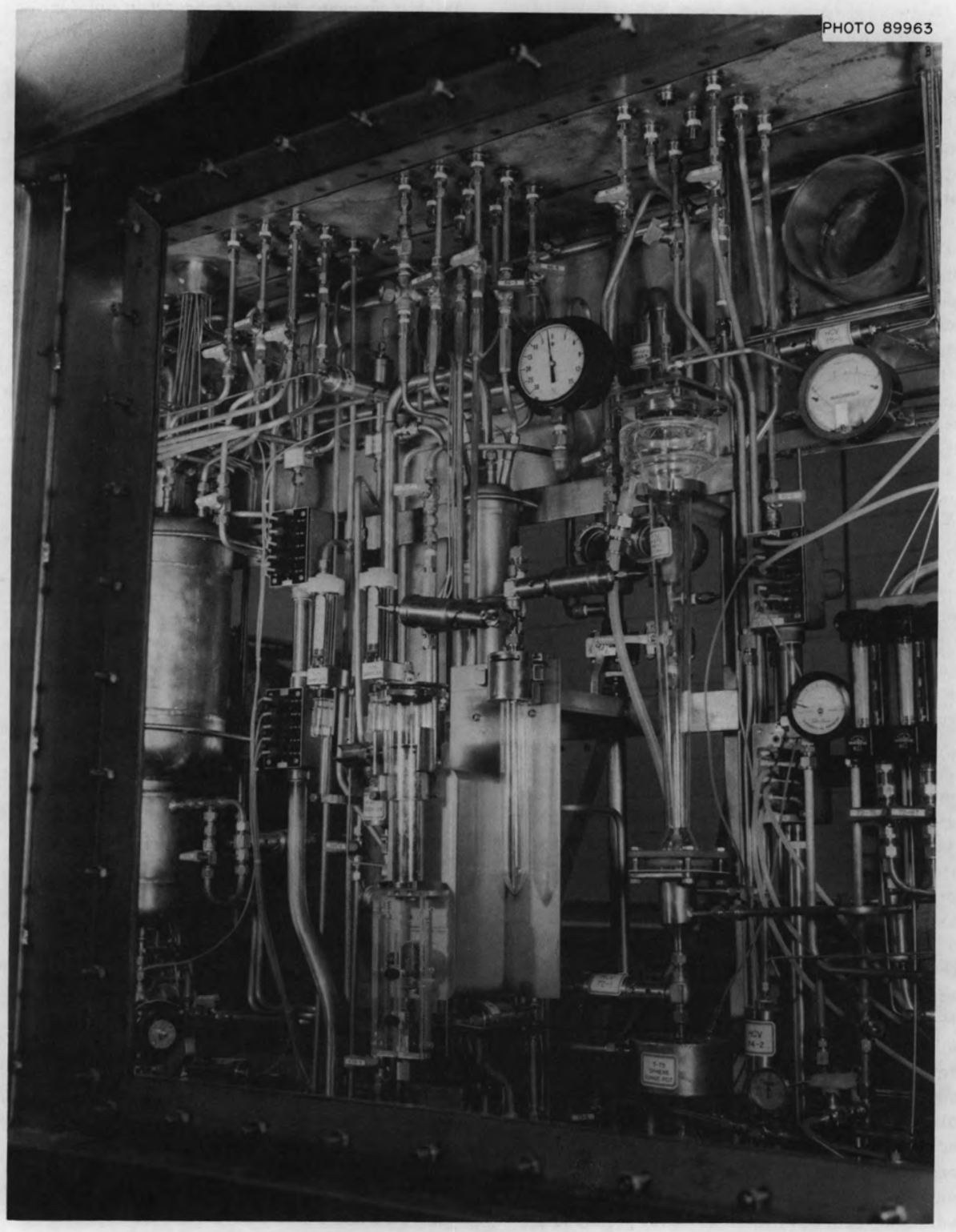

Fig. 9.8. Portion of Sol-Gel Production Unit Fabricated for Mound Laboratory.

Process Equipment

A facility to house the curium sol experiments was installed in cell 4 of Building 4507. Sol preparations were made in modified laboratory glassware; however, the equipment rack shown in Fig. 9.9 was also required. This dual-purpose unit contains the microsphere forming column, the solvent circulation system, and various process and storage vessels required for curium purification. The following refinements were built into the circulation system: (1) a bead overflow trap coupled with a solvent air-lift system, which returns solvent to the main reservoir, (2) a pressure ballast for stabilizing metered flow, and (3) a duplicate pump arrangement, which allows either of the two pumps to operate the entire system.

Sol Preparation

Prior to the preparation of sol, feed material was purified by either a single or a double oxalate-precipitation–calcination cycle. Judging by experiments to date, high purity is required for satisfactory sol preparation. The impurity level of the original feed, which contained 150 mg of zirconium per gram of curium and smaller amounts of other ionic impurities, prevented sol formation. A single oxalate cycle reduced the zirconium concentration to less than 10 mg per gram of curium.

Batch sizes in these experiments varied from 4 to 9 g of total metal. In initial efforts to prepare curium-americium oxide sols, a stock solution that had been purified by one oxalate cycle was used. The procedure that had been used to prepare ^{241}Am oxide sols consisted in precipitating the metal hydroxide by adding a dilute solution of the metal nitrate to a large excess of 8 *M* NH_4OH, filtering and washing with water (in a jacketed filter funnel) to a final pH of 8–9, and heating for 1 to 2 hr at 85°C. During heating, the paste converted to a fluid sol, which could be collected by filtration. Yields of final curium-americium oxide sols prepared in this way were very low (10 to 15%). It appeared that prolonged contact between the sintered-glass frit and the hydroxide, under static conditions, produced a thick cake that would not convert to sol. In subsequent experiments, essentially complete conversion to sol was obtained by fluidizing the filter cake during the washing step and removing the hydroxide from the filter immediately at the end of this step. The hydroxide was digested at 85°C in a glass beaker. Conversion to a fluid sol required about 2 hr under these conditions. These sols were milk-white, had NO_3^-/metal mole ratios of 0.4 to 0.7, and exhibited only a slight tendency to form radiolytic-gas-generated foam. The sols were quite fluid at concentrations of 0.1 to 0.15 *M* but tended to thicken at a concentration of about 0.2 *M*.

Subsequent sol preparations were made using stock solution that had been highly purified by a double oxalate-precipitation cycle. Three consecutive high-yield runs produced sols that were superior to previous preparations in several respects. For example, the NO_3^-/metal mole ratios were reduced from about 0.7 to 0.2, the digestion time required for converting washed hydroxide to crystalline sol was reduced from 2 hr to 1 hr or less, and the sols were very fluid at metal concentrations of 0.2 to 0.25 *M*. The sols were characterized by excellent colloidal stability. No foaming was observed.

Preparation of Microspheres

Gel microspheres were formed from 0.1 to 0.25 *M* curium-americium oxide sols, using standard sphere-forming techniques. Plugging of the column feed line, which was experienced in early runs, was virtually eliminated by using a larger orifice in the column nozzle and by water-cooling the sol during storage.

The gel spheres were removed from the column and air-dried overnight in an open container prior to calcination in air at 1150°C. The calcined spheres were free flowing, dust free, and showed no tendency to crack or disintegrate. A photomicrograph of these spheres is shown in Sect. 6.3. The particle size varied from 40 to 177 μ in diameter. The characteristic pit seen in the larger spheres is believed to be a result of low sol concentration, since similar effects are observed when dilute rare-earth sols are formed.

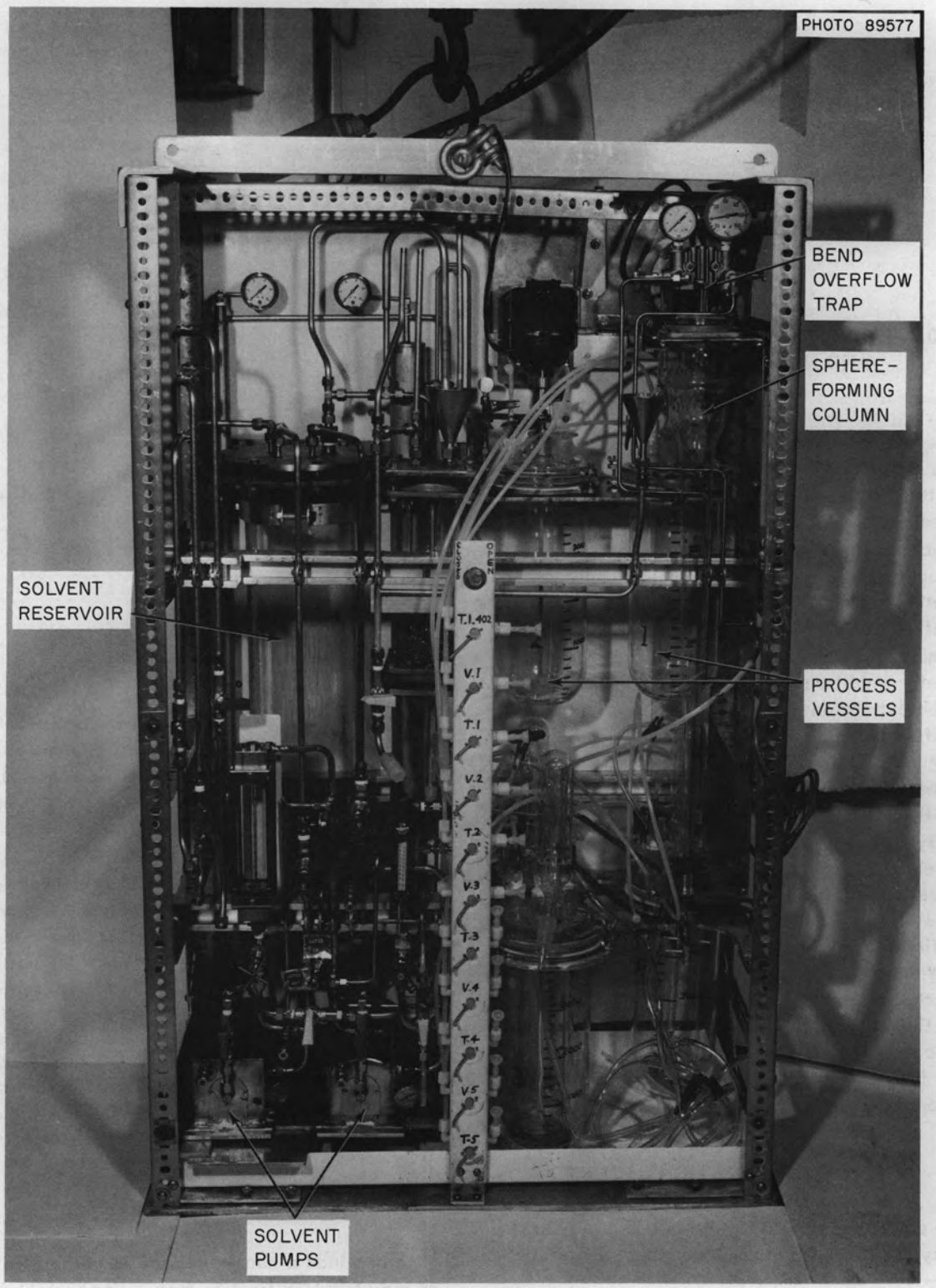

Fig. 9.9. Curium Sol Equipment Rack.

10. Separations Chemistry Research

10.1 EXTRACTION OF METAL SULFATES AND NITRATES BY AMINES

In view of the potential for increased use of amine extractants, a systematic survey is being made of the characteristics of the extraction of metals from various acid and salt solutions with representative amines. The study of metal chloride extractions from hydrochloric acid and acidified lithium chloride solutions has been completed and reported.[1] Data for the extraction of metals from acidified lithium nitrate solutions and acidified lithium sulfate solutions have been partially reported.[2] Additional data have now been obtained for the extraction of Co(II), V(IV), and hafnium from acidified lithium sulfate solutions.

Figure 10.1 shows data for the extraction of V(IV) and hafnium from acidified lithium sulfate solutions with 0.1 *M* solutions of representative primary, secondary, tertiary, and quaternary amines in diethylbenzene. Extraction coefficients for V(IV) were highest for the quaternary amine but were less than 1 at all sulfate concentrations; with hafnium, the coefficients for Primene JM ranged from 2000 at 0.3 *N* SO_4^{2-} to 2.4 at 5 *N* SO_4^{2-}, while those for the other three amines were much lower (3 to 6) over the same sulfate concentration range. Extraction coefficients for Co(II) (not shown in the figure) were less than 0.02 over the total sulfate concentration range studied.

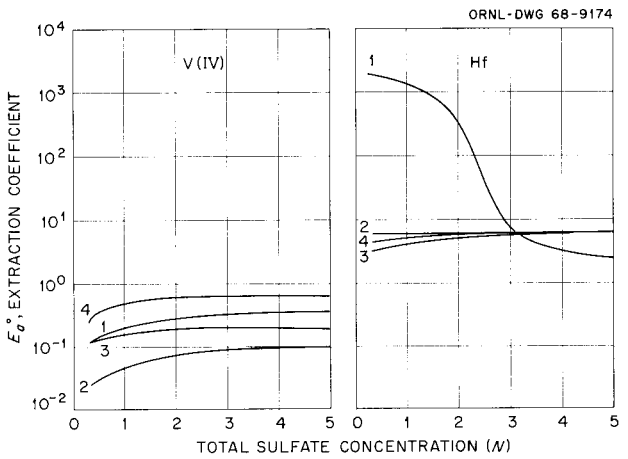

Fig. 10.1. Extraction of Metals from Sulfate Solutions with Amines. Organic phase: 0.1 *M* solutions of (1) Primene JM ($RR'R''CNH_2$, 18 to 24 carbon atoms); (2) Amberlite LA-1 ($RR'R''CNHC_{12}H_{23}$, 24 to 27 carbon atoms); (3) Adogen 364 (R_3N, R = *n*-octyl, *n*-decyl mixture); (4) Adogen 464 [$R_3(CH_3)N^+$, R = *n*-octyl, *n*-decyl mixture] in diethylbenzene. With Adogen 464, 3 vol % of tridecanol was added to the solvent phase to prevent the formation of a third phase. Amines were in the sulfate form. Aqueous phase: 0.01 *M* metal ion in Li_2SO_4–0.2 *N* H_2SO_4. Contact time: 10 min at a phase ratio of 1:1.

10.2 NEW SEPARATIONS AGENTS

We are continuing to investigate, for potential utility in solvent extraction or other separations methods, compounds that are: (1) newly available commercially, (2) submitted by manufacturers for testing, or (3) specially procured for testing of class or structure.

Carboxylic and Sulfonic Acids

We obtained a narrow mixture of carboxylic acids as a distillation fraction from a commercial developmental product, "Versatic Acid 1519." This product contains 15- to 19-carbon isomeric and homologous α,α-dialkylcarboxylic acids,

[1] F. G. Seeley and D. J. Crouse, *J. Chem. Eng. Data* 11(3), 424 (1966).

[2] *Chem. Technol. Div. Ann. Progr. Rept. May 31, 1967*, ORNL-4145, pp. 208–9.

$RR'MeCCO_2H$, that were produced by the Koch synthesis from cracked paraffin. The distillation fraction has a neutral equivalent of 262 ($C_{16}H_{33}CO_2H$ = 270). The sodium salt is soluble in water; however, the solubility of the acid in water, or of the sodium salt in 5 *M* sodium nitrate solution, is less than 10^{-5} *M*. In the pH range of 8 to 9, it is a strong extractant for alkaline earths (see Sect. 10.5).

One new commercial sulfonic acid, nominally tridecylbenzenesulfonic acid (neutral equivalent: 341, theoretical; 303, experimental) showed acceptable solubility in hydrocarbons, but its sodium salt is excessively soluble in aqueous phases even at high ionic strengths.

Organophosphorus Acids

We prepared 1-methylheptyl phenylphosphonic acid, HMeH[ϕP], by controlled hydrolysis of dicapryl phenylphosphonate with ethanolamine. Preliminary tests indicate that it has significant advantages over other organophosphorus acids that have been used for intraseries separations of lanthanides and actinides. (The most important other organophosphorus acids are di(2-ethylhexyl)phosphoric acid, HDEHP, and 2-ethylhexyl phenylphosphonic acid, HEH[ϕP]). It gave higher separation factors (1.5 to 4 times those for the other acids) for several metal pairs in both nitrate and chloride solutions. The enhancement of extractions by zirconium, a disadvantage in these separations, is considerably less with HMeH[ΦP] than with HEH[ΦP] (Sect. 10.5).

β-Diketones

Three diketones of higher molecular weight than has been previously available were synthesized for testing as lithium extractants: tridecanoylacetylmethane or tridecanoylacetone, TDA:

$$CH_3(CH_2)_{12}\overset{\overset{\displaystyle O}{\|}}{C}CH_2\overset{\overset{\displaystyle O}{\|}}{C}CH_3 ,$$

2-ethylhexanoylpivalylmethane, 2EHPM:

$$CH_3(CH_2)_3\underset{\underset{\displaystyle C_2H_5}{|}}{CH}\overset{\overset{\displaystyle O}{\|}}{C}CH_2\overset{\overset{\displaystyle O}{\|}}{C}(CH_3)_3 ,$$

Table 10.1. Extraction of Alkali Metals by β-Diketones[a]

Reagent	Extraction Coefficient for:[b]			Separation Factor for:	
	Li	Ma	K	Li from Na	Li from K
TDA	95	0.1	0.02	930	5000
2EHPM	20	0.03	<0.01	700	>2000
DPM	8	0.06	<0.01	130	>800
NTDPM	6	0.09	<0.01	70	>600

[a]TDA: tridecanoylacetone; 2EHPM: 2-ethylhexanoylpivalylmethane; DPM: dipivalylmethane; NTDPM: neotridecanoylpivalylmethane. 0.1 *M* diketone + 0.1 *M* tri-*n*-octylphosphine oxide in *n*-hexane.

[b]Extraction from 1 *M* KCl + 0.1 *M* NaOH + 0.03 *M* LiCl; equal volumes of aqueous and organic phases.

neotridecanoylpivalylmethane, NTDPM:

$$CH_3(CH_2)_8\underset{\underset{\displaystyle (CH_3)_2}{|}}{C}\overset{\overset{\displaystyle O}{\|}}{C}CH_2\overset{\overset{\displaystyle O}{\|}}{C}(CH_3)_3 .$$

At a concentration of 0.1 *M* in *n*-hexane, NTDPM extracted lithium from alkaline chloride solution. The other two diketones extracted lithium when 0.1 *M* tri-*n*-octylphosphine oxide (TOPO) was added to the organic phase, but they precipitated the lithium in the absence of TOPO. All three showed high selectivity for lithium over sodium and especially over potassium (Table 10.1). The separation factors with NTDPM were similar to those with the previously studied dipivalylmethane, DPM, which has an analogous structure, while separation factors with the less extensively branched TDA and 2EHPM were higher.

10.3 BERYLLIUM PURIFICATION BY SOLVENT EXTRACTION

New and potentially less expensive methods are being studied for preparing high-purity beryllium compounds for reactor use, starting with beryllium

concentrates such as those obtained by amine extraction[3] or di(2-ethylhexyl)phosphoric acid extraction[4] of low-grade beryllium ore leach liquors. Major emphasis has been on the development of a purification process[5] that uses quaternary ammonium extractants to recover beryllium from dilute carbonate liquors. The beryllium is stripped from the solvent with ammonium bicarbonate solution and is recovered as a pure hydroxide product by heating the strip solution.

Status and Progress

The development of the quaternary ammonium extraction process was completed. Recent experimental work included comparing the extraction abilities of quaternary ammonium compounds of various structures and studying the effect of diluent type on extraction results. The preparation of pure products (<100 ppm total metal impurities) was successfully demonstrated in batch countercurrent extraction tests. Based on this small-scale evaluation, the process appears to offer an attractive route for preparing high-purity beryllium compounds.

Preparation of Feed Solutions

We have prepared both sodium beryllium carbonate and ammonium beryllium carbonate feed solutions by a two-stage batch countercurrent leaching-decantation procedure. Beryllium hydroxide that had been freshly precipitated from an impure beryllium sulfate solution was dissolved in 0.8 *M* $NaHCO_3$–0.2 *M* Na_2CO_3 at 70°C or in 0.8 *M* NH_4HCO_3–0.2 *M* $(NH_4)_2CO_3$ at 55°C to give feed solutions containing about 2 g of beryllium per liter. In each case, more than 97% of the beryllium was dissolved by using about 3.5 moles of bicarbonate and 0.8 mole of carbonate per mole of beryllium. Only small percentages of most of the metal contaminants were dissolved. The undissolved solids settled rapidly and were easily separated from the carbonate liquor by decantation.

[3]D. J. Crouse, K. B. Brown, and F. G. Seeley, "Primary Amine Extraction of Beryllium from Sulfate Liquors," pp. 327–41 in *Solvent Extraction Chemistry of Metals*, Macmillan, London, 1965.

[4]L. Crocker *et al.*, U.S. Bureau of Mines Reports RI-6173 and RI-6469 (1963).

[5]*Chem. Technol. Div. Ann. Progr. Rept. May 31, 1967*, ORNL-4145, pp. 215–17.

Beryllium Extraction

A number of quaternary ammonium compounds of different structures were tested for their ability to extract beryllium from 0.8 *M* Na_2CO_3–0.2 *M* $NaHCO_3$ solution (pH 10). Of the compounds tested, those containing either one or two *N*-methyl groups were found to be the most effective (Table 10.2). Compounds with four long chains attached to the nitrogen were completely ineffective. Both Adogen 464 and Aliquat 336, which are similar commercially available quaternary ammonium compound mixtures, showed adequate extraction power and also have other desirable characteristics. Phase separation with Adogen 464 was slightly better than with Aliquat 336; therefore, the former was used in most of the testing.

The comparison of diluents for use with Adogen 464 showed that several different types are suitable. When aliphatic hydrocarbons (dodecane, Varsol) are used, a small amount (2 to 5 vol %) of a

Table 10.2. Extraction of Beryllium with Quaternary Ammonium Compounds

Organic phase: 0.1 *N* quaternary ammonium carbonate in diethylbenzene

Aqueous phase: 0.01 *M* Be (plus ^7Be tracer), 0.8 *M* Na_2CO_3, 0.2 *M* $NaHCO_3$

Contact: 10 min at a phase ratio of 1 : 1

Quaternary Ammonium Carbonate	Beryllium Extraction Coefficient (E_a^o)
Tetraheptyl	0.008
Trioctylpropyl	0.008
Dilauryldimethyl	7.4[a]
Adogen 464 ($[R_3N\text{-}CH_3]_2CO_3$, where the R's are mixed *n*-octyl and *n*-decyl)	5.3
Aliquat 336 (mixture similar to Adogen 464)	5.5
Altered Aliquat 336 (methyl group replaced with a dodecylbenzyl group)	0.003
N-Benzyl-*N*,*N*-dimethyl-(1-hendecyldodecyl)	4.3

[a]Extractant concentration was 0.07 *N*.

long-chain alcohol (e.g., tridecanol) must be added to prevent formation of a third liquid phase during extraction. With these diluents, the beryllium extraction coefficients were about the same as those obtained for Solvesso 100 (aromatic petroleum product) and diethylbenzene; however, they were a factor of 1.5 to 2 lower than those obtained by using benzene, toluene, and carbon tetrachloride.

The recovery of beryllium from an ammonium carbonate–ammonium bicarbonate solution (pH 9.2) that was 0.8 *M* in total carbonate and contained 1.65 g of beryllium per liter was demonstrated in a batch countercurrent test with 0.57 *N* Adogen 464 in 95% diethylbenzene–5% tridecanol. The scrub solution was 0.2 *M* NH_4HCO_3, and the aqueous feed : solvent : scrub ratio was 1.5 : 1 : 0.25. Beryllium recovery in four extraction and two scrub stages was 99.8%. The beryllium extraction coefficients were about 3 in the feed stage and 20 in the raffinate stage. Similar results were obtained in a test with a sodium carbonate–sodium bicarbonate feed.

Beryllium Stripping and Product Recovery

Beryllium is stripped efficiently from 0.5 *N* Adogen 464 with 1.5 to 2 *M* NH_4HCO_3 or 2.5 to 3 *M* $(NH_4)_2CO_3$ solutions. The former solution is slightly more efficient and is preferred. In a test with 0.5 *N* Adogen 464 containing 2.4 g of beryllium per liter, more than 99% of the beryllium was stripped by contacting the solvent with five one-tenth volumes of 1.9 *M* NH_4HCO_3. Heating the strip solution to 90 to 95°C in an open vessel precipitated the beryllium almost quantitatively in 15 to 30 min. Most of the ammonia and carbon dioxide were volatilized during the precipitation and could be recovered from the vessel off-gas for recycle.

Process Demonstrations

To determine the purity of the product obtainable from the process, a batch countercurrent demonstration run was made in which all the equipment was constructed of either plastic or Teflon-lined glass. The feed solution was prepared by precipitating beryllium (with ammonia) from sulfuric acid containing 20 different metal contaminants (total of 1.3×10^5 parts of metal contaminants per million parts of BeO), washing the precipitate to remove occluded sulfate, and dissolving the precipitate in NH_4HCO_3-$(NH_4)_2CO_3$ solution. The beryllium was extracted with 0.5 *N* Adogen 464 in a batch countercurrent system and was scrubbed with 0.2 *M* NH_4HCO_3. One portion of the scrubbed organic extract was stripped with 1.9 *M* NH_4HCO_3, and a beryllium hydroxide product was recovered by heating the strip solution. Detectable metal contaminants in the product, in parts per million parts of BeO, were: B, 20; Ca, 100; Cr, 200; Cu, 10; Fe, 300; Mg, 50; Mo, 20; Na, 20; Si, 30; Ti, 5; and V, 100. A product was obtained from a second portion of the extract in the same manner except that both the strip solution and the 0.2 *M* NH_4HCO_3 solution used to wash the $Be(OH)_2$ precipitate were 0.02 *M* in EDTA. This greatly improved the purity of the product. Detectable metal contaminants in the product, in parts per million parts of BeO, were: Al, 20; B, 30; Mg, <10 (trace); and Si, 60.

10.4 RECOVERY OF URANIUM FROM COMMERCIAL PHOSPHORIC ACID

The production of commercial phosphoric acid is increasing very rapidly. The acid produced from Florida phosphate rock contains 50 to 200 ppm of uranium and, by 1970, will represent a potential source of about 2000 tons of U_3O_8 annually. Because of the strong complexing action of the phosphate in this concentrated solution (~5 *M* H_3PO_4), well-known uranium extractants, such as tributyl phosphate and long-chain amines, are not effective. A solvent extraction process employing pyrophosphoric acids (the reaction product of P_2O_5 and a long-chain alcohol) was used for several years for by-product uranium recovery in Florida phosphoric acid plants. Pyrophosphoric acids, however, are unstable and have other undesirable characteristics for economical industrial application. Preliminary screening tests made at ORNL several years ago to find a more suitable extractant were not very encouraging. Because of the poor results, and because the annual production of phosphoric acid at that time was not large, the program was discontinued. Now, in view of the expanding production of phosphoric acid and the corresponding increase in the total amount of solubilized uranium, we are reexamining extractants to determine if an economical process for uranium recovery can be found.

Screening Tests

A large number of organophosphorus reagents of different types and structures were tested for their ability to extract hexavalent and tetravalent uranium from 5.3 *M* H_3PO_4 (reagent grade, containing 200 ppm of uranium). Most of these compounds showed very low extraction power and were thus of little interest. The highest uranium extraction coefficients (>500) were obtained with two organophosphorus compounds that were synthesized at ORNL. These compounds, however, rapidly lost their extraction power after contact with successive volumes of fresh phosphoric acid, thereby indicating that they are either unstable or have a high distribution loss to the aqueous phase. Favorable results have been obtained in preliminary tests with the synergistic uranium extraction combination di(2-ethylhexyl)phosphoric acid (D2EHPA) plus tri-*n*-octylphosphine oxide (TOPO), which is known to have good stability and to exhibit low losses to the aqueous phase. In addition, it is readily stripped with sodium or ammonium carbonate solutions, thus providing an attractive route to the preparation of a relatively high-grade uranium concentrate. Uranium extraction coefficients with this reagent combination, although comparatively low, appear to be high enough for process use; therefore, the combination has been selected for detailed study.

Extraction of Uranium with D2EHPA-TOPO

D2EHPA-TOPO extracts hexavalent uranium much more strongly than tetravalent uranium. In all tests described subsequently, the uranium was present as U(VI). The uranium extraction coefficients decrease rapidly as the phosphoric acid concentration increases. For example, in extractions of uranium from "pure" phosphoric acid (containing 0.2 g of uranium per liter) by 0.18 *M* D2EHPA–0.05 *M* TOPO in *n*-dodecane (phase ratio, 1 : 1), the extraction coefficients were 185, 18, and 2.7 for acid concentrations of 1.5, 3.3, and 5.3 *M* respectively. When the D2EHPA concentration was held constant at 0.18 *M* and the TOPO concentration was varied from 0.01 to 0.14 *M*, the maximum extraction of uranium from 5.3 *M* H_3PO_4 occurred at a D2EHPA : TOPO mole ratio of about 4 : 1. Increasing the D2EHPA concentration from 0.1 to 1 *M* (while maintaining the D2EHPA : TOPO mole ratio constant at 4 : 1) increased the uranium extraction coefficient from 1.2 to 30. The extraction is very rapid, with equilibrium being reached within 1 min.

Isotherms for the extraction of uranium from 5.3 *M* H_3PO_4 containing 0.2 g of uranium per liter by 0.2, 0.3, 0.5, and 1.0 *M* D2EHPA in *n*-dodecane (modified with 0.25 mole of TOPO per mole of D2EHPA) showed maximum uranium loadings for these solvents of about 0.58, 1.0, 1.9, and 4.1 g/liter respectively. Indicated uranium recoveries obtainable in five ideal extraction stages, with the solvent being loaded to 80% of these maximum values, increased from 92% for 0.2 *M* D2EHPA–0.05 *M* TOPO to 97% for 1 *M* D2EHPA–0.25 *M* TOPO. It appears that this small gain in extraction efficiency, obtained by using the more concentrated solvent, would be more than offset by the increase in solvent costs at the higher solvent concentration.

ORNL-DWG 68-9175

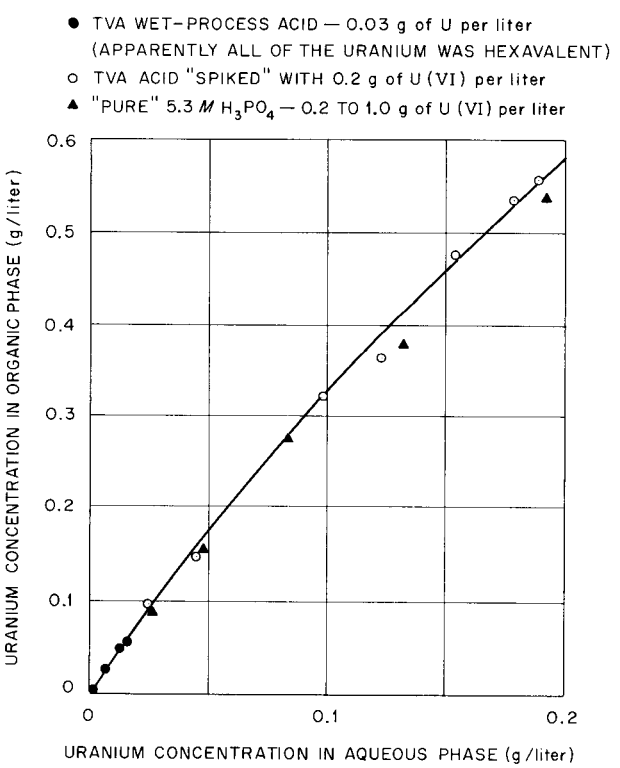

Fig. 10.2. Extraction of U(VI) from TVA Wet-Process Acid (5.3 *M* H_3PO_4) by 0.2 *M* D2EHPA–0.05 *M* TOPO in *n*-Dodecane.

We studied the effects of the presence of iron and fluoride, which are important contaminants in wet-process phosphoric acid, on the extraction of uranium by D2EHPA-TOPO. Adding 0.5 to 1.0 *M* fluoride to 5.3 *M* H_3PO_4 had no effect on the extraction of uranium. For some reason, as yet unexplained, adding 0.07 to 0.16 *M* Fe(III) by dissolving ferric oxide or ferric sulfate in the liquor increased the extraction coefficients by about 25%.

Extractions from Commercial Phosphoric Acid. – Data for the extraction of uranium from a sample of wet-process phosphoric acid (produced at the TVA fertilizer pilot plant in Muscle Shoals, Ala.) by 0.2 *M* D2EHPA–0.05 *M* TOPO in *n*-dodecane were in agreement with those obtained in extractions from "pure" phosphoric acid (Fig. 10.2). The sample of liquor, which was several years old, contained 28 ppm of uranium and the following impurities (approximate concentrations in grams per liter): 12 Fe(III), 3.5 Al, 0.4 Ca, 16 SO_4, 0.6 F, and 5 Si. To extend the range of data, the liquor was "spiked" with uranium in some tests. The oxidation state of the liquor was not adjusted prior to extraction, but it is known that some oxidation of the iron in the liquor occurred after receipt of the sample. The extraction results indicate that essentially all of the uranium was hexavalent. Samples of commercial phosphoric acid from other sources are being obtained for testing.

10.5 EQUILIBRIA AND MECHANISMS OF EXTRACTION

Zirconium Enhancement of the Extraction of Metal Ions by Organophosphorus Acids

We previously[6] reported that small amounts of zirconium cause significantly enhanced extractions of some trivalent lanthanides and actinides by 2-ethylhexyl phenylphosphonic acid and thus interfere with a projected process for separating berkelium and californium from americium and curium. The study of this effect was extended to most of the metals and to a variety of extractants. A paper comparing several monoesters of phosphonic acids (see Table 10.3) has been accepted for publication in the *Journal of Inorganic and Nuclear Chemistry*. Its abstract follows:

[6] *Chem. Technol. Div. Ann. Progr. Rept. May 31, 1967*, ORNL-4145, p. 221.

Table 10.3. Zirconium Enhancement of the Extraction of Cerium by Phosphonic Acid Esters

Organic phase: 0.1 *M* extractant in *n*-octane

Aqueous phase: 0.2 *N* HNO_3, tracer $^{144}Ce(III)$

Phosphonic Acid Ester	E_a^o for Ce(III)		Enhancement Factor
	No Zr	0.5 mg Zr/ml[a]	
2-Ethylhexyl phenyl	9.1	810	90
1-Methylheptyl phenyl	0.59	9.2	16
Butyl cyclohexyl	0.018	115	6,400
Butyl butyl	0.025	280	11,000
Amyl amyl	0.034	269	7,500
Hexyl hexyl	0.076	340	4,500
Decyl decyl	0.019	11.5	600

[a] Zr: extractant mole ratio = 1 : 18.

Boyd Weaver, "Enhancement by Zirconium of Extractions of Cations by Organophosphorus Acids. I. Mono-Acidic Phosphonates." *Abstract*: "The extraction of zirconium from aqueous solutions by monoacidic phosphonates (monoesters of phosphonic acids) produces compounds which are much stronger extractants for many cations than are the simple acidic phosphonates. The most highly enhanced extractions observed are those of some of the alkaline earths and the lighter trivalent lanthanides and actinides. With 2-ethylhexyl phenylphosphonic acid (HEH[ϕP]) containing zirconium, extraction enhancement factors as high as 10^4 have been observed for some alkaline earths. Other cations for which zirconium increases extraction include Li(I), Ag(I), Tl(I), Mn(II), Co(II), Fe(III) in chloride, Y(III), Pb(IV), and Pu(IV), but not Cs(I), Be(II), Cu(II), Ni(II), Zn(II), Cr(III), Fe(III) in nitrate, nor Sc(III). Enhancements vary with the anionic constituent of the aqueous solution. Enhancement is a complex function of the zirconium concentration. Hafnium and titanium are the only elements other than zirconium so far known to produce this enhancement. A suggested mechanism involves cation exchange with the hydrogen of a hydroxyl group on a complex zirconic acid."

Zirconium also enhanced the extraction of cerium from hydrochloric acid solution by dihexyl phosphoric acid, from nitric acid solution by di(2-ethyl-

hexyl) phosphorous acid and several dialkyl phosphoric acids (hexyl, 2-ethylhexyl, 2-ethyl-4-methylpentyl, decyl, tridecyl), but not by monododecyl phosphoric acid or di(2-ethylhexyl)phosphinic acid.

Alkali and Alkaline Earth Extractions by Carboxylic Acids

The equilibria of extraction of sodium and strontium from sodium nitrate solutions by a branched carboxylic acid of moderately high molecular weight have been determined and compared with the parallel extractions by dialkylphosphoric acid. A paper has been written and will be submitted for publication in the *Journal of Inorganic and Nuclear Chemistry*. Its abstract follows:

W. J. McDowell and H. D. Harmon, "Sodium and Strontium Extraction from Sodium Nitrate Solutions by *n*-Octane Solutions of a Branched Aliphatic Monocarboxylic Acid." *Abstract*: "Sodium and strontium are extracted from 5.0 *M* $NaNO_3$ solutions by *n*-octane solutions of a highly branched aliphatic carboxylic acid (RR′MeCCOOH), a fraction distilled from a developmental mixture 'Versatic Acid 1519.' From the dependence of the extraction on pH and extractant concentration, from extractant and extract aggregation in the organic phase, and from infrared absorption studies of the extract complexes, the most probable extraction reactions are:

$$Na^+ + 1.5(HA)_2 \rightleftharpoons NaA \cdot 2HA + H^+$$

and

$$Na^+ + 2(HA)_2 \rightleftharpoons NaA \cdot 3HA + H^+$$

$$Sr^{2+} + 2(HA)_2 \rightleftharpoons SrA_2 \cdot 2HA + 2H^+$$

and

$$Sr^{2+} + 2.5(HA)_2 \rightleftharpoons SrA_2 \cdot 3HA + 2H^+$$

The carboxylic acid extraction of sodium and strontium from sodium salted systems is in several ways similar to di(2-ethylhexyl)phosphoric acid (HDEHP) extraction of these ions. Similar salt-plus-coordinated-acid complexes are formed, and this results in the curves of strontium extraction coefficient vs pH having the same general shapes including well defined maxima. The maximum strontium extraction coefficients and separation factors from sodium are nearly 100 times greater with this carboxylic acid than with HDEHP. Maximum extraction with the carboxylic acid occurs, however, at pH 8.5 to 9.5, while with HDEHP it occurs in the pH range 5 to 6. Thus, the advantage in extraction coefficient may be limited to extraction of the more basic ions."

Sulfuric Acid Activity in Acid-Salt Mixtures

The investigation of aqueous sulfate complex systems by means of amine extraction (cf. Sect. 6.5) requires knowledge of the sulfuric acid activity, the true sulfate ion concentration, and the ionic strength in solutions containing sulfuric acid and sodium sulfate at known gross concentrations. This information is available through a relationship developed by Baes[7] for sulfate solutions over the ionic strength range of 0.2 to 1.5 *m* (e.g., 0.08 to 0.5 *m* Na_2SO_4). We subsequently found, experimentally, that the relationship is valid at higher concentrations, up to total sulfate concentrations of 1.5 *m*.[8] We now have available two computer programs, SULFATE and CALACT, to speed up and refine the calculations.

When given a desired sulfuric acid activity and the set of total sulfate concentrations required for a series of solutions, together with an initial estimate of the sulfuric acid concentration needed, program SULFATE will calculate the sulfuric acid concentration, its activity coefficient, the true sulfate ion concentration, and the ionic strength for each solution of the series. We believe that the calculated compositions are correct to within ±5% in the optimum range of 0.075 to 1.5 *m* total sulfate concentrations. At lower concentrations the uncertainty rises to 10 or 15%, because of increasing divergence between the two activity coefficient curves on whose similarity the working relationship is based.

The companion program CALACT uses the same relationship to calculate the sulfuric acid activity and activity coefficient, the true sulfate ion concentration, and the ionic strength when the gross concentrations of sodium sulfate and sulfuric acid are given.

---

[7] C. F. Baes, Jr., *J. Am. Chem. Soc.* **79**, 5611 (1957).

[8] K. A. Allen and W. J. McDowell, *J. Phys. Chem.* **67**, 1138 (1963).

10.6 KINETICS OF METAL-ION EXTRACTION BY ORGANOPHOSPHORUS ACIDS

Iron Extraction

It was previously reported[9] that the observed kinetics of iron(III) extraction by di(2-ethylhexyl)phosphoric acid (HDEHP or HA) in hydrocarbon solutions from aqueous acid perchlorate solutions was usefully well fitted by two empirical proportionalities,

$$k \propto [\Sigma HA]^{0.5}/[H^+] \quad \text{at } [\Sigma HA] < 0.2\ M\ , \qquad (A)$$

$$k \propto [\Sigma HA]^{1.5}/[H^+]^2 \quad \text{at } [\Sigma HA] > 0.5\ M\ , \qquad (B)$$

for the net reaction

$$Fe(H_2O)_6{}^{3+} + \underset{\cdots\cdots}{3(HA)_2} \rightleftharpoons \underset{\cdots\cdots\cdots\cdots}{FeA_3 \cdot 3HA} + 3H^+ + 6H_2O\ , \qquad (C)$$

where k is defined by $-d[Fe]/dt = k[Fe]$. It was also shown that Eq. (A) can result from rate control by the first step in the reaction

$$Fe(H_2O)_6{}^{3+} + A^- \rightleftharpoons (H_2O)_5FeOH^{2+} + HA \rightleftharpoons (H_2O)_5FeA^{2+} + H_2O\ , \qquad (D)$$

occurring at the interface. All the measurements were limited to extraction of a small quantity of iron in order to avoid loading the extractant and were also limited to extraction of a small fraction of the iron in order to keep the reverse reaction negligible.

We subsequently found that Eq. (B) can result from a shift of the rate control to an analogous first step in the introduction of the second ligand:

$$(H_2O)_5FeA^{2+} + HA_2{}^- \rightleftharpoons (H_2O)_4FeAOH^+ + (HA)_2 \rightleftharpoons (H_2O)_4FeA_2{}^+ \cdot HA + H_2O\ . \qquad (E)$$

However, it was obvious that control by these two steps could not account for the complete mechanism. Since the transition from (A) to (B) is to a higher rate and also to a higher log slope with respect to HDEHP concentration, that is, since the k-vs-$[\Sigma HA]$ curves represented by (A) plus (B) are concave upward, the transition must occur between steps that are parallel. But transition from control by (D) to control by (E) is a transition between steps in series. Hence, there must be at least one more controlling step between (D) and (E).

Detailed geometric analysis of the shapes of the experimental curves in the transition region indicated that the parallel transition is actually from log slope zero (rate independent of HDEHP concentration) to 1.5, instead of from 0.5 to 1.5. Zero slope implies rate control involving a saturation with some critical species, and saturation with the most plausible species proved to imply that the kinetics should be zero order instead of first order with respect to iron. Tests over a range of iron concentrations[10] showed that the extraction rate is indeed zero order with respect to iron in the transition region, although it is first order at lower and higher HDEHP concentrations.

At present, the best model for the extraction mechanism involves the following reactions, all limited to the interface:

$$Fe(H_2O)_6{}^{3+} + HA_2{}^- \overset{1d}{\rightleftharpoons} (H_2O)_5FeOH^{2+} + (HA)_2 \rightleftharpoons (H_2O)_5FeA^{2+} \cdot HA + H_2O \qquad (F)$$

$$HA \Big\updownarrow \qquad (G)$$

$$Fe(H_2O)_6{}^{3+} + A^- \overset{1m}{\rightleftharpoons} (H_2O)_5FeOH^{2+} + HA \rightleftharpoons (H_2O)_5FeA^{2+} + H_2O \qquad (D)$$

$$HA \quad H^+ \Big\updownarrow \qquad (H)$$

$$(H_2O)_5FeA^{2+} \cdot HA \rightleftharpoons (H_2O)_5FeA^{2+} \cdot H^+ + A^- \overset{2,2s}{\rightleftharpoons} (H_2O)_4FeAOH^+ + HA + H^+ \rightleftharpoons (H_2O)_4FeA_2{}^+ + H_2O + H^+ \qquad (J)$$

$$(H_2O)_5FeA^{2+} + HA_2{}^- \overset{2d}{\rightleftharpoons} (H_2O)_4FeAOH^+ + (HA)_2 \rightleftharpoons (H_2O)_4FeA_2{}^+ \cdot HA + H_2O\ . \qquad (E)$$

---

[9] *Chem. Technol. Div. Ann. Progr. Rept. May 31, 1967*, ORNL-4145, p. 229.

[10] The conventional test for reaction order, by linearity of either ΔM vs t or $\Delta \log M$ vs t, failed because most tests were limited to a small fraction (<5%) of the equilibrium extraction. For either order, both plots appear essentially linear at least up to 10% reaction. Extension of the test runs until definite curvature appeared would not be useful unless we made a detailed study of the reverse reaction, which could also introduce curvature.

The steps that can control the rate are labeled accordingly as they involve introduction of the first or the second ligand, via reactions starting with dimer ion, monomer ion, or no independent ion. When step 2 of (*J*) is rate controlling because the interface is saturated with $(H_2O)_5FeA^{2+} \cdot HA$, it is designated 2*s*. Apparently the diligand species $(H_2O)_4FeA_2^+$, etc., enter the bulk organic phase for further (fast) reactions to produce $FeA_3 \cdot 3HA$.

The foregoing reactions, together with the dimerization and ionization equilibria of HA, show that the steps 1*d*, 1*m*, and 2*d* give rates that are first order with respect to aqueous-phase iron:

$$\text{rate} = -d[\text{Fe}]/dt = d[\text{Fe}]_{\text{org}}/dt = k[\text{Fe}] ,$$

$$\text{rate}/[\text{Fe}] = k_{1m} \propto [\Sigma\text{HA}]^{0.5}/[\text{H}^+]$$

$$k_{1d} \propto [\Sigma\text{HA}]/[\text{H}^+]$$

$$k_{2d} \propto [\Sigma\text{HA}]^{1.5}/[\text{H}^+]^2 .$$

Step 2 gives a rate that is zero order with respect to aqueous-phase iron:

$$\text{rate} = k_2 \propto [\Sigma\text{FeA}^{2+}]_{\text{interface}}/[\text{H}^+]$$

$$\propto [\Sigma\text{HA}]^{0.5}/[\text{H}^+]^2 .$$

As the interface approaches saturation so that $[\Sigma\text{FeA}^{2+}] \approx$ constant, this becomes:

$$\text{rate} = k_{2s} \propto 1/[\text{H}^+] .$$

At low $[\Sigma\text{HA}]$, the path is through 1*m* (plus 1*d*) and 2. Step 1*m* is rate controlling at HA concentrations below 0.004 *M*; it is faster than 1*d* (parallel) and slower than 2 (series). As $[\Sigma\text{HA}]$ is increased, the rate increases in proportion to a power of $[\Sigma\text{HA}]$ between square root (1*m*) and first power (1*d*). At an intermediate ΣHA concentration, most of the interface becomes covered by first-step products, so that control shifts from 1*m* and 1*d* to 2*s*. Then, as $[\text{HA}_2^-]$ increases with increasing $[\Sigma\text{HA}]$, control shifts to 2*d*. At high $[\Sigma\text{HA}]$, the path is through 1*d* and 2*d* (plus 2); 2*d* is controlling because it is slower than 1*d* (series) and faster than 2 (parallel).

These parallel and series steps combine so that the net observed rate/[Fe] is:

$$r = \frac{(r_{1m} + r_{1d})(r_{2s} + r_{2d})}{r_{1m} + r_{1d} + r_{2s} + r_{2d}} . \qquad (K)$$

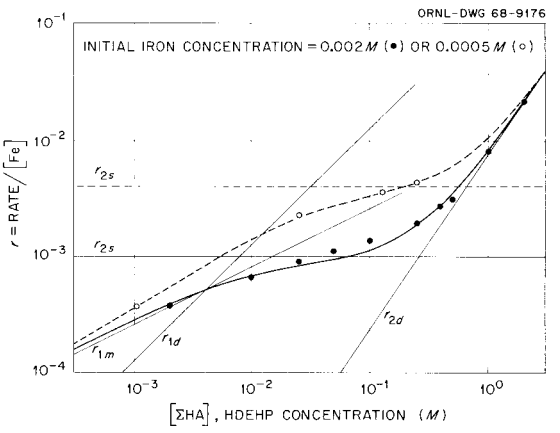

Fig. 10.3. Kinetics of Iron(III) Extraction from Acid Perchlorate Solution by HDEHP (HA) in *n*-Octane. Initial acid concentration = 0.052 *M*. Points: experimental; curves: calculated from

$$-\frac{d[\text{Fe}]/dt}{[\text{Fe}]} = r = \frac{(r_{1m} + r_{1d})(r_{2s} + r_{2d})}{r_{1m} + r_{1d} + r_{2s} + r_{2d}} ,$$

where

$$r_{1m} = 4.0 \times 10^{-4}[\Sigma\text{HA}]^{0.5}/[\text{H}^+],$$

$$r_{1d} = 6.8 \times 10^{-3}[\Sigma\text{HA}]/[\text{H}^+],$$

$$r_{2s} = 1.03 \times 10^{-7}/[\text{H}^+][\text{Fe}],$$

$$r_{2d} = 2.1 \times 10^{-5}[\Sigma\text{HA}]^{1.5}/[\text{H}^+]^2.$$

Each r_i is established by its theoretical log slope vs $[\Sigma\text{HA}]$ and an empirically fitted coefficient which is its intercept at unit $[\Sigma\text{HA}]$ (see Fig. 10.3). These four empirical coefficients were evaluated by least-squares fitting to the experimental data at two acidities and several iron concentrations. Figure 10.3 shows plots of the resulting Eq. (*K*) at one acidity and two iron concentrations, together with the corresponding experimental points. Points at higher and lower acidities also agree with Eq. (*K*).

The nature of reactions (*D*) through (*J*) suggests further analogous reaction steps that might be involved, especially

$$(H_2O)_5FeA^{2+} + A^- \overset{2m}{\rightleftharpoons} (H_2O)_4FeAOH^+ + HA$$

$$\rightleftharpoons (H_2O)_4FeA_2^+ + H_2O ,$$

$$k_{2m} \propto [\Sigma\text{HA}]/[\text{H}^+]^2 ;$$

$$(H_2O)_5FeA^{2+} \cdot HA + HA_2^-$$
$$\overset{2df}{\rightleftharpoons} (H_2O)_4FeAOH^+ + HA + (HA)_2$$
$$\rightleftharpoons (H_2O)_4FeA_2^+ \cdot HA + H_2O ,$$

$$k_{2df} \propto [\Sigma HA]^2/[H^+]^2 .$$

However, the fitting of coefficients so far indicates that these are less important.

It was previously shown,[9] in support of reactions (*D*) and (*F*), that the iron extraction at low $[\Sigma HA]$ is faster when proton-accepting complexers such as acetate are present, in accordance with the predicted reactions

$$Fe(H_2O)_6^{3+} + X^- \rightleftharpoons (H_2O)_5FeOH^{2+} + HX$$
$$\rightleftharpoons (H_2O)_5FeX^{2+} + H_2O ,$$

$$(H_2O)_5FeX^{2+} + HA \rightleftharpoons (H_2O)_5FeA^{2+} + HX .$$

This was found to be true at high $[\Sigma HA]$ also, which supports reaction (*E*). As shown below, addition of 1 *M* acetate to the aqueous solution (pH 1) doubled the rate/[Fe] at 1 *M* HA:

$[\Sigma HA]_{org}$	$[Acetate]_{aq}$	Rate/[Fe]
0.1	0	0.0006
	0.1	0.0105
1	0	0.0066
	0.1	0.0128

It is also noteworthy that the rate with 0.1 *M* HA and 0.1 *M* acetate nearly equaled that with 1 *M* HA and 0.1 *M* acetate. This is consistent with the hypothesis that the slow steps through A^- or HA_2^- are bypassed by a faster parallel path through the acetate.

Zirconium-Synergized Extractions

The extraction of various metal ions by several organophosphorus acids is synergistically enhanced by the presence of small amounts of zirconium or hafnium (Sect. 10.5). Qualitatively, equilibration appeared to be slower in at least some of the synergistic extractions than in the corresponding extractions without zirconium. Hence, we have started measurements of the kinetics of this system. Initial tests confirmed a decrease in the rate of cerium(III) extraction by 0.5 *M* 2-ethylhexyl phenylphosphonic acid, HEH[ϕP], in *n*-octane from a 0.5 *M* HCl–0.5 *M* NaCl solution that was 0.08 *M* in zirconium. The extractant HEH[ϕP] was chosen for this study because it has been used extensively in the equilibrium studies and because it gives a large synergistic shift. However, the HEH[ϕP] of highest purity available at present still contains a component that slowly precipitates zirconium; thus, the kinetic measurements are being delayed until we can obtain a higher-purity extractant.

10.7 AGGREGATION AND ACTIVITY COEFFICIENTS IN SOLVENT PHASES

Techniques for Measuring Vapor-Pressure Depression

For several years, a commercial matched-thermistor vapor-pressure osmometer[11] has been used increasingly for determining the effective molecular weights of solutes in organic solutions. We have found it to be rapid and convenient for estimating aggregation numbers but less reproducible than is desirable for calculating activity coefficients.[12] Recently, another matched-thermistor vapor-pressure osmometer has been introduced;[13] its sensitivity is advertised to be ten times that of the earlier instrument while remaining constant over a broad range of molecular weights. In a test of this instrument, we confirmed its sensitivity and found results to be reproducible down to solute concentrations of 0.002 *M*. However, the failure of the two low-slope curves in Fig. 10.4 to approach $\bar{n} = 1$ as the amine salt concentration approaches zero suggests that a systematic error in calibration or performance became significant below about 0.01 *M*. The instrument was simple and rapid to use, except for a tendency of the solution delivery tube system to plug and the susceptibility to failure of one electronic component. An inherent disadvantage, which would seriously limit the instrument's applicability to our work, is that it must be used at a temperature at least 10°C above ambient temperature (i.e., $\gtrsim$35°C).

---

[11] Mechrolab, Inc., Mountain View, Calif.

[12] *Chem. Technol. Div. Ann. Progr. Rept. May 31, 1967*, ORNL-4145, p. 231.

[13] Hitachi Perkin-Elmer model 115 osmometer.

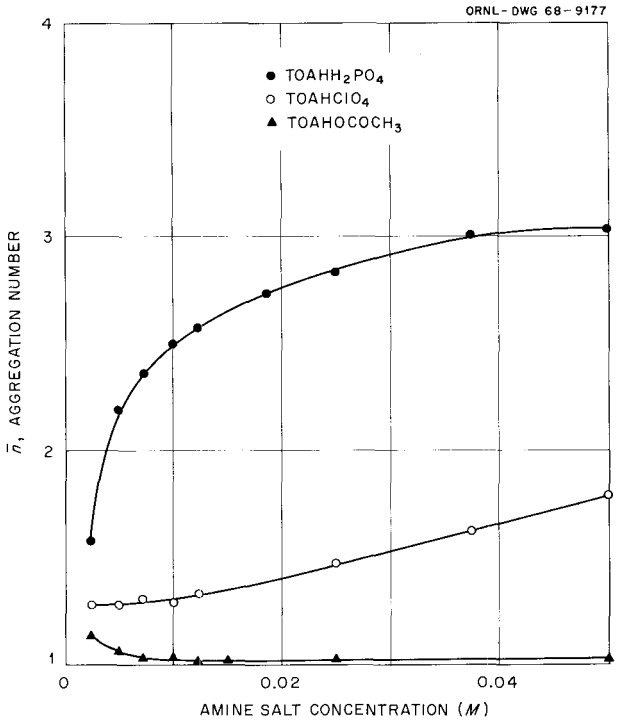

Fig. 10.4. Degree of Aggregation of Tri-*n*-octylamine Salts in Dry Benzene at 35.5°C. Measured in trials of Hitachi Perkin-Elmer Osmometer, which was calibrated against triphenylmethane.

Benzil as a Reference Standard

Benzil (dibenzoyl, $C_6H_5COCOC_6H_5$) is widely used as a standard for calibrating matched-thermistor osmometers and promises to be a useful reference solute in isopiestic vapor-pressure balancing measurements. We determined its osmotic behavior in dry benzene solutions at 25°C by isopiestic balancing against triphenylmethane (TPM), for which the osmotic coefficient $\phi = 1 - 0.5743m_{TPM} + 0.3583m^2_{TPM}$, $m \leq 0.33$. The measured values fit the following equation for the osmotic coefficient of the benzil solutions:

$$\phi = 1 - 0.8197m_{benzil} + 0.7970m^2_{benzil},$$

which is valid at benzil concentrations up to 0.33 *m*. The benzil deviates from ideality by 7 and 18%, respectively, at concentrations of 0.1 and 0.33 *m*; these deviations are only slightly more than those observed for triphenylmethane (5 and 15%) at the same concentrations.

Aggregation Numbers for a Carboxylate Extractant

Aggregation numbers for a carboxylate extractant dissolved in an aliphatic hydrocarbon, needed in equilibrium extraction studies (Sect. 10.5), were measured by means of a matched-thermistor vapor-pressure osmometer.[11] The extractant is a mixture of α,α-dialkylcarboxylic acids, containing about 17 carbons, that were obtained as a narrow distillation fraction from a developmental acid mixture, "Versatic Acid 1519." *n*-Hexane was used as the diluent because the preferred diluent, *n*-octane, is not sufficiently volatile. The instrument was calibrated against azobenzene, assumed to be ideal in the concentration range used, 0 to 0.05 *M*. (A benzene solution of azobenzene deviates from ideality by less than 5% at 0.05 *M*.[14] The aggregation number was initially 2, as expected for carboxylic acids in general, and increased rapidly with conversion of the acid to the sodium salt (Fig. 10.5). There was no significant difference between total carboxylate concentrations of 0.05 and 0.10 *M*. The aggregation number reached 4 at 25% neutralization ($NaA/\Sigma A = 0.25$), which is in agreement with the proposed composition of one of the species, NaA • 3HA (Sect. 10.5), in the extract. Beyond 40% neutralization, the aggregation number exceeded the sensitivity of the instrument.

[14] *Chem. Technol. Div. Ann. Progr. Rept. May 31, 1964*, ORNL-3627, p. 207.

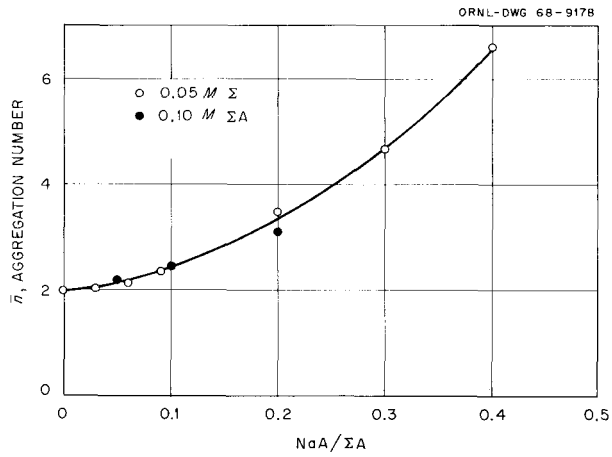

Fig. 10.5. Degree of Aggregation, $\bar{n}$, of Carboxylic Acid–Sodium Carboxylate Mixtures in *n*-Hexane. Mixture of branched acids, $HA = RR'R''CCO_2H \approx C_{16}H_{33}CO_2H$, a fraction from "Versatic Acid 1519."

Water in Extractant Phases

In the continued study of the role of water in organic solutions of extractants, the solubility of water in benzene solutions of tri-*n*-octylamine (TOA) and several of its salts was measured as a function of water activity and amine concentration.

Diluent. – Calculation of the amount of water associated with each solute requires accurate knowledge of the amount of water dissolved by the diluent itself. We developed a sensitive gravimetric determination for water in benzene and other volatile diluents. A paper describing this technique has been accepted for publication in *Talanta*. Its abstract follows:

J. W. Roddy and C. F. Coleman, "Solubility of Water in Hydrocarbons as a Function of Water Activity." *Abstract*: "A method is described for determination of low solubilities of water in organic liquids (such as are used in solvent extraction) by vacuum distillation of a suitable-sized equilibrated sample through magnesium perchlorate in a conventional weighing tube. Tritium tracer is used to estimate completeness of water absorption. At the same time, the results serve to evaluate the ratio of tritium and water distribution coefficients for use in collateral determinations of water solubility by simple liquid-liquid distribution. The solubility of water in benzene, *n*-hexane, and cyclohexane is respectively 0.0363, 0.00362, and 0.00345 *M*. The dissolved water follows Henry's law constants respectively 0.00323, 0.000476, and 0.000375 (mole fraction scale)."

Measurements by this method showed a bias in the previously reported[15] measurements by liquid-liquid distribution in several diluents. Table 10.4 gives the corrected values, together with the separation factor found for water over tritium, $\alpha = D_a^o(H_2O)/D_a^o(HTO)$, in extractions from aqueous solutions.

This method also shows promise as a means for accurately determining the concentration of water in nonvolatile materials that can be dispersed in a dry volatile diluent. To test this possibility, we saturated tributyl phosphate (TBP) with water, dissolved 5-ml samples of the water-saturated TBP in 50-ml volumes of dry benzene, and proceeded as described in the paper cited above. The water content of the TBP averaged 3.61 ± 0.02 *M* for three runs; this value is in excellent agreement with the previous carefully determined value[16] of 3.58 ± 0.02 *M*.

Table 10.4. Solubility of Water in Common Diluents at 25°C

Diluent	Solubility[a] (*M*)	Henry's Law Constant (mole fraction scale)	α^b
Chloroform[c]	0.0753		1.17
Benzene	0.0363	0.00323	1.07
Cyclohexane	0.00345	0.000375	1.27
n-Hexane	0.00362	0.000476	1.23
n-Octane	0.00317	0.000518	1.22

[a]For each diluent except chloroform, the molar solubility is also the Henry's law constant on the molarity scale.

[b]α = ratio of distribution coefficients, $D_a^o(H_2O)/D_a^o(HTO)$.

[c]Measured immediately after scrubbing stabilizing alcohol from the chloroform.

Free-Base Amine. – The water extracted by benzene solutions of tri-*n*-octylamine, corrected for the water extracted by benzene alone, proved to vary linearly both with water activity and with amine concentration up to 0.0138 *M* water at 0.5 *M* amine. Thus, the water solubility may be summarized by the equation

$$\Delta M_w = M_w - M_{w/benzene}$$

$$= 0.0275 M_{TOA} a_w , \qquad M_{TOA} \leq 0.5 .$$

This linearity suggests that the water is associated with the amine principally in a 1 : 1 mole ratio (i.e., as amine monohydrate). Accordingly, the following equations were fitted and solved by a nonlinear least-squares method to evaluate $Q_{Bw} = [TOA \cdot w]/[TOA][w]$, the concentration quotient for formation of the hydrate:

$$\Delta M_w = Q_{Bw} C_B C_w ,$$

$$M_{TOA} = C_B Q_{Bw} C_B C_w ,$$

$$C_w = 0.0363 a_w ,$$

where C_B and C_w are the concentrations of unassociated amine and water, respectively, and 0.0363

[15]*Chem. Technol. Div. Ann. Progr. Rept. May 31, 1967*, ORNL-4145, p. 232.

[16]J. W. Roddy and J. E. Mrochek, *J. Inorg. Nucl. Chem.* **28**, 3019 (1966).

is the concentration (M) of water in benzene at $a_w = 1$. These equations are valid if the amine monohydrate is the only complex present and if each solute species follows Henry's law. These assumptions are supported by the good degree of fit, as shown by the standard error of the resulting value of the formation quotient:

$$Q_{Bw} = 0.858 \pm (\sigma = 0.006) .$$

Since Mohr *et al.*[17] have reported that organic bases tend to form dimer hydrates, $B_2 \cdot H_2O$, at higher base concentrations, we attempted to fit the same data to equations for formation of both $B \cdot H_2O$ and $B_2 \cdot H_2O$. However, the best fit that could be obtained, $Q_{Bw} = 0.875 \pm (\sigma = 0.024)$, $Q_{B_2w} = -0.046 \pm (\sigma = 0.062)$, did not change Q_{Bw} significantly except to increase its standard error. It could not distinguish Q_{B_2w} from zero, thus indicating that very little, if any, dimer hydrate is formed at 0.5 M TOA.

Amine Salts. – The solubility of water in 0.1 N benzene solutions of tri-*n*-octylamine salts (water extracted, corrected for the water extracted by benzene alone, Fig. 10.6) conformed to Henry's law, at least over a short range, with all the salts tested except the perchlorate.

Salt	Henry's Law Constant (molarity scale)	Maximum Applicable a_w
TOAHCl	0.101	1
$TOAHHSO_4$	0.09	0.6
$TOAHNO_3$	0.064	0.85
$(TOAH)_2SO_4$	0.02	0.4
$TOAHOCOCH_3$	0.012	1

The linear response with the chloride, nitrate, and acetate suggests that monohydrates are formed; that is, one water molecule associates with one monomer or polymer unit of the amine salt. The sharply breaking solubility curves for the sulfate and bisulfate suggest that higher hydrates are also formed; that is, $(TOAH)_2SO_4 \cdot 4H_2O$ and $(TOAHHSO_4)_3 \cdot 8H_2O$ are estimated to be present from the slopes of the corresponding logarithmic plots. At higher concentrations of normal amine sulfate, the solubility curves were similar to the curve in Fig. 10.6, with higher water : sulfate mole

[17] S. C. Mohr, W. D. Wilk, and G. M. Barrow, *J. Am. Chem. Soc.* **87**, 3048 (1965).

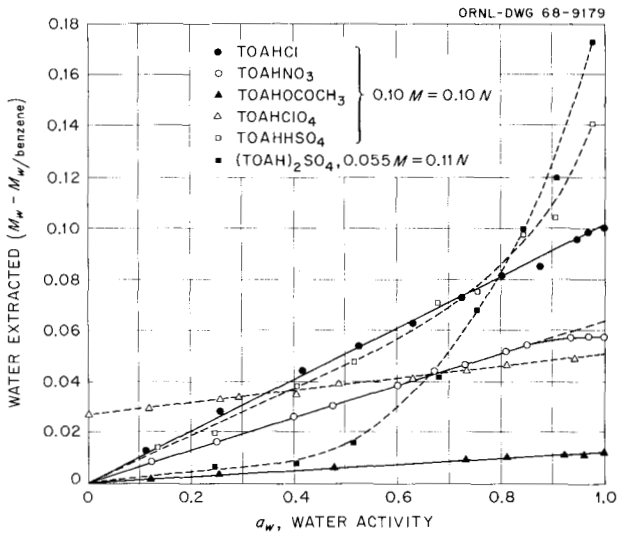

Fig. 10.6. Extraction of Water by Tri-*n*-octylamine Salts in Benzene Solution from Aqueous Solutions at 25°C and at Various Water Activities.

Table 10.5. Mole Ratio of Water to Tri-*n*-Octylamine Normal Sulfate in Benzene

$[(TOAH)_2SO_4]$ (M)	$[H_2O]/[(TOAH)_2SO_4]$	
	$a_w = 0.5$	$a_w = 0.9$
0.055	0.32	2.3
0.075	0.65	3.4
0.503	1.10	5.1

ratios (Table 10.5), but still indicating the formation of both monohydrate and tetrahydrate.

The concentration of water in the 0.1 N TOA perchlorate was also a linear function of water activity but did not decrease to zero at $a_w = 0$. The residual water content (0.027 M), as measured by tritium tracer and corrected for the exchangeable proton of the trialkylammonium ion, could not be removed by treatment with magnesium perchlorate, either by direct contact or through the vapor phase. This appears to indicate a very stable hydrate with a water : perchlorate mole ratio of 1 : 3 or 1 : 4 and hence aggregation of the amine perchlorate to at least the trimer or the tetramer. However, 0.0206 N $TOAHClO_4$ similarly has a water content of 0.0064 M (mole ratio = 0.31), which again appears to indicate aggregation to at least trimer or tetramer, while vapor-pressure measurements, on the other hand (see Fig. 10.4), showed that 0.02 M $TOAHClO_4$ is not aggregated even to dimer.

11. Chemical Applications of Nuclear Explosions

The purpose of this program is to provide research and development in selected areas of the Plowshare Program, especially those areas requiring knowledge of chemistry or metallurgical engineering to determine feasibility. Areas in which research was performed during the past year included:

1. studies of the distribution and possible fate of radionuclides formed during the use of nuclear devices to aid in the recovery of copper from ore deposits,
2. studies of the distribution and possible fate of radionuclides formed during the use of nuclear devices to aid in the recovery of oil from shales.

Knowledge of the thermal stability and the high-temperature reactions of actinide compounds is pertinent to the possible production of these compounds through the use of thermonuclear devices. A description of related studies to determine some of these data by differential thermal analysis and thermogravimetric analysis techniques appears in Sect. 6 of this report.

11.1 COPPER ORES

Fracturing of copper ores with nuclear explosives, followed by leaching in place, is being studied for the AEC by Lawrence Radiation Laboratory (LRL) and by the U.S. Bureau of Mines at Tucson, Arizona. The Oak Ridge National Laboratory is cooperating in this program by studying potential problems that might arise from the presence of radioactive contaminants in the processing cycle. The proposed flowsheet for recovering copper includes percolating a leaching solution of dilute sulfuric acid down through the nuclear-broken ore to dissolve the copper, collecting the leach liquor at the bottom of the ore body and pumping it to the surface, recovering a copper concentrate from the solution by cementation on iron, and recycling the barren solution, after fortifying it with acid, for use in the leaching step. The cement copper is then smelted into a consumable anode and purified by electrolysis.

Status and Progress

Previous studies have indicated that ^{106}Ru is probably the only radioisotope of importance with respect to radiocontamination of the cement copper.[1] The ruthenium follows the copper through the smelting step but is separated efficiently from it during electrolysis. Recent test results showed, as expected, that essentially ruthenium-free copper products can also be produced by electrowinning copper from solutions prepared by dissolving the contaminated cement copper in sulfuric acid. This is an alternative to the smelting-electrolysis method. Treating the cell electrolyte with ozone (to oxidize and volatilize ruthenium) offers a means of isolating ^{106}Ru, which tends to build up in the cell electrolyte.

Purification of Cement Copper

As an alternative to processing cement copper by smelting-electrolysis, cement copper contaminated with ^{106}Ru was purified by dissolution in aerated 1 *N* sulfuric acid at 80°C and subsequent electrolysis of the solution to deposit the copper on a copper anode. "Electrowinning" is the term generally applied to such an operation. In the sulfuric acid dissolution step, about two-thirds of the ^{106}Ru dissolved. About 0.5% of the cement copper, which was insoluble in the acid solution, settled out as a finely divided black sludge that contained

[1] *Chem. Technol. Div. Ann. Progr. Rept. May 31, 1967*, ORNL-4145, p. 234.

the remaining one-third of the ^{106}Ru. The copper products contained less than 2% of the ruthenium that was initially present in the cement copper.

Control of Ruthenium

When air or oxygen containing ozone was passed through heated electrolyte solution, up to 78% of the ruthenium was volatilized from the solution and was subsequently sorbed on activated carbon. This suggests a method for limiting the buildup of ^{106}Ru in the cell electrolyte and providing for its eventual disposal. In a series of small-scale continuous tests, a preheated solution (simulated electrolyte) that was 1 *N* in H_2SO_4 and contained 25 g of copper and 0.032 μc of ^{106}Ru per milliliter was fed at the rate of 3 ml/min to a heated reactor, where it was mixed with a stream of ozonized air or oxygen. The removal of ruthenium from the solution was more efficient at 90°C than at 80°C. With a solution residence time of 15 min at 90°C, the amount of volatilized ruthenium increased only slightly (from 73 to 78%) when the ozone feed rate was increased from 3.7 to 7.8 mg/min. The gas contained 26 to 46 mg of ozone per liter, and the gas flow rate varied from 140 to 270 cc/min in these tests. The efficiency of ozone utilization (only about 5% of the ozone was consumed in the reactor) can undoubtedly be improved by changing the reactor design to improve the gas-liquid contact and by optimizing the temperature, contact time, ozone concentration, and gas flow. Activated carbon was highly effective for removing ruthenium from the gas stream. A 1-g sample of activated carbon (type OL, 20 × 50 mesh, Pittsburgh Chemical Company) sorbed 5 μc of ^{106}Ru without measurable breakthrough. In a test to measure the loading capacity of the carbon, a 0.01-g sample was loaded with 21 μc of ^{106}Ru, which is equivalent to more than 2 mc per gram of carbon.

Calculations indicate that the ^{106}Ru concentration in the cell electrolyte could be maintained at a tolerable level by processing only a small fraction of the total cell electrolyte daily. For example, assuming an ^{106}Ru concentration in the cement copper of 0.1 $\mu c/g$ (probably the maximum concentration that would be encountered) and a removal efficiency of 70% in the ozone treatment, the daily processing of about 6% of the electrolyte would limit the steady-state ^{106}Ru concentration in the electrolyte to 0.1 $\mu c/ml$; the processing of 15% would limit the concentration to only 0.04 $\mu c/ml$. These calculations are based on the assumption that no electrolyte would be lost from the cell.

An equivalent removal of ruthenium from the electrolyte solution was obtained by using sodium persulfate solution as the oxidant and passing a stream of preheated air through the solution. However, in this case, the ruthenium that was released from the solution plated on the equipment walls and, therefore, was not carried out of the system in the air stream.

Tritium Behavior in Copper Leaching

Assuming that a thermonuclear device is used to aid in recovering copper from ore deposits, tritium (as tritiated water) will be the dominant radionuclide in the chimney of nuclear-broken ore. Previously, when a column of copper ore was wetted with tritiated water and then leached, the tritiated water was readily washed from the ore before any significant amount of copper was dissolved.[2] Consequently, the initial portions of effluent could be discarded to reduce the tritium hazard in the copper processing operation. The previous results were confirmed in a test made under conditions that more closely resemble those expected in an actual chimney. Before being leached with dilute sulfuric acid, the copper ore was heated at 85°C for one week in a tightly stoppered column containing tritiated water (0.6 μc per gram of ore) to provide an opportunity for the tritiated water to exchange with bound water in the ore. As in the earlier test, most of the tritium was washed from the ore in the first portions of column effluent. The first 0.5 bed volume of effluent contained more than 80% of the tritiated water and less than 0.5% of the copper that was initially present in the column.

11.2 RECOVERY OF OIL FROM SHALE

The feasibility of recovering oil from Green River oil shales by using a nuclear device to fracture the shale and then retorting the oil in place is being studied by several government agencies and commercial companies. The Oak Ridge National Laboratory is participating in this program by studying

[2] *Chem. Technol. Div. Ann. Progr. Rept. May 31, 1966*, ORNL-3945, p. 192.

the oil recovery system with regard to the behavior of the radioactive contaminants that would be formed in the nuclear detonation.

Status and Progress

Results of scoping tests indicated that the contamination of shale oil by fission products should not be a serious obstacle to using a nuclear device to break the shale. Oil that had been heated with test-shot debris and had become slightly contaminated could be effectively decontaminated by distillation. Most of the radioactive material, which was initially present in the oil as finely dispersed solids, remained in the pot residue.

The problem concerning the contamination of the oil by tritium (from a fusion device) appears to be more serious. Oil retorted from shale after prolonged exposure to tritiated water vapor (in a sealed flask at elevated temperatures) contained tritium; when the oil was distilled, each of the fractions also contained tritium. Tritium apparently is incorporated in the hydrocarbons of the shale during the exposure to tritiated water vapor.

Behavior of Tritium

In an earlier test, the retorting of shale that had simply been moistened with tritiated water just prior to retorting was found to produce oil that was contaminated with tritium.[3] In the most recent tests, the shale was heated with tritiated water vapor in a sealed flask. Then it was washed thoroughly with water and was dried to remove entrained water preparatory to retorting. Tritium contamination of the oil increased as the time of exposure of the shale to tritiated water vapor at 85°C increased and as the tritium concentration in the water increased (Table 11.1). It decreased as the water-to-shale ratio (milliliter of water per 100 g of shale) increased. The oil derived from retorting shale that had been exposed for 29 days at 85°C to tritiated water vapor at a level of 1 μc of tritium per gram of shale contained 0.92 μc of tritium per gram. Oil retorted from shale that had been equilibrated under these same conditions for one or eight days contained tritium at a concentration that was 61 or 83%, respectively, of that obtained in 29 days. For a constant water-to-shale ratio, the degree of tritium contamination of the oil varied almost linearly with the tritium concentration of the water. When the tritium-to-shale ratio was held at 1 μc/g and the water-to-shale ratio was increased by a factor of 3.3, the tritium concentration in the oil (after equilibration for eight days in each case) was lower by a factor of 2.3.

None of the tritium was removed from the oil by contacting it with solid drying agents ($CaCO_3$, $CaCl_2$, Na_2SO_4) or washing with water; this tended

[3] *Chem. Technol. Div. Ann. Progr. Rept. May 31, 1967*, ORNL-4145, p. 239.

Table 11.1. Tritium Concentration in Shale Oil

Shale Treatment Conditions[a]			Tritium in Oil Retorted[b] from Treated Shale (μc per gram of oil)
Water/Shale Ratio (ml of H_2O per 100 g of shale)	Tritium/Shale Ratio (μc of tritium per gram of shale)	Days at 85°C	
1	1	1	0.56
1	1	8	0.76
1	1	29	0.92
1	0.1	25	0.078
1	12	25	9.6
3.3	1	8	0.33

[a] 100 g of shale (−0.31 +0.19 in.) heated at 85°C with tritiated water in a sealed 1-liter flask.

[b] In small retort described previously;[3] 12 to 13 g of oil per 100 g of shale is produced in the temperature range 300 to 430°C.

Table 11.2. Distillation of Tritium-Contaminated Shale Oil

Distillation Fraction				Tritium Concentration (% of the concentration in the feed shale oil)
Descriptive Name	Pressure	Temperature (°C)	Percent by Volume	
Naphtha	Atmospheric	To 200	10	91
Light oil	40 mm Hg	To 225	26	66
Heavy oil	40 mm Hg	225–300	29	84
Residuum	40 mm Hg		33	98

Table 11.3. Results of Leaching Test-Shot Debris with Shale Oil

Procedure: 5.2 g of test-shot debris heated successively with three 25-ml portions and two 50-ml portions of shale oil at 220°C under reflux. The contact time for each leach was 4 hr. The oil was centrifuged before analysis

Radionuclide	Concentration in Debris (dis min^{-1} g^{-1})	Radioactivity of Combined Oil Samples (% of initial)
^{95}Zr-Nb	9.3×10^7	2.0
^{103}Ru	1.9×10^7	5.2
^{141}Ce	1.4×10^7	2.1
^{140}Ba-La	2.8×10^6	1.1
Gross gamma[a]	3.5×10^7	7.6

[a]Gross gamma activity measured in counts min^{-1} g^{-1}.

to confirm that the tritium in the oil is not present in the form of entrained tritiated water. It suggests that the tritium is present as part of the hydrocarbon structure, since bound tritiated water would be expected to exchange with water in the water washes. The concentrations of tritium, expressed as percentages of the tritium concentration in the feed shale oil, in each of the volatile fractions of a sample of tritiated oil and in the residuum are shown in Table 11.2. Surprisingly, the data show practically no fractionation of the tritiated species. The concentration of tritium in the residuum was approximately equal to that found in the oil before distillation.

The level of tritium (1 μc per gram of shale) used in most of these tests was probably not much different from that which might be expected in an actual operation. However, a very large extrapolation would have to be made from the conditions of these tests to the conditions that would apply in a nuclear test; therefore, the data, rather than having quantitative significance, should be used only to support the contention that appreciable contamination of the oil with tritium may occur.

Results of preliminary tests indicate that it may be possible to remove most of the tritium from tritiated shale by passing water-saturated air through the chimney of broken ore prior to retorting. Evaluation of this possibility is being emphasized in present test work.

Fission Product Behavior

When a 5.2-g sample of test-shot debris (several months old) was heated successively with three 25-ml portions and two 50-ml portions of shale oil at 220°C under reflux, the combined oil samples contained 7.6% of the gross gamma activity of the debris (Table 11.3). Most of the activity of the oil

was due to ^{95}Zr-Nb (60%) and ^{103}Ru (30%), the dominant radionuclides detected in the debris. The combined oil samples contained about 2% of the ^{95}Zr-Nb and 5% of the ^{103}Ru, along with 2% of the ^{141}Ce, initially present in the debris. The longer-lived radionuclides ^{106}Ru, ^{137}Cs, and ^{144}Ce were not detected in this analysis of the debris because of interference with the radiometric analysis by the high concentrations of the shorter-lived radionuclides. The results confirm and extend those from earlier tests with longer-cooled debris.[3] Much of the radioactivity of the oil was due to finely dispersed solids rather than dissolved radionuclides. When the contaminated crude oil was dissolved in hexane, an insoluble residue remained. This residue contained about 40% of the radioactive material but amounted to only 0.2% of the initial sample weight. An additional 45% of the radioactive material (0.9% of the sample weight) was filtered from the hexane on a Millipore filter containing stacked papers of 8-, 0.8-, and 0.1-μ pore sizes. Most of these solids were collected on the 8-μ paper. Further, when the contaminated oil was distilled, essentially all the radioactive material remained in the residuum.

12. Biochemical Separations

Macromolecular Separations

12.1 DEVELOPMENT OF REVERSED-PHASE CHROMATOGRAPHY SYSTEMS FOR TRANSFER RIBONUCLEIC ACID SEPARATIONS

During the past year the research and development activities associated with the biochemical separations program have continued to be directed toward the separation of *E. coli* transfer RNA's and related problems. Two new reversed-phase chromatography systems, RPC-3 and RPC-4 (see Table 12.1), were developed during a systematic evaluation of new quaternary ammonium salts for the separation of tRNA's. No diluent is employed in these systems; instead, the quaternary ammonium compound is deposited directly on the hydrophobic Chromosorb W support. The earlier systems, RPC-1 and RPC-2 (Table 12.1), have been described in preceding progress reports. All of these systems are similar in principle; essentially they consist of two-dimensional anion exchange materials (all the active exchanger is on the surface of the inert support) confined in a column. A sodium chloride gradient (i.e., a solution of gradually increasing NaCl concentration) is used to sequentially elute the individual tRNA's. Not all of these systems are equally useful for the preparation of the same purified individual tRNA's; frequently they can best be used in combination (rechromatography) to yield purified tRNA's.

A typical chromatogram of *E. coli* B crude tRNA on a 1- by 240-cm RPC-3 column (37°C) is shown in Fig. 12.1. Approximately 100 mg of crude tRNA was applied to the column and was eluted with a 3-liter elution gradient that was 0.25 to 0.70 *M* in NaCl, 0.01 *M* in $MgCl_2$, and 0.01 *M* in sodium acetate buffer and had a pH of 4.5. Excellent resolution of individual tRNA's was achieved; also, most, if not all, of the tRNA's displayed multiple peaks (i.e., the tRNA's were heterogeneous). The RPC-3 system has proved to be

Table 12.1. Reversed-Phase Chromatographic Systems

System Designation	Description	Reference
RPC-1	Dimethyldilaurylammonium chloride in isopentyl acetate; on Chromosorb W (AW-DMCS)[a]	*J. Biol. Chem.* **240**, 3979 (1965)
RPC-2	Tricaprylylmethylammonium chloride in tetrachlorotetrafluoropropane; on Chromosorb W (AW-DMCS)	*Biochemistry* **6**, 2507 (1967)
RPC-3	Trioctylpropylammonium bromide on Chromosorb W (AW-DMCS)	
RPC-4	Dimethyldilaurylammonium chloride on Chromosorb W (AW-DMCS)	

[a]Acid-washed dimethyldichlorosilane.

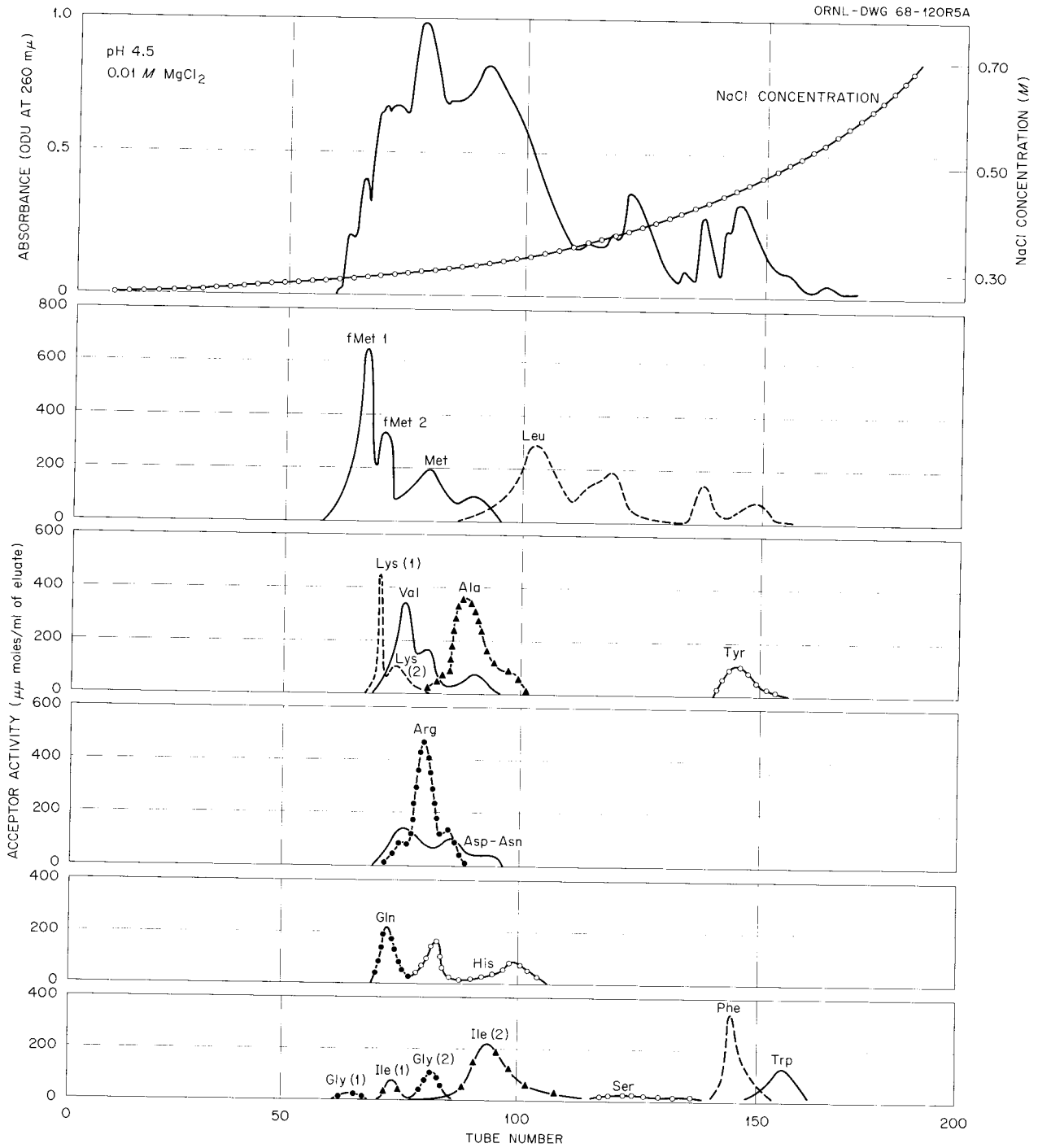

Fig. 12.1. Chromatogram of *E. coli* B Crude tRNA on an RPC-3 Column.

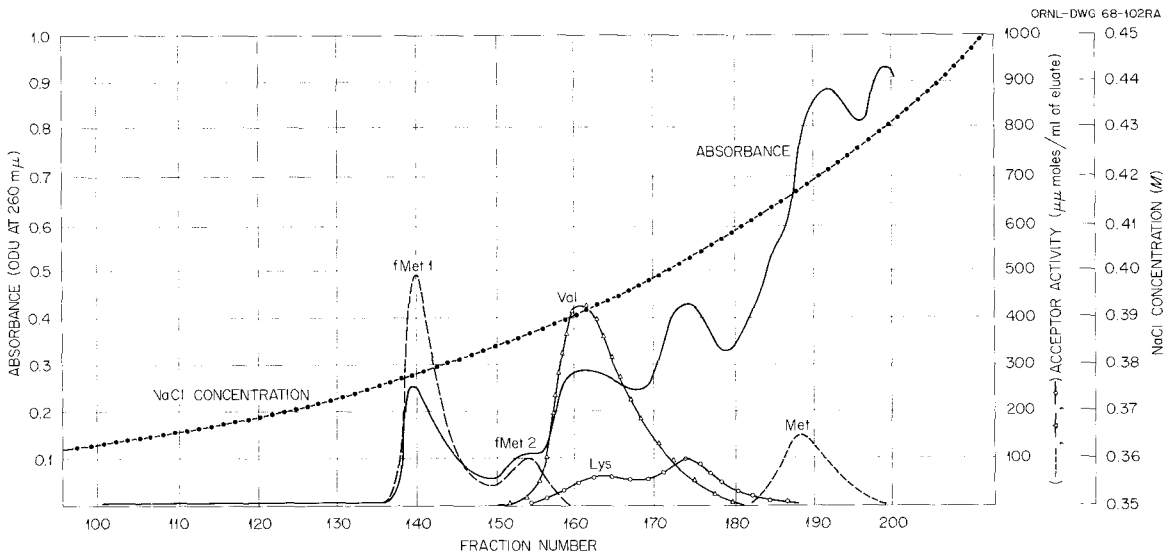

Fig. 12.2. Chromatogram of Methionine tRNA's from *E. coli* B Crude tRNA on a 1- by 240-cm RPC-3 Column. In addition to containing NaCl, the eluent was 0.01 *M* in $MgCl_2$ and 0.01 *M* in Tris buffer at pH 7.0.

particularly useful for the resolution of the methionine tRNA's. The initial portion of a chromatogram of *E. coli* B crude tRNA is shown in Fig. 12.2. It is obvious that individual amino acid-accepting peaks coincide with A_{260} peaks. The identification of the three methionine tRNA's, carried out in cooperation with Dr. Lee Shugart of the Biology Division, showed that the first two are formylmethionine tRNA's (i.e., tRNA's that are involved in the initiation of protein chains), while the third is the normal methionine tRNA.

12.2 ENGINEERING SCALE-UP OF BIOCHEMICAL SEPARATIONS TECHNIQUES

The principal aim of this portion of the program is the development and demonstration of engineering-scale procedures for the separation of large (gram) quantities of relatively pure transfer ribonucleic acids (tRNA's) from *E. coli* bacteria. As described last year, approximately 0.5 ton of *E. coli* (strain B) was grown in a fermenter at the Biology Division and processed to yield approximately 500 g of mixed tRNA's. This mixture was separated on RPC-1 columns to obtain the purified phenylalanine tRNA. The bulk of the tRNA's that were eluted ahead of the phenylalanine tRNA were reserved for further processing. One gram of phenylalanine tRNA product was recovered and has been distributed to scientific investigators throughout the world by the sponsoring agency, the National Institute of General Medical Science.

Since the phenylalanine acceptance activity of the product from these runs was not as high as predicted from previous laboratory experiments, a more detailed study has been made of the effects of various chemical and operating parameters on the performance of the RPC-1 column. Also, a method has been developed for pretreating tRNA feed on a diethylaminoethyl (DEAE) cellulose column to effect partial separation of several of the tRNA's from the phenylalanine tRNA; this pretreatment will simplify the subsequent separation of phenylalanine tRNA on RPC-1. By using the information obtained from these studies, we made an intermediate-scale test of the phenylalanine tRNA separation. The product obtained was more active than that prepared in the engineering-scale runs.

Effect of Process Parameters on the Separation of Phenylalanine tRNA on RPC-1 Columns

The elution sequence and the recovery of both tyrosine tRNA and tryptophan tRNA on RPC-1 columns were found to be strongly affected by the pH of the eluent. At a pH of 4.5, the tryptophan

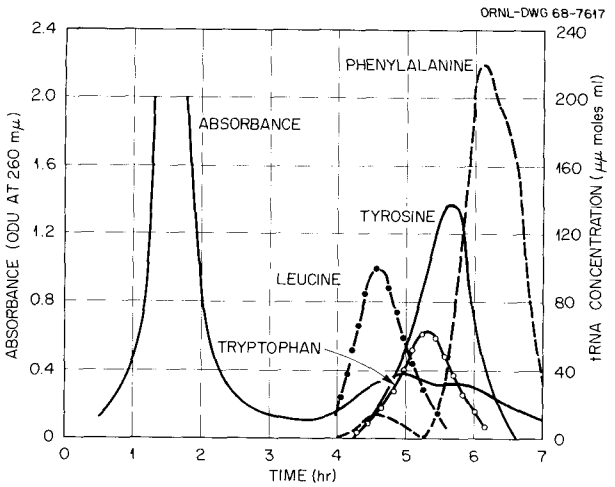

Fig. 12.3. Elution Sequence of tRNA's on RPC-1 Column. pH = 8.5.

tRNA was eluted with the phenylalanine tRNA, whereas the tyrosine tRNA was held on the column and only a trace was eluted just behind the phenylalanine tRNA peak. As the pH was increased, the tyrosine tRNA began to be eluted as a distinct chromatographic peak; however, both it and the tryptophan tRNA were moved forward with respect to the phenylalanine tRNA. At pH 8.5, the elution positions of the tyrosine tRNA and the tryptophan tRNA were sufficiently far ahead of the phenylalanine tRNA that it was possible to obtain a phenylalanine tRNA peak free of tryptophan and virtually free of tyrosine tRNA (see Fig. 12.3). Thus, operation at a pH of 8.5 is one feasible method for obtaining a product that is free of tryptophan tRNA. Operation at a pH above 8.5 is not practical since the recovery of both phenylalanine tRNA and tyrosine tRNA declines drastically, presumably as a result of hydrolysis of the tRNA's.

In an investigation of the significant operating parameters of the RPC-1 column, the following conclusions were drawn:

1. Within wide limits, the length of the column is not a significant variable; virtually the same separation of phenylalanine tRNA was achieved on 6-in.- and 24-ft-long columns. Also, the use of sequential columns of diminishing diameter did not improve the separation.
2. Columns can be operated at a relatively high flow rate (10 ml min^{-1} cm^{-2} as compared with a normal flow rate of 2 ml min^{-1} cm^{-2}) with only a slight loss in resolution.
3. When the column load is increased, the sodium chloride concentration of the eluent must be adjusted proportionally in order to achieve the same separation.
4. The resolving ability of a column deteriorates with its use, presumably because of gradual contamination of the column by materials in the tRNA feed.
5. If the feed to a column is 0.55 *M* in NaCl instead of 0.5 *M*, a greater quantity of phenylalanine tRNA can be loaded on the column.

Pretreatment of tRNA Feed on DEAE Cellulose

The elution sequence of several tRNA's on a DEAE cellulose column is shown in Fig. 12.4. The bulk of the tryptophan tRNA was eluted ahead of the phenylalanine tRNA, and the bulk of the tyrosine tRNA was eluted behind the phenylalanine tRNA. Thus, if the mixed tRNA is pretreated on a DEAE cellulose column, the major fractions of the two tRNA's that are most difficult to separate from phenylalanine tRNA can be removed; the subsequent separation on the reversed-phase column then becomes much easier. In general, the DEAE cellulose separation appears to be a useful method for concentrating a given tRNA and can be readily carried out on a macro scale, 100 g of tRNA per run, with almost quantitative recovery.

Demonstration of Phenylalanine tRNA Separation

A small amount of mixed tRNA (~600,000 ODU), from *E. coli* (strain B), that had not been processed during the original production runs was used for an intermediate-scale test of the improved techniques that had been developed initially for recovering phenylalanine tRNA.

The mixed tRNA was processed in two runs on a 4-in. DEAE cellulose column. The product was pooled in three fractions (see Fig. 12.4): a tyrosine tRNA pool (tubes 241 to 340), a phenylalanine tRNA pool (tubes 201 to 240), and a methionine tRNA pool (tubes 140 to 200). The tRNA in each of these fractions was recovered by precipitation with ethanol and subsequent centrifugation. The methionine and tyrosine tRNA pools were set aside

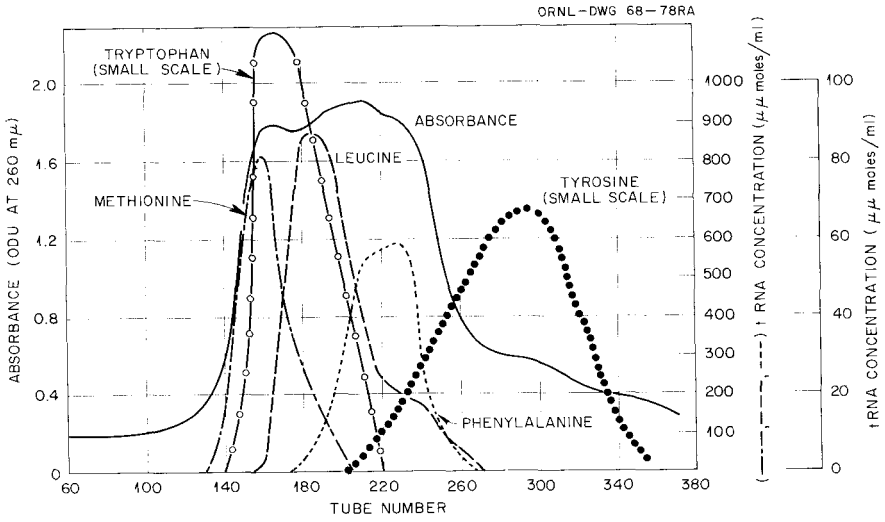

Fig. 12.4. Partial Separation of tRNA's on DEAE Cellulose Column.

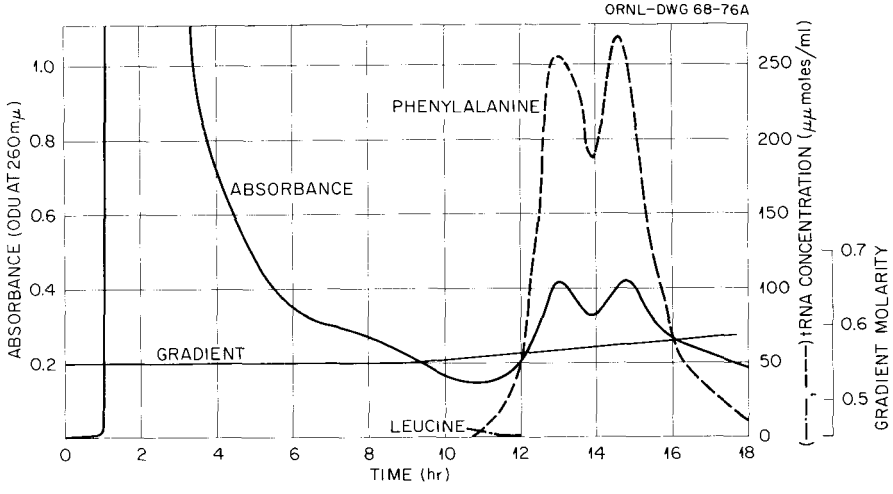

Fig. 12.5. Chromatographic Separation of Phenylalanine tRNA on Reversed-Phase Columns.

for future study. The phenylalanine tRNA pool was processed further on RPC-1 columns.

The RPC-1 columns used for phenylalanine tRNA separation were 2 in. in diameter and 3 ft long. The flow rate was 16 ml/min (0.8 ml min^{-1} cm^{-2}) at a pH of 4.5, and the loading in each run was about 30,000 A_{260} units of crude tRNA, which contained about 35 mg of phenylalanine tRNA. A chromatogram of one of the runs (see Fig. 12.5) shows only a trace of leucine tRNA and partial resolution of the phenylalanine tRNA into two chromatographic peaks. No tyrosine tRNA was found. Eluates associated with the phenylalanine tRNA peaks from this and other runs were pooled separately; then the pools were desalted on a G-25 gel column, concentrated by evaporation and ethanol precipitation, and combined into two fractions: a composite sample of the front phenylalanine tRNA peak and a composite sample of the rear phenylalanine tRNA peak. The specific activity of the sample of the front phenylalanine tRNA peak was 1120 micromicromoles/ODU, while that of the sample of the

rear phenylalanine tRNA peak was 940 micromicromoles/ODU. After concentration of the phenylalanine tRNA and removal of high-molecular-weight contaminants on a G-100 gel column, the specific activities were increased to 1220 and 1150 micromicromoles/ODU respectively. These values compare favorably with 1320 micromicromoles/ODU, the activity previously obtained in laboratory-scale experiments.

12.3 ISOLATION OF PURIFIED TRANSFER RIBONUCLEIC ACIDS

Intermediate-sized RPC-3 columns have been operated to prepare samples of the valine tRNA and the two formylmethionine tRNA's that are eluted early in the chromatographic run. Figure 12.6 shows the results obtained from the fractionation of 20,000 A_{260} units of *E. coli* B tRNA (i.e., tRNA recovered after the removal of phenylalanine tRNA by RPC-1, as described in the last annual report) on a 5- by 90-cm RPC-3 column (37°C) at pH 7.0. The bulk of the $tRNA^{Met}_{F1}$ (first formylmethionine tRNA) was directly pooled to yield a purified sample. The $tRNA^{Met}_{F2}$ and the valine tRNA were contained in a separate pooled fraction. The position of the valine tRNA in the chromatogram shown in Fig. 12.6 has shifted forward slightly, as compared with that in Fig. 12.2, as the result of a higher tRNA loading. (It has been shown that higher loads of tRNA selectively displace the valine tRNA with respect to the two formylmethionine tRNA's.) The second formylmethionine tRNA and the valine tRNA were separated by rechromatography on a 1- by 240-cm RPC-4 column (37°C) at pH 7.0, as shown in Fig. 12.7. Thus, by using both RPC-3 and RPC-4 columns, three purified tRNA's were obtained. Further scale-up of this method is being carried out in conjunction with the Unit Operations Section. All of the *E. coli* B tRNA on hand will be processed to prepare larger purified samples of these three tRNA's.

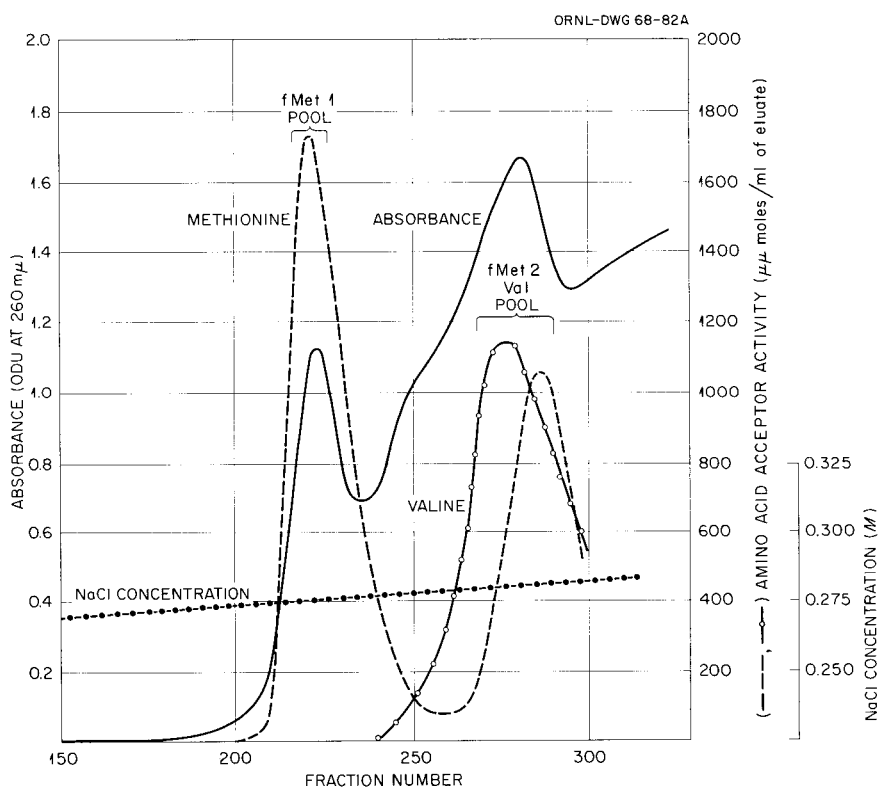

Fig. 12.6. Chromatogram Showing Separation of Two Formylmethionine tRNA's on an Intermediate-Sized RPC-3 Column.

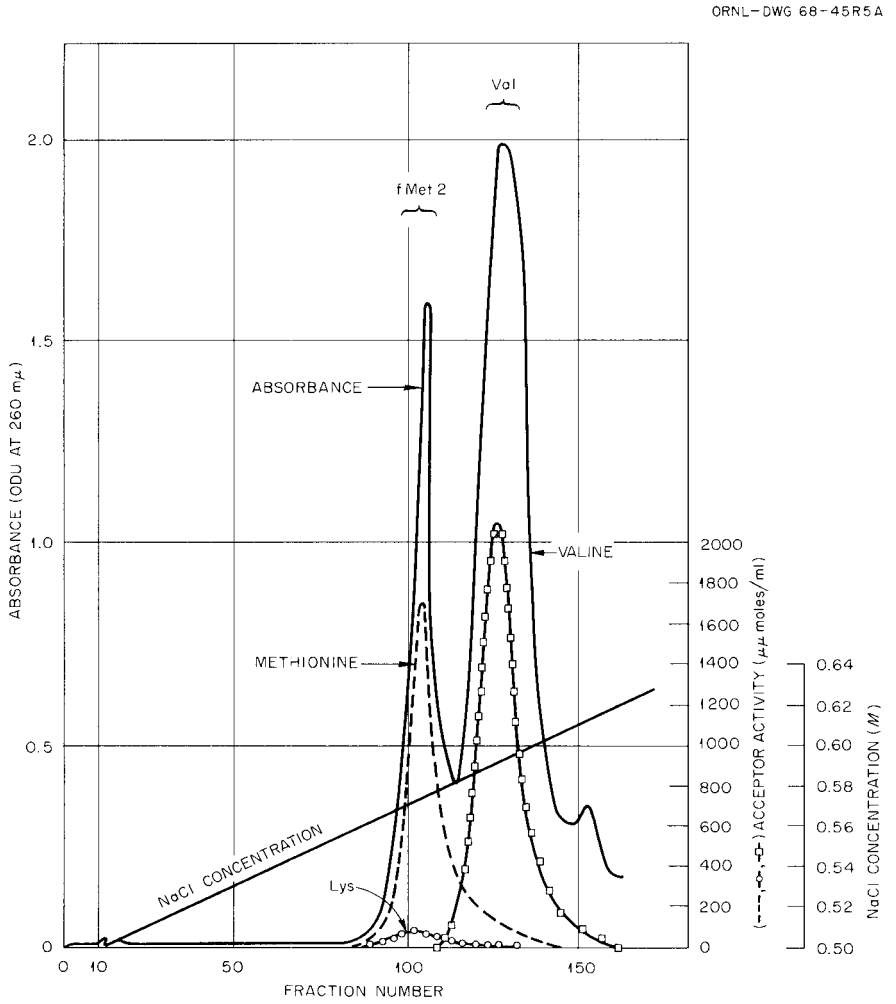

Fig. 12.7. Chromatogram Showing Separation of Formylmethionine-2 tRNA and Valine tRNA on an RPC-4 Column.

12.4 SOLVENT EXTRACTION OF TRANSFER RIBONUCLEIC ACIDS

The selective extraction of tRNA's by water-insoluble quaternary ammonium salts has been reported by Khym.[1] Similar compounds have been applied successfully in reversed-phase chromatographic systems to give sharp separations of tRNA's (see Sect. 12.1 and preceding annual reports). Solvent extraction studies were initiated for two reasons: (1) to attempt to provide a separation technique as an alternative to reversed-phase chromatography and (2) to elucidate the mechanisms involved in the separation of tRNA's.

Generally, each extraction was carried out by vigorously shaking a specified volume of an organic solution with an equal volume of an aqueous solution. The organic solution contained Adogen 464, a tetraalkylammonium chloride, in Freon 214 diluent. The aqueous solution contained mixed tRNA's from *E. coli* B and was 0.05 *M* in Tris-HCl buffer and 0.01 *M* in $MgCl_2$; its NaCl concentration varied. The tRNA's were completely extracted at NaCl concentrations below 0.1 *M*. The extraction coefficients decreased with increasing NaCl concentration (Fig. 12.8); consequently, the tRNA's could be stripped from the organic phase with an

[1] J. X. Khym, *J. Biol. Chem.* 241, 4529 (1966).

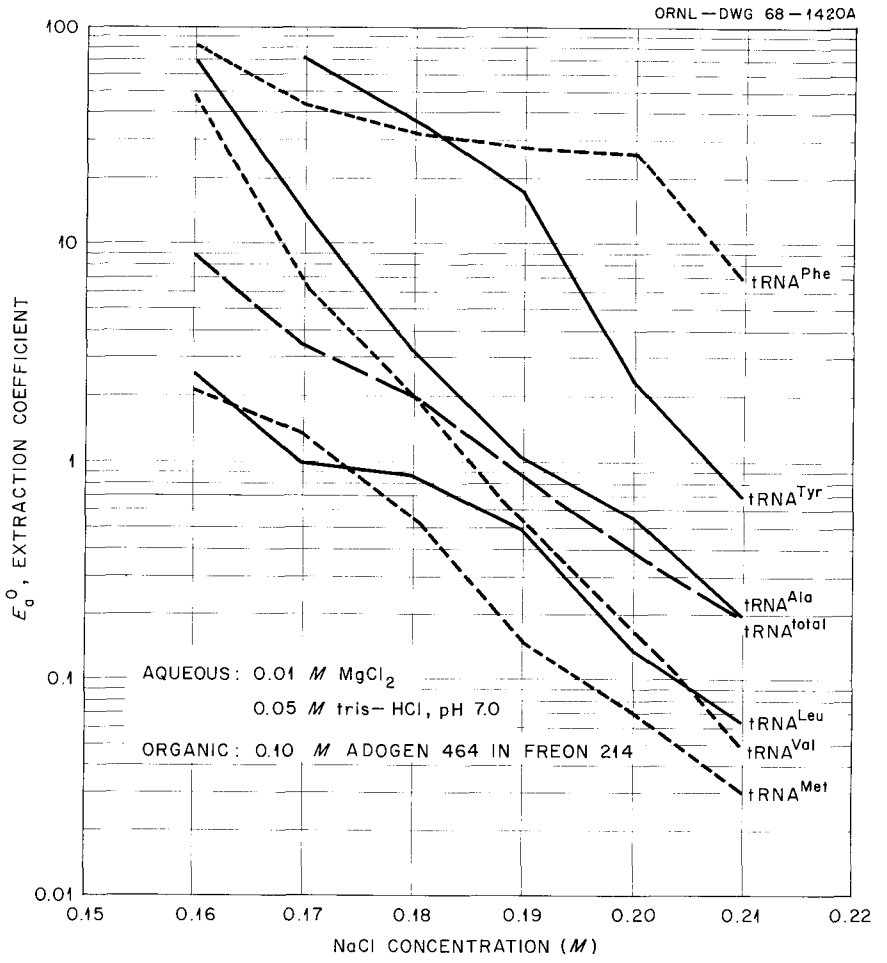

Fig. 12.8. Dependence of Extraction Coefficients of Specific tRNA's on the NaCl Concentration in the Aqueous Phase.

aqueous solution of higher salt concentration (e.g., 0.5 *M* NaCl). For the sake of clarity, not all the tRNA's are shown in Fig. 12.8; however, the values of the extraction coefficients of the other tRNA's usually fell between those for methionine tRNA and tyrosine tRNA. At NaCl concentrations of 0.2 *M* and higher, tyrosine tRNA was less extractable than phenylalanine. Since the behavior of the different tRNA's is not parallel, the separation factors are not the same at different NaCl concentrations. This behavior probably reflects the heterogeneity of the tRNA's.

The extraction coefficient of mixed tRNA, as measured by the absorbance at 260 mμ, increased with increasing temperature (Fig. 12.9). It is necessary, therefore, to maintain a constant temperature during the extraction process in order to keep the extraction coefficients (and separation factors) constant. Conversely, advantage can be taken of the temperature dependence of the extraction coefficient to strip the tRNA's from the organic phase at lower temperatures.

Other parameters that influence the extraction coefficients are the amine concentration in the organic phase and the Mg^{2+} concentration in the aqueous phase. With other conditions constant, the extraction coefficients for 0.1 *M* and 0.5 *M* amine solutions were 3.75 and 15.1 respectively. The NaCl concentration for the useful extraction range was higher in the absence of $MgCl_2$ than in its presence.

The order of extractability of the specific tRNA's can be correlated with the order of elution from a reversed-phase chromatographic column (Sect. 12.1).

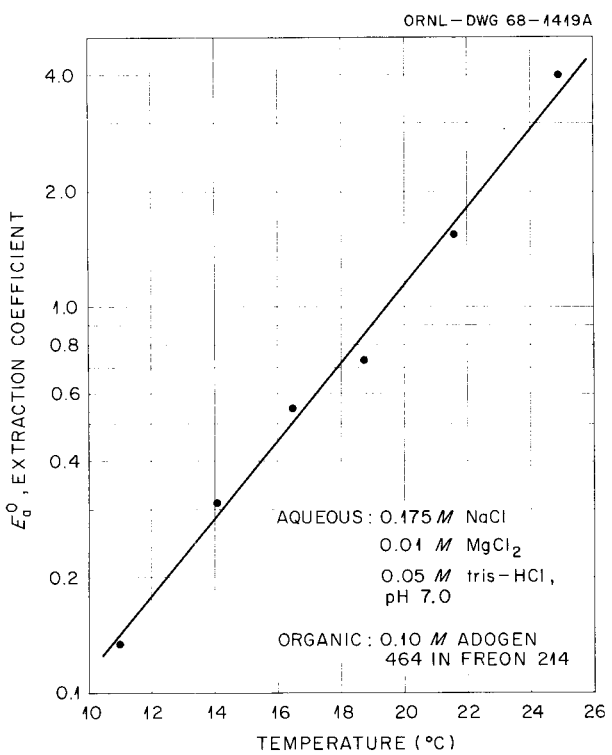

Fig. 12.9. Dependence of the Extraction Coefficient of Mixed tRNA on Temperature.

In general, the tRNA's that are eluted first are the least extractable, whereas those that are eluted last are the most extractable.

A computer program has been written to analyze, in an idealized situation, the separation of mixtures into individual products by countercurrent distribution techniques. For example, in the case of tRNA, the separation of a component having a typical separation factor of 1.5 (relative to adjacent components) would require 200 stages in order to achieve 95% recovery and to obtain a product containing less than 5% impurity (sum of adjacent components).

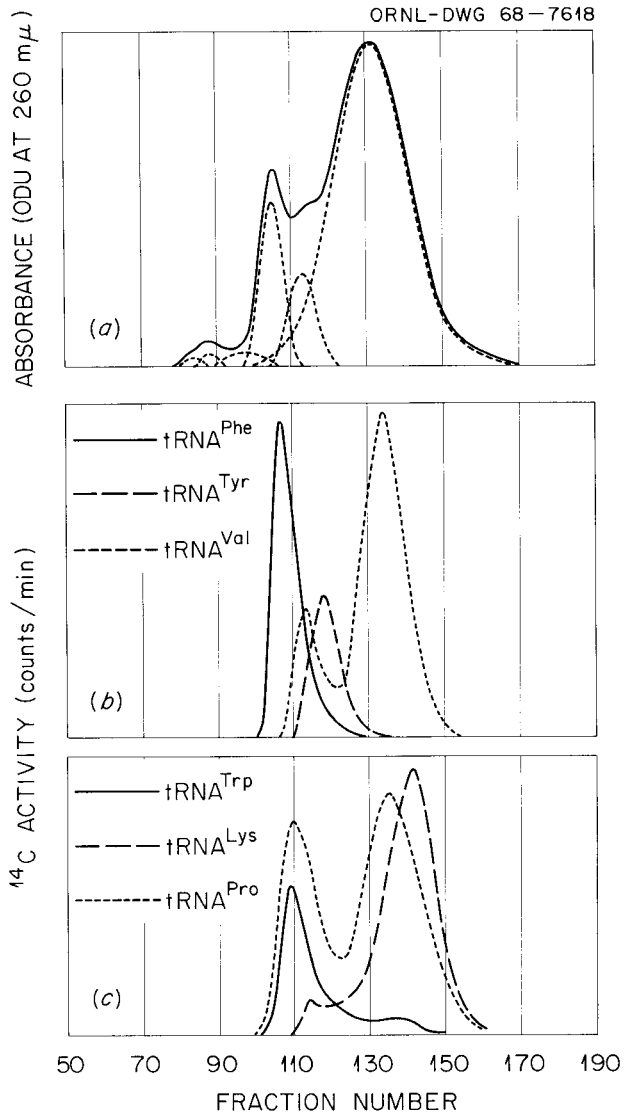

Fig. 12.10. Gel-Permeation Chromatography of tRNA's on Bio-Gel P-100. Column, 2.5 by 231 cm; temperature, 5°C; eluent: 0.4 *M* in NaCl, 0.01 *M* in $MgCl_2$, 0.05 *M* in Tris-HCl, pH 7.4. (*a*) Solid line: absorbance of effluent fractions at 260 mμ; dashed line: resolution by curve analysis into three major peaks. (*b*) and (*c*) ^{14}C activity of selected amino acids accepted by the fractions.

12.5 BEHAVIOR OF TRANSFER RIBONUCLEIC ACIDS ON POLYACRYLAMIDE GEL COLUMNS

Transfer ribonucleic acids were partially separated at 5°C by elution from a Bio-Gel P-100 polyacrylamide gel column with a solution that was 0.4 *M* in NaCl, 0.01 *M* in $MgCl_2$, and 0.05 *M* in Tris-HCl buffer and had a pH of 7.4. The tRNA's are usually located in one or more of three major groups or elution positions. Figure 12.10 shows representative groups. A more effective separation of the tRNA's was obtained at 5°C than at 45°C, although, at the higher temperature, an RNA impurity that would not accept amino acids was eluted separately in front of the tRNA's.

Separation of tRNA's by gel-permeation chromatography may be considered to occur as the result of charge effects or differences in the sizes of the solute particles. The relatively high ionic strength of the solution that is used to selectively elute the tRNA's tends to minimize the charge effects. Size differences, including differences due to molecular aggregation, may be considered as differences either in the shapes of the tRNA's or in their molecular weights.

Since the shape of a tRNA is generally determined by its intramolecular interactions, melting curves (i.e., curves of the absorbance at 260 mμ vs temperature) may provide evidence for the amount of structure (or intramolecular interaction) and, therefore, the shape of tRNA's. Differences in structure (shape) would presumably be reflected in differences in hyperchromicity (change of absorbance on heating), melting point, or the temperature at which "melting-out" begins. Melting curves of selected fractions of tRNA from a P-100 chromatogram are shown in Fig. 12.11. The degree of hyperchromicity of the various fractions is similar. The shapes of the curves are different; those fractions that were eluted early in the chromatographic run began to melt at lower temperatures, and consequently the melting was spread over a wider temperature range. The midpoints of the melting temperature curves are slightly lower for the fractions that were eluted first. These results indicate that tRNA's in the first fractions have less conformational stability; however, it should be pointed out that the presence of an impurity with a less-complicated structure in the early part of the chromatogram could produce the same result.

The molecular weight of a tRNA can be quantitatively related to its osmotic pressure. If the specific absorbance of a tRNA is assumed to be constant throughout the tRNA region of the chromatogram, the molecular weight, as calculated from osmotic pressure per absorbance unit, of a fraction near point 2 in Fig. 12.11 is less than 1.2 times the molecular weight of fractions near point 4. Therefore, it is unlikely that the different peaks result from aggregation of tRNA's.

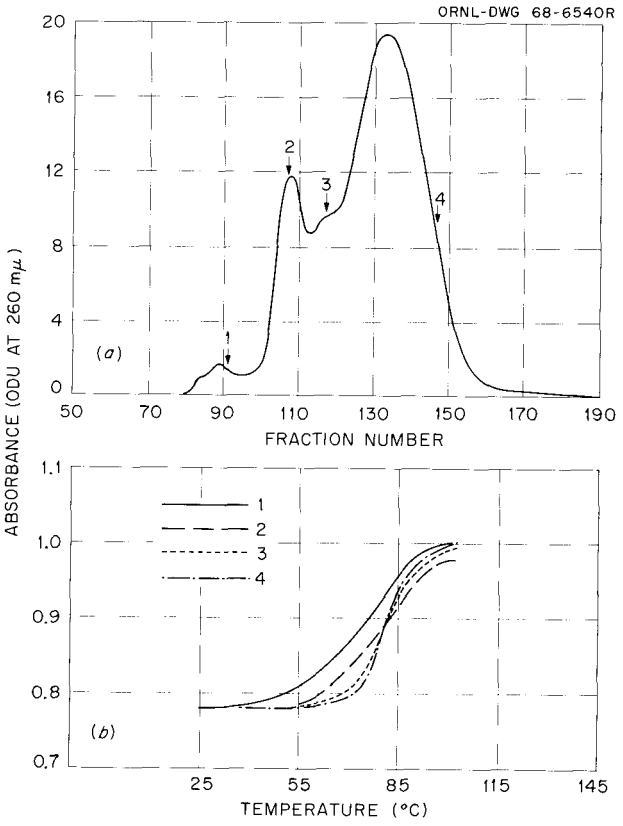

Fig. 12.11. (*a*) **Chromatography of tRNA's on Bio-Gel P-100;** (*b*) **Melting Curves of Selected Fractions from Chromatogram.**

While tRNA separations by gel-permeation chrotography are still not clearly understood, this technique appears to be useful for partially separating the tRNA's into groups prior to complete separation and purification by other techniques such as reversed-phase chromatography (Sect. 12.1).

Body Fluid Analysis

In order to take advantage of recent advancements in the medical sciences, the supporting clinical laboratory must have more-selective and more-sensitive analytical techniques. Increasing demands for medical services will also require that these techniques and other laboratory procedures be highly automated, accurate, and as rapid as is practical. Development of instrumentation to meet these needs is the objective of the Body Fluid Analysis Program.

At present, our efforts are directed toward the development of high-resolution, automated analyzers for clinical application; emphasis is on techniques that result in the determination of large numbers of constituents. The initial effort has involved the determination of low-molecular-weight constituents of body fluids and has resulted in the development of two separate analytical systems: an analyzer for ultraviolet (uv)-absorbing constituents and an analyzer for carbohydrates.

12.6 PROTOTYPE ANALYZERS

Prototype systems for both the uv analyzer and the carbohydrate analyzer, each of which is designated model Mark II, have been designed. The designs have been documented, and one of each of these systems is being built for evaluation.

The uv prototype system will be placed in the Duke University Medical School prior to June 1, 1968, and the carbohydrate prototype system will be placed in the Clinical Center of NIH prior to July 1, 1968. Both institutions have been visited, and space and maintenance requirements have been discussed with personnel who will operate the analyzers. Complete sets of construction prints will be available for interested commercial concerns by July 1, 1968.

Both analytical systems use heated high-pressure (up to 4000 psi) anion exchange columns for separation, elution with a buffer whose concentration increases with time for separating and transporting the constituents of the sample, and a recording photometer for detection. Samples are introduced into each system by injecting a measured volume (0.5 to 2.0 ml) of the sample, via an automatic six-port injection valve, into the high-pressure eluent stream just ahead of the separation column.

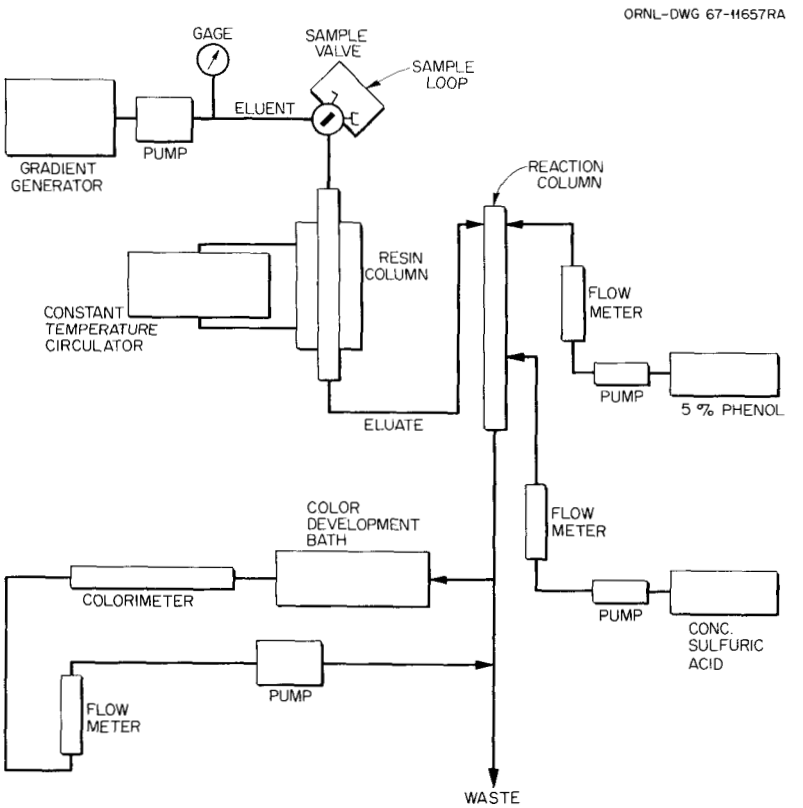

Fig. 12.12. High-Pressure Anion Exchange Chromatograph for Analyzing Carbohydrate Constituents of Body Fluids.

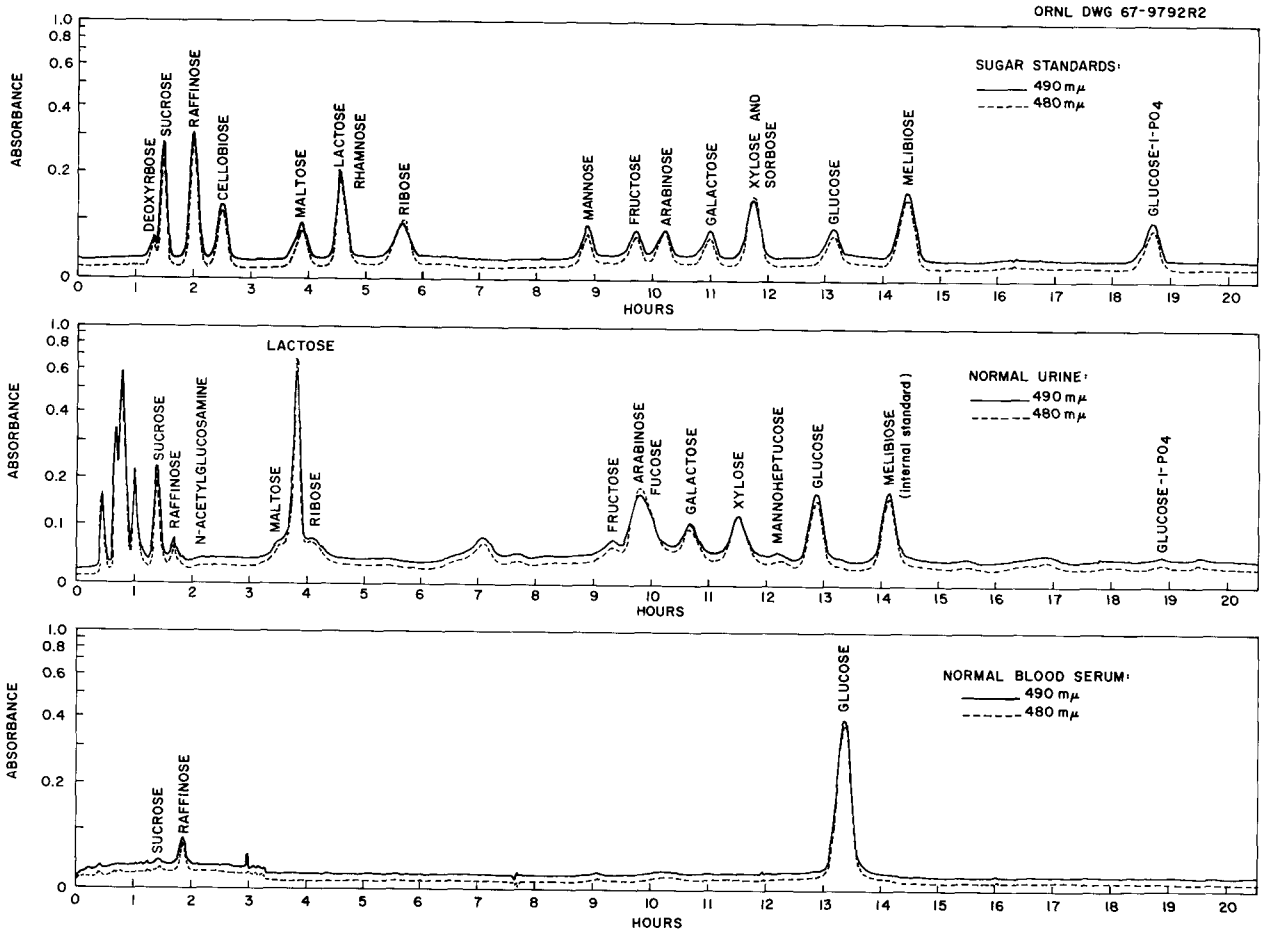

Fig. 12.13. Carbohydrate Chromatograms of Sugar Standards and of Urine and Blood Serum of a Normal Human Male, 38 Years Old. Run conditions: column, 0.62 cm ID × 150 cm stainless steel; resin, Dowex 1-X8, 6–12 μ diam; temperature, 55°C; pressure, 600–900 psig; 24-hr elution gradient, 0.029 *M* $Na_2B_4O_7$–0.057 *M* H_3BO_3 to 0.147 *M* $Na_2B_4O_7$–0.283 *M* H_3BO_3; sugar standard sample size, 0.62 micromole, except 1.25 micromoles melibiose and glucose-1-phosphate; urine sample size, 12.4 ml; blood serum sample size, 1.6 ml.

The uv analyzer has been described previously.[2,3] In the carbohydrate analyzer (Fig. 12.12), a sodium tetraborate–boric acid buffer (pH 8.4) is used for elution, and the separation column, 0.68 cm ID × 150 cm, is maintained at a temperature of 55°C. A color is developed in the detection system by the phenol–sulfuric acid reaction with carbohydrates. This system consists of a trickle-bed glass bead column in which the column effluent, 5% phenol, and concentrated sulfuric acid are mixed; a reaction section maintained at 100°C; and a continuous-flow colorimeter that measures the absorbance of the reaction mixture at 480 and at 490 mμ.

Samples for carbohydrate analysis are pretreated by concentrating (by factors of 2 to 10) via vacuum evaporation, mixing with the concentrated buffer to form a borate complex, adjusting the pH to 8.5, and centrifuging to remove precipitates.

The carbohydrate chromatogram, which shows the absorbance of the column effluent as a function of

[2]C. D. Scott, J. E. Attrill, and N. G. Anderson, "Automatic, High-Resolution Analysis of Urine for Its Ultraviolet-Absorbing Constituents," *Proc. Soc. Exptl. Biol. Med.* **125**, 181 (1967).

[3]D. E. Ferguson *et al.*, *Chem. Technol. Div. Ann. Progr. Rept. May 31, 1967*, ORNL-4145, p. 253.

time, is developed by elution with the borate buffer (see above) at a rate of about 1.14 ml/min. The final borate concentration of this buffer is higher, by a factor of 5, than its initial concentration. Flow rates for 5% phenol and concentrated sulfuric acid are 0.43 and 2.67 ml/min respectively. The carbohydrate chromatogram of a physiological sample requires about 20 hr, and up to 48 peaks can be resolved from a single urine sample (Fig. 12.13).[4,5]

12.7 SYSTEM COMPONENTS

Several components of the analytical systems have limitations that either make automated operation difficult or contribute to a high incidence of maintenance. The separation and detection portions of the analyzers are perhaps the most critical in this respect. Improvements are constantly being made to these parts of the analyzers, as well as to components such as the concentration gradient generators, reagent metering devices, and column temperature controllers.

Separation Systems

In selecting a column material, an anion exchange resin such as Dowex 1 or its equivalent[3] has been found to provide the most satisfactory separation properties. This resin is a polystyrene divinylbenzene (DVB) copolymer with quaternary ammonium active sites. In order to evaluate the effects of DVB cross-linkage and chloromethylation on separation, we obtained five different batches of this type of resin. These batches had different degrees of initial DVB cross-linkage, 2% and 8% (see Table 12.2), and different amounts of chloromethylation, as indicated by the change in percentage of cross-linkage after chloromethylation (final vs initial cross-linkages).

After the resin was separated into 5- to 20-μ fractions by a continuous elutriation process,[6] resin from each batch was changed to the acetate form and was dynamically loaded into identical high-pressure columns. Standard analyses were then made with each column, using the uv analyzer. The resolution (number of chromatographic peaks resolved) for each resin was established with a reference urine sample.

Resin in which the final cross-linkage was 7 to 10% provided satisfactory resolution; the resin with an initial cross-linkage of 8% and a final cross-linkage of 10% was optimum (see Table 12.2). This

[4]R. L. Jolley and M. L. Freeman, "Automated Carbohydrate Analysis of Physiological Fluids," *Clin. Chem.* (in press).

[5]J. G. Green, "Automated Carbohydrate Analyzer: Experimental Prototype," *Natl. Cancer Inst. Monograph* 21, 447 (1966).

[6]C. D. Scott, "Continuous Separation of Ion Exchange Resin into Size Fractions by Elutriation with Water," *Anal. Biochem.* (in press).

Table 12.2. Resolution of Urinary Constituents by Several Special Anion Exchange Resins Manufactured by Bio-Rad Laboratory[a]

Batch	Cross linkage (% DVB)		Capacity		Number of Chromatographic Peaks
	Initial	Final	meq/g	meq/ml	
BRX 48001	2	4	4.26	1.08	0[b]
BRX 48002	2	7	4.79	1.65	90
BRX 48003	8	8	1.68	0.90	88
BRX 48004	8	10	3.15	1.50	94
BRX 48005	8	12	4.16	2.26	60

[a]Run conditions: column, 0.62-cm-diam × 150 cm type 316 stainless steel; resin size range, 5–20-μ-diam; sample, 1.0 ml of 62-f urine; temperature, 40°C; 33 ml/hr; initial pressure, 1350–3000 psi; elutriant, sodium acetate-acetic acid buffer, pH = 4.4, varying from 0.015 *M* to 6 *M* at an average initial flowrate of 33 ml/hr.

[b]The flowrate was less than 1 ml/hr at pressures up to 3500 psi. The resin evidently collapsed.

resin also had separation properties very similar to the most satisfactory anion exchange resin found previously. Results with resin having a higher cross-linkage (due to additional chloromethylation) were much less satisfactory, while resin with a final cross-linkage of only 4% did not have enough structural strength to prevent bed collapse and a high pressure drop.

Detection Systems

The detection or monitoring portion of an analyzer greatly affects sensitivity and selectivity. At present, a modified double-beam uv spectrophotometer is used as the detector in the uv analyzer, and a small continuous-flow colorimeter is used as the detector in the carbohydrate analyzer.

UV Detector. – A double-beam uv photometer that is designed specifically for a flow system and that has the capability of multiple-wavelength operation would be desirable for this application. The photometer should have solid-state electronics in order to avoid the high maintenance requirements of vacuum tube circuitry; also, it should be small so that it can be used near the exit of the column and with microanalytical systems.

We have designed such a photometer, and it will be built in the near future (see Fig. 12.14). It will be of modular construction so that the sizes of the path lengths of the sample and reference streams can be varied. The detection head will be sufficiently small ($1 \times 1 \times 1\frac{1}{2}$ in.) to allow installation of the photometer near the exit of the column and to permit its use with microanalytical systems. The same conceptual design will be used for small flow colorimeters and small flow fluorimeters.

Other Detection Systems. – Two potentially useful flow detection systems – a differential electrical conductivity cell and an adsorption cell – are being developed.

The differential conductivity cell functions by comparing the electrical signal from a bridge circuit, two legs of which are conductivity probes, in the eluent stream ahead of the separation column and in the column eluate (see Fig. 12.15). As the separated constituents leave the column, they progress through one side of the conductivity cell, thus causing the electrical conductivity there to be different from that of the reference side. This difference in conductivity alters the current flow in the bridge circuit, and a differential measurement of the bridge potential results in a signal that is a function of the concentration of the eluted compound.

The adsorption cell measures the heat of sorption or desorption of the separated constituents as they pass through a small bed of the separation media immediately downstream from the column. Theoretically, it should be capable of detecting any constituent that is separated by the column.

ORNL-DWG 68-816RA

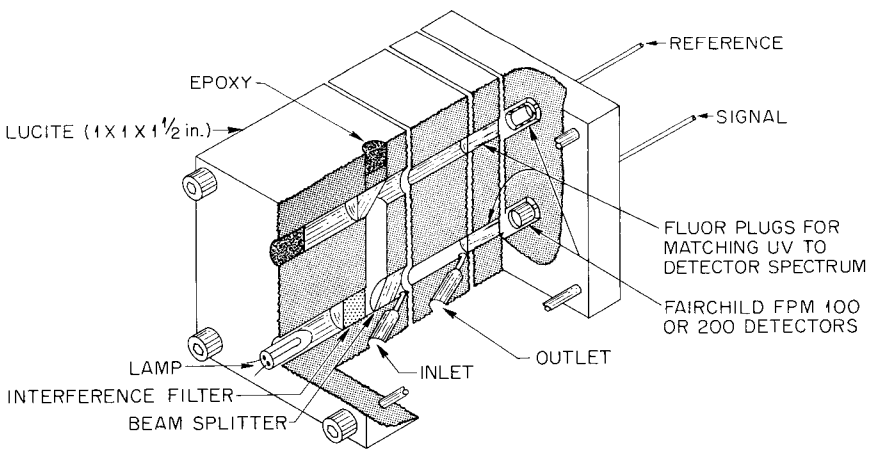

Fig. 12.14. Miniature Flow Photometer.

ORNL-DWG 68-806A

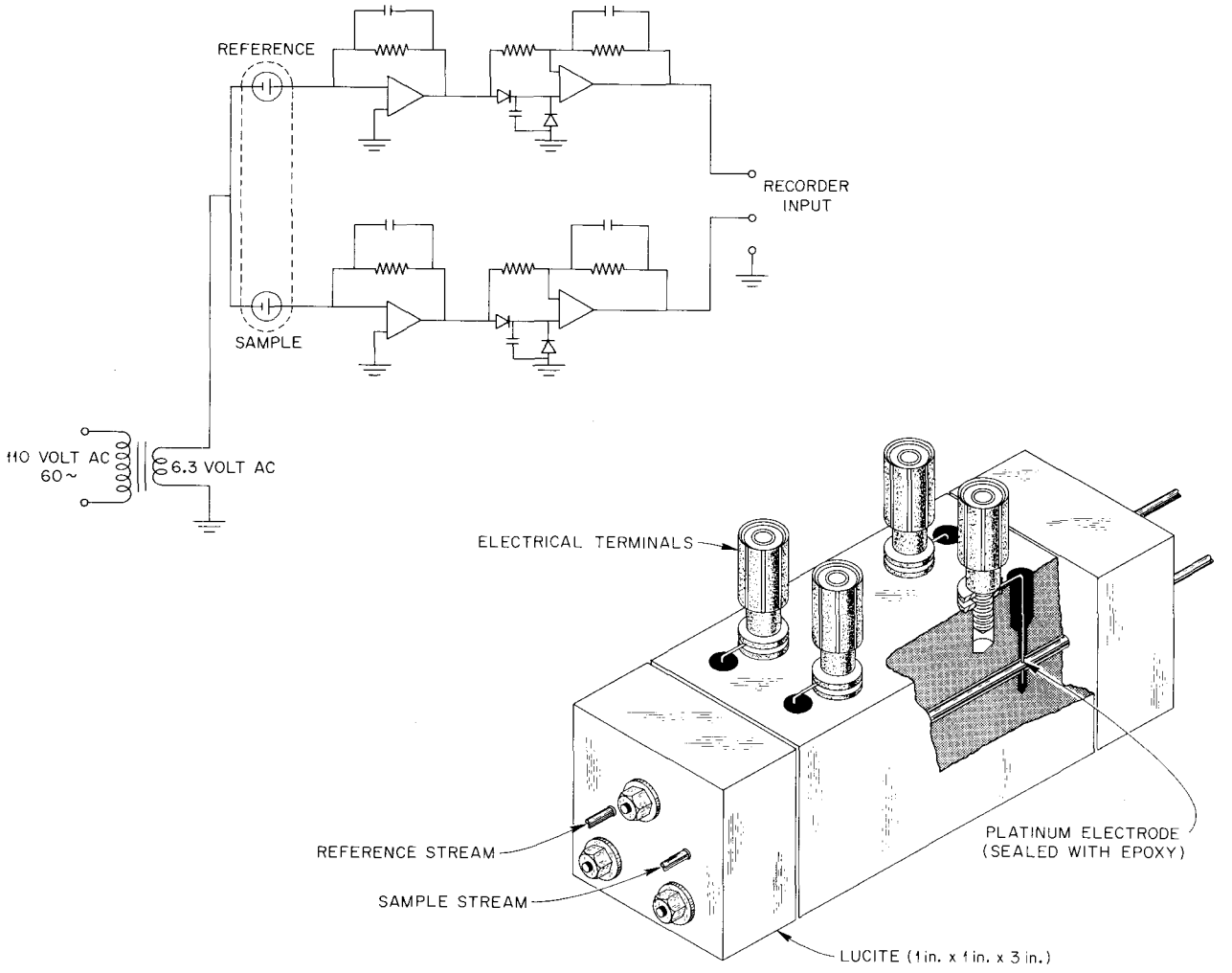

Fig. 12.15. Differential Conductivity Detector.

Two thermistors, one in a nonadsorbing bed of solids and one in an adsorbing bed, constitute two legs of a bridge circuit, and a change in temperature due to sorption produces an electrical signal (see Fig. 12.16).

Concentration Gradient Generation

In both analytical systems, the concentration of the buffer solution used as the eluent gradually increases with time. Elution with this type of buffer is usually referred to as "concentration gradient" elution. The "concentration gradient" can be generated by connecting, in series, two or more chambers containing buffer solutions of different concentration. The concentration output from such a system varies with the volume removed and thus depends only on the relative cross-sectional areas of the chambers and the fluid properties. Such devices with chambers of constant cross section (nine-chamber gradient boxes) are now being used routinely with both the uv analyzer and the carbohydrate analyzer. A computer program that calculates the concentration gradient from these gradient boxes has been written. The use of these devices is limited by two major disadvantages: (1) reproducibility is very dependent on the operator, and (2) automation will be difficult and expensive.

A different method for generating the concentration gradient is also under development. In this

ORNL-DWG 68-815A

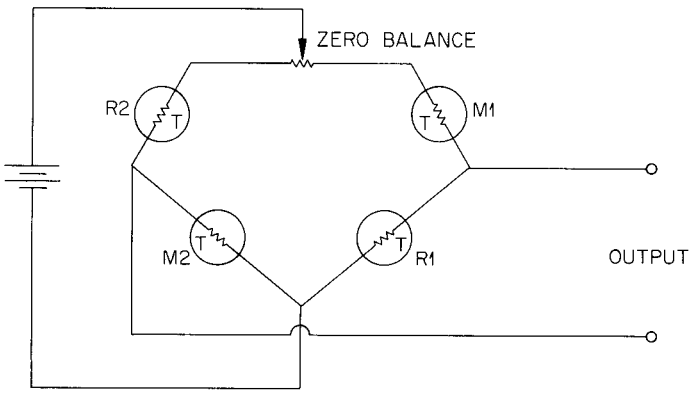

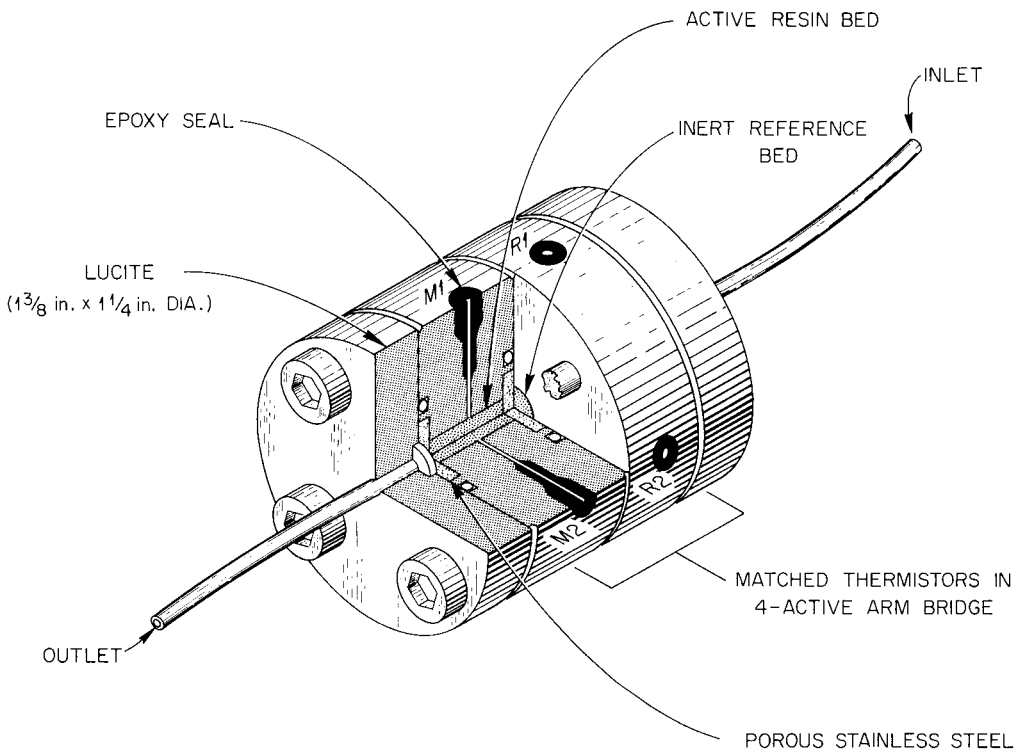

Fig. 12.16. Adsorption Detector.

method, the operation can be completely automated, and the equipment is relatively inexpensive. Two coupled reservoirs, one containing distilled water and the other containing concentrated buffer, have varying cross sections that will generate the desired eluent. By properly choosing the shape of the reservoirs, any concentration gradient can be generated; however, once the shape is fixed, the reservoirs will not have general applicability and cannot be used to generate other concentration gradients.

The solutions are fed, simultaneously, by gravity from each chamber to a small mixing chamber, which then becomes the feed reservoir for the high-pressure pump.[7] The eluent concentration depends

[7]C. D. Scott, *Body Fluid Analysis Program Progress Report for the Period March 1, 1967, to March 1, 1968*, ORNL-TM-2184 (April 1968).

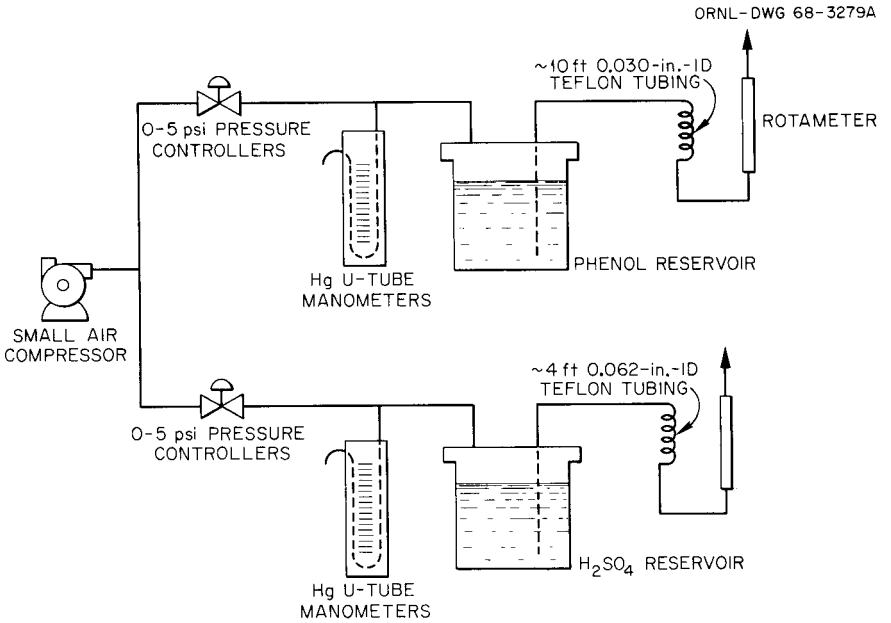

Fig. 12.17. System for Metering Reagents for the Carbohydrate Analyzer by Use of Pressurized Reservoirs and Flow Resistances.

on the cross-sectional areas of the two reservoirs and on the concentration and densities of the solutions in the reservoirs.

Metering of Reagents

In several chromatographic systems, chemical reagents are continuously added to the column effluent to produce a color that can be detected and quantified.[4,5,8] In the carbohydrate analyzer, a 5% phenol solution and concentrated sulfuric acid are metered and are continuously mixed with the effluent from the anion exchange column. A carbohydrate in the effluent produces a colored derivative that can be detected by a continuous-flow colorimeter.

In the past, positive-displacement metering pumps were used to control the flow of the reagent; however, they produced pulsations that contributed to background noise, and they frequently failed after service with corrosive reagents such as concentrated sulfuric acid.

A means of producing constant reagent flow, utilizing a controlled pressure and a fixed pressure drop across a length of capillary tubing, has recently been developed and tested in the carbohydrate analyzer. A schematic of this system is shown in Fig. 12.17. The reagent reservoirs are filled and a small amount of pressure is imposed on the reservoirs by means of an air compressor and pressure-reducing valves. A dip tube (in each reservoir) attached to a length of small-diameter tubing provides enough resistance to the reagent flow (pressure drop) to control the flow rate. U-tube manometers attached to each reservoir act as "safety valves" for each reservoir.

12.8 PARAMETRIC STUDIES

In previous reports[3,9] the effects of resin size and the type of buffer concentration gradient on column resolution were noted. The effects of the change of column dimensions and of the temperature of the column on resolution and pressure drop in the column have also been studied.

[8]S. More and W. H. Stein, "Procedures for the Chromatographic Determination of Amino Acids on Four Percent Cross-Linked Sulfonated Polystyrene Resins," *J. Biol. Chem.* 211, 893 (1954).

[9]C. D. Scott, "Analysis of Urine for Its Ultraviolet-Absorbing Constituents by High-Pressure Anion Exchange Chromatography," *Clin. Chem.* (in press).

Table 12.3. Effect of Column Dimensions on Column Resolution[a]

Column Dimensions (cm)		Number of Chromatographic Peaks
Inside Diameter	Length	
0.15	200	68
0.45	150	56
0.45	200	84
0.62	100	60
0.62	150	76
0.62	200	89
0.78	150	58
0.78	200	87
0.94	200	83

[a]All analytical tests were made with the following standard conditions: ion exchange resin, Dowex 1X-8, 10–20 μ; temperature, 40°C; buffer, sodium acetate-acetic acid, pH = 4.4, varying from 0.15 *M* to 6 *M*; eluent flow-rate of 100 ml/cm^2-hr; and urine sample size was approximately 6.4 ml/cm^2 of column cross-sectional area.

Resolution

Column Dimensions. – The resolution (separation of chromatographic peaks) of a chromatographic column can be increased by increasing its length, at least up to 200 cm (Table 12.3). If resolution is defined as the number of chromatographic peaks that can be resolved from a standard urine sample when the system is operated under similar conditions, a 200-cm column can resolve about 15% more peaks than a 150-cm column and about 50% more peaks than a 100-cm column. Column diameter had only a minimal effect on resolution in the range 0.45 to 0.94 cm; however, a 0.15-cm-diam column gave poor resolution.

Pressure Drop

The effects of column and operating parameters on the pressure drop of low-pressure ion exchange chromatographic columns can essentially be disregarded; however, these factors become very important in high-pressure chromatography. The major parameters that influence the pressure across an ion exchange column are particle diameter, flow rate, column length, and fluid properties such as density and viscosity.

A series of tests were made in which the effects of resin size, eluent flow rate, and column length were studied. The pressure drop across the ion exchange column was found to be inversely dependent on the square of the mean ion exchange resin particle diameter and linearly dependent on the specific flow rate and the column length. Additional tests are needed to establish the exact functional relationships and to determine the effects of column diameter, buffer concentration, and temperature.

12.9 IDENTIFICATION OF BODY FLUID CONSTITUENTS

Three primary methods are being used to identify chromatographically separated body fluid constituents: (1) comparison with chromatographic properties of reference compounds, (2) spectrometric analysis of isolated constituents, and (3) chemical analyses or testing of isolated constituents.[7,10]

[10]C. A. Burtis and K. S. Warren, "Identification of Urinary Constituents Isolated by Anion Exchange Chromatography," *Clin. Chem.* 14, 290 (1968).

Chromatographic Properties

Chromatographic properties, mainly chromatographic position, of reference compounds can be used to tentatively identify many of the chromatographic peaks from body fluids. Photometric data such as the ratio of the absorbance of two wavelengths can also be used.

UV Analyzer. – The chromatographic positions and the relative uv absorbance of 60 uv-absorbing chemicals known to be present in urine have been established by using the uv analyzer. This was done by chromatographing samples of mixtures of reference compounds, determining the chromatographic position of the resulting peaks, and comparing the uv absorption spectra of the separated constituents with reference spectra compiled from reference solutions of pure compounds. The elution positions of 25 ^{14}C-labeled biochemicals found in urine have also been determined by using a radioactivity monitor on the column effluent.

Positions of 53 of the uv-absorbing biochemicals have been established in urine chromatograms by cochromatography, and it is now possible to give a quantitative estimate for these compounds in urine samples. Such techniques have resulted in the tentative identification of at least 35 of the chromatographic peaks in urine; many of these peaks are shown in Fig. 12.18.

Carbohydrate Analyzer. – The chromatographic positions of 40 sugars or sugar derivatives known to be in urine or blood serum have been determined with the carbohydrate analyzer. Fourteen chromatographic peaks from urine have been tentatively identified by cochromatography. Figure 12.13 shows a typical reference sugar chromatogram, as well as urine and blood-serum chromatograms for a normal 38-year-old male. Several of the chromatographic peaks are identified.

Spectrometric Analysis

Spectrometric analysis of the isolated constituents is another method used to identify unknown chromatographic peaks. Since the analytical systems operate with a maximum sample volume of 2.0 ml, the total amount of any one urinary constituent that is separated by the chromatograph is very small (1 mg or less). This quantity of material may be sufficient for a uv spectrometric analysis, mass spectrometry, or infrared spectroscopy, but not for nuclear magnetic resonance. For the latter three types of analyses, the separated constituent must be purified; this further decreases the amount of available sample. To circumvent the problem of small sample size, a preparative column (1.25 × 200 cm, stainless steel) is now being used to separate up to 20 ml of the body fluids into their molecular constituents. Resolution in this large column is not as good as that for the analytical columns, mainly because a slightly larger anion exchange resin is used.

The acetate buffer, which contaminates all of the separate molecular constituents, is removed by gel filtration chromatography using Sephadex G-10. The column fraction that is related to a chromatographic peak of interest is isolated, collected, and concentrated by vacuum distillation if necessary. Then it is placed on the top of the gel column (typically 2.5 × 100 cm) and eluted with distilled water. This results in separation of the urinary constituent from both of the constituents of the acetate buffer.

Chemical Testing

Many analytical procedures routinely used in clinical and chemical laboratories for analyzing serum and urine may be adapted to the qualitative analysis of chromatographic column eluate fractions.[11] These procedures may be particularly useful if they are simple spot tests using a small amount of column eluate. The chemical basis of most spot tests is oxidation of the unknown compound. Certain functional groups (i.e., amino acids, phenols, etc.) may form colored substances if present; however, the disappearance of color from an originally colored reactant is equally useful. In either case, the test may be carried out in a test tube or on a spot test plate with only a few drops of eluate.

Fourteen such chemical tests have been evaluated by using 75 uv-absorbing compounds known to be in urine. None of the color reactions were specific for a single urinary component; however, ten of them may be useful in identifying the separated compounds.

Spot testing of individual column fractions has been hampered by the presence of the acetate

[11] R. J. Henry, *Clinical Chemistry, Principles and Technics*, Hoeber Medical Division, Harper and Row, New York, 1964.

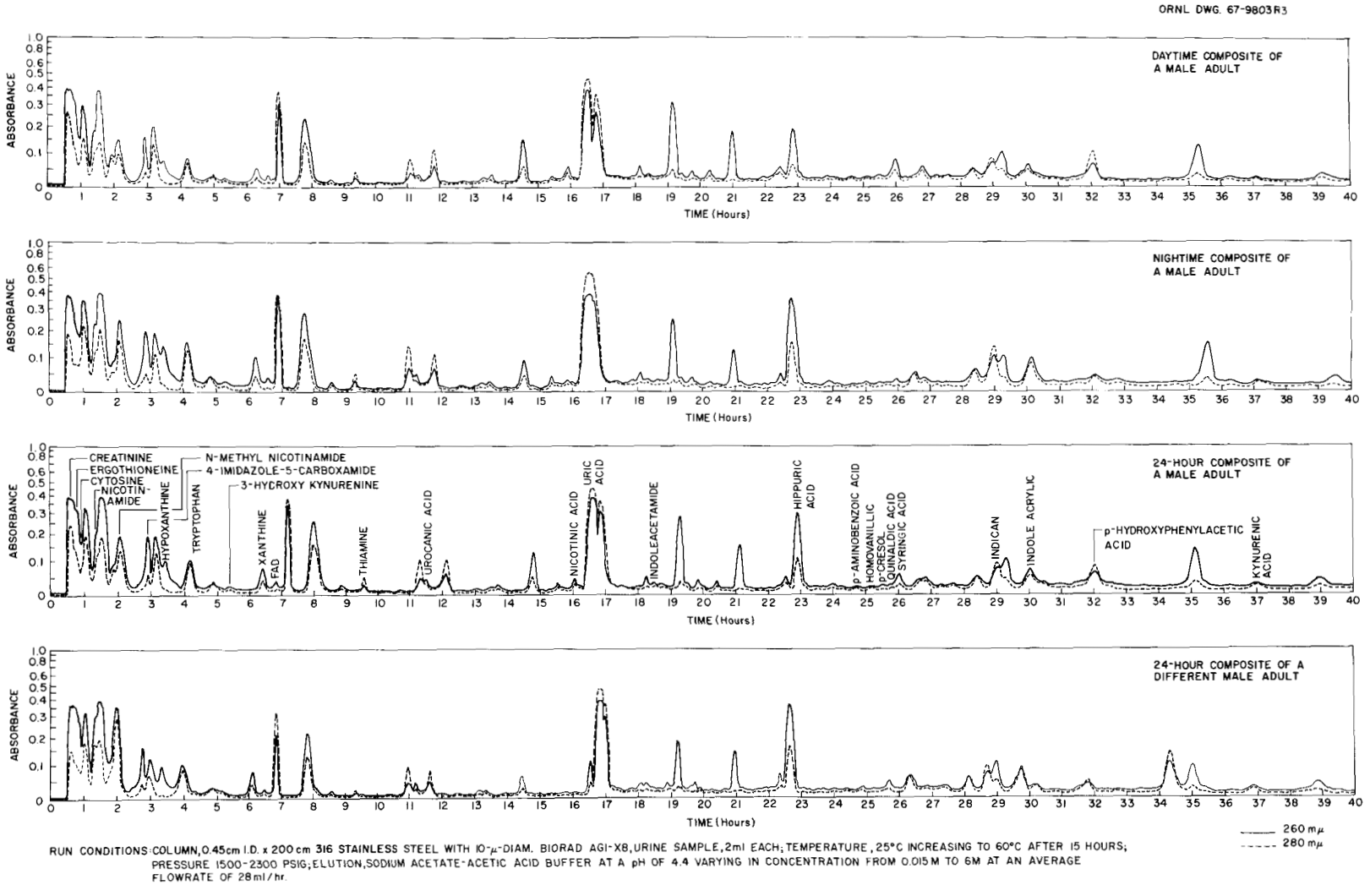

RUN CONDITIONS: COLUMN, 0.45 cm I.D. x 200 cm 316 STAINLESS STEEL WITH 10-μ-DIAM. BIORAD AGI-X8, URINE SAMPLE, 2 ml EACH; TEMPERATURE, 25°C INCREASING TO 60°C AFTER 15 HOURS; PRESSURE 1500-2300 PSIG; ELUTION, SODIUM ACETATE-ACETIC ACID BUFFER AT A pH OF 4.4 VARYING IN CONCENTRATION FROM 0.015 M TO 6 M AT AN AVERAGE FLOWRATE OF 28 ml/hr.

Fig. 12.18. Typical Chromatograms for the Ultraviolet Analyzer, Showing Reproducibility, Difference in Diurnal Cycle, and Similarity Between Different Urine Samples.

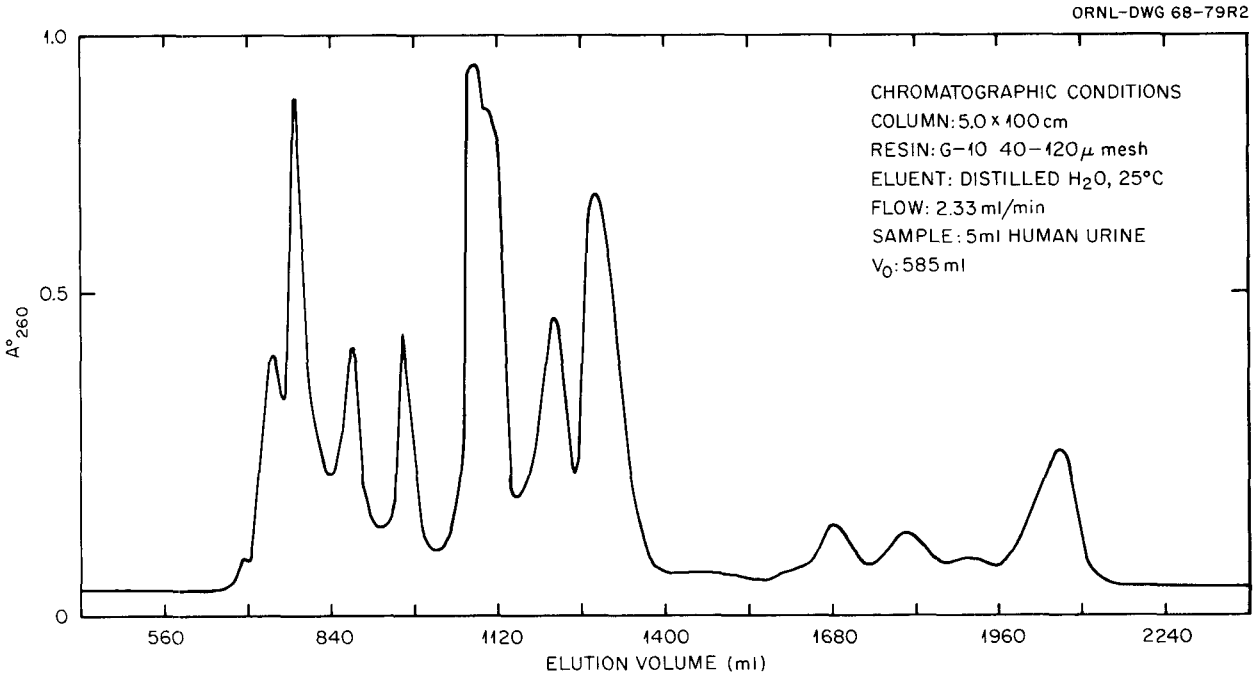

Fig. 12.19. Fractionation of Urine by Gel-Filtration Chromatography.

buffer. Also, many of the tests are not sensitive to the concentrations of constituents found in the column eluate.

Other Techniques

Since many excreted urinary constituents are known to exist as conjugates (with glucuronic acid, with sulfuric acid, or, in the case of aromatic acids, with amino acids), the effect of enzymatic hydrolysis on these compounds was investigated. For example, hydrolysis of urine by a mixture of glucuronidase and sulfatase resulted in the disappearance of nine chromatographic peaks from a normal urine chromatogram and the appearance of two new peaks. Hydrolysis with pepsin resulted in the disappearance of nine peaks and the appearance of eight new ones.

To solve the problem of multiple compounds per column fraction, gel filtration chromatography was used to initially separate the urine into several fractions, each of which was then further separated via the uv analyzer or the preparative system. Separation of urine by gel filtration chromatography with Sephadex G-10 yielded up to ten fractions (Fig. 12.19). After concentration, these fractions were further separated, using the analytical and preparative systems, to give well-defined chromatographic peaks. The column eluate fraction associated with these peaks should be of sufficient purity for spectral analysis.

During the past year, Davis *et al.*[3,12] developed a computer program for determining the quantities of uv-absorbing constituents in a mixture by a least-squares resolution technique. This technique may be useful for determining the quantities of the components in a fraction of the column effluent.

12.10 ANALYTICAL RESULTS

Concurrent with progress in the development of improvements in the uv and the carbohydrate analyzers, a program to evaluate these instruments in their present state is under way. A large number of analyses have been made to establish "base-line" urine and sugar chromatograms of eight normal male subjects. In these

[12]W. Davis, Jr., E. Schonfeld, and A. H. Kibbey, "Determination of Urinary Constituents in Solutions by Least-Squares Resolution of Ultraviolet Spectra," *Clin. Chem.* 14, 310 (1968).

tests, urine and blood serum from the normal subjects were analyzed by both of the analytical systems.

A limited number of analyses are also being made in cooperative research projects. These projects include the study of the effects of total-body ionizing radiation on urinary constituents, the use of urine analysis to show genetic differences in mice, and the analyses of urinary constituents of laboratory rats undergoing tests for lipid metabolism.

Normal Body Fluid Program

In order to differentiate between the normal and the pathological states by analyses of body fluids, it is necessary to establish normal excretion rates of body fluid constituents, or the normal chromatographic patterns for the two high-resolution analytical systems under development. Several individuals were clinically screened, and eight males were chosen as normal subjects. (Normal subjects were defined as males between the ages of 25 and 40, having no clinical manifestations of disease or physical abnormality.) Blood and urine samples were obtained from these subjects and are being analyzed by both analytical systems.

Analysis of Blood Serum. – The blood serum of one subject was chromatographed on the uv analyzer and tentatively was found to contain (per 100 ml of blood) 0.7 mg of creatinine, 0.08 mg of uracil, 0.1 mg of hypoxanthine, and 5.0 mg of uric acid.

Carbohydrate chromatograms for the fasting blood serum samples for all eight subjects revealed 7 to 12 carbohydrates, of which glucose is the major component. The mean concentration and the standard deviation of the blood-serum glucose for the eight subjects were 66.5 mg/100 ml and 11.1 mg/100 ml respectively.

Analysis of Urine. – Since variations in the urine chromatographic pattern had been noted during the diurnal cycle (Fig. 12.18), 24-hr composites were evaluated with both the uv analyzer and the carbohydrate analyzer. In each case, a similar pattern was noted in the chromatograms; minor variations in peak size were evident.

UV Analysis. – The normal uv chromatograms have as many as 100 peaks, of which 50 to 60 are common to each subject and 80 to 100 are common to most. A tentative quantification has been made for 18 uv constituents (see Table 12.4). Most of our values agree reasonably well with those cited in the literature; however, the tentative nature of these values precludes any definitive evaluation at this time.[13–16]

A computer program was written for statistically evaluating the data from the normal chromatograms. This program determined the mean values of either the peak heights or the quantity of material represented by the peak height, the standard deviation, and the percentage standard deviation for 50 chromatographic peaks in the eight normal samples. The percentage standard deviation of the 50 peaks ranged from about 15 to 100%. This type of statistical information will ultimately be useful in determining the normal limits.

Carbohydrate Analysis. – As many as 48 chromatographic peaks were resolved by the carbohydrate analyzer. Forty of these were common to most of the eight normal chromatograms, while 23 peaks were common to all eight chromatograms. The mean values and the standard deviations for the quantities of 12 selected sugars are given in Table 12.5.

Diurnal Variation. – The two 12-hr portions of the 24-hr urine composite, designated day and night samples, for each normal subject were analyzed by both the uv analyzer and the carbohydrate analyzer. Preliminary results indicate higher excretion rates of total solids and of uv-absorbing components for the night samples.

Cooperative Testing Programs

Although routine clinical use of these high-resolution analytical systems is not yet feasible, it is desirable to test the equipment with "unusual" or potentially abnormal body fluid samples. Information is needed on the magnitude of the differences between normal and abnormal specimens as represented by their chromatograms. We are also interested in applications of these instruments to the field of biology in general.

---

[13] P. L. Alman and D. S. Dittmer, *Blood and Other Body Fluids*, Federation of American Societies for Experimental Biology, Washington, D.C., 1961.

[14] P. L. Alman and D. S. Dittmer, *Biology Data Book*, Federation of American Societies for Experimental Biology, Washington, D.C., 1964.

[15] H. D. Damm, ed., *Handbook of Clinical Laboratory Data*, Chemical Rubber Co., Cleveland, 1965.

[16] C. Long, ed., *Biochemists' Handbook*, E. & F. N. Spon, Ltd., London, 1961.

Table 12.4. Normal Urine Study: Excretion Rate of Selected UV-Absorbing Constituents

Mg compound/(kg body weight)/(day)

Tentative Peak Identification	Computer Write-Out Identity	Normals							
		1	2	3	4	5	6	7	8
Aconitic acid	K2	0.1	0.09	0.08	0.1	0.08	0.04	0.04	0.06
Anthranilic acid	I7	Int	Int	Int	Int	0.08	0.06	Int	Int
p-Cresol	H5	NF	Int	NF	0.04	NF	0.04	0.04	NF
Hippuric acid	H	4.4	7.8	4.4	4.0	1.2	1.8	2.2	2.0
Homovanillic acid	H5[1]	0.003	0.002	0.003	NF	0.005	0.003	0.004	0.008
p-Hydroxybenzoic acid	L1	0.008	NF	0.009	0.006	0.008	NF	0.004	0.016
p-Hydroxyphenylacetic acid	I8	0.08	0.04	0.08	0.10	0.08	0.16	0.06	0.08
Hypoxanthine	D5	0.1	0.07	0.07	0.06	0.05	0.04	0.04	0.09
Kynurenic acid	K	0.07	0.10	0.04	Int	0.012	0.03	0.03	0.06
Maleuric acid	U10	NF	0.014	0.008	NF	NF	0.01	0.003	NF
Phenol	U9	Int	0.04	Int	Int	Int	Int	Int	Int
Pseudouridine peak[a]	C*	<1.4	<1.4	<1.0	<1.2	<1.0	<1.0	<0.7	<1.3
Syringic acid	I_0'	NF	NF	NF	NF	NF	NF	NF	0.02
Theophylline	D7	0.007	0.02	NF	0.014	NF	NF	0.006	NF
Uracil peak[a]	C2*	0.2	0.4	0.2	0.2	0.12	Int	0.14	0.3
Uric acid	U	6.6	6.4	5.8	6.0	6.0	5.6	3.4	5.6
Urocanic acid	F7	0.04	0.04	0.008	0.02	0.02	Int	0.03	0.04
Xanthine	E	0.06	0.05	0.04	0.03	0.05	0.05	0.04	0.06
Sample taken, ml		1.3	1.45	1.12	1.1	0.91	1.7	1.65	0.67
Volume of daily excretion, ml		1584	2058	1528	1208	1184	1320	986	750
Body weight, kg		69.5	88.7	79.54	77.3	81.8	60.9	75.0	70.45

[a]This peak may contain several compounds, and excretion values are probably higher than actual quantities.

NF – not found. Int – interference of other peaks prevented quantification.

UV Analyzer. – In the past, comparisons have been made between the uv chromatograms of normal subjects and those from patients with schizophrenia and various types of cancer.[2] There were significant differences between urine from the latter subjects and those who were normal. Additional pathological urine samples have now been analyzed.

Effects of Radiation. – Urine was obtained from a 60-year-old male, who had been diagnosed as having polycythemia rubra vera, both before and after he received a total-body radiation exposure of about 100 r at the Medical Division of ORAU. Analyses were made with the uv analyzer.

Comparison of the chromatograms of this patient's urine before and after radiation and with that of a healthy person showed: (1) Of the 11 peaks selected for comparison, 6 may be considered constant; that is, no significant differences exist between the three urine specimens.

Table 12.5. Normal Urine Study: Excretion Rate of Selected Carbohydrates

Excretion rate of selected carbohydrates, mg sugar/(kg body weight × day)

	Normal Subjects								Mean ER[a]	Standard Deviation	Percent Standard Deviation
	N-1	N-2	N-3	N-4	N-5	N-6	N-7	N-8			
Sucrose	0.22	0.50	0.32	0.22	0.35	0.26	0.49	0.19	0.32	0.11	35
Raffinose	0.053	0.062	0.047	0.019	0.031	0.051	0.054	0.014	0.041	0.016	40
Maltose	0.19	0.27	0.14	0.25	0.13	0.22	0.15	0.38	0.22	0.077	36
Lactose	3.0	0.88	1.5	0.53	1.6	2.1	1.1	0.35	1.4	0.82	59
Rhamnose	0	0	0	0.073	0	0	0	0.092	0.021	0.036	175
Ribose	0.38	0	0	0	0.12	0	0.13	0.18	0.10	0.13	124
Fructose	0.14	0.12	0.36	0.15	0.23	0.15	0.26	0.64	0.26	0.16	63
Arabinose	1.20	0.76	1.14	0.70	0.80	0.90	0.84	0.73	0.88	0.17	20
Galactose	0.78	0.48	0.81	0.38	0.42	0.89	0.54	0.24	0.57	0.22	38
Xylose	0.98	0.71	0.34	0.24	0.23	0.29	0.21	0.28	0.41	0.26	64
Mannoheptulose	0.099	0.066	0.052	0.045	0.079	0.074	0.041	0.045	0.063	0.019	30
Glucose	0.61	0.64	0.65	0.81	0.63	0.61	0.45	0.50	0.61	0.10	16
Sample volume, ml	16	16	16	16	16	16	16	12.50			
Volume of daily excretion, ml	1584	2085	1528	1208	1184	1320	986	750	1327		
Body weight, kg	69.5	88.7	79.5	77.3	81.8	60.9	75.0	70.4	75.4		

[a]ER = excretion rate.

(2) The urocanic acid peak, which is present to a slight extent in normal urine, is not present in the polycythemic urine. (3) Four peaks were unchanged by the radiation therapy but were somewhat smaller than in the case of the normal urine. (4) One peak was apparently reduced by the radiation dose.

Additional data will be gathered on similar patients in the future.

Genetic Differences in Mice. – During the past year a cooperative effort with the ORNL Biology Division involved a brief comparative study of urines from two inbred strains of mice, T-stock albino and 101 × C3H hybrid. Chromatographic analyses of 0.5-ml samples were made with the uv analyzer. The mice had been subjected to identical environments.

Six significant differences between the two chromatograms were noted. The 101 × C3H hybrid strain produced urine that yielded at least six constituents not found in the urine from the T-stock albino. Also, significant quantitative differences in a number of corresponding peaks were noted in the chromatographic patterns of the two specimens.

Carbohydrate Analyzer. – The urine of a 67-year-old male with a diseased liver was analyzed for carbohydrates, and the results were compared with three normal urine samples. Of the 13 carbohydrates quantified, almost all the values determined for the normal subjects fell within the reported normal ranges; however, the amount of *N*-acetylglucosamine was significantly greater in the subject with the diseased liver.

Urine samples from individuals having diabetes mellitus, both controlled and uncontrolled, were also chromatographed (Fig. 12.20). Because of the large quantity of glucose in these urines, the sample size had to be reduced to a minimum, and, consequently, very little chromatographic structure

ORNL DWG 67-11655RI

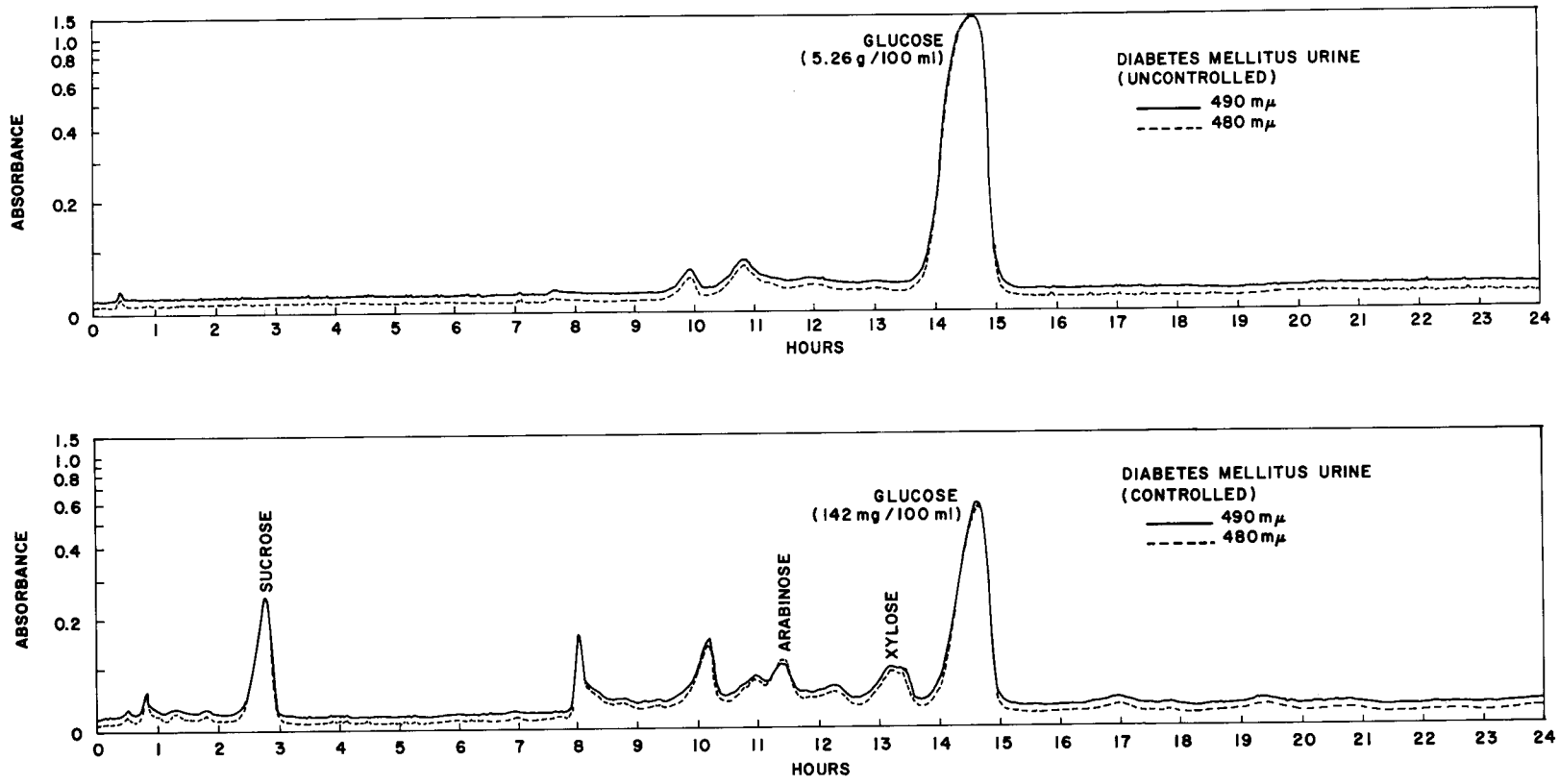

Fig. 12.20. Urine Chromatograms of Individuals with Uncontrolled and Controlled Diabetes Mellitus. Run conditions: column, 0.62 cm ID × 150 cm stainless steel; resin, Dowex 1-X8, 10–20 μ diam; temperature, 55°C; pressure, 700–800 psig; 24-hr elution gradient, 0.029 *M* $Na_2B_4O_7$–0.057 *M* H_3BO_3 to 0.147 *M* $Na_2B_4O_7$–0.283 *M* H_3BO_3; urine (uncontrolled) sample size, 0.125 ml; urine (controlled) sample size, 1.6 ml.

is shown. The glucose concentration in the urine of the controlled diabetic was 142 mg/100 ml, as compared with 5.26 g/100 ml in the urine of the uncontrolled diabetic. Normal glucose concentration is considered to be 1 to 12 mg/100 ml.[13–16]

12.11 DATA ACQUISITION AND ANALYSIS

The high-resolution analytical systems generate a large amount of data. To facilitate the use of these data, automated methods of data acquisition and data analysis must be developed. In turn, these methods will allow data to be acquired in a form that is usable by modern computers and, therefore, will necessitate the development of computer programs to analyze the data and to provide quantitative information.

Automated Data Acquisition

A data acquisition system that digitizes the electrical signal from the uv analyzer detection system and records it on punched paper tape has been built. This system uses a multipoint strip-chart recorder as the control for switching the spectrophotometer to different wavelengths. The wavelength changes with each successive recorder point. A readout control then directs the printer and paper-tape punch to record the digitized signal from the spectrophotometer as each recorder point is printed. The wavelength is also encoded and punched with each data point.

Data Analysis

Analysis of Complex Chromatograms. – A rather simple computer program was written to convert the reading of the digital voltmeter, from complex chromatograms having more than 100 peaks, into transmission and absorbance values. Originally, the background noise from the digital voltmeter was equivalent to about 0.002 absorbance unit. However, this has been reduced to about 0.00005 absorbance unit by mathematical methods that include least-squares smoothing of the absorbances and then calculating the smoothed first derivatives of the absorbances.

Peak areas are determined by numerical integration, and a correction is made for the base line by two different methods. In the first method, the base line is assumed to be a straight line; in the other method, it is assumed to be an exponential function. The exponential function is a good approximation of the lower part of a tail (of a major peak) that interferes with a small peak.

Partially separated, or overlapping, peaks are resolved by extending a line from the valley between the peaks to the base line. Other methods, such as nonlinear least-squares resolution, proportioning the areas, extrapolation techniques, and the use of an analog curve resolver, are in the process of being evaluated.

Identification of Chromatographic Peaks. – After the position and the area of the individual components in the chromatogram are determined, a name or label is assigned to each peak. To correct for spectral shifts due to variations of flow rates, temperature, etc., correction or normalization methods are used. The simplest method is to normalize to a well-defined peak. This method was evaluated for chromatograms obtained with the carbohydrate analyzer. The normalization peak used was that of glucose, which is eluted at about 12.6 hr. Normalization improved considerably the positions of the compounds eluting between 6 and 21 hr. Even better results were obtained by using a second normalization procedure, which is based on the assumption that a proportional shift plus a constant shift occurs in the elution time of each peak. To calculate these shifts it is necessary to use two well-defined peaks such as those of sucrose and glucose.

12.12 LITERATURE SURVEY

An annotated bibliography containing about 4000 literature references concerned with the determination of low-molecular-weight organic constituents in normal and pathological human urines is being prepared. The references have been collected from volumes 59–65 of *Chemical Abstracts* (July 1963 through December 1966), *Biological Abstracts* for the years 1964–66, *Index Medicus* for the year 1965, and by an automated search by the MEDLARS system for the year 1966. The last two sources were found to be relatively nonproductive and will not be extended over the entire 1964–66 period. References to more than 300 low-molecular-weight urinary constituents have been noted; more than 200 of these are thought to have pathological significance.

13. Irradiation Effects on Heterogeneous Systems

For several years the study of irradiation effects on heterogeneous systems has been focused on the radiolysis of adsorbed water. In initial experiments, silica gel was used as the adsorbent; recently, however, attention has been centered on molecular sieves of various types. This study is now complete; at present our efforts are aimed at investigating irradiation effects on colloidal systems, using the recently acquired streaming current detector.

13.1 THE RADIOLYSIS OF ADSORBED WATER

The study of the radiolysis of water adsorbed on high-surface-area solids has been completed, and a paper has been prepared for publication in the *Journal of Physical Chemistry:* "The Radiolysis of Adsorbed Water," by N. A. Krohn.

Abstract. – "The yield of hydrogen from the radiolytic decomposition of water by beta or gamma radiation is much greater than expected when the water is adsorbed on a high-surface-area solid such as silica gel, silica-alumina, or molecular sieve. It appears that energy absorbed initially by the solid is transferred in the form of electrons to the surface, where the electrons react primarily with acid hydrogen sites to yield H atoms and, subsequently, hydrogen gas. The efficiency of this process depends on the Brönsted acidity of the surface and the amount of water adsorbed on it.

"In the absence of adsorbed water, no gaseous hydrogen is detected. As the water content increases, the hydrogen yield rises rapidly, reaches a maximum, and then decreases. The height of the maximum depends on the surface acidity and can attain values approaching 30 times that calculated by apportioning the radiant energy between the adsorbent and the water on the basis of their electron fractions. The hydrogen yield also decreases with total radiation dose, probably because of the destruction of active sites. These sites may be restored by heating the adsorbent-water system to 150°C for a few hours. The activation energy for H_2 production is 1.8 kcal/mole, which is in reasonable agreement with recently reported values for reactions of the hydrated electron in aqueous solutions.

"The oxidizing species that are necessarily formed result in the formation of CO_2 from carbonaceous surface impurities, the release of molecular oxygen, and a residual oxidizing capacity, probably in the form of O_2^- radicals, on the irradiated surface itself. The distribution of these products depends on the particular surface and the total radiation dose."

14. Spectrophotometric Studies of Solutions of Alpha-Active Materials

The major objective of this program is to develop and exploit spectrophotometric techniques for studying the chemical properties of aqueous solutions, especially of the lanthanide, actinide, and transition elements, over wide ranges of experimental conditions. Efforts thus far have been concentrated principally on the uranyl ion and the correlation of its spectra with those of the penta- and hexavalent transuranium elements. A specially modified Cary model 14 spectrophotometer system[1,2] has been built and installed for studying the more highly alpha-active actinides. This system is designed to provide safe containment for such materials and to operate at temperatures up to the critical point of water (372°C) and at pressures up to 10,000 psi.

14.1 SPECTRAL CORRELATIONS OF THE ACTINYL IONS

The ultraviolet and visible spectra of the uranyl ion were resolved into seven major absorption bands and a number of vibrationally perturbed bands.[3–5] These seven bands were assigned as representations of the energy levels of the nonbonding orbitals in the molecular orbital model for the uranyl ion. The seven energy levels were then correlated with the absorption bands of penta- and hexavalent neptunium, plutonium, and americium.[6] This correlation showed that the one to four extra electrons of these actinyl ions (as compared with the uranyl ion) are located in the first and second nonbonding orbitals of the model (Fig. 14.1). Thus, by the continuous addition of electrons to the nonbonding orbitals, one model can be applied to all of the known actinyl ions. Theoretically, an increase in the number of nonbonding electrons should decrease the stability of the molecular species; the observed decreasing stability of the higher actinyl ions is in agreement with this theory.

14.2 MODIFICATION AND TESTING OF THE SPECTROPHOTOMETER SYSTEM FOR HIGH ALPHA LEVELS

The high-temperature, high-pressure spectrophotometer system for use in the study of alpha-active materials has been operated at temperatures up to 390°C with dummy cells. Leakage at the sapphire-window–titanium-flange junction of the actual cells led to a modification in the sealing design; that is, a groove was cut in the face flange to allow a Haskel seal to be installed between the window and the flange. One modified cell, filled with water, has been thermally recycled between 25 and 267°C and then tested at up to 320°C; no leakage has been observed.

The surface of the Resistoflex unions for connecting the heat-transfer fluid lines to the absorption cells was found to deteriorate with usage.

---

[1] *Chem. Technol. Div. Ann. Progr. Rept. May 31, 1966*, ORNL-3945, pp. 221–27.

[2] *Chem. Technol. Div. Ann. Progr. Rept. May 31, 1965*, ORNL-3830, pp. 236–47.

[3] J. T. Bell and R. E. Biggers, *J. Mol. Spectry.* 18, 247 (1965).

[4] J. T. Bell and R. E. Biggers, *J. Mol. Spectry.* 22, 262 (1967).

[5] J. T. Bell and R. E. Biggers, *J. Mol. Spectry.* 25, 312–29 (1968).

[6] J. T. Bell, "Continuities in the Spectra and Structure of the Actinyl Ions," submitted for publication in *J. Inorg. Nucl. Chem.*

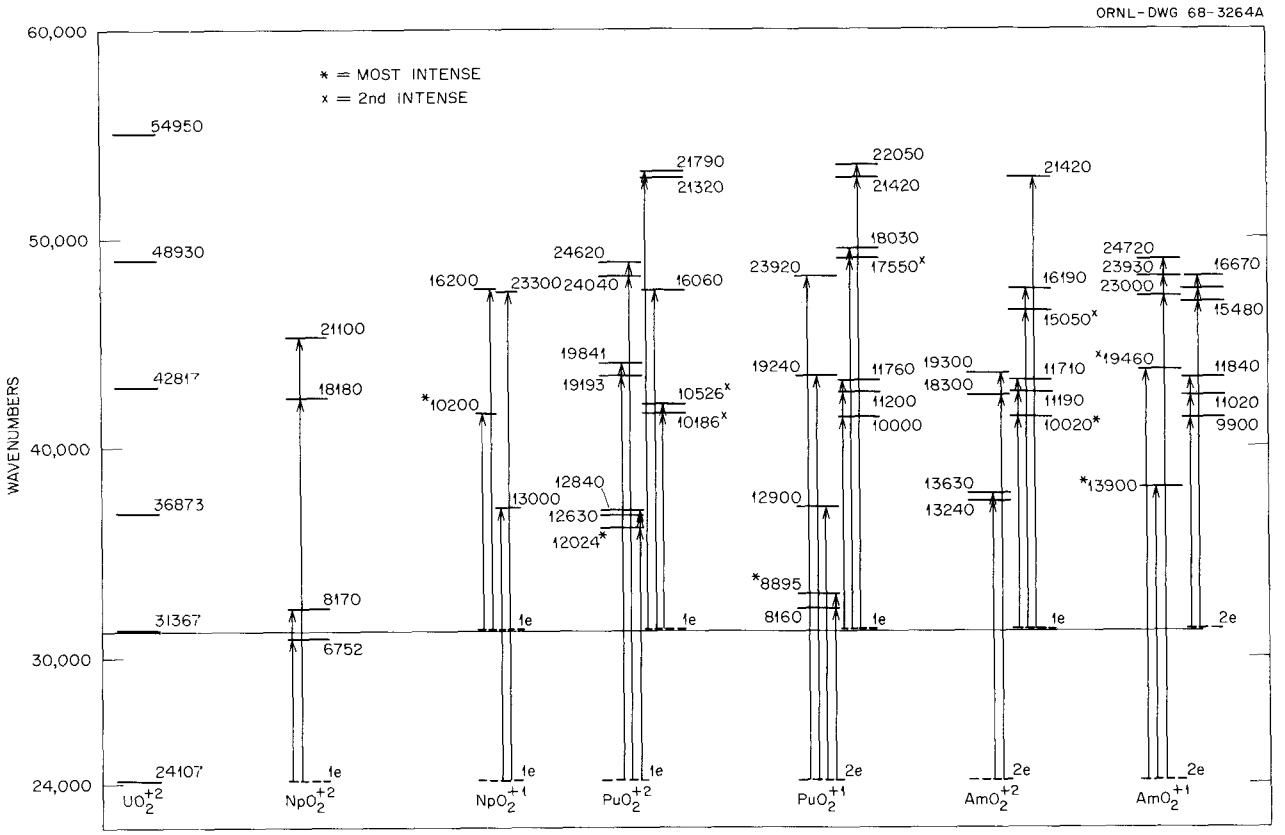

Fig. 14.1. Relative Energy Levels of the Actinyl Molecular Orbitals and the Electron Transitions.

This situation was corrected by inserting a 5-mil-thick gold washer between the mating surfaces. In a test at temperatures as high as 320°C, the oil line union appeared to be adequately sealed.

Studies of nonradioactive and low-level-radioactive systems (i.e., uranium, lanthanides, and other transition elements) have begun. Uranium solutions were selected for the first investigations because we already have some of the necessary density data for these solutions up to 320°C.

The spectrum of 0.01 *M* UCl_4 in 0.5 *M* HCl is greatly affected by increasing temperature. New absorption bands that cannot be seen at room temperature appear, and, at the same time, bands that are obvious at 25°C almost disappear at 120°C. We believe that these effects are associated with the equilibria of the U(IV) chloride complexes, and hence we predict that the complexes will not exist at temperatures much higher than 120°C. After this preliminary study is concluded, some of the lanthanide systems that should correspond closely to the trivalent actinide systems will be investigated.

14.3 EMISSION SPECTRA OF THE TRANSURANIUM ELEMENTS

The visible and near-infrared absorption spectra of Am^{3+} and Cm^{3+} indicate that americium and curium may have properties similar to those of laser materials. We are cooperating with personnel of the Transuranium Research Laboratory in studying these properties. The first step in the investigation was a study of the emission spectrum of 1 mole % Am_2O_3 embedded in $CaWO_4$. Two groups of the observed emission bands are encouraging. The bands of one group, near 7000 A, are sharp and narrow (~25 A) and are within 100 A of the wavelength of ruby laser light. The bands of the other group, near 10,000 A, have approximately the same intensities and bandwidths as the first group and are close to the wavelength of neodymium laser light. Further investigations will include refining the measurements of the emission lines and calculating the quantum values pertinent to evaluating Am_2O_3 as a laser material. Similar investigations of Cm_2O_3 will follow.

15. Chemical Engineering Research

15.1 DEVELOPMENT OF THE STACKED-CLONE CONTACTOR

The stacked-clone contactor is a multistaged countercurrent solvent extraction device featuring a high flow capacity, a very short residence time per stage, and high stage efficiencies. The ultimate objective of the stacked-clone development program is to apply this device to radiochemical systems that demand minimal solvent radiation exposure [e.g., the processing of short-cooled fast breeder reactor (FBR) fuels]. At this time the contactor holds promise of being highly suitable for this application.[1,2]

Other desirable features of the stacked-clone contactor include rapid response and rapid recovery from process perturbations. Its ability to attain steady-state operation from startup in a matter of a few minutes will undoubtedly bring about its application in short or varied processing campaigns, nuclear or nonnuclear, where small batches of feed must be processed quickly and efficiently at near-steady-state conditions.[3] Its very high throughput-to-internal-volume ratio allows extraction-scrubbing-stripping (i.e., full-cycle operation) to proceed with a very low solvent inventory. During a period of several weeks we used a total of only 30 liters of *n*-hexane as the diluent for TBP (in the extraction of uranyl nitrate) at solvent flow rates as high as 2 liters/min in both extraction and stripping contactors. The entire solvent inventory was recycled every 15 min.

The 18-stage (14 extraction and 4 polishing stages) prototype contactor,[3] 8.5 in. in diameter and 9 ft long, has been tested with simulated FBR fuel processing solutions. An aqueous feed that was 3 *M* in HNO_3 and contained 70 g of uranium per liter was contacted with 15 vol % TBP in an aliphatic hydrocarbon diluent. The solvent was scrubbed with 2 *M* HNO_3. Uranium processing rates as high as 41 kg/day were realized in the aqueous-continuous mode at mass-transfer stage efficiencies of about 50%. Uranium losses were less than 0.1% when more than ten stages were used for extraction. The solution residence time per stage was about 6 to 10 sec. Normally, extraction efficiencies in the aqueous-continuous mode are about 60%; however, solution backmixing imposed by the flow ratios, which were dictated by the FBR flowsheet conditions, limited mass transfer to the extent indicated and prevented solvent scrubbing. Organic-phase-continuous extraction efficiencies averaged about 30%. Previous experience with another system, although scant, showed 30 to 40% to be a normal value. Scrubbing did occur in the organic-phase-continuous mode; efficiencies were similar to extraction efficiencies.

As an outgrowth of the dimensional scaling studies completed last year, an 11-stage contactor, with nine hydroclones (i.e., clones) per stage, has been designed and is now being fabricated. The clones in this contactor are three-eighths of the size of the standard clones used in the prototype. The clones in each stage are driven by a single pump. The projected flow capacity of this new machine is higher than that of the prototype by a factor of 2.7. Stage efficiencies are expected to be about 10% higher, based on our experience with 0.5-scale clones. The solution residence time will be less

[1] M. E. Whatley *et al.*, *Unit Operations Section Quarterly Progress Report, July–September 1967*, ORNL-4234 (in preparation).

[2] M. E. Whatley *et al.*, *Unit Operations Section Quarterly Progress Report, October–December 1967*, ORNL-4235 (in preparation).

[3] W. S. Groenier and M. E. Whatley, *The Stacked-Clone Contactor: A High-Performance Solvent Extraction Machine Having Potential for Use in the Processing of Highly Radioactive Nuclear Fuels*, ORNL-4267 (July 1968).

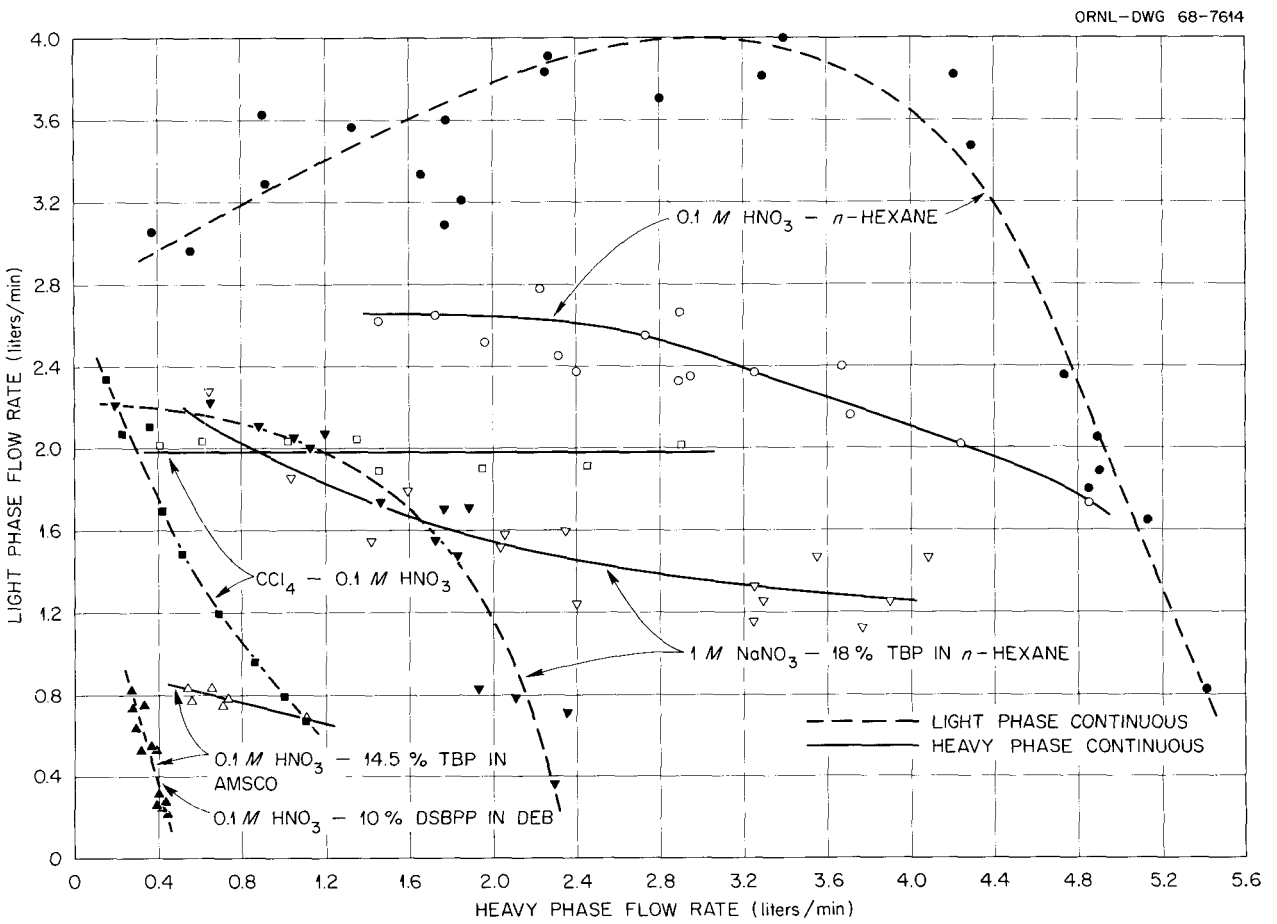

Fig. 15.1. Flow Capacities of the Prototype Stacked-Clone Contactor.

than 1 sec per stage. The new device is only 8 in. in diameter and 39 in. long.

Although the stacked-clone contactor possesses many unique capabilities, it also has limitations. Among these are a sensitivity to the viscosity of the aqueous phase and an inability to operate satisfactorily at very low flow ratios. The contactor will operate in the aqueous-continuous mode over a wide range of flow ratios (aqueous:organic) up to 50; however, at ratios of less than 1, backmixing of the phases becomes significant. Since many reprocessing flowsheets require flow ratios that are less than 1, increased efforts to evaluate the contactor for organic-continuous operation have been made. Recent performance data, in addition to data from simulated FBR processing runs, are listed in Table 15.1. Flow capacity data of special interest appear in Fig. 15.1. The range of physical properties represented by all solutions that have been tested in the stacked-clone contactor to date is as follows:

Density of continuous phase, g/ml	0.656–1.585
Density of dispersed phase, g/ml	0.656–1.585
Density difference between phases, g/ml	0.121–0.592
Viscosity of continuous phase, centipoises	0.31–4.17
Viscosity of dispersed phase, centipoises	0.31–116
Interfacial tension, dynes/cm	7.1–52.7

Organic-phase-continuous operation has proved to be beneficial with regard to increased flow capacity at low aqueous:organic flow ratios and with viscous aqueous systems. This mode of operation also allows solvent scrubbing to be accomplished. Since mass-transfer efficiencies have been quite low in the few tests made thus far, additional runs are being made to verify efficiencies in this mode.

Table 15.1. Performance Data for the Prototype Stacked-Clone Contactor

Heavy Phase	Light Phase	Continuous Phase	Flow Capacity at Flooding (liters/min) Continuous:Dispersed Phase Flow Ratio ½	1	2	3	5	Mass Transfer Efficiency (%)
0.5 *M* $Al(NO_3)_3$, 0.1 *M* HNO_3	Diethylbenzene (DEB)	Heavy	0.97	1.05	1.19	1.36		
		Light		2.06	2.31	2.39	2.28	
0.1 *M* HNO_3	Diethylbenzene (DEB)	Heavy		1.25	1.65			
		Light	1.40	1.68	1.98	2.03	1.95	
0.1 *M* HNO_3	10 vol % di-sec-butyl phenylphosphonate (DSBPP) in DEB	Light	0.66	0.78	0.96	1.08		
0.1 *M* HNO_3	Amsco 125-82	Heavy	2.85	3.12				
		Light	1.44	1.58	1.76	1.86	1.98	
0.1 *M* HNO_3	5.5 vol % tributyl phosphate (TBP) in Amsco	Heavy	1.76	2.11				
		Light	1.60	1.74	1.91	2.00	2.11	
0.1 *M* HNO_3	14.5 vol % TBP in Amsco	Heavy	1.29	1.54				
		Light	0.66	0.78	0.96	1.08		
1 *M* $NaNO_3$	18 vol % TBP in Amsco	Heavy[a]		1.00	1.31	1.56	1.95	
		Heavy	1.67	2.00	2.50	2.85	3.33	64.5
0.1 *M* HNO_3	*n*-Hexane	Heavy[a]	3.99	5.17	6.10	6.68		
		Light[a]	7.14	7.62	5.59	4.49	3.70	
1 *M* $NaNO_3$	18 vol % TBP in *n*-hexane	Heavy[a]	2.81	3.24	4.18	5.25		
		Light[a]	3.04	3.32	3.11	2.89	2.65	
1 *M* $NaNO_3$, 3 g of U per liter	18 vol % TBP in *n*-hexane, 10 g of U per liter	Heavy[a]		2.01	2.73	3.30	4.23	55.7
		Light[a]	2.12	2.15				36.7
CCl_4	0.1 *M* HNO_3	Heavy[a]	2.98	3.97	5.96			
		Light[a]	1.77	1.81	1.90	2.00	2.19	
20 vol % DSBPP in CCl_4	0.1 *M* HNO_3	Heavy[a]	2.41	2.97	4.44			
		Light[a]	2.28	2.11	2.00	2.02	2.10	

[a]Temperature 25 to 30°C; other data at 40 to 45°C.

Flow capacities in the organic-continuous mode decreased sharply as the concentration of extractant in diluent was increased. No significant flow capacities were obtained at extractant concentrations above about 15 vol % TBP in Amsco or about 10 vol % di-sec-butyl phenylphosphonate (DSBPP) in diethylbenzene. Operation with an internal interface, with no loss in throughput, is possible in this mode with certain systems. This type of operation is desirable from the standpoint of reducing the total solvent inventory, since no external settlers are required. Systems containing TBP or DSBPP at levels below those noted suffer some loss in capacity when an internal interface is used. We feel that modifications could be made in the design of those stages that contain the internal interface; in this way, the usefulness of this feature could be extended to other systems.

Two organic liquids that have potential as diluents by virtue of their unique physical properties are *n*-hexane and CCl_4. The extremely low viscosity of *n*-hexane (0.31 centipoise) rates it as an excellent candidate for organic-phase-continuous systems. It is currently in routine use by the British. High flow capacities are achieved when pure *n*-hexane and TBP-hexane systems are used (see Table 15.1). Carbon tetrachloride, which is heavier than most aqueous liquids, allows organic-phase-continuous operation to proceed with the heavy phase as the continuous phase. This diluent is currently under serious consideration for use in a ^{233}U recovery scheme at Battelle Northwest Laboratory. Its major disadvantage, the release of chloride on decomposition, would be minimized by the low residence time in the stacked-clone contactor.

16. Reactor Evaluation Studies

This program, which is a joint effort with other ORNL Divisions, especially the Reactor Division and the Metals and Ceramics Division, consists of studies of various advanced reactor and fuel-cycle systems to determine engineering and economic feasibility. The work in this Division during the past year included cost studies of shipping fresh and spent nuclear fuel, reprocessing spent fuel, and preparing various virgin and recycle fuel materials (oxides, metals, fluorides, etc.), primarily in support of the USAEC evaluation of civilian nuclear power for the period 1970–2020. Computer codes were developed to calculate rational growth patterns for the fuel cycle industry and to make projections of cost vs time for the various steps in the fuel cycle, based on both marketplace (nonoptimal) and optimal economic models. A computer code, RIBDOR, was written to calculate individual fission product isotopes, fission product elements, groups of chemically similar elements, and their gross totals, as well as beta and gamma decay heat release rates. The program also calculates gamma photon release rates in terms of 16 energy groups for use in shielding calculations.

16.1 WORK IN SUPPORT OF THE AEC EVALUATION OF CIVILIAN NUCLEAR POWER FOR THE PERIOD 1970–2020

From August 1966 to April 1968, the AEC, the national laboratories, and various industrial representatives were engaged in a large-scale economic evaluation of civilian nuclear power production. Representatives of Oak Ridge National Laboratory participated in this study, as members of various task forces, subcommittees, and working groups. The Chemical Technology Division was represented on the Systems Analysis Task Force (SATF) and the Fuel Recycle Task Force (FRTF) and on the working groups of these two task forces, the Advanced Converter Task Force, and the Alternate-Coolant Fast Breeder Reactor Task Force. We had the primary responsibility for preparing the preliminary report of the FRTF[1] and also contributed to the reports of the other three task forces mentioned.[2–11]

Work done for the SATF included: (1) collection of data from the various task forces and transmission to the SATF, (2) formulation of economic

---

[1] *Report of the Fuel Recycle Task Force*, USAEC Civilian Nuclear Power Series, WASH-1099 (in preparation).

[2] *Report of the Systems Analysis Task Force*, US AEC Civilian Nuclear Power Series, WASH-1100 (in preparation).

[3] *An Evaluation of Advanced Converter Reactors*, USAEC Civilian Nuclear Power Task Force Report, WASH-1086 (in preparation).

[4] *An Evaluation of Alternate Coolant Fast Breeders*, USAEC Civilian Nuclear Power Task Force Report, WASH-1090 (in preparation),

[5] R. S. Carlsmith, J. T. Roberts, R. Salmon, *et al.*, *An Evaluation of High-Temperature Gas-Cooled Reactors*, ORNL-4194 (in preparation).

[6] L. L. Bennett, J. T. Roberts, R. Salmon, *et al.*, *An Evaluation of Gas-Cooled Fast Breeders*, ORNL-4206 (in preparation).

[7] W. R. Gall, J. T. Roberts, R. Salmon, *et al.*, *An Evaluation of Steam-Cooled Fast Breeders*, ORNL-4245 (in preparation).

[8] R. D. Cheverton, J. T. Roberts, R. Salmon, *et al.*, *An Evaluation of a Heavy-Water-Moderated Boiling-Light-Water-Cooled Reactor*, ORNL-4258 (in preparation).

[9] P. R. Kasten, J. T. Roberts, R. Salmon, *et al.*, *An Evaluation of Heavy-Water-Moderated Organic-Cooled Reactors*, ORNL-3921 (January 1967).

[10] P. R. Kasten, J. T. Roberts, R. Salmon, W. G. Stockdale, *et al.*, *An Evaluation of Heavy-Water-Moderated Organic-Cooled Reactors*, suppl. A to ORNL-3921 (in preparation).

[11] E. H. Gift, J. T. Roberts, R. Salmon, *et al.*, *An Evaluation of Heavy-Water-Moderated Organic-Cooled Reactors*, suppl. B to ORNL-3921 (in preparation).

ground rules through the Ground Rules Subcommittee of the SATF, (3) participation in formulating and building the mathematical simulation model of the nuclear power economy in collaboration with the Model Subcommittee of the SATF, (4) review and evaluation of the calculational results, and (5) participation in writing the final report of the task force. The ORNL computer code POWERCO[12,13] was made a part of the simulation model. This code calculates the levelized power costs of the various reactors and determines the annual cash flows associated with the operation of these reactors over a 30-year lifetime. In combination with the PNL code PACTOLUS, POWERCO can be used to evaluate competing reactors on a levelized power cost basis without using the linear programming portion of the systems analysis model.

POWERCO was also used to calculate the fixed charge rates on depreciable and nondepreciable capital used by the Fuel Recycle, Advanced Converter, and Alternate-Coolant Task Forces in their economic evaluations.

One of the major tasks of Chemical Technology Division personnel, as members of the FRTF and its working group, was to supply fuel cycle cost data for various reactors. These data were required to be expressed both as a function of process throughput and as a function of time over the period 1968–2039. The computer code FUELCO was developed as a means of simulating the growth of the nuclear fuel-cycle industry and estimating the costs of the various individual operations. Starting with the total demands for fuel cycle services, this code determines a reasonable building schedule for the fuel preparation, fabrication, reprocessing, and reconversion plants that are required to meet these demands. From the sizes of the plants and their building schedules, the code then calculates the unit costs of the various fuel cycle services as a function of time. FUELCO is documented to some extent in the report of the Fuel Recycle Task Force[1] and will be described in detail in a forthcoming ORNL report. It was used by the SATF as a part of the input cost coefficient calculation.

Shipping costs for fresh and spent fuels were estimated for each reactor in the study; previously described computer codes and methods were used.

16.2 FUEL SHIPPING COST STUDIES

Estimates of fuel shipping costs were made for a large number of reactors. The methods used were generally the same as those that were described in previous reports[9,14,15] and were based mainly on the use of the computer code MYRA.[16] Typical estimates are summarized in Table 16.1.

The estimates for spent fuels were based on rail shipment, a distance of 1000 miles each way, and the use of casks weighing up to 120 tons. Casks were assumed to be purchased at a cost of $1.25 per pound; capital charges were based on a fixed charge rate of 15% per year. Property insurance was included at a rate of 0.0005 times the value of the shipment.

Estimates of the cost of shipping spent fast breeder reactor (FBR) fuel were based on the assumption that the fuel assemblies were sealed in individual liquid-metal-filled steel canisters in the manner suggested by the General Electric Company in 1964.[17] The steel shipping cask was assumed to carry four to six of these canisters at a given time. Because of the high value of the FBR core fuel, the optimal cooling time before shipment will be quite short, possibly 20 to 30 days. This short period will intensify the problem of removing decay heat, which is already difficult because of the high level of radioactivity of the fuel and the compact geometry of the fuel assemblies. A circulating-liquid cooling system outside the canisters would provide adequate heat removal during normal conditions of shipment. Under the accident conditions specified in the

[12] R. Salmon, *A Procedure and a Computer Code (POWERCO) for Calculating the Cost of Electricity Produced by Nuclear Power Stations*, ORNL-3944 (June 1966).

[13] R. Salmon, *Revision of Computer Code POWERCO (Calculation of Cost of Electricity Produced by Nuclear Power Stations)*, ORNL-4116 (in preparation).

[14] M. W. Rosenthal *et al.*, *A Comparative Evaluation of Advanced Converters*, ORNL-3686 (January 1965).

[15] R. Salmon, *Estimation of Fuel-Shipping Costs for Nuclear Power Cost-Evaluation Purposes*, ORNL-3943 (March 1966).

[16] R. Salmon, *A Computer Code for Calculating the Cost of Shipping Spent Reactor Fuels*, ORNL-3648 (August 1964).

[17] M. J. McNelly, *Liquid Metal Fast Breeder Reactor Design Study (1000 Mwe UO_2-PuO_2 Fueled Plant)*, vols. I and II, GEAP-4418 (January 1964).

Table 16.1. Estimated Costs for Shipping Spent Fuel

Dollars per kilogram of heavy metal charged to the reactor.
Where two figures are given, the upper figure is for core plus axial blanket, and the lower is for radial blanket.

Fuel Type	Near-Term			Long-Term		
	Spent Fuel	Fresh Fuel	Recycled Fuel	Spent Fuel	Fresh Fuel	Recycled Fuel
PWR – UO_2	4.01	0.65		3.37	0.50	
PWR – Pu recycle	4.01		1.10	3.37		0.95
HWBLW	1.80	0.45		1.67	0.40	
HTGR (reference design)	17.00	2.50	8.00	16.00	2.20	7.00
HWOCR – enriched UC	2.80	0.50		2.50	0.40	
HWOCR – ThO_2	3.30	0.50		2.91	0.40	
HWOCR – Th metal	4.30	0.50		3.77	0.40	
HWOCR – natural UC	1.80	0.55		1.50	0.45	
HWOCR – natural U	1.25	0.50		1.12	0.40	
GCFR (reference design)	14.30	2.00	2.60	13.00	1.70	2.30
	2.80	0.60		2.40	0.50	
SCBR – low pressure	12.00	1.70	2.40	11.00	1.50	2.10
	2.50	0.55		2.10	0.45	
SCBR – intermediate pressure	10.00	1.20	2.00	9.00	1.00	1.80
	2.20	0.50		1.80	0.40	
SCBR – high pressure	18.00	2.00	2.70	16.00	1.70	2.40
	3.00	0.60		2.50	0.50	
HTGR (backup design)	17.00	2.50	8.00	16.00	2.20	7.00
GCFR – advanced carbide	14.30	2.00	2.60	13.00	1.70	2.30
	2.80	0.60		2.40	0.50	
LMFBR – advanced oxide	33.20	2.30	3.20	29.88	2.07	2.88
	3.70	0.80		3.33	0.72	
LMFBR – carbide	25.70	1.80	2.70	23.13	1.62	2.43
	3.00	0.80		2.70	0.72	
LMFBR – advanced carbide	23.10	1.70	2.50	20.79	1.53	2.25
	2.80	0.70		2.52	0.63	
LMFBR – carbide converter	22.80	1.60	2.40	20.52	1.44	2.16
	4.50	1.00		4.05	0.90	
LMFBR – reference oxide (AI)	42.90	3.00	4.00	38.61	2.70	3.60
	4.90	0.85		4.41	0.77	
LMFBR – advanced oxide (AI)	29.50	2.10	3.10	26.55	1.89	2.79
	3.50	0.80		3.15	0.72	
LMFBR – oxide converter (CE)	28.70	2.00	2.80	25.83	1.80	2.52
	3.90	0.85		3.51	0.77	
GCFR (derated design)	14.30	2.00	2.60	13.00	1.70	2.30
	2.80	0.60		2.40	0.50	

AEC-ICC shipping regulations,[18,19] the circulating cooling system would become inoperative, and all heat would have to be removed by natural means. In making the cost estimates, it was assumed that the canisters could be made strong enough to avoid leakage or rupture under accident conditions. The demonstration of this point is of crucial importance in the design of a system for shipping spent fuel from fast breeders.

[18]Code of Federal Regulations, Title 10, Part 71, as published in the Federal Register, vol. 31, No. 141, July 22, 1966.

[19]Interstate Commerce Commission Order No. 70, Nov. 18, 1965, amended Apr. 14, 1966, as reported in the Federal Register, vol. 31, No. 83, Apr. 29, 1966.

16.3 COST ESTIMATES FOR THE PREPARATION, REPROCESSING, AND RECONVERSION OF FUEL

Cost Estimates for the Preparation and Reconversion of Fuel

Table 16.2 summarizes estimates of the capital investment and the annual operating costs that will be associated with the preparation and reconversion of fuel for various reactors. These estimates were used in our recent reactor evaluation studies. Empirical cost-scaling equations of the following form were fitted to the estimates by choosing the best values for the parameters

Table 16.2. Summary of Fuel Preparation and Reconversion Cost Estimates Used as Bases for FUELCO Cost Equations

FUELCO Identification No.	Process	Plant Capacity (metric tons/day)	Capital Investment (dollars)	Annual Operating Costs (dollars)
			$\times 10^6$	$\times 10^6$
46	$UF_6 \rightarrow UO_3$	1	2.54	0.615
		10	7.53	1.91
		30	13.4	3.91
47	$UO_3 + Pu(NO_3)_4 \rightarrow UO_2 \cdot PuO_2$	0.907	3.93	0.765
		9.07	11.6	2.26
		27.2	24.3	4.73
48	$U_3O_8 \rightarrow UO_3$	0.907	2.06	0.425
		9.07	5.36	1.12
		27.2	9.40	2.51
49	$UO_3 \rightarrow UO_2$	1	1.11	0.364
		10	3.41	1.12
50	$UO_2 \rightarrow U(metal)$	1	2.00	1.00
		10	10.7	5.72
		30	23.9	13.2
51	$UO_2(NO_3)_2 + Pu(NO_3)_4 \rightarrow UO_2 \cdot PuO_2$	2.25	2.46	0.395
		6.76	3.98	0.660
53	$Th(NO_3)_4 + {}^{233}UO_2(NO_3)_2 + {}^{235}UF_6 \rightarrow ThO_2 \cdot UO_2$	1	5.82	1.16
		4	11.0	2.19
54	$Th(NO_3)_4 + {}^{233}UO_2(NO_3)_2 + {}^{235}UF_6 \rightarrow Th(metal) + U(metal)$	1	6.84	2.00
		4	12.1	4.51
58	$UO_2(NO_3)_2 \cdot 6H_2O \rightarrow UF_6$	1	2.53	1.27
		5	6.74	2.45

Table 16.3. Typical Fuel Preparation and Reconversion Costs Calculated by FUELCO

FUELCO Identification No.	Year	Number of Plants	Total Throughput (metric tons)	Unit Cost (dollars/kg)
46	1972	3	1,961	3.19
	1995	6	14,085	1.64
	2020	6	42,203	1.03
47	1977	3	1,010	5.00
	1995	5	8,801	3.76
	2020	12	58,876	2.07
48	1977	3	825	3.93
	1987	3	1,200	3.93
	1997	1	377	3.93
49	1972	3	1,961	1.77
	1995	5	12,135	0.87
	2020	3	16,059	0.59
53	1980	4	932	11.02
	1990	5	1,495	10.35
	2000	3	1,299	8.16
58	1975	3	1,358	5.23
	1990	3	4,721	3.72
	2005	2	1,427	3.66

A, B, C, D, E, and F:

$$\text{C.I.} = AS^B + CS ,$$

$$\text{A.O.C.} = D(0.5S + 0.5S^*)^E + FS ,$$

where

C.I. = total capital investment, millions of dollars,

A.O.C. = annual operating cost, millions of dollars per year,

S = nominal plant capacity, metric tons/day,

S^* = actual average production rate, metric tons/day = (actual metric tons/year) ÷ 260.

These equations, together with the amounts and types of reactor fuels that are assumed to be required over the next 50 years, are used in the FUELCO code to predict the number and the size of fuel preparation and reconversion plants, and the associated unit costs, that will be required in the future.

The results for typical cases are summarized in Table 16.3. The capital investment figures were converted to equivalent annual capital charges, using a fixed-charge rate (FCR) of 24%/year. This FCR, which was calculated by using the POWERCO[12,13] code, can be subdivided as follows:

1. Cost of money	
70% equity capital at 16%/year	11.20%
30% debt capital at 5%/year	1.50
	12.70%
2. Other capital charges (present-worth levelized)	
Depreciation (sinking fund, 15 years at 12.7%)	2.54%
Federal income tax (50% rate, based on sum-of-the-years'-digits depreciation)	5.69
State and local taxes	2.51
Interim replacement	0.35
Property insurance	0.25
Total	24.04%

Cost Estimates for Fuel Reprocessing and Waste Disposal

The spent-fuel reprocessing cost estimates for our recent reactor evaluation studies were based on the following cost estimates (in millions of dollars) for standard light-water-reactor fuels:

	1.0-metric-ton/day Plant	10.0-metric-ton/day Plant
Construction of facilities, including field engineering and construction interest, but *not* including waste storage facilities	23.0	51.0
Plant site, working capital, and preoperational testing	3.0	7.0
	26.0	58.0
Contingencies	3.0	7.0
Total capital investment (exclusive of waste disposal)	29.0	65.0
Annual capital charges at 24% FCR	6.96	15.6
Annual operating costs	2.57	6.76

We fitted these estimates to empirical cost-scaling equations as follows:

$$\text{C.I.} = A(S)^{0.35} ,$$

$$\text{A.O.C.} = 0.084(\text{C.I.}) + (0.13 \times 10^6)\,(S^*) ,$$

where C.I., A.O.C., S, and S^* have the same meanings as given previously, and A is the capital cost estimate for a 1.0-metric-ton/day reprocessing plant to handle spent fuels of the types specified, in millions of dollars.

Multipurpose plants were assumed for the FUELCO reprocessing cost calculation. Costs were added, as necessary, for head-end and tail-end modifications to the nominal 1.0-metric-ton/day LWR fuel plant; throughputs were reduced for some fuels. The resulting modified capital investment was scaled with the 0.35 power for plants having sizes other than 1.0 metric ton/day (260 metric tons/year). In the case of plutonium-recycle-LWR fuel or HWOCR-thorium fuel, an estimated $2.5 million was added to the basic $29 million capital investment for the 1-metric-ton/day LWR fuel plant. The throughput was assumed to remain at 1000 kg/day for the plutonium-recycle fuel but to be reduced to 500 kg/day for the thorium fuel. In the case of FBR fuel, $5.0 million was added to the basic capital investment, and fuel throughput was assumed to be 500 kg/day. An additional $1.0 million each was added for: (1) SAP-clad fuels (some HWOCR types), (2) carbide fuels (some HWOCR and some FBR types), and (3) sodium-bonded fuels (some FBR types). An estimated additional $9.0 million was added for HTGR fuels, and the HTGR fuel throughput was assumed to be 500 kg/day. We also assumed that the ^{235}U-^{236}U particles were separated from the Th-^{233}U particles in the head-end portion of the process and that the two types of uranium were recovered separately. No extra capital charges were assessed for handling HWBLWR or HWOCR-U(metal) fuels.

In the worst case (i.e., for the case in which all fuel types are to be handled in the same plant), this scheme for estimating the capital investment would give $46 million for a nominal 1.0-metric-ton/day plant (handling 0.5 metric ton of FBR or thorium fuel per day), $103 million for a nominal 10-metric-ton/day plant (handling 5 metric tons of FBR or thorium fuel per day), or $169 million for a 41-metric-ton/day plant (the largest size considered, after about year 2018). The scheme used by computer code FUELCO for assigning fuels to the various reprocessing plants tends to "overdiversify"; for example, in a typical study of LWR's, advanced converters, and FBR's, 35 of the 55 reprocessing plants built were provided with the capability for handling HTGR fuels, whereas a much smaller number would have sufficed. Twenty-two of the fifty-five plants were capable of handling *all* fuel

types. This means that the FUELCO estimates are conservative, at least in this respect.

Single-purpose reprocessing plants, which are designed to handle only one type of fuel, are potentially a more economical choice for some fuel types if a sufficient amount of fuel of that type is available to support a large plant. ORNL-estimated costs for a single-purpose plant are built into the FUELCO capital cost calculation scheme, although the present fuel assignment scheme only rarely calls for a single-purpose plant. The 1.0-metric-ton/day single-purpose plant estimates (with *no* throughput reductions required) that are currently provided in FUELCO are as follows:

	Millions of Dollars
LWR or HWBLWR or HWOCR-U(metal U(metal)	29
LWR-Pu-recycle	31.5
HWOCR-Th(metal)	30
HWOCR-UC (SAP-clad) or HWOCR-ThO_2 (SAP-clad) or HTGR	31
FBR-oxide (no Na bond)	37
LMFBR-carbide (Na bond)	39.5

The absence of a "thorium penalty" in the single-purpose plant costs is based on a Du Pont estimate for the HWOCR evaluation.[9] This estimate reveals that a 9.07-metric-ton/day remote-maintenance plant for reprocessing HWOCR-Th fuel would cost approximately the same as Du Pont's original 9.07-metric-ton/day uranium plant, that is, $60 million on the original basis, after taking into consideration that larger equipment would be needed but that fewer cycles of decontamination would be required. Remote fabrication of the recycle thorium and uranium would be necessary, in any event, because of the presence of the gamma-active daughters of ^{228}Th, ^{234}Th, and ^{232}U.

For the recent evaluations, our reprocessing cost estimates show a separate annual charge for total waste disposal costs, including the capital and operating costs for the waste processing plant, as well as the subsequent "perpetual-maintenance" costs. Some form of government (state or federal) ownership of the waste disposal facilities has been assumed in that we have used a 4% cost of money and a tax-free basis and have assumed that the total waste disposal costs are charged to the processing plant on an amortized annual payment basis. In FUELCO, the construction-date–size schedule is developed for the reprocessing plant, and the basic capital and operating costs are calculated; then the waste costs are calculated separately and are added to give a total reprocessing cost for each type of fuel.

The annual high-level waste disposal charge (A.H.L.W.C.) was calculated from the following empirical cost-scaling equation, obtained by fitting TASCO[20] results for reprocessing plants of sizes in the range assumed in FUELCO:

$$\text{A.H.L.W.C.} = (\$1.46 \text{ million}) \times \left[\frac{\sum_j (\text{metric tons/year})_j \, (\text{Mwd/metric ton})_j}{10^7}\right]^{0.844} .$$

The numerator inside the brackets is, for a particular plant, the sum (over all the fuel types processed) of the products of the amount of fuel of each given type and the burnup of that fuel type. The numerical value of the numerator is thus the number of thermal megawatt-days per year represented by the fuel processed and is approximately equal to the number of grams of fission products handled per year in the plant. The 10^7 in the denominator is a normalizing factor, such that the $1.46 million coefficient represents the annual high-level waste charge to a plant handling, annually, the equivalent of 1000 metric tons of fuel that has been irradiated to a burnup of 10^4 Mwd/metric ton.

An annual intermediate-level waste disposal charge (A.I.L.W.C.) was assessed to fuels requiring a chemical decladding step. In this study, such a cost was applied only to SAP-clad fuels (HWOCR-UC and HWOCR-ThO_2). This charge was calculated from an empirical cost-scaling law based on TASCO[20] calculations for long-term tank storage of neutralized low-heat-level wastes:

$$\text{A.I.L.W.C.} = (\$336{,}000) \left[\frac{\text{metric tons/year}}{10^3}\right]^{0.844} .$$

[20] J. O. Blomeke, E. J. Frederick, R. Salmon, and E. D. Arnold, *The Cost of Permanent Disposal of Power-Reactor Fuel-Processing Wastes in Tanks*, ORNL-2873 (September 1965).

The numerator inside the brackets represents the amount of HWOCR-UC and HWOCR-ThO_2 fuel processed per year in a particular reprocessing plant. The denominator is a normalizing factor.

A storage charge was assessed for thorium and depleted uranium recovered in reprocessing. Recovered thorium was assumed to be stored for ten years or more to allow its gamma activity to decay to that of natural thorium before being returned to the fuel cycle. Depleted uranium was assumed to be stored semi-indefinitely. Based on TASCO-type calculations, the estimated annual storage charges for thorium (A.Th.S.C.) and depleted uranium (A.D.U.S.C.) were expressed by the following empirical cost scaling equation:

$$\text{A.Th.S.C., or A.D.U.S.C.} = (\$1.53 \text{ million}) \times \left[\frac{\text{metric tons/year}}{10^3}\right]^{0.844}$$

The numerator inside the brackets is the total amount of thorium and depleted uranium handled each year by a reprocessing plant.

Using these cost-scaling equations, together with assumed amounts and types of spent fuels to be processed over the next 50 years, we used the FUELCO code to predict the number and the sizes of plants, and the associated unit costs, that will be required in the future. Table 16.4 shows one projection of spent-fuel discharge, by geographical region, with time. This particular projection was based on a mixture of uranium-fueled LWR's, recycle-plutonium-fueled LWR's, and carbide-fueled FBR's. The FUELCO projection of the number of multipurpose reprocessing plants (for handling all three of these fuel types) that will be in operation by the designated years was:

Year	Number of Multipurpose Reprocessing Plants
1980	4
1990	6
2000	8
2010	10
2020	12

These numbers do not include the plants that would cease operation after a nominal 15-year life.

The projected unit reprocessing costs for reference LWR fuel irradiated to a burnup of 20,000 Mwd/metric ton were:

Year		Dollars per Kilogram
1972	Basic reprocessing	27.33
	High-level waste	3.24
		30.57
1990	Basic reprocessing	10.75
	High-level waste	2.34
		13.09
2010	Basic reprocessing	5.57
	High-level waste	2.08
		7.65

These unit charges would correspond to fully loaded single-purpose plant sizes of about 1.6, 6.9, and 20.6 metric tons/day respectively; however, they actually result from calculations made for larger plants which are, on the average, less than fully loaded and which may have multipurpose capability.

In another study, which included advanced converters and oxide-fueled FBR's, reprocessing charges were calculated for the various types of fuel expected to be used in 1990 (see Table 16.5). The basic charge was $13.20 or $26.40 per kilogram; the latter charge is based on a throughput reduction factor (disadvantage factor) of 2 for thorium fuels and FBR fuels (mixed core and blanket). The high-level waste cost is related to burnup. The intermediate-level waste cost, for SAP-decladding waste, is small and applies to only one type of fuel in this case. The charge for storing thorium or depleted uranium is higher, adding about 5% to the totals. The LWR reprocessing cost estimate is higher here than in the previously mentioned case because more fuel types are included. Thus higher head-end and tail-end costs are required in the multipurpose reprocessing plants, with these costs being shared by all of the fuels. Also, the total load (in equivalent tons of LWR fuel) is lower, as a result of more high-burnup fuels. This leads to higher unit costs.

Table 16.4. Projected Geographical Distribution of Spent-Fuel Discharges

Units are "equivalent" metric tons[a] discharged during year

Year	FPC[b] Region Designation								Total in U.S.A.
	I	II	III	IV	V	VI	VII	VIII	
1970	94	3	0	21	0	0	24	15	157
1971	127	9	13	72	0	0	25	16	262
1972	228	21	86	163	0	0	33	21	553
1973	308	28	202	182	0	11	31	19	782
1974	370	78	285	224	0	36	30	54	1,078
1975	426	105	348	260	15	43	46	108	1,351
1976	529	125	455	303	25	50	75	150	1,711
1977	633	141	545	347	24	53	102	198	2,042
1978	781	175	684	414	39	55	134	273	2,556
1979	889	192	803	458	47	67	159	336	2,950
1980	1,204	258	1,090	606	54	88	219	481	4,001
1982	1,694	397	1,589	819	115	140	315	738	5,807
1984	2,079	554	2,002	995	187	177	400	971	7,365
1986	2,694	808	2,674	1,301	316	238	539	1,344	9,914
1988	3,525	1,195	3,602	1,747	540	327	742	1,866	13,544
1990	4,358	1,672	4,633	2,253	896	429	981	2,474	17,697
1992	4,847	2,113	5,349	2,629	1,339	508	1,174	2,947	20,907
1994	5,362	2,640	6,074	3,061	1,940	599	1,420	3,475	24,571
1996	5,923	3,262	6,855	3,544	2,598	701	1,696	4,043	28,623
1998	6,414	3,897	7,556	4,001	3,305	799	2,006	4,586	32,564
2000	7,376	4,840	8,735	4,739	4,277	955	2,484	5,437	38,842
2002	8,301	5,791	9,896	5,446	5,289	1,109	3,049	6,233	45,114
2004	9,343	6,832	11,135	6,187	6,360	1,270	3,600	7,063	51,791
2006	11,115	8,461	13,282	7,467	7,953	1,543	4,490	8,398	62,708
2008	12,200	9,617	14,564	8,291	9,098	1,720	5,131	9,190	69,812
2010	13,791	11,168	16,481	9,456	10,640	1,970	5,999	10,284	79,789
2012	15,214	12,585	18,181	10,474	12,071	2,203	6,799	11,176	88,703
2014	16,550	13,899	19,732	11,428	13,369	2,417	7,552	11,955	96,902
2016	18,605	15,843	22,111	12,878	15,298	2,736	8,648	13,245	109,365
2018	19,557	16,868	23,246	13,602	16,291	2,905	9,237	13,775	115,480
2020	20,419	17,822	24,274	14,274	17,278	3,056	9,778	14,214	121,116

[a]One metric ton of (mixed core and blanket) FBR fuel is assumed to be equivalent to two metric tons of LWR fuel for reprocessing purposes.

[b]Federal Power Commission.

Table 16.5. Estimates of Reprocessing Costs in 1990, as Calculated by FUELCO for Multipurpose Plants

Fuel Type	Average Burnup (Mwd/metric ton)	Costs[a] for –				Total Costs
		Basic Reprocessing	High-Level Waste	Intermediate-Level Waste	Storing Th or Depleted U	
LWR	20,300	13.20	2.27			15.47
LWR-Pu	33,900	13.20	3.79		1.46	18.45
HTGR	61,600	26.40	6.89		1.46	34.75
HWOCR-UC	17,000	13.20	1.90	0.35	1.46	16.91
FBR-oxide (GCFR; SCBR; LMFBR-Ox.)	33,000	26.40	3.68		1.46	31.54
FBR-carbide (LMFBR, Na-bond)	47,300	26.40	5.29		1.46	33.15

[a]Costs are given in dollars per kilogram, based on amount of heavy metal (U + Pu + Th) charged to reactor. (Unit costs would be somewhat higher if based on amount of heavy metal discharged from reactor.)

The differences in the totals, especially between thorium and fast breeder reactors on the one hand and all the uranium-fueled thermal reactors on the other, may or may not be exaggerated from an evaluation point of view. In such a "system," it might be more economical to have a greater number of single-purpose reprocessing plants; this would tend to increase the lower totals, as well as to decrease some of the higher totals, in Table 16.5.

16.4 OPTIMIZATION STUDIES OF THE REPROCESSING INDUSTRY IN AN EXPANDING NUCLEAR ECONOMY

The FUELCO rationale for calculating reprocessing costs as a function of time is based on an arbitrary, intuitive "marketplace" model of an expanding economy. Optimization (cost minimization) of the sizes and dates of construction of plants is not considered explicitly, although costs could be minimized by using large values for the maximum-plant-size sequence and an optimal "look-ahead" time. The possibility of backlogging (inventorying) spent fuel prior to building a reprocessing plant, in order to permit the construction of larger plants with better load factors, is not considered. Also, the locations of plants are not considered.

Studies have shown that significant savings are potentially available, on paper at least, by optimization of the sizes, locations, and dates of construction of reprocessing plants and of the backlogging of spent fuel. These studies assume centralized coordinated planning for the entire nation, with no requirement of free competition (although ownership of the various plants by different commercial companies is not excluded). Thus, the results indicate only a theoretical optimal strategy; however, they are interesting and informative for evaluation purposes and for comparison with alternative strategies.

A linear-programming (LP) model of the United States spent-fuel reprocessing economy during the period 1970–2039 has been developed at ORNL and used for two types of problems, one in which no limits were placed on reprocessing plant sizes and another in which "intuitive" limits were placed on plant size in each year (the limits increasing with time). The present method used for correcting for nonlinearities in reprocessing costs does not necessarily yield true global optima (minimum-cost solutions); however, it is thought that the solutions obtained probably are near optimal as far as present-work total cost

Table 16.6. Schedule Showing the Locations, Sizes, and Dates of Construction of Processing Plants, as Indicated by a Linear-Programming Model[a]

First Year of Operation	Results with No Limits Placed on Individual Plant Size (size, metric tons/day)	Results with Upper Limits Placed on Individual Plant Size with Time (size, metric tons/day)
1972		3.5 (I)
1974	18.4 (III)	
1976		6.5 (III)
1980		9.5 (I)
1983		12.5 (III)
1986	77.0 (III)	15.0 (VIII)
1988		18.0 (IV)
1990		20.0 (II)
1992		22.0 (III)
1995		25.0 (I)
1997		26.5 (V)
1998	18.5 (III)	
1999		28.5 (III)
2001		31.5 (VIII)
2002	178 (III)	
2003		33.5 (IV)
2004		35.0 (VII)
2005		36.0 (II)
2007		39.5 (III)
2008		40.0 (I)
2010		40.0 (V)
2011		40.0 (I)
2012	43.4 (VIII)	40.0 (II)
2014		40.0 (III)
2015		40.0 (V)
2016		40.0 (VIII)
2017	185 (III)	40.0 (IV)
2018		40.0 (III)
2019		40.0 (VII)
2020		40.0 (II)
2021	65.5 (I)	
2022		40.0 (I), 40.0 (III)
2023		40.0 (IV), 40.0 (VIII)
2025		40.0 (I), 40.0 (V)
2026	118 (II), 68.7 (VIII)	40.0 (I)
2027		40.0 (II)
2029		40.0 (III)
2030		40.0 (II), 40.0 (V), 40.0 (VI), 40.0 (VII)
2031		40.0 (VIII)
2032		40.0 (IV)
2033		40.0 (III)
2035		40.0 (VII)
2037		40.0 (I), 40.0 (II), 40.0 (III)
2038		40.0 (IV), 40.0 (VIII)
Total No. of plants	9	49

[a]Basis: Spent-fuel discharge schedules based on Table 16.4. Sizes are expressed in "equivalent" metric tons/day, with 1 metric ton of FBR or thorium fuel assumed to be equivalent to 2 metric tons of PWR fuel. Backlogging of spent fuel for one or more years before reprocessing is permitted if economically justified. Reprocessing plant life assumed to be 15 years. Intra- and interregional shipping costs, backlogging costs, and reprocessing costs (varying with scale) as estimated by ORNL. Radioactive waste disposal costs not included in optimization. Roman numeral in parentheses indicates FPC region designation number.

(of shipping, inventorying, and reprocessing) is concerned.

The estimated amount of spent fuel to be discharged from nuclear reactors in each of eight geographical regions of the United States in each of the 70 years during the period 1970–2039 (Table 16.4, extrapolated an additional 20 years to minimize "end effects") was supplied as input to the IBM-360-75 "MPS" LP code, together with intra- and interregional shipping costs, estimated costs of inventorying spent fuel prior to processing, and the estimated cost-scaling laws for reprocessing. The code decides whether (and how much) fuel backlogging is economically optimal prior to building a plant and determines the locations and the sizes of the plants.

Table 16.6 gives the solutions obtained both with and without limits on individual plant sizes. The present-worth-averaged cost over the 70 years of shipping, backlogging, and reprocessing (but not including waste disposal) for the no-limits case was about $10.90 per kilogram, assuming that only nine plants were built during the entire time period. When arbitrary "intuitive" plant size limits were imposed (starting at 2 metric tons/day for plants coming on stream in 1970 and increasing to 5 metric tons/day, 10 metric tons/day, and 40 metric tons/day by 1974, 1980, and post-2010 respectively), the present-worth-levelized cost increased to about $12.10 per kilogram; the number of plants built increased to 49.

Essentially the same problem was run using the FUELCO code. The FUELCO solution indicated a greater number of smaller plants (a total of 52) and gave an overall present-worth-averaged reprocessing cost of $11.40 per kilogram. This cost would have to be adjusted to approximately $14.80 per kilogram for comparison with the optimized LP results (adding $3.30 per kilogram for shipping costs, but not including waste disposal costs).

The LP results that do not stipulate any limit on plant size are not felt to be realistic because the cost-scaling laws are not valid up to the very large sizes indicated (e.g., 178 metric tons/day) and also because siting and other considerations may limit individual plant sizes. It is, however, economically important to determine what limits really are applicable to this problem on some better basis than "arbitrary" or "intuitive" judgment. Apparently, the optimal solution to the LP model will be to build plants mostly at the upper limit imposed on size, with the code deciding the locations and the dates of construction.

In this model, 1 kg of FBR fuel is assumed to be equivalent to 2 kg of LWR fuel; thus the unit costs mentioned above must be doubled for FBR. The "average" costs apply, roughly, to the period 1985–90.

The present method for handling nonlinear costs in the linear program probably distorts the results involving location more than those involving size and date of construction. An improved version of the LP code, using the separable-variables method for handling nonlinearities, is also under current development at ORNL and is expected to greatly increase the probability of arriving at a true minimum-cost solution (with regard to the sizes, locations, and dates of construction of the plants, and to the backlogging of spent fuel) instead of a "local" optimum.

16.5 RIBDOR FISSION PRODUCT CODE

A computer code, RIBDOR, has been written to calculate activities and concentrations of individual fission product isotopes, fission product elements, groups of chemically similar elements, and their gross totals, as well as beta and gamma decay heat release rates. The program also calculates gamma photon release rates in terms of 16 energy groups for use in shielding calculations.

Fission-yield and cross-section data have been obtained for the thermal and fast fission of both ^{235}U and ^{239}Pu. The fast-reactor data have been used to evaluate fission product production and heat generation rates for the fast-reactor program.

Beta and gamma energy group data for ^{239}Pu fission products have been calculated by the RIBDOR program to be used as permanent data for PHOEBE.[21]

A set of calculations for a fast-reactor plutonium-fueled core operating at a specific power of 133 Mw/metric ton, irradiated to a burnup of 80,000 Mwd/metric ton, were made by using RIBDOR. The results were compared with those obtained by using the PHOEBE code and ^{235}U

[21] E. D. Arnold, *PHOEBE – a Code for Calculating Beta and Gamma Activity and Spectra for ^{235}U Fission Products*, ORNL-3931 (July 1966).

release rate data. RIBDOR results for the release of heat from fast-reactor plutonium fuel agree, within 10% for decay times of 1 to 120 days, with those of PHOEBE for thermal ^{235}U. However, the RIBDOR results are 37% higher than those of PHOEBE after one year's decay. This represents the difference, for the two cases, in yields of fission products (e.g., ^{106}Ru and ^{144}Ce) having intermediate (approximately one-year) half-lives. Results of these calculations are shown in Table 16.7 and in Figs. 16.1 and 16.2.

Table 16.7. Heat Release Rates from Fast-Reactor Plutonium-Fueled Core Irradiated to a Burnup of 80,000 Mwd/metric ton at a Specific Power of 133 Mw/metric ton

Decay Time (days)	Heat Source	Calculated Fission Product Heat Release Rate (kw per kilogram of fuel)	
		RIBDOR	PHOEBE
1	Beta	230.5	248.7
	Gamma	362.7	328.2
	Total	593.2	576.9
4	Beta	150.0	160.2
	Gamma	245.9	222.6
	Total	395.9	382.7
10	Beta	116.1	120.9
	Gamma	174.6	165.5
	Total	290.7	286.4
30	Beta	81.3	84.2
	Gamma	97.6	94.4
	Total	178.9	178.6
60	Beta	63.5	63.0
	Gamma	60.5	58.2
	Total	124.0	121.2
90	Beta	54.9	51.5
	Gamma	43.9	42.0
	Total	98.7	93.5
100	Beta	52.7	48.6
	Gamma	39.8	38.2
	Total	92.5	86.8
120	Beta	49.1	43.8
	Gamma	33.2	32.0
	Total	82.3	75.8
180	Beta	41.0	33.5
	Gamma	20.3	19.8
	Total	61.3	53.3
365	Beta	26.6	18.0
	Gamma	6.8	6.4
	Total	33.4	24.4

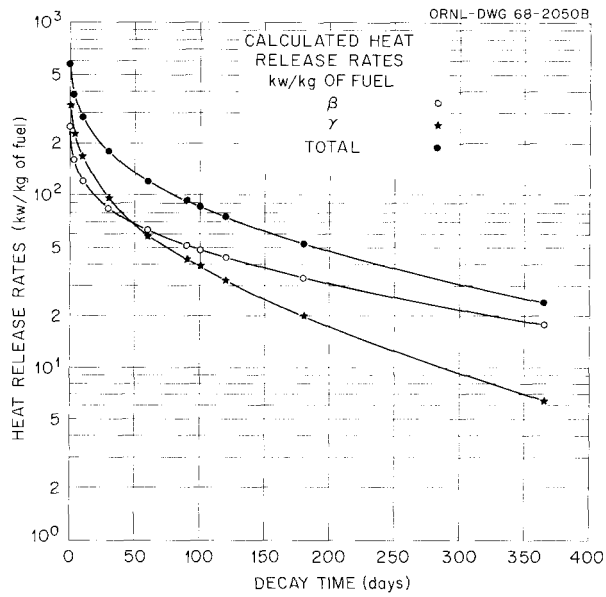

Fig. 16.1. Calculated Heat Release Rates for Thermal Fission of ^{235}U as Calculated by PHOEBE. Specific power = 133 Mw/metric ton; burnup = 80,000 Mwd/metric ton.

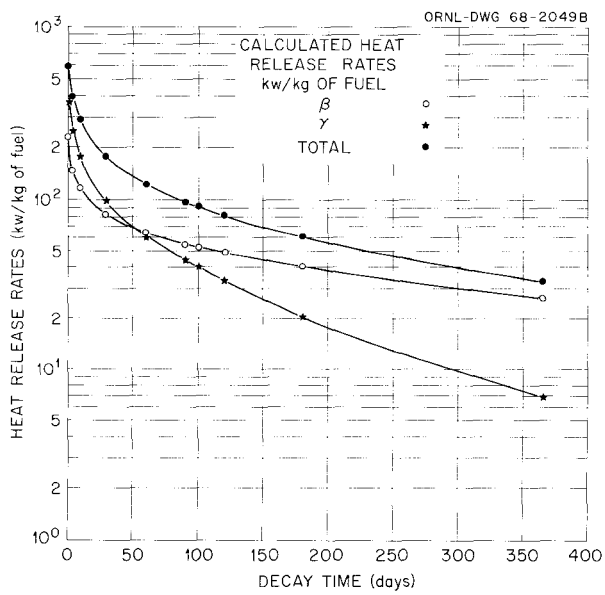

Fig. 16.2. Calculated Heat Release Rates for Fast Fission of ^{239}Pu as Calculated by RIBDOR. Specific power = 133 Mw/metric ton; burnup = 80,000 Mwd/metric ton.

17. Preparation and Properties of Actinide Oxides

The purpose of this program is to find ways of influencing the microstructural, surface-chemical, and colloid-chemical properties which control the behavior of the metal hydroxides and oxides that are important in sol-gel processes. Techniques developed for thoria (and also used for urania) are being extended to plutonia and other actinide oxides and to the corresponding lanthanide oxides.

17.1 FUNDAMENTAL STUDIES OF URANIA SOLS

Electrophoretic Studies

Studies of the charge on colloidal UO_2 particles were continued, using both the Beckman model H electrophoresis instrument (with a Tiselius cell) and a Waters streaming current detector. Most of the work was done with chloride-stabilized sols, in order to minimize the U(VI) content.[1] For measurements of the electrophoretic mobility with the regular optical system of the Beckman model H electrophoresis apparatus, the concentrations of the nearly opaque urania sols were limited to approximately 0.02 *M*. At higher concentrations, insufficient light was transmitted to give Rayleigh fringes or schlieren patterns; at lower concentrations, the refractive index gradient was insufficient to obtain the patterns. For measurements at higher concentrations, an external water bath assembly was made to accommodate the Tiselius cell assembly, and the boundary velocities were measured by means of a cathetometer. The ascending boundary usually moved faster than the descending boundary; the electrophoretic mobilities were dependent on sol concentration and the voltage gradient applied (Tables 17.1 and 17.2). With this technique it is impossible to see any extraneous boundaries that may be present; however, the more rapid movement of the ascending boundary indicates nonideal behavior. In one experiment with 0.35 *M* chloride-stabilized sol, electrophoresis was performed until the ascending and descending boundaries were at exactly the same height. The cell arms were then isolated and opened, and their contents were submitted for analysis. Results showed that the sol in the descending arm was depleted in U(VI) and that the sol in the ascending arm was enriched in U(VI); the U(VI)/U(IV) ratios were 0.066 and 0.113 respectively. These results indicate that the distribution of U(VI) on the U(IV) sol particles is nonuniform and that the more highly oxidized particles have a higher charge (and thus should be more stable). This reasoning is in conflict

Table 17.1. Effect of Sol Concentration on the Measured Electrophoretic Mobility of Urania Sols

Sol Concentration[a] (*M*)	Electrophoretic Mobility[b] ($cm^2\ v^{-1}\ sec^{-1}$)	Voltage Gradient (v/cm)
	$\times 10^{-4}$	
0.02	2.71	1.23
0.175	1.51	1.48
0.35	1.18	1.16
0.70	1.02	1.02
1.50	0.71	0.75

[a]Chloride-stabilized UO_2; 1.12% oxidized to U(VI); pH 1.8.

[b]Calculated from the velocity of the descending boundary.

[1]D. M. Helton, J. T. Bell, and N. A. Krohn, *Preparation and Preliminary Studies of Chloride-Stabilized UO_2 Sols*, ORNL-TM-2056 (February 1968).

Table 17.2. Effect of Voltage Gradient on the Measured Electrophoretic Mobility of Urania Sols

Type of Urania Sol	Voltage Gradient (v/cm)	Electrophoretic Mobility ($cm^2\ v^{-1}\ sec^{-1}$)
		$\times 10^{-4}$
Nitrate-formate-stabilized	0.57	5.30
[~0.02 *M*; 15% U as U(VI)]	1.14	3.35
	2.28	2.38
	4.56	2.19
Chloride-stabilized	0.62	4.48
[~0.02 *M*; 1.12% U as U(VI)]	1.23	2.71
	6.15	2.36

with the general observation that exposure of nitrate-stabilized urania sols to air causes them to gel, but it agrees with the viscosity results previously reported for the effect of the addition of UO_3 to concentrated chloride-stabilized UO_2 sols.[1,2] Thus a major difference between chloride-stabilized and nitrate-formate-stabilized sols may have been established.

Streaming Current Studies

The newly acquired Waters streaming current detector was used to study the effect of oxidation on both chloride- and nitrate-stabilized sols. This detector is a recently developed instrument which gives a current reading that is proportional to the zeta potential of the sol particles. The assembly is small and can be readily sealed into a chamber that can be flushed with any desired gas. In studies of the effect of oxidation on the streaming current of urania sols, CO_2-free air was continuously passed over each sol, and the streaming current (in arbitrary units) was measured as a function of time. Preliminary results shown in Table 17.3 indicate a difference in behavior of the two sols. The current measured with the chloride-stabilized system changed only slightly, showing a small decrease followed by an increase. The nitrate-formate-stabilized sol, on the other hand, showed a continuous and marked current decrease, and the sol ultimately flocculated.

Another interesting effect on the streaming current occurred when the chloride-stabilized UO_2 sol was placed in a CO_2 atmosphere. The current decreased rapidly until it reached a constant value, which persisted until the CO_2 was swept away with an inert gas. Once the blanket of CO_2 was removed, the current increased to its original value. Whether this current change was caused by changes in pH or by surface adsorption of CO_2 is not yet known. A similar rapid decrease in the current was observed in a thoria sol when it was exposed to CO_2, but under similar conditions its dialyzate showed no change in current. These results indicate that the change in current observed when either thoria sol or urania sol is blanketed with CO_2 is due to surface adsorption. If this is true, it suggests a method for determining the surface area of the sol particles without drying the sol.

Theoretical Study of Colloidal Particles

Thoria crystallites sometimes join together to form strings containing six to eight crystallites each.[3] This arrangement of the crystallites occurs as a result of their electrical potential fields. The potential field is described by a differential equation that cannot be solved exactly, although it has been solved numerically for a single particle.[4]

[2] *Chem. Technol. Div. Ann. Progr. Rept. May 31, 1967*, ORNL-4145, pp. 287–88.

[3] K. H. McCorkle, *Surface Chemistry and Viscosity of Thoria Sols* (thesis), ORNL-TM-1536 (July 1966).

[4] A. L. Loeb, J. T. Overbeek, and P. H. Wiersema, *The Electrical Double Layer Around a Spherical Colloid Particle*, pp. 3–17, M.I.T. Press, Cambridge, Mass., 1961.

Table 17.3. Effect of Oxidation on the Streaming Current of UO_2 Sols

0.7 *M*, Chloride-Stabilized Sols			0.2 *M*, Nitrate-Formate-Stabilized Sols		
Exposure to Air (min)	Current[a]	Percent of U as U(VI)	Exposure to Air (min)	Current[a]	Percent of U as U(VI)
0	5.96	4.23	0	17.5	~10.0
20	5.93	5.34	20	15.0	*b*
40	5.96	8.19	40	13.0	
60[c]	5.93	8.53	50	12.0	
120	5.42	9.29	60	11.2	
150	5.62	12.13	80	10.0	
180	6.20	12.58	105	10.5	
			d	7.0	51.5

[a]Arbitrary units adjusted to ×1 scale of Waters streaming current detector.

[b]Insufficient material for intermediate sampling.

[c]Stored overnight under argon.

[d]Stored overnight in stagnant air. Sol flocculated; color of supernate, yellow.

However, a fairly good description of the potential field can be obtained by using approximate expressions for the potential.

A program to compute the potential field about a string of crystallites has been written for the IBM 360/75 computer. Preliminary results with the use of an approximate expression for the potential indicate that the repulsive potential of the string is smallest at the ends, which are thus the most likely positions for addition of other crystallites.

17.2 PREPARATION OF CERMETS FROM MIXED SOLS

Investigations of methods for preparing cermets or dispersion-hardened metals by sol-gel processes were continued. Thermal conductivity data for an iron–2% thoria sample were previously reported.[5] Recently, elevated-temperature hardness tests were made on the same material. At 1000°C its diamond pyramid hardness (488-g load) was 31, about 20 points higher than that of Armco iron. Because of the small size of the sample, only one traverse could be made; therefore, the significance of the single value is in doubt.

A cermet of Fe–5% Al_2O_3 was prepared by mixing a sol of α-Fe_2O_3 with a suspension of Alon C, a commercial alumina with a nominal particle diameter of 0.02 μ. The sol was dried, fired in H_2 at 700°C to reduce the iron to metal, sintered in H_2 for 1 hr, and extruded at 600°C after being enclosed in a billet. A second sample of the iron sol, with no alumina added, was treated in the same way. A room-temperature diamond pyramid hardness (1-kg load) of 2239 was found for the Fe–5% Al_2O_3 vs 1478 for the iron alone. The alumina was much more uniformly dispersed than the thoria (above) and was easier to work with since alpha containment was not required. These results indicate that sol-gel techniques can be used to prepare dispersion-hardened metals.

17.3 FUNDAMENTAL STUDIES OF URANIA GELS

The work reported in this section was done under subcontract with the University of Utah, under the direction of M. H. Wadsworth. Most of the past year was occupied in the assembly of glove boxes containing equipment for the preparation and the study of urania gels under an inert atmosphere, especially with respect to their behavior upon heating. Instruments were acquired to measure shrinkage, pore size, and surface area

[5]*Chem. Technol. Div. Ann. Progr. Rept. May 31, 1967*, ORNL-4145, pp. 284–85.

and to determine the composition of the gases evolved and the extent of oxidation of U(IV) to U(VI). Except for calibration of the sorptometer and the subsequent measurement of a few surface areas with it, experimental work was limited to studies of the gases evolved upon heating a urania gel.

Evolution of Gases from the Pyrolysis of Urania Gel

A urania gel, UUA-1, which had been prepared from a nitrate-formate-stabilized sol, was used in this study. Gases evolved upon heating the gel to successively higher temperatures from 100 to 660°C were analyzed in a Perkin-Elmer model 820 gas chromatograph equipped with a pyrolysis unit. Three columns were used: (1) 12 ft of $\frac{1}{8}$-in. stainless steel tubing packed with 60/80 mesh Chrom W coated with 5 wt % Carbowax 1500 for the separation of NO_2, water, and some organic compounds such as HCOOH, HCHO, and CH_3OH; (2) 12 ft of $\frac{1}{8}$-in. stainless steel tubing packed with 80/100 mesh 13X molecular sieve for the separation of H_2, N_2, O_2, CH_4, NO, and CO; and (3) 20 ft of $\frac{1}{4}$-in. stainless steel tubing packed with 60/80 mesh Gas Chrom RZ coated with 40% dimethyl sulfoxide for the separation of CO_2 and N_2O. The gases evolved in 15 min at each temperature were chromatographed; residual gases were flushed out before each temperature increase.

The components separated by each column were identified by comparing the retention time of the unknown with that of a standard. In addition to water, rather large amounts of CO_2, CO, N_2, and O_2 were found, with smaller amounts of N_2O, NO_2, HCOOH, CH_3OH, and H_2 and traces of HCHO and an unidentified gas. The evolution of water was greatest between 100 and 220°C, after which it decreased continuously with increasing temperature. The evolution of CO_2 reached a rather sharp maximum at 260°C and then declined, though it was still in evidence at 660°C. The evolution of CO reached a maximum at 320°C, decreased to 480°C, and then showed a secondary peak around 600°C. The evolution of nitrogen was almost constant from 100 to 260°C but then declined at higher temperatures. The evolution of oxygen was lower and declined to an approximately constant level above 260°C. The ratio of oxygen to nitrogen was less than that in air. Of the minor components, N_2O, HCHO, H_2, and the unknown gas appeared at about 320°C. The N_2O became undetectable above 610°C, the HCHO stayed fairly constant, and the unknown gas disappeared at 470°C. However, the H_2 showed a very broad peak centering around 470°C. (It should be noted that measuring H_2 with helium as the carrier gas is a poor method, because of the small difference in their thermal conductivities and because H_2-He gas mixtures exhibit anomalous thermal conductivities.) The evolution of formic acid stayed approximately constant from 100 to 320°C, rose slightly at 390°C, and then decreased. The evolution of NO_2 and CH_3OH showed rather sharp peaks at 320 and 470°C respectively.

17.4 COMPARATIVE INVESTIGATION OF LANTHANIDE AND ACTINIDE SOLS

A study of several lanthanide hydroxide sols was begun, using both the Beckman model H electrophoresis apparatus and the Waters streaming current detector. The former device measures the electrophoretic mobility of the sol particles, from which their zeta potential may be calculated; the latter device gives a direct meter reading that is proportional to the zeta potential with an unknown proportionality constant. Therefore, several different sols were examined by both methods to see if an empirical correlation factor between the electrophoretic mobility and the streaming current could be found. The results are shown in Fig. 17.1.

Although a good correlation was obtained for many systems, there were exceptions. The streaming current values for both the titania and the thoria sols fell to the left of the correlation line but tended to approach it over a period of time. The other sols gave stable readings within a few seconds. Further correlation studies, varying sol concentration and ionic strength for a given sol, are needed.

Other results for lanthanide sols investigated by the streaming current method are shown in Table 17.4. The striking difference between the -I-C and the -II-H samples was the result of digesting the latter at 80°C for two to four weeks, whereas the -I-C samples were aged at room temperature. Heating caused release of base from the crystallites, as shown by the increase in pH and reversal of the sign of the charge on the particles. To see

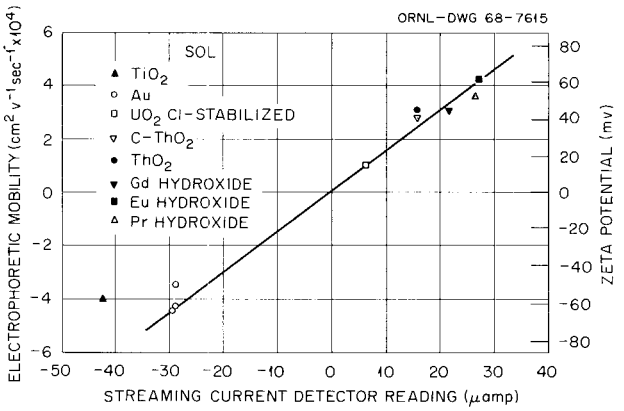

Fig. 17.1. Correlation of Electrophoretic Mobilities of Various Sols with the Waters Streaming Current Detector Readings. Zeta potential scale was calculated by assuming a constant dielectric constant of 78.

if the pH change was solely responsible for the latter effect, NaOH was added to the positively charged sols. The charge decreased as anticipated and could be made slightly negative at a pH of 12 to 13, but not as negative as in the sols digested at 80°C. The pH at the isoelectric point decreased as the atomic number of the lanthanide increased (Table 17.5). All of the sols in Table 17.5 were aged at room temperature for at least a month; however, there was some indication that slow changes in pH and streaming current were still occurring at the time these measurements were made. We will continue the investigations of the effects of aging by using sols that have been prepared under closely controlled conditions.

Table 17.4. Streaming Current Detector Readings for Yttrium Lanthanide Hydroxide Sols[a]

Sample No.[b]	pH	SCD Reading (μa)
D-Y-I-C	7.36	27.5
D-Ho-I-C	6.66	29.0
D-Er-I-C	6.96	31.0
D-Er-II-H	10.12	−37.0
D-Yb-I-C	6.62	25.0
D-Yb-II-H	9.98	−40.5
D-Lu-II-H	10.95	−26.3

[a]Samples obtained from R. G. Haire, Chemical Technology Division.

[b]Symbol following D indicates the element.

Table 17.5. The pH of Yttrium and Lanthanide Hydroxide Sols at the Isoelectric Point

Element	Atomic Number	pH at Isoelectric Point
Y	39	11.4
Pr	59	12.3
Eu	63	11.8
Gd	64	11.8
Ho	67	10.6
Er	68	10.4
Yb	70	9.0

18. Chemistry of Carbides and Nitrides

The basic chemistry of the carbides, nitrides, and carbonitrides of uranium and thorium is being investigated, with emphasis on reactions in aqueous systems. This work has application to the processing of power reactor fuels, reactor safety, high-temperature materials development, and the manufacture of chemicals in an agro-industrial complex. Previous studies were primarily concerned with the reactions of the uranium and thorium carbides with water and nonoxidizing acids. The reactions of the uranium carbides with nitric acid and of the thorium carbides with sodium hydroxide solutions have also been examined. During the past year we studied the reactions of: (1) the uranium carbides with sodium hydroxide solutions, (2) uranium mononitride and thorium monocarbide with nitric acid, and (3) uranium monocarbide and thorium monocarbide with ammonium fluoride solutions. A program to determine the chemical properties of uranium carbonitride was initiated. Work already reported in the open literature[1–3] has only been briefly summarized here.

Since the uranium carbide specimens used in the chemical studies had been carefully characterized by chemical, x-ray diffraction, and metallographic techniques, a natural by-product of this work was to correlate the microstructures with their compositions and heat treatments. Optical photomicrographs, at magnifications of 250 and 1000×, of 78 different arc-cast and heat-treated uranium carbide specimens, together with their compositions and heat treatments, are discussed in ref. 3. The major emphasis was on the monocarbide-dicarbide, monocarbide-sesquicarbide, and sesquicarbide-dicarbide regions of the phase diagram; however, specimens with total carbon:uranium atom ratios ranging from 0.4 to 2.4 (2 to 11 wt % carbon) were included. The phases present were identified by x-ray diffraction analysis of the specimens at room temperature and, in many instances, were further confirmed by determining products of hydrolysis. Specimens were also analyzed for total uranium, total carbon, free carbon, oxygen, nitrogen, and tungsten.

Reactions of Uranium Carbides with Sodium Hydroxide Solutions

The reactions of the uranium carbides with 2 to 18 *M* NaOH solutions at 80°C produced some uranium(IV) oxide, hydrogen, gaseous hydrocarbons, and, in the case of the sesqui- and dicarbides, some wax.[1] These reactions were unique in that part of the uranium was oxidized to the hexavalent state, with the accompanying evolution of hydrogen, as follows:

$$U(IV) + 2H^+ \xrightarrow{OH^-} U(VI) + H_2 \ .$$

The hydrocarbons produced in reactions with uranium monocarbide and sesquicarbide were the same as those produced in reactions with water. With uranium dicarbide, some of the hydrogen resulting from oxidation of the uranium reacted with the carbide carbon to form more gaseous hydrocarbons than were obtained with water. Oxidation of some of the uranium to the hexavalent state by the NaOH solutions was unexpected. Hydrates of UO_2, the products formed in the water reactions, can be prepared by

[1] M. B. Sears, Merle D. Pattengill, and L. M. Ferris, "Reactions of Uranium Carbides with Aqueous Sodium Hydroxide Solutions," to be published in the *Journal of Inorganic and Nuclear Chemistry*.

[2] L. M. Ferris, "Reactions of Uranium Mononitride, Thorium Monocarbide, and Uranium Monocarbide with Nitric Acid and Other Aqueous Reagents," presented at the 155th National Meeting, American Chemical Society, San Francisco, Calif., Mar. 31–Apr. 5, 1968, and to be published in the *Journal of Inorganic and Nuclear Chemistry*.

[3] M. B. Sears, R. J. Gray, L. M. Ferris, and B. C. Leslie, *Correlation of Composition and Heat-Treatment with the Microstructures of Uranium Carbides*, ORNL-3515 (July 1968).

precipitation from U(IV) solutions with alkalis,[4] and thermodynamic calculations show that "UO_2 cannot be expected to reduce water."[5] Experiments confirmed that the addition of NaOH to a uranous chloride solution merely precipitated a UO_2 hydrate, but the in situ addition of NaOH to the amorphous residue from the hydrolysis of a uranium monocarbide specimen resulted in the oxidation of some of the uranium to the hexavalent state, accompanied by the evolution of hydrogen.

Reactions of UN, ThC, and UC with Nitric Acid and Other Aqueous Reagents

The results of these studies will be reported in detail in the literature.[2] A summary of the work follows.

Studies were made of the reactions of uranium mononitride and thorium monocarbide with nitric acid and of uranium monocarbide and thorium monocarbide with ammonium fluoride solutions, using gas chromatography to analyze for most of the gaseous products. The behavior of these heavy-metal compounds in several other aqueous reagents was also tested. Uranium mononitride was inert at 80°C in water, 3 to 12 *M* HCl, 1 *M* H_2SO_4, 1 *M* NaOH, 1 *M* $NaNO_3$, and 5 *M* NH_4NO_3; however, it did react in 1 to 2.5 *M* $Al(NO_3)_3$. The nitride reacted with 0.5 to 15.8 *M* HNO_3 to give gaseous mixtures of N_2, N_2O, NO, and NO_2 (the NO_2 was produced only when the HNO_3 concentration was 6 *M* or higher). In reactions of thorium monocarbide with 0.1 to 1 *M* HNO_3 at 90°C, both hydrolysis (yielding mainly methane) and oxidation (yielding CO_2, N_2, and nitrogen oxides) of the carbide took place; at higher HNO_3 concentrations, only oxidation occurred. The principal reaction of UC or ThC with 4 and 6 *M* NH_4F at 80°C was:

$$(\text{U or Th})C(s) + 5NH_4F(aq) \longrightarrow$$

$$(\text{U or Th})F_4 \cdot NH_4F(s) + 4NH_3(g) + CH_4(g) .$$

[4] J. J. Katz and E. Rabinowitch, *The Chemistry of Uranium the Element, Its Binary, and Related Compounds*, p. 281, McGraw-Hill, New York, 1951.

[5] *Ibid.*, p. 309.

Reactions of Uranium Carbonitride with Aqueous Reagents

Uranium monocarbide forms a complete series of solid solutions with UN. These solutions, called carbonitrides, are stable at high temperatures, have high melting points, and are moderately good thermal conductors; therefore, they are of interest as possible fuels for nuclear reactors. No literature reference to the chemistry of the carbonitrides could be found.

In cooperation with R. A. Potter of the Metals and Ceramics Division, a uranium carbonitride specimen was prepared by the reaction:

$$UN + xC \longrightarrow UC_xN_{1-x} + \frac{x}{2} N_2 .$$

The product had a chemical composition of $UC_{0.23}N_{0.77}O_{0.003}$ and contained less than 0.01% unreacted carbon. It was single-phase by x-ray diffraction analysis and had a lattice constant of 4.908 A. Under the microscope the material consisted of very small crystallites that, individually, seemed to be quite dense even though the specimen had not been sintered during preparation. The specimen was broken to a −10 + 100 mesh powder for the chemical studies. Preliminary qualitative tests were made with a number of solutions. The uranium carbonitride was inert both in water and in 6 *M* NaOH at 25°C (1-hr tests) and at 80°C (4-hr tests). Quantitative experiments were then made with the more-promising reagents.

The reaction of this uranium carbonitride powder (U, 3.97 mg-atoms per gram of carbonitride; C, 0.90 mg-atom/g; N, 3.06 mg-atoms/g) with 6 *M* HCl at 80°C exhibited an induction period of about 30 min, during which no visible attack occurred. After the induction period, a rapid reaction ensued, with 90% of the total gas being evolved within the next hour (Fig. 18.1). The primary products were CH_4 (0.70 millimole per gram of carbonitride), H_2 (1.96 millimoles/g), NH_4^+ (3.10 meq/g), and U^{4+} (3.97 mg-atoms/g) in accordance with the equations:

$$UC + 4HCl \longrightarrow UCl_4 + CH_4 ,$$

$$2UN + 10HCl \longrightarrow 2UCl_4 + 2NH_4Cl + H_2 .$$

Small quantities of ethane, propane, butane, and propyne (totaling 0.07 mg-atom of carbon per gram of carbonitride) were also detected in the gas. The UO_2 impurity in the carbonitride did not react and

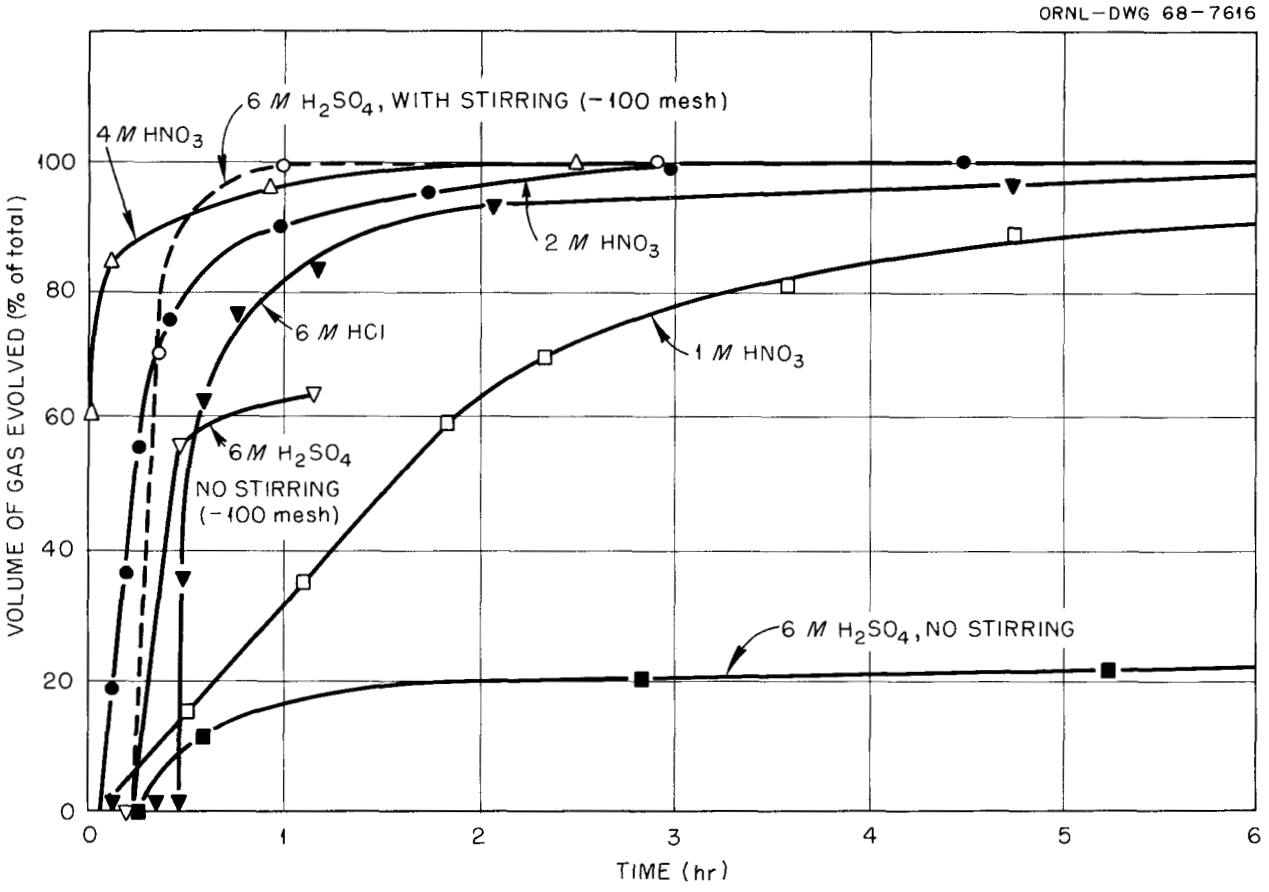

Fig. 18.1. Rates of Gas Evolution in the Reaction of $UC_{0.23}N_{0.77}$ (−10 +100 Mesh) with Acids at 80°C.

was insoluble in the final hydrochloric acid solution.

There was an induction period of about 14 min in the reaction of the uranium carbonitride with 6 *M* H_2SO_4 at 80°C. The induction period was followed by a brief surge of gas that tapered off as insoluble uranous sulfate formed on the surface of the carbonitride (Fig. 18.1). After seven days, less than 50% of the −10 +100 mesh carbonitride powder had reacted with the sulfuric acid. Grinding to a −100 mesh powder increased the reaction rate, but complete reaction (within a reasonable time) could be obtained only by mechanically stirring the mixture to expose fresh carbonitride to the acid. The reaction of the −100 mesh powder was 99% complete in 1 hr when stirring was used, vs 64% complete without stirring (Fig. 18.1). Mechanical agitation had no effect on the induction period. The primary products were CH_4 (0.94 millimole per gram of carbonitride), H_2 (1.56 millimoles/g), NH_4^+ (2.79 millimoles/g), $U(SO_4)_2 \cdot 4H_2O$ (3.35 millimoles/g), and U^{4+} 0.68 mg-atom/g) in accordance with the equations:

$$UC + 2H_2SO_4 + 4H_2O \longrightarrow U(SO_4)_2 \cdot 4H_2O + CH_4 ,$$

$$2UN + 5H_2SO_4 + 8H_2O \longrightarrow 2U(SO_4)_2 \cdot 4H_2O + (NH_4)_2SO_4 + H_2 .$$

Small quantities of ethane, propane, butane, and propyne (totaling 0.02 mg-atom of carbon per gram of carbonitride) were also detected in the gas.

The uranium carbonitride reacted exothermally with nitric acid solutions to produce a yellow uranyl nitrate solution, carbon dioxide, nitrogen, nitrogen oxides, nitrous acid, unidentified nitric acid–soluble organic compound(s), and, in some cases, NH_4^+ (Fig. 18.1 and Table 18.1). About half of the carbonitride carbon was found as carbon dioxide.

Table 18.1. Data for the Reaction of $UC_{0.23}N_{0.77}O_{0.003}$[a] with HNO_3

Expt. No.	HNO_3 Concentration (M)	Temperature (°C)	Volume of Gas Evolved [milliliters (STP) per gram of carbonitride]	Gaseous Products (millimoles/g)						Species in Solution			Time Required to Dissolve All Solids	Time[b] Allowed for Reaction
				N_2	NO	N_2O	NO_2	CO	CO_2	NH_4^+ (millimoles/g)	NO_2^- (millimoles/g)	C (mg-atoms/g)		
1	1	25	107	1.0	3.4				0.5	1.6	2.0	0.6	>2 days	6 days
2	1	35	109	1.2	3.2				0.5	1.5	2.0	0.8	>2 days	6 days
3	1	80	164	3.5	3.4				0.5	0.02	0.7	0.7[c]	5 hr < x < 22 hr	2 days
4	2	25	94	1.3	2.4				0.5	1.4	3.0	0.7	1¼ days	7 days
5	2	35	115	1.7	2.8			0.07	0.6	0.8	1.7	0.7	1¼ days	7 days
6	2	80	156	3.0	3.3	0.02		0.02	0.5	0.04	0.6	0.7	1½ hr	4½ hr
7	2	80	129	1.8	3.4				0.6	1.0	0.7	0.8	50 min	50 min
8	4	25	104	2.4	1.7	0.1			0.5	0.5	0.1	0.2	5 hr	6 days
9	4	25	80	1.4	1.7	0.1			0.5	1.5[d]	0.01[d]	0.5	6 hr	23 hr
10	4	35	117	2.8	1.9	0.1			0.5	0.01	1.3	0.3	1½ hr	7 days
11	4	35	71[e]	0.9[e]	1.9[e]	0.1			0.3	1.6	1.7	0.8	50 min	50 min
12	4	80	133	2.7	2.2	0.2	0.4		0.5	0.001	0.02	0.7	<6 min	4 hr
13	8	25	133	2.6	2.0	0.3	0.4	0.02	0.6	0.02	2.4[c]	0.4	2 min	6 days
14	8	25	114	1.9	1.9	0.3	0.4	0.04	0.5	0.3	1.4	0.4	<3 min	22 hr

[a]Elemental analyses: U, 3.97 mg-atoms per gram of carbonitride; N, 3.06 mg-atoms/g; C, 0.90 mg-atom/g.

[b]All solids dissolved, but not necessarily all gas evolved.

[c]Poor agreement between duplicate experiments.

[d]Values may be low since solution was analyzed 19 days after the reaction was terminated.

[e]Gas was released during filtration but was not collected. It could have been NO from the decomposition of HNO_2 or N_2 from the decomposition of NH_4NO_3.

The amount of nitric acid–soluble organic compound(s) was too small to isolate or identify. These organic compounds differ from the products of the uranium monocarbide–nitric acid reaction in that no highly colored species were formed. The quantities of the nitrogen-containing compounds produced by the reaction varied as a function of both the acid concentration and the temperature (Table 18.1). From the standpoint of the process engineer who is primarily concerned with dissolving the fuel in nitric acid, time is an additional variable since gas may be evolved from the solution for several days after all the solids have disappeared. Many of the experiments summarized in Table 18.1 were arbitrarily terminated after six or seven days; at that time, the solutions were still evolving 1 or 2 ml of gas per gram of carbonitride per day. The values reported in Table 18.1 for NO_2^- are probably low, since nitrous acid is in equilibrium with NO_2 and/or NO according to:[6]

$$2HNO_2 \rightleftharpoons NO + NO_2 + H_2O \ ,$$

$$3HNO_2 \rightleftharpoons H^+ + NO_3^- + 2NO + H_2O \ .$$

Thus, nitrous acid was probably lost from the solutions when gas samples containing NO were withdrawn for analysis.

The reaction of the nitride nitrogen in uranium carbonitride at 25 or 35°C appears to be a two-step process in which the nitride nitrogen is first converted to NH_4^+ and then the NH_4^+ is oxidized slowly to form free N_2. For example, in experiment 11 with 4 *M* HNO_3 at 35°C, the reaction was terminated after 50 min when all the carbonitride had visually dissolved. At this point, 0.9 millimole of N_2 per gram of carbonitride had been evolved. A sudden release of gas occurred when the solution touched a sintered glass filter; this gas could have been either NO from the decomposition of nitrous acid or N_2 from the decomposition of NH_4NO_2. After filtration, the solution contained 1.5 millimoles of NH_4^+ per gram of carbonitride. In experiment 10 with 4 *M* HNO_3 at 35°C, the reaction was allowed to continue for seven days; the products then included 2.7 millimoles of N_2 per gram and practically no NH_4^+. The amounts of NO, N_2O, and CO_2 that formed were about the same in both experiments (Table 18.1), but three times as much N_2 was obtained after seven days as in 1 hr. Although overlapping of the two steps in the oxidation of the nitride nitrogen was greater in the reactions with 1 and 2 *M* HNO_3 at 25 and 35°C than with 4 *M* HNO_3, significant quantities of the NH_4^+ intermediate were found; some gas was evolved from the solutions after all the solids had disappeared, and the final gas sample was always richer in N_2 than the first sample. Within the limits of experimental error (±10%), in the experiments at 25 and 35°C, all the nitride nitrogen may be accounted for as either NH_4^+ or free N_2 formed by the following reaction involving NH_4^+:

$$5NH_4^+ + 3NO_3^- \longrightarrow 4N_2 + 2H^+ + 9H_2O \ ,$$

and no N_2 was formed by any other reaction (Table 18.2). Reactions involving the uranium and the carbide portions of the carbonitride must, therefore, produce only nitrogen oxides and nitrous acid at 25 and at 35°C.

At 80°C the nitride nitrogen again appears to react by a two-step process, with NH_4^+ as the intermediate, and free N_2 as the final, product (experiments 6 and 7, Tables 18.1 and 18.2); however, in the case of 1 *M* HNO_3 (and possibly also with 2 *M* HNO_3), more free N_2 is produced than can be accounted for solely by the nitride reactions (Table 18.2). Thus, with the dilute acids, the uranium and carbide portions of the carbonitride may yield a small amount of free N_2 at 80°C, although NO and nitrous acid are still the primary products.

Elemental N_2 is not a common product from nitric acid oxidations. It is never obtained with one-electron reducing agents and only under special conditions with two-electron reducing agents such as cold stannous ion or hydrazine.[6] No N_2 was found in the reactions of the uranium carbides with nitric acid,[7] and only 2 to 4 vol % was found in the reaction of thorium monocarbide with 2 to 4 *M* HNO_3.[2] Nitrogen was produced in the reaction of uranium mononitride with nitric acid in approximately the quantities reported here, based on the amount of nitride present.[2] No NH_4^+ was detected in the uranium mononitride studies; however, those experiments were not conducted under conditions where NH_4^+ was found in the carbonitride experiments.

[6]W. M. Latimer, *Oxidation Potentials*, pp. 92–105, Prentice-Hall, New York, 1952.

[7]L. M. Ferris and M. J. Bradley, *J. Am. Chem. Soc.* **87**, 1710 (1965).

Table 18.2. Data for the Reaction of $UC_{0.23}N_{0.77}O_{0.003}$[a] with HNO_3

Experiment No.	HNO_3 Concentration (M)	NH_4^+ (millimoles/g)	$\frac{5}{4}N_2$ (millimoles/g)	$NH_4^+ + \frac{5}{4}N_2$ (millimoles/g)	
		25°C			
1	1	1.6	1.2	2.8	Av = 3.1
4	2	1.4	1.6	3.0	
8	4	0.5	3.0	3.5	
9	4	1.5	1.8	3.3	
13	8	0.02	3.3	3.3	
14	8	0.3	2.4	2.7	
		35°C			
2	1	1.5	1.5	3.0	
5	2	0.8	2.1	2.9	
10	4	0.01	3.5	3.5	
11	4	1.6	1.1	2.7	
		80°C			
3	1	0.02	4.4	4.4	
6	2	0.04	3.8	3.8	
7	2	1.0	2.2	3.2	
12	4	0.001	3.4	3.4	

[a]Elemental analysis: 3.06 mg-atoms of nitrogen per gram of carbonitride.

As expected for reactions with dilute nitric acid, NO was the principal nitrogen oxide formed (Table 18.1). In the experiments with 8 M HNO_3, the NO_2 (N_2O_4) concentration varied as a function of the time, with the intensity of the brown color rising to a maximum at about 3 min. This was followed by a rapid decrease in the intensity of the color and a 10% decrease in the total volume of gas evolved. After 20 or 30 min the gas volume increased slowly, presumably as the NH_4^+ was oxidized to N_2, although this has not been proved experimentally. Additional work on the reactions of the uranium carbonitrides is in progress.

19. Safety Studies of Fuel Transport

19.1 THE *CRITERIA*

This program was organized in the early part of 1966 to develop an *Irradiated Fuel Shipping Cask Criteria* for the Division of Reactor Development and Technology (DRDT). The *Criteria* will provide the AEC with a series of cask design standards and specifications that, if followed, should ensure adherence to the requirements set forth in AEC regulations.

The *Criteria* will establish suitable engineering standards for the design, fabrication, and inspection of irradiated fuel shipping casks by providing information on structural integrity, shielding, heat transfer, criticality, materials of construction, and fabrication techniques. Specifications and standards presented in the *Criteria* will be based on data that have been developed from experiments and analyses.

Approximately 85% of the *Criteria* has been written. Specifically, Chap. 2, "Structural Design and Philosophy," is about 65% complete; Chaps. 3, 4, 5, 6, and 7, covering "Materials of Construction," "Fabrication," "Heat Transfer," "Criticality," and "Shielding," are finished.

Structural Design

In the last annual report we presented equations that will permit a designer to determine the minimum inner and outer steel shell thicknesses for a lead-shielded cask. Additional information and work in the past year has led to an improvement in the equation that predicts the outer shell thickness, t_s; this equation, which is suitable for both carbon and stainless steel, is given below:

$$t_s \leq \left(\frac{W}{S}\right)^{0.71},$$

where W is the cask weight in pounds and S is the ultimate tensile strength of the material. The only restriction on the use of this equation is that the material must have an ultimate elongation greater than 40%.

The kinetic energy of a cask in an impact must be dissipated in the cask, since regulations stipulate that the impact surface must be unyielding. Thus the energy will be absorbed by elastic and plastic deformation of the cask and/or any shock-absorbing shield built to absorb such impacts. The properties of the shielding material must, therefore, be known in order to study, analytically, the effect of impact on a cask.

Limited test data indicate that the steel weldment of a well-built lead-shielded cylindrical cask will withstand a 30-ft impact on end without rupture or excessive distortion of the shells. Most of the impact energy appears to be dissipated in the deformation of the lead shielding. The lead behaves like an extremely viscous fluid; that is, it tends to expand against the outer steel shell and collapse the inner one. If the lead is not bonded to the steel shells and if the lead receives no support from the inner and outer shells (such as in a corner drop or from internal fins), the lead will settle the maximum amount, thereby creating a void in the end opposite the point of impact.

The change in the height of a column of lead contained in a steel jacket may be estimated from the following equation:

$$\Delta H = \frac{RWH}{\pi(R^2 - r^2)\,\{t_s\sigma_s + R\sigma_{Pb}\,[1 - (r/R)^2]\}},$$

where

R = outer radius of lead, in.;

r = inner radius of lead, in.;

W = cask weight, lb;

H = drop height, in.;

σ_s = static yield point stress of the shell, psi;

σ_{Pb} = dynamic flow pressure of lead, ~5500 psi.

Investigators at the University of Tennessee, under subcontract, are studying closure and tie-down design. A report covering the drop tests performed on several closure types will be issued in the near future; a report on cask tie-downs has already been received. Both topics will be incorporated into Chap. 2 of the *Criteria*.

Heat Transfer

All shipping casks should be evaluated to determine their expected responses in normal thermal environments and during accidents. Specifically, the temperatures that should be determined are the maximum cask surface temperature and the maximum fuel element temperature under normal conditions, the temperature distribution through the shield, and the maximum fuel element temperature under accident conditions.

Many aspects of the heat-transfer problem have been analyzed by workers at Battelle Memorial Institute. In their recent report, two heat sources were discussed: the decay heat from the radioactive source and the solar heat load to which the cask is exposed.

The decay heat load for a fuel element that is operated at a known power level can be determined from Fig. 19.1 by selecting a specified irradiation time on the ordinate, proceeding horizontally to a cooling time, and then moving upward to the decay heat/operating power scale. The latter value,

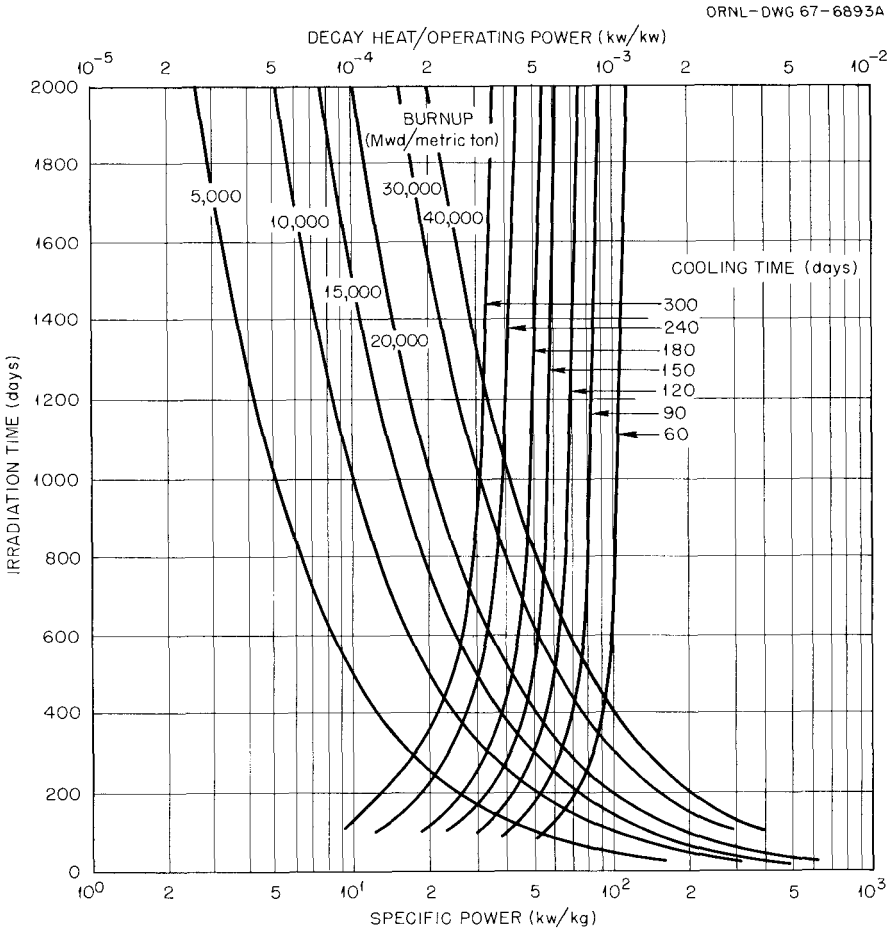

Fig. 19.1. Ratio of Decay Heat to Power for Spent Fuel Elements.

when multiplied by the operating power of the element, gives the desired answer.

In the analysis of external heat transfer, the rejection of both the decay heat and the solar heat from the cask surface to the environment was considered. Analytical procedures were developed to analyze heat transfer from the cask surface by taking into account the variations in cask geometry and orientation (i.e., the cask may be finned or unfinned, and it may be transported either vertically or horizontally).

It is difficult to make generalized statements regarding heat transfer inside cask cavities. Maximum element temperatures are quite dependent upon the internal geometry of the cask and fuel. Heat transfer through the fuel cladding, the primary coolant region, the inner shell, the shield, and the outer shell must also be considered.

Temperature maps of two fuel element geometries (square arrays of 36 pins and 144 pins per fuel assembly respectively) were studied to determine the effect of varying several parameters. The data were developed by using a heat-transfer computer code that considers conductive, convective, and radiative heat transfer simultaneously and solves the problem by a relaxation technique.

The internal geometry of each assembly was assumed to be an "egg crate" arrangement, with steel plates forming the compartments. Each fuel element "saw" only the four sides of the compartment; heat was transferred through the coolant (air) to the steel and was then conducted to the inner surface of the inner shell. Figure 19.2 shows the maximum temperature of the center fuel pin vs linear heat generation rate for a square array of nine fuel elements in which the steel "egg crate," or webbing, is $\frac{1}{4}$ in. thick (unless otherwise noted).

The cask for base case 1 (36-pin assembly) has an outer diameter of approximately 44 in., while the cask for base case 2 (144-pin assembly) has an outer diameter of approximately 47 in. In one analysis, copper shot, which was used to fill interior voids, enhanced the heat transfer and reduced the maximum temperature.

The fire analysis described in the *Criteria* is concerned with the thermal phenomena occurring in the cask during a 30-min 1475°F fire. The objectives of the analysis are to determine the temperature profile through the lead shield as a function of time and to determine what portion of the shield melts.

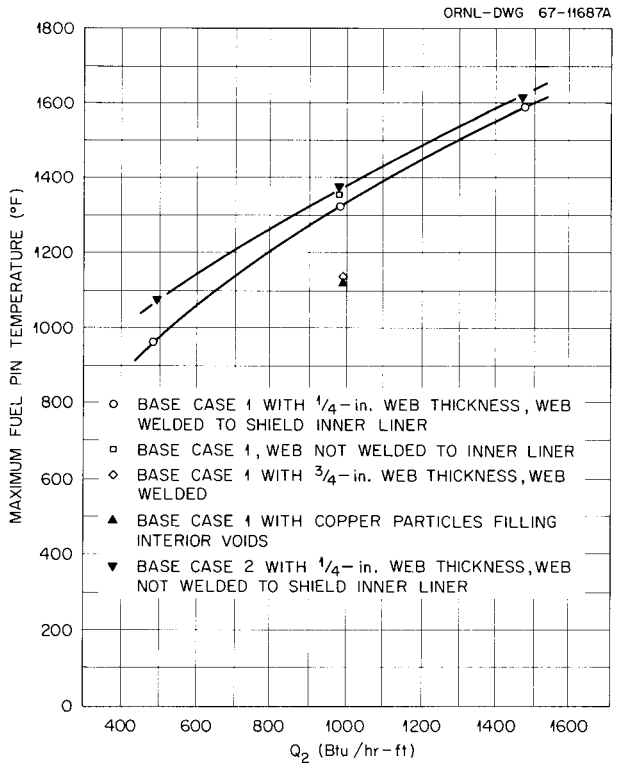

Fig. 19.2. Maximum Temperature of Center Fuel Pin vs Linear Heat Generation Rate. A square array of nine fuel elements in an "egg crate" arrangement is assumed.

Several procedures that may be used to treat this problem are discussed; among them are empirical, analog, graphical, and finite difference methods. Heat transfer equations written in finite difference form and applied to the accident fire conditions have been programmed for the CDC 6400 and the IBM 360/75; it can account for a change in phase if the lead shielding melts.

Criticality

The AEC regulations require every shipment of fissile material to remain subcritical at all times during normal transport, including loading and unloading, and under hypothetical accident conditions leading to the most reactive credible configuration. In order to comply with AEC regulations, shippers of irradiated reactor fuels normally make a criticality evaluation of their shipping containers. A need exists for a guide to good practice in such evaluations.

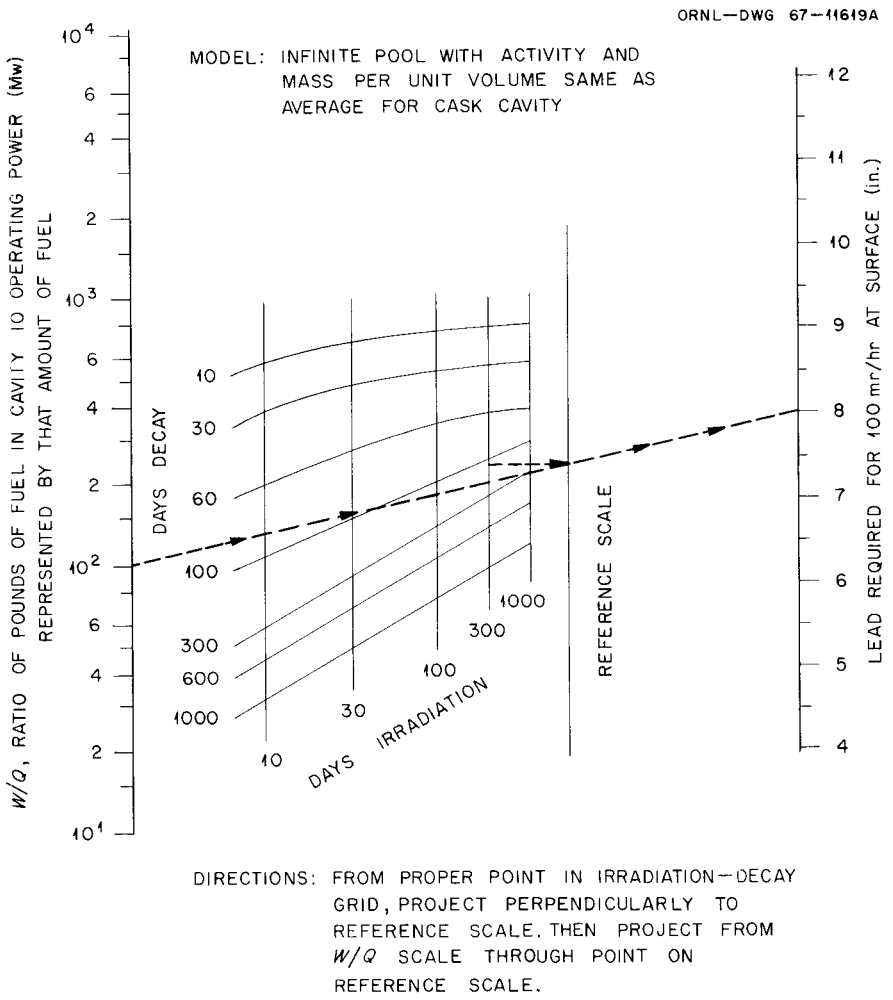

Fig. 19.3. Nomograph for Estimating Amount of Shielding for Casks.

The criticality evaluation problem, as discussed here, is not as much concerned with the method of maintaining subcriticality as it is with the proof of adherence to the requirement of subcriticality. In the interests of economy and practicality, a shipper should be allowed to exercise any practical controls he desires in rendering a system subcritical; however, he must present proof that these controls are adequate. Therefore, the chapter on criticality deals with the determination of the kinds of evidence that should be considered as acceptable for proving that a system conforms to the criticality requirements of existing federal regulations. For example, proof of the subcriticality of a system can hardly be better substantiated than with an experiment using the fuel in question, arranged in the most reactive credible configuration with respect to the design of the shipping cask. However, such information is often unavailable, and proof of subcriticality must be based on calculational methods; the ground rules for such methods are discussed in the *Criteria*.

Shielding

The shielding around any shipping cask must reduce the external irradiation dose rate from the largest expected source to less than specified tolerance levels. It is obvious that the cask itself should be as light as possible, since unnecessary weight adds both to the initial cost and the recurring shipping charges.

In the United States the shielding of highly radioactive materials, such as spent fuel elements, is usually accomplished with lead. Therefore, the chapter on shielding will be devoted, primarily, to the use of this material, although steel and depleted uranium can be used to advantage under certain circumstances. The purpose of this chapter is to provide AEC personnel with a rapid and reasonably accurate method for determining whether the shielding offered by a given cask will be adequate for the specified source.

Figure 19.3 is a nomograph[1] that will permit reviewers to estimate the amount of shielding that would be required to reduce the dose rate from spent fuel elements to 100 mr/hr on a cask surface. Surface dose rates other than 100 mr/hr can be estimated by noting that the rate changes by a factor of 2 for about every 0.6-in. change in lead thickness.

Figure 19.3 is based on the assumptions that a large source has the same activity and mass per unit volume as the average for a cask cavity and that the fuel is either fairly well distributed or is approximately centered in the cavity. This model is suitable when the product wD exceeds about 200, where w (lb/ft^3) is the average density of the cask contents and D (ft) is the minimum cross-sectional dimension of the cavity. For values of wD as small as 100, however, the conservatism of the method results in less than $\frac{1}{2}$ in. of added thickness.

Comparison of Nomograph and Machine Code

Calculations made to determine the shielding thickness required to produce a dose rate of 100 mr/hr on the cask surface were determined by means of the QAD-P5A code,[2] which uses a kernel technique; the buildup factor was calculated by the moments method and compared with those values obtained in Fig. 19.3. It was found that the nomograph gave values of lead thicknesses that were generally accurate to within 5% of those calculated using the QAD-A5A code; the widest limits were −7.6% and +5.4%.

19.2 AEC ASSISTANCE PROGRAM

We have been involved with seven AEC cask projects this past year. These projects are briefly summarized in Table 19.1. Only two, namely, the PM-1 Navy cask project and the uranium cask testing program at Paducah, are still in progress. It

[1] L. L. Zahn *et al.*, "Transportation of Radioactive Materials," *Reactor Technology, Selected Reviews – 1965*, TID-8541.

[2] R. E. Malenfant, *QAD; a Series of Point Kernel General Purpose Shielding Programs*, LA-3573 (Apr. 5, 1967).

Table 19.1. Summary of AEC Cask Projects

Project	Sites Concerned	Principal Cask Consultation Effort
Hallam[a]	AI, AEC	Review of overall design, including fabrication, lead bonding, and cask repair problems
PM-1 and 3A	Navy, AEC	Design review, including redesign recommendations
Piqua/Elk River[a]	AEC-COO	Complete analyses indicating compliance with AEC and IAEA regulations
BONUS/LACBWR[a]	AEC-COO	Specifications review
AARR[a]	Argonne	Complete review of safety analysis resulting in specific recommendations
Uranium cask	Paducah	Continuing program and cask design review
TREAT[a]	Argonne	Complete review of safety analysis resulting in specific recommendations

[a] Completed.

seems probable that the AEC will continue to request assistance for review of various cask projects in the future.

19.3 CTD CASK EVALUATION PROGRAM

The Department of Transportation (DOT) requires that all radioactive material shipping casks in use after December 31, 1968, meet their regulations. The new regulations are concerned, primarily, with ensuring that a given cask can adequately contain and shield its contents under both normal and accident conditions, including a 30-ft free fall, a puncture, and a fire followed by submersion in water. Evaluation involves stress calculations of the structures and components of the cask. In addition, effects of the accident conditions on the welds and the shielding material must be considered.

All of the casks available in the Chemical Technology Division are presently being examined to determine what modifications will be required to meet the regulations. Four shipping containers have already been reviewed, and a request for their certification has been forwarded to the AEC. One of these containers, the TRU 10-ton californium shipping cask (see Fig. 19.4), was designed to transport isotopes of Am, Cm, Bk, Cf, Es, and Fm

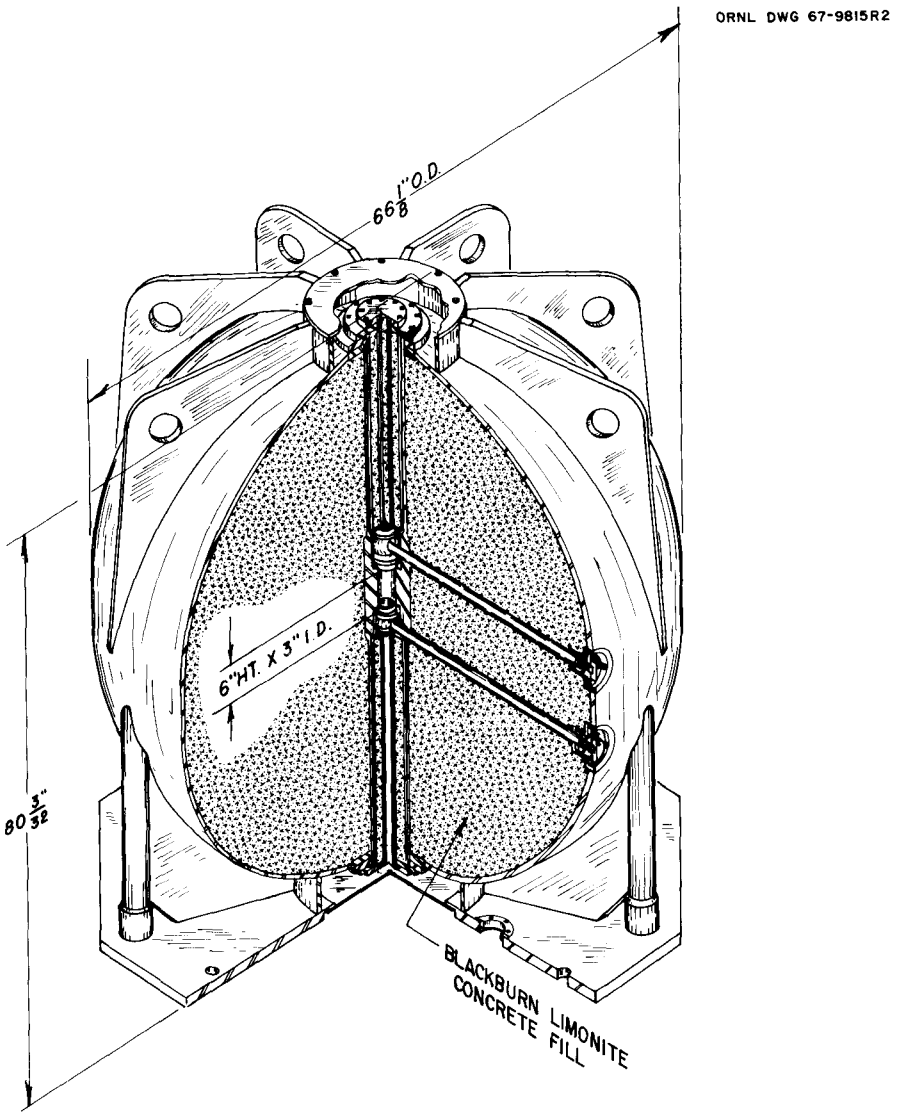

Fig. 19.4. TRU 10-ton Shipping Container.

in solid form. This cask is fabricated of stainless steel and is shielded by 32 in. of Blackburn limonite concrete.

Studies of the transportation problem associated with the fast breeder reactor project are under way. Economic considerations dictate that shipment should be made after very short cooling times. Under such circumstances the removal of heat will be quite difficult, and the normal operating cask temperatures will probably be above the melting point of lead. This consideration makes all-steel casks appear attractive in spite of the extra weight penalty. An economic study is now under way to determine quantitatively the advantages of an all-steel cask. To this end, cost estimates are being prepared for a new steel-shielded cask that will weigh approximately 110 tons. It will have an outside diameter of 77 in. and a height of 183 in. and will contain six 11-in.-diam, 153-in.-long holes.

20. The Nuclear-Powered Agro-Industrial Complex: Special Study Project

Work by the Chemical Technology Division on a special study project, "The Nuclear-Powered Agro-Industrial Complex," is described in detail in reports issued by the Nuclear Desalination Program and in the final project report, ORNL-4290, which is now in preparation by members of the study group; consequently, only an abstract appears in this report (see the Summary).

21. Water Research Program

Work by the Chemical Technology Division on the Water Research Program is reported directly to the Office of Saline Water, and only an abstract appears in this report (see the Summary).

22. Assistance Programs

The Division provided assistance to others on several projects, principally the Eurochemic Assistance Program and a program in which the radiation resistance of several protective coatings is being determined.

22.1 EUROCHEMIC ASSISTANCE PROGRAM

The Laboratory continued to coordinate the Eurochemic Assistance Program to provide an exchange of information between Eurochemic and the several AEC sites included in the program. In addition, the Laboratory is supplying the services of a resident U.S. Technical Advisor, E. M. Shank, who will remain at Mol, Belgium, during the initial hot operations of the Eurochemic plant.

Eurochemic has successfully completed five test runs with spent fuels from European reactors EL-1, -2, -3, Diorit, FR-2, and BR-1. The product purity easily met USAEC specifications. The product was returned, without incident, to the reactor operators in CEA type 2100-1 containers. These runs constitute Eurochemic's first highly enriched uranium (HEU) campaign. A second HEU campaign, planned for late April 1968, will probably be completed by mid-1968. During the past year, 154 USAEC-originated documents and miscellaneous items of information were sent to Eurochemic. Thirteen Eurochemic documents written in English were received, reproduced, and distributed.

22.2 EVALUATION OF THE RADIATION RESISTANCE OF SELECTED PROTECTIVE COATINGS (PAINTS)

Tests to evaluate commercial protective coatings were continued. Thirty-seven coatings, specimens of which were supplied by five different manufacturers, are being evaluated by exposure in air and in deionized water to a ^{60}Co gamma source (intensity, 6×10^5 r/hr; temperature range, 40 to 50°C). The results at the current exposure level are presented in Table 22.1. Tests of these coatings will be continued until they have failed or until they have received a dose of 1×10^{10} rads. Additional tests are planned for coatings supplied by manufacturers that have not previously participated in the "radiation damage" evaluations.

A United States of America Standards Institute standard, N5.9-1967, "Protective Coatings (Paints) for the Nuclear Industry," was issued under the sponsorship of the American Institute of Chemical Engineers. The committee that was responsible for the standard was comprised of industrial, USAEC, and USAEC contractual and operating personnel. Members of the committee were: C. D. Watson (chairman), G. A. West, and H. B. Graham (secretary), Oak Ridge National Laboratory; H. W. Bishop, Koppers Company; R. J. Christl and E. A. Rachal, E. I. du Pont de Nemours and Company; J. H. Kleinpeter, Battelle Northwest Laboratory; W. H. McMahon, Amercoat Corporation; L. E. Parks, Lloyd E. Parks Company; B. J. Newby and K. Rohde, Idaho Nuclear Corporation; F. D. Reali, General Services Administration; C. W. Sisler, Monsanto Company; A. B. Smith, Celanese Coatings Company; H. D. Tarlas, Carboline Company; and R. F. Wiseman, Kaiser Engineers.

A newly organized committee has begun work on a related standard, "Protective Coatings (Paints) for Nuclear Power Reactor Containment Facilities," which is scheduled for completion by June 1969.

Table 22.1. Gamma Radiation Resistance of Several Protective Coatings

Radiation source: ^{60}Co at 6×10^5 r/hr and 40–50°C temperature

Coating	Generic Type	Manufacturer[a]	Substrate	Exposure[b] in Demineralized Water		Exposure[b] in Air	
				Dose (rads)	Effect[c]	Dose (rads)	Effect[c]
Phenoline 368(A)[d]	Modified phenolic	1	Concrete	1.2×10^9 [e]	B	9×10^9	
Phenoline 368(B)[d]	Modified phenolic	1	Steel	2.6×10^9 [e]	A	9×10^9	
Phenoline 368(C)[f]	Modified phenolic	1	Concrete	1.2×10^9 [e]	B	9×10^9	
Phenoline 368(D)[f]	Modified phenolic	1	Steel	2.6×10^9 [e]	A	9×10^9	
Phenoline 368(E)[f]	Modified phenolic	1	Concrete	2.6×10^9 [e]	A	9×10^9	
Phenoline 368(F)[f]	Modified phenolic	1	Steel	2.6×10^9 [e]	A	9×10^9	
Phenoline 368(G)[f]	Modified phenolic	1	Concrete	2.6×10^9 [e]	B	9×10^9	
Phenoline 368(H)[f]	Modified phenolic	1	Steel	2.6×10^9 [e]	A	9×10^9	
Phenoline 368(I)	Modified phenolic	1	Concrete	7.8×10^8 [e]	B	9×10^9	
Phenoline 368(J)	Modified phenolic	1	Masonite	7.8×10^8 [e]	B	7.7×10^9	B,C
Phenoline 368(O)[d]	Modified phenolic	1	Concrete	7.9×10^8 [e]	B	9×10^9	
Phenoline 368(P)[d]	Modified phenolic	1	Steel	7.9×10^8 [e]	B	9×10^9	
Q-Kote	Phenolic	2	Concrete	1.9×10^8 [e]	B	8×10^9	
Q-Kote	Phenolic	2	Steel	1.9×10^8 [e]	B	8×10^9	
Topping 285	Epoxy	3	Concrete	1.8×10^9	B	3.8×10^9	
Topping 2036	Epoxy	3	Concrete	1.8×10^9	B	3.8×10^9	
Absorption process topping		3	Concrete	5×10^8	A	3.8×10^9	
No. 1, Hi-Build (HB), stainless steel (SS) flake enamel	Epoxy	4	Concrete	4×10^8	B	2.3×10^9	
No. 2, 7230 HB, SS flake enamel	Phenolic	4	Concrete	2.3×10^9	A	2.3×10^9	
No. 3, 7239 (catalyzed), SS flake enamel	Urethane	4	Concrete	4×10^8	B	2.3×10^9	
No. 4, 4130 top coat, SS flake enamel	Epoxy	4	Concrete	1×10^9	B	2.3×10^9	
No. 5, HB, SS flake enamel	Epoxy	4	Concrete	1×10^9	B	2.3×10^9	
No. 6, 4130 top coat, HB primer	Epoxy	4	Steel	1×10^9	B	2.3×10^9	

Table 22.1 (continued)

Coating	Generic Type	Manufacturer[a]		Exposure[b] in Demineralized Water		Exposure[b] in Air	
				Dose (rads)	Effect[c]	Dose (rads)	Effect[c]
No. 7, white enamel (RCI), HB primer	Epoxy	4	Steel	1×10^9	A,B	2.3×10^9	
No. 8, epoxy HB, SS flake enamel	Epoxy	4	Steel	1×10^9	B	2.3×10^9	
No. 9, 7230 HB white enamel	Phenolic	4	Steel	4×10^8	B	2.3×10^9	
No. 10, 7239 (catalyzed), SS flake enamel	Urethane	4	Steel	4×10^8	B	2.3×10^9	D
No. 11, 7230 over 6820 primer	Phenolic and chlorinated rubber	4	Steel	4×10^8	B	2.3×10^9	
No. 12, 7230 over 6040 primer	Phenolic and oxidized alkyd	4	Steel	4×10^8	B	2.3×10^9	
No. 13, 2952 over 6040 primer	Chlorinated rubber and oxidized alkyd	4	Steel	4×10^8	B,D	2.3×10^9	
No. 14, epoxy white enamel	Epoxy	4	Steel	2.3×10^9	?	2.3×10^9	A,D
No. 15, 6002 (oxidized)	Alkyd	4	Steel	4×10^8	B	2.3×10^9	
No. 16, 6002 (oxidized) over 6040 primer	Alkyd	4	Steel	4×10^8	B	2.3×10^9	
No. 17, white enamel over 6040 primer	Alkyd	4	Steel	4×10^8	B	2.3×10^9	
No. 18, 4130 over HB primer	Epoxy	4	Concrete	1.5×10^9	A	2.3×10^9	
No. 19, white enamel over HB primer	Epoxy	4	Concrete	1.5×10^9	A	2.3×10^9	
Plastite 1120 over 1100 primer	Inorganic	5	Steel	1.3×10^9		1.3×10^9	

[a]Manufacturers: 1, Carboline Co.; 2, Chemline Coatings Co., Division of Dixie Paint and Varnish Co.; 3, Kalman Floor Co., Inc.; 4, Keeler and Long, Inc.; Wisconsin Protective Coating Co.

[b]The materials were inspected for radiation damage at various dose intervals: $\sim 1 \times 10^7$, $\sim 5 \times 10^7$, $\sim 1 \times 10^8$, $\sim 2.5 \times 10^8$, $\sim 5 \times 10^8$, and each additional 5×10^8 rads thereafter. The exposure values listed represent the cumulative irradiation dose that had been received at the time the adverse effects were first observed.

[c]Effects: A, chalked; B, blistered; C, embrittled; D, loss of adhesion.

[d]Coating reinforeed with woven glass fabric laminate.

[e]Reported previously in ORNL-4145.

[f]Coating filled with chopped Fiberglas.

Publications, Speeches, and Seminars

ASSISTANCE PROGRAMS

Shank, E. M., W. E. Unger, and D. D. Robinson, *List of Information Sent to and Received from the Eurochemic Co., January 1, 1967, Through December 31, 1967 (Categorized)*, ORNL-TM-685, suppl. 8 (Jan. 25, 1968).

BIOCHEMICAL SEPARATIONS

Burtis, C. A., and K. S. Warren, "Identification of Urinary Constituents Isolated by Anion-Exchange Chromatography," presented at the Symposium on Urinary Constituents of Low Molecular Weight, held at ORNL, Nov. 30–Dec. 1, 1967; published in *Clin. Chem.* **14**, 290 (1968).

Davis, W., E. Schonfeld, and A. H. Kibbey, "Determination of Urinary Constituents in Solutions by Least-Squares Resolution of Ultraviolet Spectrums," presented at the Symposium on Urinary Constituents of Low Molecular Weight, ORNL, Nov. 30–Dec. 1, 1967; published in *Clin. Chem.* **14**, 310 (1968).

Davis, W., E. Schonfeld, and A. H. Kibbey, *Determination of Urinary Constituents in Solutions by Least-Squares Resolution of Ultraviolet Spectra*, ORNL-4232 (July 1968).

Egan, B. Z., "Selectivity of Polyacrylamide and Dextran Gels for Simple Cations and Anions," *J. Chromatog.* **34**, 382 (1968).

Jolley, R. L., and M. L. Freeman, "Column Chromatography of Carbohydrates in Physiological Fluids," presented at Tennessee Academy of Science Annual Meeting, Cookeville, Tenn., Nov. 17–18, 1967.

Jolley, R. L., and M. L. Freeman, "Automated Carbohydrate Analysis of Physiological Fluids," presented at Symposium on Urinary Constituents of Low Molecular Weight, ORNL, Nov. 30–Dec. 1, 1967; published in *Clin. Chem.* **14**(6), 538 (1968).

Kelmers, A. D., "Fractionation of Transfer Ribonucleic Acids," presented at U.S. Army Nuclear Science Seminar, Oak Ridge, Tenn., July 24, 1967.

Kelmers, A. D., "Separation of Transfer Ribonucleic Acids," presented at Gordon Research Conference on Ion Exchange, New London, N.H., Aug. 21–25, 1967.

Kelmers, A. D., "Macromolecular Separations," presented at Oak Ridge–Knoxville Section of AIChE, ORINS Special Training Building, Oak Ridge, Tenn., Sept. 12, 1967.

Kelmers, A. D., R. L. Pearson, and J. F. Weiss, "Preparation of 2-Formylmethionine Transfer RNA's from *E. coli* B by a New Reversed-Phase Chromatographic Method," presented at the Federation of American Societies for Experimental Biology, Atlantic City, N.J., Apr. 15–20, 1968.

Kelmers, A. D., and J. F. Weiss, "Comparison of Two Reversed Phase Chromatographic Systems for Separation of Individual *E. coli* Transfer Ribonucleic Acids," presented at the Southeastern Regional American Chemical Society Meeting, Atlanta, Ga., Nov. 1–3, 1967.

Scott, C. D., "Automated High Resolution of Body Fluids for Molecular Constituents," presented at ORAU Medical Staff Meeting, Oak Ridge, Tenn., Oct. 10, 1967.

Scott, C. D., "Analysis of Urine for Its Ultraviolet-Absorbing Constituents by High-Pressure Anion Exchange Chromatography," presented at Symposium on Urinary Constituents of Low Molecular Weight, ORNL, Nov. 30–Dec. 1, 1967; published in *Clin. Chem.* 14(6), 521 (1968).

Scott, C. D., and R. S. Melville,[1] "Introduction to the Proceedings of the Symposium on Urinary Constituents of Low Molecular Weight," *Clin. Chem.* 14(4), 287–89 (1968).

Weiss, J. F., and A. D. Kelmers, "A New Chromatographic System for Increased Resolution of Transfer Ribonucleic Acids," *Biochemistry* **6**, 2507 (1967).

CHEMICAL ENGINEERING RESEARCH

Groenier, W. S., and M. E. Whatley, *The Stacked-Clone Contactor: A High-Performance Solvent Extraction Machine Having Potential for Use in the Processing of Highly Radioactive Nuclear Fuels,* ORNL-4267 (July 1968).

McAllister, R. A.,[2] W. S. Groenier, and A. D. Ryon, "Correlation of Flooding in Pulsed, Perforated-Plate, Extraction Columns," *Chem. Eng. Sci.* **22**, 931–44 (1967).

CHEMICAL PROCESSING FOR THE MOLTEN-SALT BREEDER REACTORS

Carter, W. L., and M. E. Whatley, *Fuel and Blanket Processing Development for Molten Salt Breeder Reactors,* ORNL-TM-1852 (June 1967).

Hightower, J. R., Jr., and L. E. McNeese, *Measurement of the Relative Volatilities of Fluorides of Ce, La, Pr, Nd, Sm, Eu, Ba, Sr, Y, and Zr in Mixtures of LiF and* BeF_2, ORNL-TM-2058 (January 1968).

Whatley, M. E., W. L. Carter, R. B. Lindauer, L. E. McNeese, C. D. Scott, and J. R. Hightower, "Engineering Development of On-Site Processing for Molten Salt Breeder Reactors," *Thorium Fuel Cycle, Proceedings of Second International Thorium Fuel Cycle Symposium, Gatlinburg, Tennessee, May 3–6, 1966,* pp. 653–70, USAEC, February 1968.

DEVELOPMENT OF THE THORIUM FUEL CYCLE

Haas, P. A., W. D. Bond, M. H. Lloyd, and J. P. McBride, "Sol-Gel Process Development and Microsphere Preparation," *Thorium Fuel Cycle, Proceedings of Second International Thorium Fuel Cycle Symposium, Gatlinburg, Tennessee, May 3–6, 1966,* pp. 391–415, USAEC, February 1968.

Nicholson, E. L., L. M. Ferris, J. R. Flanary, J. H. Goode, B. A. Hannaford, J. W. Landry, J. G. Moore, R. H. Rainey, C. D. Watson, and H. O. Witte, "Recent Developments in Thorium Fuel Processing," *Thorium Fuel Cycle, Proceedings of Second International Thorium Fuel Cycle Symposium, Gatlinburg, Tennessee, May 3–6, 1966,* pp. 589–616, USAEC, February 1968.

Roberts, J. T., "Introduction to Thorium Fuel Cycles," lecture presented at Netherlands'-Norwegian Reactor School, Advanced Course on Reprocessing of Fuel from Present and Future Power Reactors, at the Institutt for Atomenergi, Kjeller, Norway, Aug. 21–Sept. 1, 1967 (to be published, together with other lecture notes, by the Institutt in 1968).

---

[1]National Institute of General Medical Sciences.

[2]Lamar State College of Technology, Beaumont, Tex.

FLUORIDE VOLATILITY PROCESSING

Miles, F. W., *Choice of a Neutron Poison for Criticality Protection of the Process Scrubber Tank in the Fluidized-Bed Volatility Pilot Plant,* ORNL-TM-2093 (April 1968).

Nicol, R. G., and W. T. McDuffee, *Molten-Salt Fluoride Volatility Pilot Plant: Equipment Performance During Processing of Aluminum-Clad Fuel Elements,* ORNL-4251 (July 1968).

Youngblood, E. L., and F. W. Miles, *Hazards Evaluation for the Fluidized-Bed Volatility Pilot Plant,* ORNL-TM-2092 (June 17, 1968).

MISCELLANEOUS

Bell, J. T., and R. E. Biggers, "Absorption Spectrum of the Uranyl Ion in Perchlorate Media. III. Resolution of the Ultraviolet Band Spectra; Some Conclusions Concerning the Excited State of UO_2^{2+}," *J. Mol. Spectry.* **25**, 312–29 (1968).

Blake, C. A., Jr., and D. J. Crouse, "Project Bronco Feasibility Study: Potential Problems Due to Radioactive Contaminants in In-Situ Retorting of Nuclear-Broken Oil Shale," in *The Bronco Oil Shale Study,* PNE-1400 (Oct. 13, 1967).

Blanco, R. E., W. C. Yee, W. E. Clark, J. M. Holmes, and R. Salmon, *A Closed-Cycle Process for Preventing Scale Formation in Evaporators and Producing Industrial Chemicals at a Nuclear Desalination Plant,* ORNL-4057 (September 1967).

Burch, W. D., and T. A. Arehart, "Safety Review Procedures for Hot Cell and Radiochemical Processing Facilities at ORNL," presented at the Winter ANS Meeting, Chicago, Ill., Nov. 5–9, 1967.

Coleman, C. F., "Properties of Organic-Water Mixtures. VIII. Dielectric Constants of *N,N*-Dialkylamides Containing Water," published as a note in *J. Phys. Chem.* **72**, 265–67 (1968).

Coleman, C. F., "Solubilities and Activity Coefficients of Sodium Chloride and Potassium Chloride in Organic-Water Mixtures. Methyl(2-ethylhexyl)sulfoxide and Several Quaternary Ammonium Chlorides and Carboxylates Containing Water," *J. Chem. Eng. Data* **13**(2), 267–71 (1968).

Davis, W., Jr., *A FORTRAN Program to Draw Isometric-Type Projections with the Calcomp Plotter,* ORNL-4137 (July 1967).

Davis, W., Jr., *Present Costs of Amino Acids and a Proposal for Their Production in an Agro-Industrial Complex,* ORNL-TM-2037 (Nov. 6, 1967).

Farrell, J. B., and P. A. Haas, "Oxidation of Nuclear-Grade Graphite by Nitric Acid and Oxygen," *I&EC Process Design and Development* **6**(3) (1967).

Ferris, L. M., "Reactions of Uranium Mononitride, Thorium Monocarbide, and Uranium Monocarbide with Nitric Acid and Other Aqueous Reagents," presented at the 155th National ACS Meeting, San Francisco, Calif., Mar. 31–Apr. 5, 1968.

Goeller, H. E., "Industrial Processes and Complexes," presented to Water and Desalination Information Meeting at ORNL, May 7–8, 1968.

Goode, J. H., and J. G. Moore, *Adsorption of Protactinium on Unfired Vycor: Final Hot-Cell Experiments,* ORNL-3950 (June 1967).

Haas, P. A., and H. F. Johnson, "Model and Experimental Results for Drainage of Solution Between Foam Bubbles," *Ind. Eng. Chem., Fundamentals* **6**, 225 (1967).

Klima, B. B., L. B. Shappert, and W. C. T. Stoddart, *Structural Analysis of Shipping Casks. Vol. 6 – Impact Testing of a Long Cylindrical Lead-Shielded Cask Model,* ORNL-TM-1312 (Jan. 23, 1968).

Landry, J. W., "Project Plowshare," presented at the Exhibit Managers Training Course sponsored by the Oak Ridge Associated Universities, Oak Ridge, Tenn., July 28, 1967.

Landry, J. W., "Peaceful Nuclear Explosives," presented to the Nuclear Engineering Seminar, University of Tennessee, Knoxville, Oct. 11, 1967.

Landry, J. W., "The Big Bomb – Once Bane, Now Boon," presented to joint meeting of Mathematics, Chemistry, and Science Clubs of Roane County High School, Kingston, Tenn., Oct. 16, 1967.

Landry, J. W., "Taming the H-Bomb for Mining and Other Industrial Applications," presented to the East Tennessee Section of The American Institute of Mining, Metallurgical, and Petroleum Engineers, Knoxville, Tenn., Nov. 10, 1967.

Landry, J. W., "Nuclear Canal Blast Pondered," interview with William Greenburg of the *Nashville Tennesseean*, published in the March 24, 1968, edition.

Landry, J. W., "Peaceful Nuclear Explosives – Objects of Optimistic Outlook," presented to Oak Ridge Optimist Club, Oak Ridge, Tenn., Apr. 9, 1968.

Landry, J. W., "A Big Boom That Is Just Ahead in Nuclear Engineering," presented to School of Nuclear Engineering, Georgia Institute of Technology, Atlanta, Apr. 25, 1968.

Landry, J. W., "Chemical and Other Industrial and Scientific Applications of Nuclear Explosives," presented to Assembly Division, Y-12 Plant, Oak Ridge, Tenn., May 2, 1968.

Landry, J. W., "Nuclear Canals and Harbors – Bigger, Better, and Bargains," presented to U.S. Navy Research Reserve, Clinton, Tenn., May 22, 1968.

Long, J. T., *Engineering for Nuclear Fuel Reprocessing* (book sponsored by USAEC Division of Technical Information), Gordon and Breach, New York, 1968.

Perona, J. J., "Multistage Hyperfiltration," presented at Water Desalination Information Meeting, ORNL, May 7, 1968.

Perona, J. J., "Hyperfiltration. Processing of Pulp Mill Sulfite Wastes with a Membrane Dynamically Formed from Feed Constituents," *Environ. Sci. Technol.* **1**, 991–96 (December 1967).

Robinson, R. A.,[3] J. P. Nichols, *et al.*, *Brayton-Cycle Radioisotope Heat-Source Design Study – Phase II (Preliminary Design) Report*, ORNL-TM-1829 (August 1967).

Rom, A. M., *Design of a Jet-Actuated Vacuum System for Use in the Coated Particle Development Laboratory, Building 4508*, ORNL-TM-1902 (June 26, 1967).

Schonfeld, E., "ALPHA M – an Improved Computer Program for Determining Radioisotopes by Least-Squares Resolution of the Gamma-Ray Spectra," *Nucl. Instr. Methods* **52**, 177 (1967).

Schonfeld, E., "Pulse-Height Analysis of Gamma-Ray Spectra of Samples Containing Very Low Levels of Radioactivity," *Nucl. Appl.* **3**, 635 (1967).

Schonfeld, E., "Equilibrium Constants and Concentrations for the Reactions of Nitrogen and Oxygen at 127 to 4727°C," *J. Chem. Educ.* **45**, 173 (1968).

Schonfeld, E., *LINEAR – A Computer Program to Fit Data Easily to Many Models by the Weighted Least-Squares Method*, ORNL-4264 (Aug. 18, 1968).

Scott, C. D., and J. S. Newman,[4] "Heat Storage in Tunnel Walls," *I&EC Fundamentals* **6**(3), 473–74 (August 1967).

Sears, M. B., and L. M. Ferris, "Reactions of Uranium and Thorium Carbides with Aqueous Solutions of Hydrochloric Acid and Sulfuric Acid," *J. Inorg. Nucl. Chem.* **29**, 1548–52 (1967).

Sears, M. B., R. J. Gray,[5] L. M. Ferris, and B. C. Leslie,[5] *Correlation of Composition and Heat-Treatment with the Microstructures of Uranium Carbides*, ORNL-3515 (July 1968).

---

[3]Isotopes Division.

[4]University of California, Berkeley.

[5]Metals and Ceramics Division.

Shappert, L. B., "Status Report on the Shipping Cask Acceptance Criteria," presented to Nuclear Safety Information Meeting at ORNL, Feb. 7, 1968.

Strain,[6] J. E., W. J. Ross,[6] G. A. West, and J. W. Landry, *The Design and Evaluation of a Delayed-Neutron Leached-Hull Monitor,* ORNL-4135 (February 1968).

Watson, C. D., G. A. West, and H. B. Graham, *et al., USA Standard Protective Coatings (Paints) for the Nuclear Industry,* USASI Standard N5.9-1967, copyright 1968 by American Institute of Chemical Engineers.

Watson, J. S., "Measurements of Enhanced Mass Transfer Rates," presented to UT Chemical Engineering Department, spring of 1967.

Watson, J. S., "Detached Turbulence Promoters," presented to UT Engineering Mechanics Department, summer of 1967.

Watson, J. S. and D. G. Thomas,[7] "Forced Convection Mass Transfer; Part IV. Increased Mass Transfer in Aqueous Medium Caused by Detached Cylindrical Turbulence Promoters in a Rectangular Channel," *A.I.Ch.E. J.* 13(4), 676–77 (July 1967).

Wymer, R. G., "Chemistry of the Nuclear Fuel Cycle," presented in two 1-hr seminars at the Ten-Week Health Physics Course, ORAU, June 3–4, 1968.

ORAU TRAVELING LECTURE PROGRAM

Landry, J. W., "The Big Bomb Bringeth Bold Benefits," presented at Oakland City College, Oakland City, Ind., Nov. 2, 1967.

Wymer, R. G., "Elements Beyond Plutonium – Their Production and Isolation," presented at University of Virginia, Charlottesville, Oct. 23, 1967.

Wymer, R. G., "A Broad View of the Nuclear Fuel Cycle," presented at Lowell Technological Institute, Lowell, Mass., Apr. 4, 1968.

POWER REACTOR FUEL PROCESSING

Blake, C. A., *Solvent Stability in Nuclear Fuel Processing: Evaluation of the Literature, Calculation of Radiation Dose, and Effects of Iodine and Plutonium,* ORNL-4212 (March 1968).

Finney, B. C., R. S. Lowrie, and C. D. Watson, *A Conceptual Design and a Cost Estimate of an On-Site Facility for Cleaning, Disassembling, and Canning Short-Cooled LMFBR Fuel in Preparation for Shipment to a Central Reprocessing Plant,* ORNL-TM-2050 (May 20, 1968).

Flanary, J. R., and J. H. Goode, *Hot-Cell Evaluation of the Grind-Leach Process. I. Irradiated HTGR Candidate Fuels: Pyrocarbon-Coated* $(Th,U)C_2$ *Particles Dispersed in Graphite,* ORNL-4117 (August 1967).

Goode, J. H., and J. R. Flanary, *Hot-Cell Evaluation of the Grind-Leach Process. II. Recovery of Uranium and Thorium from Irradiated Pyrolytic-Carbon-Coated Sol-Gel Thoria-Urania Particles,* ORNL-4213 (March 1968).

Roberts, J. T., "Reprocessing of Thorium Fuels," lecture presented at Netherlands'-Norwegian Reactor School, Advanced Course on Reprocessing of Fuel from Present and Future Power Reactors, at the Institutt for Atomenergi, Kjeller, Norway, Aug. 21–Sept. 1, 1967 (to be published, together with other lecture notes, by the Institutt in 1968).

---

[6]Analytical Chemistry Division.

[7]Reactor Division.

Roberts, J. T., "Technical and Economic Evaluation of Aqueous and Nonaqueous Reprocessing," lecture presented at Netherlands'-Norwegian Reactor School, Advanced Course on Reprocessing of Fuel from Present and Future Power Reactors, at the Institutt for Atomenergi, Kjeller, Norway, Aug. 21–Sept. 1, 1967 (to be published, together with other lecture notes, by the Institutt in 1968).

Unger, W. E., "Potential Problems in Application of Aqueous Processing to Fast Reactor Fuel," presented to Chemical Engineering Division of Argonne National Laboratory, Argonne, Ill., June 9, 1967.

Unger, W. E., F. E. Harrington, J. R. May,[8] S. F. Scott,[9] and T. N. Washburn,[5] *On-Site Fuel Processing and Recycle Plant – Design Study,* ORNL-3959 (April 1967).

West, G. A., and C. D. Watson, *Safety Studies of the Shear-Leach Processing of Zircaloy-2-Clad Spent Nuclear Fuels,* ORNL-4061 (October 1967).

PROGRESS REPORTS

Arnold, W. D., C. A. Blake, Jr., and D. J. Crouse, *Chemical Applications of Nuclear Explosions (CANE): Progress Report for July 1 to September 30, 1967,* ORNL-TM-2062 (Nov. 17, 1967).

Arnold, W. D., C. A. Blake, Jr., and D. J. Crouse, *Chemical Applications of Nuclear Explosions (CANE): Progress Report for October 1 to December 31, 1967,* ORNL-TM-2119 (Feb. 2, 1968).

Arnold, W. D., C. A. Blake, Jr., and D. J. Crouse, *Chemical Applications of Nuclear Explosions (CANE): Progress Report for January 1 to March 31, 1968,* ORNL-TM-2198 (Apr. 10, 1968).

Blake, C. A., Jr., and D. J. Crouse, *Chemical Applications of Nuclear Explosions (CANE): Progress Report for January 1 to March 31, 1967,* ORNL-TM-1886 (June 2, 1967).

Blake, C. A., Jr., D. J. Crouse, and W. D. Arnold, *Chemical Applications of Nuclear Explosions (CANE): Progress Report for April 1 to June 30, 1967,* ORNL-TM-1932 (Aug. 3, 1967).

Blanco, R. E., and F. L. Parker,[10] *Waste Treatment and Disposal Semiannual Progress Report, July–December 1966,* ORNL-TM-1887 (November 1967).

Ferguson, D. E., and staff, *Chemical Technology Division Annual Progress Report for Period Ending May 31, 1967,* ORNL-4145 (October 1967).

Scott, C. D., *Body Fluid Analysis Program, Progress Report for the Period March 1, 1967, to March 1, 1968,* ORNL-TM-2184 (April 1968).

Whatley, M. E., *et al., Unit Operations Section Quarterly Progress Report, April–June 1966,* ORNL-4074 (April 1967).

Whatley, M. E., *et al., Unit Operations Section Quarterly Progress Report, October–December 1966,* ORNL-4094 (February 1968).

Whatley, M. E., *et al., Unit Operations Section Quarterly Progress Report, January–March 1967,* ORNL-4139 (February 1968).

Whatley, M. E., *et al., Unit Operations Section Quarterly Progress Report, April–June, 1967,* ORNL-4204 (May 1968).

---

[8]Guest Scientist from Australia.

[9]Co-op student.

[10]Health Physics Division.

SEPARATIONS CHEMISTRY RESEARCH

Davis, W., Jr., and J. Mrochek, "Activities of Tributyl Phosphate in Tributyl Phosphate–Uranyl Nitrate–Water Solutions," pp. 283–95 in *Solvent Extraction Chemistry, Proceedings of the International Conference Held at Gothenburg, Sweden, 27 Aug.–1 Sept., 1966,* ed. by D. Dyrssen, J.-O. Liljenzin, and J. Rydberg, North-Holland, 1967.

McDowell, W. J., *Dielectric Constants and Refractive Indices of Solutions of Some Organophosphorus Compounds in* n-*Octane,* ORNL-TM-1893 (June 13, 1967).

Roddy, J. W., and C. F. Coleman, "Extraction of Water by Tri-*n*-octylamine Salts in Benzene and Phenylcyclohexane," presented at the 155th National ACS Meeting, San Francisco, Calif., Mar. 31–Apr. 5, 1968.

Weaver, B., "Enhancement by Zirconium of Extraction of Cations by Organophosphorus Acids I. Monoacidic Phosphonates," presented at the 155th National ACS Meeting, San Francisco, Calif., Mar. 31–Apr. 5, 1968; accepted for publication in *J. Inorg. Nucl. Chem.*

Weaver, B., and F. A. Kappelmann, "Preferential Extraction of Lanthanides over Trivalent Actinides by Monoacidic Organophosphates from Carboxylic Acids and from Mixtures of Carboxylic and Aminopolyacetic Acids," *J. Inorg. Nucl. Chem.* **30**, 263–72 (1968).

SOL-GEL STUDIES

Haas, P. A., C. C. Haws, Jr., F. G. Kitts, and A. D. Ryon, *Engineering Development of Sol-Gel Processes at the Oak Ridge National Laboratory,* ORNL-TM-1978 (January 1968); also presented at the C.N.E.N. Symposium on "Sol-Gel Processes for the Production of Ceramic Nuclear Fuels," Turin, Italy, Oct. 2–3, 1967.

Haas, P. A., F. G. Kitts, and H. Beutler, "Preparation of Reactor Fuels by Sol-Gel Processes," *Chem. Eng. Progr., Symp. Ser.* **63**(80), 16–27 (1967).

Hardy, C. J., S. R. Buxton, and M. H. Lloyd, *Preparation of Lanthanide Oxide Microspheres by Sol-Gel Methods,* ORNL-4000 (August 1967).

Helton, D. M., J. T. Bell, and N. A. Krohn, *Preparation and Preliminary Studies of Chloride-Stabilized* UO_2 *Sols,* ORNL-TM-2056 (Nov. 8, 1967).

Kitts, F. G., R. B. Fitts, and A. R. Olsen, "Sol-Gel Urania-Plutonia Microsphere Preparation and Fabrication into Fuel Rods," presented at the 1967 Nuclear Metallurgy Symposium on Plutonium Fuels Technology, Phoenix, Ariz., Oct. 4–6, 1967; to be published as a volume in Nuclear Metallurgy series of IMD Special Reports.

McBride, J. P., W. D. Bond, M. H. Lloyd, K. H. McCorkle, L. E. Morse, J. G. Moore, and R. G. Haire, *Laboratory Studies of Sol-Gel Processes at the Oak Ridge National Laboratory,* ORNL-TM-1980 (September 1967); also presented at the C.N.E.N. Symposium on Sol-Gel Processes for the Production of Ceramic Nuclear Fuels, Turin, Italy, Oct. 2–3, 1967.

Meservey, A. B., *Preparation of Sols and Microspheres of* ThO_2, UO_2, ThO_2-UO_2, *and* ThO_2-UO_3 *by Sol-Gel Techniques,* ORNL-TM-2128 (Feb. 6, 1968).

Moore, J. G., *A Sol-Gel Process for Preparing* ThO_2-UO_3 *Sols from Nitrate Solutions by Solvent Extraction with Amines,* ORNL-4095 (October 1967).

Washburn, T. N.,[5] A. L. Lotts,[5] and F. E. Harrington, *Comparative Evaluation of Sol-Gel Fuel Fabrication Costs,* ORNL-TM-1979 (September 1967).

Wymer, R. G., "Laboratory and Engineering Studies of Sol-Gel Processes at Oak Ridge National Laboratory," presented at Panel on Sol-Gel Processes held by IAEA, Vienna, Austria, May 6–10, 1968; published as ORNL-TM-2205.

THESES

Clinton, S. D., *Mass Transfer of Water from Single Thoria Sol Droplets Fluidized in 2-Ethyl-1-hexanol,* M.S. thesis, University of Tennessee, Knoxville; also published as ORNL-TM-2163 (June 1968).

Watson, J. S., *A Study of Detached Turbulence Promoters for Increasing Mass Transfer Rates in Aqueous Channel Flow,* Ph.D. dissertation, University of Tennessee, Knoxville; also published as ORNL-TM-1912 (August 1967).

TRANSURANIUM ELEMENT PROCESSING

Baybarz, R. D., and P. B. Orr, *Final Purification of the Heavy Actinides from the First Four Campaigns of the TRU Program,* ORNL-TM-2083 (Nov. 20, 1967).

Baybarz, R. D., and P. B. Orr, "Final Purification of the Heavy Actinides from the Transuranium Processing Plant," presented at the 155th National ACS Meeting, San Francisco, Calif., Mar. 31–Apr. 5, 1968.

Burch, W. D., "Transuranium Program," presented at Second International Symposium on Nucleonics in Aerospace, Columbus, Ohio, July 12, 1967; also published in Proceedings.

Burch, W. D., F. R. Chattin, and O. O. Yarbro, "Operating Experience in the Transuranium Processing Plant," presented at the 155th National Meeting of the ACS, San Francisco, Calif., Mar. 31–Apr. 5, 1968.

Buxton, S. R., and D. O. Campbell, *Application of High-Pressure Ion Exchange Column to the Separation of Trivalent Actinides and Lanthanides,* ORNL-TM-1876 (May 9, 1967).

Campbell, D. O., and S. R. Buxton, "Rapid Separation of Actinides or Lanthanides Using Finely Divided Ion Exchange Resin," presented at the 155th National ACS Meeting, San Francisco, Calif., Mar. 31–Apr. 5, 1968.

Chilton, J. M., and J. J. Fardy, "The Use of Anion Exchange Resin for the Quantitative Separation of Plutonium," presented at the 11th Annual Conference on Analytical Chemistry in Nuclear Technology, Gatlinburg, Tenn., Oct. 10–12, 1967.

Haire, R. G., "Installation and Operation of Thermogravimetric and Differential Thermal Analysis Instrumentation for Studying the Transplutonium Elements," presented at the 11th Annual Conference on Analytical Chemistry in Nuclear Technology, Gatlinburg, Tenn., Oct. 10–12, 1967.

Keller, O. L.,[11] D. E. Ferguson, and J. P. Nichols, "Prospects of Transuranium Isotopes as Neutron Sources," presented at ORAU Symposium on Radioisotopes in Medicine: In Vitro Studies, Oak Ridge, Tenn., Nov. 13–16, 1967; to be published in Proceedings.

King, L. J., *et al., Safety Analysis for the Transuranium Processing Plant, Building 7920,* ORNL-3954 (April 1968).

Matherne, J. L., E. D. Collins, and W. W. Evans, "Problems and Successes in the First Major Maintenance Performed in the Transuranium Processing Plant," presented at the Winter ANS Meeting, Chicago, Ill., Nov. 5–9, 1967.

McDuffee, W. T., and L. J. King, *Summary of the Campaign to Process Four Prototype HFIR Targets in the Transuranium Processing Plant,* ORNL-TM-1938 (April 1968).

Nichols, J. P., "Design Data for ^{252}Cf Neutron Source Experiments," *Nucl. Appl.* 4(6), 382–87 (June 1968).

---

[11]Chemistry Division.

Nugent, L. J.,[11] J. R. Tarrant,[11] J. L. Burnett,[11] R. D. Baybarz, G. K. Werner,[12] and O. L. Keller,[11] "Intra-Molecular Energy Transfer in Actinide Beta-Diketones. Exchange of Lanthanide and Actinide Ions in a Convenient Method of Scanning Actinide Complexes for Application to Liquid Lasers," presented at the 155th National ACS Meeting, San Francisco, Calif., Mar. 31–Apr. 5, 1968; submitted to *J. Phys. Chem.*

Vaughen, V. C. A., W. T. McDuffee, E. Lamb, and R. A. Robinson, "The Preparation of Multigram Quantities of ^{242}Cm for SNAP-11," presented at the Winter ANS Meeting on Remote Systems Technology, Chicago, Ill., Nov. 5–9, 1967.

Weaver, B., "Precipitation of Berkelium(IV) Iodate from Homogeneous Solution," presented at the 155th National ACS Meeting, San Francisco, Calif., Mar. 31–Apr. 5, 1968; accepted for publication in *Anal. Chem.*

URANIUM FUEL CYCLE SOL-GEL PROCESSES

Morse, L. E., "The Preparation of Aqueous Urania Sols by Solvent Extraction," presented at the 155th National ACS Meeting, San Francisco, Calif., Mar. 31–Apr. 5, 1968.

Parrott, J. R., and R. E. Brooksbank, "The Handling of Kilogram Quantities of ^{233}U by Direct and Remote Methods at the Oak Ridge National Laboratory Central Dispensing Facility," presented at the Winter ANS Meeting on Remote Systems Technology, Chicago, Ill., Nov. 5–9, 1967.

WASTE TREATMENT AND DISPOSAL

Blanco, R. E., "General Discussion on Fuel Processing and Waste Disposal," presented at the Second Annual Tennessee Industries Week Meeting, University of Tennessee, Sept. 11–15, 1967.

Blomeke, J. O., and F. E. Harrington, *Management of Radioactive Wastes at Nuclear Power Stations,* ORNL-4070 (January 1968).

Bradshaw, R. L.,[10] J. J. Perona, J. O. Blomeke, and W. J. Boegly, Jr.,[10] *Evaluation of Ultimate Disposal Methods for Liquid and Solid Radioactive Wastes. VI. Disposal of Solid Wastes in Salt Formations,* ORNL-3358 (May 1968).

Clark, W. E., D. N. Hess, P. D. Neumann, L. Rice, and J. L. English, *Laboratory Development of Processes for Fixation of High-Level Radioactive Wastes in Glassy Solids. (4) Corrosion Studies on Candidate Materials of Construction,* ORNL-3816 (July 1967).

Fitzgerald, C. L., H. W. Godbee, M. H. Davis, and W. E. Clark, *A Computer Code for Storing and Retrieving Data and Developing Improved Solids for Fixation of Highly Radioactive Wastes,* ORNL-3824, suppl. 1 (March 1968).

Godbee, H. W., N. M. Davis, and W. E. Shockley, *Dispersion of Simulated High-Level Radioactive Waste Powders in a Glass Matrix,* ORNL-TM-1897 (Aug. 4, 1967).

Goode, J. H., and J. R. Flanary, *Fixation of Intermediate-Level Radioactive Waste Concentrates in Asphalt: Hot-Cell Evaluation,* ORNL-4059 (January 1968).

King, L. J., A. Shimozato, and J. M. Holmes, *Pilot Plant Studies of the Decontamination of Low-Level Process Waste by a Scavenging-Precipitation Foam Separation Process,* ORNL-3803 (July 1968).

---

[12]Physics Division.

SEMINARS

1967		
Dec. 12	Processing of Fast Reactor Fuels:	
	Solvent Extraction	D. E. Horner
	Plutonium Partition by Hydrogen Reduction	R. H. Rainey
Dec. 19	Radiolysis of Adsorbed Water	N. A. Krohn
1968		
Jan. 9	Design of Solex Equipment	J. W. Snider
	A Pilot Plant for Plutonium Sol Gel	F. E. Harrington
Jan. 16	The Current Outlook for Nuclear Power in the U.S.	J. A. Lane
Jan. 26	Competitive Equilibria in Molecular Complex Systems	C. C. Thompson[13]
Jan. 30	Reversed-Phase Chromatographic Separation of tRNAs	J. F. Weiss
	Preparation of Two Formylmethionine tRNAs	R. L. Pearson
Feb. 6	Studies in the Unit Operations Section on the Separation of tRNAs	H. O. Weeren C. W. Hancher
Feb. 20	Status of Development of Automated Analytical Systems for Body Fluids	C. D. Scott R. L. Jolley
Feb. 27	Use of Nuclear Explosives in Processing Copper Ores and Oil Shales	W. D. Arnold C. A. Blake
Mar. 5	Incorporation of Radioactive Wastes in Asphalt:	
	Laboratory Development	H. W. Godbee
	Engineering Development	J. T. Long
	Radiation Stability	J. H. Goode
Mar. 12	Electron Microscope Studies of Lanthanide and Actinide Hydroxides	R. G. Haire
	Rapid Separation of Actinides or Lanthanides Using Finely Divided Ion Exchange Resin	D. O. Campbell
Mar. 27	Final Purification of Heavy Actinides from the Transuranium Processing Plant	P. B. Orr
	Plutonium Isolation from Chloride Solutions by Di(2-ethylhexyl)phosphoric Acid and by Anion Exchange	J. J. Fardy
Apr. 10	Processing of a MSBR by Fluorination and Distillation:	
	Relative Volatilities of Components of MSR Salt Using Recirculating Stills	J. R. Hightower
	Relative Volatilities by a Transpiration Technique	F. J. Smith
	Frozen Wall Protection Against Corrosion	B. A. Hannaford
Apr. 24	Status of TRU	O. O. Yarbro
	Some Recent Cross Section Data Obtained from Californium Irradiation in HFIR	J. E. Bigelow
May 1	Distillation of MSRE Carrier Salt	L. E. McNeese
	The Preparation of ^{233}U-Bearing Fuel for the MSRE	J. M. Chandler
May 29	Possible Impact of Agro-Industrial Developments in India	H. E. Goeller

[13]Middle Tennessee State University.

CHEMICAL TECHNOLOGY DIVISION

D. E. FERGUSON, DIRECTOR
K. B. BROWN, ASSISTANT DIRECTOR
NANCY BEACH, SECRETARY
ELAINE HICKMAN, SECRETARY
JANE WEBB, SECRETARY
J. B. RUCH, RADIATION AND SAFETY CONTROL OFFICER
R. L. JOLLEY, RADIATION AND SAFETY CONTROL OFFICER
A. T. GRESKY, SPECIAL ASSIGNMENT
MARTHA STEWART,[1] REPORTS EDITOR

H. B. GRAHAM, ADMINISTRATIVE ASSISTANT
JUNE REDMOND, SECRETARY
W. O. GREEVER, PROCUREMENT
LUCILLE KUYKENDALL, SECRETARY

LONG RANGE PLANNING COMMITTEE
J. T. ROBERTS, CHAIRMAN
E. D. ARNOLD
S. C. JACOBS
R. SALMON
O. L. CULBERSON, CONSULTANT, U.T.
JO DeCARLO, SECRETARY
TECHNICIAN: P. P. HAYDON

CHEMICAL DEVELOPMENT SECTION A

R. G. WYMER, SECTION CHIEF
R. E. LEUZE, ASSISTANT SECTION CHIEF
C. F. COLEMAN,[2] ASSISTANT SECTION CHIEF
ALICE McWILLIAMS, SECRETARY
CAROLYN WHEAT, SECRETARY
TECHNICIANS: C. F. KECK
D. E. HEATHERLY[3]
LINDA GILES,[4] PUBLICATION ASSISTANT
R. G. MANSFIELD, TRANSLATIONS

SOL-GEL STUDIES

J. P. McBRIDE, GROUP LEADER
K. H. McCORKLE
L. E. MORSE
W. L. PATTISON
TECHNICIAN: J. F. TALLEY

FUEL CYCLE STUDIES

W. D. BOND, GROUP LEADER
A. B. MESERVEY
K. J. NOTZ
TECHNICIANS: C. W. GREENE
A. S. LYLE

HEAVY ELEMENT SEPARATIONS AND ANALYSES

D. O. CAMPBELL, PROBLEM LEADER

SEPARATIONS CHEMISTRY RESEARCH

C. F. COLEMAN,[2] GROUP LEADER
W. J. McDOWELL
J. W. RODDY
TECHNICIANS: G. N. CASE
J. E. THOMPSON

HEAVY ELEMENT SEPARATIONS

M. H. LLOYD, COORDINATOR[2]
J. R. FLANARY, *TRU FLOWSHEETS*
B. WEAVER, GROUP LEADER, *SEPARATIONS AND CHEMISTRY OF ACTINIDES AND LANTHANIDES*
J. B. KNAUER, JR.
TECHNICIAN: R. R. SHOUN

R. D. BAYBARZ, GROUP LEADER, *TRU FINAL SEPARATIONS AND RESEARCH*
A. DELLE SITE[5]
F. A. KAPPELMANN
P. B. ORR
TECHNICIANS: E. C. HENDREN[6]
R. L. HICKEY
J. T. WIGGINS

M. H. LLOYD,[2] GROUP LEADER, *TRU PROCESS RESEARCH AND DEVELOPMENT*
S. R. BUXTON
J. M. CHILTON
J. J. FARDY[5]
R. G. HAIRE
J. D. HOESCHELE
O. K. TALLENT
TECHNICIANS: S. A. McCOSH
C. H. JONES

ACTINIDE ELEMENT OXIDES AND RADIATION EFFECTS

N. A. KROHN,[2] GROUP LEADER
I. L. THOMAS
TECHNICIAN: D. H. NEWMAN

ACTINIDE ELEMENT SPECTROPHOTOMETRY

N. A. KROHN,[2] GROUP LEADER
J. T. BELL
TECHNICIAN: D. M. HELTON

BIOCHEMICAL SEPARATIONS

A. D. KELMERS, GROUP LEADER
B. Z. EGAN
R. W. RHEAR
R. L. PEARSON
J. F. WEISS
TECHNICIANS: J. P. EUBANKS
J. B. OVERTON

BODY FLUIDS ANALYSES

C. D. SCOTT, GROUP LEADER
K. S. WARREN
R. L. JOLLEY[7]
C. A. BURTIS[6]
W. W. PITT
S. KATZ
E. SCHONFELD
TECHNICIANS: M. L. FREEMAN
N. E. LEE

CHEMICAL DEVELOPMENT SECTION B

R. E. BLANCO, SECTION CHIEF
D. J. CROUSE,[2] ASSISTANT SECTION CHIEF
L. M. FERRIS,[2] ASSISTANT SECTION CHIEF
W. E. CLARK[8]
SUE DAMEWOOD, SECRETARY
BEA GARBER, SECRETARY
J. E. FARMER, DRAFTSMAN

SOLVENT DEGRADATION PRODUCTS – FORMATION AND REACTIONS

W. DAVIS, JR., GROUP LEADER
A. H. KIBBEY
J. E. MROCHEK[9]
H. F. SOARD

WASTE STUDIES

H. W. GODBEE, GROUP LEADER
C. L. FITZGERALD
W. C. YEE[9]
TECHNICIAN: W. E. SHOCKLEY

POWER REACTOR FUEL PROCESSING

V. C. A. VAUGHEN, GROUP LEADER, *FLOWSHEET DEMONSTRATION ON RADIO-ACTIVE FBR, HTGR, AND LWR FUELS*
J. H. GOODE
TECHNICIANS: L. A. BYRD
G. D. DAVIS
O. L. KIRKLAND

L. M. FERRIS,[2] GROUP LEADER, *MOLTEN-SALT REACTOR PROCESSING*
J. J. LAWRANCE[5]
J. C. MAILEN
E. D. NOGUEIRA[5]
C. E. SCHILLING
M. B. SEARS[4]
F. J. SMITH
TECHNICIANS: J. F. LAND
C. T. THOMPSON
D. E. SPANGLER

R. H. RAINEY, GROUP LEADER, *FBR AND HTGR REACTOR PROCESSING AND NOBLE GAS REMOVAL*
D. E. HORNER
TECHNICIANS: J. R. COLLINS
R. C. LOVELACE

G. I. CATHERS, GROUP LEADER, *VOLATILITY PROCESSING*
M. R. BENNETT
TECHNICIAN: C. J. SHIPMAN

SEPARATIONS PROCESSES

D. J. CROUSE,[2] GROUP LEADER
W. D. ARNOLD
F. J. HURST
F. G. SEELEY
J. G. MOORE
TECHNICIAN: W. B. HOWERTON

RADIOIODINE CHEMISTRY – RADIATION STABILITY OF SOLVENT

C. A. BLAKE,[2] GROUP LEADER
J. M. SCHMITT

PLOWSHARE PROGRAM

C. A. BLAKE[2]
D. J. CROUSE[2]
W. D. ARNOLD[2]
F. J. HURST[2]

UNIT OPERATIONS SECTION

M. E. WHATLEY, SECTION CHIEF
A. D. RYON, ASSISTANT SECTION CHIEF
JANE POSEY, SECRETARY
JANICE SHANNON, SECRETARY

FUEL CYCLE STUDIES AND THORIUM UTILIZATION

P. A. HAAS, GROUP LEADER
S. D. CLINTON
C. C. HAWS, JR.
J. T. LONG
R. E. NORMAN[10]
TECHNICIANS: R. D. ARTHUR
D. A. McWHIRTER
D. E. WILLIS
E. R. JOHNS[11]

MOLTEN SALT PROCESSING

L. E. McNEESE, GROUP LEADER
J. R. HIGHTOWER, JR.
B. A. HANNAFORD
M. S. LIN
J. S. WATSON
TECHNICIANS: J. BEAMS
V. L. FOWLER
R. O. PAYNE

BIOCHEMICAL SEPARATIONS

C. D. WATSON, GROUP LEADER
C. W. HANCHER
H. O. WEEREN
H. F. JOHNSON[12]
TECHNICIANS: G. B. DINSMORE
J. S. TAYLOR

POWER REACTOR FUEL PROCESSING

C. D. WATSON, GROUP LEADER
B. C. FINNEY
R. S. LOWRIE
G. A. WEST
S. H. JURY[13]
TECHNICIANS: F. G. KILPATRICK
F. L. ROGERS
J. C. ROSE

DESALINATION STUDIES

J. C. SUDDATH
J. J. PERONA
TECHNICIAN: W. G. SISSON

[1]ON LOAN FROM TECHNICAL INFORMATION DIVISION
[2]DUAL CAPACITY
[3]EDUCATIONAL LEAVE
[4]PART-TIME EMPLOYEE
[5]GUEST SCIENTIST FROM ABROAD
[6]ASSIGNED TO THIS PROBLEM BY THE ANALYTICAL CHEMISTRY DIVISION
[7]RADIATION SAFETY OFFICER
[8]LEAVE OF ABSENCE
[9]ON LOAN TO AGRO-INDUSTRIAL SURVEY
[10]ON LOAN FROM GULF GENERAL ATOMIC
[11]ON LOAN FROM CHEMICAL SECTION A
[12]CONSULTANT, U.T.
[13]ON LOAN FROM GENERAL ENGINEERING DIVISION
[14]CONTRACT EMPLOYEE FROM SOUTHERN TECHNICAL SERVICES
[15]PART TIME FROM PILOT PLANT SECTION
[16]ON LOAN FROM PLANT AND EQUIPMENT DIVISION
[17]ON LOAN FROM PROCESS DESIGN SECTION
[18]ON LOAN FROM METALS AND CERAMICS DIVISION
[19]ON LOAN TO METALS AND CERAMICS DIVISION
NOTE: CO-OP AND SUMMER EMPLOYEES NOT INCLUDED ON CHART

PROCESS DESIGN SECTION

H. E. GOELLER,[2] SECTION CHIEF
W. E. UNGER, ASSISTANT SECTION CHIEF
H. E. GOELLER,[2] *AGRO-INDUSTRIAL STUDY*
E. M. SHANK, *EUROCHEMIC ASSISTANCE*
DOROTHY D. ROBINSON,[2] CORRESPONDENT
J. W. LANDRY,[2] *PLOWSHARE PROGRAM*
W. G. STOCKDALE,[2] *ECONOMIC STUDIES*
P. L. ROBERTSON, *COST ESTIMATES*
J. M. HOLMES,[3] *INDUSTRIAL CHEMICAL STUDIES*
F. E. HARRINGTON,[2] *PLUTONIUM SOL-GEL STUDIES*
A. M. ROM,[2] *PLUTONIUM SOL-GEL STUDIES*
W. F. SCHAFFER, JR.,[2] *WATER CLEANUP STUDIES*
W. L. CARTER,[2] *NOBLE GAS MEMBRANE SEPARATION STUDIES*
J. P. NICHOLS,[2] *NUCLEAR ENGINEERING STUDIES*
F. L. PEISHEL, *TRANSURANIUM ASSISTANCE*
F. N. BROWDER[8]
MAY E. PEPPER, SECRETARY
MARY S. BROWN, SECRETARY
DOROTHY D. ROBINSON,[2] SECRETARY
K. F. STOOKSBURY, CLERK

DRAFTSMEN

D. E. DUNNING,[13] DRAFTING SUPERVISOR

J. W. DAY	L. C. HUBBARD[13]
B. G. DeVALL	R. D. NIPPER[13]
H. W. FALLON[13]	J. M. O'KEEFE[13]
R. G. FARLEY[13]	R. P. OLIVER[13]
A. J. FARMER	H. B. PERKINSON[14]
DONNA S. FITZGERALD	J. D. PHILLIPS[13]
G. K. FORD[13]	N. D. ROBERTS[13]
M. R. JOHNSON[14]	W. W. SHEWBROOKS[13]
BARBARA A. HISE	J. N. WHEELER[13]

THORIUM FUEL CYCLE

A. R. IRVINE,[2] GROUP LEADER
J. W. ANDERSON,[13] *CONSTRUCTION LIAISON*
J. P. JARVIS,[13] *CONSTRUCTION LIAISON*
J. M. CHANDLER,[13] *PROCESS EQUIPMENT*
J. W. SNIDER,[2] *PROCESS EQUIPMENT*
F. L. HANNON,[13] *PROCESS EQUIPMENT*
G. B. BERRY,[2,13] *PROCESS EQUIPMENT*
R. V. FOLTZ,[2,13] *PROCESS EQUIPMENT*
J. H. FREELS,[13] *CRITICAL PATH SCHEDULE*

VOLATILITY STUDIES

R. P. MILFORD,[2] GROUP LEADER
S. MANN, *SAMPLING AND ACCOUNTABILITY*
F. W. MILES,[2] *RADIATION AND PLUTONIUM*
E. L. YOUNGBLOOD,[2] *SAFETY ANALYSIS*
B. B. KLIMA,[2] *PROCUREMENT*
G. E. PIERCE,[14] *PROJECT LIAISON*
J. T. HUFFSTETLER,[13] *CRITICAL PATH SCHEDULE*

WASTE STUDIES

J. O. BLOMEKE, GROUP LEADER
E. J. FREDERICK,[2] *FBVPP WASTE STUDIES*
A. M. ROM,[2] *ASPHALT WASTE STUDIES*

MSR STUDIES

E. L. NICHOLSON, GROUP LEADER
W. L. CARTER,[2] *MSBR FUEL PROCESSING*
J. P. NICHOLS,[2] *COMPUTER STUDIES*
W. F. SCHAFFER, JR.,[2] ^{233}U *MSRE LOADING*
E. L. YOUNGBLOOD,[2] *EQUIPMENT DESIGN*
M. J. BELL, *SAFETY STUDIES*

AQUEOUS FBR FUEL PROCESSING

A. R. IRVINE,[2] GROUP LEADER
W. G. STOCKDALE,[2] *OFF-GAS STUDIES*
F. E. HARRINGTON,[2] *DESIGN ANALYSIS*
J. W. SNIDER,[2] *PROCESS EQUIPMENT DESIGN*
G. B. BERRY,[2] *PROCESS EQUIPMENT*
F. W. MILES,[2] *CONTAINMENT STUDIES*

FUEL TRANSPORT STUDIES

L. B. SHAPPERT, GROUP LEADER
E. J. FREDERICK,[2] *TECHNICAL ANALYSIS*
W. C. T. STODDART,[13] *STRUCTURAL ANALYSIS*
B. B. KLIMA,[2] *CASK DESIGN COMPLIANCE*

Y-12 ENGINEERING ASSISTANCE

B. F. BOTTENFIELD
J. W. LANDRY[2]
R. P. MILFORD[2]
A. M. ROM[2]
J. B. RUCH[2]
R. V. FOLTZ[2,13]

PILOT PLANT SECTION

R. E. BROOKSBANK, SECTION CHIEF
W. D. BURCH, ASSISTANT SECTION CHIEF
R. B. LINDAUER, *MSRE PROCESSING PLANT DESIGN*
BOBBIE HOYLE, SECRETARY
JANET MASON, SECRETARY
JOYCE WALDEN, SECRETARY
NANCY WEXLER, SECRETARY
E. C. BRANTLEY, CLERK
R. B. WATERS, DRAFTSMAN

TRANSURANIUM FACILITY

W. D. BURCH, GROUP LEADER
O. O. YARBRO, *OPERATIONS*
L. J. KING, *TECHNICAL GROUP*
J. L. MATHERNE, *ENGINEERING, PLANT SAFETY*
F. L. PEISHEL[17]
J. E. BIGELOW
E. D. COLLINS
W. W. EVANS
J. E. VAN CLEVE[15]

PROCESS SUPERVISORS

C. E. WADDELL
B. J. STRADER[18]
R. C. SHIPWASH
C. L. SHEPHERD

TECHNICIANS

W. G. BARRETT	R. R. LAXSON
K. P. BAYNE[18]	D. B. OWSLEY
W. J. BRYAN	R. E. POTTER[19]
H. S. CALDWELL	K. R. SANGER
T. L. DOUGLASS	J. R. SLAVEN[18]
J. T. EAST[18]	W. M. SPROULE
J. H. GROOVER	H. C. THOMPSON
J. C. HILL[18]	A. V. WILDER
M. C. HILL	G. E. WOODALL

FLUORIDE VOLATILITY

W. H. CARR, GROUP LEADER

RADIOCHEMICAL OPERATIONS

J. R. PARROTT, GROUP LEADER
R. G. NICOL, ^{233}U *DISPENSING, CONSTRUCTION*
F. R. CHATTIN, *SOL-GEL PILOT PLANT PROJECTS*
W. T. McDUFFEE, *SOL-GEL PREPARATION*

PROCESS SUPERVISORS

W. A. SHANNON
R. J. SHANNON

TECHNICIANS

J. H. BROCK	C. W. MARTIN
C. W. BOATMAN	R. E. PURKEY
W. H. LEWIS, JR.	S. E. SHELL
W. A. LINDSEY	D. R. TAYLOR
J. H. WALKER	

HOT CELL FACILITY

V. C. A. VAUGHEN, GROUP LEADER, *PLANT SAFETY*

MSRE FUEL PREPARATION

J. M. CHANDLER[19]
S. MANN
TECHNICIANS: W. T. BOSTIC
E. W. BROWN
B. G. DeVALL[17]
A. J. FARMER[17]

SPECIAL PROJECTS

F. G. KITTS, *MOUND ASSISTANCE*
W. R. WHITSON, *IN-PLANT DESIGN*
R. W. HORTON, *ACCOUNTABILITY, COMPUTER PROGRAMS*

ORNL-4272
UC-10 – Chemical Separations Processes for Plutonium and Uranium

INTERNAL DISTRIBUTION

1. Biology Library
2–4. Central Research Library
5. Laboratory Shift Supervisor
6–7. ORNL – Y-12 Technical Library Document Reference Section
8. MIT Practice School
9–28. Laboratory Records Department
29. Laboratory Records, ORNL R.C.
30–31. R. D. Baybarz
32. S. E. Beall
33. Arnold Berman
34. D. S. Billington
35. C. A. Blake
36. R. E. Blanco
37. J. O. Blomeke
38. W. D. Bond
39. C. J. Borkowski
40. G. E. Boyd
41. R. E. Brooksbank
42. J. C. Bresee
43. R. B. Briggs
44. F. N. Browder
45. K. B. Brown
46. F. R. Bruce
47. W. D. Burch
48. D. O. Campbell
49. W. H. Carr
50. G. I. Cathers
51. J. M. Chandler
52. W. E. Clark
53. C. F. Coleman
54. J. A. Cox
55. D. J. Crouse
56. F. L. Culler
57. J. E. Cunningham
58. W. Davis, Jr.
59. D. A. Douglas
60. J. J. Fardy
61–210. D. E. Ferguson
211. L. M. Ferris
212. J. R. Flanary
213. J. L. Fowler
214. J. H. Frye, Jr.
215. R. C. Fuller
216. J. H. Gillette
217. H. W. Godbee
218. H. E. Goeller
219. H. B. Graham
220. A. T. Gresky
221. W. R. Grimes
222. P. A. Haas
223. J. P. Hammond
224. C. S. Harrill
225. R. W. Horton
226. A. R. Irvine
227. R. L. Jolley
228. W. H. Jordan
229. M. A. Kastenbaum
230. C. P. Keim
231. M. T. Kelley
232. A. D. Kelmers
233. F. Kertesz
234. R. F. Kimball
235. N. A. Krohn
236. E. Lamb
237. J. A. Lane
238. C. E. Larson
239. R. E. Leuze
240. R. B. Lindauer
241. J. L. Liverman
242. R. S. Livingston
243. M. H. Lloyd
244. H. G. MacPherson
245. F. C. Maienschein
246. J. P. McBride
247. W. J. McDowell
248. L. E. McNeese
249. R. A. McNees
250. A. B. Meservey
251. R. P. Milford
252. D. R. Miller
253. E. C. Miller
254. K. Z. Morgan
255. M. L. Nelson
256. J. P. Nichols
257. E. L. Nicholson

258. R. E. Norman
259–260. R. B. Parker
261. J. R. Parrott
262. Helen Raaen
263. R. H. Rainey
264. M. E. Ramsey
265. J. T. Roberts
266. A. D. Ryon
267. A. F. Rupp
268. C. D. Scott
269. H. E. Seagren
270. E. M. Shank
271. L. B. Shappert
272. M. J. Skinner
273. A. H. Snell
274. M. G. Stewart
275. J. C. Suddath
276. D. A. Sundberg
277. E. H. Taylor
278. W. E. Unger
279. V. C. A. Vaughen
280. F. C. Von der Lage
281. C. D. Watson
282. B. S. Weaver
283. A. M. Weinberg
284. M. E. Whatley
285. J. C. White
286. G. C. Williams
287. R. G. Wymer
288. B. J. Young
289. Gale Young
290. E. L. Youngblood
291. P. H. Emmett (consultant)
292. J. J. Katz (consultant)
293. E. A. Mason (consultant)
294. J. L. Margrave (consultant)
295. R. B. Richards (consultant)

EXTERNAL DISTRIBUTION

296. D. F. Cope, RDT Site Office (ORNL)
297. Richard Hamburger, AEC, Washington
298. J. A. Swartout, 270 Park Avenue, New York 17, New York
299. Sylvania Electric Products, Inc.
300. Dr. Barendregt, c/o COMPRIMO, Europahuis, James Wattstraat 79, Amsterdam, Holland
301. Giacomo Calleri, CNEN, c/o Vitro via Bacdisseras, Milano, Italy
302. D. J. Carswell, Radiochemical Laboratory, The New South Wales University of Technology, P.O. Box 1, Kensington, Sydney, N.S.W., Australia
303. E. Cerrai, Laboratori CISE, Casella Postale N. 3986, Milano, Italy
304. David Dryssen, The Royal Institute of Technology, Department of Inorganic Chemistry, Kemisträgen 37, Stockholm 70, Sweden
305. Syed Fareeduddin, Indian Rare Earths Ltd., Army and Navy Building, 148 Mahatma Gandhi Road, Bombay 1, India
306. W. Wild, United Kingdom Atomic Energy Authority, Atomic Energy Research Establishment, Harwell, Berks, England
307. W. A. Graf, Manager, Plant Design, Atomic Products Division, General Electric Company, Box 450, Palo Alto, Calif.
308. H. Irving, Department of Inorganic Chemistry, University of Leeds, Leeds, England
309. T. Ishihara, Division of Fuel Research and Development, Tokai Research Establishment, JAERI, Tokai-mura, Ibaraki-ken, Japan
310. A. S. Kertes, Hebrew University, Jerusalem
311. Jorgen Klitgaard, Atomic Energy Commission Res. Estab. Risö, Roskilde, Denmark
312. Y. Marcus, Israel Atomic Energy Commission, Tel Aviv, Israel
313. E. Glueckauf, Atomic Energy Research Establishment, Harwell, Berks, England
314. P. Regnaut, C.E.N. Fontenay-aux-Roses, Boite Postale No. 6, Fontenay-aux-Roses, Seine, France
315. R. Rometsch, Eurochemic, Mol. Belgium
316. A. J. A. Roux, Director of Atomic Energy Research, South African Council for Scientific and Industrial Research, Box 395, Pretoria, South Africa

317. Jan Rydberg, Department of Nuclear Chemistry, Chalmers Tekniska Hogskola, Gibraltargatan 5 H. Goteborg, Sweden
318. M. Shaw, AEC, Washington
319. Erik Svenke, Director, Department of Chemistry, Atomic Energy Company, Stockholm 9, Sweden
320. D. G. Tuck, Associate Professor, Department of Chemistry, Simon Fraser University, Burnaby 2, British Columbia, Canada
321. B. F. Warner, United Kingdom Atomic Energy Authority, Production Group, Windscale and Calder Works, Sellafield, Seascale, Cumberland, England
322. R. A. Wells, Dept. of Scientific and Industrial Research, National Chemical Laboratory, Teddington, Middlesex, England
323. M. Zifferero, Comitato Nazionale per l'Energia, Nucleare, Laboratorio Trattamento Elementi Combustibili, c/o Instituto di Chemica Farmaceutica e Tossicologica dell 'Universita, Piazzale delle Scienze, 5, Rome, Italy
324. M. Claude Jean Jouannaud, Department Head, Plutonium Extraction Plant, Marcoule (Gard), France
325. Prof. Louis Gutierrez-Jadra, Director de Planta Pilotos e Industriales, Junta de Energia Nuclear, Ciudad Universitaris, Madrid (3), Spain
326. W. G. Belter, AEC, Washington
327. J. A. Lieberman, AEC, Washington
328. W. H. Regan, AEC, Washington
329. H. Bernard, AEC, Washington
330. P. Schmid, Federal Institute for Reactor Research, Wurenlingen, AG, Switzerland
331. Atou Shimozato, Nuclear Reactor Design Section, Nuclear Power Plant Department, Hitachi Ltd., Hitachi Works, Hitachi-Shi, Ibaraki-Ken, Japan
332. R. S. Brodsky, Division of Naval Reactors, Atomic Energy Commission, Washington, D.C. 20545
333. R. W. Barber, AEC, Washington
334. Theodore Rockwell III, Chairman AIF Safety Task Force, MPR Associates, Inc., 815 Connecticut Avenue, N.W., Washington, D.C. 20006
335. Guenther Wirths, NUKEM, Hanau, Germany
336. Riki Kobayashi, Professor, Rice University
337. W. Pollard, Oak Ridge Associated Universities
338. G. R. Hall, Nuclear Technology Laboratories, Department of Chemical Technology, Imperial College, Prince Consort Road, London, S.W. 7, England
339. Giuseppe Orsenigo, CNEN, Via Belisario 15, Rome, Italy
340. Laboratory and University Division, AEC, ORO
341. Dr. Werner Muller, European Transuranium Institute, Euratom, Postfach 2266, 75 Karlsruhe, West Germany
342. Prof. F. Baumgartner, Heidelberg University, Karlsruhe, Postfach 947, West Germany
343. Dr. Hugo Schumacher, Swiss Federal Institute for Reactor Research, Ch-5303 Wurenlingen, Switzerland
344. B. L. Vondra, NUMEC, Apollo, Pa.
345. W. H. McVey, AEC, Washington
346. E. E. Sinclair, AEC, Washington
347. A. R. Van Dyken, AEC, Washington
348. C. L. Sumrall, Gilbert Associates, Reading, Pa.
349. Dr. Narayanan Srinivasan, Head of Fuel Reprocessing Division, Bhabha Atomic Research Center, Bombay 74, India
350. D. M. Rafi, Pakistan Institute of Nuclear Science and Technology, P.O. Box Nilore, Rawal Pindi, Pakistan
351. D. E. Bloomfield, Battelle Northwest, Richland Washington
352. P. A. DeJonghe, Centre d'Etude de l'Energie Nucleaire, Mol, Belgium
353. T. W. McIntosh, Division of Reactor Development and Technology, USAEC, Washington, D.C. 20545
354. R. E. Pahler, AEC, Washington

355–499. Given distribution as shown in TID-4500 under Chemical Separations Processes for Plutonium and Uranium (25 copies – CFSTI)